frontiers | Research Topics

# Translational applications of neuroimaging

**Edited by**
Stavros Skouras, David M. A. Mehler and Amelie Haugg

**Published in**
Frontiers in Neuroscience

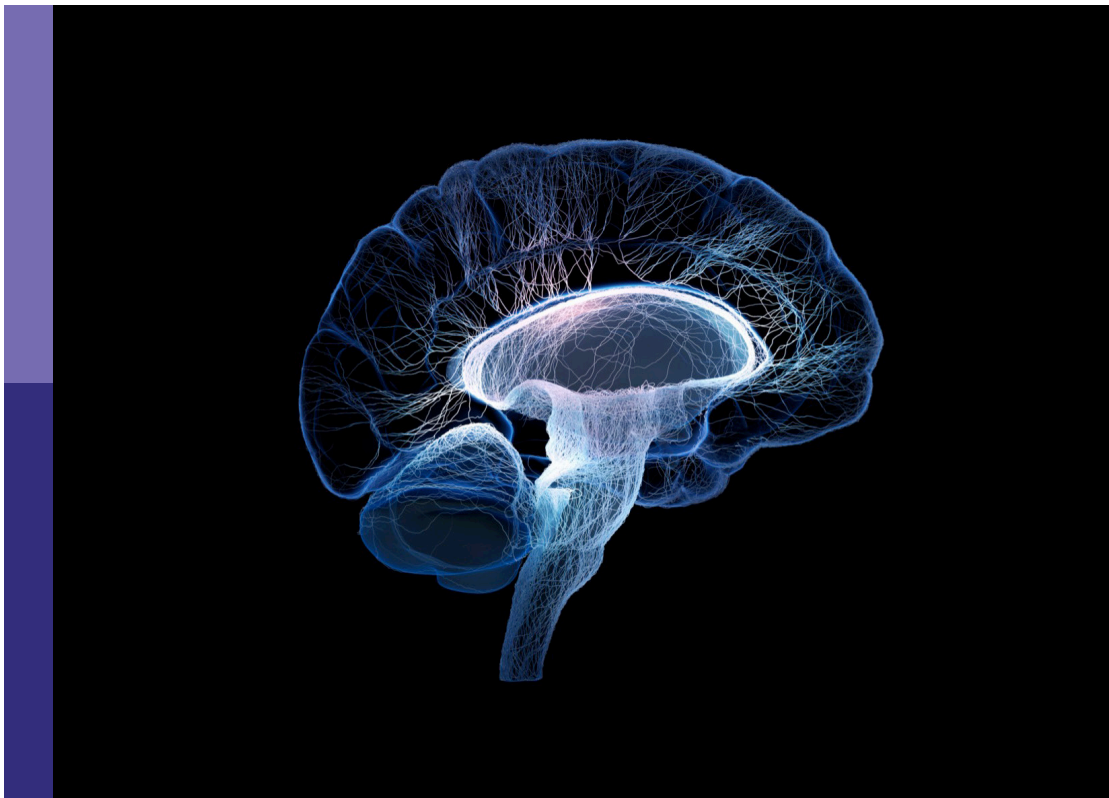

ISSN 1664-8714
ISBN 978-2-8325-4733-5
DOI 10.3389/978-2-8325-4733-5

## About Frontiers

Frontiers is more than just an open access publisher of scholarly articles: it is a pioneering approach to the world of academia, radically improving the way scholarly research is managed. The grand vision of Frontiers is a world where all people have an equal opportunity to seek, share and generate knowledge. Frontiers provides immediate and permanent online open access to all its publications, but this alone is not enough to realize our grand goals.

## Frontiers journal series

The Frontiers journal series is a multi-tier and interdisciplinary set of open-access, online journals, promising a paradigm shift from the current review, selection and dissemination processes in academic publishing. All Frontiers journals are driven by researchers for researchers; therefore, they constitute a service to the scholarly community. At the same time, the *Frontiers journal series* operates on a revolutionary invention, the tiered publishing system, initially addressing specific communities of scholars, and gradually climbing up to broader public understanding, thus serving the interests of the lay society, too.

## Dedication to quality

Each Frontiers article is a landmark of the highest quality, thanks to genuinely collaborative interactions between authors and review editors, who include some of the world's best academicians. Research must be certified by peers before entering a stream of knowledge that may eventually reach the public - and shape society; therefore, Frontiers only applies the most rigorous and unbiased reviews. Frontiers revolutionizes research publishing by freely delivering the most outstanding research, evaluated with no bias from both the academic and social point of view. By applying the most advanced information technologies, Frontiers is catapulting scholarly publishing into a new generation.

## What are Frontiers Research Topics?

Frontiers Research Topics are very popular trademarks of the *Frontiers journals series*: they are collections of at least ten articles, all centered on a particular subject. With their unique mix of varied contributions from Original Research to Review Articles, Frontiers Research Topics unify the most influential researchers, the latest key findings and historical advances in a hot research area.

Find out more on how to host your own Frontiers Research Topic or contribute to one as an author by contacting the Frontiers editorial office: frontiersin.org/about/contact

# Translational applications of neuroimaging

**Topic editors**

Stavros Skouras — University of Bergen, Norway

David M. A. Mehler — University Hospital RWTH Aachen, Germany

Amelie Haugg — Psychiatric University Hospital Zurich, Switzerland

**Citation**

Skouras, S., Mehler, D. M. A., Haugg, A., eds. (2024). *Translational applications of neuroimaging*. Lausanne: Frontiers Media SA. doi: 10.3389/978-2-8325-4733-5

# Table of contents

frontiers | Frontiers in Neuroscience

TYPE Editorial
PUBLISHED 26 March 2024
DOI 10.3389/fnins.2024.1400383



OPEN ACCESS

EDITED AND REVIEWED BY
Guo-Yuan Yang,
Shanghai Jiao Tong University, China

*CORRESPONDENCE
Amelie Haugg
✉ amelie.haugg@uzh.ch

†These authors have contributed equally to this work

RECEIVED 13 March 2024
ACCEPTED 18 March 2024
PUBLISHED 26 March 2024

CITATION
Haugg A, Mehler DMA and Skouras S (2024) Editorial: Translational applications of neuroimaging. *Front. Neurosci.* 18:1400383. doi: 10.3389/fnins.2024.1400383



# Editorial: Translational applications of neuroimaging

Amelie Haugg[1*†], David M. A. Mehler[2,3,4†] and Stavros Skouras[5†]

[1]Department of Child and Adolescent Psychiatry, Psychiatric Hospital, University of Zürich, Zürich, Switzerland, [2]Department of Psychiatry, Psychotherapy and Psychosomatics, Faculty of Medicine, RWTH Aachen University, Aachen, Germany, [3]Institute for Translational Psychiatry, University of Münster, Münster, Germany, [4]Cardiff University Brain Research Imaging Centre, School of Psychology, Cardiff University, Cardiff, United Kingdom, [5]Department of Fundamental Neurosciences, Faculty of Medicine, University of Geneva, Geneva, Switzerland

KEYWORDS

**translational applications, neuroimaging, psychiatry, neurology, EEG, MRI, CT, multimodal neuroimaging**

Editorial on the Research Topic
Translational applications of neuroimaging

Despite substantial progress in the development of neuroimaging methodologies, translational applications of neuroimaging remain scarce. This Research Topic focuses on the latest efforts to transform scientific insights into clinical solutions, highlighting a wide range of promising neuroimaging applications and techniques aimed at improving health outcomes.

Five original studies featured here investigated the use of electroencephalography (EEG) to identify potential neurophysiological biomarkers for the diagnosis and prognosis of neurological and psychiatric disorders. Rockholt et al. conducted a narrative literature review to explore how EEG combined with machine learning algorithms can be utilized as a tool for investigating the neural underpinnings of chronic pain. They underscored the advantages of EEG for studying chronic pain and highlighted the role of machine learning in developing possible biomarkers for this condition. The authors concluded that, in combination with the acquisition of large-scale datasets through collaborative efforts, EEG holds promise for providing valuable information for chronic pain diagnostics in the future. Kenefati et al. empirically assessed the association between EEG oscillations and altered acute pain in chronic pain patients. They observed that chronic pain enhanced pain perception in both pain-affected and pain-unaffected body sites and that distinct brain regions and oscillations were involved in localized hypersensitivity and generalized hyperalgesia. Tao et al. investigated the potential of a limited frontoparietal EEG montage to predict favorable or unfavorable outcomes for comatose patients. Using a retrospective analysis, the authors observed a significant association between a suppressed phase-lag index derived from electrodes F3 and P4 and an unfavorable coma outcome for both stroke patients and patients with traumatic brain injury, demonstrating the value of a limited frontoparietal EEG montage for prognosing coma outcomes. Wang et al. demonstrated how the power of convolutional neural network optimization techniques can be harnessed toward the development of automatic epileptic seizure detection systems for clinical applications. Lastly, Carrle et al. addressed the ubiquitous data science challenge of limited training data in the context of classifying patients suffering from major depressive disorder

(MDD) vs. healthy controls using EEG resting-state. First, the authors systematically reviewed existing EEG literature for data augmentation techniques and found reports of classification accuracy improvements ranging between 1 and 40%. They then used data augmentation to generate EEG time-series based on two publicly available case-control EEG data sets that both contained recordings obtained from MDD patients and healthy controls. Their results yielded an improved classification accuracy of up to 10% for one of the two case-control data sets. The authors discuss important challenges worth considering for data augmentation in MDD and other clinical contexts.

Another area with translational potential for neuroimaging is concerned with monitoring changes in brain structure following disease or interventions. Molinski et al. (2024) used deep learning to detect hypoxic ischemic encephalopathy after cardiac arrest based on computer tomography (CT) images. Their overall sample comprised 168 CT images, of which about half (52.4%) showed radiological signs, according to expert ratings that were used as ground truth labels. Classification performance on a testing set of 34 independent images revealed accuracies of ∼79% with an area under the curve of 93–94%. The authors further provided data that helped interpret the machine learning process by visualizing image features that contributed to the classifier's decision. Further, Shao et al. provide a clinical review emphasizing the role of diffusion tensor imaging for studying the arcuate fasciculus, a key white matter tract implicated in language function. The authors highlight its relevance for exploring potential targets for interventions, as well as for assessing therapeutic progress from neural plasticity, following major brain injuries due to stroke or tumors.

Multimodal brain imaging approaches allow for combining strengths of individual brain imaging techniques and partly overcoming limitations of single modality approaches. Reviews help aggregate such knowledge and highlight new insights that complementary imaging modalities provide for a research field or use case of interest. Korivand et al. contributed a systematic review of studies on the neural correlates of human locomotion. EEG was the most commonly used neuroimaging technique to study locomotion, followed by fMRI, functional near-infrared spectroscopy (fNIRS), and positron emission tomography (PET). Ecologically valid tasks, such as cycling and walking in real-world settings are noted as particularly promising for translational purposes. A key insight is that neural correlates of locomotion have thus far mostly been in healthy individuals. The review concludes with recommendations for the future development of the locomotion imaging research field. Konrad et al. (2023) performed a review of neurostimulation and neuroimaging methods used to promote Interpersonal Neural Synchrony, which is considered a key facilitator of empathy, emotion regulation, and prosocial commitment. The review highlights the potential of hyperscanning to investigate neural mechanisms of impaired social interactions in Autism Spectrum Disorder (ASD), Reactive Attachment Disorder (RAD), and Social Anxiety Disorder (SAD). Current limitations and future steps toward clinical utility are presented, including a potential role for combining hyperscanning and neurofeedback (hyperfeedback) as a potential new intervention to target impaired social interactions.

Particularly, the use of real-time fMRI neurofeedback (rt-fMRI-NFB) is emerging as a promising neuroimaging-based intervention technique aiming to normalize dysfunctional brain signals associated with clinical symptoms. With an original rt-fMRI-NFB study, Lieberman et al. tested the feasibility of downregulating activity in the amygdala or the posterior cingulate cortex (PCC) in a sample of patients suffering from post-traumatic stress disorder (PTSD). Both groups showed similar downregulation performance. However, compared to the amygdala downregulation group, patients in the PCC group showed decreased neural activity in areas associated with PTSD psychopathology, including higher visual cortices as well as temporoparietal regions. Behavioral data indicated that only the PCC group showed improvements in PTSD symptoms, suggesting that observed network changes following PCC downregulation may have therapeutic effects. Watve et al. investigated the feasibility of a rt-fMRI-NFB application that coupled ongoing amygdala activity with a visual feedback display of dynamic emotional faces. Healthy participants, divided into four groups, were instructed to either upregulate or downregulate their amygdala activity based on feedback ranging from either fearful to neutral or neutral to happy faces. Amygdala activity in groups receiving feedback based on fearful faces, but not happy faces, showed signal modulations. Further, valence-dependent changes in effective connectivity between the fusiform face area and the amygdala were observed. However, neurofeedback training did not lead to changes in clinical and behavioral measures.

Concluding, this Research Topic draws together diverse findings from the latest research across multiple neuroimaging modalities and clinical use cases. According to this, particularly promising near-future applications of translational neuroimaging include the use of machine learning approaches and real-time interventions in the management of chronic and acute pain, epilepsy, encephalopathy, coma, stroke, MDD, PTSD, ASD, RAD, and SAD.

## Author contributions

AH: Writing – original draft, Writing – review & editing. DM: Writing – original draft, Writing – review & editing. SS: Writing – original draft, Writing – review & editing.

## Funding

The author(s) declare financial support was received for the research, authorship, and/or publication of this article. AH was supported by the NCCR Evolving Language with Swiss National Science Foundation Agreement #51NF40_180888 and the Foundation Adrian et Simone Frutiger. DM was supported by the RWTH Junior Principal Investigator (JPI) fellowship funded by the Excellence Strategy of the Federal Government and the Laender (Grant No. JPI074-21).

## Conflict of interest

The authors declare that the research was conducted in the absence of any commercial or financial relationships that could be construed as a potential conflict of interest.

## Publisher's note



## References

Konrad, K., Gerloff, C., Kohl, S. H., Mehler, D. M., Mehlem, L., Volbert, E. L., et al. (2023). Interpersonal neural synchrony and mental disorders: unlocking potential pathways for clinical interventions. *Front. Neurosci.* 18:1286130. doi: 10.3389/fnins.2024.1286130

Molinski, N. S., Kenda, M., Leithner, C., Nee, J., Scheel, M., and Meddeb, A. (2024). Deep learning-enabled detection of hypoxic–ischemic encephalopathy after cardiac arrest in CT scans: a comparative study of 2D and 3D approaches. *Front. Neurosci.* 18:1245791. doi: 10.3389/fnins.2024.1245791

frontiers | Frontiers in Neuroscience

TYPE Systematic Review
PUBLISHED 01 March 2023
DOI 10.3389/fnins.2023.1051500



OPEN ACCESS

EDITED BY
David M. A. Mehler,
University Hospital RWTH Aachen, Germany

REVIEWED BY
Shanshan Yao,
Stony Brook University, United States
Johanna Wagner,
University of California, San Diego,
United States

*CORRESPONDENCE
Jiaqi Gong
✉ jiaqi.gong@ua.edu

SPECIALTY SECTION
This article was submitted to Translational Neuroscience, a section of the journal Frontiers in Neuroscience

RECEIVED 22 September 2022
ACCEPTED 06 February 2023
PUBLISHED 01 March 2023

CITATION
Korivand S, Jalili N and Gong J (2023) Experiment protocols for brain-body imaging of locomotion: A systematic review. *Front. Neurosci.* 17:1051500. doi: 10.3389/fnins.2023.1051500



# Experiment protocols for brain-body imaging of locomotion: A systematic review

Soroush Korivand[1,2], Nader Jalili[1] and Jiaqi Gong[2]*

[1]Department of Mechanical Engineering, The University of Alabama, Tuscaloosa, AL, United States, [2]Department of Computer Science, The University of Alabama, Tuscaloosa, AL, United States

**Introduction:** Human locomotion is affected by several factors, such as growth and aging, health conditions, and physical activity levels for maintaining overall health and well-being. Notably, impaired locomotion is a prevalent cause of disability, significantly impacting the quality of life of individuals. The uniqueness and high prevalence of human locomotion have led to a surge of research to develop experimental protocols for studying the brain substrates, muscle responses, and motion signatures associated with locomotion. However, from a technical perspective, reproducing locomotion experiments has been challenging due to the lack of standardized protocols and benchmarking tools, which impairs the evaluation of research quality and the validation of previous findings.

**Methods:** This paper addresses the challenges by conducting a systematic review of existing neuroimaging studies on human locomotion, focusing on the settings of experimental protocols, such as locomotion intensity, duration, distance, adopted brain imaging technologies, and corresponding brain activation patterns. Also, this study provides practical recommendations for future experiment protocols.

**Results:** The findings indicate that EEG is the preferred neuroimaging sensor for detecting brain activity patterns, compared to fMRI, fNIRS, and PET. Walking is the most studied human locomotion task, likely due to its fundamental nature and status as a reference task. In contrast, running has received little attention in research. Additionally, cycling on an ergometer at a speed of 60 rpm using fNIRS has provided some research basis. Dual-task walking tasks are typically used to observe changes in cognitive function. Moreover, research on locomotion has primarily focused on healthy individuals, as this is the scenario most closely resembling free-living activity in real-world environments.

**Discussion:** Finally, the paper outlines the standards and recommendations for setting up future experiment protocols based on the review findings. It discusses the impact of neurological and musculoskeletal factors, as well as the cognitive and locomotive demands, on the experiment design. It also considers the limitations imposed by the sensing techniques used, including the acceptable level of motion artifacts in brain-body imaging experiments and the effects of spatial and temporal resolutions on brain sensor performance. Additionally, various experiment protocol constraints that need to be addressed and analyzed are explained.

KEYWORDS

**human locomotion, observational constraints, brain body imaging, experimental design methodology, cognitive demands, locomotive task, brain muscle functional connectivity**

# 1. Introduction

About 28% of American adults older than 50 in the general community presented with impaired locomotion and its prevalence increased with age ($p < 0.001$) (Mahlknecht et al., 2013). The causes of impaired locomotion are divided into neurological (e.g., Parkinson's disease, stroke, Multiple Sclerosis, and dementia) (Allali et al., 2018; Buckley et al., 2019) and/or musculoskeletal drivers, such as arthritis and cardiovascular conditions (Blyth et al., 2019; Andonian and Huffman, 2020; Minetto et al., 2020). Among these neurological and musculoskeletal impacts, previous research has identified different patterns of gait disorders, such as parkinsonian (De Bartolo et al., 2020; Guayacán and Martínez, 2021), frontal (Hülser et al., 2022), or spastic gait (Muñoz-Lasa et al., 2019; Norbye et al., 2020). Furthermore, researchers have argued that locomotion should be defined as a syndrome for pre-clinical outcomes, such as motoric cognitive risk syndrome for pre-dementia (Xiang et al., 2021; Li et al., 2022a). Because of the neurological and musculoskeletal correlates of locomotion, rehabilitation treatments have been explored to utilize locomotion training, such as treadmill gait exercise, to improve patients' musculoskeletal ability and further induce neurological benefits (Smania et al., 2011; Hornby et al., 2016; Bassiri et al., 2022). Therefore, each human locomotion contains unique features of neural and musculoskeletal drivers, clinical conditions, the complexities of human development and aging, and signifiers of physical activity for health and wellness (Runge and Hunter, 2006; Pons et al., 2013; Kerkman et al., 2018).

Understanding the neurological and musculoskeletal correlates of locomotion is a pivotal need to pave the way for successful rehabilitation, improve performing locomotion tasks, especially in older adults, or create a digital twin of humans while doing a locomotion task (Dai et al., 2022). Various techniques, such as electroencephalography (EEG), functional near-infrared spectroscopy (fNIRS), and magnetic resonance imaging (MRI), have been developed and deployed to study age-related changes and specific diseases in the neurological and musculoskeletal correlates (Lewis et al., 2019). These various techniques enable us access to the movement phenotypes, such as brain structures (Chenausky and Tager-Flusberg, 2022), the functional substrates (Magrinelli et al., 2021), and motion signatures (Klibaite et al., 2022), in locomotion control during different experimental settings. However, these neuroimaging techniques present advantages and limitations, such as sensitivity to motion artifacts (Abtahi et al., 2020; Bonnal et al., 2022), portability (Sejdić et al., 2019), and spatial and temporal resolutions (Martini et al., 2020; Kumar and Michmizos, 2022). These limitations set up constraints on the design of the experimental protocols. For instance, MRI studies mainly investigated imagined locomotion rather than real-world locomotion (Stolbkov et al., 2019; Skinner et al., 2022). Although the sensitivity of fNIRS and EEG to artifacts has been improved, still most existing studies focus on low-intensity movement (e.g., walking) rather than high intensity, such as running.

To overcome these challenges and limitations of traditional brain imaging techniques, most recent research argued that brain-body imaging techniques that enable simultaneous measurements of dynamics of brain activities and body movements could be a promising method to reveal the profound relationship between brain, body, and behavior (Makeig et al., 2009; Gramann et al., 2010; Gwin et al., 2010; Wagner et al., 2012). The brain/body imaging techniques integrated portable devices, reliable sensing methods against motion artifacts, and capable of monitoring brain activities and locomotion with appropriate temporal and spatial resolutions, and sophisticated data analysis approaches for multi-modal data preprocessing and curation. Thus far, some specialized centers and clinics such as GE HealthCare (HealthCare, 2023), SCL Health (Group, 2023), Stratus (Stratus, 2023), Zeto (Zeto, 2023), CMS (CMS, 2023), CNS (Calyx, 2023), NordicNeuroLab (NordicNeuroLab, 2023), and NIRx (NIRx, 2023) have adopted these brain/body imaging tools. With multiple-channel EEG (more than 64) capturing brain activities, these tools track spatial information of brain correlates of human motion and provide high-precision data at a sampling rate of 200–5,00 Hz (Cortney Bradford et al., 2019). Simultaneously, they utilized standard locomotion tools, such as optical motion capture systems (Divya and Peter, 2022), inertial measurement units (Khaksar et al., 2021), and EMG sensors (Hallett et al., 2021) to capture the locomotion data at the same sampling rate as brain activity data. As a result, sophisticated data analysis approaches have been developed to study the relationship between brain, body, and behavior, such as cognitive-motor interference and coherence (Zhu et al., 2022).

However, before these brain-body imaging tools can truly be adopted for clinical use, their effectiveness must be carefully assessed. From a technical point of view, reproducing human locomotion experiments has been problematic due to the lack of protocols, standardization, and benchmarking tools, which ultimately impairs the evaluation of previous research quality and validation of prior understandings (Parmentier et al., 2020; Kameli et al., 2021). Notably, only a few studies focused on developing standard protocols and related design methodology as an open research issue. Therefore, this paper focuses on reviewing the settings of existing experiment protocols, such as locomotion intensity, duration, distance, brain sensor technologies, and corresponding brain activation expressions. First, we develop a conceptual framework to identify the design methodology of experiment protocols. Limitations of each brain-body imaging technique and the corresponding constraints on protocol design are then characterized and mapped into the scope of the systematic review approach. Next, we review existing studies that implement various types of experiment protocols, demonstrating the current gaps in design methodology. Finally, metrics for evaluating the research quality and implications for reproducing prior knowledge are proposed.

Overall, we aim to provide a roadmap for the future development of locomotion analysis methods based on brain-body imaging techniques, including highlighting current progress, identifying various constraints, and suggesting potential research directions. The main contributions of this review paper are to:

- Establish intrinsic links between neurological and musculoskeletal correlates of locomotion characteristics and quantifiable measures that brain-body imaging tools can capture;

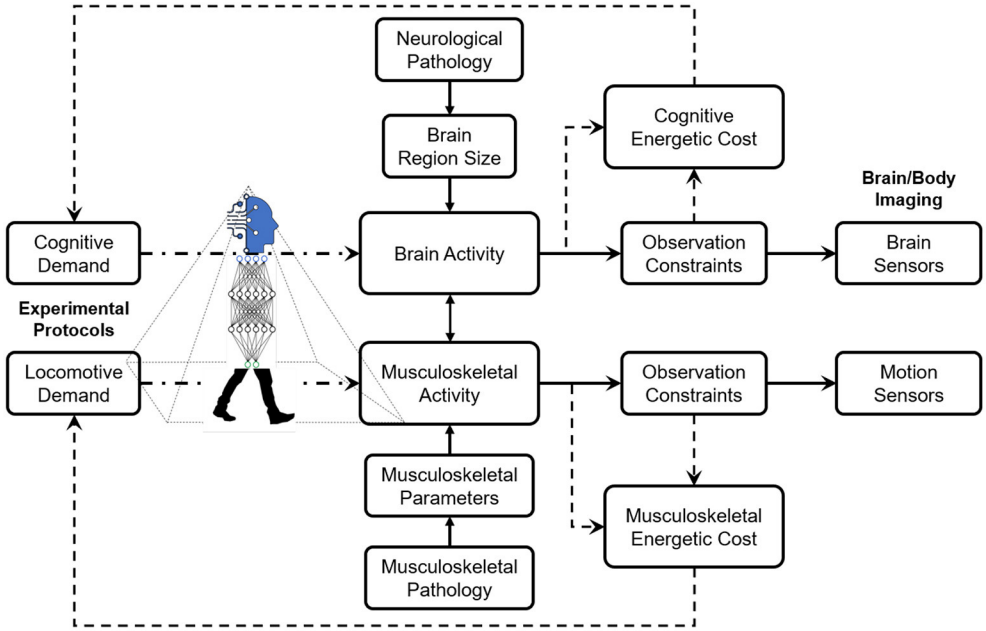


FIGURE 1
The design methodology of experimental protocols is based on comprehensive considerations of cognitive and locomotive demands, observation constraints by the sensing technology, and energetic costs determined by the human subjects.

- Review existing experimental protocols for studying neurological and musculoskeletal correlates of locomotion;
- Examine the feasibility of replicating the experiments in the laboratory systems, and finally,
- Identify gaps and lay out a roadmap for the design methodology of experiment protocols.

## 2. Methodology

The design methodology of experimental protocols for studies on neurological and musculoskeletal correlates of human locomotion is based on careful considerations of cognitive and locomotive demands, observation constrained by the sensing technology, the pathology derived from the research interests, and energetic costs invested by the human subjects. Ideally, the cognitive and locomotive demands are designed in specific thresholds to stimulate certain intertwined relationships between neurological and/or musculoskeletal activities. However, the sensing technology's thresholds of these demands are constrained, including sensitivity to motion artifacts, portability in different environments, and spatial and temporal resolutions for capturing dynamics. For instance, current sensing techniques, such as EEG and fNIRS, claim they have lowered their sensitivity to motion artifacts. Still, most researchers design low-intensity locomotion (e.g., slow walking) to avoid difficulty in denoising efforts. Sometimes, in high-intensity locomotion experiments (e.g., running), the data become useless due to a high amount of movement artifacts (Gwin et al., 2011). Figure 1 illustrates the conceptual framework of the design methodology of experimental protocols.

We developed a systematic search of existing studies based on the conceptual framework. To find the papers, these keywords were searched for in Google Scholar: human brain locomotion/locomotion, OR EEG, OR nirs, OR MRI/ Brain-Body Imaging. Then, all the papers were examined, and the related papers were added to the tables of this paper. The criteria for a paper to be reviewed are: 1) it must examine the brain's signals while the participants perform a locomotion task. 2) The experiment participants should be healthy; the results of this systematic search are shown in Figure 2. Although exploring walking disorders is highly valuable, there are thorough reviews for each locomotion disease. Then, the critical information on protocol design has been extracted and inserted into the tables. In this respect, these parameters in each protocol have been extracted: the type of the surface or the device used for experimenting (e.g., overground and treadmill), the speed of performing the task, the distance that participants have moved, the duration of the task, the type of the sensors used in the experiment (it is more focused on the sensors to read the brain's data), number and age of the participants, special conditions of each research, and the contribution of the research.

All the results were converted to the same units to make the protocols comparable. Accordingly, the distance is stated in meters (m), the speed is in kilometers per hour (km/h), and the duration of the task is in minutes (min); otherwise, the unit is stated.

## 3. Locomotive and cognitive demands

To examine neural activities during human locomotion, single tasks without cognitive demands (e.g., walking) and dual tasks with cognitive demands (e.g., talking while walking) are examined. In this paper, the tasks are divided into walking, running, cycling, and

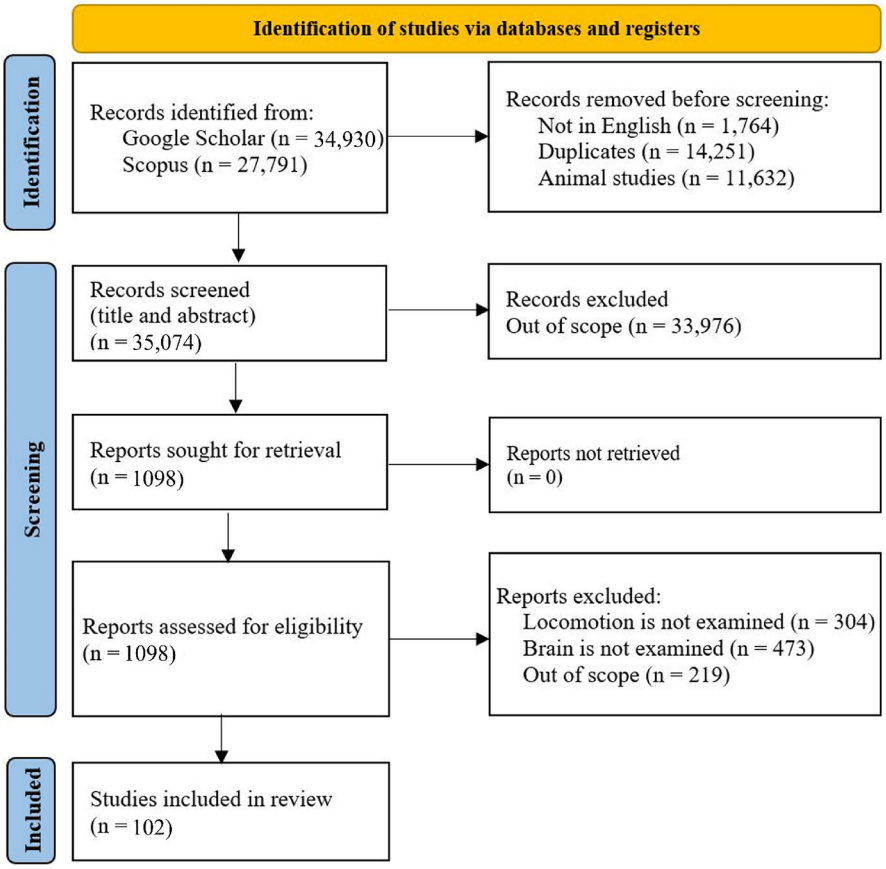


FIGURE 2
Mobile body imaging study selection: Preferred items for systematic reviews and meta-analyzes (PRISMA) flow diagram.

**TABLE 1** Abbreviation table.

| Abbreviation | Term | Abbreviation | Term |
|---|---|---|---|
| B | Board with pedals | deoxyHb | De-Oxygenated Hemoglobin |
| EEG | Electroencephalogram | EMG | Electromyography |
| Erg | Ergometer | IM | Imaginary locomotion |
| M1 | Primary Motor Cortex | min | Minute |
| MRI | Magnetic Resonance Imaging | NIRS | Near-Infrared Spectroscopy |
| OA | Older Adults | OG | Overground |
| oxyHb | Oxygenated Hemoglobin | PET | Positron Emission Tomography |
| PFC | Pre-Frontal Cortex | PMC | Pre-Motor Cortex |
| rpm | Revolution Per Min | s | Second(s) |
| S1 | Primary Sensorimotor Cortex | SMA | Supplementary Motor Area |
| SMC | Sensorimotor Cortex | SVM | Support Vector Machine |
| SW | Single Walking | T | Tesla |
| Tr | Treadmill | YA | Younger Adults |

Dual-Task-Walking (DTW). The abbreviations used in this paper are explained in Table 1.

- In the participant section, M shows the number of male participants and the rest are Females.

- a ± b is used to describe the participants' age statistics in which a is mean and b is standard deviation.
- If participants are older than 60, they are considered as OA.

### 3.1. Type 1: Walking

Walking has been examined in different forms: actual walking, imaginary walking, and simulated walking. Nonetheless, the common point between these studies is the activation of the brain and involvement of higher cognition control areas (Al-Yahya et al., 2011). The studies that have investigated the walking as the human locomotion are shown in Table 2.

### 3.2. Type 2: Running

Only one paper was found that merely focused on examining running as a locomotion task and studying brain activities. This paper's information is described in Table 3.

### 3.3. Type 3: Cycling

Cycling is another locomotive task to study the brain correlates of locomotion. The locomotive demands span from low to high intensity, with various cycling speeds, while few studies gave self-paced instructions to participants. Most studies expected to utilize the locomotive demands to stimulate the dynamics of brain activities for identifying neurological and musculoskeletal benefits. The research studies related to the cycling are demonstrated in Table 4.

### 3.4. Type 1-2: Walking-running

In this section, three research were found that have investigated both walking and running their studies, which meet the defined criteria for research selection in this review. These studies are investigated in Table 5.

### 3.5. Type 1–2: Walking-cycling

Only one paper shown in Table 6 was found that has examined both walking and cycling.

### 3.6. Type 4: Dual walking task-spontaneous locomotive and cognitive demands

By switching from single tasks to dual tasks, the age-related gait changes are more distinguished (Beurskens and Bock, 2012) the reason roots in the fact that the cognitive resources should compensate for the motor impairments (Mirelman et al., 2017). Because of this reason, in this type of locomotion task, usually both young adults (YA) and old adults (OA) are examined. The Dual task walking studies are presented in Table 7.

## 4. Results

### 4.1. Task analysis

The filtered papers based on the mentioned criteria are 102 papers. Most of the papers, 65, conducted research on low-intensity locomotion, walking, only 4 papers examined running, 17 papers examined cycling, and 18 papers conducted the experiment on dual task, which considers the locomotive and cognitive demands simultaneously. Figure 3 shows the visualization of the tasks, the surface that the experiment has been conducted on, and the brain sensor that has been employed for the experiment. In this regard, the most outer layer of the circle shows the investigated locomotion tasks (walking, running, cycling, and dual-task walking). The middle circle demonstrates the type of the surface (Tr: treadmill, IM: imaginary, OG: overground, Erg: Ergometer bicycle, B: on a board). The type of brain sensor used in the research are shown in the most inner circle (EEG, NIRS, MRI, and PET).

### 4.2. Analysis of locomotive intensity

Among the researches that have declared the intensity (e.g., speed) that locomotion has been performed, the papers that have stated their speed (or an average of speed) have been compared with each other. However, the researches that the speed was not defined quantitatively and constant (e.g., the speed was dependent on the length of the participants' feet length Wagner et al., 2012, 2014; Seeber et al., 2014) were excluded from the visualization. Accordingly, the rotational velocities when the brain-body imaging experiment is using an ergometer or a pedaling board are visualized in Figure 4. The experiment using 60 rpm in cycling has been considered a reference speed for most researchers. Besides the rotational velocities of Figure 4, the linear speed for SW and DTW on different surfaces (i.e., Tr and OG) for YA and OA are shown in Figure 5. The bigger the bulb, the more repetition on reported speed. For example, walking at the speed of 2 Km/h is the main standard for researchers on the treadmill when the participants are YA. In addition, in each experiment surface, a trend of using a higher speed for YA compared to the speed used for OA can also be observed in the reviewed papers in this figure. For instance, in DTW OG, the maximum speed reported for YA is 4.6 Km/h, although the maximum speed reported for OA in DTW OG is about 3.8 Km/h.

TABLE 2 Brain-body imaging in walking.

| References | Surface | Dist. (m) | Speed Km/h | Duration (min) | Sensors | Participants No. and age | Special condition | Contribution |
|---|---|---|---|---|---|---|---|---|
| Vitorio et al. (2018) | Treadmill | - | Self-paced | 5 min: 5 trials of 30 s SW and 30 s rhythmic auditory cueing walking | 40-channel fNIRS | 15 YA Range: 20–40, 15 OA Older than 60 | A digital metronome was used to create rhythmic auditory cueing with preferred frequency | In OA, rhythmic auditory cueing enhances walking, which is achieved through increased activity in multiple cortical areas (PMC, SMA, and M1). In OA, cortical response reduction with repeated exposure indicates OA's ability to adapt to a new task. |
| Kurz et al. (2012) | Treadmill | - | 1.62 | 5 min: five blocks consisting of 30 s standing still and 30 s walking | 24-channel fNIRS | 13, 23.7 ± 1.4 | Forward or backward walking condition is placed in five alternating blocks of standing still or walking. Backward walking needs more SMC and increases the variability of the stride time compared to forward walking. | Amount of oxyHb during forward walking is correlated with the variability of stride time in forward walking in the pre-central gyrus and SMA of the brain. |
| Khan et al. (2018) | Treadmill | - | Self-paced | 10 s walking and 20 s for rest intervals | 12-channel fNIRS, 4 detector and 5 sources | 9M (30 ± 3) | The fNIRS data were collected from M1 only on the left hemisphere | Initiation and stopping commands received from M1 in the left hemisphere obtained by fNIRS are classified with different ML algorithms. |
| Berger et al. (2019) | Treadmill | - | 2.8 | One block of each walking condition consisted of 5 trials and each trail lasts for 1 min with 1 min interval. | fNIRS with 16 optodes (8×8) and ground reaction forces | 12 right-handed (3M), 25±4 | Two conditions of unassisted walking and robot assisted walking are compared. Body weight support is adjusted to 30%. | Using robot assisted walking causes an increase in gait variability, which is correlated with increasing brain activity in SMC. |
| Suzuki et al. (2008) | Treadmill | - | 3 | Two walking tasks and total duration of each task was 240 s | fNIRS (42 channels) with 28 optodes, consisting of 12 light-source fibers and 16 detectors | 7 right-handed (4M), 31.3 ± 4.8 | Duration of rest period was selected randomly (10, 15, 20, and 25). The walking tasks were repeated 4 times. | When walking triggers with a verbal instruction ("ready"), the brain's frontal activation during the preparation, execution, and walking performance improves. |
| Miyai et al. (2001) | Treadmill | - | 1 | Each task or rest period lasted 32 s (8 scans). each series contained 80 scans with a complete duration of 5 min 20 s. | NIRS (21 optodes), which consist of nine light source fibers and 12 detectors | 8 (4M), 35 ± 8, Range: 24–46 | Performing each of these tasks for 30 s (1) walking on the treadmill at 1.0 km/h and rest, (2) alternating arm swing without walking and rest in standing position, (3) alternating dorsiflexion and plantar flexion movement of the feet at a pace of 1 Hz and rest in sitting position, and (4) motor imagery of gait in standing position | Using local oxyHb measured by NIRS topography, cortical activation patterns of human gait is visualized. Total and increased level of oxygenated hemoglobin in the medial S1 and SMA are coupled with walking activities. |
| Harada et al. (2009) | Treadmill | - | High gait capacity: 3.6 ± 1, 5.8 ± 1, 6.9 ± 1 Low gait capacity: 3.1 ± 1, 4.4 ± 1, 5.2 ± 0.7 | 20 s rest, 60 s walking, 20 s rest | NIRS (42 channel) with 28 optodes consisting of 12 light sources and 16 detectors | 15 (2M), 63 ± 4 | Dividing the participants to two groups based on incremental walking test: 1-low gait capacity ($n$ = 8) 2-high gait capacity ($n$ = 7) | In higher speeds, left PFC and the SMA consists of higher oxyHb. The degree of medial SMC and SMA activations are associated with the locomotor speed and cadence. Heart rate is only depended on left PFC. Left PFC, SMA, and SMC control gait speed, and that the involvement of the left PFC may rely on reduction of gait capacity in elder adults. |

*(Continued)*





10.3389/fnins.2023.1051500

TABLE 2 (Continued)

| References | Surface | Dist. (m) | Speed Km/h | Duration (min) | Sensors | Participants No. and age | Special condition | Contribution |
|---|---|---|---|---|---|---|---|---|
| Sipp et al. (2013) | Treadmill (customized by adding a beam to evaluate the stability) | - | 0.792 | 25 min, two times | EEG (256 channels), Vicon motion capture with 28 reflective markers | 26 (14M), 23 ± 5, All of them right-handed and right footed | To avoid the effect of fatigue on the experiment, participants could walk whenever they wanted. Accordingly, the time of experiment could last between 60 to 120 min. | Walking involves baseline theta band activity that significantly increases with loss of balance. Also, in the right-handed and footed participants, the left SMC plays a larger role in sensing loss of balance during walking than the right SMC. |
| Gwin et al. (2011) | Treadmill | - | 2.88 (slow walking) and 4.5 (fast walking) | 5 min standing 10 min slow walking 10 min fast walking | EEG (248 channel), force measuring on the treadmill with 25 reflective markers | 8 (1M) range: 21–31 | The experiments start with 5 min standing followed by three random conditions: slow walking, fast walking, or running. Collected data from running was not used because of large mechanical artifacts | Alpha and beta band spectral power increase around sensorimotor and dorsal anterior cingulate cortex at the end of the stance phase. But, their increase around the sensorimotor during the push off is more noticeable. Changes in anterior cingulate, posterior parietal, and SMC were pronounced in intra-stride high-gamma spectral power. |
| Bruijn et al. (2015) | Treadmill (split-belt) | - | 3.6 | 30 min | EEG (64 channel), ground force sensors, 2 pairs of bipolar EMG, cluster-markers and Optotrack | 10 (7M), 31.4 ± 6.6 | The experiment consists 5 conditions: Sitting with open eyes (1 min), sitting while receiving stimuli to the medial nerve (7 min), normal walking on treadmill (10 min), supported walking on treadmill (10 min), walking while receiving stimuli (10 min) | During stabilized walking, beta band increases in the left M1 indicating the role of the part in steady state gait stability. Confirming that medio-lateral foot placement is determined during push-off to some degree. |
| Bradford et al. (2016) | Treadmill | - | 2.7 | 30 min walk at 0% grade | EEG (264 channel), EMG (6 channel), ground forces | 22 (12M), 23.1 ± 3.9 | Subjects walked for a total of 1 h at 0.75 m/s. Subjects alternately walked in 7.5-min blocks of time at 0% grade and at 15% grade, for a total of 30 min at each condition | Comparison of walking with 0% and 15% grades shows greater gamma power during level walking in the left sensorimotor and anterior cingulate clusters. Also, comparison of frequency activation of the artifacts during walking conditions shows that the differences between walking conditions were cortically driven rather than a residual artifact of the experiment. |
| Salazar-Varas et al. (2015) | Treadmill | - | 2 | 12 min combination of different reactions to the appeared obstacles. | EEG (32 channel), 7 IMU | 5M, range: 24–29 | To create obstacles, in one scenario a line laser is projected over the treadmill to simulate the appearance of the obstacle. In the second scenario, a screen placed in front of the treadmill changes its color to simulate the appearance of the obstacle | EEG role can be developed to detect the unexpected obstacles as EEG potential over the fronto-central area of the subjects' brain change. An accuracy of 79.5% was reported for obstacle detection. |

*(Continued)*





10.3389/fnins.2023.1051500

TABLE 2 (Continued)

| References | Surface | Dist. (m) | Speed Km/h | Duration (min) | Sensors | Participants No. and age | Special condition | Contribution |
|---|---|---|---|---|---|---|---|---|
| Bulea et al. (2015) | Treadmill | - | 3.24 (slow walking) 5.4 (fast waking) and self- adjusted speed | 1 min data collection by EEG cap in two modes of passive and active. | EEG (64 channels), Vicon MX motion capture system | 10 (4M) 28.9 ± 6.3 | The experiment consists of passive walking (defined speed) in which the speed periodically changes. Or active walking (self-adjusted). In the active mode, combination of feedforward and feedback controllers were implemented. Each participant completed 6 trials | Gamma band power increases during double support and early swing phases. This indicates that pre-frontal and posterior parietal networks are engaged to leverage lower limb control during walking. The cortical network engagement evoked by active treadmill indicates the possibility of enhancing neuroplasticity for more effective motor training. |
| Yokoyama et al. (2018) | Treadmill | - | 2 | 7 min and 30 s | 64-channel EEG and 13-channel EMG also 3D ground reaction forces | 12M, Range: 23–31 | The last 7 min of walking and 30 channels' data of EEG cap were used for analysis | During walking cerebral cortex controls multiple muscles hierarchically through a few muscle synergies. Locomotor muscle synergies activation can be decoded from slow cortical waves. |
| Presacco et al. (2011) | Treadmill | - | Self-paced | 5 min to find the comfort speed, 2 min rest, 5 min precise walking, then normal walking | EEG (60 channel), EMG, infrared optical motion capture system | 6 (3M), Rang: 18–45 | To increase attentional demand during precision walking condition, participants were instructed to avoid stepping on the white stripe (2 in. wide) glued diagonally on the treadmill's belt by using the monitor's video to keep track of foot placement relative to the white stripe | Confirming that a plurality of cortical brain areas controls the walking. Decoding human walking using EEG data in two conditions: 1- walking while providing foot placement guide visually (precise walking) 2- normal walking |
| Presacco et al. (2012) | Treadmill | - | Self-paced | 5 min to find the comfort speed, 2 min rest, 5 min precise walking, then normal walking | EEG (60 channel), EMG, infrared optical motion capture system | 6 (3M), Rang: 18–45 | To increase attentional demand during precision walking condition, participants were instructed to avoid stepping on the white stripe (2 in. wide) glued diagonally on the treadmill's belt by using the monitor's video to keep track of foot placement relative to the white stripe | Activation of ankle, knee, and hip during walking on treadmill are decoded by recording 12 EEG signal channel placed on pre-frontal, motor, parietal, and occipital areas. |
| Castermans et al. (2014) | Treadmill | - | 1.5, 3, and 4.5 | About 12 min | EEG (32 channel), piezoelectric accelerometer, 6 infrared cameras to record lower limb movements | 7 (5M), Range: 25–33 | The piezoelectric accelerometer was fixed firmly on top of the participants' head | The role of cortical origin of low-delta and high-gamma bands during walking may not be valid. Depending on the electrodes' locations, motion artifacts in phase with walking frequency can affect the EEG data up to 15 Hz. Accelerometer and EEG data have similar time-frequency characteristics during walking. |
| Petersen et al. (2012) | Treadmill | - | Self-paced between 3.5 to 4 | 5 min epochs of continuous treadmill walking and 2 min of static contraction | EEG (28 electrode), EMG | 9 (4M), 23.4 ± 4.1 | additional walking with speed of 1 km/h (slow walking) and static dorsiflexion for seven of the participants | Rhythmic cortical activity in the 24–40 Hz frequency band is transmitted *via* the corticospinal tract to the active muscles. In steady state treadmill walking, motor cortex and corticospinal tract contribute directly to the muscle activities. |

*(Continued)*





10.3389/fnins.2023.1051500

TABLE 2 (Continued)

| References | Surface | Dist. (m) | Speed Km/h | Duration (min) | Sensors | Participants No. and age | Special condition | Contribution |
|---|---|---|---|---|---|---|---|---|
| Quiroz et al. (2017) | Treadmill | - | 4.83 and 8.05 | 5 min | EEG (9 channels) | 3 | Each participant repeated the experiment 10 times: 1 min low speed, 1 min higher speed, then 1 min low speed also 1 min between transitions | Compared to imager locomotion, during lower limb control, neural activity in cortical sensorimotor areas increases. Also, pre-motor and sensorimotor areas' show high neural activities compared to resting. |
| Artoni et al. (2017) | Treadmill | - | 2.5 and 3.5 | 20 min (10 min for each speed) and also 5-min rest between the tasks | EEG (64 Channels), EMG (6 channels) | 11, 30 ± 4 | 3-min preliminary walking was performed for the purpose of acclimation | A significant casual unidirectional drive from contralateral motor cortex to muscles in the swing leg and control of muscles during stereotyped treadmill locomotion is found using SVM. Highest accuracy was reported as 0.78 ± 0.04. |
| Tortora et al. (2020) | Treadmill | - | 2.5 and 3.5 | 20 min (10 min for each speed) and also 5-min rest between the tasks | EEG (64 Channels), EMG (6 channels) | 11, 30 ± 4 | 3-min preliminary walking was performed for the purpose of acclimation. A specific set of channels was removed for each of the 11 participants. | Decoding swing and stance of both legs together, or of each leg independently by deep learning and using the method of LSTM recurrent and EEG signals of motor cortex. An average accuracy of 90.4±1.4% is reported. |
| Wei et al. (2021) | Treadmill | - | 1.4, 2 and 2.6 | 7.5 min: walking at three speed in 15 30-s blocks | 24-channel EEG, 8-channel EMG, motion capture, | 9 (7M), Range: 23–26 | To divide the gait cycle, 3D markers in five positions were employed | Activation of cerebral cortex during gait phases is examined. During pre-swing and terminal-stance, cerebral cortex is more actively involved in the control of eight examined muscles. |
| Nordin et al. (2019a) | Treadmill | - | 1.8, 3.6, 5.4, 7.2 | 3 min for each speed and considering rest between each experiment | Dual layer EEG and 8-channel EMG | 9 (6M), 27 ± 4 | As the speed is close to running, the subjects were asked to walk even in high speeds. A standing baseline trial was recorded prior to changing speed experiments. | Dual-layer EEG isolates the changes in sensorimotor electrocortical dynamics across walking speeds. Also, dual-layer EEG is beneficial to remove residual artifacts while gait speeds change. In addition, a correlation between different walking phases and alpha/beta spectral power is drawn. |
| Luu et al. (2017b) | Treadmill | - | 1.6 | 2 min rest, 15 min Gonio-ctrl walking, 5 min BCI-ctrl walking, 2 min rest | 64-channel EEG | 8 (3M), Range: 19–29 | Goni-ctrl: the avatar was driven by a goniometer. goniometer sensor placed at hip, knee, and ankle joint angles. BCI-ctrl: the avatar was controlled by BCI. The participants could see the avatar on the 52-inch TV. | In closed-loop walking using BCI and avatar, cortical involvement during walking increases as $\alpha/\mu$ are subdued in the posterior parietal cortex and inferior parietal lobe. Low $\gamma$ modulations in the anterior cingulate cortex and superior temporal gurus may show the increasing voluntary control of human gait. |

*(Continued)*





10.3389/fnins.2023.1051500

TABLE 2 (Continued)

| References | Surface | Dist. (m) | Speed Km/h | Duration (min) | Sensors | Participants No. and age | Special condition | Contribution |
|---|---|---|---|---|---|---|---|---|
| Lin et al. (2014) | Treadmill | - | 1.6, 3.2, 4.8 | Less than 30 min | 14-channel EEG | 17 (14M), Range: 22–32 Mean age: 26.76 | Each subject participated in four sessions (standing and three speeds). Each session repeated a run 10 times analysis. | The centro-parietal was not covered with the sparse 14-channel electrodes and no spectral changes were observed in SMC. steady-state visual-evoked potential-based BCI can be used to mimic natural walking using consumer-level EEG. |
| Úbeda et al. (2014) | Treadmill | - | 2,3, and 4 | 24 min | 32-channel EEG, IMU | 3M, 26.3 ± 3.8 Range: 22–29 | Each participant performed 8 runs. Each run includes walking at three speeds and each for 1 min | Using the linear regression model, a correlation between EEG signal recorded from central and parietal cortex and knee angle during walking has been found |
| Severens et al. (2012) | Treadmill | - | 2.8 ± 0.2 | 10 min | 62-channel EEG, EMG channel, occipital channel | 6, 21.6 ± 2.3 Range: 20- 26 | To help the subject to synchronize the step frequency, a metronome was used for 15 s. The step frequency was about 1.4 Hz. | ERD has been examined and measured during walking. Beta ERD is strongest above the lateral motor cortex, with mu at the central motor cortex. Also, desynchronization is strongest in the swing phase of the contralateral leg above the motor cortex. |
| Wagner et al. (2016) | Treadmill | 12 trials of 10 blocks of 120 steps | Self-paced between 3.0 and 3.7 | - | 108-channel EEG, EMG channel | 18 (10M), 29.1 ± 2.7 (Wagner et al., 2019a), Range: 22–35 | the walking was synchronized with a series of cue pacing cue tones and thus the step rate and length were changed based on the pacing cue tempo | Analyzing beta band power in the right dorsolateral prefrontal cortex shows two recognizable patterns. One pattern may help in starting and executing the movement and the other one has control and inhibition functions (Wagner et al., 2016). Also, in the posterior medial frontal cortex, an EEG step-cue delay negatively is generated with a peak at 250 ms after anomalous cue tone onsets (Wagner et al., 2019b). |
| De Sanctis et al. (2023) | Treadmill | - | Self-paced | 28 min (eight 3.5-min blocks) | 160-channel EEG, optitrack motion capture with 9 cameras | 26 (12M), 74.9 | High and low cognitive impairment risk is defined by Montreal Cognitive Assessment battery (MoCA, range: 0-30): high (22–26) and low (27+) | Characterizing the neural signature of walking: an increase in frontomedial theta in high-risk cognitive impairment individuals was observed. Left sensorimotor beta in low-risk cognitive impairment individuals decreases when visual perturbation is used during walking. |

*(Continued)*





10.3389/fnins.2023.1051500

TABLE 2 (Continued)

| References | Surface | Dist. (m) | Speed Km/h | Duration (min) | Sensors | Participants No. and age | Special condition | Contribution |
|---|---|---|---|---|---|---|---|---|
| Wagner et al. (2012) | Treadmill/ robotic gait orthosis | - | Speed = 0.54 (leg length in cm)/ 27.8 The speed varied between 1.8 to 2.2 | 6 min for walking session; 3 min resting session | Combining four 32-channel amplifiers for recording data from 120 sites using EEG and EMG data | 14 (8M), 24.3 ± 2.7, Range: 22–28 | Each participant completed 8 runs of robot-assisted walking (four in each of two active/passive walking conditions) and three runs of upright standing. | To compensate for the differences between active and PW in robot-assisted walking, cortical activities related to lower limb movements were shown. Depending on the gait cycle, the power in the mu and beta bands decreases during active walking. Also, depending on the gait cycle, cortical activity was localized in the M1 in the lower gamma band. (passive walking: participants let the robot move their legs) |
| Seeber et al. (2015) | Treadmill/ robotic gait orthosis | - | Speed = 0.54(leg length in cm)/ 27.8 The speed varied between 1.8 and 2.2 | 6 min for the walking session (4 times); 3 min standing (3 times) | Combining four 32-channel amplifiers for recording data from 120 sites using EEG and EMG data | 10 (5M), 25.6 ± 3.5, Range: 22–28 | Each participant completed 4 runs of robot-assisted walking (each 6 min), 3 runs of standing (each 3 min) | When high gamma oscillations are increased artificially by transcranial alternating current stimulation (tACS) in the central sensorimotor cortex, motor performance during walking enhances. |
| Seeber et al. (2014) | Treadmill/ robotic gait orthosis | - | Depending on the leg length, ranging from 1.8 to 2.2 | 4 runs (6 min each) of active walking and 3 runs of upright standing (3 min each). | EEG (120 channel), EMG | 10 (5M), 25.6 ± 3.5 | Participants completed Body weight support adjusted to less than 30% | $\mu$ (10–12 Hz) and $\beta$ (18–30 Hz) oscillations in active walking is significantly less than upright standing. Depending on the gait phase, supported $\mu$ and $\beta$ ERD indicate a movement-related state change of cortical excitability. While generated frequencies in $\mu$ and $\beta$ have overlaps, the center of generations is different. |
| Wagner et al. (2014) | Treadmill/ robotic gait orthosis | - | Speed = 0.54 (leg length in cm)/27.8. The speed varied between | Participants walked 4 min in each of the five conditions and walking was repeated two times during the experiment | EEG (61 channel), EOG (3 channel) electrodes by two 32-channel amplifiers | 11 (7M), 26 ± 2 | Walking in five different conditions: 1-looking at a black mirror 2- looking at white graphical objects 3- watching their mirrored walking 4- 3rd person in Virtual environment 5-1st person in a virtual environment | In conditions that require adjusting the steps based on the visual input, $\mu$, $\beta$, and lower $\gamma$ frequencies in pre-motor and parietal cortices are reduced, which shows these brain areas' activation increase. This activation is higher compared to mirror feedback and a visual attention task, which may indicate additional motor planning and visuomotor processing. |
| Alchalabi et al. (2019) | Treadmill real walking/ imagining/ observing | - | - | 8.5 s for each trial | 19-channel EEG and 15 rigid body reflective motion-capture and 12-camera Vicon optoelectronic motion capture system | 20 (7M), 23.3 ± 3.93 | The participants performed the experiments in three conditions of 1-controlling an avatar in virtual reality 2-imagining the avatar 3- observing the avatar. Each condition consisted of 240 trials. | It is shown that it is feasible to use pre-motor, motor and parietal areas' EEG data to measure the level of embodiment during physically or mentally controlling an avatar's walking. |

*(Continued)*





10.3389/fnins.2023.1051500

TABLE 2 (Continued)

| References | Surface | Dist. (m) | Speed Km/h | Duration (min) | Sensors | Participants No. and age | Special condition | Contribution |
|---|---|---|---|---|---|---|---|---|
| Severens et al. (2014) | Treadmill/ imaginary | - | 3 | 48 s for the task | 62-channel EEG | 12, 29 ± 5.6 | Four tasks' EED data: forward walking and backward walking in actual and imaginary manners were recorded on a treadmill. | Although walking is automatic, brain signals, especially the cortical area, can be classified to walking and non-walking signals reliably with high speed. Also, actual waking classification has a higher accuracy compared to imaginary walking. |
| Nojiri and Iwane (2014) | Imaginary | - | - | 2 min: 30 s walking, standing, turning left, and turning right | 11-channel EEG | 1 participant | For imagination, a movie shows three kinds of arrows and stop sign | Providing a method to estimate walking direction using power spectrum density data of motor area's EEG signals. |
| Malouin et al. (2003) | Imaginary | - | Qualitat-ively: fast and slow | Each subject experienced eight PET scans within a single session that took approximately 2 h | PET. EMG and ECG were recorded for 1 min just before and during each scan. ANOVA to record heart rate | 6 right-handed (1M) Range: 41–70, Mean age: 55.9 | Brain scanning while participants imagine Standing, initiating gait, walking, walking with obstacles. The results of these conditions were compared to a rest (control) condition | When the cognition demand of the task and the need for processing sensory information increase, the higher brain centers become more engaged. |
| Iseki et al. (2008) | Imaginary | - | Observa-tion of virtual walking with the speed of 3.2–3.6 | Duration of each clip was 5 s, with the frame rate of 29.97 frame/s | 3-Tesla MRI with an 8-channel phased-array head coil | 16 healthy, right-handed (13M), 34.3 ± 4.6 | Tasks: observation of 1- Gait movement 2- normal stepping in a standing position 3- standing still 4- scrambled gait 5- virtual walking 6- scrambled virtual walking | During imagine of walking (first person) or observing other people's walking (third person), the planning center of gait, including SMA and dorsal M1 are activated. |
| Labriffe et al. (2017) | Imaginary | - | 120 step/min | 5 min and 42 s | MRI-compatible Korvit simulator and EMG | 18 (11M), 27 ± 4.7, Range: 20–40 | The experiment has two modes: 1- organized: sequential activation of muscles related to walking 2-chaotic: non-gait-like pattern activation of muscles. Each experiment repeated 9 times. | There is no difference between activation of chaotic and organized patterns of stimulation. Activation pattern of mental imagery and gait-like plantar stimulation are similar especially in SMA-proper bilaterally and right pre-SMA. |
| Wang et al. (2009) | Imaginary | - | - | 3 min and 40 s for each session | fMRI | 21 right-handed gender-balanced, 21.5 ± 1.2, Range: 20–25 | The experiment includes ten fMRI sessions consisting of three blocks. Walking and stand positions were randomly shown. | In major gait-related task especially at initiation of a gait, SMA is activated. During termination and stepping over an obstacle, a significant visuomotor network is required. |
| Sacco et al. (2006) | Imaginary | - | 90 step/min | 12 s for each active condition | fMRI | 12 right-handed and right-footed (7M), Range: 20.8–34.9, mean: 27.5 | Each participant completed 25 blocks: 13 rest and 12 active conditions | Imagery training expands active bilateral motor areas and reduces visuospatial activation in the posterior right brain. |

*(Continued)*





10.3389/fnins.2023.1051500

TABLE 2 (Continued)

| References | Surface | Dist. (m) | Speed Km/h | Duration (min) | Sensors | Participants No. and age | Special condition | Contribution |
|---|---|---|---|---|---|---|---|---|
| Kline et al. (2020) | 1)Imagining walking 2) using board and pedals connected to the fMRI board | - | 50 step/min | 90 s: 10 blocks consisting 5 rest block and 5 display of walking block. Each block: 18 s | fMRI: T2*-weighted echo planar imaging | 16M healthy, right-handed 24.7 ± 3.31, Range: 19–31 | The visual stimulus was generated by Daz 3D. Before starting experiment, high-resolution structural brain scan obtained for anatomical structure of fMRI data | The executed task is coupled with more activation in M1 and the medial cerebellum while imagined task has higher activation in somatosensory cortex, M1, and lateral cerebellum. |
| Ikeda et al. (2016) | Horizontal free walking on a board/ treadmill | - | 60 step/min | 500 s: treadmill gait for 100 s and 25 s gait-like motion repeated four times | fMRI and EMG for five muscles treadmill gait | 8M, 24.0 ± 0.82 | The difference between gait-like motion and real walking which is intention for moving lower extremities and biceps femoris. | It is shown that lower-extremity motion simulator by providing gait-like motion incites motor sensation in cerebellum, brainstem, and spinal. |
| Sahyoun et al. (2004) | Board (a purpose-built wooden apparatus in MRI device) | - | - | 12.5 min for a total experiment | 3T Varian INOVA MRI, EMG | 12 (7M) healthy right-handed. Mean age: 25.4 Range: 20-31 | Only one degree of freedom for foot movement is studied: extension-flexion at the ankle joint | Anterior pre-frontal regions are involved in the decision making for moving forward. |
| Takahiro et al. (2013) | On board | - | 1.8 s for each gait | Four reparations of 25-s rest and 25-s gait-like motion | fMRI | 1 subject | Three degree of freedom were created on the board for each leg. | The activation of the brain's area in sensory motor is higher in PW compared to active walking due to processing of the unanticipated sensory feedback and not-imaged movement |
| Wieser et al. (2010) | Board with adjustable tilt angle | - | 44 step/min | 7 min rest at $\alpha$=0 and 30 min stepping at $\alpha$=76 and again 7 min rest at $\alpha$=0 | 64-Channel EEG and record of EMG for Four muscles | 20 (9M), 28.6 ± 8.3 | Task: Stepping (gait -like), the experimental board was vertical ($\alpha$=0) and then tilted ($\alpha$=76°) | S1, M1 and SMA mainly control the human's gait. Also, most of the cortical capacity is used for changing the direction between flexion and extension phase. |
| Xu et al. (2017b) | OG | 4.4 m | Qualitat-ively: Low/ medium/ high | About 4.5–6 s | 22-channel fNIRS | 30, 21 ± 1 | To train the algorithm 15 individuals' data was used and 15 individuals' data was used for validation. | Decoding the walking speeds categorized in three speeds based on PFC, M1, frontal eye cortices, and SMA by oxyHB data and SVM algorithm. |
| Xu et al. (2017a) | OG | 4.4 m | Qualitat-ively: Low/ medium/ high | - | 22-channel fNIRS | 21, 21 ± 1 | 12 set of data is used for training and 9 for validation | Classification of walking speed based on oxyHB characteristics using SVM. |
| Lacerenza et al. (2021) | OG | - | Self-paced | 20 s standing then 20 s performing the task and 20 s recovery for five times | Single channel fNIRS | 3M (age 30, 55, and 50 years) | The task is combination of standing still, forward walking, and backward walking | Time domain fNIRS during freely walking is measured. Diverse cortical response during forward and backward walking can be related to the different motor cortex involvement. |

*(Continued)*



10.3389/fnins.2023.1051500

TABLE 2 (Continued)

| References | Surface | Dist. (m) | Speed Km/h | Duration (min) | Sensors | Participants No. and age | Special condition | Contribution |
|---|---|---|---|---|---|---|---|---|
| Li et al. (2020) | OG | 10.5 self-paced, 10.5 gait adjusted, (two times) | - | - | 20-channel fNIRS | 30 (16M), 21 ± 1 | Gait adjusted walking included: speed increase, speed reduction, strep increase, and step reduction | Showing the feasibility of decoding the walking intention from a motion state using M1, PFC, and supplementary motor areas by fNIRS system. |
| Peters et al. (2020) | OG | 10 mactive and 10 m PW | - | 51.4±5.2 (Active) to 52.8±3.6 (Passive) seconds | 54-channel fNIRS and EMG | 14 (7M) 34±8 | In PW, participants were instructed to be relax so that the exoskeleton could perform the walking. | Finding the partial activation of parietal cortex during passive robotics exoskeleton gait |
| Brantley et al. (2016) | OG, and stairs | 7.92 | self-paced | - | EEG (64 channel), surface EMG (12 electrodes) | 1M, 31 | The subject has performed 20 trials. Each trial consists of 26ft level ground walking followed by an 8-step staircase (13.4 cm height) | During level ground walking, EEG-led coupling between electrodes and sEMG (tibialis anterior) in the frequency band of (3–5 Hz) indicates the command signal is sent from cortex to peripheral motor neurons. A higher coherence was observed for frequencies less than 2 Hz during stair ascent in which EMG was the leading signal for biceps femoris and gastrocnemius. |
| Mehra et al. (2021) | OG, and stairs | - | Self-paced | One-min data recording | EEG (60 channels), EOG (4 channels), EMG (6 channels), IMU sensors. | 6 (5M) | Each participant completes 20 trials of level ground walking, slope descends, and stair ascends, then 180° return to the starting point and resting. | Decoding the transition of walking conditions 3.0 ± 1.63 s in advance using EOG signals. This decoding is faster than decoding reported by Luu et al. (2017a) using occipital EEG signals. |
| Luu et al. (2017a) | OG, and stairs | - | Self-paced | One-min data recording | EEG (60 channels), EOG (4 channels), EMG (6 channels), IMU sensors. | 6 (5M) | Each participant completes 20 trials of level ground walking, slope descends, and stair ascends, then 180° return to the starting point and resting | Decoding the transition of walking conditions 1.27 s in advance by observing the changes in the cortical dynamics |
| Velu and de Sa (2013) | OG | 1.5 | - | - | 64-channel EEG data and two EOG electrodes and 8-channel EEG | 9 (7M) right-handed subjects, Range: 18–27 | The experiment consisted of 60 trials for 6 conditions (standing still, pointing left or right, walking left or right or front). | Walking, pointing, and standing can be classified using EEG data. Spatial and spectral contributions were from areas related to motor planning and mostly from low frequency cortical activity. |
| Budde et al. (2016) | OG | 10 | Self-paced | 2 min | 64-channel EEG and OptoGait-System | 12 (6M), Range: 20–28 | The experiments had three conditions: 1- normal walking 2- cognitive interface task: press a button based when a high-pitch sound is heard and ignore the low-pitch sound 3- motor interface task: preventing connection of the rings placed on a stick | Doing tasks that involve the brain's motor interface reduces gait velocity and stride length and increases the stride time and temporal-spatial variability. These changes don't occur in tasks require cognitive interface involvement. |

*(Continued)*





10.3389/fnins.2023.1051500

TABLE 2 (Continued)

| References | Surface | Dist. (m) | Speed Km/h | Duration (min) | Sensors | Participants No. and age | Special condition | Contribution |
|---|---|---|---|---|---|---|---|---|
| do Nascimento et al. (2005) | OG | - | Self-paced | 6 s for each task. Each task was repeated 60 times | 40-channel EEG and 4-channel EMG | 8 right-handed (4M), 23.5 ± 4, Range: 21 to 33 | The experiments' tasks are oriented stepping toward: forward, backward, lateral, right side, and forward-oriented gait initiation, backward-oriented gait initiation. | Variations in the directional orientation of gait and stepping (especially backward-oriented tasks) are coupled with changes in movement-related potentials, according to recorded data from cortical motor areas. |
| Li et al. (2016) | OG | - | Self-paced | - | 62-channel EEG 2-channel EOG 4-channel EMG | 7M, 23.57 ± 1.51 | The experiments were performed in free walking, using exoskeleton with and without applying assistive torque | The activation pattern during walking when the exoskeleton is used and when it is not used is different, which can affect the rehabilitation procedure and further orthosis development. Though somewhat similar in spatial pattern distribution in the medium occipital cortex and parietal cortex, and the lateral temporal cortices, assistive walking shows higher activation in the frontal part compared to two other conditions |
| Li et al. (2019) | OG | 21 | Self-paced | - | 62-channel EEG, 1-channel EOG, 4-channel EMG | 27M, 4 ± 2.32 | The participants performed four overground walking: free walking, walking with exoskeleton without applying force and with low and high applied load force | Power spectral density is different in sensorimotor and posterior parietal areas in four different walking conditions. Power spectral density of the brain in conditions of walking while wearing the exoskeleton have more similarities together than free walking. |
| Nakagome et al. (2017) | OG | - | Self-paced | - | 64-channel EEG, 6-channel EMG, 17 IMU | 6 (5M) | Level ground walking, stair descent, stair ascent, ramp ascent, and ramp descent are the activities that participants performed. Each participant performed the tasks for 20 times. | Unscented Kalman Filter was used to predict limbs activation using EEG signals. |
| Weersink et al. (2019) | OG | 150 | Self-paced | - | 32-channel EEG | 20 (7M), 64.95 ± 7.2 | The participants performed two experiments with 10 min in between: 1-walking normal (with swinging arm) 2-walking without swinging arm. | The relation between arm swing in walking and a step ERD-ERS pattern in high-beta/low-gamma band with the SMA shows the SMA's role in integration of cyclic anti-phase movement of upper and lower limbs. |
| Hasan et al. (2019) | - | - | Self-paced | 1.5 s before the event and 0.5 s of post event | 8-channel EEG and one-channel EMG and 9 IMU sensors | 7 (5M), 27.4 ± 3.1 | Each participant completed 140 trials, which consists of rest, start walking, stop walking and rest again. | Classification of walking intention (active) and non-intention (in-active) by SVM |





10.3389/fnins.2023.1051500

10.3389/fnins.2023.1051500

TABLE 3 Brain-body imaging in running.

| References | Surface | Dist. (m) | Speed Km/h | Duration (min) | Sensors | Participants No. and age | Special condition | Contribution |
|---|---|---|---|---|---|---|---|---|
| Giles et al. (2018) | Treadmill | - | As fast as heart rate is within 75–85% of age adjusted heart rate | 90 min for the main task | 20-channel fNIRS | 24 (9M) right-handed individuals, Range: 18–33 | Emotion regulation were performed before warming up and was reminded every 15 min during running | An emotion regulation strategy is suggested to benefit psychological state during endurance exercise. This benefit may not be reflected in oxygenation of PFC. |

## 4.3. Analysis of participants' age

To analyze the age of the participants, when the age of the participant is unknown, the research is excluded in the visualization of Figure 6. In this regard, there is a significant gap in the ages between 40 and 60 years old as only studies had participants in this range of age.

## 4.4. Analysis of locomotion duration

The duration of locomotion task varies from seconds to hours (Figure 7). In this regard, when it comes to single walking, the experiment on the treadmill with a duration of 12 min is the primary source for experiments. To make the results of studies with different duration comparable, the effect of fatigue on the muscles needs to be studied, and one solution could be recording the data after the locomotion task for a specific time.

## 4.5. Analysis of locomotion distance

Besides the duration, another parameter for assessing the locomotion demands is the distance when the participants were asked to walk overground. The walk distance falls in a range of 1 to 150 meters. For better demonstration, only the distances up to 30 meters are shown in Figure 8.

## 4.6. Brain activation in brain-body imaging experiments

In this section, the corresponding brain activation to the locomotion is presented. Comparison of the brain activation areas for the locomotion tasks are shown in Figure 9. In this figure, we have only shown the results of the reviewed papers that have specifically mentioned the brain regions' activation sources and their effects. However, if a study generally describes the cortex area is excluded from this visualization. In this figure, $\propto$ is the proportional symbol, $\uparrow$ shows increasing, and $\downarrow$ shows reduction of an item. For instance, when the OA's walk speed increases, oxyHB in the Supplementary Motor Area increases.

# 5. Discussion

In this section, the configurations of locomotive and cognitive demands, the research interests regarding neurological and musculoskeletal drivers, and the observational constraints from the sensing techniques are discussed concerning the impact of brain-body imaging sensors on the design methodology of experimental protocols for measuring dynamics of brain, body, and behavior. Since few papers in the field have adopted a conceptual framework to evaluate the quality of the neurological and musculoskeletal correlates of human locomotion extracted using various methods, it is not easy to compare these state-of-the-art methods. Therefore, in this section, we focus on establishing the elements of the proposed

TABLE 4 Brain-body imaging in cycling.

| References | Surface | Speed Km/h | Duration (min) | Sensors | Participants No. and age | Special condition | Contribution |
|---|---|---|---|---|---|---|---|
| Billaut et al. (2013) | Ergometer cycle | 128.7 ± 12.5 | Fifteen 5-s cycling sprints interspersed with 25 s of rest | 2 pairs of NIRS and EMG from three muscles. | 10M athlete 22.8 ± 4.4 | All of the participants are from sports clubs and have cycling experience | According to PFC data recorded by fNIRS, during intermittent, short, sprints, central; nervous system regulates quadriceps muscle recruitment and limits the development of muscle fatigue. |
| Keramidas et al. (2011) | Ergometer cycle | Self-paced (60–90) | 30 min for the constant power testing | 3-pairs of NIRS | 8, 23.9 ± 4.6 | The experiments consisted of three parts: 1- maximal oxygen uptake 2- a control constant power test 3- a constant power test | Performing respiratory work before an exercise test affects the oxygenation of the legs and respiratory muscles but not the frontal cortex. |
| Radel et al. (2017) | Ergometer cycle | - | The participants performed 10 min or 60 min exercising | 2-channel NIRS | 22 (15M), 21.27 ± 2.07 | Attentional focus as assessed three times during performing exercise by indicating a point in an analog range of completely on task to completely off task. | Based on oxyHb in right dorsolateral PFC and right medial frontal cortex, the brain's region associated with mental effort is disengaged with the brain's region linked to resting activity in order to keep mental resources for the maintenance of exercise. |
| Racinais et al. (2014) | Ergometer cycle | Not below 70 | - | 2-channel NIRS and 4-channel EMG | 25 cyclists, 37 ± 8 years | The workload was increased by 25 W/min until the cycling rate drops below 70 | Metabolic and ventilatory events may affect both muscle and cerebral oxygenation levels, and in turn, muscle employment |
| Smith and Billaut (2010) | Ergometer cycle | Qualitat-ively: Low/ medium/ high | Ten set of 10-s cycling with 30 s of rest | 2-channel NIRS and EMG electrodes | 13M soccer and rugby players, 23.6 ± 3.7 | Subjects were exposed to a gas for 10-min while sitting on the ergometer. The gases used in this experiment were: normoxia, and hypoxia | During repeated short sprint cycling, although $O_2$ availability influences the PFC, it doesn't affect the muscles. |
| Shibuya et al. (2004) | Ergometer cycle | 90 to find the maximal oxygen uptake | 147.2 ± 3.4 s | NIRS | 5M, 24.6 ± 0.4 | Subjects breathed through mask connected to hot wire flow meter to measure the respiratory flow. | Exhaustive exercise induces the decrease of cerebral function. Fatigue resulting from dynamic exercise decreases the cerebral cortex activity. |
| Subudhi et al. (2007) | Ergometer cycle | Above 50 | Until the participants get exhausted | 2-channel NIRS | 13M cyclist, 30 ± 7 | Subjects inhaled gas for less than 2 min before the experiment. Gas: normoxic or hypoxic | NIRS study on athletes show that incremental exercise performance under normoxic conditions is not possible to be limited by changes in cerebral oxygenation. |
| Subudhi et al. (2009) | Ergometer cycle | - | Until the participants get exhausted | Multi-channel NIRS | 25 (23M) | For the experiments two gases of normoxic and hypoxic were used | During high-intensity, cortical deoxygenation is not restricted to the brain's pre-frontal part. It is possible that deoxygenation in pre-motor and motor cortices contribute to fatigue and/or decision to stop exercising. |

*(Continued)*



10.3389/fnins.2023.1051500

TABLE 4 (Continued)

| References | Surface | Speed Km/h | Duration (min) | Sensors | Participants No. and age | Special condition | Contribution |
|---|---|---|---|---|---|---|---|
| Thomas and Stephane (2008) | Ergometer cycle | Above 60 | 13.3 ± 0.3 min | 2-channel NIRS and EMG | 13M right-handed, 24.9 ± 1.5 | All participants had 6.1 ± 0.9 h/week training | During progressive maximal cycling exercise, a reduction in PFC oxygenation before motor performance failure is reported. |
| Pires et al. (2016) | A speed bicycle attached to a cycle-simulator | Self-paced 4 km time trial (TT4km) and maximal control-pace incremental test (MIT) with 80 | 699 ± 67 s for MIT and 359 ± 17 s for TT4km | 32-channel EEG and 32×32 NIRS and a pair of EMG and gas analyzer for recording Cardiopulmonary Data | 9M trained road cyclists, 32.9 ± 7.3 | 7 min warm up was performed before the experiment. This includes 5-min TT4km and 2-min MIT at 80 | According to oxyHb in PFC and vastus lateralis muscle, at the closing stage of different cycling task, when the oxygen level ($VO_{2MAX}$) is matched, similar motor output (EMG and motor output) is recorded though existence of different disturbances before the final point. Activation of M1 in through the exercises may represent that this part plays a role in centrally-coordinated exercise regulation. |
| Fumoto et al. (2010) | Ergometer cycle | 60 | 15 min | 24-channel NIRS | 10 (9M), 32 ± 2.2 | To assess psychological mood, subjects were asked to answer questionnaires. | Cycling task increases the brain's activity in ventral PFC region. This may cause a reduction in negative mood. |
| Ludyga et al. (2016) | Ergometer cycle | 60, 90, and 120 | 3-min for each speed | 32-channel EEG | 36 (24M) cyclists 27 ± 3 | The participants had at least 4 h cycling training per week within the last 6 months before the experiment. | Improvement in cycling training is closely related to brain cortical activity. Also, the higher cadence, the greater brain functional response. |
| Jain et al. (2013) | Stationary bicycle with a rigid, reclined backboard | 2.1 s/cycle (±0.5 s/cycle) | 20 min with a short break after 10 min | EEG: 64 channels EMG: 10 Channels | 10, Range: 22-32 Median: 26 | A warm-up consisting of 5-min self-paced walking and 2-min cycling at 100 W with pedal cadence of 80 rpm was performed | During pedaling, the brain processes a great amount of sensory activities. Cortical activities in pedaling reaches to its maximum in transitioning the legs from flexion to extension and vice versa |
| Schneider et al. (2013) | Ergometer cycle | Five pedaling exercises at 90 | 2 | 32-channel EEG and 7 muscle recording by EMG and electronically braked cycle ergometer | 8, 5M aged 27 ± 4 and 3 female aged 24 ± 2 | A standardized warm-up (i.e., 5 min at 1 W/kg, 2 min at 3 W/kg, and 1 min at 5 W/kg) and a 5-min recovery period was used before doing the task. | Besides showing the possibility of localizing brain cortical activity during pedaling activity, it is shown that motor cortex activity increases with the increasing of power level and significantly mirrored muscle activity. |
| Enders et al. (2016) | Ergometer cycle | 97 by average (between 90 and 100) | 7:04 min by average (range: 6:01 to 8:58 min) | 64-channel EEG cap EMG | 10M experienced cyclists | Each subject performed the tests on 3 different days. First day: finding the maximum aerobic power of participants Second day: perfuming the test at 85% of individual ability and familiarization. Third day: repeating the second day test and data recording | By increasing the fatigue, EEG power increases. The maximum increase occurs in frontal area of the cortex. timing of event-related desynchronization occurring in SMA denotes the source of producing force and its transition from flexion to extension in pedaling. |
| Fontes et al. (2020) | Ergometer cycle | 60 | 30 s cycling and 30 s rest for four times | fMRI | 22M, 24.4 ± 7.1 | The intensity of the cycling was increased by 25 W at each round | By increasing the exercise's intensity, PFC activities decreases. Cerebellum was activated only in low-intense activity while motor cortex is activated in low and high intense activities. |



10.3389/fnins.2023.1051500

TABLE 5 Brain-body imaging in walking-running.

| References | Surface | Dist. (m) | Speed Km/h | Duration (min) | Sensors | Participants No. and age | Special condition | Contribution |
|---|---|---|---|---|---|---|---|---|
| Suzuki et al. (2004) | Treadmill | - | Walking: 3, 5, and running: 9 | 30 s rest, 90s locomotion, 30 s rest. Three repetition for each subject | NIRS (42 channel) with 28 optodes consisting of 12 light-source fibers and 16 detectors | 9, right-handed, healthy subjects (7M 28.1 ± 7.4, Range 22–46 | Starting task was selected randomly between 3 or 5 km/h speed. Participants could swing their hands freely. | In the frontal cortices, in contrast to deoxyHb, oxyHb increases in acceleration period proceeded by locomotion task. This change in oxygenated hemoglobin is greater in PFC and M1 at high-speed locomotion and there is less change in SMC. Consequently, to adapt to locomotor speed, PFC and M1 play crucial roles. |
| Nordin et al. (2019b) | Treadmill | - | Walking: 1.8, 3.6, 5.4, 7.2 and running 7.2, 9 | 18 min (3 min for each speed) | 128-channel EEG, 8-channel EMG, optitrack with 10 cameras | 9 (6M) | random obstacles were added to during walking/running on the treadmill | The dual-layer EEG cap reduced the artifacts effects on the data. Spectral power of delta, theta, and alpha frequency bands in SMA and PMC increased within 200 ms after the obstacle presence. |
| Jahn et al. (2004) | Imaginary | - | Walking: 3.6 and running: 9 | 0.33 | fMRI (34 slices of brain was covered) | 13, mean: 27.3 range: 21–35 | Imaginary walking with closed eyes in supine condition: tasks: rest, standing, walking, and running in 20-s sequences | In slow walking spatial navigation plays a more significant role and this role is played by the parahippocampal cortex. In an unhindered locomotion such as running vestibular and somatosensory cortex get deactivated and this prevents the disruptive effect on the spinal pattern and sensory signals. |



10.3389/fnins.2023.1051500

10.3389/fnins.2023.1051500

TABLE 6 Brain-body imaging in walking-cycling.

| References | Surface | Dist. (m) | Speed Km/h | Duration (min) | Sensors | Participants No. and age | Special condition | Contribution |
|---|---|---|---|---|---|---|---|---|
| Storzer et al. (2016) | OG/ Ergometer bicycle | - | 40 strides per min ($41.5 \pm 2.88$) for walking and 40 rpm: ($40.9 \pm 1.72$) for bicycling | 10 s movement (bicycling or walking) then 10 s rest for 50 times. Then, continues 2 min movement. | 18-channel EEG and 6-channel EMG | 14 (8M), $24.9 \pm 3.0$ | The speed adjustment is based on prior instruction. | cortical activation during bicycling and walking are compared. During movement, while bicycling is associated with stronger decrease in beta power, walking is associated with alpha power reduction. |

conceptual framework and discuss how to assess the neurological and musculoskeletal measures extracted from brain-body imaging sensors for further clinical use.

## 5.1. Neurological and musculoskeletal drivers

According to our systematic review results, most studies followed the philosophy of medical diagnosis that is rooted in conducting statistical analysis between different groups (e.g., young vs. old, control vs. patient). These groups were asked to perform specific behavioral protocols under which their performances were supposed to show neurological and musculoskeletal differences reflected by the brain-body imaging data. Therefore, various experimental protocols were explored to capture the differences in statistical norms among groups (Kashuba et al., 2020; Warmerdam et al., 2020). The typical statistical analysis approaches include comparisons of statistical norms (e.g., *p*-value, effect size) and classifications based on machine learning (e.g., accuracy, precision) (Figueiredo et al., 2018; Hatami et al., 2019; Patil et al., 2019; Hausmann et al., 2021). Few studies adopted representation learning methods based on deep neural networks to explore patterns and features of brain and motion signals to show the group differences (Vásquez-Correa et al., 2018; Talo et al., 2019; Song et al., 2021). Furthermore, specific quantitative assessments, such as clinical outcomes or symptoms, were identified as ground truth so that the same reference could examine both groups. However, no consensus on experimental protocols caused challenges in determining reliable ground truth or references. Otherwise, few studies provided explanations and rationales for the design methodology of behavioral experiments.

Although it lacks standardization of experimental protocols, existing studies still generated consistent conclusions on neurological and musculoskeletal correlates of human locomotion. For example, most studies revealed that the active brain regions during various walking protocols include the motor, sensory, and prefrontal cortexes. The brain areas involved in walking behavior span SMA, premotor cortex, sensorimotor, M1, and left and right prefrontal cortex. Notably, the age-related changes showed that the involvement of PFC increased among old adults, especially during high-speed walking. When the subjects need to adjust their postures for cycling, the involvement of PFC decreases in order to keep mental resources for the maintenance of these additional requirements during exercise. The PFC has been implicated in planning complex cognitive behavior, especially in the resting status. Few studies explored the running protocols; therefore, there is little consistent knowledge regarding neurological and musculoskeletal correlates of human running. It is noteworthy that when subjects are required to conduct spontaneous cognitive tasks, the PFC activation increases in all age populations, and its increase is more significant in older adults with and without cognitive impairment. These conclusions have motivated many hypothesis-driven research projects on disease-related changes in neurological and musculoskeletal correlates of human locomotion.

Besides the consistent understanding of neurological correlates of human locomotion, mixed results and conclusions exist due

TABLE 7 Brain-body imaging in dual-task walking.

| References | Surface | Dist. (m) | Speed Km/h | Duration (min) | Sensors | Participants No. and age | Special condition | Contribution |
|---|---|---|---|---|---|---|---|---|
| Mirelman et al. (2017) | OG/ Mat | 30 | SW-YA: 1.349 ± 0.157 SW-OA: 1.069 ± 0.1137 DTW-YA: 1.238 ± 0.136 DTW-OA: 1.058 ± 0.123 | - | fNIRS (6 channel), walkway gait pressure mat | YA: 23 (10M): 30.9 ± 3.7 and OA: 20 (10M): 69.7 ± 5.8 | Each round started and ended with 20 s of standing quietly, with the instruction to refrain from talking and moving the head. More complex walking: negotiating with two physical obstacles during walking. DTW: walking while talking (subtracting 3 s from a 3 digit, predefined number) | Needed cognition increases for both young and older people but for older people is more significant. Gait variability in older adults increases with the increase in pre-frontal activation. pre-frontal activation in older people is higher indicating older people rely more on their cognitive resources during walking. Neural activation in the PFC increases with task complexity, similarly, in both younger and older adults. |
| Holtzer et al. (2011) | OG/ Room | 4.572 | SW-YA: 0.1222 ± 0.175 SW-Old 0.716 ± 0.177 DTW-YA: 0.810 ± 0.175 DTW-OA: 0.362 ± 0.131 | - | fNIRS (16 channels) | YA: 11 (4M): range: 19–29 OA: 11 (4M): range: 69–88 | quiet room wearing comfortable footwear with the fNIRS attached to the front of the head. DTW: walking while talking alternate letters of the alphabet | PFC activation increases in WWT compared to mere walking. This increase is higher in young adults than older adults (contradiction with Mirelman et al., 2017). The results are compared to the WWT and shown that single walking task needs less cognitive resources. |
| Lu et al. (2015) | OG | - | Self-paced walking | 1 min | fNIRS 8×8 | 17 (9M), 23.1 ± 1.5 | WCT: subtracting 7 from a 3-digit number and speaking out the number. WMT: carrying a 600-ml bottle on a tray while walking | PFC, M1, and supplemental motor areas data obtained by fNIRS show that left-PFC has the highest oxyHb during WCT and there is a minor increase in oxyHb in initial phases of NW and WMT. M1 and supplementary areas get more activated during WCT and WMT. WCT cause a reduction in cadence, stride time, and stride length while WMT only diminishes the stride length. |
| Makizako et al. (2013) | OG | - | Self-paced walking (SW: 3.5 ± 0.6, DTW: 3.1 ± 0.7) | 20 s for performing a SW or DTW | 16-channel fNIRS (6 emitters and 6 detectors) | 16 right-handed OA (10M) with 65 years or older | Each participant completed three SW and DTW. 10 s rest before the task and 20 s rest after the task were considered. | During DTW, pre-frontal activation is observed among older adults with mild cognitive impairment |
| Mirelman et al. (2014) | OG/ 7-meter sensor-carpet | 5 walks of 30 meters for each trial | SW (4.86 ± 0.36), walking while counting (4.64±0.54), walking while S7 (4.43 ± 0.50) | 20 s during the task | 6-channel NIRS | 23 (10M), 30.9±3.7 | The conditions are: 1-SW 2-walking while counting forward 3- walking while subtracting 7 from a 3-digit number (S7) 4-standing while S7 | It is shown that DTW is coupled with frontal brain activation. The observed changes are directly related to the cognition during walking and not verbalization. |
| Talamonti et al. (2021) | OG | - | SW: 4.169 ± 0.130 DT: 3.859 ± 0.144 | 5 min combination 30 s walking/ cognition task/ dual task walking | 256-channel fNIRS | 24, Older than 60, Participants were divided to two groups of high and low cardiovascular risk factors (HCVRFs and LCRFS) based on Framingham score. | Cognitive task: remembering 2-back heard number. Dual task walking: performing cognitive task while walking | HCVRFs show greater task-related cortical response specifically in pre-frontal caudal and rostral dorsal regions in the beginning of 12-month training. Physical training had more cortical activation reduction for HCVRFs. Cognitive performance and stable gait speed throughout are associated with 12-month physical training. |

*(Continued)*





10.3389/fnins.2023.1051500

TABLE 7 (Continued)

| References | Surface | Dist. (m) | Speed Km/h | Duration (min) | Sensors | Participants No. and age | Special condition | Contribution |
|---|---|---|---|---|---|---|---|---|
| Pizzamiglio et al. (2017) | OG | - | Self-paced walking, walking while conversing with a friend and lastly walking while texting with a smartphone. | - | 64-EEG channel, 2 digital force sensing resistor sensors for recording movement. A digital button (1-to-0 active edge) to distinguish start and end points | 14 (5M), 26 ± 3 | 3 min of resting standing still (i.e., baseline) with their eyes open looking at a standard spot on a blank wall. Then walking for the purpose of familiarization and then recording for mere walking, then walking while conversing, finally walking while texting | Real-life activities are associated with different frequency-specific neural biomarkers. Walking while conversing is integrated with an increase of theta and beta neural power in electrodes located over left-frontal and right parietal regions. However, walking while texting is accompanied with a decrease of $\beta$ neural power in a cluster of electrodes over the frontal-M1 and SMC. |
| de Tommaso et al. (2015) | OG | 10 | Self-paced | 15 min | 21-channel EEG, 4-channel EMG | 17 (5M), Range: 18-65 | Each subject did: sitting (5 min), standing (5 min), walking (5 min), P300 oddball was performed during standing and walking | P300 component amplitude increases during walking compared to standing. There is a negative correlation between age and P300 component vanishing during walking. According to motor-cortex and EMG activities, abnormal gait is distinguished from normal ones. |
| Meester et al. (2014) | Treadmill | - | SW: 4.39 ± 0.86 faster walking: 5.33 ± 0.94 | 30 s for performing the task and 20–40 s for rest. For five times at two speeds | 4-channel fNIRS with two sources and two detectors and spinal cord reflex activity measured by soleus H-reflex | 17 (7M), 15 right-handed and 2 left-handed. 27.8 ± 6.3, Range: 22–44 | The cognitive task was counting backward in steps of seven from a defined number. | Although PFC activation doesn't change by increasing the walking speed, it would be activated in response to cognitive loads. |
| Eggenberger et al. (2016) | Treadmill | - | 0.2, 3, 5 for walking | 9 min walk 30 min exergame | fNIRS (2 sensors) | 19, 74.9 ± 6.9 for exergame, 14, 74.9 ± 6.9 for balance | intermittent Interventions of exergame and balance during walking | Intermittent of exergame and balance reduce the oxygenation of the PFC. This reduction is more significant in exergame. This reduction could be relevant to improve mobility and falls prevention in the elderly. |
| Fraser et al. (2016) | Treadmill | - | YA: 2.64 OA: 1.78 And also preferred speed | 2 min | fNIRS (16 detector) | 19 YA 21.83 ± 1.92 14 OA: 66.85 ± 5.26 | DTW: Walking and talking and remembering words and report immediately (1-back or 2-back) | After controlling the walking speed, the difference between YA and OA could be revealed as when the difficulty of task was increased, oxyHb in PFC of OA was increased. |
| Lau et al. (2014) | Treadmill | - | 2.88 and 4.5 | 5 min standing and 10 min walking | 248-channels EEG | 8 (7M), Range: 20-31 | Task: visual oddball discrimination, 20% target and 80% standard stimuli were displayed on a monitor to the participants at eye level 1 m in front of them. | Walking has lower functional connectivity between SMC areas than standing. |
| Castermans et al. (2011) | Treadmill | - | 1.5, 3, and 4.5 | 6.5 min | 32-channel EEG | 7, Range: 25–33 | The dual task was counting the green letters appearing during 3 s on a screen in front of the participants. Task: 0.2 s flashing light, 0.1 s between two flashes and 1 s interval and repeating that for 12 times for 25 target letters. | Feasibility of suing P300 during walking while recording EEG signals from parietal and occipital areas is shown, which can be beneficial for ambulatory conditions. |

*(Continued)*





10.3389/fnins.2023.1051500

TABLE 7 (Continued)

| References | Surface | Dist. (m) | Speed Km/h | Duration (min) | Sensors | Participants No. and age | Special condition | Contribution |
|---|---|---|---|---|---|---|---|---|
| Malcolm et al. (2015) | Treadmill | - | YA: 2.4 and 5 OA: 2.4 to 4.8 (3.5 by average) | About 4 min for a block | EEG (72 channel) | 17 YA (9M), 27.2 ± 4.6 Range: 21.8–36.1, 16 OA (7M), 63.9 ± 4.0, Range: 57.7- 71.0 | OA performed five blocks of the response inhibition task while sitting, 9 or 10 blocks while walking and two blocks only walking. YA completed three or four blocks sitting, a minimum of four blocks walking slowly (range: 4-8 blocks), at least four blocks walking quickly (range: 4-8 blocks) and two blocks of each speed walking without the task. Task: speeded visual Go/No-Go task | By examining the variability and time of stride in different configurations, only the OA's accuracy drops significantly when performing inhibitory task while walking. Also, the brain's performance in YA is more modulated than OA according to the EEG data of cortical activities. The reason might be an age-associated loss in flexible resource allocation across multiple tasks. |
| De Sanctis et al. (2014) | Treadmill | - | 2.4, 5 | About 4 min for a block | EEG (72 channel) | 18 (10M) Range: 21.8-36.1, Mean: 27.2 | Doing a Go/No-Go task by shown pictures and selecting by mouse while sitting, walking slowly and walking briskly | When walking while doing another task, stride time in walking grows by increasing the cognition load of the task. Also, by increasing the age, the cortical motor behavior shifts from automatic to more controlled process. |
| Mazurek et al. (2021) | Treadmill | - | 2.4, 5 | About 4 min for a block | EEG (64 channels and 128 channels) | 10, Range: 20–72 | Doing Go/No-Go task while walking similar to De Sanctis et al. (2014) 16 blocks: one training block at the beginning, seven sitting blocks, seven walking blocks, and one task-free block (walking on the treadmill without a task) | Developing and easy customizing method for configuration EEG electrodes, which is improving the spatial localization of without specialized hardware or software. |
| Lau et al. (2012) | Treadmill | - | 2.88 | 5 min standing followed by 10 min walking | 248-channel EEG | 8, Range: 20–31 | Showing stimulus while the participants stand/walk should press a button when seeing the target stimuli. | Based on studying visual cortex in visual oddball discrimination during standing and walking, Weighted Phase Lag Index introduced as a potential method for recovering cognitive brain dynamics in the presence of gait-related artifacts. |
| Gramann et al. (2010) | Treadmill | - | 2.88, 4.5 | Two 10-min for each condition (60 min in total) | 248-Channel EEG | 11 (10M), 24.2 ± 3.4 | A computer screen 50cm away from participants showed 80% non-target and 20% target stimuli, vertical or 45° rotated black cross for 500 ms. Three conditions were standing, slow walking, fast walking, and running (removed because of artifacts) | Inside or near right-lateral occipital cortex, and superior and inferior parietal cortex, according to ICA, are activated in the target -stimulus ERPs. In contrast, 40% of variance in 350–500 ms of the target-response ERPs was accounted for all movement conditions with activation in or near anterior cingulate cortex. |





10.3389/fnins.2023.1051500

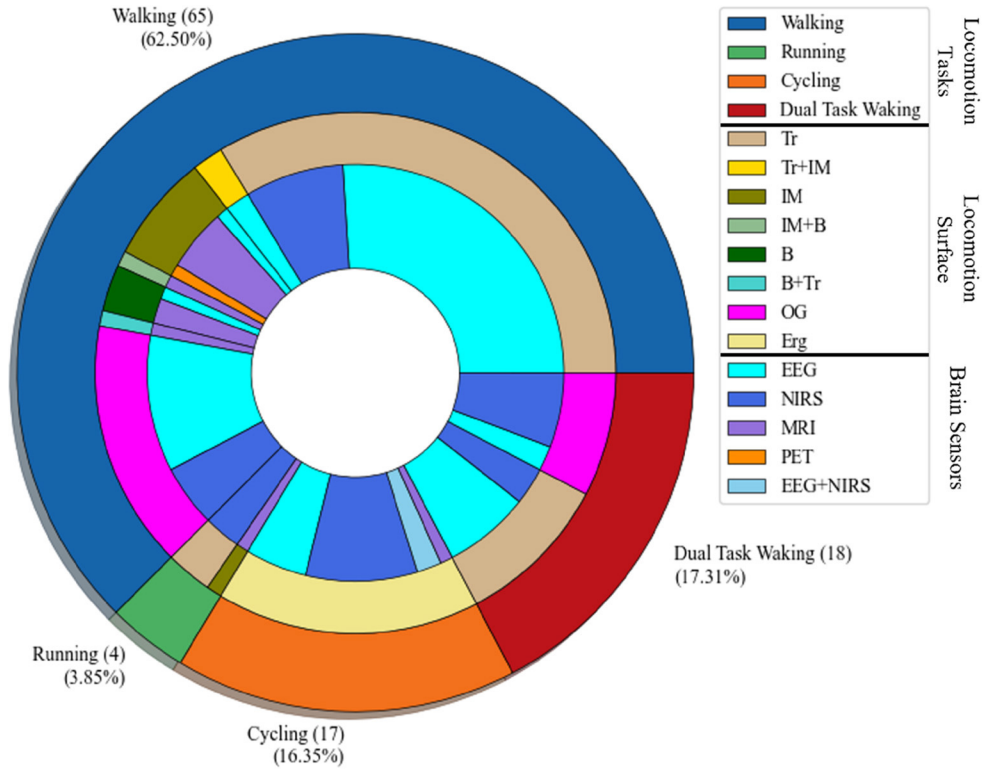


FIGURE 3
Task-Surface-Brain sensor visualization: the most outer layer shows the type of the locomotion task; walking, running, cycling, and dual-task walking. The middle layer shows the type of the surface used for the body-brain imaging experiment, which are Tr: treadmill, IM: imaginary task, B: Board with pedals, OG: overground, Erg: Ergometer cycling. The most inner layer shows the type of the brain sensor used in the brain-body imaging.

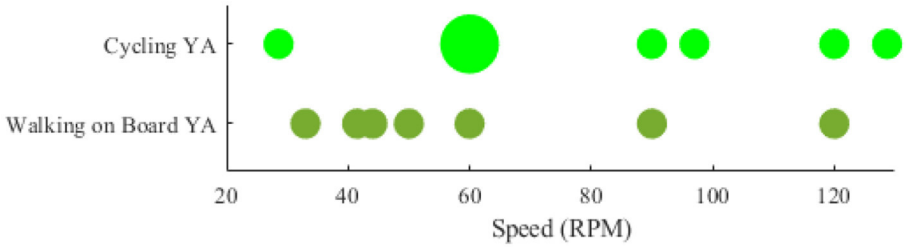


FIGURE 4
Comparing locomotive intensity in two types of brain-body imaging tasks performed with different rotational speeds: 1) cycling 2) walking on a board with pedals. Only younger adults have been employed to perform these tasks.

to the heterogeneity of participants' neurological expressions, musculoskeletal variance under imprecise experimental protocols, and observation constraints by the sensing techniques. For instance, some studies concluded that the cerebral cortex controls multiple muscles hierarchically through a few synergies during walking. In contrast, few studies argued that the role of cortical control during walking might not be valid due to the motion artifacts of EEG. Furthermore. Subjects that conducted actual walking were more accurately classified than subjects with imaginary walking. Subjects that walked on a treadmill showed different band activities captured by EEG compared to subjects who walked over the ground. These inconsistent results require further investment in establishing protocols, standardization, and benchmarking tools, which also motivated this research work.

## 5.2. Locomotive and cognitive demands

The primary assumption underlying the experimental protocols is that the locomotive and cognitive demands could stimulate changes and patterns in neural activity, which the brain-body sensors could pick up (Ladouce et al., 2019). Thus, the knowledge of the simulation mechanisms further guides the treatment and rehabilitation strategies for potential clinical

outcomes. However, most experimental protocols involve low-intensity locomotion tasks, such as walking and cycling, while few studies conducted high-intensity locomotion tasks, such as running. In addition, little research explained the design methodology of the experimental protocol, especially the research hypothesis of which types of neural activities might be expected under the experimental configurations, such as duration, intervals, and frequency. Also, conducting behavioral studies on human subjects is always challenging, even more, if considering psychological factors such as state of mind, concentration, and technical dexterity. Therefore, some studies integrated cognitive demands into locomotive tasks, such as avoiding obstacles, determining walking directions, or following an avatar. Other studies developed a dual-task paradigm to examine the involvement of cognition in human locomotion.

As illustrated in Figure 1, the conceptual framework argued that more work is needed to examine the simulation mechanisms, thus developing a better design methodology for experimental protocols. The systematic review results showed that several challenging questions remain in the research field. First, benchmarking the locomotive and cognitive demands will be needed. Locomotive tasks have several configurable parameters, such as duration, intervals, and frequency, which need to divide into several levels or intensities. Cognitive tasks also have configurable parameters, such as type and complexity, depending on working memory and executive functions. For instance, for a specific subpopulation's demographic, locomotion and cognition capacity, researchers in designing experimental protocol need a basic understanding of which levels of demands might stimulate the anticipated brain activity. Knowledge of locomotion disorder patterns and corresponding brain areas has helped establish experimental protocols for several neurological diseases, such as parkinsonian gait for Parkinson disease (Ghai et al., 2018) and NIH cognitive toolbox for cognitive impairment (Gershon et al., 2010). Second, manipulation of the tasks needs more research investment. Existing studies rarely consider how the sequential configuration of the tasks stimulates neural activity. Most protocols conducted a heuristic-designed sequence of locomotive tasks and anticipated the brain-body sensors could capture the subtle changes or patterns of neural activities. However, the loop from demands to brain and musculoskeletal activities to sensors, in Figure 1, shows that manipulation of the demands could generate richer information than the heuristic-designed protocol. Third, the experimental protocols should be easily administered to avoid confusion and distraction for participants. Few studies gave a clear description of how the protocols are being instructed. Cueing the participants toward specific tasks could have influenced the expected neural activity and cognitive performance. Therefore, most researches argued that when the experiment protocol is administered and instructed by assistance of a computer is less likely that neural activity and cognitive performance get adversely affected compared to the case that the experiment is controlled and instructed by interference of a human. Hence, replication of previous experiment protocols that were controlled by a human as examiner with a computer-assisted administration provides a high-quality data with removal of the human interference affects (Vrana and Vrana, 2017; Dror, 2020; Young et al., 2022). Moreover, computer assistance in the cognitive load assessment could make it feasible to conduct

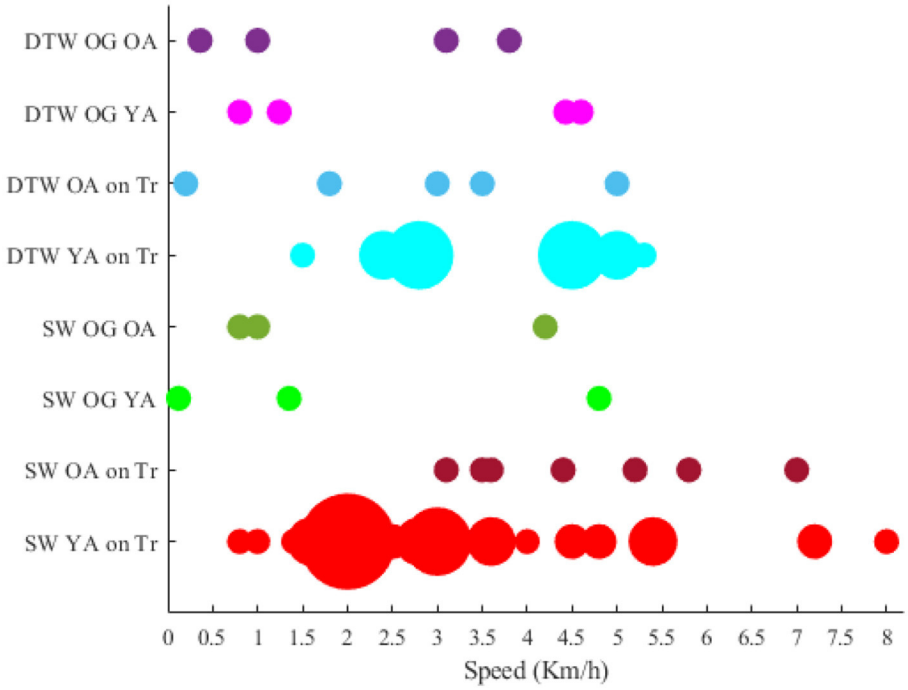


FIGURE 5
Intensity of locomotion in existing experiment protocols.

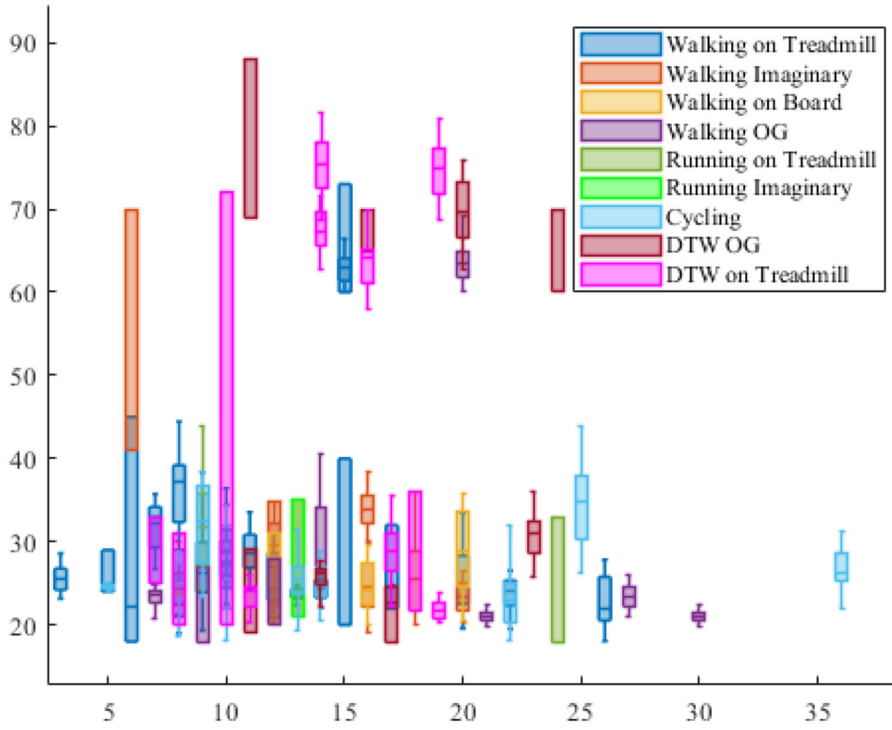


FIGURE 6
The participants' age distribution in each locomotion experiment. The vertical axis shows the age of the participants and the horizontal axis shows the number of participant in the reported experiment protocol.

the experiment at places out of the clinics and laboratories. These places (e.g., participants' home or a local clinic) are accessible to the participants and individuals are comfortable to perform the experiment with assistance of a computer without interference of an examiner. As positive side effects of the computer-assisted experiment administration, high-quality and cost-effective patient care could be provided (Porrselvi, 2022; Young et al., 2022).

## 5.3. Observation constraints by the sensing techniques

Another dimension of our systematic review results is illustrating the impacts of the observation constraints by the brain-body sensing techniques. Previous work has reviewed and discussed the advantages and disadvantages of these techniques, including tolerance of motion artifacts and spatial and temporal resolutions. However, most studies reviewed in this work did not explain the rationale for selecting specific sensing techniques in experimental protocol design. According to our review results, it is obvious to see the impacts of sensing techniques on the research results and generated knowledge. Therefore, we summarize these impacts for enabling guidelines for future researchers to design experimental standards and benchmarks.

### 5.3.1. Tolerance of motion artifacts

Prior knowledge of sensing techniques has concluded that among three of them, MRI has the lowest tolerance to motion artifacts, EEG less, and fNIRS the highest. Despite efforts in signal processing and denoising to improve each technique's tolerance to motion artifacts, most studies still followed the knowledge and showed different experimental results. Studies that adopted MRI has considered its limited tolerance of motion artifacts and mainly designed imaginary locomotion or simulated surrogate tasks rather than actual locomotion in their experiments (Stolbkov et al., 2019; Amemiya et al., 2021). The central assumption of

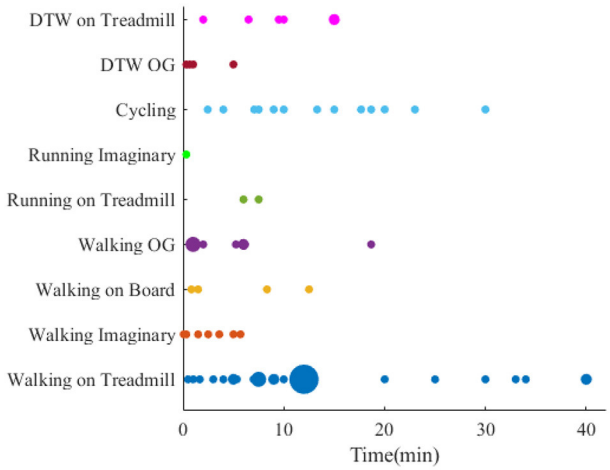


FIGURE 7
Brain-body imaging experiments' duration.

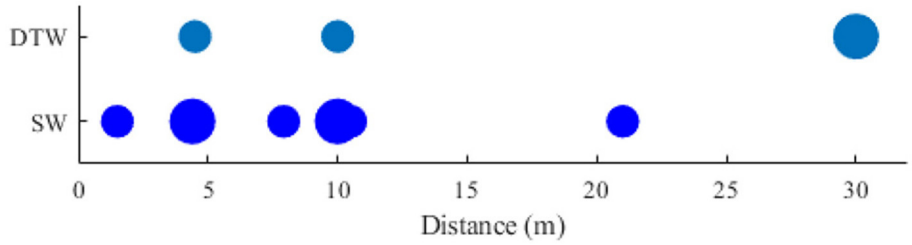


FIGURE 8
Comparing distance the walk distance in two types of Brain-body imaging experiments: 1) DTW and 2) SW.

these studies is that neurological correlates of these imaginary or surrogate tasks are closely related to neurological activation during actual locomotion. However, our summarized results in locomotion tables and Figure 9 showed that these imaginary or surrogate tasks could not simulate the complex dynamics the brain must execute to adjust and maintain the musculoskeletal patterns during actual locomotion. Especially studies that utilized EEG have shown that actual walking stimulated brain activation patterns that could be classified with higher precision than imagery walking. Therefore, studies that adopted EEG sensors designed a more comprehensive range of locomotion tasks, from imaginary walking and cycling to running. Furthermore, the fNIRS studies are preferred in high-intensity locomotion experiments. More than 50% of studies reviewed in this work that conducted cycling and running tasks adopted fNIRS sensors.

Sensitivity of EEG data to motion artifacts is a research concern and the results of some previous published research due to not considering an extensive removal of motion artifacts has been questioned. For instance, the reported EEG results indicating the changes in high-gamma frequency band during walking (Gwin et al., 2011) could be caused by motion artifacts as well (Castermans et al., 2014). To address the considerable drawback, different denoising methods to employ during or after data collection have been developed. During data collection, artifact removal is associated with hardware modifications. In this respect, one effective way has been introduced to separate electrophysiological signals from non-neural signals. To this end, in one approach, two layers are used below the EEG cap. A silicone layer is used on top of the scalp to block electrophysiological signal. Then, a simulated conductive scalp with similar impedance to human scalp is used to measure the voltage differences generated by gait dynamics (Snyder et al., 2015). In another approach, well-known as a EEG dual electrode design, simultaneously EEG data and isolated motion artifacts are recorded by pairs of the electrodes that are electrically independent and mechanically coupled (Nordin et al., 2018; Clark et al., 2020). After the data collection, denoising is coupled with software data processing. In this regard, Independent Component Analysis (ICA), low, high, and band band pass filter are routinely applied. Besides these remedies, ICA-based methods such as adaptive ICA mixture model algorithm (Palmer et al., 2006), extended infomax ICA (Lee et al., 1999) and multiple mixture ICA (Allen et al., 2000) approaches are utilized (Gwin et al., 2010). Moreover, a developed conductive head phantom and robotic motion platform has emerged as a powerful tool to analyze the artifact removal methods through generating a ground truth for EEG signal. This device is used to evaluate artifact removal methods such as dual-layer EEG and Artifact Subspace Reconstruction (Richer et al., 2020). Also, this device is used to show that electrodes with larger surface reduces the electrodes vulnerability to motion artifacts (Symeonidou et al., 2018). In addition, this device is employed to assess the effect of the motion artifacts parameters such as frequency and amplitude (Oliveira et al., 2016).

### 5.3.2. Spatial and temporal resolutions

MRI has the highest spatial resolution among the three sensing techniques while fNIRS has the lowest (only centimeters under the skull) (Li et al., 2022b). Accordingly, MRI studies discussed their results with a detailed description of the brain cortex, such as SMA and the dorsal premotor cortex. Nonetheless, lacking the portability feature has significantly limited the application of the MRI in the brain-body imaging of locomotion studies mostly to imaginary task and thus, this scope of study has been deprived from the high spatial resolution of the MRI imaging technique. On the other hand, although EEG has lower spatial resolution than MRI, appropriate source localization approaches could improve its spatial resolution at a cortical level. When source localization is used, the spatial resolution of the fNIRS and EEG are comparable. However, EEG has the highest temporal resolution among the three methods and permits the highest and the most precise data brain investigation compared to the fNIRS and MRI methods. Thus, Looking into the results summarized in our work, we can see that studies that adopted EEG sensors provided the neurological and musculoskeletal correlates on a fine-grained temporal scale, such as neural activation patterns during different movement periods (e.g., swing, stance). These features has made the EEG the most popular technique in the explorations of the brain-body imaging of human locomotion.

### 5.3.3. Miscellaneous constraints

We also observed other constraints in the design methodology of experimental protocols, such as imbalanced ages of participants. For example, most studies recruited participants aged below 40, while fewer recruited participants older than 60. A significant age gap (40–60) among the participants involved in these studies existed. However, the adults within this age range are baby boomers in the U.S., a large sector of the population, a group deemed by

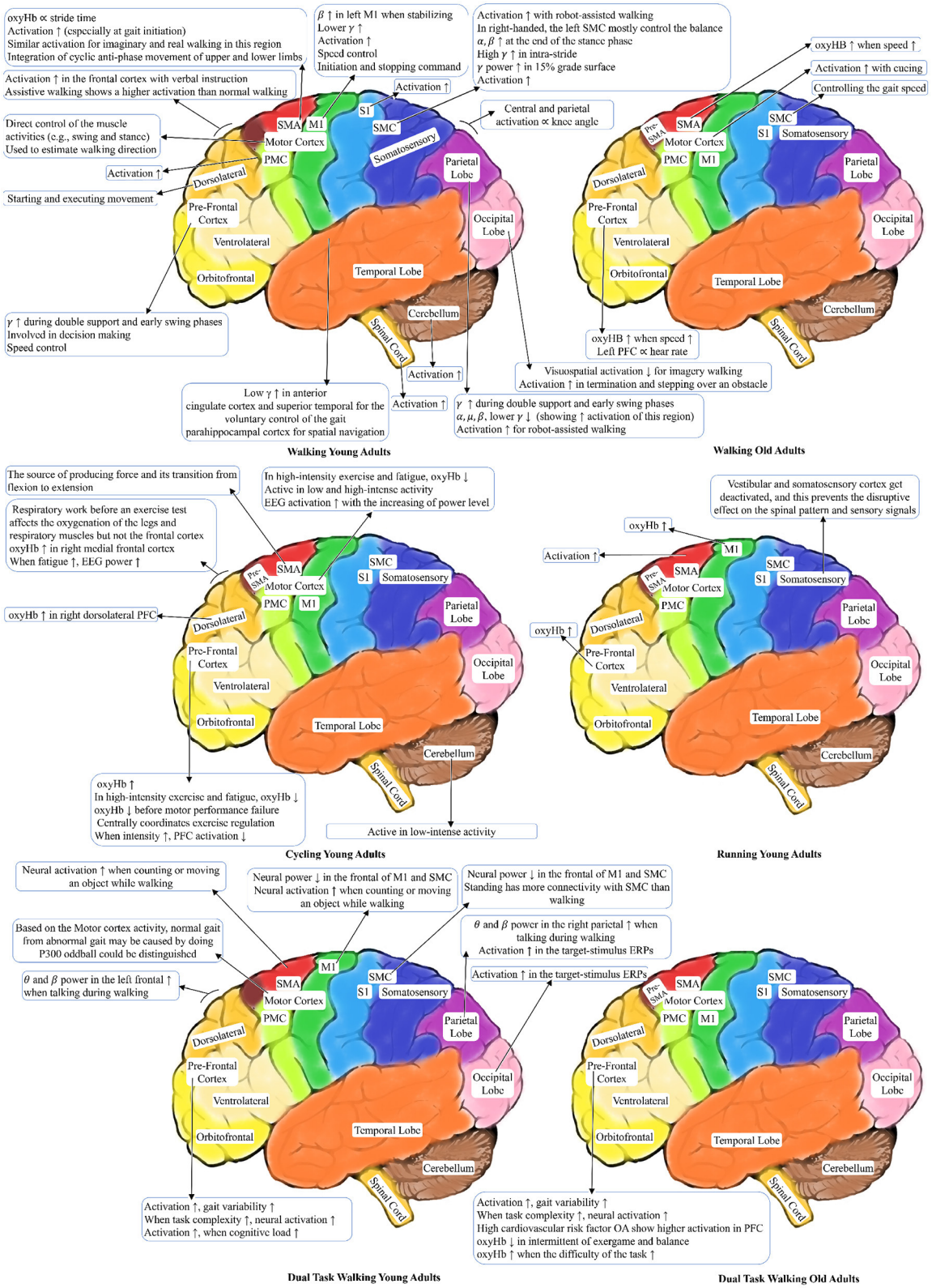


FIGURE 9
Brain areas activation patterns during locomotion tasks.

the Centers for Disease Control and Prevention (CDC) as mid-life stage adults. This age population is facing an increase in clinical and other preventive services to support maintaining good health into older age (Pearson-Stuttard et al., 2019; Doubeni et al., 2021), which means this age group should be a critical population for studies on neurological and musculoskeletal correlates of human locomotion. Although there might exist real-world challenges to recruiting this specific age population, additional investment in balancing the age distribution of the participants is needed to fulfill a cross-lifespan understanding of human locomotion and its neurological and musculoskeletal correlates.

## 6. Conclusion

This paper explores the topic of the design methodology of experimental protocols that aim to study neurological and musculoskeletal correlates of human locomotion using brain-body sensing techniques. The review of many types of neural activities stimulated by human locomotion demonstrates the importance of quantitative analysis using brain-body sensors in potential healthcare applications. By reviewing the current design methodology of experimental protocols, this paper illustrates that the protocol design significantly impacts the experimental results due to the heterogeneity of participants' neurological expressions, musculoskeletal variance under the imprecise locomotive and cognitive demands, and observation constraints by the sensing techniques. Finally, the impacts of the experimental protocols are discussed by reviewing the practical issues to provide implications and guidelines for future researchers to design experimental standards and benchmarks.

Brain-body imaging of human locomotion is a vast area of research. This paper focused on a significant research issue: how to reproduce human locomotion experiments. Therefore, we conducted a systematic review of existing experiment protocols to examine various settings and conditions, such as locomotion intensity, locomotion duration, locomotion distance, brain sensing technologies, and corresponding brain activation expressions. In future work, technologies for locomotion sensing and their advantages and disadvantages will be further examined and discussed. Also, upper-limb locomotion, such as shoulder, elbow, wrist, and finger movement, is a broad study that will be examined in another work. Finally, as the participants of this systematic review are healthy, similar brain-body imaging experiment exploration for neuromechanical disorders would be a valuable work to extend.

## Data availability statement

The original contributions presented in the study are included in the article/supplementary material, further inquiries can be directed to the corresponding author.

## Author contributions

JG designed the study, created the research question, and finalized the manuscript. SK implemented the study process, collected and analyzed the data, and initiated the manuscript. NJ developed the study motivation and significance, guided the data analysis, and revised the manuscript. All authors contributed to the article and approved the submitted version.

## Conflict of interest

The authors declare that the research was conducted in the absence of any commercial or financial relationships that could be construed as a potential conflict of interest.

## Publisher's note

All claims expressed in this article are solely those of the authors and do not necessarily represent those of their affiliated organizations, or those of the publisher, the editors and the reviewers. Any product that may be evaluated in this article, or claim that may be made by its manufacturer, is not guaranteed or endorsed by the publisher.

## References


Abtahi, M., Borgheai, S. B., Jafari, R., Constant, N., Diouf, R., Shahriari, Y., et al. (2020). Merging fnirs-eeg brain monitoring and body motion capture to distinguish parkinsons disease. *IEEE Trans. Neural Syst. Rehabil. Eng.* 28, 1246–1253. doi: 10.1109/TNSRE.2020.2987888

Alchalabi, B., Faubert, J., and Labbe, D. R. (2019). "EEG can be used to measure embodiment when controlling a walking self-avatar," in *2019 IEEE Conference on Virtual Reality and 3D User Interfaces (VR)* (Osaka: IEEE), 776–783.

Allali, G., Blumen, H. M., Devanne, H., Pirondini, E., Delval, A., and Van De Ville, D. (2018). Brain imaging of locomotion in neurological conditions. *Neurophysiol. Clin.* 48, 337–359. doi: 10.1016/j.neucli.2018.10.004

Allen, P. J., Josephs, O., and Turner, R. (2000). A method for removing imaging artifact from continuous eeg recorded during functional mri. *Neuroimage* 12, 230–239. doi: 10.1006/nimg.2000.0599

Al-Yahya, E., Dawes, H., Smith, L., Dennis, A., Howells, K., and Cockburn, J. (2011). Cognitive motor interference while walking: a systematic review and meta-analysis. *Neurosci. Biobehav. Rev.* 35, 715–728. doi: 10.1016/j.neubiorev.2010.08.008

Amemiya, K., Morita, T., Hirose, S., Ikegami, T., Hirashima, M., and Naito, E. (2021). Neurological and behavioral features of locomotor imagery in the blind. *Brain Imaging Behav.* 15, 656–676. doi: 10.1007/s11682-020-00275-w

Andonian, B. J., and Huffman, K. M. (2020). Skeletal muscle disease in rheumatoid arthritis: the center of cardiometabolic comorbidities? *Curr. Opin. Rheumatol.* 32, 297–306. doi: 10.1097/B.O.R.0000000000000697

Artoni, F., Fanciullacci, C., Bertolucci, F., Panarese, A., Makeig, S., Micera, S., et al. (2017). Unidirectional brain to muscle connectivity reveals motor cortex control of leg muscles during stereotyped walking. *Neuroimage* 159, 403–416. doi: 10.1016/j.neuroimage.2017.07.013

Bassiri, Z., Austin, C., Cousin, C., and Martelli, D. (2022). Subsensory electrical noise stimulation applied to the lower trunk improves postural control during visual perturbations. *Gait Posture* 96, 22–28. doi: 10.1016/j.gaitpost.2022.05.010

Berger, A., Horst, F., Steinberg, F., Thomas, F., Müller-Eising, C., Schöllhorn, W. I., et al. (2019). Increased gait variability during robot-assisted walking is accompanied by increased sensorimotor brain activity in healthy people. *J. Neuroeng. Rehabil.* 16, 1–13. doi: 10.1186/s12984-019-0636-3

Beurskens, R., and Bock, O. (2012). Age-related deficits of dual-task walking: a review. *Neural Plast*. 2012, 608. doi: 10.1155/2012/131608

Billaut, F., Kerris, J. P., Rodriguez, R. F., Martin, D. T., Gore, C. J., and Bishop, D. J. (2013). Interaction of central and peripheral factors during repeated sprints at different levels of arterial $O_2$ saturation. *PLoS ONE* 8, e77297. doi: 10.1371/journal.pone.0077297

Blyth, F. M., Briggs, A. M., Schneider, C. H., Hoy, D. G., and March, L. M. (2019). The global burden of musculoskeletal pain–where to from here? *Am. J. Public Health* 109, 35–40. doi: 10.2105/AJPH.2018.304747

Bonnal, J., Monnet, F., Le, B.-T., Pila, O., Grosmaire, A.-G., Ozsancak, C., et al. (2022). Relation between cortical activation and effort during robot-mediated walking in healthy people: a functional near-infrared spectroscopy neuroimaging study (fnirs). *Sensors* 22, 5542. doi: 10.3390/s22155542

Bradford, J. C., Lukos, J. R., and Ferris, D. P. (2016). Electrocortical activity distinguishes between uphill and level walking in humans. *J. Neurophysiol.* 115, 958–966. doi: 10.1152/jn.00089.2015

Brantley, J. A., Luu, T. P., Ozdemir, R., Zhu, F., Winslow, A. T., Huang, H., et al. (2016). "Noninvasive eeg correlates of overground and stair walking," in *2016 38th Annual International Conference of the IEEE Engineering in Medicine and Biology Society (EMBC)* (Orlando, FL: IEEE), 5729–5732.

Bruijn, S. M., Van Dieën, J. H., and Daffertshofer, A. (2015). Beta activity in the premotor cortex is increased during stabilized as compared to normal walking. *Front. Hum. Neurosci*. 9, 593. doi: 10.3389/fnhum.2015.00593

Buckley, C., Alcock, L., McArdle, R., Rehman, R. Z. U., Del Din, S., Mazzà, C., et al. (2019). The role of movement analysis in diagnosing and monitoring neurodegenerative conditions: Insights from gait and postural control. *Brain Sci*. 9, 34. doi: 10.3390/brainsci9020034

Budde, H., Wegner, M., Soya, H., Voelcker-Rehage, C., and McMorris, T. (2016). Neuroscience of exercise: neuroplasticity and its behavioral consequences. *Neural Plast*. 2016, 3643879. doi: 10.1155/2016/3643879

Bulea, T. C., Kim, J., Damiano, D. L., Stanley, C. J., and Park, H.-S. (2015). Prefrontal, posterior parietal and sensorimotor network activity underlying speed control during walking. *Front. Hum. Neurosci*. 9, 247. doi: 10.3389/fnhum.2015.00247

Calyx (2023). ©*Calyx*. Available online at: https://www.calyx.ai/ (accessed February 14, 2023).

Castermans, T., Duvinage, M., Cheron, G., and Dutoit, T. (2014). About the cortical origin of the low-delta and high-gamma rhythms observed in eeg signals during treadmill walking. *Neurosci. Lett*. 561, 166–170. doi: 10.1016/j.neulet.2013.12.059

Castermans, T., Duvinage, M., Petieau, M., Hoellinger, T., De Saedeleer, C., Seetharaman, K., et al. (2011). Optimizing the performances of a p300-based brain-computer interface in ambulatory conditions. *IEEE J. Emerg. Select. Top. Circ. Syst*. 1, 566–577. doi: 10.1109/JETCAS.2011.2179421

Centers for Medicare & Medicaid Services. (2023). *CMS.gov*. Available online at: https://www.cms.gov/ (accessed February 14, 2023).

Chenausky, K. V., and Tager-Flusberg, H. (2022). The importance of deep speech phenotyping for neurodevelopmental and genetic disorders: a conceptual review. *J. Neurodev. Disord*. 14, 1–14. doi: 10.1186/s11689-022-09443-z

Clark, D. J., Manini, T. M., Ferris, D. P., Hass, C. J., Brumback, B. A., Cruz-Almeida, Y., et al. (2020). Multimodal imaging of brain activity to investigate walking and mobility decline in older adults (mind in motion study): hypothesis, theory, and methods. *Front. Aging Neurosci*. 11, 358. doi: 10.3389/fnagi.2019.00358

Cortney Bradford, J., Lukos, J. R., Passaro, A., Ries, A., and Ferris, D. P. (2019). Effect of locomotor demands on cognitive processing. *Sci. Rep*. 9, 1–12. doi: 10.1038/s41598-019-45396-5

Dai, Y., Wang, J., and Gao, S. (2022). Advanced electronics and artificial intelligence: must-have technologies toward human body digital twins. *Adv. Intell. Syst*. 2022, 2100263. doi: 10.1007/978-3-031-14054-9

De Bartolo, D., Morone, G., Giordani, G., Antonucci, G., Russo, V., Fusco, A., et al. (2020). Effect of different music genres on gait patterns in parkinson's disease. *Neurol. Sci*. 41, 575–582. doi: 10.1007/s10072-019-04127-4

De Sanctis, P., Butler, J. S., Malcolm, B. R., and Foxe, J. J. (2014). Recalibration of inhibitory control systems during walking-related dual-task interference: a mobile brain-body imaging (mobi) study. *Neuroimage* 94, 55–64. doi: 10.1016/j.neuroimage.2014.03.016

De Sanctis, P., Wagner, J., Molholm, S., Foxe, J. J., Blumen, H. M., and Horsthuis, D. J. (2023). Neural signature of mobility-related everyday function in older adults at-risk of cognitive impairment. *Neurobiol. Aging* 122, 1–11. doi: 10.1016/j.neurobiolaging.2022.11.005

de Tommaso, M., Vecchio, E., Ricci, K., Montemurno, A., De Venuto, D., and Annese, V. F. (2015). "Combined EEG/EMG evaluation during a novel dual task paradigm for gait analysis," in *2015 6th International Workshop on Advances in Sensors and Interfaces (IWASI)* (Gallipoli: IEEE), 181–186.

Divya, R., and Peter, J. D. (2022). Smart healthcare system-a brain-like computing approach for analyzing the performance of detectron2 and posenet models for anomalous action detection in aged people with movement impairments. *Complex Intell. Syst*. 8, 3021–3040. doi: 10.1007/s40747-021-00319-8

do Nascimento, O. F., Nielsen, K. D., and Voigt, M. (2005). Influence of directional orientations during gait initiation and stepping on movement-related cortical potentials. *Behav. Brain Res*. 161, 141–154. doi: 10.1016/j.bbr.2005.02.031

Doubeni, C. A., Simon, M., and Krist, A. H. (2021). Addressing systemic racism through clinical preventive service recommendations from the us preventive services task force. *JAMA* 325, 627–628. doi: 10.1001/jama.2020.26188

Dror, I. E. (2020). Cognitive and human factors in expert decision making: six fallacies and the eight sources of bias. *Anal. Chem*. 92, 7998–8004. doi: 10.1021/acs.analchem.0c00704

Eggenberger, P., Wolf, M., Schumann, M., and De Bruin, E. D. (2016). Exergame and balance training modulate prefrontal brain activity during walking and enhance executive function in older adults. *Front. Aging Neurosci*. 8, 66. doi: 10.3389/fnagi.2016.00066

Enders, H., Cortese, F., Maurer, C., Baltich, J., Protzner, A. B., and Nigg, B. M. (2016). Changes in cortical activity measured with eeg during a high-intensity cycling exercise. *J. Neurophysiol*. 115, 379–388. doi: 10.1152/jn.00497.2015

Figueiredo, J., Santos, C. P., and Moreno, J. C. (2018). Automatic recognition of gait patterns in human motor disorders using machine learning: a review. *Med. Eng. Phys*. 53, 1–12. doi: 10.1016/j.medengphy.2017.12.006

Fontes, E. B., Bortolotti, H., da Costa, K. G., de Campos, B. M., Castanho, G. K., Hohl, R., et al. (2020). Modulation of cortical and subcortical brain areas at low and high exercise intensities. *Br. J. Sports Med*. 54, 110–115. doi: 10.1136/bjsports-2018-100295

Fraser, S. A., Dupuy, O., Pouliot, P., Lesage, F., and Bherer, L. (2016). Comparable cerebral oxygenation patterns in younger and older adults during dual-task walking with increasing load. *Front. Aging Neurosci*. 8, 240. doi: 10.3389/fnagi.2016.00240

Fumoto, M., Oshima, T., Kamiya, K., Kikuchi, H., Seki, Y., Nakatani, Y., et al. (2010). Ventral prefrontal cortex and serotonergic system activation during pedaling exercise induces negative mood improvement and increased alpha band in eeg. *Behav. Brain Res*. 213, 1–9. doi: 10.1016/j.bbr.2010.04.017

GE HealthCare. (2023). ©*General Electric HealthCare*. Available online at: https://www.gehealthcare.com/ (accessed February 14, 2023).

Gershon, R. C., Cella, D., Fox, N. A., Havlik, R. J., Hendrie, H. C., and Wagster, M. V. (2010). Assessment of neurological and behavioural function: the nih toolbox. *Lancet Neurol*. 9, 138–139. doi: 10.1016/S1474-4422(09)70335-7

Ghai, S., Ghai, I., Schmitz, G., and Effenberg, A. O. (2018). Effect of rhythmic auditory cueing on parkinsonian gait: a systematic review and meta-analysis. *Sci. Rep*. 8, 1–19. doi: 10.1038/s41598-017-16232-5

Giles, G. E., Cantelon, J. A., Eddy, M. D., Brunyé, T. T., Urry, H. L., Taylor, H. A., et al. (2018). Cognitive reappraisal reduces perceived exertion during endurance exercise. *Motiv. Emot*. 42, 482–496. doi: 10.1007/s11031-018-9697-z

Gramann, K., Gwin, J. T., Bigdely-Shamlo, N., Ferris, D. P., and Makeig, S. (2010). Visual evoked responses during standing and walking. *Front. Hum. Neurosci*. 4, 202. doi: 10.3389/fnhum.2010.00202

Guayacán, L. C., and Martínez, F. (2021). Visualising and quantifying relevant parkinsonian gait patterns using 3d convolutional network. *J. Biomed. Inform*. 123, 103935. doi: 10.1016/j.jbi.2021.103935

Gwin, J. T., Gramann, K., Makeig, S., and Ferris, D. P. (2010). Removal of movement artifact from high-density EEG recorded during walking and running. *J. Neurophysiol*. 103, 3526–3534. doi: 10.1152/jn.00105.2010

Gwin, J. T., Gramann, K., Makeig, S., and Ferris, D. P. (2011). Electrocortical activity is coupled to gait cycle phase during treadmill walking. *Neuroimage* 54, 1289–1296. doi: 10.1016/j.neuroimage.2010.08.066

Hallett, M., DelRosso, L. M., Elble, R., Ferri, R., Horak, F. B., Lehericy, S., et al. (2021). Evaluation of movement and brain activity. *Clin. Neurophysiol*. 132, 2608–2638. doi: 10.1016/j.clinph.2021.04.023

Harada, T., Miyai, I., Suzuki, M., and Kubota, K. (2009). Gait capacity affects cortical activation patterns related to speed control in the elderly. *Exp. Brain Res*. 193, 445–454. doi: 10.1007/s00221-008-1643-y

Hasan, S. S., Siddiquee, M. R., and Bai, O. (2019). "Supervised classification of eeg signals with score threshold regulation for pseudo-online asynchronous detection of gait intention," in *2019 18th IEEE International Conference on Machine Learning and Applications (ICMLA)* (Boca Raton, F: IEEE), 1476–1479.

Hatami, T., Hamghalam, M., Reyhani-Galangashi, O., and Mirzakuchaki, S. (2019). "A machine learning approach to brain tumors segmentation using adaptive random forest algorithm," in *2019 5th Conference on Knowledge Based Engineering and Innovation (KBEI)* (Tehran: IEEE), 076–082.

Hausmann, S. B., Vargas, A. M., Mathis, A., and Mathis, M. W. (2021). Measuring and modeling the motor system with machine learning. *Curr. Opin. Neurobiol*. 70, 11–23. doi: 10.1016/j.conb.2021.04.004

Holtzer, R., Mahoney, J. R., Izzetoglu, M., Izzetoglu, K., Onaral, B., and Verghese, J. (2011). fnirs study of walking and walking while talking in young and old individuals. *J. Gerontol. A Biomed. Sci. Med. Sci*. 66, 879–887. doi: 10.1093/gerona/glr068

Hornby, T. G., Moore, J. L., Lovell, L., and Roth, E. J. (2016). Influence of skill and exercise training parameters on locomotor recovery during stroke rehabilitation. *Curr. Opin. Neurol.* 29, 677. doi: 10.1097/WCO.0000000000000397

Hülser, M., Spielmann, H., Oertel, J., and Sippl, C. (2022). Motor skills, cognitive impairment, and quality of life in normal pressure hydrocephalus: early effects of shunt placement. *Acta Neurochir.* 164, 1765–1775. doi: 10.1007/s00701-022-05149-2

Ikeda, T., Matsushita, A., Saotome, K., Hasegawa, Y., Matsumura, A., and Sankai, Y. (2016). Muscle activity during gait-like motion provided by MRI compatible lower-extremity motion simulator. *Adv. Robot.* 30, 459–475. doi: 10.1080/01691864.2015.1122552

Iseki, K., Hanakawa, T., Shinozaki, J., Nankaku, M., and Fukuyama, H. (2008). Neural mechanisms involved in mental imagery and observation of gait. *Neuroimage* 41, 1021–1031. doi: 10.1016/j.neuroimage.2008.03.010

Jahn, K., Deutschländer, A., Stephan, T., Strupp, M., Wiesmann, M., and Brandt, T. (2004). Brain activation patterns during imagined stance and locomotion in functional magnetic resonance imaging. *Neuroimage* 22, 1722–1731. doi: 10.1016/j.neuroimage.2004.05.017

Jain, S., Gourab, K., Schindler-Ivens, S., and Schmit, B. D. (2013). EEG during pedaling: evidence for cortical control of locomotor tasks. *Clin. Neurophysiol.* 124, 379–390. doi: 10.1016/j.clinph.2012.08.021

Kameli, N., Dragojlovic-Kerkache, A., Savelkoul, P., and Stassen, F. R. (2021). Plant-derived extracellular vesicles: current findings, challenges, and future applications. *Membranes* 11, 411. doi: 10.3390/membranes11060411

Kashuba, V., Stepanenko, O., Byshevets, N., Kharchuk, O., Savliuk, S., Bukhovets, B., et al. (2020). The formation of human movement and sports skills in processing sports-pedagogical and biomedical data in masters of sports. *Int. J. Human Movement Sport Sci.* 8, 249–257. doi: 10.13189/saj.2020.080513

Keramidas, M. E., Kounalakis, S. N., Eiken, O., and Mekjavic, I. B. (2011). Muscle and cerebral oxygenation during exercise performance after short-term respiratory work. *Respiratory Physiol. Neurobiol.* 175, 247–254. doi: 10.1016/j.resp.2010.11.009

Kerkman, J. N., Daffertshofer, A., Gollo, L. L., Breakspear, M., and Boonstra, T. W. (2018). Network structure of the human musculoskeletal system shapes neural interactions on multiple time scales. *Sci. Adv.* 4, eaat0497. doi: 10.1126/sciadv.aat0497

Khaksar, S., Pan, H., Borazjani, B., Murray, I., Agrawal, H., Liu, W., et al. (2021). Application of inertial measurement units and machine learning classification in cerebral palsy: randomized controlled trial. *JMIR Rehabil. Assist. Technol.* 8, e29769. doi: 10.2196/29769

Khan, R. A., Naseer, N., Qureshi, N. K., Noori, F. M., Nazeer, H., and Khan, M. U. (2018). fnirs-based neurorobotic interface for gait rehabilitation. *J. Neuroeng. Rehabil.* 15, 1–17. doi: 10.1186/s12984-018-0346-2

Klibaite, U., Kislin, M., Verpeut, J. L., Bergeler, S., Sun, X., Shaevitz, J. W., et al. (2022). Deep phenotyping reveals movement phenotypes in mouse neurodevelopmental models. *Mol. Autism* 13, 1–18. doi: 10.1186/s13229-022-00492-8

Kline, A., Pittman, D., Ronsky, J., and Goodyear, B. (2020). Differentiating the brain's involvement in executed and imagined stepping using fmri. *Behav. Brain Res.* 394, 112829. doi: 10.1016/j.bbr.2020.112829

Kumar, N., and Michmizos, K. P. (2022). A neurophysiologically interpretable deep neural network predicts complex movement components from brain activity. *Sci. Rep.* 12, 1–12. doi: 10.1038/s41598-022-05079-0

Kurz, M. J., Wilson, T. W., and Arpin, D. J. (2012). Stride-time variability and sensorimotor cortical activation during walking. *Neuroimage* 59, 1602–1607. doi: 10.1016/j.neuroimage.2011.08.084

Labriffe, M., Annweiler, C., Amirova, L. E., Gauquelin-Koch, G., Ter Minassian, A., Leiber, L.-M., et al. (2017). Brain activity during mental imagery of gait versus gait-like plantar stimulation: a novel combined functional mri paradigm to better understand cerebral gait control. *Front. Hum. Neurosci.* 11, 106. doi: 10.3389/fnhum.2017.00106

Lacerenza, M., Spinelli, L., Buttafava, M., Dalla Mora, A., Zappa, F., Pifferi, A., et al. (2021). Monitoring the motor cortex hemodynamic response function in freely moving walking subjects: a time-domain fnirs pilot study. *Neurophotonics* 8, 015006. doi: 10.1117/1.NPh.8.1.015006

Ladouce, S., Donaldson, D. I., Dudchenko, P. A., and Ietswaart, M. (2019). Mobile eeg identifies the re-allocation of attention during real-world activity. *Sci. Rep.* 9, 1–10. doi: 10.1038/s41598-019-51996-y

Lau, T. M., Gwin, J. T., and Ferris, D. P. (2014). Walking reduces sensorimotor network connectivity compared to standing. *J. Neuroeng. Rehabil.* 11, 1–10. doi: 10.1186/1743-0003-11-14

Lau, T. M., Gwin, J. T., McDowell, K. G., and Ferris, D. P. (2012). Weighted phase lag index stability as an artifact resistant measure to detect cognitive eeg activity during locomotion. *J. Neuroeng. Rehabil.* 9, 1–9. doi: 10.1186/1743-0003-9-47

Lee, T.-W., Girolami, M., and Sejnowski, T. J. (1999). Independent component analysis using an extended infomax algorithm for mixed subgaussian and supergaussian sources. *Neural Comput.* 11, 417–441. doi: 10.1162/089976699300016719

Lewis, R., Gómez Álvarez, C. B., Rayman, M., Lanham-New, S., Woolf, A., and Mobasheri, A. (2019). Strategies for optimising musculoskeletal health in the 21st century. *BMC Musculoskeletal Disord.* 20, 1–15. doi: 10.1186/s12891-019-2510-7

Li, C., Su, M., Xu, J., Jin, H., and Sun, L. (2020). A between-subject fnirs-bci study on detecting self-regulated intention during walking. *IEEE Trans. Neural Syst. Rehabil. Eng.* 28, 531–540. doi: 10.1109/TNSRE.2020.2965628

Li, J., Chen, G., Thangavel, P., Yu, H., Thakor, N., Bezerianos, A., et al. (2016). "A robotic knee exoskeleton for walking assistance and connectivity topology exploration in eeg signal," in *2016 6th IEEE International Conference on Biomedical Robotics and Biomechatronics (BioRob)* (Singapore: IEEE), 1068–1073.

Li, J., Dimitrakopoulos, G. N., Thangavel, P., Chen, G., Sun, Y., Guo, Z., et al. (2019). What are spectral and spatial distributions of eeg-emg correlations in overground walking? an exploratory study. *IEEE Access* 7, 143935–143946. doi: 10.1109/ACCESS.2019.2945602

Li, R., Wang, X., Lawler, K., Garg, S., Bai, Q., and Alty, J. (2022a). Applications of artificial intelligence to aid detection of dementia: a scoping review on current capabilities and future directions. *J. Biomed. Inform.* 2022, 104030. doi: 10.1016/j.jbi.2022.104030

Li, R., Yang, D., Fang, F., Hong, K.-S., Reiss, A. L., and Zhang, Y. (2022b). Concurrent FNIRS and EEG for brain function investigation: a systematic, methodology-focused review. *Sensors* 22, 5865. doi: 10.3390/s22155865

Lin, Y.-P., Wang, Y., and Jung, T.-P. (2014). Assessing the feasibility of online ssvep decoding in human walking using a consumer eeg headset. *J. Neuroeng. Rehabil.* 11, 1–8. doi: 10.1186/1743-0003-11-119

Lu, C.-F., Liu, Y.-C., Yang, Y.-R., Wu, Y.-T., and Wang, R.-Y. (2015). Maintaining gait performance by cortical activation during dual-task interference: a functional near-infrared spectroscopy study. *PLoS ONE* 10, e0129390. doi: 10.1145/2818302

Ludyga, S., Gronwald, T., and Hottenrott, K. (2016). Effects of high vs. low cadence training on cyclists' brain cortical activity during exercise. *J. Sci. Med. Sport* 19, 342–347. doi: 10.1016/j.jsams.2015.04.003

Luu, T. P., Brantley, J. A., Zhu, F., and Contreras-Vidal, J. L. (2017a). "Cortical features of locomotion-mode transitions via non-invasive EEG," in *2017 IEEE International Conference on Systems, Man, and Cybernetics (SMC)* (Banff, AB: IEEE), 2437–2441.

Luu, T. P., Nakagome, S., He, Y., and Contreras-Vidal, J. L. (2017b). Real-time eeg-based brain-computer interface to a virtual avatar enhances cortical involvement in human treadmill walking. *Sci. Rep.* 7, 1–12. doi: 10.1038/s41598-017-09187-0

Magrinelli, F., Balint, B., and Bhatia, K. P. (2021). Challenges in clinicogenetic correlations: one gene-many phenotypes. *Mov. Disord. Clin. Pract.* 8, 299–310. doi: 10.1002/mdc3.13165

Mahlknecht, P., Kiechl, S., Bloem, B. R., Willeit, J., Scherfler, C., Gasperi, A., et al. (2013). Prevalence and burden of gait disorders in elderly men and women aged 60-97 years: a population-based study. *PLoS ONE* 8, e69627. doi: 10.1371/journal.pone.0069627

Makeig, S., Gramann, K., Jung, T.-P., Sejnowski, T. J., and Poizner, H. (2009). Linking brain, mind and behavior. *Int. J. Psychophysiol.* 73, 95–100. doi: 10.1016/j.ijpsycho.2008.11.008

Makizako, H., Shimada, H., Park, H., Tsutsumimoto, K., Uemura, K., Suzuki, T., et al. (2013). Brain activation during dual-task walking and executive function among older adults with mild cognitive impairment: a fnirs study. *Aging Clin. Exp. Res.* 25, 539–544. doi: 10.1007/s40520-013-0119-5

Malcolm, B. R., Foxe, J. J., Butler, J. S., and De Sanctis, P. (2015). The aging brain shows less flexible reallocation of cognitive resources during dual-task walking: a mobile brain/body imaging (mobi) study. *Neuroimage* 117, 230–242. doi: 10.1016/j.neuroimage.2015.05.028

Malouin, F., Richards, C. L., Jackson, P. L., Dumas, F., and Doyon, J. (2003). Brain activations during motor imagery of locomotor-related tasks: a pet study. *Hum. Brain Mapp.* 19, 47–62. doi: 10.1002/hbm.10103

Martini, M. L., Oermann, E. K., Opie, N. L., Panov, F., Oxley, T., and Yaeger, K. (2020). Sensor modalities for brain-computer interface technology: a comprehensive literature review. *Neurosurgery* 86, E108-E117. doi: 10.1093/neuros/nyz286

Mazurek, K. A., Patelaki, E., Foxe, J. J., and Freedman, E. G. (2021). Using the mobi motion capture system to rapidly and accurately localize EEG electrodes in anatomic space. *Eur. J. Neurosci.* 54, 8396–8405. doi: 10.1111/ejn.15019

Meester, D., Al-Yahya, E., Dawes, H., Martin-Fagg, P., and Piñon, C. (2014). Associations between prefrontal cortex activation and h-reflex modulation during dual task gait. *Front. Hum. Neurosci.* 8, 78. doi: 10.3389/fnhum.2014.00078

Mehra, D., Tiwari, A., and Joshi, D. (2021). Investigating neural correlates of locomotion transition via temporal relation of eeg and eog-recorded eye movements. *Comput. Biol. Med.* 132, 104350. doi: 10.1016/j.compbiomed.2021.104350

Minetto, M. A., Giannini, A., McConnell, R., Busso, C., Torre, G., and Massazza, G. (2020). Common musculoskeletal disorders in the elderly: the star triad. *J. Clin. Med.* 9, 1216. doi: 10.3390/jcm9041216

Mirelman, A., Maidan, I., Bernad-Elazari, H., Nieuwhof, F., Reelick, M., Giladi, N., et al. (2014). Increased frontal brain activation during walking while dual tasking: an fnirs study in healthy young adults. *J. Neuroeng. Rehabil.* 11, 1–7. doi: 10.1186/1743-0003-11-85

Mirelman, A., Maidan, I., Bernad-Elazari, H., Shustack, S., Giladi, N., and Hausdorff, J. M. (2017). Effects of aging on prefrontal brain activation during challenging walking conditions. *Brain Cogn.* 115, 41–46. doi: 10.1016/j.bandc.2017.04.002

Miyai, I., Tanabe, H. C., Sase, I., Eda, H., Oda, I., Konishi, I., et al. (2001). Cortical mapping of gait in humans: a near-infrared spectroscopic topography study. *Neuroimage* 14, 1186–1192. doi: 10.1006/nimg.2001.0905

Muñoz-Lasa, S., de Silanes, C. L., Atín-Arratibel, M., Á., Bravo-Llatas, C., Pastor-Jimeno, S., et al. (2019). Effects of hippotherapy in multiple sclerosis: pilot study on quality of life, spasticity, gait, pelvic floor, depression and fatigue. *Med. Clin.* (*English Edition)* 152, 55–58. doi: 10.1016/j.medcle.2018.11.012

Nakagome, S., Luu, T. P., Brantley, J. A., and Contreras-Vidal, J. L. (2017). "Prediction of emg envelopes of multiple terrains over-ground walking from eeg signals using an unscented kalman filter," in *2017 IEEE International Conference on Systems, Man, and Cybernetics (SMC)* (Banff, AB: IEEE), 3175–3178.

NIRx. (2023). ©*NIRx Medical Technologies.* Available online at: https://nirx.net/ (accessed February 14, 2023).

NordicNeuroLab. (2023). ©*NordicNeuroLab*. Available online at: https://www.nordicneurolab.com/ (accessed February 14, 2023).

Nojiri, K., and Iwane, F. (2014). "Motion direction estimation of walking base on eeg signal," in *2014 IEEE/ASME International Conference on Advanced Intelligent Mechatronics* (Besacon: IEEE), 542–547.

Norbye, A. D., Midgard, R., and Thrane, G. (2020). Spasticity, gait, and balance in patients with multiple sclerosis: a cross-sectional study. *Physiother. Res. Int*. 25, e1799. doi: 10.1002/pri.1799

Nordin, A. D., Hairston, W. D., and Ferris, D. P. (2018). Dual-electrode motion artifact cancellation for mobile electroencephalography. *J. Neural Eng.* 15, 056024. doi: 10.1088/1741-2552/aad7d7

Nordin, A. D., Hairston, W. D., and Ferris, D. P. (2019a). Faster gait speeds reduce alpha and beta eeg spectral power from human sensorimotor cortex. *IEEE Trans. Biomed. Eng*. 67, 842–853. doi: 10.1109/TBME.2019.2921766

Nordin, A. D., Hairston, W. D., and Ferris, D. P. (2019b). Human electrocortical dynamics while stepping over obstacles. *Sci. Rep*. 9, 1–12. doi: 10.1038/s41598-019-41131-2

Oliveira, A. S., Schlink, B. R., Hairston, W. D., König, P., and Ferris, D. P. (2016). Induction and separation of motion artifacts in EEG data using a mobile phantom head device. *J. Neural Eng.* 13, 036014. doi: 10.1088/1741-2560/13/3/036014

Palmer, J. A., Kreutz-Delgado, K., and Makeig, S. (2006). "Super-gaussian mixture source model for ICA," in *International Conference on Independent Component Analysis and Signal Separation. ICA 2006,* eds J. Rosca, D. Erdogmus, J. C. Príncipe, and S. Haykin (Berlin; Heidelberg: Springer). doi: 10.1007/11679363_106

Parmentier, T., Monteith, G., Cortez, M. A., Wielaender, F., Fischer, A., Jokinen, T. S., et al. (2020). Effect of prior general anesthesia or sedation and antiseizure drugs on the diagnostic utility of wireless video electroencephalography in dogs. *J. Vet. Internal Med*. 34, 1967–1974. doi: 10.1111/jvim.15856

Patil, P., Kumar, K. S., Gaud, N., and Semwal, V. B. (2019). "Clinical human gait classification: extreme learning machine approach," in *2019 1st International Conference on Advances in Science, Engineering and Robotics Technology (ICASERT)* (Dhaka: IEEE), 1–6.

Pearson-Stuttard, J., Ezzati, M., and Gregg, E. W. (2019). Multimorbidity–a defining challenge for health systems. *Lancet Public Health* 4, e599-e600. doi: 10.1016/S2468-2667(19)30222-1

Peters, S., Lim, S. B., Louie, D. R., Yang, C.-L., and Eng, J. J. (2020). Passive, yet not inactive: robotic exoskeleton walking increases cortical activation dependent on task. *J. Neuroeng. Rehabil.* 17, 1–12. doi: 10.1186/s12984-020-00739-6

Petersen, T. H., Willerslev-Olsen, M., Conway, B. A., and Nielsen, J. B. (2012). The motor cortex drives the muscles during walking in human subjects. *J. Physiol.* 590, 2443–2452. doi: 10.1113/jphysiol.2012.227397

Pires, F. O., Dos Anjos, C. A., Covolan, R. J., Pinheiro, F. A., St Clair Gibson, A., Noakes, T. D., et al. (2016). Cerebral regulation in different maximal aerobic exercise modes. *Front. Physiol.* 7, 253. doi: 10.3389/fphys.2016.00253

Pizzamiglio, S., Naeem, U., Abdalla, H., and Turner, D. L. (2017). Neural correlates of single-and dual-task walking in the real world. *Front. Hum. Neurosci.* 11, 460. doi: 10.3389/fnhum.2017.00460

Pons, J. L., Moreno, J. C., Torricelli, D., and Taylor, J. (2013). "Principles of human locomotion: a review," in *2013 35th Annual International Conference of the IEEE Engineering in Medicine and Biology Society (EMBC)* (Dhaka: IEEE), 6941–6944.

Porrselvi, A. P. (2022). Tam battery: development and pilot testing of a tamil computer-assisted cognitive test battery for older adults. *Clin. Neuropsychol.* 15, 1–20. doi: 10.1080/13854046.2022.2156396

Presacco, A., Forrester, L. W., and Contreras-Vidal, J. L. (2012). Decoding intra-limb and inter-limb kinematics during treadmill walking from scalp electroencephalographic (EEG) signals. *IEEE Trans. Neural Syst. Rehabil. Eng.* 20, 212–219. doi: 10.1109/TNSRE.2012.2188304

Presacco, A., Goodman, R., Forrester, L., and Contreras-Vidal, J. L. (2011). Neural decoding of treadmill walking from noninvasive electroencephalographic signals. *J. Neurophysiol.* 106, 1875–1887. doi: 10.1152/jn.00104.2011

Quiroz, G., Espinoza-Valdez, A., Salido-Ruiz, R., and Mercado, L. (2017). Coherence analysis of eeg in locomotion using graphs. *Revista mexicana de ingeniería biomédica* 38, 235–246.

Racinais, S., Buchheit, M., and Girard, O. (2014). Breakpoints in ventilation, cerebral and muscle oxygenation, and muscle activity during an incremental cycling exercise. *Front. Physiol.* 5, 142. doi: 10.3389/fphys.2014.00142

Radel, R., Brisswalter, J., and Perrey, S. (2017). Saving mental effort to maintain physical effort: a shift of activity within the prefrontal cortex in anticipation of prolonged exercise. *Cognit. Affect. Behav. Neurosci.* 17, 305–314. doi: 10.3758/s13415-016-0480-x

Richer, N., Downey, R. J., Hairston, W. D., Ferris, D. P., and Nordin, A. D. (2020). Motion and muscle artifact removal validation using an electrical head phantom, robotic motion platform, and dual layer mobile eeg. *IEEE Trans. Neural Syst. Rehabil. Eng*. 28, 1825–1835. doi: 10.1109/TNSRE.2020.3000971

Runge, M., and Hunter, G. (2006). Determinants of musculoskeletal frailty and the risk of falls in old age. *J. Musculoskeletal Neuronal Interact*. 6, 167.

Sacco, K., Cauda, F., Cerliani, L., Mate, D., Duca, S., and Geminiani, G. C. (2006). Motor imagery of walking following training in locomotor attention. The effect of 'the tango lesson'. *Neuroimage* 32, 1441–1449. doi: 10.1016/j.neuroimage.2006.05.018

Sahyoun, C., Floyer-Lea, A., Johansen-Berg, H., and Matthews, P. M. (2004). Towards an understanding of gait control: brain activation during the anticipation, preparation and execution of foot movements. *Neuroimage* 21, 568–575. doi: 10.1016/j.neuroimage.2003.09.065

Salazar-Varas, R., Costa, Á., Iáñez, E., Úbeda, A., Hortal, E., and Azorín, J. (2015). Analyzing eeg signals to detect unexpected obstacles during walking. *J. Neuroeng. Rehabil.* 12, 1–15. doi: 10.1186/s12984-015-0095-4

Schneider, S., Rouffet, D., Billaut, F., and Strüder, H. (2013). Cortical current density oscillations in the motor cortex are correlated with muscular activity during pedaling exercise. *Neuroscience* 228, 309–314. doi: 10.1016/j.neuroscience.2012.10.037

Seeber, M., Scherer, R., Wagner, J., Solis-Escalante, T., and Müller-Putz, G. R. (2014). Eeg beta suppression and low gamma modulation are different elements of human upright walking. *Front. Hum. Neurosci.* 8, 485. doi: 10.3389/fnhum.2014.00485

Seeber, M., Scherer, R., Wagner, J., Solis-Escalante, T., and Müller-Putz, G. R. (2015). High and low gamma eeg oscillations in central sensorimotor areas are conversely modulated during the human gait cycle. *Neuroimage* 112, 318–326. doi: 10.1016/j.neuroimage.2015.03.045

Sejdić, E., Godfrey, A., McIlroy, W., and Montero-Odasso, M. (2019). "Engineering human gait and the potential role of wearable," in *Falls and Cognition in Older Persons*, eds M. Montero-Odasso, and R. Camicioli (Cham: Springer). doi: 10.1007/978-3-030-24233-6_22

Severens, M., Nienhuis, B., Desain, P., and Duysens, J. (2012). "Feasibility of measuring event related desynchronization with electroencephalography during walking," in *2012 Annual International Conference of the IEEE Engineering in Medicine and Biology Society* (San Diego, CA: IEEE), 2764–2767.

Severens, M., Perusquia-Hernandez, M., Nienhuis, B., Farquhar, J., and Duysens, J. (2014). Using actual and imagined walking related desynchronization features in a bci. *IEEE Trans. Neural Syst. Rehabil. Eng.* 23, 877–886. doi: 10.1109/TNSRE.2014.2371391

Shibuya, K., Tanaka, J., Kuboyama, N., Muraj, S., and Ogaki, T. (2004). supramaximal exhaustive exercise. *J. Sports Med. Phys. Fitness* 44, 2.

Sipp, A. R., Gwin, J. T., Makeig, S., and Ferris, D. P. (2013). Loss of balance during balance beam walking elicits a multifocal theta band electrocortical response. *J. Neurophysiol.* 110, 2050–2060. doi: 10.1152/jn.00744.2012

Sisters of Charity of Leavenworth Health Services Corporation. (2023). ©*SCL Health Medical Group*. Available online at: https://www.sclhealth.org/locations/medical-group/ (accessed February 14, 2023).

Skinner, J. W., Lee, H. K., and Hass, C. J. (2022). Evaluation of gait termination strategy in individuals with essential tremor and parkinson's disease. *Gait Posture* 92, 338–342. doi: 10.1016/j.gaitpost.2021.12.007

Smania, N., Bonetti, P., Gandolfi, M., Cosentino, A., Waldner, A., Hesse, S., et al. (2011). Improved gait after repetitive locomotor training in children with cerebral palsy. *Am. J. Phys. Med. Rehabil.* 90, 137–149. doi: 10.1097/PHM.0b013e318201741e

Smith, K. J., and Billaut, F. (2010). Influence of cerebral and muscle oxygenation on repeated-sprint ability. *Eur. J. Appl. Physiol.* 109, 989–999. doi: 10.1007/s00421-010-1444-4

Snyder, K. L., Kline, J. E., Huang, H. J., and Ferris, D. P. (2015). Independent component analysis of gait-related movement artifact recorded

using EEG electrodes during treadmill walking. *Front. Hum. Neurosci.* 9, 639. doi: 10.3389/fnhum.2015.00639

Song, S., Kidziński, Ł., Peng, X. B., Ong, C., Hicks, J., Levine, S., et al. (2021). Deep reinforcement learning for modeling human locomotion control in neuromechanical simulation. *J. Neuroeng. Rehabil.* 18, 1–17. doi: 10.1186/s12984-021-00919-y

Stolbkov, Y., Moshonkina, T., Orlov, I., Tomilovskaya, E., Kozlovskaya, I., and Gerasimenko, Y. P. (2019). The neurophysiological correlates of real and imaginary locomotion. *Hum. Physiol.* 45, 104–114. doi: 10.1134/S0362119719010146

Storzer, L., Butz, M., Hirschmann, J., Abbasi, O., Gratkowski, M., Saupe, D., et al. (2016). Bicycling and walking are associated with different cortical oscillatory dynamics. *Front. Hum. Neurosci.* 10, 61. doi: 10.3389/fnhum.2016.00061

Stratus. (2023). ©*Stratus.* Available online at: https://stratusneuro.com/clinical-trials/ (accessed February 14, 2023).

Subudhi, A. W., Dimmen, A. C., and Roach, R. C. (2007). Effects of acute hypoxia on cerebral and muscle oxygenation during incremental exercise. *J. Appl. Physiol.* 103, 177–183. doi: 10.1152/japplphysiol.01460.2006

Subudhi, A. W., Miramon, B. R., Granger, M. E., and Roach, R. C. (2009). Frontal and motor cortex oxygenation during maximal exercise in normoxia and hypoxia. *J. Appl. Physiol.* 106, 1153–1158. doi: 10.1152/japplphysiol.91475.2008

Suzuki, M., Miyai, I., Ono, T., and Kubota, K. (2008). Activities in the frontal cortex and gait performance are modulated by preparation. An fnirs study. *Neuroimage* 39, 600–607. doi: 10.1016/j.neuroimage.2007.08.044

Suzuki, M., Miyai, I., Ono, T., Oda, I., Konishi, I., Kochiyama, T., et al. (2004). Prefrontal and premotor cortices are involved in adapting walking and running speed on the treadmill: an optical imaging study. *Neuroimage* 23, 1020–1026. doi: 10.1016/j.neuroimage.2004.07.002

Symeonidou, E.-R., Nordin, A. D., Hairston, W. D., and Ferris, D. P. (2018). Effects of cable sway, electrode surface area, and electrode mass on electroencephalography signal quality during motion. *Sensors* 18, 1073. doi: 10.3390/s18041073

Takahiro, I., Akira, M., Kousaku, S., Yasuhisa, H., and Yoshiyuki, S. (2013). "Preliminary report of brain activities during active and passive gait-like motion," in *2013 6th International IEEE/EMBS Conference on Neural Engineering (NER)* (San Diego, CA: IEEE), 1566–1569

Talamonti, D., Vincent, T., Fraser, S., Nigam, A., Lesage, F., and Bherer, L. (2021). The benefits of physical activity in individuals with cardiovascular risk factors: a longitudinal investigation using fnirs and dual-task walking. *J. Clin. Med.* 10, 579. doi: 10.3390/jcm10040579

Talo, M., Yildirim, O., Baloglu, U. B., Aydin, G., and Acharya, U. R. (2019). Convolutional neural networks for multi-class brain disease detection using mri images. *Comput. Med. Imaging Graphics* 78, 101673. doi: 10.1016/j.compmedimag.2019.101673

Thomas, R., and Stephane, P. (2008). Prefrontal cortex oxygenation and neuromuscular responses to exhaustive exercise. *Eur. J. Appl. Physiol.* 102, 153–163. doi: 10.1007/s00421-007-0568-7

Tortora, S., Ghidoni, S., Chisari, C., Micera, S., and Artoni, F. (2020). Deep learning-based bci for gait decoding from eeg with lstm recurrent neural network. *J. Neural Eng.* 17, 046011. doi: 10.1088/1741-2552/ab9842

Úbeda, A., Planelles, D., Costa, A., Hortal, E., Iáñez, E., and Azorín, J. M. (2014). "Decoding knee angles from EEG signals for different walking speeds," in *2014 IEEE International Conference on Systems, Man, and Cybernetics (SMC)* (San Diego, CA: IEEE), 1475–1478.

Vásquez-Correa, J. C., Arias-Vergara, T., Orozco-Arroyave, J. R., Eskofier, B., Klucken, J., and Nöth, E. (2018). Multimodal assessment of parkinson's disease: a deep learning approach. *IEEE J. Biomed. Health Inform.* 23, 1618–1630. doi: 10.1109/JBHI.2018.2866873

Velu, P. D., and de Sa, V. R. (2013). Single-trial classification of gait and point movement preparation from human EEG. *Front. Neurosci.* 7, 84. doi: 10.3389/fnins.2013.00084

Vitorio, R., Stuart, S., Gobbi, L. T., Rochester, L., Alcock, L., and Pantall, A. (2018). Reduced gait variability and enhanced brain activity in older adults with auditory cues: a functional near-infrared spectroscopy study. *Neurorehabil. Neural Repair.* 32, 976–987. doi: 10.1177/1545968318805159

Vrana, S. R., and Vrana, D. T. (2017). Can a computer administer a wechsler intelligence test? *Profess. Psychol. Res. Pract.* 48, 191. doi: 10.1037/pro0000128

Wagner, J., Makeig, S., Gola, M., Neuper, C., and Müller-Putz, G. (2016). Distinct $\beta$ band oscillatory networks subserving motor and cognitive control during gait adaptation. *J. Neurosci.* 36, 2212–2226. doi: 10.1523/JNEUROSCI.3543-15.2016

Wagner, J., Martinez-Cancino, R., Delorme, A., Makeig, S., Solis-Escalante, T., Neuper, C., et al. (2019a). High-density eeg mobile brain/body imaging data recorded during a challenging auditory gait pacing task. *Scientific Data* 6, 1–9. doi: 10.1038/s41597-019-0223-2

Wagner, J., Martínez-Cancino, R., and Makeig, S. (2019b). Trial-by-trial source-resolved eeg responses to gait task challenges predict subsequent step adaptation. *Neuroimage* 199, 691–703. doi: 10.1016/j.neuroimage.2019.06.018

Wagner, J., Solis-Escalante, T., Grieshofer, P., Neuper, C., Müller-Putz, G., and Scherer, R. (2012). Level of participation in robotic-assisted treadmill walking modulates midline sensorimotor eeg rhythms in able-bodied subjects. *Neuroimage* 63, 1203–1211. doi: 10.1016/j.neuroimage.2012.08.019

Wagner, J., Solis-Escalante, T., Scherer, R., Neuper, C., and Müller-Putz, G. (2014). It's how you get there: walking down a virtual alley activates premotor and parietal areas. *Front. Hum. Neurosci.* 8, 93. doi: 10.3389/fnhum.2014.00093

Wang, J., Wai, Y., Weng, Y., Ng, K., Huang, Y.-Z., Ying, L., et al. (2009). Functional mri in the assessment of cortical activation during gait-related imaginary tasks. *J. Neural Transm.* 116, 1087–1092. doi: 10.1007/s00702-009-0269-y

Warmerdam, E., Hausdorff, J. M., Atrsaei, A., Zhou, Y., Mirelman, A., Aminian, K., et al. (2020). Long-term unsupervised mobility assessment in movement disorders. *Lancet Neurol.* 19, 462–470. doi: 10.1016/S1474-4422(19)30397-7

Weersink, J. B., Maurits, N. M., and de Jong, B. M. (2019). EEG time-frequency analysis provides arguments for arm swing support in human gait control. *Gait Posture* 70, 71–78. doi: 10.1016/j.gaitpost.2019.02.017

Wei, P., Zhang, J., Wang, B., and Hong, J. (2021). Surface electromyography and electroencephalogram-based gait phase recognition and correlations between cortical and locomotor muscle in the seven gait phases. *Front. Neurosci.* 15, 607905. doi: 10.3389/fnins.2021.607905

Wieser, M., Haefeli, J., Bütler, L., Jäncke, L., Riener, R., and Koeneke, S. (2010). Temporal and spatial patterns of cortical activation during assisted lower limb movement. *Exp. Brain Res.* 203, 181–191. doi: 10.1007/s00221-010-2223-5

Xiang, K., Liu, Y., and Sun, L. (2021). Motoric cognitive risk syndrome: symptoms, pathology, diagnosis, and recovery. *Front. Aging Neurosci.* 13, 728799. doi: 10.3389/fnagi.2021.728799

Xu, J., Li, C., Li, J., Zhang, H., Jin, H., Qu, W., et al. (2017a). "Classification of desired motion speed–a study based on cerebral hemoglobin information," in *2017 2nd International Conference on Advanced Robotics and Mechatronics (ICARM)* (Hefei and Tai'an: IEEE), 115–119.

Xu, J., Li, C., Zhang, H., Li, J., Jin, H., Qu, W., et al. (2017b). A pilot study based on cerebral hemoglobin information to classify the desired walking speed. *IEEE Robot. Autom. Lett.* 3, 532–536. doi: 10.1109/LRA.2017.2765002

Yokoyama, H., Kaneko, N., Ogawa, T., Kawashima, N., Watanabe, K., and Nakazawa, K. (2018). Cortical control of locomotor muscle activity through muscle synergies in humans: a neural decoding study. *bioRxiv*, 413567. doi: 10.1101/413567

Young, S. R., Maddocks, D. L., and Caemmerer, J. M. (2022). Computer-enhanced practice: The benefits of computer-assisted assessment in applied clinical practice. *Profess. Psychol. Res. Pract.* 2022, 449. doi: 10.1037/pro0000449

Zeto (2023). ©*Zeto.* Available online at: https://zeto-inc.com/ (accessed February 14, 2023).

Zhu, X., Korivand, S., Hamill, K., Jalili, N., and Gong, J. (2022). A comprehensive decoding of cognitive load. *Smart Health* 26, 100336. doi: 10.1016/j.smhl.2022.100336

frontiers | Frontiers in Neuroscience

TYPE Review
PUBLISHED 14 June 2023
DOI 10.3389/fnins.2023.1186418



OPEN ACCESS

EDITED BY
Amelie Haugg,
Psychiatric University Hospital Zurich, Switzerland

REVIEWED BY
Paul Theo Zebhauser,
Technical University of Munich, Germany
Luz Maria Alonso-Valerdi,
Monterrey Institute of Technology and Higher Education (ITESM), Mexico

*CORRESPONDENCE
Jing Wang
✉ Jing.Wang2@nyulangone.org

RECEIVED 14 March 2023
ACCEPTED 12 May 2023
PUBLISHED 14 June 2023

CITATION
Rockholt MM, Kenefati G, Doan LV, Chen ZS and Wang J (2023) In search of a composite biomarker for chronic pain by way of EEG and machine learning: where do we currently stand?
*Front. Neurosci.* 17:1186418.
doi: 10.3389/fnins.2023.1186418



# In search of a composite biomarker for chronic pain by way of EEG and machine learning: where do we currently stand?

Mika M. Rockholt[1], George Kenefati[1], Lisa V. Doan[1], Zhe Sage Chen[2,3,4] and Jing Wang[1,3,4]*

[1]Department of Anesthesiology, Perioperative Care and Pain Management, New York University Grossman School of Medicine, New York, NY, United States, [2]Department of Psychiatry, New York University Grossman School of Medicine, New York, NY, United States, [3]Department of Neuroscience & Physiology, Neuroscience Institute, New York University Grossman School of Medicine, New York, NY, United States, [4]Department of Biomedical Engineering, New York University Tandon School of Engineering, Brooklyn, NY, United States

Machine learning is becoming an increasingly common component of routine data analyses in clinical research. The past decade in pain research has witnessed great advances in human neuroimaging and machine learning. With each finding, the pain research community takes one step closer to uncovering fundamental mechanisms underlying chronic pain and at the same time proposing neurophysiological biomarkers. However, it remains challenging to fully understand chronic pain due to its multidimensional representations within the brain. By utilizing cost-effective and non-invasive imaging techniques such as electroencephalography (EEG) and analyzing the resulting data with advanced analytic methods, we have the opportunity to better understand and identify specific neural mechanisms associated with the processing and perception of chronic pain. This narrative literature review summarizes studies from the last decade describing the utility of EEG as a potential biomarker for chronic pain by synergizing clinical and computational perspectives.

KEYWORDS

**chronic pain, biomarkers, neurobiomarkers, EEG, machine learning, neurophysiology, biomarker, composite biomarker**

## 1. Introduction

Pain is a complex and multi-dimensional process resulting from dynamic interactions of neural processes. It includes sensory-discriminative, affective-emotional, and cognitive-evaluative components (Rainville et al., 1997; Price, 2000; Perl, 2007; Sun et al., 2021). All pain initiates as acute pain but can become maladaptive and persist into a chronic phase (Gan et al., 2014; Chapman and Vierck, 2017; Gan, 2017). Numerous studies have demonstrated clear evidence that chronic pain continues to be a global public health issue, with an estimated prevalence of around 30% in adults (Johannes et al., 2010; Gardner and Sachdeva, 2019; Yong et al., 2022; Zimmer et al., 2022). The condition is not only known to significantly reduce quality of life (Yong et al., 2022) but is also associated with long-term disability; this typically requires multimodal treatment approaches, commonly results in reliance on opioid analgesics, and contributes to the opioid epidemic (Kehlet et al., 2006; Ataoğlu et al., 2013; Ladha et al., 2016;

Gan, 2017; Schuchat et al., 2017; Hollmann et al., 2019). Hence, advances in pain research are urgently needed to address these healthcare issues.

By observing the brain activity that occurs during pain and trying to decode its underlying mechanism, it is believed that these pathways could be targeted earlier and more precisely, preventing pain from chronification, and thus reducing the consumption of addictive analgesics (Mouraux and Iannetti, 2018).

Over the last 20 years, advancing research has contributed to an increased understanding of the spinal, peripheral, and cortical mechanisms of pain (Apkarian et al., 2005; Rosa and Seymour, 2014; Tu et al., 2016; Ploner et al., 2017; Mouraux and Iannetti, 2018). In contrast to other sensory perceptions that are associated with a specific sensory cortex, a specific "pain cortex" associated with pain perception does not exist (Kucyi and Davis, 2015). Instead, it is the result of an activation of a distributed network of cortical and subcortical areas (Besson, 1999; Sawamoto et al., 2000; Mouraux and Iannetti, 2018; Liberati et al., 2020; Chen et al., 2022). Because of its complex nature, further research is required to better understand the mechanisms behind pain and to propose an adequate biomarker for chronic pain in particular (Tracey et al., 2019; Chen, 2021).

Studies using modern neuroimaging techniques such as functional magnetic resonance imaging (fMRI) and positron emission tomography have identified brain regions involved in sensory processing of acute pain. These brain regions include the primary somatosensory cortex (S1), anterior cingulate cortex (ACC), and insular cortex (Isnard et al., 2011; Duerden and Albanese, 2013; Vierck et al., 2013; Boccard et al., 2014; Mouraux and Iannetti, 2018; Van Der Miesen et al., 2019; Lamichhane et al., 2021; Sun et al., 2021). These techniques have limited temporal resolution, making it difficult to capture the dynamic nature of pain perception and experience (Wager et al., 2013). Therefore, some study groups have shifted focus to explore less invasive and more cost-effective alternatives with a higher temporal resolution, such as electroencephalography (EEG) (Pinheiro et al., 2016; Ploner et al., 2017; Levitt and Saab, 2019; Van Der Miesen et al., 2019; Xu and Huang, 2020; Millard et al., 2022; Chowdhury et al., 2023).

With an increasing number of human neuroimaging studies investigating the mechanism of pain, the field is steadily moving toward the development of a viable biomarker for pain (Furman et al., 2018; Seminowicz et al., 2018; Furman et al., 2019; Seminowicz et al., 2019; Furman et al., 2020). For instance, modern source localization techniques have substantially improved anatomical precision for EEG studies to enable circuit-level analysis, further facilitating the potential of biomarker development (Ferracuti et al., 1994; Le Pera et al., 2000; Chang et al., 2001; Seminowicz et al., 2019; Furman et al., 2020; Sun et al., 2021; Chowdhury et al., 2023). Recent reports have indicated that enhanced nociceptive response in EEG is manifested as abnormally elevated power in theta and gamma oscillations, suggesting that EEG could potentially predict the presence of pain and analgesic response (Babiloni et al., 2002; Wang et al., 2011; Schulz et al., 2012a, b; Rouleau et al., 2015; Peng and Tang, 2016; Taesler and Rose, 2016; Martel et al., 2017; Fallon et al., 2018; Tan et al., 2021). This provides further support for the feasibility of an EEG-based biomarker (Zhang et al., 2017; Dinh et al., 2019; May et al., 2019; Zis et al., 2022).

By applying machine learning (ML) to analyze functional brain imaging data such as EEG, we now have the capability to better identify response features to a given experiment—or stimulus, as well as to predict subjective perception and response to the same experiment (Hu and Iannetti, 2016; Lötsch et al., 2017; Fernandez Rojas et al., 2019). Hence, ML is a promising tool for the future development of biomarkers for chronic pain (Lamichhane et al., 2021; Harland et al., 2022). Recently, numerous studies have presented findings with considerable accuracy, working toward developing algorithms with improved generalizability and interpretability (Harland et al., 2022; Mari et al., 2022). The number of studies coupling ML algorithms with subjective reports on pain perception is increasing, and there is an impetus for data-sharing and collaboration within the pain research community to improve the sensitivity and efficacy of biomarker developmental methods (Van Der Miesen et al., 2019). While obstacles remain, it is clear that "decisions based on neural data will only be as good as the science behind them" (Hu and Iannetti, 2016). Hence, for the science to get better, it is imperative that we validate the results of past studies, identify the state-of-the-art methods, and provide updates on ongoing studies.

Today, the probability of presenting a non-composite, single biomarker capturing "pain" in its entirety is increasingly appearing unlikely (Tracey et al., 2019). It remains difficult to identify a standard way to qualify brain responses as specifically pain responses, especially without a dedicated pain cortex. However, by further exploring advanced analytical tools like neural networks, artificial intelligence, and machine-learning algorithms, it may be possible to combine multiple objective biomarkers into one composite pain biomarker (Tracey, 2021). Such approach could expedite success in understanding the mechanisms for pain as well as providing clinically relevant biomarkers (Baskin et al., 2016; Su et al., 2019; Eldabe et al., 2022).

To support the field in future research, we have conducted a narrative literature review by combining the following search terms: "electroencephalography" and "chronic pain" and "machine learning" using PubMed (including MEDLINE), Ovid (including EMBASE), Web of Science and the Cochrane Library. While several review articles have appeared in the literature (Reckziegel et al., 2019; Van Der Miesen et al., 2019; Mari et al., 2022; Zebhauser et al., 2023), our review focuses on studies published in the last decade (from 2012 to 2023), describing the practical utility of combining physiological data, EEG, and ML to study the mechanisms of chronic pain. Specifically, our review aims to appraise the role and potential utility of EEG as a biomarker for chronic pain. Hence, this review discusses a limited cohort and does not cover the entire breadth of publications in the pain research field. Nonetheless, we show how different computational methods and ML algorithms can help in the discovery of EEG biomarkers for chronic pain. We also discuss the future utility of today's cutting-edge methods and how we can incorporate further analyses and neurophysiological data into an integrated biomarker model. Lastly, we discuss challenges in the chronic pain research field and offer insight on potential future directions.

## 2. The benefits of EEG for biomarker studies on chronic pain

### 2.1. Measurement of pain-related brain activity

Behavior arising from the experience of pain is seldom obscure, often manifested physically in the form of facial expressions, changes in body language, or changes in mood (Dansie and Turk, 2013). Thus,

the presence of pain can be observed and measured – to a certain extent. Pain perception is a highly subjective experience (Kinnealey and Fuiek, 1999). Pain does not only vary between subjects but can vary in the same subject across time. For this reason, a number of pain assessments are available for the quantification of pain.

### 2.1.1. Bottom-up measurements based on pain-induced behavior

The current standard for self-reported pain intensity is assessed using the visual analog scale (VAS, typical range: 0–100 mm) (Boonstra et al., 2008) or the numeric rating scale (NRS, range: 0–10) (Haefeli and Elfering, 2006). Although these behavioral scales offer a degree of standardization across the population, individuals can still exhibit considerable and unpredictable variability in painful percepts in response to the same nociceptive stimulus (Quiton and Greenspan, 2008). Furthermore, self-reported pain intensity has been shown to at times correlate poorly with the stimulus intensity in experimental studies (Nickel et al., 2017). The mechanisms underlying such within-subject and between-subject variability in experimental pain remain insufficiently understood. The objective of top-down measurements of pain experience is to identify neural indicators that explain such perceptual variability in all types of pain (Hu and Iannetti, 2016).

### 2.1.2. Top-down measurements based on brain activity

A wide variety of neuroimaging techniques are used to record brain signals, at varying levels of invasiveness and across a range of spatial and temporal resolutions. For instance, microelectrode implants can record neural spikes from a single neuron or local field potentials from a small population of neurons, though at the cost of invasiveness and highly rapid time courses (Einevoll et al., 2013; Nurse et al., 2016; Merk et al., 2022). At the other end of the spectrum, whole brain imaging technologies such as fMRI can noninvasively image blood-oxygen dynamics as a proxy to region-specific activity, yet with relatively low temporal resolution and mid-range spatial resolution (Logothetis, 2008; Power et al., 2017; Woo et al., 2017; Siddiqi et al., 2022). In this review, we focus solely on EEG which measures extracellular current but at a larger spatial scale, reflecting the activity of hundreds of millions of neurons (Jackson and Bolger, 2014). EEG is noninvasive: the signal is recorded from an array of surface electrodes placed on a subject's scalp, at a microvolt (μV) scale (Rosa and Seymour, 2014). Despite anatomical impedances, such as the presence of hair and variations in skull conductivity, EEG electrodes are capable of detecting the electrical activity of similarly oriented groups of cerebral cortical neurons near the scalp. The majority of the electrical activity sensed by scalp electrodes represents the summation of the inhibitory or excitatory postsynaptic potentials from thousands of pyramidal cells near each electrode (Britton et al., 2016). This trait enables researchers and clinicians a view into the cortical activity of the brain with low cost and effort.

EEG can be recorded using one of two methods: resting-state EEG (rs-EEG) or stimulus-evoked EEG. rs-EEG is recorded while a participant is awake but not engaged in any specific task. Though rs-EEG studies do not typically include stimuli, they may be used to evaluate the functional activity of the brain before and after a treatment or intervention, as well as to study chronic behavioral or pathological conditions such as chronic pain. Stimulus-evoked EEG, in contrast, is recorded in response to a specific stimulus. Typically, participants are subject to a set of repeated stimuli to study the dynamics of one or more regions involved in responding to said stimulus. Thus, stimulus-evoked EEG provides temporally specific information in a dynamic behavioral context, and it also offers insights into how an underlying disease condition such as chronic pain can alter temporal sensory processing. Both techniques are equally important, even as they enable fundamentally different approaches to studying chronic pain which are discussed in the next section.

## 2.2. Advantages and disadvantages of EEG for chronic pain studies

Despite the advances in pain research using other neuroimaging techniques, such as fMRI and PET, numerous studies have described the advantages of leveraging the non-invasiveness of EEG as a potential path to a biomarker for pain (Ploner et al., 2017; Liberati et al., 2018; Mouraux and Iannetti, 2018; May et al., 2019; Sun et al., 2021; Tracey, 2021; Vuckovic et al., 2022).

First, because of its high temporal resolution, it allows us to assess the oscillatory activity of neural pain processing. High temporal resolution is critical for understanding pain since it is a highly dynamic process (Schulz et al., 2012a,b). At the same time, correlating oscillatory activities across different brain areas enables us to detect specific brain areas associated with chronic pain. As such, in chronic pain studies, scalp EEG recordings present spontaneous synchronized postsynaptic neuronal activity of the brain cortex (Huber et al., 2006; Stern et al., 2006; Jobert et al., 2012; Mouraux and Iannetti, 2018).

A second advantage of EEG in the study of pain is that it is portable, easy to perform, well tolerated by patients, and more cost-effective than other neuroimaging modalities (Katsigiannis and Ramzan, 2017; Krigolson et al., 2017; Mussigmann et al., 2022). The ease of placement and mobility of EEG systems allows for continuous recordings of primary cortical activities in clinical settings, enabling the potential to develop a variety of biomarkers for chronic pain from a single modality (Byrom et al., 2018; Xu and Huang, 2020).

Meanwhile, a number of potential obstacles in using EEG to assess chronic pain should also be considered (Tracey, 2021). First, there are some limitations seen in past studies, where most have analyzed potentials from rs-EEG (as presented in Table 1). These potentials provide a basis for further analyses, allowing us to explore the dynamic of neural circuits involved in pain processing. The use of rs-EEG alone in understanding pain, however, can become problematic, since rs-EEG potentials may be confounded by other brain processes. As suggested by Hansen et al. (2017) studying evoked EEG potentials allows for a better understanding of the mechanism underlying nociception, which is especially important when studying a complex condition such as chronic pain (Cao et al., 2020). Thus, when studying chronic pain, rs-EEG can provide us with insights into baseline differences, whereas evoked EEG potentials can contain information about acute changes in neural pain processing, which can be more informative (Plaghki and Mouraux, 2005). Regardless of the types for potentials studied, uncertainties around whether recorded EEG responses are directly related to pain still exist, prompting the need for further research (Mouraux and Iannetti, 2018).

Second, since evoked potentials of EEG signals are usually brief in duration, the ability to establish generalizable features can be difficult (Iannetti et al., 2008). Instead, studies have suggested longer sensory

TABLE 1 Summary of recent studies utilizing EEG as a potential biomarker for chronic pain (review articles are excluded from this summary).

| Author | Subjects | Chronic pain | EEG State[a] | Feature/Machine learning analysis | Findings (significance, $p$-value; accuracy, %) | Biomarker type |
|---|---|---|---|---|---|---|
| **2012** | | | | | | |
| Graversen et al. | $N_{pain} = 31$ | Pancreatitis | rs-EEG | PSD, SVM | Pregabalin: decreased pain / increased theta power ($p = 0.03$; 85.7%) | Monitoring |
| Mendonça-de-Souza et al. | $N_{pain} = 11$ $N_{healthy} = 7$ | Migraine | rs-EEG eEEG | FBP | Differences in cortical coherence before and after photic stimulation ($p < 0.05$) | Diagnostic, prognostic |
| Schmidt et al. | $N_{pain} = 37$ $N_{healthy} = 37$ | Low Back Pain | rs-EEG | Peak frequency, PSD | No significant findings observed ($p > 0.05$) | N/A |
| **2013** | | | | | | |
| Jensen et al. | $N_{pain} = 10$ | Any | rs-EEG eEEG | PSD | Neurofeedback treatment: decreased pain/decreased theta ($p = 0.004$), increased alpha power ($p = 0.002$) | Monitoring |
| van den Broeke et al. | $N_{pain} = 8$ $N_{healthy} = 11$ | Post Mastectomy | rs-EEG eEEG | CoG | Enhanced alpha activity (7–13 Hz) in parietal and occipital cortices ($p < 0.05$) | Diagnostic |
| De Vries et al. | $N_{pain} = 16$ $N_{healthy} = 16$ | Pancreatitis | rs-EEG | Peak alpha frequency | Decreased peak alpha frequencies ($p = 0.049$) | Diagnostic |
| **2014** | | | | | | |
| Vuckovic et al. | $N_{pain} = 10$ $N_{healthy} = 20$ | Central Neuropathic Pain | rs-EEG eEEG | PSD | Increased ERD in theta, alpha and beta bands (16–24 Hz) ($p = 0.0085$) | Diagnostic[b] |
| Sufianov et al. | $N_{pain} = 30$ $N_{healthy} = 10$ | FBSS | rs-EEG | PSD | Differences in peak alpha frequency, beta and theta power after epidural spinal cord stimulation ($p < 0.05$) | Diagnostic, monitoring |
| **2015** | | | | | | |
| Navarro López et al. | $N_{pain} = 13$ $N_{healthy} = 13$ | Fibromyalgia | rs-EEG | PSD | Decreased theta and absolute alpha power, increased beta power ($p < 0.05$) | Diagnostic |
| Schmidt et al. | $N_{pain} = 21$ | Back Pain | rs-EEG | Peak frequency, peak power, CoG | Mindfulness-based stress-reduction: no significance | Monitoring |
| **2016** | | | | | | |
| González-Roldán et al. | $N_{pain} = 20$ $N_{healthy} = 18$ | Fibromyalgia | rs-EEG | PSD, sLORETA, current source distribution | Negative correlation between delta band power and pain duration ($p = 0.026$). Increased theta power ($p = 0.04$), reduced alpha response ($p = 0.017$). Significant changes in beta bands ($p < 0.05$) | Diagnostic |
| Meneses et al. | $N_{pain} = 21$ $N_{healthy} = 21$ | Rheumatoid Arthritis | rs-EEG | PSD | Increased absolute and relative alpha power densities ($p < 0.05$) | Diagnostic |
| **2017** | | | | | | |
| Gram et al. | $N_{pain} = 81$ | Hip Pain | rs-EEG eEEG | PSD, functional connectivity, SVM | Frontal delta power and functional connectivity features influence post-operative treatment response (65%) | Predictive |
| Camfferman et al. | $N_{pain} = 103$ | Any | rs-EEG | Spectral band power | Negative association between alpha power and pain intensity in frontal and parietal areas ($p < 0.01$) | Diagnostic |
| Thibaut et al. | $N_{pain} = 5$ $N_{healthy} = 47$ | Pancreatitis | rs-EEG | PSD | Transcranial electrical stimulation (tPCS/tDCS): differences in alpha, beta ($p < 0.05$), and theta ($p \leq 0.002$) band power. | Diagnostic, monitoring |
| Prinsloo et al. | $N_{pain} = 62$ | Peripheral Neuropathy | rs-EEG eEEG | PSD | Neurofeedback therapy: increased alpha power ($p = 0.021$) and decreased beta power ($p = 0.021$) | Monitoring |
| **2018** | | | | | | |
| Cao et al. | $N_{pain} = 40$ $N_{healthy} = 40$ | Migraine | rs-EEG | Inherent fuzzy entropy; SVM | Changes in EEG patterns between phases of an ongoing migraine attack (76%) | Prognostic |
| Di Pietro et al. | $N_{pain} = 20$ $N_{healthy} = 20$ | Trigeminal Neuropathy | rs-EEG | PSD | Differences in theta ($p = 0.04$), beta and low alpha ranges ($p = 0.03$) | Diagnostic |
| Fallon et al. | $N_{pain} = 19$ $N_{healthy} = 18$ | Fibromyalgia | rs-EEG eEEG | sLORETA | Increased theta power in prefrontal cortex, anterior cingulate cortex and DLPFC ($p < 0.05$) | Diagnostic |
| Vanneste et al. | $N_{pain} = 78$ $N_{healthy} = 264$ | Neuropathic Pain | rs-EEG | sLORETA; SVM | Thalamocortical dysrhythmia may serve as a mechanism underlying pain (92.5%) | Diagnostic |
| Vuckovic et al. | $N_{pain} = 11$ $N_{healthy} = 31$ | Central Neuropathic Pain | rs-EEG | Band power analysis; SVM | Transferable learning classifier could detect patients developing chronic neuropathic pain based on alpha band features (> 85%) | Prognostic[c] |
| Prichep et al. | $N_{pain} = 77$ $N_{healthy} = 77$ | Any | rs-EEG | sLORETA | Overactivation of the cingulate gyrus, insula, parietal lobule, the thalamus and the DLPFC (90%) | Diagnostic, monitoring |
| Zhou et al. | $N_{pain} = 14$ $N_{healthy} = 14$ | Postherpetic Neuralgia | rs-EEG | PSD, Phase-amplitude coupling | Increased gamma power (prefrontal and cerebellar areas); positive correlation with pain intensity ($p < 0.05$) | Diagnostic, monitoring |

*(Continued)*

TABLE 1 (Continued)

| Author | Subjects | Chronic pain | EEG State[a] | Feature/Machine learning analysis | Findings (significance, *p*-value; accuracy, %) | Biomarker type |
|---|---|---|---|---|---|---|
| **2019** | | | | | | |
| Dinh et al. | $N_{pain} = 101$ $N_{healthy} = 84$ | Any | rs-EEG | Functional connectivity, SVM | Increased connectivity: theta and gamma frequencies frontally, global network reorganization (57%) | Diagnostic |
| Ahn et al. | $N_{pain} = 20$ | Low Back Pain | rs-EEG | Alpha band power | Transcranial stimulation (tACS): increased alpha power in somatosensory regions indicating pain relief ($p < 0.05$) | Diagnostic, monitoring |
| Ferdek et al. | $N_{pain} = 20$ $N_{healthy} = 17$ | Endometriosis | rs-EEG eEEG | Directed transfer function connectivity | Increased beta connectivity: left DLPFC, somatosensory, orbitofrontal and right temporal cortex ($p < 0.05$) | Diagnostic |
| Villafaina et al. | $N_{pain} = 31$ $N_{healthy} = 31$ | Fibromyalgia | rs-EEG | Spectral power | Reduced alpha-2 (11–12 Hz) power with negative VAS pain score correlations ($p < 0.05$) | Diagnostic |
| Yüksel et al. | $N_{pain} = 42$ $N_{healthy} = 21$ | Fibromyalgia | rs-EEG | PSD | Changes in anterior delta, theta, alpha and beta power with TENS and acupuncture ($p < 0.05$) | Diagnostic, Monitoring |
| **2020** | | | | | | |
| Baroni et al. | $N_{pain} = 24$ $N_{healthy} = 24$ | Orofacial Pain | rs-EEG eEEG | Z-scored PSD | Decreased alpha and increased gamma activity in central and frontal regions ($p < 0.05$) | Diagnostic |
| de Melo et al. | $N_{pain} = 31$ | Fibromyalgia | rs-EEG | PSD | Transcranial stimulation therapy (tDCS); differences in frontal and parietal alpha-2 band power bands ($p < 0.05$) | Diagnostic, monitoring |
| Levitt et al. | $N_{pain} = 37$ $N_{healthy} = 20$ | Low Back Pain | rs-EEG | PSD, Phase-amplitude coupling, SVM | Differences in low-gamma power (42–43 Hz) (82.5%) | Diagnostic |
| González-Villar et al. | $N_{pain} = 43$ $N_{healthy} = 51$ | Fibromyalgia | rs-EEG | Temporal-concatenation group connectivity, PLI | Increased beta connectivity with shorter microstate occurrence/functional connectivity ($p < 0.05$) | Diagnostic |
| Telkes et al. | $N_{pain} = 9$ | Any | rs-EEG eEEG[d] | PSD | Differences in alpha-theta spectral dynamics in prefrontal, frontal and S1 cortices ($p < 0.05$), increasing alpha band power | Monitoring |
| Uygur-Kucukseymen et al. | $N_{pain} = 26$ | Fibromyalgia | rs-EEG eEEG | PSD, ERD | Reduced alpha power in frontal, central and parietal areas, reduced beta power in central areas ($p < 0.05$), smaller ERD responses in theta and delta bands ($p < 0.05$) | Diagnostic, Predictive |
| **2021** | | | | | | |
| Patel et al. | $N_{pain} = 4$ $N_{healthy} = 4$ | Any | rs-EEG eEEG | Alpha power | Transition probabilities from low to high alpha state after alpha-neurofeedback therapy ($p < 0.05$) | Monitoring |
| Barbosa-Torres et al. | $N_{pain} = 37$ | Fibromyalgia | rs-EEG eEEG | Spectral band amplitude | Neurofeedback therapy: changes in theta wave ratio before and after treatment ($p < 0.005$) | Monitoring |
| Bernardi et al. | $N_{pain} = 15$ | Fibromyalgia | rs-EEG | Spectral power | Transcranial stimulation (tACS): increased alpha power ($p = 0.024$) and reduced pain symptoms ($p < 0.05$) | Monitoring |
| Buchanan et al. | $N_{pain} = 57$ $N_{healthy} = 54$ | Post-Concussive Syndrome | rs-EEG | PSD, SVM | Increased delta and theta power (87.6%) | Diagnostic[e] |
| Feng et al. | $N_{pain} = 27$ | Low Back Pain | rs-EEG | Alpha band power | Negative correlation between central alpha power and pain intensity ($p = 0.01$; strongest at Cz $p = 0{:}04$) | Diagnostic |
| Jensen et al. | $N_{pain} = 173$ | Any | rs-EEG | Spectral band power | Lower pain intensity across all intervention groups no significance in EEG differences | Predictive, Monitoring |
| Lee et al. | $N_{pain} = 11$ | FBSS | rs-EEG | sLORETA source-localized spectral band power | Pain improvement with increased activity in the right anterior cingulate cortex after non-invasive painless signaling therapy ($p < 0.05$) | Monitoring |
| Lendaro et al. | $N_{pain} = 16$ $N_{controls} = 10$ | Phantom Limb Pain | rs-EEG | CSP, C-support vector classification | Potential to discriminate between pain and no pain using broad-band (4–40 Hz) CSP features (93.7%, leave out cross-validation) | Diagnostic |
| Kimura et al. | $N_{pain} = 23$ | Hip Pain | eEEG | Sub-band power spectrum, SVM | Differences among subjects with different levels of hip pain at frequencies ranging from 1 to 35 Hz (79.6%) | Monitoring |
| Martín-Brufau et al. | $N_{pain} = 23$ $N_{healthy} = 23$ | Fibromyalgia | rs-EEG | sLORETA, spectral band power, coherence | Decreased amplitudes in theta and alpha and beta frequencies ($p < 0.01$), with scarce cortical interconnections for delta and beta bands and greater functional connectivity in insular and frontal regions ($p < 0.01$; 91.3–100%) | Diagnostic |
| May et al. | $N_{pain} = 101$ $N_{healthy} = 88$ | Any | rs-EEG | Microstate analysis | Decreased presence of microstate D, potentially related to dysfunctional attentional processes ($p < 0.002$) | Diagnostic |
| Parker et al. | $N_{pain} = 16$ | Neuropathic Pain | rs-EEG | Spectral band power | Dorsal root ganglia stimulation: increased frontal, central and parietal beta power ($p < 0.003$), reduced pain intensity | Monitoring |

*(Continued)*

TABLE 1 (Continued)

| Author | Subjects | Chronic pain | EEG State[a] | Feature/Machine learning analysis | Findings (significance, *p*-value; accuracy, %) | Biomarker type |
|---|---|---|---|---|---|---|
| Santana et al. | $N_{pain} = 22$ $N_{healthy} = 18$ | Hip Pain | rs-EEG eEEG | Motif synchronization | Impaired dynamic brain network with shorter full synchronization time in rest network and more pronounced diffuse connectivity ($p = 0.007$) | Diagnostic |
| Teixeira et al. | $N_{pain} = 12$ $N_{healthy} = 10$ | Peripheral Neuropathic Pain | rs-EEG | Power band analysis | Changes in GABAergic lower beta oscillation (global power spectrum decrease) ($p = 0.007$) | Diagnostic |
| Zortea et al. | $N_{pain} = 47$ | Fibromyalgia | rs-EEG | Average spectral power | Decreased theta and beta peak amplitudes in opioid users vs. non-opioid users (67–73% sensitivity, 62–72% specificity) | Monitoring |
| 2022 | | | | | | |
| Wei et al. | $N_{pain} = 70$ | Postherpetic Neuralgia | rs-EEG | Sub-band power spectral entropy, kNN | Central-parietal beta band spectral different in treatment-resistant and treatment-sensitive patients (80% ± 11.7%) | Predictive |
| Teel et al. | $N_{pain} = 121$, $N_{healthy} = 39$ | Muskuloskeletal Pain | rs-EEG eEEG | Theta band permutation entropy; radial basis functional kernel SVM | Theta permutation entropy features distinguishes between baseline and cold pressor task conditions in chronic pain (75.6%) | Diagnostic |
| Teixeira et al. | $N_{pain} = 30$ | Low Back Pain | rs-EEG eEEG | Spectral band power | Differences in EEG frequencies between pain response and higher pain over frontal, central and parietal cortices ($p < 0.05$) | Diagnostic |
| Topaz et al. | $N_{pain} = 133$, $N_{healthy} = 47$ | Diabetic Polyneuropathy | rs-EEG | Spectral correlation by MSC; C-support vector classification | Painful diabetes polyneuropathy patients present significantly higher cortical functional connectivity in theta ($p = 0.008$) and alpha ($p = 0.001$) bands, | Diagnostic |
| Heitmann et al. | $N_{pain} = 41$ | Any | rs-EEG | Peak frequencies and CoG, functional connectivity | Interdisciplinary multimodal pain treatment reduced pain and showed an increase in theta global network efficiency ($p < 0.001$) | Monitoring |

Center of Gravity (CoG); Common Spatial Pattern (CSP); Dorsolateral Frontal Cortex (DLPFC); Event-related Desynchronization (ERD); Frequency Band Power (FBP); Failed Back Surgery Syndrome (FBSS); k-Nearest Neighbors Classifier (kNN); Magnitude-Squared Coherence (MSC); Phase-Lag index (PLI); Power Spectral Density (PSD); Support Vector Machine (SVM).
[a]Resting-state EEG (rsEEG) or evoked EEG (eEEG).
[b]Suggested this type of biomarker to also serves as a prognostic biomarker.
[c]Continuation of previous study where the same data was to propose a combined diagnostic and prognostic biomarker.
[d]Intraoperative continuous EEG recordings in patients undergoing surgery for implantation of spinal cord stimulator (SCS).
[e]Findings are suggested to have a prognostic value in the future, where they could be applied to assess treatment response and guide treatment strategies.

stimuli exposure to capture the true nature of evoked pain perception, where the results have shown a positive correlation with gamma power changes in the medial prefrontal cortex (Schulz et al., 2015; Misra et al., 2017).

Third, scalp EEG electrodes only record compounded peripheral neuronal activity, meaning that the signal from deeper brain structures cannot be easily separated (Hallez et al., 2007). Further studies using depth electrodes, as in invasive intracranial EEG (iEEG) which are placed in the deep structures, such as the hippocampus, amygdala, and insula, could help us to understand better the complexities of chronic pain, and its affective-emotional and cognitive-evaluative components (Peyron et al., 2002; Mokhtari et al., 2019).

Overall, the use of EEG for chronic pain studies is appealing for its high temporal resolution, low cost, broad availability, and ease of data collection (Morton et al., 2016).

# 3. Extracting pain-related features from EEG data

With the advances in pain research, the field has made significant progress in improving and streamlining the analysis of EEG measurements. Following data acquisition, the first step in a neural data analysis pipeline is preprocessing. Preprocessing, including spectral filtering and artifact rejection, extracts the signals of interest while suppressing noise to maximize the signal-to-noise ratio (Hasenstab et al., 2015). Next, the preprocessed data is used to perform feature extraction, which aims to extract only the most discriminative information from a given signal (Pedroni et al., 2019).

## 3.1. Preprocessing: artifact removal

Human EEG recordings are highly susceptible to artifacts (e.g., head movement, eye blinks, and heartbeat). Extraction and removal of these components is typically accomplished by independent component analysis (ICA) (Urigüen and Garcia-Zapirain, 2015). Once the independent components have been identified, they can be analyzed and classified as either endogenous (e.g., muscular/ocular movement, cardiac activity) or exogenous artifacts (e.g., electronic device interference, electromagnetic radiation), and subsequently removed from the EEG data (Jas et al., 2017; Jiang et al., 2019).

## 3.2. Resting-state versus stimulus-evoked processing

The signal processing pipeline differs for resting-state and stimulus-evoked types of EEG data. While the activity recorded in evoked EEG can be associated with specific emotional, motor, sensory, perceptive and cognitive processes, that of rs-EEG cannot be associated with specific events; in relation, its activity is purely spontaneous. Accordingly, evoked data may consist of dozens to hundreds of repeated, seconds-long epochs (Aunon et al. 1978; Hu et

al. 2019) while rs-EEG data is composed of one recording ranging from a few minutes to several hours in duration (Khanna et al., 2015; Olejarczyk et al., 2017), Therefore, evoked EEG data is accompanied by trial time-stamps, trial labels, and subject responses, while rs-EEG data may only contain sparse annotations. The differences in processing pipelines for the two data types are summarized below.

Common resting-state processing techniques:

- Omit trace segments with amplitude values above a set threshold for each electrode.
- Visually or programmatically omit trace segments containing movement artifacts.
- Set a single baseline as amplitude reference
- Cropped total duration.

Common evoked signal processing techniques:

- Programmatically drop entire epochs containing movement artifacts.
- Scale amplitude values across epochs, especially for cross-subject analyses.
- Set a single baseline as reference, or independent baseline preceding each epoch.

## 3.3. EEG feature extraction

The extraction of features from EEG data involves prior knowledge of the brain activity potentially related to pain processing (Hu and Zhang, 2019). Examples of such prior knowledge may include which brain regions are involved in pain processing, the timing and synchronization of activity—both within and between regions, and the degree of connectivity between those regions. Features commonly used in EEG studies of chronic pain can be represented in the spatial, temporal, or spectral domains (or a combination of the three) and computed from either sensor space or source space data. These features are typically analyzed for temporal dynamics more than rs-EEG and the different feature representations contribute to the investigation of pain processing from distinct yet meaningful perspectives.

### 3.3.1. Spatial features

Extracting meaningful spatial patterns in EEG data by methods such as dimensionality reduction and pattern optimization allows for the identification of specific regions involved in pain processing. For instance, common spatial patterns is a linear algebra-based technique that works by finding the most discriminative EEG components between different classes in a given dataset, such as trials during painful stimulation versus trials without (Blankertz et al., 2008; Lu et al., 2010; Wu et al., 2014).

### 3.3.2. Temporal and spectral features

Pain processing is associated with complex temporal-spectral patterns of brain activity. Brain oscillations are patterns of synchronized electrical activity that arise from the coordinated activity of large populations of neurons; they can vary in amplitude, timing, and frequency. Features constructed from brain oscillations may take the form of power spectral density, relative power ratio, amplitude, phase coherence, and phase synchrony (Riaz et al., 2015). Pain-evoked event-related potentials (ERPs) are associated with an increase in theta band (4–8 Hz) power, also referred to as the theta-ERS (Pinheiro et al., 2016). In evoked pain, EEG studies have shown increased activity in the high-gamma band (60–100 Hz) (Ploner et al., 2017). In chronic pain, decreases in the power of the alpha band have also been observed (see Table 1) (De Vries et al., 2013). An increase or decrease in the power of a certain frequency band is referred to as non-phase-locked event-related synchronization (ERS) or event-related desynchronization (ERD), respectively (Pfurtscheller 2001; Hadjileontiadis, 2015). Figure 1 illustrates the differences between the ERP and ERD/ERS analysis techniques.

Higher-order information can also be extracted from both temporal and spectral features. One such example based on spectral features is the center of gravity (CoG). Assuming a defined region of interest (ROI) composed of either a subset of channels or a current source density distribution, CoG is defined as the frequency at which the whole EEG power within the empirically defined window is split into two equal parts, each part possessing the same overall power (Schmidt et al., 2012). Another example of a higher-order feature is entropy, also known as complexity. Based on information theory, entropy is a method for quantifying the irregularity of the EEG signal. When applied to the EEG power spectrum, entropy can measure the "peakedness" or "flatness" of the power distribution, representing the rhythmicity of the signal based on changes in the proportions of power at each frequency (Inouye et al., 1991).

### 3.3.3. Source localization

Source localization in EEG is a method of estimating the location and intensity of current sources generated from cortical and even subcortical regions (Seeber et al., 2019). Minimum norm estimate, Low-resolution electromagnetic tomography (LORETA), and Beamforming are some examples of source localization algorithms (Chen et al., 2002; So, 2011; Michel and Brunet, 2019). Following EEG source localization with a subsequent functional connectivity analysis is commonly done (Schoffelen and Gross, 2009; Sohrabpour et al., 2016).

### 3.3.4. Connectivity patterns

Functional connectivity (FC) analysis in EEG typically involves computing the statistical dependence or relationship between different brain regions or networks (Sakkalis, 2011). Some common examples of these algorithms include coherence, correlation, partial correlation, wavelet coherence, dynamic causal modeling (DCM), and Granger causality (Guo et al., 2020). These algorithms can provide insight into the direction and strength of connectivity between brain regions, as well as the dynamic nature of these connections. For example, FC has been used to identify long-range nociceptive information flow within the brain in chronic pain conditions (Necka et al., 2019).

# 4. Application of machine learning to EEG studies of chronic pain

## 4.1. Overview of machine learning algorithms

While the preprocessing and feature selection stages extract information from EEG data, the subsequent decoding stage utilizes the extracted features to provide insights for clinical and research

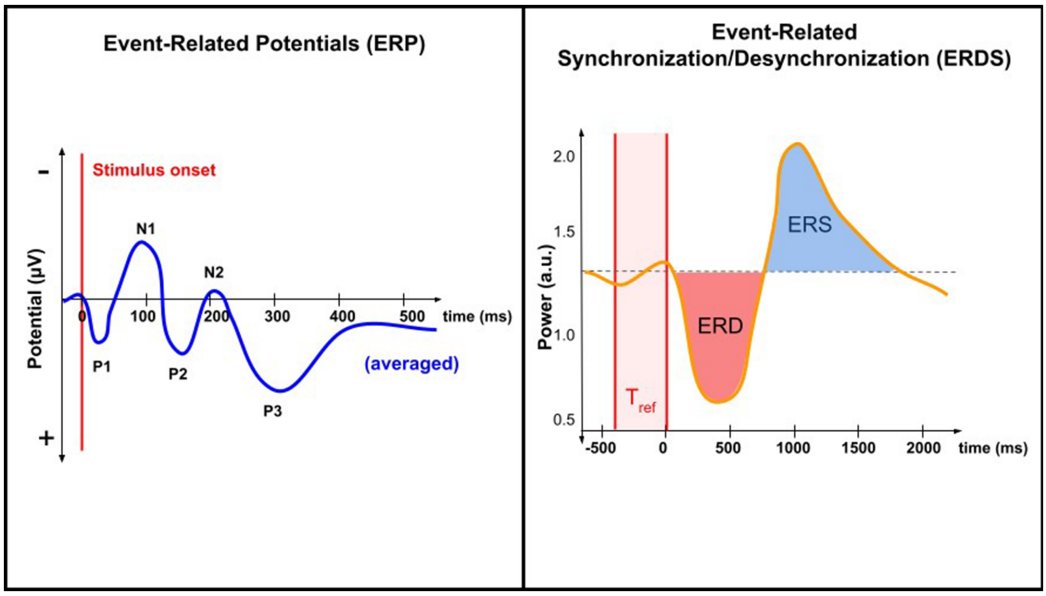


FIGURE 1
Comparing ERP and ERD/ERS analysis techniques. ERP analysis involves EEG data time-locked to a specific event. When averaged, ERPs reveal characteristic peaks and troughs (N1, P1, etc.). ERDS analysis involves quantifying changes in the power (rather than potential) of specific frequency bands in the EEG signal relative to a baseline period, $T_{ref}$. Both techniques study changes in neural activity associated with a specific task or event, but only ERP is time-locked.

applications. The application of ML facilitates tasks such as classification, detection, prediction, and risk assessment to identify meaningful features from EEG data (Müller et al., 2008; Hosseini et al., 2020). Then, after meeting certain criteria such as specificity, sensitivity, and generalizability, these features can be deemed biomarkers. In the context of chronic pain, this would allow us to identify patterns in EEG that could serve as putative neural codes for diagnosis, prognosis, monitoring, or prediction of chronic pain (Brodersen et al., 2012; Wager et al., 2013; Chen, 2021; Tracey, 2021; Harland et al., 2022).

Supervised and unsupervised ML approaches remain the most common approaches used in EEG studies of chronic pain cohorts (Alloghani et al., 2020). However, semi-supervised learning involves a small portion of labeled samples and a large number of unlabeled samples from which a model must learn and make predictions on new samples (Jia et al., 2014; She et al., 2019). Currently, the majority of published studies apply supervised learning to analyze EEG findings (Hammal and Cohn, 2012; Jenssen et al., 2021; Harland et al., 2022). By identifying spatial, temporal, or spectral features from the EEG data, one can train a parametric or nonparametric classifier on the labeled data to accomplish a certain task (Matsangidou et al., 2021). Examples of such tasks are described in Figure 1.

## 4.2. Supervised versus unsupervised learning approaches

Supervised and unsupervised learning methods differ primarily in their approaches to training, specifically in their reliance on labels (Aggarwal and Chugh, 2022). In the context of pain studies using stimulus-evoked EEG, the availability of labeled samples is dependent on many factors. For one, the collection of a sufficiently large number of trials (>100) in human subjects is time-consuming and often difficult for chronic pain patients who generally experience a heightened level of discomfort. Additionally, the selection of pain stimulus device, method, and intensity is limited and requires approval due to considerations of safety and ethics (Gatchel et al., 2016). To alleviate overfitting, both regularization and dimensionality reduction techniques are often employed. Another common concern in supervised learning is sample imbalance between classes. Under-sampling from the class with more trials is one way to alleviate the problem; though in pain studies, could lead to reducing an already low number of trials.

In a recent systematic review by Mari et al. (2022), they reviewed a total of 44 studies evaluating the effectiveness of ML algorithms on EEG data to explore the various aspects of pain. The continuous improvement of various performing models demonstrated high accuracies, ranging between 62 to 100%. These findings show that ML has the potential to predict pain outcomes, such as pain intensity, pain phenotype, and treatment response (Mari et al., 2022). The majority of the publications included were based on supervised ML methods, which are also known to present higher accuracies than their unsupervised counterparts (Hosseini et al., 2020).

Recently, Sun et al. developed an unsupervised learning method based on linear features extracted from EEG recordings to detect pain signals with a reported accuracy of 76% (Sun et al., 2021). By looking at source-localized ROIs using a state-space model, they observed that the unsupervised learning method requires fewer training trials and suggested that its performance is comparable—or perhaps better than the supervised method (Sun et al., 2021). However, this study assessed EEG signals from healthy pain-free subjects, with trials of acute evoked pain. To our knowledge, no studies describing the application of unsupervised learning methods to chronic pain data yet exist.

Unsupervised learning can alleviate the need for a large, balanced dataset of labeled samples. For example, in chronic pain research, cluster algorithms can be used when looking into pain intensities

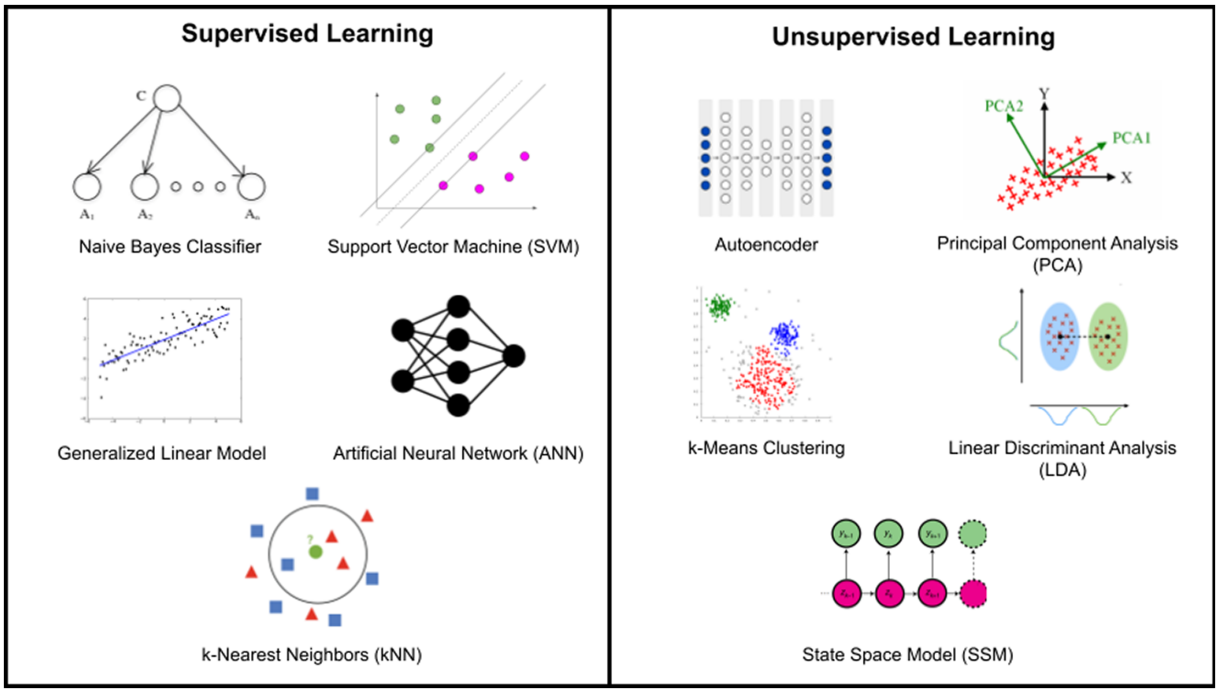


FIGURE 2
Common supervised and unsupervised classifiers applied in chronic pain research.

(Kragel et al., 2018). Furthermore, unsupervised learning methods have proven useful in extracting nonlinear features, making them more attractive as a decoding method in EEG pain research. However, further development is needed to demonstrate that unsupervised methods can support their generalizability with sufficiently high performance. Examples of common supervised and unsupervised classifiers employed in chronic pain research are described in Figure 2.

Semi-supervised learning approaches are worth exploring as they may offer practicality in the face of limitations: sparsely labeled data. EEG data requires administering stimuli (in the case of evoked data) or prolonged recording periods (in the case of resting-state data). For some chronic pain patients, prolonged sedentary periods can become overly uncomfortable, thereby resulting in diminishing returns with longer recordings due mostly to movement artifacts. Because semi-supervised learning requires significantly fewer labels over an entire dataset, individual recording sessions can be optimized and sped up, thereby resulting in data with higher quality and quantity. Such bottom-up approaches where the analysis step influences the data collection protocol can oftentimes lead to the best outcomes, facilitated by proper feedback.

### 4.3. Important considerations for ML in EEG studies of chronic pain

While choosing the right ML algorithm is indispensable, the importance of employing good ML practices cannot be understated. First-time users of ML may follow practices that lead to error-prone analyses, or to the illusion of successful results due to phenomena such as overfitting (model memorization of training data). By taking care in properly arranging input data, selecting an algorithm and its parameters deliberately, and appropriately evaluating model performance, one can be sure to maximize the potential in their dataset (Chicco, 2017).

Deep learning, a type of ML based on neural networks, can be highly effective at identifying nuanced pain-related features in EEG (Chen, 2021). However, deep learning requires a large number of labeled samples in training, restricting its use in the chronic pain cohort. While some studies have shown promising results in studying chronic pain with deep learning (Vuckovic et al., 2018), they are not as widespread because of the limited sample size.

## 5. Types of potential EEG biomarkers and their utility in chronic pain research

The most acknowledged definition of a biomarker is "a defined characteristic that is measured as an indicator of normal biological processes, pathogenic processes or responses to an exposure or intervention" (Group, 2016). In the context of chronic pain, a biomarker could thus serve to either confirm the presence of pain, identify the transition from one pain state to another, measure the risk of developing pain, estimate a prognosis, or predict and evaluate intervention responses (Van Der Miesen et al., 2019).

Clinical biomarkers can be further classified based on their presumed application and purpose (Group, 2016; Califf, 2018; Tracey et al., 2019; Van Der Miesen et al., 2019; Eldabe et al., 2022). The various types of biomarkers according to the most recent literature are presented in Figure 3. Until recently, the main objective of biomarker development has focused less on quantifying pain and more on delivering high-accuracy diagnoses and treatment algorithms,

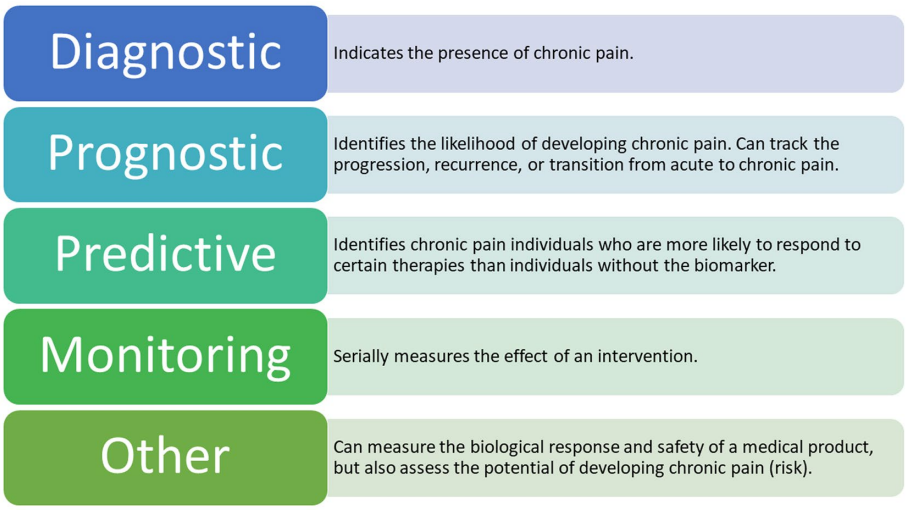


FIGURE 3
Types of Potential EEG Biomarkers for Chronic Pain. The following types of biomarkers have the potential to be clinically applicable in chronic pain management (Tracey et al., 2019; Van Der Miesen et al., 2019) A combination of these biomarkers is also a possible outcome for future research.

although based on neural mechanisms, rather than on symptoms (Dahlhamer et al., 2018; Gunn et al., 2020).

There are seven defined biomarker subtypes, each belonging to one of four categories associated with the development of biological biomarkers (Group, 2016; Tracey et al., 2019; Van Der Miesen et al., 2019). To date, the most applied biomarker subtypes in chronic pain research are diagnostic, prognostic, predictive, and monitoring (Davis et al., 2020). By identifying specific brain regions involved in the processing of chronic pain signals, we are indeed getting closer to decoding the presence of chronic pain (Graversen et al., 2012; Mendonça-de-Souza et al., 2012; Schmidt et al., 2012; De Vries et al., 2013; van den Broeke et al., 2013; Vuckovic et al., 2014; González-Roldán et al., 2016; Zebhauser et al., 2023). However, existing studies in this cohort are relatively few in number and the studies published so far have focused on the signals detected in either healthy participants exposed to acute experimental pain or in patients suffering from acute pain (Mouraux and Iannetti, 2018; Reckziegel et al., 2019). Thus, observed results mainly apply to a single type of condition at a certain point in time, which could easily be confounded with signals responsible for a long-lasting condition, such as chronic pain.

In contrast to acute pain, chronic pain involves complex peripheral and supraspinal brain mechanisms, where details on the underlying mechanisms remain incompletely known (von Hehn et al., 2012; Sun et al., 2021). Because of the multidimensional nature of chronic pain, a biomarker specific to the pathology has the potential to serve more than one purpose, thus being multifaceted and combinatorial (Ploner et al., 2017; Levitt and Saab, 2019). An overview of the studies included in this review, together with a summary of their representative features and biomarker type for each pain disease, can be seen in Tables 1–3.

## 5.1. Diagnostic biomarkers

A diagnostic biomarker indicates the presence of a condition or disease, like chronic pain. Most studies on chronic pain fall under this category (Van Der Miesen et al., 2019), primarily those associating chronic pain with group differences in EEG features (Reckziegel et al., 2019).

Studies assessing the potential of EEG as a diagnostic biomarker for chronic pain have emerged in the past decade and have led to the discovery of specific brain regions where relevant EEG changes associated with chronic pain are commonly observed. As presented in Table 1, the majority of the earlier studies recorded rs-EEG potentials in a few subjects. Nevertheless, they demonstrated promising findings indicating changes in specific frequency bands within targeted structures (De Vries et al., 2013; van den Broeke et al., 2013; Vuckovic et al., 2014; Navarro López et al., 2015; González-Roldán et al., 2016; Meneses et al., 2016). The described observations, mainly localized in the frontal, parietal, and occipital cortices, include both enhanced and reduced peak alpha frequency and theta responses, increased beta-band power, and increased ERD in the same bands—suggesting their potential as diagnostic biomarkers for chronic pain (De Vries et al., 2013; van den Broeke et al., 2013; Sufianov et al., 2014; Vuckovic et al., 2014; Navarro López et al., 2015; González-Roldán et al., 2016; Camfferman et al., 2017) (please see Table 2).

In one of the largest studies to date, Dinh et al. used SVM to demonstrate increased connectivity at theta (4–8 Hz) and gamma (50–100 Hz) frequencies in frontal regions, as well as global network reorganization (Dinh et al., 2019). Moreover, they demonstrated a decreased global efficiency at gamma frequencies in chronic pain patients. Such patterns have previously demonstrated involvement in the pathophysiology of chronic pain and are now better investigated. However, as described in Table 2, there still seems to be a continued discrepancy in the reported power responses in the theta, alpha, and beta bands, complicating the proposal of a consistent and reliable biomarker for chronic pain (Freye and Levy, 2006; Navarro López et al., 2015; Martín-Brufau et al., 2021). Moreover, the decoder performed only at 57% accuracy—close to chance-level, leaving much room for improvement. In more recent years, researchers' primary goal in improving decoding performance has been motivated primarily by the goal of optimizing model generalization, where the

TABLE 2 Representative features and their biomarker types for each pain disease reviewed. Pain disease columns are sorted by descending quantity of papers reviewed; rows are sorted by descending count of observations. Format: "*Potential biomarker* (count of shared observations/number of papers reviewed in that pain disease; biomarker type(s)) [Reference(s)]."

| Fibromyalgia | Chronic pain | Pancreatitis | Central neuropathic pain | Hip pain | Failed back surgery syndrome | Peripheral neuropathy | Low back pain | Diabetic polyneuropathy (DPN) |
|---|---|---|---|---|---|---|---|---|
| Decreased alpha band power (5/18; diagnostic, predictive) (Sufianov et al., 2014; González-Roldán et al., 2016; Meneses et al., 2016; Lancaster et al., 2017; Ferdek et al., 2019) | Decreased alpha band power (2/8; diagnostic) (Vachon-Presseau et al., 2016; Telkes et al., 2020) | Increased theta band power (2/5; monitoring) (Graversen et al., 2012; Jensen et al., 2013) | Alpha band activity (1/4; prognostic) (Vuckovic et al., 2018) | Frontal delta power (1/3; predictive) (Yüksel et al., 2019) | Decreased peak alpha frequency (2/3; diagnostic, monitoring) (Baliki et al., 2012; Uygur-Kucukseymen et al., 2020) | Decreased alpha band power (1/3; monitoring) (Prinsloo et al., 2017) | Decreased alpha band power (2/3; diagnostic, monitoring) (Gram et al., 2017; Baroni et al., 2020) | Increased theta band connectivity (1/2; diagnostic) (Martín-Brufau et al., 2021) |
| Decreased theta band power (3/18; diagnostic) (Sufianov et al., 2014; Meneses et al., 2016; Zortea et al., 2021) | Increased theta band connectivity (1/8; diagnostic) (Schulz et al., 2012a,b) | Decreased peak alpha frequency (1/5; diagnostic) (De Vries et al., 2013) | Increased ERD in alpha band (1/4; diagnostic) (Vuckovic et al., 2014) | Frontal spectral power between 1 and 35 Hz (1/3; monitoring) (Liu et al., 2015) | Increased beta band power (1/3; diagnostic, monitoring) (Baliki et al., 2012; Uygur-Kucukseymen et al., 2020) | Increased beta band power (1/3; monitoring) (Prinsloo et al., 2017) | Delta and theta bands correlated with self-reported pain intensities (1/3; diagnostic) (Parker et al., 2021) | Increased alpha band connectivity (1/2; diagnostic) (Martín-Brufau et al., 2021) |
| Increased theta band power (3/18; diagnostic) (González-Roldán et al., 2016; May et al., 2021) | Increased gamma band connectivity (1/8; diagnostic) (Dinh et al., 2019) | Increased beta band power (1/5; diagnostic, monitoring) (Jensen et al., 2013) | Increased ERD in theta band (1/4; diagnostic) (Vuckovic et al., 2014) | Increased frontal connectivity (1/3; diagnostic) (Jensen et al., 2021) | Decreased beta-2 band power (1/3; monitoring) (Uygur-Kucukseymen et al., 2020) | Low-beta band activity (1/3; diagnostic) (Kimura et al., 2021) | | |
| Increased beta band power (3/18; diagnostic) (Sufianov et al., 2014; Meneses et al., 2016; May et al., 2021) | Over-activation in frontal and parietal areas (1/8; diagnostic, monitoring) (Santana et al., 2021) | Decreased alpha/beta power ratio (1/5; diagnostic, monitoring) (Jensen et al., 2013) | Increased ERD in beta band (1/4; diagnostic) (Vuckovic et al., 2014) | | | | | |
| Decreased alpha-2 band power (1/18; diagnostic) (Villafaina et al., 2019) | Increased theta band power (1/8; monitoring) (Schouppe et al., 2020) | | | | | | | |
| Increased beta band connectivity (1/18; diagnostic) (Zhou et al., 2018) | Decreased presence of microstate D (1/8; diagnostic) (Bernardi et al., 2021) | | | | | | | |
| Decreased beta band power (1/18; diagnostic, predictive) (Lancaster et al., 2017) | Increased theta global network efficiency (1/8; monitoring) (Teixeira et al., 2021) | | | | | | | |
| Decreased SMR/theta power ratio with neuro-feedback therapy (1/18; monitoring) (Di Pietro et al., 2018) | | | | | | | | |

*(Continued)*





10.3389/fnins.2023.1186418

TABLE 2 (Continued)

| Migraine | Orofacial pain | Post-concussive pain | Postherpetic neuralgia | Trigeminal neuropathy | Endometriosis | Lumbar back pain | Musculoskeletal pain | Post-mastectomy pain | Rheumatoid arthritis |
|---|---|---|---|---|---|---|---|---|---|
| Greater cortical coherence during baseline (1/2; diagnostic, prognostic) (Mendonça-de-Souza et al., 2012) | Decreased frontal and central alpha band power (1/2; diagnostic) (Wei et al., 2022) | Increased delta band power (1/2; diagnostic) (Lendaro et al., 2021) | Central-parietal beta band spectral entropy (1/2; predictive) (Heitmann et al., 2022) | Increased theta band power (1/2; diagnostic) (de Melo et al., 2020) | Increased beta connectivity in frontal, central, and temporal areas (1/1; diagnostic) (Lee et al., 2021) | Low-gamma band activity (1/1; diagnostic) (Teel et al., 2022) | Theta band permutation entropy (1/1; diagnostic) (Camiferman et al., 2017) | Enhanced alpha band power in parietal and occipital areas (1/1; diagnostic) (van den Broeke et al., 2013) | Increased alpha band power (1/1; diagnostic) (Cao et al., 2018) |
| Higher prefrontal complexity in the preictal phase (1/2; prognostic) (Thibaut et al., 2017) | Increased frontal and central gamma band power (1/2; diagnostic) (Wei et al., 2022) | Increased theta band power (1/2; diagnostic) (Lendaro et al., 2021) | Increased prefrontal gamma band power (1/2; diagnostic, monitoring) (Barbosa-Torres and Cubo-Delgado, 2021) | | | | | | |

application of SVM classifiers has led to an improvement in accuracy with up to 93.7% (Misra et al., 2017; Kragel et al., 2018; Levitt et al., 2020; Buchanan et al., 2021; Lendaro et al., 2021; Zolezzi et al., 2021; Teel et al., 2022; Topaz et al., 2022).

With gradual improvements in the ML algorithms over the years, there is a trend of testing their applicability in clinical practice, especially for diagnostic, monitoring, and prognostic purposes in the context of chronic pain (Mendonça-de-Souza et al., 2012; Sufianov et al., 2014). These applications would allow us to detect individuals with an increased risk of developing a certain condition, for example, the transition from acute to chronic pain. More importantly, it allows us to track the trajectory of pain development after applying certain therapies. This stratification of patients could serve to guide and inform future treatment and adds an additional quantitative objective measure of pain (Thibaut et al., 2017; Ahn et al., 2019; Yüksel et al., 2019; Santana et al., 2021; Heitmann et al., 2022).

As an example, and as a continuation of previous studies, Vuckovic et al. (2022) developed and further trained their own classifiers to evaluate subjects with central neuropathic pain. They provided evidence for the potential of utilizing non-oscillatory, non-linear features of EEG not only as a diagnostic biomarker but also for prognostic purposes. Thus, their study suggests that ML models can be trained not only to determine the presence of pain but also to predict the delay after which patients start showing symptoms of pain-state transition. However, pain is a highly subjective experience and often presents itself heterogeneously. Studies so far have not been able to present a diagnostic biomarker with enough validation and generalizability for clinical settings.

The extraction of spatial patterns and the detection of changes in oscillations have moved the field one step closer to producing a diagnostic biomarker for the presence of chronic pain. We now know that a distributed network of cortical circuits regulates pain with knowledge of specific regions involved in pain processing—the S1, ACC, and insular cortex (Liberati et al., 2018; Van Der Miesen et al., 2019; Sun et al., 2021). Furthermore, we know that noxious stimulation can evoke neural responses from these regions, like changes in theta and high gamma power (Baliki et al., 2012; Liu et al., 2015; Ploner et al., 2017; Zhang et al., 2017; Prichep et al., 2018; Schouppe et al., 2020). Currently, these features are described primarily in studies of acute experimental pain—with relatively few on chronic pain. Hence, to propose a diagnostic biomarker of chronic pain, further studies are needed to identify and confirm discriminative features specific to chronic pain states.

## 5.2. Prognostic biomarkers

Prognostic biomarkers serve to identify the likelihood of developing a disease or state, to track the progression or recurrence of a disease, or to identify the transition from one disease state to another, e.g., from an acute to chronic pain state (Baliki et al., 2012; Tracey et al., 2019; Van Der Miesen et al., 2019).

In general, difficulties have been noted in the studies trying to propose the usage of EEG as a prognostic biomarker. The main concern arises from the complex, dynamic nature of pain which limits the ability to capture EEG signals of prognostic value, requiring EEG recordings over a longer period. Nonetheless, there is a possibility that features learned through ML in studies

TABLE 3 Representative features pooled across all pain disease types. Similar features are combined within the same row in column 1.

| Potential biomarker | Biomarker type (s) | Number of claims[a] (64 total features) |
|---|---|---|
| Decreased alpha band power; Decreased alpha-2 band power; Decreased peak alpha frequency; Increased ERD in alpha band; Decreased frontal and central alpha band power | Diagnostic, Predictive, Monitoring | 16 |
| Increased theta band power; Increased theta band connectivity; Theta band correlated with self-reported pain intensities | Diagnostic | 11 |
| Increased beta band power; Increased beta band connectivity; Increased beta connectivity in frontal, central, and temporal areas | Diagnostic, Monitoring | 8 |
| Decreased theta band power; Increased ERD in theta band | Diagnostic | 4 |
| Decreased beta band power; Increased ERD in beta band; Decreased beta-2 band power | Diagnostic, Predictive | 3 |
| Increased prefrontal gamma band power; Increased gamma band connectivity; Increased frontal and central gamma band power | Diagnostic, Monitoring | 3 |
| Increased alpha band power; Increased alpha band connectivity; Enhanced alpha band power in parietal and occipital areas | Diagnostic | 3 |
| Increased delta band power; Delta band correlated with self-reported pain intensities | Diagnostic | 2 |

Rows are sorted by descending number of observations. Decreased alpha power prevails among all other potential biomarkers, accounting for 25% of all those reviewed.
[a]For brevity, only showing potential biomarkers with more than one observation; fourteen (14) potential biomarkers are omitted, which can be found in Table 1.

using other neuroimaging modalities, such as fMRI (Baliki et al., 2012), can be used to monitor the transition between disease states from continuous EEG signals to be used as monitoring biomarkers. Meanwhile, only a few studies have examined this possibility in a longitudinal cohort of pain patients.

In 2018, Vuckovic et al. (2022) demonstrated the potential utility of EEG as a prognostic biomarker after using previous datasets with previously recorded EEG signals in patients with painful and non-painful central neuropathic pain. By testing three classifiers (artificial neural network, SVM, and linear discriminant analysis) on EEG band power in resting state data recorded over time, they demonstrated that a transferable learning classifier learning classifier could detect patients at risk for developing painful chronic neuropathic pain with 86% accuracy. The study also suggested that it is possible to further develop and expand the purpose of a biomarker by using already existing data sets (Vuckovic et al., 2014).

To our knowledge, there are only a handful of published studies using EEG as a potential biomarker solely for prognostic purposes in chronic pain patients. Due to its complex nature and clinical importance, a prognostic biomarker for chronic pain requires rigorous model training and validation with large data sets to achieve high sensitivity and high specificity, as well as good generalizability. With an increasing number of studies on diagnostic and monitoring biomarkers, studies investigating its prognostic counterpart are likely to increase over the coming years, potentially relying on existing data from the diagnostic and monitoring arm of the field (Vachon-Presseau et al., 2016).

## 5.3. Predictive and monitoring biomarkers

Available knowledge of neural processes and pathways associated with the presence of pain has initiated the development of ***predictive biomarkers*** *and* ***monitoring biomarkers*** for chronic pain. A ***predictive biomarker*** enables the identification of individuals who are more likely to respond to certain therapies than individuals without the biomarker (Reckziegel et al., 2019; Tracey et al., 2019; Van Der Miesen et al., 2019; Eldabe et al., 2022). A ***monitoring biomarker***, on the other hand, helps to serially measure the effect of an intervention or therapy. By combining both, we could predict a patient's response to a certain therapy, enabling the development of a customized intervention program ahead of time.

For decades, scientists have explored the clinical implication of EEG as a monitoring biomarker for chronic pain. This has been done mainly by evaluating EEG signals before and after applying certain therapies—either individually or combined across subjects. Examples of such interventions include acupuncture, analgesics and anticonvulsants, epidural cord stimulation, neurofeedback treatment, surgical treatment, and transcranial stimulation therapies (Graversen et al., 2012; Jensen et al., 2013; Sufianov et al., 2014; Prinsloo et al., 2017; Thibaut et al., 2017; Ahn et al., 2019; Yüksel et al., 2019; de Melo et al., 2020; Barbosa-Torres and Cubo-Delgado, 2021; Heitmann et al., 2022).

As presented in Table 1, only a few studies attempting to assess EEG changes after applying targeted therapies have used healthy controls for comparison, hampering the predictive potentials of the proposed biomarker (Gram et al., 2017; Prinsloo et al., 2017; Ahn et al., 2019; de Melo et al., 2020; Lee et al., 2021; Zortea et al., 2021; Wei et al., 2022).

Notably, the majority of studies evaluating potential therapies have observed noticeable, statistically significant differences in the powers of theta, alpha, beta, and gamma activity in regions associated with chronic pain states (Zhou et al., 2018; de Melo et al., 2020; Lee et al., 2021; Patel et al., 2021; Zortea et al., 2021). These findings further strengthen the potential of EEG as a monitoring biomarker. With data over longer periods, from both healthy controls and chronic pain patients, the development of a robust composite biomarker serving diagnostic, predictive, prognostic, and monitoring purposes will be more readily achievable.

# 6. The future of EEG as a biomarker for chronic pain

In the last decade, the EEG pain research field has seen rapid progress. Though as we look into the future, we predict collaborative efforts will be crucial for achieving the development of any EEG biomarker for pain, especially one that is composite. Below we list some recommendations to push the EEG pain research community forward.

Data sharing and data pooling across study groups have proven to be appealing and perhaps essential methods to address the need for large data sets for ML analysis of EEG recordings (Van Der Miesen et al., 2019; Davis et al., 2020). Research groups may test various features and ML methods on the same large dataset, making for more robust comparisons between models, and facilitating faster discovery of potential features toward a composite biomarker for chronic pain. Moreover, by pooling data across various study groups, the validity of a potential biomarker would increase as the sample size gets larger, allowing for more robust cross-validation (Davis et al., 2020). In addition, the transparency of a potential EEG biomarker would be significantly improved by homogenized reporting standards. Currently, there exists a great discrepancy between reported results, and as part of an effort to improve future outcomes, new reporting guidelines have been developed and presented (Mari et al., 2022). However, large, multi-center datasets do come with a caveat: increased subject variability may hinder the clarity of cross-subject predictors.

Another benefit of data pooling is the diversity of chronic pain conditions, making a potential biomarker more generalizable. Due to slight variations in population samples, two research groups studying the same pain disease with similar experimental and analysis techniques could arrive at contrasting results. For example, a number of the studies in this review are focused on one specific pain disease cohort: fibromyalgia patients, a condition that is much more common in women than in men, creating an obstacle for a generalizable biomarker. Thus, data pooling has the potential to reduce the impact of sample population variations in small datasets by increasing the diversity in multi-center datasets.

Another innovative approach that has emerged recently is to combine rs-EEG studies with stimulus-evoked signals (Table 1). Pain is a dynamic process, and chronic pain involves both tonic and phasic components. Thus, by analyzing both resting-state and stimulus-evoked EEG potentials, we can further reduce the risk of confounders and improve sensitivity and specificity (Hansen et al., 2017).

Furthermore, Ávila et al. published an open and fully automated pipeline (DISCOVER-EEG) enabling easy, fast, and homogenous preprocessing, analysis, and visualization of rs-EEG data. This is an important step forward and should be taken as an example for future studies—where a tool like this will most likely promote open and reproducible research on brain function (Gil Avila et al., 2023). Optimally, this tool could be further developed into an unsupervised or semi-supervised ML method, allowing us to use largely unlabeled data, which would increase the generalizability of the potential biomarker itself. Moreover, standardized ML processes could contribute to the use of good ML practices, where commonly noted mistakes in current studies are results that may reflect overfitting or other anomalies in the ML implementation. Importantly, future studies also need to focus on diversity, equity, and inclusion in both training and testing datasets to further ensure good ML practice.

Advances in EEG source localization may also help improve the validity and reliability of a potential EEG biomarker for pain. Specifically, these methods could be used to inform which scalp electrodes are best positioned to record pain-associated brain activity, improving biomarker transparency and usability. As an example, the study conducted by Cao et al. demonstrated that using just a handful of leads may be enough to detect the presence of a disease, making future studies easier to conduct, but also facilitating continuous and longer EEG recording for monitoring purposes (Cao et al., 2018). This would be further facilitated by way of a portable device (Pu et al., 2021; Eldabe et al., 2022).

## 6.1. The potential for multimodal biomarkers

Studies on multimodal biomarkers are emerging for chronic pain patients (Prichep et al., 2018; Tracey et al., 2019; Eldabe et al., 2022). The incorporation of computational methods to conventional neurophysiological techniques such as EEG can be combined with other testing modalities, such as clinical reports, blood biomarkers, and quantitative sensory testing, to quantify pain and to predict outcomes for chronic pain patients (Califf, 2018; Mari et al., 2022).

Over recent years, a shift in paradigm for decoding chronic pain has already occurred, by incorporating objective neural signals into more subjective measurements of pain such as pain and mood questionnaires, as well as physiological data such as pulse and skin conductance measurements (Lancaster et al., 2017). With our current understanding of the EEG patterns associated with chronic pain states, and with the continuous improvement of ML algorithms, we now have the tools to propose multimodal biomarkers in the future. Another development in biomarker research is that an appropriately collected and curated database could be applied to the development of multiple biomarkers serving more than one clinical purpose (Vuckovic et al., 2014, 2018).

## 6.2. Limitations of this review

As a narrative review, we did not employ a systematic set of criteria for study inclusion, in part due to the relatively disparate literature in machine learning and EEG studies in pain. By presenting concepts from the perspective of clinical applicability, we aimed to facilitate an understanding of the application of EEG and machine learning in studies of chronic pain without the use of restrictive language.

## 6.3. Summary

In summary, impactful studies have been conducted in the past decade showing the potential for an EEG-based biomarker for chronic pain. Through the establishment of standardized practices and improved collaborations between members of the field, EEG-based

techniques have the potential to become a key component of chronic pain diagnosis and treatment.

## Author contributions

MR wrote the first draft of the manuscript. GK, LD, ZC, and JW wrote sections of the manuscript. All authors contributed to the article and approved the submitted version.

## Acknowledgments

The authors acknowledge funding from the National Institutes of Health grants NS121776 (JW and ZC), MH118928 (ZC) and DA056394 (ZC). Any opinions, findings, and conclusions or recommendations expressed in this article are solely those of the authors and do not necessarily reflect the views of the funding agencies.

## Conflict of interest

JW is a cofounder of Pallas Technologies, Inc., and ZC is a scientific advisor of Pallas Technologies, Inc. JW and ZC are inventors of a pending US patent application of pain treatment technology.

The remaining authors declare that the research was conducted in the absence of any commercial or financial relationships that could be construed as a potential conflict of interest.

## Publisher's note

All claims expressed in this article are solely those of the authors and do not necessarily represent those of their affiliated organizations, or those of the publisher, the editors and the reviewers. Any product that may be evaluated in this article, or claim that may be made by its manufacturer, is not guaranteed or endorsed by the publisher.

## References

Aggarwal, S., and Chugh, N. (2022). Review of machine learning techniques for EEG based brain computer interface. *Arch. Comput. Methods Eng.* 29, 3001–3020. doi: 10.1007/s11831-021-09684-6

Ahn, S., Prim, J. H., Alexander, M. L., McCulloch, K. L., and Fröhlich, F. (2019). Identifying and engaging neuronal oscillations by Transcranial alternating current stimulation in patients with chronic low Back pain: a randomized, crossover, double-blind, Sham-Controlled Pilot Study. *J. Pain.* 20, 277.e1–277.e11. doi: 10.1016/j.jpain.2018.09.004

Alloghani, M., Al-Jumeily, D., Mustafina, J., Hussain, A., and Aljaaf, A. J. (2020). "A systematic review on supervised and unsupervised machine learning algorithms for data science" in *Supervised and unsupervised learning for data science*. ed. M. W. Berry (Heidelberg: Springer), 3–21.

Apkarian, A. V., Bushnell, M. C., Treede, R.-D., and Zubieta, J.-K. (2005). Human brain mechanisms of pain perception and regulation in health and disease. *Eur. J. Pain* 9, 463–484. doi: 10.1016/j.ejpain.2004.11.001

Ataoğlu, E., Tiftik, T., Kara, M., Tunc, H., Ersöz, M., and Akkuş, S. (2013). Effects of chronic pain on quality of life and depression in patients with spinal cord injury. *Spinal Cord* 51, 23–26. doi: 10.1038/sc.2012.51

Aunon, J., and Sencaj, R. (1978). Comparison of different techniques for processing evoked potentials. *Med. Biol. Eng. Comput.* 16, 642–650. doi: 10.1007/BF02442443

Babiloni, C., Babiloni, F., Carducci, F., Cincotti, F., Rosciarelli, F., Arendt-Nielsen, L., et al. (2002). Human brain oscillatory activity phase-locked to painful electrical stimulations: a multi-channel EEG study. *Hum. Brain Mapp.* 15, 112–123. doi: 10.1002/hbm.10013

Baliki, M. N., Petre, B., Torbey, S., Herrmann, K. M., Huang, L., Schnitzer, T. J., et al. (2012). Corticostriatal functional connectivity predicts transition to chronic back pain. *Nature Neurosci.* 15, 1117–1119. doi: 10.1038/nn.3153

Barbosa-Torres, C., and Cubo-Delgado, S. (2021). Clinical findings in SMR neurofeedback protocol training in women with fibromyalgia syndrome. *Brain Sci.* 11:1069. doi: 10.3390/brainsci11081069

Baroni, A., Severini, G., Straudi, S., Buja, S., Borsato, S., and Basaglia, N. (2020). Hyperalgesia and central sensitization in subjects with chronic orofacial pain: analysis of pain thresholds and EEG biomarkers. *Front. Neurosci.* 14:552650. doi: 10.3389/fnins.2020.552650

Baskin, I. I., Winkler, D., and Tetko, I. V. (2016). A renaissance of neural networks in drug discovery. *Expert Opin. Drug Discov.* 11, 785–795. doi: 10.1080/17460441.2016.1201262

Bernardi, L., Bertuccelli, M., Formaggio, E., Rubega, M., Bosco, G., Tenconi, E., et al. (2021). Beyond physiotherapy and pharmacological treatment for fibromyalgia syndrome: tailored tACS as a new therapeutic tool. *Eur. Arch. Psychiatry Clin. Neurosci.* 271, 199–210. doi: 10.1007/s00406-020-01214-y

Besson, J. (1999). The neurobiology of pain. *Lancet* 353, 1610–1615. doi: 10.1016/S0140-6736(99)01313-6

Blankertz, B., Tomioka, R., Lemm, S., Kawanabe, M., and Müller, K. (2008). Optimal spatial filters for robust EEG single-trial analysis. *IEEE Signal Process. Mag.* 25, 41–56. doi: 10.1109/MSP.2008.4408441

Boccard, S. G., Pereira, E. A., Moir, L., Van Hartevelt, T. J., Kringelbach, M. L., FitzGerald, J. J., et al. (2014). Deep brain stimulation of the anterior cingulate cortex: targeting the affective component of chronic pain. *Neuroreport* 25, 83–88. doi: 10.1097/WNR.0000000000000039

Boonstra, A. M., Preuper, H. R. S., Reneman, M. F., Posthumus, J. B., and Stewart, R. E. (2008). Reliability and validity of the visual analogue scale for disability in patients with chronic musculoskeletal pain. *Int. J. Rehabil. Res.* 31, 165–169. doi: 10.1097/MRR.0b013e3282fc0f93

Bressler, S. L. (2011). "Event-related potentials of the cerebral cortex. Electrophysiological recording techniques" in *Electrophysiological recording techniques, Neuromethods*. eds. P. Vertes and R. W. Stackman, vol. *54* (Heidelberg: Springer)

Britton, J. W., Frey, L. C., Hopp, J. L., Korb, P., Koubeissi, M. Z., Lievens, W. E., et al. (2016) in *Electroencephalography (EEG): An introductory text and Atlas of Normal and abnormal findings in adults, children, and infants*. eds. E. K. ST. Louis and L. C. Frey (Chicago: American Epilepsy Society)

Brodersen, K. H., Wiech, K., Lomakina, E. I., Lin, C.-S., Buhmann, J. M., Bingel, U., et al. (2012). Decoding the perception of pain from fMRI using multivariate pattern analysis. *NeuroImage* 63, 1162–1170. doi: 10.1016/j.neuroimage.2012.08.035

Buchanan, D. M., Ros, T., and Nahas, R. (2021). Elevated and slowed EEG oscillations in patients with post-concussive syndrome and chronic pain following a motor vehicle collision. *Brain Sci.* 11:537. doi: 10.3390/brainsci11050537

Byrom, B., McCarthy, M., Schueler, P., and Muehlhausen, W. (2018). Brain monitoring devices in neuroscience clinical research: the potential of remote monitoring using sensors, wearables, and mobile devices. *Clin. Pharm. Therap.* 104, 59–71. doi: 10.1002/cpt.1077

Califf, R. M. (2018). Biomarker definitions and their applications. *Exp. Biol. Med.* 243, 213–221. doi: 10.1177/1535370217750088

Camfferman, D., Moseley, G. L., Gertz, K., Pettet, M. W., and Jensen, M. P. (2017). Waking EEG cortical markers of chronic pain and sleepiness. *Pain Med.* 18, 1921–1931. doi: 10.1093/pm/pnw294

Cao, Z., Lai, K.-L., Lin, C.-T., Chuang, C.-H., Chou, C.-C., and Wang, S.-J. (2018). Exploring resting-state EEG complexity before migraine attacks. *Cephalalgia* 38, 1296–1306. doi: 10.1177/0333102417733953

Cao, T., Wang, Q., Liu, D., Sun, J., and Bai, O. (2020). Resting state EEG-based sudden pain recognition method and experimental study. *Biomed. Signal Process Control* 59:101925. doi: 10.1016/j.bspc.2020.101925

Chang, P., Arendt-Nielsen, L., Graven-Nielsen, T., Svensson, P., and Chen, A. C. (2001). Different EEG topographic effects of painful and non-painful intramuscular stimulation in man. *Exp. Brain Res.* 141, 195–203. doi: 10.1007/s002210100864

Chapman, C. R., and Vierck, C. J. (2017). The transition of acute postoperative pain to chronic pain: an integrative overview of research on mechanisms. *J. Pain* 18, e1–e38. doi: 10.1016/j.jpain.2016.11.004

Chen, Z. S. (2021). Decoding pain from brain activity. *J. Neural Eng.* 18:051002. doi: 10.1088/1741-2552/ac28d4

Chen, J. C., Yao, K., and Hudson, R. E. (2002). Source localization and beamforming. *IEEE Signal Process. Mag.* 19, 30–39. doi: 10.1109/79.985676

Chen, D., Zhang, H., Kavitha, P. T., Loy, F. L., Ng, S. H., Wang, C., et al. (2022). Scalp EEG-based pain detection using convolutional neural network. *IEEE Trans. Neural Syst. Rehabil. Eng.* 30, 274–285. doi: 10.1109/TNSRE.2022.3147673

Chicco, D. T. (2017). Quick tips for machine learning in computational biology. *BioData Mining* 10:35. doi: 10.1186/s13040-017-0155-3

Chowdhury, N. S., Skippen, P., Si, E., Chiang, A. K. I., Millard, S. K., Furman, A. J., et al. (2023). The reliability of two prospective cortical biomarkers for pain: EEG peak alpha frequency and TMS corticomotor excitability. *J. Neurosci. Methods* 385:109766. doi: 10.1016/j.jneumeth.2022.109766

Dahlhamer, J., Lucas, J., Zelaya, C., Nahin, R., Mackey, S., DeBar, L., et al. (2018). Prevalence of chronic pain and high-impact chronic pain among adults—United States, 2016. *MMWR Morb. Mortal. Wkly Rep.* 67:1001. doi: 10.15585/mmwr.mm6736a2

Dansie, E., and Turk, D. C. (2013). Assessment of patients with chronic pain. *Br. J. Anaesth.* 111, 19–25. doi: 10.1093/bja/aet124

Davis, K. D., Aghaeepour, N., Ahn, A. H., Angst, M. S., Borsook, D., Brenton, A., et al. (2020). Discovery and validation of biomarkers to aid the development of safe and effective pain therapeutics: challenges and opportunities. *Nat. Rev. Neurol.* 16, 381–400. doi: 10.1038/s41582-020-0362-2

de Melo, G. A., de Oliveira, E. A., dos Santos Andrade, S. M. M., Fernández-Calvo, B., and Torro, N. (2020). Comparison of two tDCS protocols on pain and EEG alpha-2 oscillations in women with fibromyalgia. *Sci. Rep.* 10:18955. doi: 10.1038/s41598-020-75861-5

De Vries, M., Wilder-Smith, O. H., Jongsma, M. L., van den Broeke, E. N., Arns, M., Van Goor, H., et al. (2013). Altered resting state EEG in chronic pancreatitis patients: toward a marker for chronic pain. *J. Pain Res.* 6:815. doi: 10.2147/JPR.S50919

Di Pietro, F., Macey, P. M., Rae, C. D., Alshelh, Z., Macefield, V. G., Vickers, E. R., et al. (2018). The relationship between thalamic GABA content and resting cortical rhythm in neuropathic pain. *Hum. Brain Mapp.* 39, 1945–1956. doi: 10.1002/hbm.23973

Dinh, S. T., Nickel, M. M., Tiemann, L., May, E. S., Heitmann, H., Hohn, V. D., et al. (2019). Brain dysfunction in chronic pain patients assessed by resting-state electroencephalography. *Pain* 160:2751. doi: 10.1097/j.pain.0000000000001666

Duerden, E. G., and Albanese, M. C. (2013). Localization of pain-related brain activation: a meta-analysis of neuroimaging data. *Hum. Brain Mapp.* 34, 109–149. doi: 10.1002/hbm.21416

Einevoll, G. T., Kayser, C., Logothetis, N. K., and Panzeri, S. (2013). Modelling and analysis of local field potentials for studying the function of cortical circuits. *Nat. Rev. Neurosci.* 14, 770–785. doi: 10.1038/nrn3599

Eldabe, S., Obara, I., Panwar, C., and Caraway, D. (2022). Biomarkers for chronic pain: significance and summary of recent advances. *Pain Res. Manag.* doi: 10.1155/2022/1940906

Fallon, N., Chiu, Y., Nurmikko, T., and Stancak, A. (2018). Altered theta oscillations in resting EEG of fibromyalgia syndrome patients. *Eur. J. Pain* 22, 49–57. doi: 10.1002/ejp.1076

Feng, L., Li, H., Cui, H., Xie, X., Xu, S., and Hu, Y. (2021). Low back pain assessment based on alpha oscillation changes in spontaneous electroencephalogram (EEG). *Neural Plast.* 2021. doi: 10.1155/2021/8537437

Ferdek, M. A., Oosterman, J. M., Adamczyk, A. K., van Aken, M., Woudsma, K. J., Peeters, B. W., et al. (2019). Effective connectivity of beta oscillations in endometriosis-related chronic pain during rest and pain-related mental imagery. *J. Pain* 20, 1446–1458. doi: 10.1016/j.jpain.2019.05.011

Fernandez Rojas, R., Huang, X., and Ou, K.-L. A. (2019). Machine learning approach for the identification of a biomarker of human pain using fNIRS. *Sci. Rep.* 9, 1–12. doi: 10.1038/s41598-019-42098-w

Ferracuti, S., Seri, S., Mattia, D., and Cruccu, G. (1994). Quantitative EEG modifications during the cold water pressor test: hemispheric and hand differences. *Int. J. Psychophysiol.* 17, 261–268. doi: 10.1016/0167-8760(94)90068-x

Freye, E., and Levy, J. (2006). The effects of tramadol on pain relief, fast EEG-power spectrum and cognitive function in elderly patients with chronic osteoarthritis (OA). *Acute. Pain.* 8, 55–61. doi: 10.1016/j.acpain.2006.03.001

Furman, A. J., Meeker, T. J., Rietschel, J. C., Yoo, S., Muthulingam, J., Prokhorenko, M., et al. (2018). Cerebral peak alpha frequency predicts individual differences in pain sensitivity. *NeuroImage* 167, 203–210. doi: 10.1016/j.neuroimage.2017.11.042

Furman, A. J., Prokhorenko, M., Keaser, M. L., Zhang, J., Chen, S., Mazaheri, A., et al. (2020). Sensorimotor peak alpha frequency is a reliable biomarker of prolonged pain sensitivity. *Cereb. Cortex* 30, 6069–6082. doi: 10.1093/cercor/bhaa124

Furman, A. J., Thapa, T., Summers, S. J., Cavaleri, R., Fogarty, J. S., Steiner, G. Z., et al. (2019). Cerebral peak alpha frequency reflects average pain severity in a human model of sustained, musculoskeletal pain. *J. Neurophysiol.* 122, 1784–1793. doi: 10.1152/jn.00279.2019

Gan, T. J. (2017). Poorly controlled postoperative pain: prevalence, consequences, and prevention. *J. Pain Res.* 10:2287. doi: 10.2147/JPR.S144066

Gan, T. J., Habib, A. S., Miller, T. E., White, W., and Apfelbaum, J. L. (2014). Incidence, patient satisfaction, and perceptions of post-surgical pain: results from a US national survey. *Curr. Med. Res. Opin.* 30, 149–160. doi: 10.1185/03007995.2013.860019

Gardner, J., and Sachdeva, H. (2019). Causes of pain worldwide. *Pain*, 1191–1192. doi: 10.1007/978-3-319-99124-5_253

Gatchel, R. J., Fuchs, P. N., and Allen, C. (2016). "Ethical issues in chronic pain research" in *Ethical Issues in Chronic Pain Management*. ed. M. E. Schatman (Boca Raton: CRC Press)

Gil Avila, C., Bott, F. S., Tiemann, L., Hohn, V. D., May, E. S., Nickel, M. M., et al. (2023). DISCOVER-EEG: an open, fully automated EEG pipeline for biomarker discovery in clinical neuroscience. *bioRxiv* 2023, 20:524897. doi: 10.1101/2023.01.20.524897

González-Roldán, A. M., Cifre, I., Sitges, C., and Montoya, P. (2016). Altered dynamic of EEG oscillations in fibromyalgia patients at rest. *Pain Med.* 17, 1058–1068. doi: 10.1093/pm/pnw023

González-Villar, A. J., Triñanes, Y., Gómez-Perretta, C., and Carrillo-de-la-Peña, M. T. (2020). Patients with fibromyalgia show increased beta connectivity across distant networks and microstates alterations in resting-state electroencephalogram. *NeuroImage* 223:117266. doi: 10.1016/j.neuroimage.2020.117266

Gram, M., Erlenwein, J., Petzke, F., Falla, D., Przemeck, M., Emons, M., et al. (2017). Prediction of postoperative opioid analgesia using clinical-experimental parameters and electroencephalography. *Eur. J. Pain* 21, 264–277. doi: 10.1002/ejp.921

Graversen, C., Olesen, S. S., Olesen, A. E., Steimle, K., Farina, D., Wilder-Smith, O. H., et al. (2012). The analgesic effect of pregabalin in patients with chronic pain is reflected by changes in pharmaco-EEG spectral indices. *Br J. PClin. harmacol.* 73, 363–372. doi: 10.1111/j.1365-2125.2011.04104.x

Group, F. N. B. W. (2016). "BEST (biomarkers, endpoints, and other tools) resource [internet]" in *Silver spring (MD): Food and Drug Administration (US)* (Bethesda (MD): National Institutes of Health (US))

Gunn, J., Hill, M. M., Cotten, B. M., and Deer, T. R. (2020). An analysis of biomarkers in patients with chronic pain. *Pain Physician* 23:E41. doi: 10.36076/PPJ.2020/23/E41

Guo, X., Zhang, Q., Singh, A., Wang, J., and Chen, Z. S. (2020). Granger causality analysis of rat cortical functional connectivity in pain. *J. Neural Eng.* 17:016050. doi: 10.1088/1741-2552/ab6cba

Hadjileontiadis, L. J. (2015). EEG-based tonic cold pain characterization using wavelet higher order spectral features. *I.E.E.E. Trans. Biomed. Eng.* 62, 1981–1991. doi: 10.1109/TBME.2015.2409133

Haefeli, M., and Elfering, A. (2006). Pain assessment. *Eur. Spine J.* 15, S17–S24. doi: 10.1007/s00586-005-1044-x

Hallez, H., Vanrumste, B., Grech, R., Muscat, J., De Clercq, W., Vergult, A., et al. (2007). Review on solving the forward problem in EEG source analysis. *J. Neuroeng. Rehabil.* 4, 1–29. doi: 10.1186/1743-0003-4-46

Hammal, Z., and Cohn, J. F. (2012). Automatic detection of pain intensity. *Proc ACM Int. Conf. Multimodal. Interact.* 2012, 47–52. doi: 10.1145/2388676.2388688

Hansen, T. M., Mark, E. B., Olesen, S. S., Gram, M., Frøkjær, J. B., and Drewes, A. M. (2017). Characterization of cortical source generators based on electroencephalography during tonic pain. *J. Pain Res.* 10:1401. doi: 10.2147/JPR.S132909

Harland, T., Hadanny, A., and Pilitsis, J. G. (2022). Machine learning and pain outcomes. *Neurosurg. Clin. N. Am.* 33, 351–358. doi: 10.1016/j.nec.2022.02.012

Hasenstab, K., Sugar, C. A., Telesca, D., McEvoy, K., Jeste, S., and Şentürk, D. (2015). Identifying longitudinal trends within EEG experiments. *Biometrics* 71, 1090–1100. doi: 10.1111/biom.12347

Heitmann, H., Ávila, C. G., Nickel, M. M., Dinh, S. T., May, E. S., Tiemann, L., et al. (2022). Longitudinal resting-state electroencephalography in patients with chronic pain undergoing interdisciplinary multimodal pain therapy. *Pain* 163, e997–e1005. doi: 10.1097/j.pain.0000000000002565

Herrmann, C. S., and Knight, R. T. (2001). Mechanisms of human attention: event-related potentials and oscillations. *Neurosci. Biobehav. Rev.* 25, 465–476. doi: 10.1016/s0149-7634(01)00027-6

Hollmann, M. W., Rathmell, J. P., and Lirk, P. (2019). Optimal postoperative pain management: redefining the role for opioids. *Lancet* 393, 1483–1485. doi: 10.1016/S0140-6736(19)30854-2

Hosseini, M.-P., Hosseini, A., and Ahi, K. (2020). A review on machine learning for EEG signal processing in bioengineering. *IEEE Rev. Biomed. Eng.* 14, 204–218. doi: 10.1109/RBME.2020.2969915

Hu, L., and Iannetti, G. D. (2016). Painful issues in pain prediction. *Trends Neurosci.* 39, 212–220. doi: 10.1016/j.tins.2016.01.004

Hu, L., and Zhang, Z., editors. *EEG signal processing and feature extraction*, Springer, Heidelberg (2019).

Huber, M., Bartling, J., Pachur, D. V., Woikowsky-Biedau, S., and Lautenbacher, S. (2006). EEG responses to tonic heat pain. *Exp. Brain Res.* 173, 14–24. doi: 10.1007/s00221-006-0366-1

Iannetti, G. D., Hughes, N. P., Lee, M. C., and Mouraux, A. (2008). Determinants of laser-evoked EEG responses: pain perception or stimulus saliency? *J. Neurophysiol.* 100, 815–828. doi: 10.1152/jn.00097.2008

Inouye, T., Shinosaki, K., Sakamoto, H., Toi, S., Ukai, S., Iyama, A., et al. (1991). Quantification of EEG irregularity by use of the entropy of the power spectrum. *Electroencephalogr. Clin. Neurophysiol.* 79, 204–210. doi: 10.1016/0013-4694(91)90138-t

Isnard, J., Magnin, M., Jung, J., Mauguière, F., and Garcia-Larrea, L. (2011). Does the insula tell our brain that we are in pain? *Pain* 152, 946–951. doi: 10.1016/j.pain.2010.12.025

Jackson, A. F., and Bolger, D. J. (2014). The neurophysiological bases of EEG and EEG measurement: a review for the rest of us. *Psychophysiology* 51, 1061–1071. doi: 10.1111/psyp.12283

Jas, M., Engemann, D. A., Bekhti, Y., Raimondo, F., and Gramfort, A. (2017). Autoreject: automated artifact rejection for MEG and EEG data. *NeuroImage* 159, 417–429. doi: 10.1016/j.neuroimage.2017.06.030

Jensen, M. P., Gertz, K. J., Kupper, A. E., Braden, A. L., Howe, J. D., Hakimian, S., et al. (2013). Steps toward developing an EEG biofeedback treatment for chronic pain. *Appl. Psychophysiol. Biofeedback* 38, 101–108. doi: 10.1007/s10484-013-9214-9

Jensen, M. P., Hakimian, S., Ehde, D. M., Day, M. A., Pettet, M. W., Yoshino, A., et al. (2021). Pain-related beliefs, cognitive processes, and electroencephalography band power as predictors and mediators of the effects of psychological chronic pain interventions. *Pain* 162:2036. doi: 10.1097/j.pain.0000000000002201

Jensen, M. P., Hakimian, S., Sherlin, L. H., and Fregni, F. (2008). New insights into neuromodulatory approaches for the treatment of pain. *J. Pain* 9, 193–199. doi: 10.1016/j.jpain.2007.11.003

Jenssen, M. D. K., Bakkevoll, P. A., Ngo, P. D., Budrionis, A., Fagerlund, A. J., Tayefi, M., et al. (2021). Machine learning in chronic pain research: a scoping review. *Appl. Sci.* 11:3205. doi: 10.3390/app11073205

Jia, X., Li, K., Li, X., and Zhang, A. (2014). A novel semi-supervised deep learning framework for affective state recognition on eeg signals. *IEEE Int. Conf. Bioinformatics Bioeng.*, 30–37. doi: 10.1109/BIBE.2014.26

Jiang, X., Bian, G.-B., and Tian, Z. (2019). Removal of artifacts from EEG signals: a review. *Sensors* 19:987. doi: 10.3390/s19050987

Jobert, M., Wilson, F. J., Ruigt, G. S., Brunovsky, M., Prichep, L. S., Drinkenburg, W. H., et al. (2012). Guidelines for the recording and evaluation of pharmaco-EEG data in man: the international Pharmaco-EEG society (IPEG). *Neuropsychobiology* 66, 201–220. doi: 10.1159/000343478

Johannes, C. B., Le, T. K., Zhou, X., Johnston, J. A., and Dworkin, R. H. (2010). The prevalence of chronic pain in United States adults: results of an internet-based survey. *J. Pain* 11, 1230–1239. doi: 10.1016/j.jpain.2010.07.002

Katsigiannis, S., and Ramzan, N. (2017). DREAMER: a database for emotion recognition through EEG and ECG signals from wireless low-cost off-the-shelf devices. *IEEE J. Biomedical. Health Inform.* 22, 98–107. doi: 10.1109/JBHI.2017.2688239

Kehlet, H., Jensen, T. S., and Woolf, C. J. (2006). Persistent postsurgical pain: risk factors and prevention. *Lancet* 367, 1618–1625. doi: 10.1016/S0140-6736(06)68700-X

Khanna, A., Pascual-Leone, A., Michel, C. M., and Farzan, F. (2015). Microstates in resting-state EEG: current status and future directions. *Neurosci. Biobehav. Rev.* 49, 105–113. doi: 10.1016/j.neubiorev.2014.12.010

Kimura, A., Mitsukura, Y., Oya, A., Matsumoto, M., Nakamura, M., Kanaji, A., et al. (2021). Objective characterization of hip pain levels during walking by combining quantitative electroencephalography with machine learning. *Sci. Rep.* 11, 1–10. doi: 10.1038/s41598-021-82696-1

Kinnealey, M., and Fuiek, M. (1999). The relationship between sensory defensiveness, anxiety, depression and perception of pain in adults. *Occup. Ther. Int.* 6, 195–206. doi: 10.1002/oti.97

Kragel, P. A., Koban, L., Barrett, L. F., and Wager, T. D. (2018). Representation, pattern information, and brain signatures: from neurons to neuroimaging. *Neuron* 99, 257–273. doi: 10.1016/j.neuron.2018.06.009

Krigolson, O. E., Williams, C. C., Norton, A., Hassall, C. D., and Colino, F. L. (2017). Choosing MUSE: validation of a low-cost, portable EEG system for ERP research. *Front. Neurosci.* 11:109. doi: 10.3389/fnins.2017.00109

Kucyi, A., and Davis, K. D. (2015). The dynamic pain connectome. Trends. *Neurosciences* 38, 86–95. doi: 10.1016/j.tins.2014.11.006

Ladha, K. S., Patorno, E., Huybrechts, K. F., Liu, J., Rathmell, J. P., and Bateman, B. T. (2016). Variations in the use of perioperative multimodal analgesic therapy. *Anesthesiology* 124, 837–845. doi: 10.1097/ALN.0000000000001034

Lamichhane, B., Jayasekera, D., Jakes, R., Glasser, M. F., Zhang, J., Yang, C., et al. (2021). Multi-modal biomarkers of low back pain: a machine learning approach. *Neuroimage Clin.* 29:102530. doi: 10.1016/j.nicl.2020.102530

Lancaster, J., Mano, H., Callan, D., Kawato, M., and Seymour, B. (2017). Decoding acute pain with combined EEG and physiological data. *IEEE Int. Conf. Neural. Eng.*, 521–524. doi: 10.1109/NER.2017.8008404

Le Pera, D., Svensson, P., Valeriani, M., Watanabe, I., Arendt-Nielsen, L., and Chen, A. C. (2000). Long-lasting effect evoked by tonic muscle pain on parietal EEG activity in humans. *Clin. Neurophysiol.* 111, 2130–2137. doi: 10.1016/s1388-2457(00)00474-0

Lee, C. H., Kim, H. S., Kim, Y.-S., Jung, S., Yoon, C. H., and Kwon, O.-Y. (2021). Cerebral current-source distribution associated with pain improvement by non-invasive painless signaling therapy in patients with failed back surgery syndrome. *Korean J. Pain.* 34, 437–446. doi: 10.3344/kjp.2021.34.4.437

Lendaro, E., Balouji, E., Baca, K., Muhammad, A. S., and Ortiz-Catalan, M. (2021). Common spatial pattern EEG decomposition for phantom limb pain detection. *Ann. Int. Conf. IEEE Eng. Med. Biol. Soc.* 2021, 726–729. doi: 10.1109/EMBC46164.2021.9630561

Levitt, J., Edhi, M. M., Thorpe, R. V., Leung, J. W., Michishita, M., Koyama, S., et al. (2020). Pain phenotypes classified by machine learning using electroencephalography features. *NeuroImage* 223:117256. doi: 10.1016/j.neuroimage.2020.117256

Levitt, J., and Saab, C. Y. (2019). What does a pain 'biomarker'mean and can a machine be taught to measure pain? *Neurosci. Lett.* 702, 40–43. doi: 10.1016/j.neulet.2018.11.038

Liberati, G., Klöcker, A., Algoet, M., Mulders, D., Maia Safronova, M., Ferrao Santos, S., et al. (2018). Gamma-band oscillations preferential for nociception can be recorded in the human insula. *Cereb. Cortex* 28, 3650–3664. doi: 10.1093/cercor/bhx237

Liberati, G., Mulders, D., Algoet, M., van den Broeke, E. N., Santos, S. F., Ribeiro Vaz, J. G., et al. (2020). Insular responses to transient painful and non-painful thermal and mechanical spinothalamic stimuli recorded using intracerebral EEG. *Sci. Rep.* 10:22319. doi: 10.1038/s41598-020-79371-2

Liu, C., Chien, J., Chang, Y., Kim, J., Anderson, W., and Lenz, F. (2015). Functional role of induced gamma oscillatory responses in processing noxious and innocuous sensory events in humans. *Neuroscience* 310, 389–400. doi: 10.1016/j.neuroscience.2015.09.047

Logothetis, N. K. (2008). What we can do and what we cannot do with fMRI. *Nature* 453, 869–878. doi: 10.1038/nature06976

Lötsch, J., Ultsch, A., and Kalso, E. (2017). Prediction of persistent post-surgery pain by preoperative cold pain sensitivity: biomarker development with machine-learning-derived analysis. BJA. *Br. J. Anaesth.* 119, 821–829. doi: 10.1093/bja/aex236

Lu, H., Eng, H.-L., Guan, C., Plataniotis, K. N., and Venetsanopoulos, A. N. (2010). Regularized common spatial pattern with aggregation for EEG classification in small-sample setting. *IEEE Trans. Biomed. Eng.* 57, 2936–2946. doi: 10.1109/TBME.2010.2082540

Mari, T., Henderson, J., Maden, M., Nevitt, S., Duarte, R., and Fallon, N. (2022). Systematic review of the effectiveness of machine learning algorithms for classifying pain intensity, phenotype or treatment outcomes using electroencephalogram data. *J. Pain.* doi: 10.1016/j.jpain.2021.07.011

Martel, M., Harvey, M.-P., Houde, F., Balg, F., Goffaux, P., and Léonard, G. (2017). Unravelling the effect of experimental pain on the corticomotor system using transcranial magnetic stimulation and electroencephalography. *Exp. Brain Res.* 235, 1223–1231. doi: 10.1007/s00221-017-4880-0

Martín-Brufau, R., Gómez, M. N., Sanchez-Sanchez-Rojas, L., and Nombela, C. (2021). Fibromyalgia detection based on EEG connectivity patterns. *J. Clin. Med.* 10:3277. doi: 10.3390/jcm10153277

Matsangidou, M., Liampas, A., Pittara, M., Pattichi, C. S., and Zis, P. (2021). Machine learning in pain medicine: an up-to-date systematic review. *Pain Ther.*, 10, 1067–1084. doi: 10.1007/s40122-021-00324-2

May, E. S., Ávila, C. G., Dinh, S. T., Heitmann, H., Hohn, V. D., Nickel, M. M., et al. (2021). Dynamics of brain function in patients with chronic pain assessed by microstate analysis of resting-state electroencephalography. *Pain* 162:2894. doi: 10.1097/j.pain.0000000000002281

May, E. S., Nickel, M. M., Ta Dinh, S., Tiemann, L., Heitmann, H., Voth, I., et al. (2019). Prefrontal gamma oscillations reflect ongoing pain intensity in chronic back pain patients. *Hum. Brain Mapp.* 40, 293–305. doi: 10.1002/hbm.24373

Mendonça-de-Souza, M., Monteiro, U. M., Bezerra, A. S., Silva-de-Oliveira, A. P., Ventura-da-Silva, B. R., Barbosa, M. S., et al. (2012). Resilience in migraine brains: decrease of coherence after photic stimulation. *Front. Hum. Neurosci.* 6:207. doi: 10.3389/fnhum.2012.00207

Meneses, F. M., Queirós, F. C., Montoya, P., Miranda, J. G., Dubois-Mendes, S. M., Sá, K. N., et al. (2016). Patients with rheumatoid arthritis and chronic pain display enhanced alpha power density at rest. *Front. Hum. Neurosci.* 10:395. doi: 10.3389/fnhum.2016.00395

Merk, T., Peterson, V., Köhler, R., Haufe, S., Richardson, R. M., and Neumann, W.-J. (2022). Machine learning based brain signal decoding for intelligent adaptive deep brain stimulation. *Exp. Neurol.*:113993. doi: 10.1016/j.expneurol.2022

Michel, C. M., and Brunet, D. (2019). EEG source imaging: a practical review of the analysis steps. *Front. Neurol.* 10:325. doi: 10.3389/fneur.2019.00325

Millard, S. K., Furman, A. J., Kerr, A., Seminowicz, D. A., Gao, F., Naidu, B. V., et al. (2022). Predicting postoperative pain in lung cancer patients using preoperative peak alpha frequency. *Br. J. Anaesth.* 128, e346–e348. doi: 10.1016/j.bja.2022.03.006

Misra, G., Wang, W., Archer, D. B., Roy, A., and Coombes, S. A. (2017). Automated classification of pain perception using high-density electroencephalography data. *J. Neurophysiol.* 117, 786–795. doi: 10.1152/jn.00650.2016

Mokhtari, T., Tu, Y., and Hu, L. (2019). Involvement of the hippocampus in chronic pain and depression. *Brain Sci. Adv.* 5, 288–298. doi: 10.26599/BSA.2019.90500

Morton, D. L., Sandhu, J. S., and Jones, A. K. (2016). Brain imaging of pain: state of the art. *J. Pain Res.* 9:613. doi: 10.2147/JPR.S60433

Mouraux, A., and Iannetti, G. D. (2018). The search for pain biomarkers in the human brain. *Brain* 141, 3290–3307. doi: 10.1093/brain/awy281

Müller, K.-R., Tangermann, M., Dornhege, G., Krauledat, M., Curio, G., and Blankertz, B. (2008). Machine learning for real-time single-trial EEG-analysis: from brain–computer interfacing to mental state monitoring. *J. Neurosci. Methods* 167, 82–90. doi: 10.1016/j.jneumeth.2007.09.022

Mussigmann, T., Bardel, B., and Lefaucheur, J.-P. (2022). Resting-state electroencephalography (EEG) biomarkers of chronic neuropathic pain. A systematic review. *NeuroImage*:119351. doi: 10.1016/j.neuroimage.2022.119351

Navarro López, J., Moral Bergós, R., and Marijuán, P. C. (2015). Significant new quantitative EGG patterns in fibromyalgia. *Eur. J. Psychiat.* 29, 277–292. doi: 10.4321/S0213-61632015000400005

Necka, E. A., Lee, I.-S., Kucyi, A., Cheng, J. C., Yu, Q., and Atlas, L. Y. (2019). Applications of dynamic functional connectivity to pain and its modulation. *Pain Rep.*:4:e752. doi: 10.1097/PR9.0000000000000752

Nickel, M. M., May, E. S., Tiemann, L., Postorino, M., Dinh, S. T., and Ploner, M. (2017). Autonomic responses to tonic pain are more closely related to stimulus intensity than to pain intensity. *Pain* 158, 2129–2136. doi: 10.1097/j.pain.0000000000001010

Nurse, E., Mashford, B. S., Yepes, A. J., Kiral-Kornek, I., Harrer, S., and Freestone, D. R. (2016). Decoding EEG and LFP signals using deep learning: heading TrueNorth. *ACM Int. Conf. Comut. Front.*, 259–266. doi: 10.1145/2903150.2903159

Olejarczyk, E., Marzetti, L., Pizzella, V., and Zappasodi, F. (2017). Comparison of connectivity analyses for resting state EEG data. *J. Neural Eng.* 14:036017. doi: 10.1088/1741-2552/aa6401

Parker, T., Raghu, A., Huang, Y., Gillies, M. J., FitzGerald, J. J., Aziz, T., et al. (2021). Paired acute invasive/non-invasive stimulation (PAINS) study: a phase I/II randomized, sham-controlled crossover trial in chronic neuropathic pain. *Brain Stimul.* 14, 1576–1585. doi: 10.1016/j.brs.2021.10.384

Patel, K., Henshaw, J., Sutherland, H., Taylor, J. R., Casson, A. J., Lopez-Diaz, K., et al. (2021). Using EEG alpha states to understand learning during alpha neurofeedback training for chronic pain. *Front. Neurosci.* 14:620666. doi: 10.3389/fnins.2020.620666

Pedroni, A., Bahreini, A., and Langer, N. (2019). Automagic: standardized preprocessing of big EEG data. *NeuroImage* 200, 460–473. doi: 10.1016/j.neuroimage.2019.06.046

Peng, W., and Tang, D. (2016). Pain related cortical oscillations: methodological advances and potential applications. *Front. Comput. Neurosci.* 10:9. doi: 10.3389/fncom.2016.00009

Perl, E. R. (2007). Ideas about pain, a historical view. *Nat. Rev. Neurosci.* 8, 71–80. doi: 10.1038/nrn2042

Peyron, R., Frot, M., Schneider, F., Garcia-Larrea, L., Mertens, P., Barral, F.-G., et al. (2002). Role of operculoinsular cortices in human pain processing: converging evidence from PET, fMRI, dipole modeling, and intracerebral recordings of evoked potentials. *NeuroImage* 17, 1336–1346. doi: 10.1006/nimg.2002.1315

Pfurtscheller, G. (2001). Functional brain imaging based on ERD/ERS. *Vision Res* 41:125760. doi: 10.1016/s0042-6989(00)00235-2

Pinheiro, E. S. D. S., Queirós, F. C. D., Montoya, P., Santos, C. L., Nascimento, M. A. D., Ito, C. H., et al. (2016). Electroencephalographic patterns in chronic pain: a systematic review of the literature. *PLoS One* 11:e0149085. doi: 10.1371/journal.pone.0149085

Plaghki, L., and Mouraux, A. (2005). EEG and laser stimulation as tools for pain research. *Curr. Opin. Investig. Drugs* 6, 58–64.

Ploner, M., Sorg, C., and Gross, J. (2017). Brain rhythms of pain. *Trends Cogn. Sci.* 21, 100–110. doi: 10.1016/j.tics.2016.12.001

Power, J. D., Plitt, M., Laumann, T. O., and Martin, A. (2017). Sources and implications of whole-brain fMRI signals in humans. *NeuroImage* 146, 609–625. doi: 10.1016/j.neuroimage.2016.09.038

Price, D. D. (2000). Psychological and neural mechanisms of the affective dimension of pain. *Science* 288, 1769–1772. doi: 10.1126/science.288.5472.1769

Prichep, L. S., Shah, J., Merkin, H., and Hiesiger, E. M. (2018). Exploration of the pathophysiology of chronic pain using quantitative EEG source localization. *Clin. EEG Neurosci.* 49, 103–113. doi: 10.1177/1550059417736444

Prinsloo, S., Novy, D., Driver, L., Lyle, R., Ramondetta, L., Eng, C., et al. (2017). Randomized controlled trial of neurofeedback on chemotherapy-induced peripheral neuropathy: a pilot study. *Cancer* 123, 1989–1997. doi: 10.1002/cncr.30649

Pu, L., Lion, K. M., Todorovic, M., and Moyle, W. (2021). Portable EEG monitoring for older adults with dementia and chronic pain - a feasibility study. *Geriatr. Nurs.* 42, 124–128. doi: 10.1016/j.gerinurse.2020.12.008

Quiton, R. L., and Greenspan, J. D. (2008). Across-and within-session variability of ratings of painful contact heat stimuli. *Pain* 137, 245–256. doi: 10.1016/j.pain.2007.08.034

Rainville, P., Duncan, G. H., Price, D. D., Carrier, B., and Bushnell, M. C. (1997). Pain affect encoded in human anterior cingulate but not somatosensory cortex. *Science* 277, 968–971. doi: 10.1126/science.277.5328.968

Reckziegel, D., Vachon-Presseau, E., Petre, B., Schnitzer, T. J., Baliki, M., and Apkarian, A. V. (2019). Deconstructing biomarkers for chronic pain: context and hypothesis dependent biomarker types in relation to chronic pain. *Pain* 160:S37. doi: 10.1097/j.pain.0000000000001529

Riaz, F., Hassan, A., Rehman, S., Niazi, I. K., and Dremstrup, K. (2015). EMD-based temporal and spectral features for the classification of EEG signals using supervised learning. *IEEE Trans. Neural Syst. Rehabil. Eng.* 24, 28–35. doi: 10.1109/TNSRE.2015.2441835

Rosa, M. J., and Seymour, B. (2014). Decoding the matrix: benefits and limitations of applying machine learning algorithms to pain neuroimaging. *Pain* 155, 864–867. doi: 10.1016/j.pain.2014.02.013

Rouleau, R. D., Lagrandeur, L., Daigle, K., Lorrain, D., Léonard, G., Whittingstall, K., et al. (2015). Significance of non-phase locked oscillatory brain activity in response to noxious stimuli. *Can. J. Neurol. Sci.* 42, 436–443. doi: 10.1017/cjn.2015.294

Sakkalis, V. (2011). Review of advanced techniques for the estimation of brain connectivity measured with EEG/MEG. *Comput. Biol. Med.* 41, 1110–1117. doi: 10.1016/j.compbiomed.2011.06.020

Santana, J. E. R., Baptista, A. F., Lucena, R., Lopes, T. D. S., do Rosário, R. S., Xavier, M. R., et al. (2021). Altered dynamic brain connectivity in individuals with sickle cell disease and chronic pain secondary to hip osteonecrosis. *Clin. EEG Neurosci.*:15500594211054297. doi: 10.1177/15500594211054297

Sawamoto, N., Honda, M., Okada, T., Hanakawa, T., Kanda, M., Fukuyama, H., et al. (2000). Expectation of pain enhances responses to nonpainful somatosensory stimulation in the anterior cingulate cortex and parietal operculum/posterior insula: an event-related functional magnetic resonance imaging study. *J. Neurosci.* 20, 7438–7445. doi: 10.1523/JNEUROSCI.20-19-07438.2000

Schmidt, S., Gmeiner, S., Schultz, C., Löwer, M., Kuhn, K., Naranjo, J. R., et al. (2015). Mindfulness-based stress reduction (MBSR) as treatment for chronic back pain-an observational study with assessment of thalamocortical dysrhythmia. *Complement. Med. Res.* 22, 298–303. doi: 10.1159/000440687

Schmidt, S., Naranjo, J. R., Brenneisen, C., Gundlach, J., Schultz, C., Kaube, H., et al. (2012). Pain ratings, psychological functioning and quantitative EEG in a controlled study of chronic back pain patients. *PLoS One* 7:e31138. doi: 10.1371/journal.pone.0031138

Schoffelen, J. M., and Gross, J. (2009). Source connectivity analysis with MEG and EEG. *Hum. Brain Mapp.* 30, 1857–1865. doi: 10.1002/hbm.20745

Schouppe, S., Van Oosterwijck, S., Danneels, L., Van Damme, S., and Van Oosterwijck, J. (2020). Are functional brain alterations present in low back pain? A systematic review of EEG studies. *J. Pain* 21, 25–43. doi: 10.1016/j.jpain.2019.06.010

Schuchat, A., Houry, D., and Guy, G. P. (2017). New data on opioid use and prescribing in the United States. *JAMA* 318, 425–426. doi: 10.1001/jama.2017.8913

Schulz, E., May, E. S., Postorino, M., Tiemann, L., Nickel, M. M., Witkovsky, V., et al. (2015). Prefrontal gamma oscillations encode tonic pain in humans. *Cereb. Cortex* 25, 4407–4414. doi: 10.1093/cercor/bhv043

Schulz, E., Tiemann, L., Witkovsky, V., Schmidt, P., and Ploner, M. (2012a). Gamma oscillations are involved in the sensorimotor transformation of pain. *J. Neurophysiol.* 108, 1025–1031. doi: 10.1152/jn.00186.2012

Schulz, E., Zherdin, A., Tiemann, L., Plant, C., and Ploner, M. (2012b). Decoding an individual's sensitivity to pain from the multivariate analysis of EEG data. *Cereb. Cortex* 22, 1118–1123. doi: 10.1093/cercor/bhr186

Seeber, M., Cantonas, L.-M., Hoevels, M., Sesia, T., Visser-Vandewalle, V., and Michel, C. M. (2019). Subcortical electrophysiological activity is detectable with high-density EEG source imaging. *Nat. Commun.* 10:753. doi: 10.1038/s41467-019-08725-w

Seminowicz, D. A., Thapa, T., Furman, A. J., Summers, S. J., Cavaleri, R., Fogarty, J. S., et al. (2018). Slow peak alpha frequency and corticomotor depression linked to high pain susceptibility in transition to sustained pain. *BioRxiv*:278598. doi: 10.1101/278598

Seminowicz, D. A., Thapa, T., and Schabrun, S. M. (2019). Corticomotor depression is associated with higher pain severity in the transition to sustained pain: a longitudinal exploratory study of individual differences. *J. Pain* 20, 1498–1506. doi: 10.1016/j.jpain.2019.06.005

She, Q., Hu, B., Luo, Z., Nguyen, T., and Zhang, Y. (2019). A hierarchical semi-supervised extreme learning machine method for EEG recognition. *Med. Biol. Eng. Comput.* 57, 147–157. doi: 10.1007/s11517-018-1875-3

Siddiqi, S. H., Kording, K. P., Parvizi, J., and Fox, M. D. (2022). Causal mapping of human brain function. *Nat. Rev. Neurosci.* 23, 361–375. doi: 10.1038/s41583-022-00583-8

So, H. C. (2011). "source localization: algorithms and analysis" in *Handbook of position location: Theory, practice, and advances*. eds. S. A. Zekavat and M. R. Buehrer (Hoboken, Wiley), 25–66.

Sohrabpour, A., Ye, S., Worrell, G. A., Zhang, W., and He, B. (2016). Noninvasive electromagnetic source imaging and granger causality analysis: an electrophysiological connectome (eConnectome) approach. *IEEE Trans. Biomed. Eng.* 63, 2474–2487. doi: 10.1109/TBME.2016.2616474

Stern, J., Jeanmonod, D., and Sarnthein, J. (2006). Persistent EEG overactivation in the cortical pain matrix of neurogenic pain patients. *NeuroImage* 31, 721–731. doi: 10.1016/j.neuroimage.2005.12.042

Su, Q., Song, Y., Zhao, R., and Liang, M. (2019). A review on the ongoing quest for a pain signature in the human brain. *Brain Sci. Adv.* 5, 274–287. doi: 10.26599/BSA.2019.9050024

Sufianov, A., Shapkin, A., Sufianova, G., Elishev, V., Barashin, D., Berdichevskii, V., et al. (2014). Functional and metabolic changes in the brain in neuropathic pain syndrome against the background of chronic epidural electrostimulation of the spinal cord. *Bull. Exp. Biol. Med.* 157, 462–465. doi: 10.1007/s10517-014-2591-0

Sun, G., Wen, Z., Ok, D., Doan, L., Wang, J., and Chen, Z. S. (2021). Detecting acute pain signals from human EEG. *J. Neurosci. Methods* 347:108964. doi: 10.1016/j.jneumeth.2020.108964

Taesler, P., and Rose, M. (2016). Prestimulus theta oscillations and connectivity modulate pain perception. *J. Neurosci.* 36, 5026–5033. doi: 10.1523/JNEUROSCI.3325-15.2016

Tan, L. L., Oswald, M. J., and Kuner, R. (2021). Neurobiology of brain oscillations in acute and chronic pain. *Trends Neurosci.* 44, 629–642. doi: 10.1016/j.tins.2021.05.003

Teel, E. F., Ocay, D. D., Blain-Moraes, S., and Ferland, C. E. (2022). Accurate classification of pain experiences using wearable electroencephalography in adolescents with and without chronic musculoskeletal pain. *Front. Pain. Res.* 3:162. doi: 10.3389/fpain.2022.991793

Teixeira, M., Mancini, C., Wicht, C. A., Maestretti, G., Kuntzer, T., Cazzoli, D., et al. (2021). Beta electroencephalographic oscillation is a potential GABAergic biomarker of chronic peripheral neuropathic pain. *Front. Neurosci.* 15:594536. doi: 10.3389/fnins.2021.594536

Teixeira, P. E., Pacheco-Barrios, K., Uygur-Kucukseymen, E., Machado, R. M., Balbuena-Pareja, A., Giannoni-Luza, S., et al. (2022). Electroencephalography signatures for conditioned pain modulation and pain perception in nonspecific chronic low back pain—an exploratory study. *Pain Med.* 23, 558–570. doi: 10.1093/pm/pnab293

Telkes, L., Hancu, M., Paniccioli, S., Grey, R., Briotte, M., McCarthy, K., et al. (2020). Differences in EEG patterns between tonic and high frequency spinal cord stimulation in chronic pain patients. *Clin. Neurophysiol.* 131, 1731–1740. doi: 10.1016/j.clinph.2020.03.040

Teplan, M. (2002). Fundamentals of EEG measurement. *Meas. Sci. Rev.* 2, 1–11.

Thibaut, A., Russo, C., Hurtado-Puerto, A. M., Morales-Quezada, J. L., Deitos, A., Petrozza, J. C., et al. (2017). Effects of transcranial direct current stimulation, transcranial pulsed current stimulation, and their combination on brain oscillations in patients with chronic visceral pain: a pilot crossover randomized controlled study. *Front. Neurol.* 8:576. doi: 10.3389/fneur.2017.00576

Topaz, L. S., Frid, A., Granovsky, Y., Zubidat, R., Crystal, S., Buxbaum, C., et al. (2022). Electroencephalography functional connectivity—a biomarker for painful polyneuropathy. *Eur. J. Neurol.* doi: 10.1111/ene.15575

Tracey, I. (2021). Neuroimaging enters the pain biomarker arena. *Sci. Transl. Med.* 13:eabj7358. doi: 10.1126/scitranslmed.abj7358

Tracey, I., Woolf, C. J., and Andrews, N. A. (2019). Composite pain biomarker signatures for objective assessment and effective treatment. *Neuron* 101, 783–800. doi: 10.1016/j.neuron.2019.02.019

Tu, Y., Tan, A., Bai, Y., Hung, Y. S., and Zhang, Z. (2016). Decoding subjective intensity of nociceptive pain from pre-stimulus and post-stimulus brain activities. *Front. Comput. Neurosci.* 10:32. doi: 10.3389/fncom.2016.00032

Urigüen, J. A., and Garcia-Zapirain, B. (2015). EEG artifact removal—state-of-the-art and guidelines. *J. Neural Eng.* 12:031001. doi: 10.1088/1741-2560/12/3/031001

Uygur-Kucukseymen, E., Castelo-Branco, L., Pacheco-Barrios, K., Luna-Cuadros, M. A., Cardenas-Rojas, A., Giannoni-Luza, S., et al. (2020). Decreased neural inhibitory state in fibromyalgia pain: a cross-sectional study. *Neurophysiol. Clin.* 50, 279–288. doi: 10.1016/j.neucli.2020.06.002

Vachon-Presseau, E., Centeno, M., Ren, W., Berger, S., Tétreault, P., Ghantous, M., et al. (2016). The emotional brain as a predictor and amplifier of chronic pain. *J. Dent. Res.* 95, 605–612. doi: 10.1177/0022034516638027

van den Broeke, E. N., Wilder-Smith, O. H., van Goor, H., Vissers, K. C., and van Rijn, C. M. (2013). Patients with persistent pain after breast cancer treatment show enhanced alpha activity in spontaneous EEG. *Pain Med.* 14, 1893–1899. doi: 10.1111/pme.12216

Van Der Miesen, M. M., Lindquist, M. A., and Wager, T. D. (2019). Neuroimaging-based biomarkers for pain: state of the field and current directions. *Pain Rep* 4:e751. doi: 10.1097/PR9.0000000000000751

Vanneste, S., Song, J.-J., and De Ridder, D. (2018). Thalamocortical dysrhythmia detected by machine learning. *Nat. Commun.* 9, 1–13. doi: 10.1038/s41467-018-02820-0

Vierck, C. J., Whitsel, B. L., Favorov, O. V., Brown, A. W., and Tommerdahl, M. (2013). Role of primary somatosensory cortex in the coding of pain. *Pain* 154, 334–344. doi: 10.1016/j.pain.2012.10.021

Villafaina, S., Collado-Mateo, D., Fuentes-Garcia, J. P., Cano-Plasencia, R., and Gusi, N. (2019). Impact of fibromyalgia on alpha-2 EEG power spectrum in the resting condition: a descriptive correlational study. *Biomed. Res. Int.* 2019:7851047. doi: 10.1155/2019/7851047

von Hehn, C. A., Baron, R., and Woolf, C. J. (2012). Deconstructing the neuropathic pain phenotype to reveal neural mechanisms. *Neuron* 73, 638–652. doi: 10.1016/j.neuron.2012.02.008

Vuckovic, A., Gallardo, V. J. F., Jarjees, M., Fraser, M., and Purcell, M. (2018). Prediction of central neuropathic pain in spinal cord injury based on EEG classifier. *Clin. Neurophysiol.* 129, 1605–1617. doi: 10.1016/j.clinph.2018.04.750

Vuckovic, A., Hasan, M. A., Fraser, M., Conway, B. A., Nasseroleslami, B., and Allan, D. B. (2014). Dynamic oscillatory signatures of central neuropathic pain in spinal cord injury. *J. Pain* 15, 645–655. doi: 10.1016/j.jpain.2014.02.005

Vuckovic, A., Jarjees, M. S., Hasan, M. A., Purcell, M., and Fraser, M. (2022). "EEG biomarkers of pain and applications of machine learning" in *Spinal Cord Injury Pain*. eds. C. Sang and C. Hulsebosch (Amsterdam: Elsevier), 199–225.

Wager, T. D., Atlas, L. Y., Lindquist, M. A., Roy, M., Woo, C.-W., and Kross, E. (2013). An fMRI-based neurologic signature of physical pain. *N. Engl. J. Med.* 368, 1388–1397. doi: 10.1056/NEJMoa1204471

Wang, J., Li, D., Li, X., Liu, F.-Y., Xing, G.-G., Cai, J., et al. (2011). Phase–amplitude coupling between theta and gamma oscillations during nociception in rat electroencephalography. *Neurosci. Lett.* 499, 84–87. doi: 10.1016/j.neulet.2011.05.037

Wei, M., Liao, Y., Liu, J., Li, L., Huang, G., Huang, J., et al. (2022). EEG beta-band spectral entropy can predict the effect of drug treatment on pain in patients with herpes zoster. *J. Clin. Neurophysiol.* 39, 166–173. doi: 10.1097/WNP.0000000000000758

Woo, C.-W., Chang, L. J., Lindquist, M. A., and Wager, T. D. (2017). Building better biomarkers: brain models in translational neuroimaging. *Nat. Neurosci.* 20, 365–377. doi: 10.1038/nn.4478

Wu, W., Chen, Z., Gao, X., Li, Y., Brown, E. N., and Gao, S. (2014). Probabilistic common spatial patterns for multichannel EEG analysis. *IEEE Trans. Pattern Anal. Mach. Intell.* 37, 639–653. doi: 10.1109/TPAMI.2014.2330598

Xu, X., and Huang, Y. (2020). Objective pain assessment: a key for the management of chronic pain. *F1000Res* 9:F1000. doi: 10.12688/f1000research.20441.1

Yong, R. J., Mullins, P. M., and Bhattacharyya, N. (2022). Prevalence of chronic pain among adults in the United States. *Pain* 163, e328–e332. doi: 10.1097/j.pain.0000000000002291

Yüksel, M., Ayaş, Ş., Cabıoğlu, M. T., Yılmaz, D., and Cabıoğlu, C. (2019). Quantitative data for transcutaneous electrical nerve stimulation and acupuncture effectiveness in treatment of fibromyalgia syndrome. *Evid. Based Complement. Alternat. Med.* 2019:9684649. doi: 10.1155/2019/9684649. doi:10.1155/2019/9684649

Zebhauser, P. T., Hohn, V. D., and Ploner, M. (2023). Resting-state electroencephalography and magnetoencephalography as biomarkers of chronic pain: a systematic review. *Pain* 164, 1200–1221. doi: 10.1097/j.pain.0000000000002825

Zhang, Q., Manders, T., Tong, A. P., Yang, R., Garg, A., Martinez, E., et al. (2017). Chronic pain induces generalized enhancement of aversion. *elife* 6:e25302. doi: 10.7554/eLife.25302

Zhou, R., Wang, J., Qi, W., Liu, F.-Y., Yi, M., Guo, H., et al. (2018). Elevated resting state gamma oscillatory activities in electroencephalogram of patients with post-herpetic neuralgia. *Front. Neurosci.* 12:750. doi: 10.3389/fnins.2018.00750

Zimmer, Z., Fraser, K., Grol-Prokopczyk, H., and Zajacova, A. (2022). A global study of pain prevalence across 52 countries: examining the role of country-level contextual factors. *Pain* 163, 1740–1750. doi: 10.1097/j.pain.0000000000002557

Zis, P., Liampas, A., Artemiadis, A., Tsalamandris, G., Neophytou, P., Unwin, Z., et al. (2022). EEG recordings as biomarkers of pain perception: where do we stand and where to go? *Pain Ther.* 11, 369–380. doi: 10.1007/s40122-022-00372-2

Zolezzi, D. M., Alonso-Valerdi, L. M., Naal-Ruiz, N. E., and Ibarra-Zarate, D. (2021). Identification of Neuropathic Pain Severity Based on Linear and Non-Linear EEG Features. *Annu Int. Conf. IEEE Eng. Med. Biol. Soc. (EMBC)*, 169–173. doi: 10.1109/EMBC46164.2021.9630101

Zortea, M., Beltran, G., Alves, R. L., Vicuña, P., Torres, I. L., Fregni, F., et al. (2021). Spectral Power density analysis of the resting-state as a marker of the central effects of opioid use in fibromyalgia. *Sci. Reports* 11:22716. doi: 10.1038/s41598-021-01982-0

frontiers | Frontiers in Neuroscience

TYPE Original Research
PUBLISHED 02 October 2023
DOI 10.3389/fnins.2023.1219133



OPEN ACCESS

EDITED BY
David M. A. Mehler,
University Hospital RWTH Aachen, Germany

REVIEWED BY
Ge Shi,
University of California, Davis, United States
Caglar Uyulan,
Izmir Kâtip Çelebi University, Türkiye

*CORRESPONDENCE
Alexandra Reichenbach
✉ alexandra.reichenbach@hs-heilbronn.de

†These authors have contributed equally to this work and share first authorship

RECEIVED 08 May 2023
ACCEPTED 05 September 2023
PUBLISHED 02 October 2023

CITATION
Carrle FP, Hollenbenders Y and Reichenbach A (2023) Generation of synthetic EEG data for training algorithms supporting the diagnosis of major depressive disorder. *Front. Neurosci.* 17:1219133. doi: 10.3389/fnins.2023.1219133



# Generation of synthetic EEG data for training algorithms supporting the diagnosis of major depressive disorder

Friedrich Philipp Carrle[1,2†], Yasmin Hollenbenders[1,2†] and Alexandra Reichenbach[1,2*]

[1]Center for Machine Learning, Heilbronn University, Heilbronn, Germany, [2]Medical Faculty Heidelberg, University of Heidelberg, Heidelberg, Germany

**Introduction:** Major depressive disorder (MDD) is the most common mental disorder worldwide, leading to impairment in quality and independence of life. Electroencephalography (EEG) biomarkers processed with machine learning (ML) algorithms have been explored for objective diagnoses with promising results. However, the generalizability of those models, a prerequisite for clinical application, is restricted by small datasets. One approach to train ML models with good generalizability is complementing the original with synthetic data produced by generative algorithms. Another advantage of synthetic data is the possibility of publishing the data for other researchers without risking patient data privacy. Synthetic EEG time-series have not yet been generated for two clinical populations like MDD patients and healthy controls.

**Methods:** We first reviewed 27 studies presenting EEG data augmentation with generative algorithms for classification tasks, like diagnosis, for the possibilities and shortcomings of recent methods. The subsequent empirical study generated EEG time-series based on two public datasets with 30/28 and 24/29 subjects (MDD/controls). To obtain baseline diagnostic accuracies, convolutional neural networks (CNN) were trained with time-series from each dataset. The data were synthesized with generative adversarial networks (GAN) consisting of CNNs. We evaluated the synthetic data qualitatively and quantitatively and finally used it for re-training the diagnostic model.

**Results:** The reviewed studies improved their classification accuracies by between 1 and 40% with the synthetic data. Our own diagnostic accuracy improved up to 10% for one dataset but not significantly for the other. We found a rich repertoire of generative models in the reviewed literature, solving various technical issues. A major shortcoming in the field is the lack of meaningful evaluation metrics for synthetic data. The few studies analyzing the data in the frequency domain, including our own, show that only some features can be produced truthfully.

**Discussion:** The systematic review combined with our own investigation provides an overview of the available methods for generating EEG data for a classification task, their possibilities, and shortcomings. The approach is promising and the technical basis is set. For a broad application of these techniques in neuroscience research or clinical application, the methods need fine-tuning facilitated by domain expertise in (clinical) EEG research.

KEYWORDS

**major depressive disorder, electroencephalography, generative adversarial network, deep learning, data augmentation, synthetic data, biomarker, diagnosis**

## 1. Introduction

Major depressive disorder (MDD) is the most common mental disorder worldwide (World Health Organization, 2017) and characterized by episodes of mild to severe loss of motivation in various areas of life and cognitive deficits, leading to impairment in quality and independence of life (Otte et al., 2016). Even though systematic alterations in the affected organ, the brain, can be assessed quantitatively (Dev et al., 2022), MDD is routinely still diagnosed using interviews and questionnaires based on DSM-5 criteria (Bundesärztekammer (BÄK) et al., 2022). This approach is based on the patients' symptoms, leading to diagnosis only after severe symptoms have already manifested and usually at least one acute phase has already been suffered (Zhang X. et al., 2022). Early diagnosis, however, can help the patient to receive prevention and early treatment to soften the disorder's impact on the patient's life (Habert et al., 2016). Clinicians have started complementing their diagnostic repertoire with electroencephalography (EEG) recordings, but to date, they still need the expertise and time to judge these recordings visually (Mahato and Paul, 2019). Therapy success is monitored using the same methods, leading to delayed detection of ineffective treatment (Zhang X. et al., 2022). In order to increase the sensitivity and objectivity of an MDD diagnosis, biomarkers based on neuroimaging have been explored in the last decade (Yasin et al., 2021; Dev et al., 2022).

The development of biomarkers based on machine learning (ML) methods applied to EEG data is a promising approach with diagnostic accuracies ranging from 70 to 99% (Yasin et al., 2021). The task of diagnosing a patient is here usually formulated as a classification problem, separating patients from healthy control (HC) subjects based on the EEG data. However, the generalizability of the results, as a basic requirement for clinical application, is often restricted by small datasets, leading to overfitting and, therewith, overestimating the diagnostic capability (Rakić et al., 2020). This is a common problem in the application of ML to clinical use cases since ML algorithms need large and diverse datasets to produce generalizable results with high fidelity. In particular, the latest generation of algorithms with deep learning (DL) that are well suited for complex problems like detecting small and distributed disease-induced changes in high-dimensional data like EEG are very data-greedy (Cho et al., 2015). The collection of clinical data, especially with recordings that are not routinely produced such as EEG in MDD patients, is time consuming and expensive. Furthermore, strict privacy policies in most countries protect patient data and prevent data sharing. Therefore, clinical datasets tend to be rather small from an ML perspective and/or only accessible to few researchers. One approach to train machine learning models with small datasets but still attain good generalizability is complementing the original data with artificially produced data (Nikolenko, 2019), a process termed data augmentation (DA). Data can be augmented by simple methods, such as the addition of noise or domain specific distortions, or more complex methods, like generating synthetic data with generative ML algorithms (Talavera et al., 2022). An additional advantage of synthetic data obtained with generative models is the possibility of publishing the data for other researchers to use to train their diagnostic models without the risk of violating patient data privacy.

Algorithms suitable for generating synthetic data that have been applied successfully to the creation of EEG data are generative adversarial networks (GAN), generative pre-trained transformers (GPT), and variational autoencoders (VAE) (Lashgari et al., 2020; He et al., 2021). GANs comprise two neural networks, a generator producing synthetic data from random noise and a discriminator judging whether the presented data is real or synthetic (Goodfellow et al., 2014). The training process gradually shifts the distribution of data produced by the generator toward the distribution of the real data. GPTs are models adapted from language understanding and production that learn the structure of arbitrary sequences and then synthesize the next data point in this sequence, therewith generating increasingly longer continuous data step-by-step (Radford et al., 2018). VAEs consist of an encoder network compressing the data into a low dimensional distribution from which the decoder network draws samples and expands them into the original data space, therewith generating data preserving the structure of the original data (Kingma and Welling, 2014). Even though the generation of synthetic time-series EEG data has been demonstrated successfully (Hartmann et al., 2018), the application for the clinical use case of augmenting EEG data for two clinical populations, patients and HC subjects, with synthetic data in order to train a "diagnosis classifier" is still sparse. Song et al. (2021) synthesized features derived from EEG for Alzheimer's disease diagnosis with a GAN and demonstrated that they successfully generated data resembling patients and HC data distributions. Sobahi et al. (2022) constructed images from EEG features and created synthetic images with an extreme learning machine based autoencoder (ELM-AE). Augmenting the data with these images increased classification accuracy for schizophrenia diagnosis. Synthesizing time-series data from EEG directly has not yet been demonstrated for the clinical use case of a diagnosis classifier. However, this approach of generating the original data format from EEG for two clinical populations preserves most degrees of freedom for later data processing, e.g., for testing new biomarkers or publishing the data for further biomarker research.

In order to provide a comprehensive overview of current approaches for generating synthetic EEG data used for a classification task and an in-depth analysis of their advantages and potential pitfalls in a clinical use case, we first conducted a systematic review. In contrast to three previous reviews (Lashgari et al., 2020; He et al., 2021; Habashi et al., 2023), we focused on the clinical application of these methods rather than on the technical aspects. Therefore, we included studies that used all kinds of ML algorithms for classification instead of restricting the search to deep learning only. Most importantly, we focused on studies using generative methods only, i.e., creating truly synthetic data. This allowed for much deeper analyses of the methods specific to generative models and carves out the current shortcomings and next steps necessary specifically for the clinical use case of generating data for two or more clinical populations.

We conclude our work with an empirical study generating time-series EEG data for two clinical populations based on two publicly available datasets containing EEG data from MDD patients and HC (Mumtaz, 2016; Cai et al., 2020). For the generator and discriminator, we used convolutional neural networks (CNN) because of the complexity of the data. In order to improve the training stability of the discriminator, we adapted the Wasserstein GAN (WGAN) architecture (Arjovsky et al., 2017), frequently used for EEG data generation. In a WGAN, a *critic* minimizing the Wasserstein distance between real and

synthetic data replaces the discriminator. For the generation of two datasets, MDD patients and HC, we adopted the frequently used conditional approach (Mirza and Osindero, 2014). For this approach, both the generator and critic get the label of the data, i.e., whether the data originated from a patient or HC, and the critic makes its judgment conditioned on this label. In order to judge the quality of the data, we first evaluated the signal qualities of the synthetic data qualitatively and quantitatively. Subsequently, we evaluated its usefulness by augmenting the real data for a diagnosis classifier. We compared the performance of the classifiers trained on the real data alone with the performance when trained on different ratios between real and synthetic data. Directly comparing the results based on two publicly available datasets allowed us to make conclusions about the generalizability of the findings and enables reproducibility.

# 2. Materials and methods

## 2.1. Systematic review

### 2.1.1. Search strategy

We conducted a systematic review according to PRISMA guidelines (Liberati et al., 2009) in the databases PubMed and IEEE Xplore on 12 August 2022 (Figure 1). The two databases were chosen to cover medical as well as technical literature. Originally, we were only interested in the clinical use case of generating synthetic EEG data for patients and their healthy counterparts in order to train a "diagnosis classifier" on the data. However, such clinical use cases were too rare, with only two studies found in the first search round. Therefore, we included any study that synthesized EEG data for a classification task. This included within-subjects studies with healthy volunteers performing some kind of cognitive task as well. We adapted the syntax of the two search strings for the respective databases and joined the results. Search strings: (1) "data augmentation" AND EEG AND diagnosis AND (ADHD OR Alzheimer OR dementia OR depression); (2) "data augmentation" AND EEG – only in abstract. We included the other diagnoses in the first search string because EEG-based biomarkers are suggested for these diseases as well (Leiser et al., 2011). After the removal of duplicates and papers after abstract screening, we added further papers based on cross-referencing. For full text assessment, three inclusion criteria were used: (1) EEG data were used for a classification task, (2) EEG data or features derived from EEG data were subjected to data augmentation, and (3) the studies were original research papers; and three exclusion criteria were used: (1) the data augmentation method was not specified, (2) there was no generative method for data augmentation, or other data than EEG data was generated, and (3) papers not published in the English language.

### 2.1.2. Analysis

We aimed for a quantitative analysis of the aspects important for generating synthetic EEG data in a clinical use case. The **use case** *per se* informs whether the classification is conducted for a clinical purpose, about the paradigm used for data recording, and whether the experimental design was a within- or between-subjects design. A diagnosis classifier is always based on a between-subjects design. Regarding the input data, we needed to focus on the information specific for generating synthetic data. The **input/output** of the generator, i.e., whether it produces time-series or features and in which format, is reported in detail. However, the plethora of methodological details for EEG data recording and preprocessing is a general methodological issue when analyzing EEG data and would inflate the review. We, therefore, only comment on the breadth of methods here. The **generative model,** with its possible variants and their advantages and pitfalls, constitutes the core of the analysis. The next important item was the **evaluation** of the synthetic data with qualitative and quantitative methods. Finally, we investigated the **effect** of data augmentation on the original **classification task** with a special focus on the impact of the quantity of data generated.

## 2.2. Data augmentation

### 2.2.1. Data

Two publicly available datasets were used for the empirical study (Mumtaz, 2016; Cai et al., 2020). Separately processing the datasets provided the possibility of direct replication of the results and therewith an account on the robustness of the methods. Both datasets contained 5-min resting-state EEG time-series from HC and MDD patients with eyes closed (Table 1). All patients were diagnosed based on the DSM-IV manual.

For cleaning and preprocessing the EEG data, we used the Python toolbox *MNE* (Gramfort et al., 2014). To match the two datasets more closely, only the intersections of electrodes from both datasets were chosen, resulting in 13 channels: the frontal electrodes Fp1/2, F3/4, F7/8, and Fz, the central electrodes C3/4, parietal P3/4, and occipital O1/2. Both datasets were re-referenced to average (Yao et al., 2019). Preprocessing proceeded with band pass filtering (1 to 40 Hz) and automatic artifact removal with ICLabel (Li et al., 2022). One patient from dataset 2 was excluded because EEG was only recorded for 3 min. Both datasets were subsampled to the smaller class, with 24 and 28 subjects for each class, respectively.

Data were $z$-normalized per subject and channel separately. The time-series were then split into 8 s windows and outlier windows were removed. Any window with minimum or maximum values below or above 2* standard deviation of the average minimum or maximum values, respectively, was regarded as an outlier. The data of each window were then normalized between −1 and 1. The data resulting from the preprocessing are termed *real data* in the remainder of the article.

For dataset 1, the data frames used for both the classification and as input for the generative model were 2D matrices consisting of 13 (channels) rows and 250 (Hz) * 8 (s) = 2,000 columns. For dataset 2, respectively, the matrices had the shape (13, 256*8). For data generation, we used all available windows from the subjects to maximize the sample data. For the classification, we subsampled the number of windows to the respective smallest numbers of windows available, resulting in 18 windows per subject for dataset 1 and 16 windows for dataset 2. The channels were ordered based on head topology with the left hemisphere electrodes first (Fp1, F3, C3, P3, O1, and F7), then the central (Fz), and finally the corresponding right ones (Fp2, F4, C4, P4, O2, and F8).

### 2.2.2. Data generation

The baseline for data augmentation not using generative methods was obtained with **noise addition** (Yang et al., 2023), the simplest and

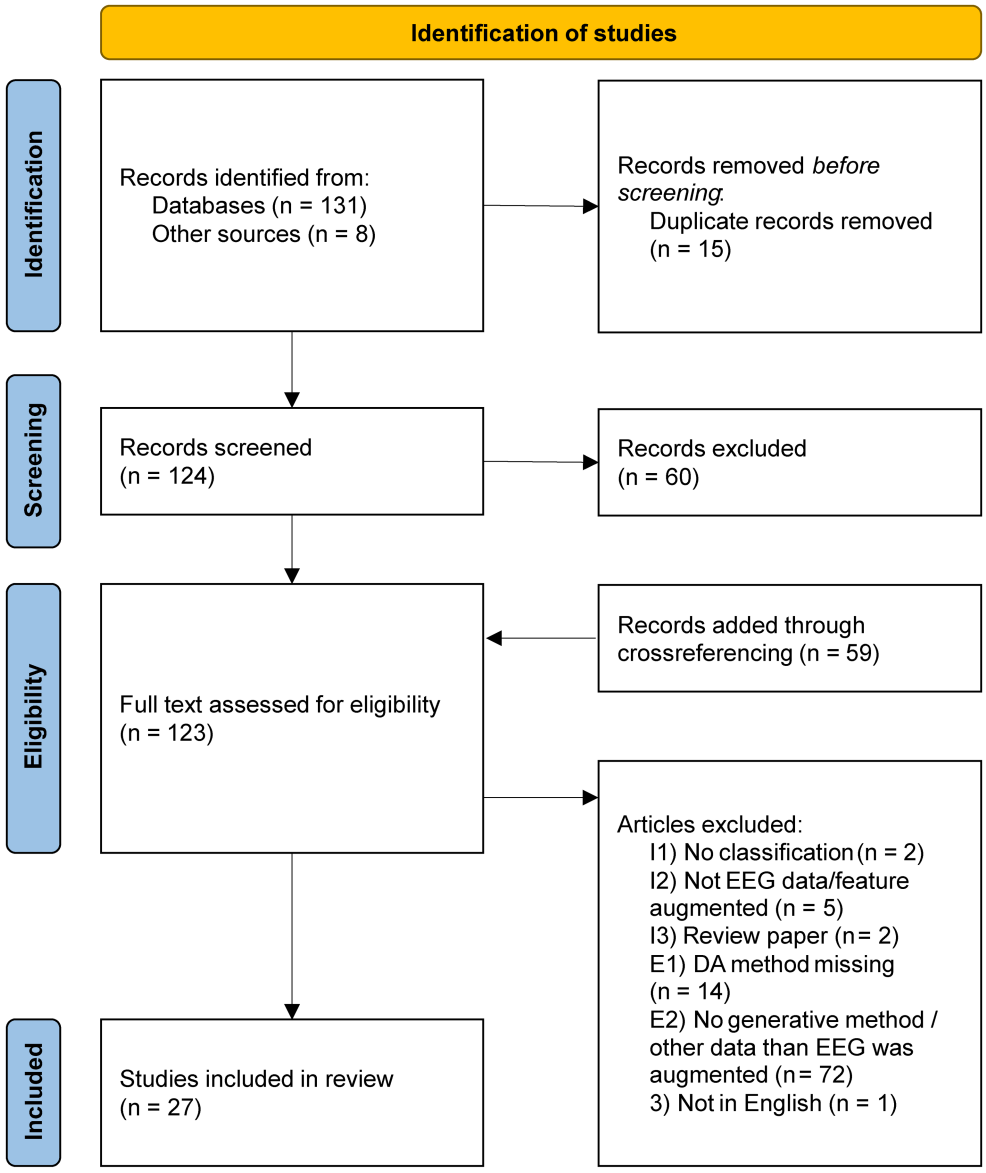


FIGURE 1
PRISMA flowchart for the paper search and selection process.

most frequently used method for generating artificial EEG data without a generative approach (Lashgari et al., 2020). We added uniform noise between −0.1 and + 0.1, corresponding to 10% of the normalized original signal amplitude, to the preprocessed time-series signal. After noise addition, the data was again normalized between −1 and 1. The data resulting from this procedure are termed *noise data* in the remainder of the paper.

The **generative method** for creating the *synthetic data* was a conditional Wasserstein GAN with a generator and critic consisting of CNNs loosely adapted from the work of Panwar et al. (2019, 2020) and optimized for our use case (for the detailed architectures, *cf.* Appendix Tables A1, A2). The generator input was a latent vector of size 100 initialized from a standard normal distribution. The input was reshaped to represent the channels in one and discrete sample times in the other dimension. The generator had four transposed convolutional layers that upsample and resize and one convolutional layer that only resizes the input. In between those layers, Leaky Rectified Linear Unit (ReLU) activation and batch normalization were used. The final output had the same shape as the real data. The activation function in the last layer was the hyperbolic tangent to obtain values ranging from −1 to 1 analog to the real data.

The input layer of the critic had the same shape as the real data and the generator output. Before it was downsampled, a Gaussian noise layer augmented the real and synthetic data to prevent the critic from memorizing the real data, which is likely to happen for small datasets (Zhao et al., 2020). Afterward, the critic reduced the dimension of the input data with two convolutional layers featuring strides of (2, 2) and a third convolutional layer featuring a stride of (1, 2). In between those layers, Leaky ReLU activation was used. The final two layers were a dropout layer to prevent overfitting (Lee and Lee, 2020) and a dense layer with linear activation returning the critic score. The Wasserstein distance was used as a loss

TABLE 1 Characteristics of the two publicly available datasets used for data augmentation.

| | Dataset 1 (Cai et al., 2020) | Dataset 2 (Mumtaz, 2016) |
|---|---|---|
| # Subjects in dataset / after preprocessing | HC: 29/24<br>MDD: 24 | HC: 28<br>MDD: 30/28 |
| Medication | No | Unknown |
| Age [years] mean ± std | HC: 31.5 ± 9.2<br>MDD: 30.9 ± 10.4 | HC: 38.2 ± 15.6<br>MDD: 40.3 ± 12.9 |
| Location | Gansu Provincial Key Laboratory of Wearable Computing<br>Lanzhou University, China | Hospital Universiti Sains Malaysia (HUSM)<br>Malaysia |
| # Electrodes | 128 | 19 |
| Electrode referencing | Cz-referenced | Linked-ear-referenced |
| Sample frequency | 250 Hz | 256 Hz |

TABLE 2 Number of data frames used for each fold of the classifiers.

| | Dataset 1 | | Dataset 2 | |
|---|---|---|---|---|
| | Train data | Test data | Train data | Test data |
| Real data | 13 × 46 × 18 | 13 × 2 × 18 | 13 × 54 × 16 | 13 × 2 × 16 |
| Noise data or synthetic data | 13 × 46 × 18 | 13 × 2 × 18 | 13 × 54 × 16 | 13 × 2 × 16 |
| 50% real + 50% noise/synt | 13 × (23 + 23) × 18 | 13 × 2 × 18 | 13 × (27 + 27) × 16 | 13 × 2 × 16 |
| 100% real +100% noise/synt | 13 × (46 + 46) × 18 | 13 × 2 × 18 | 13 × (54 + 54) × 16 | 13 × 2 × 16 |
| 100% real +200% noise/synt | 13 × (46 + 92) × 18 | 13 × 2 × 18 | 13 × (54 + 108) × 16 | 13 × 2 × 16 |

The numbers result from number of electrodes (13) × 2*number of "subjects" × number of windows per "subject".

function (Rüschendorf, 1985) with weight clipping. For the optimizer, the Adam algorithm (Kingma and Ba, 2014) was chosen with a learning rate of 0.0005, $\beta1 = 0.0$, $\beta2 = 0.999$, and $\varepsilon = 10-7$ (Hartmann et al., 2018). During training of the generator and critic, the latter was trained for five iterations for each iteration of the generator, as proposed in the original Wasserstein paper (Arjovsky et al., 2017). This helps the critic to detect poorly augmented data more easily.

### 2.2.3. Diagnosis/classification

For classification of the real data and evaluation of the augmented data, the preprocessed and/or generated EEG time-series windows were subjected to a CNN with an architecture adapted from *DeprNet* (Seal et al., 2021). The network consists of five convolutional, max-pooling, and batch normalization layers each, followed by three fully connected layers. *DeprNet* was optimized for the diagnosis of MDD from time-series EEG data and can therefore be utilized with only small modifications to accommodate the difference in number of channels, window size, and sample frequency. For the last fully connected layer, we implemented a sigmoid activation function because pretests yielded better results than the original softmax function. The initial parameters for *DeprNet* were chosen based on the values from the original study: binary cross entropy as loss function; Adam optimizer (Kingma and Ba, 2014) with learning rate 0.0005, $\beta1 = 0.9$, $\beta2 = 0.999$, and $\varepsilon = 10–7$; classification accuracy as evaluation metric. The classification accuracies with their confidence estimated were obtained with leave-two-subjects-out cross-validation, i.e., each test fold included one HC and one MDD. This procedure resulted in subject-wise cross-validation (Saeb et al., 2017).

### 2.2.4. Evaluation of the synthetic data

First, generated time-series data samples and their spectra were inspected visually. We chose the frontal electrodes as examples because abnormalities in frontal electrodes are frequently reported for MDD (Stewart et al., 2010). The exemplary single time-series from electrodes F3 and F4 served as the visual impression of the smoothness and form of the signal, while the mean time-series signals and their 95% confidence interval across subjects gave an impression of the general distribution of the continuous data over time. For the mean signals, we randomly chose one window from ten randomly chosen subjects and ten random synthetic data windows.

The frequency spectra based on the periodograms of the synthetic data reveal how well the generated signals resemble the real data in the frequency domain. Here, we only present mean and 95% confidence intervals across subjects because this data can be averaged meaningfully, resulting in an estimate of the population's spectrum. For each subject, we calculated the mean across all windows as a robust individual estimate and then matched the number of synthetic data frames with the number of subjects from each clinical group and dataset. For a quantitative assessment of commonalities and differences between spectra of real and synthetic data, we also present the averages of the commonly used frequency bands delta (0.3–4 Hz), theta (4–8 Hz), alpha (8–12 Hz), and beta (12–30 Hz). Analyses of variance (ANOVA) within datasets and frequency bands with between-subjects factors data type (real/synthetic) and diagnosis (HC/MDD) further qualify whether differences between real and synthetic data predominate or whether differences between diagnostic groups outweigh these.

Finally, the most important metric for the synthetic data was the performance of the classifier diagnosing either based on the synthetic data only or on combinations of real and synthetic data. Four classifiers were **trained** for both types of data augmentation, and all were **tested** on real data only (Table 2). Note that the first two classifiers with augmented data were trained on the same amount of data as the classifier trained on the real data only (Table 2, first row). The two remaining classifiers were trained on two or three times as much data, respectively.

The performance of the classifiers was compared using one-sided t-tests with $p = 0.05$, not corrected for multiple comparisons, considered significant. The classifiers trained on the synthetic data and the ones trained on the combination of real and synthetic data were expected to perform better than the classifiers based on the real data alone and better than the respective classifier trained on noise data. All reported results are mean values with 95% confidence intervals unless stated otherwise.

# 3. Results

## 3.1. Systematic review

The database search yielded 27 papers eligible for this review (Figure 1). The first paper appeared in 2018 (Hartmann et al., 2018).

### 3.1.1. Use case for classification and EEG paradigm

Only two studies reported the **clinical use case** of supporting the diagnosis of a psychiatric or neurodegenerative disease: diagnosing Alzheimer's disease (Song et al., 2021) or schizophrenia (Sobahi et al., 2022) (*cf.* Figure 2, violet and red segment in the outer ring). Five more studies in the clinical field (*cf.* Figure 2, red segment in the middle ring) revolved around epilepsy (*cf.* Figure 2, orange segments in the outer ring). Two studies aimed to detect an ongoing seizure or its onset (Haradal et al., 2018; Wei et al., 2019), two studies aimed to predict an upcoming seizure (Niu et al., 2021; Rasheed et al., 2021), and the last one aimed at detecting spikes occurring between seizures (Geng and Chen, 2021). Note that all five epilepsy studies had a within-subjects design, i.e., all patients contributed data for all classes.

The third and last **between-subjects study** used EEG data for identifying a person, i.e., biometric identification (Piplani et al., 2018) (*cf.* Figure 2, gray segment in the outer ring). This study and the remaining ones, using behavioral paradigms to elicit different cognitive states that were then classified, collected data from healthy subjects only (*cf.* Figure 2, dark blue segment in the middle ring).

The nature of the EEG time-series in the four studies utilizing the rapid serial visual presentation (RSVP) paradigm (Panwar et al., 2019, 2020; Xu et al., 2022; Zhang R. et al., 2022) (*cf.* Figure 2, light green segment in the outer ring) differed to most other EEG recordings in the reviewed studies with respect to the continuity in the signal. This was a **time locked paradigm** (*cf.* Figure 2, light green segment in the inner ring) assessing the P300 component of visual evoked potentials. The only other studies with time locked data were the epilepsy study for spike detection and two of the motor task studies (Abdelfattah et al., 2018; Fahimi et al., 2021) (*cf.* Figure 2, dark blue segment in the outer ring). The remaining study with a motor task recorded continuous EEG data during left hand movement vs. rest (Hartmann et al., 2018).

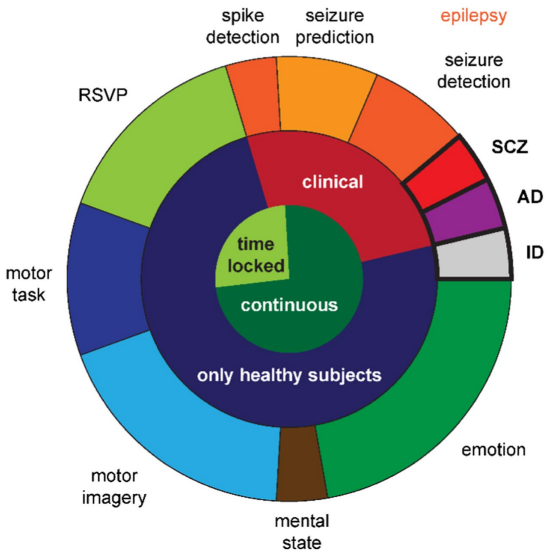


FIGURE 2
Distribution of use cases across studies. The inner circle denotes whether the EEG time-series is locked to an event or continuous. The middle ring denotes whether the classification serves a clinical purpose. The outer ring details the specific use cases with the between-subjects class designs emphasized with bold outlines and font. Note that the shades of orange further differentiate the epilepsy use cases into three types of classification goals. RSVP: rapid serial visual presentation; SCZ: schizophrenia; AD: Alzheimer's disease; ID: identification.

The remaining 12 studies generated data based on **continuous EEG data** (*cf.* Figure 2, dark green segment in the inner ring) during **cognitive tasks**. Bird et al. (2021) elicited the three mental states relaxed, neutral, and concentrated, which they later classified (*cf.* Figure 2, brown segment in the outer ring). The five studies in the field of motor imagery (Ko et al., 2019; Yang et al., 2019; Zhang et al., 2020, 2021; *cf.* Figure 2, light blue segment in the outer ring) all used public data provided for the brain–computer-interface (BCI) competitions (Sajda et al., 2003): BCI competition II dataset 3 with left and right hand movements (Schlögl et al., 1997) and BCI competition IV datasets 1 with two out of left hand, right hand, or foot movements (Blankertz et al., 2007), 2a with left and right hand, feet, and tongue movements (Naeem et al., 2006), and 2b with left and right hand movements (Leeb et al., 2007). From the six studies in the field of emotion recognition (*cf.* Figure 2, dark green segment in the outer ring), one recorded their own data with positive and negative emotions (Chang and Jun, 2019), while the remaining five (Luo and Lu, 2018; Luo et al., 2019, 2020; Pan and Zheng, 2021; Kalashami et al., 2022) used the publicly available datasets Database for Emotion Analysis using Physiological Signals (DEAP) with the two orthogonal dimensions valence and arousal, allowing for two different two-class classifiers or a four-class classifier (Koelstra et al., 2011), SJTU Emotion EEG Dataset (SEED) with positive, neutral, and negative emotions (Zheng and Lu, 2015), and SEED-V with the five emotions happiness, sadness, disgust, neutral, and fear (Liu et al., 2021).

Altogether, 18 studies used publicly available datasets and did not record their own data.

### 3.1.2. Input/output data

For recording and preprocessing EEG data, a wide variety of methods exists (Robbins et al., 2020). Since these differences are common to all EEG analyses and not just data synthetization, we only comment on the variety but refrain from analyzing them in depth in order to keep the review concise. Data were recorded from three to roughly 100 subjects using one to 256 EEG channels in different sampling frequencies. Common preprocessing steps included re-sampling, filtering, artifact removal, normalization, and splitting the EEG time-series into overlapping or non-overlapping windows.

The data format finally fed into the generative model equals the format of the generated data. The majority of studies ($n = 15$) used **time-series data**. Generating raw time-series provides the highest degree of freedom for processing the synthetic data afterward. Six studies used 2D matrices with time (samples) in the one dimension and location (channels) in the other dimension, similar to our study. Five further studies used 1D vectors in the time dimension: two studies used data from only one channel overall, two studies based on intracranial EEG used the time-series

independent of the recording electrode, and the last study modeled each channel independently. In the remaining four studies, we were not able to determine the detailed format of the input data. All seven studies with a time locked paradigm used time-series data; the remaining eight used continuous EEG like our study.

From the remaining studies, seven calculated **features** from the time-series used as 1D input vectors for data generation. The most common features were differential entropy (DE) and/or power spectral density (PSD) for delta (if possible), theta, alpha, beta, and gamma bands (n = 4). One study used the raw power spectrum and the remaining two utilized more complex sets of features that had been developed for previous studies. The study on Alzheimer's diagnosis (Song et al., 2021) belongs to the latter.

From the five studies that converted their time-series to **images**, the majority (n = 4) used time frequency representation (TFR), either one image per channel or channels stacked in the frequency domain. The remaining study was the one conducting the Schizophrenia diagnosis (Sobahi et al., 2022) and constructed an image from frequency features.

Due to conflicting information in the papers, there is some uncertainty in the assignment of two studies.

### 3.1.3. Generative model

The most popular model for generating synthetic EEG data for a classification task was by far the GAN ($n = 24$, Table 3). Only two studies adapted the GPT principle from language processing, and we found one autoencoder that was used in its own right and not just as comparison for a GAN-based approach. When several generative algorithms were compared in a study, we only extracted the one with the best result. For generating labeled data, i.e., distinct data for each class, five approaches were applied. The most popular was the conditioning of generator and discriminator with the class label ($n = 10$). The intuitive approach of simply generating the data of each class separately was adopted in seven studies. In six studies, the GAN was used for boosting the minority class, hence only the minority class was generated. The auxiliary discriminator that feeds the result of the data classification in generator and discriminator learning as well was used in three studies. The last study generated one distribution from all data and assigned class labels posthoc based on a classifier trained on the real data.

#### 3.1.3.1. Generative adversarial network

The first proposed architecture of a GAN (Goodfellow et al., 2014), often referred to as *Vanilla GAN*, comprises two multi-layer perceptrons (MLP), the generator and discriminator, competing against each other (*cf.* Figure 3). The generator transforms values $z$ randomly drawn from a standard normal distribution into synthetic data $G(z)$. The goal of the generator is to generate data the discriminator cannot distinguish from the real data $x$. With training, the discriminator maximizes its loss while the generator minimizes its loss using the Jensen–Shannon divergence between real and synthetic data distributions in the case of the Vanilla GAN.

Common variations of a GAN feature another network architecture for the generator and/or discriminator (*cf.* Table 3 and Figure 3 green rounded boxes). CNNs are a popular choice due to their hierarchical structure, successively combining groups of local data points, which resembles neural organization principles and makes them well suited for processing biological data (LeCun et al., 2015). When a CNN architecture is used, the input is often organized in two dimensions, and all studies feeding images into the GAN use CNNs (Figure 4). Note that the spatial neighborhood plays a critical role in CNN architectures since neighboring data points are combined *via* the convolution layers. The Vanilla GAN uses an MLP, and this architecture is still a popular choice. However, especially for this category, the detailed network architecture was often hard to determine, and we included a study in this category when the architecture was called a neural network or deep neural network (DNN), but the description did not sound like a CNN or recurrent neural network (RNN). Therefore, networks with one or more hidden layers were subsumed in this category. Most studies using MLP feed a 1D vector as input (Figure 4). Using an RNN as generator is motivated by the inherent properties of RNNs to deal with time dependencies, and the EEG signal has that property (Abdelfattah et al., 2018). Consequently, all studies utilizing an RNN fed time-series data into the GAN (Figure 4).

The next variations address the instabilities in training (*cf.* Figure 3 green ellipse) sometimes encountered with the Vanilla GAN. Mode collapse occurs when the generator produces very small variations of

TABLE 3 Overview of generative models and their frequency of use.

| | Class differentiation: | Only minority | 1 Generator/ class | Conditional | Auxiliary | Posthoc selection | Total |
|---|---|---|---|---|---|---|---|
| GAN | CNN total (WD, GP, select) | 4 (2, 2, 1) | 1 | 5 (2, 2, 0) | 1 (1, 1, 0) | 1 (1, 1, 1) | **12 (6, 6, 2)** |
| | MLP total (WD, GP, select) | 2 (1, 0, 0) | 1 | 5 (4, 2, 3) | | | **8 (5, 2, 3)** |
| | RNN | | 2 | | 2 | | **4** |
| GPT | | | 2 | | | | **2** |
| AE | | | 1 | | | | **1** |
| **Total** | | **6** | **7** | **10** | **3** | **1** | ***27*** |

The GAN models are further differentiated by the network making up the generator and discriminator. The five ways to generate class-specific data (columns) are explained further in the text. The number of studies improving their training with the Wasserstein distance and/or gradient-penalty are added, as well as the number of studies using selective augmentation. GAN: generative adversarial network; GPT: generative pre-trained transformer; AE: autoencoder; CNN: convolutional neural network; MLP: multi-layer perceptron; RNN: recurrent neural network; WD: Wasserstein distance; GP: gradient penalty.

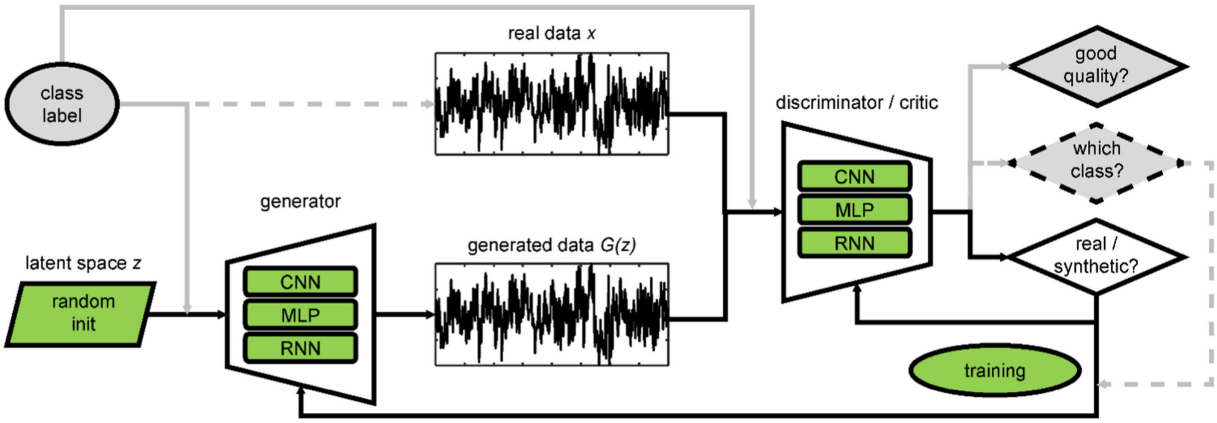


FIGURE 3
Overview of GAN architectures with variants (green) and optional elements (gray). The dashed elements belong to the GAN with auxiliary classification. Please refer to the text for details. CNN: convolutional neural network; MLP: multi-layer perceptron; RNN: recurrent neural network.

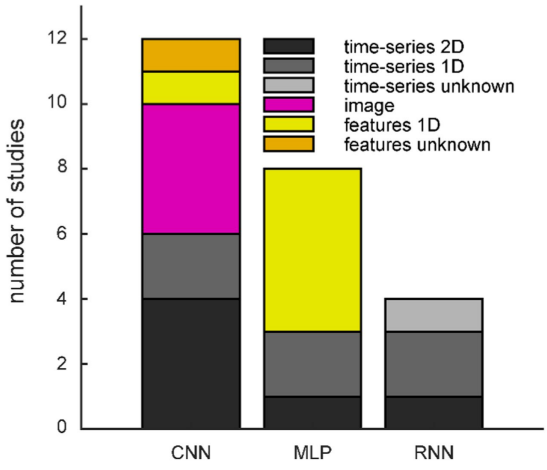


FIGURE 4
Frequency of generator/discriminator networks split by input/output formats. CNN: convolutional neural network; MLP: multi-layer perceptron; RNN: recurrent neural network.

the data because only those are recognized as real data by the discriminator (Saatci and Wilson, 2017). This problem is overcome by using a different loss function; the most popular choice here is the Wasserstein distance (WD, Table 3) (Arjovsky et al., 2017), sometimes combined with gradient penalty (GP) (Gulrajani et al., 2017) to enforce Lipschitz continuity instead of weight clipping. In a Wasserstein GAN, the discriminator is called the critic. Along with using the WD, Arjovsky et al. (2017) also proposed a training regimen in which the critic iterates several times before the generator runs again, leading to even more stability in training. This adaptation can be observed in some of the studies as well. Other modifications observed are (1) gradually increasing data resolution with training (Hartmann et al., 2018), (2) augmenting the synthetic and real data with a Gaussian noise layer before feeding them into the discriminator (Zhao et al., 2020), or (3) initializing the weights of the generator and discriminator with the weights of the decoder and encoder of a VAE (Xu et al., 2022).

Most often, the generator is initialized with random uniform noise, but we also found variations using, for example, Gaussian noise (*cf.* Figure 3 green parallelogram) (Yang et al., 2019). For the last step in the process, there is an optional addition selecting only good quality data for the synthetic dataset (Table 3, Figure 3 top right rhombus).

Finally, two approaches extend the GAN architecture to generate more than one class of data (Table 3, Figure 3). The most popular method is conditioning the generator and discriminator with the class label (Mirza and Osindero, 2014). In contrast, the auxiliary approach feeds the result of a data-label classification into the training process in addition to the results from the real vs. synthetic classification. The reviewed studies achieved the data-label classification by extending the architecture of the existing discriminator (*cf.* Figure 3 dashed elements) (Panwar et al., 2020; Geng and Chen, 2021). Note that other methods exist, e.g., utilizing an extra classifier that gets only the generated data as input (Liao and Dong, 2022).

Some authors give the variation of their GAN acronyms according to the aspect that is important to them. However, the acronyms often do not fully describe the architecture. E.g., a GAN with a CNN using the Wasserstein distance may be referred to as DCGAN, emphasizing the deep convolutional architecture of the generator and discriminator. Alternatively, it may be called WGAN, emphasizing the training based on the Wasserstein distance. Other common acronyms are RGAN for using RNN in the generator, WGAN-GP for the Wasserstein GAN using gradient penalty, cGAN for conditional GANs, or AC-GAN for GANs with auxiliary classifiers.

#### 3.1.3.2. Generative pre-trained transformer

The two studies using GPT models (Bird et al., 2021; Niu et al., 2021) based their architecture on GPT-2 (Radford et al., 2018) trained on natural language from millions of websites. Both used continuous time-series data (data format not otherwise specified) as input.

#### 3.1.3.3. Autoencoders

Only one study utilized a variant of the autoencoder as only generative model (Sobahi et al., 2022). They used an extreme learning machine based autoencoder (ELM-AE) on an image constructed from

frequency features. Four more studies (Luo et al., 2020; Zhang et al., 2020; Fahimi et al., 2021; Song et al., 2021) compared their GAN architectures against the performance of data generated with a VAE but found the GAN results superior.

### 3.1.4. Evaluation metrics and methods

The purpose of the synthetic data of all reviewed papers was to improve the training of a classifier. However, the good quality of the generated data is a prerequisite for a meaningful improvement of the classification. Furthermore, the stability of the training process might be of interest in some cases as well. Nonetheless, seven papers did not perform any kind of evaluation. Seven papers evaluated only **training stability** quantitatively to demonstrate the presence or absence of convergence failure (Zhang et al., 2018) or mode collapse by showing or describing generator and/or discriminator loss curves or discriminator accuracy. For two of those studies, this was the only evaluation at all.

The **quantitative evaluation metrics** for the generated data were rather sparse and scattered. They fall into roughly two categories: the first judges the similarity between time-series, or their respective diversity, based on cross-correlation (n = 1) or Euclidian distance (n = 1), or, in the case of time locked data, with dynamic time warping (DTW) with Manhattan distance (n = 1). The second provides metrics for describing the distances between the data distributions either using an inception classifier and reporting Fréchet inception distance (FID) (Heusel et al., 2017) ($n = 2$) or inception score (IS) (Salimans et al., 2016) ($n = 1$), or the Gaussian mixture model (GMM) log-likelihood distance ($n = 2$), maximum mean discrepancy (MMD) ($n = 1$), Kullback–Leibler (KL) divergence ($n = 1$), or sliced Wasserstein distance (Peyré and Cuturi, 2017) ($n = 1$). One paper reported the reconstruction accuracy of the signal.

Thirteen out of 18 papers, presenting **qualitative evaluation** of the generated data, provided them in addition to quantitative metrics. The most common visual representation for qualitative assessment of the synthetic data were figures of exemplary single time-series data (Figure 5). Presenting the mean of the time-series serves two purposes, dependent on the type of data: for time locked paradigms, the mean time-series reveals whether the expected response shape is present in the synthetic data. For continuous paradigms, the mean time-series shows the distribution at each time point of the arbitrary frames, and one might detect systematic differences between the time-series. Transforming data from time to frequency space and showing frequency spectra reveals whether the frequency content of the original signal is captured properly. The power spectral density (PSD) was shown in three studies. Three more studies illustrated the data in time frequency representation (TFR), with two of them generating the data already in this format and the third performing the transformation for visual inspection only. Topographic maps are a common way of depicting EEG data and were used for visual inspection by four studies. A 2D mapping of the generated data by various algorithms (*cf.* Figure 5) provides an overview of whether the distribution of the synthetic data matches the real data and was conducted by seven studies overall. Three studies had individual visual representations for their data (*cf.* Figure 5 "other").

From the eight studies using continuous EEG time-series as input/output like our study, three did not perform any kind of evaluation, and one study presented only generator and discriminator loss. The remaining four studies all showed single exemplary time-series, and two transformed the data to frequency space for a visual comparison (Hartmann et al., 2018; Bird et al., 2021). Only one study provided quantitative metrics with FID, IS, Euclidean, and sliced Wasserstein distances (Hartmann et al., 2018).

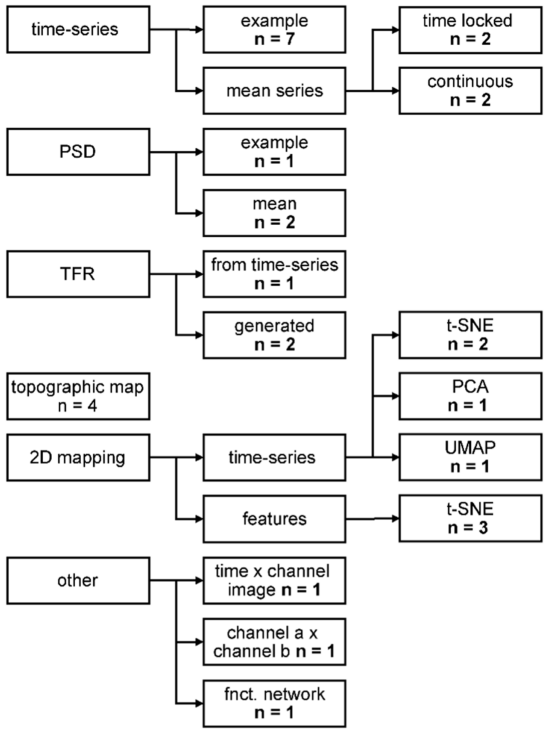


FIGURE 5
Categorization of the qualitative evaluation methods. PSD: power spectral density; TFR: time frequency representation; t-SNE: *t*-distributed Stochastic Neighbor Embedding; PCA: principal component analysis; UMAP: uniform manifold approximation and projection. For further description, see text.

### 3.1.5. Effect on classification

Since the data was generated to improve a classification task, most studies trained one or several classification algorithms with the augmented data to demonstrate the effect of the augmentation on the classification. The manifold of ML algorithms used for classifying EEG data is not the focus of this review, therefore, we only provide a brief summary here. Eighteen studies used some kind of DL algorithm directly on the data generated, with the CNN being the most popular by far. Ten studies used classical ML approaches, mainly support vector machine (SVM) but also a variety of decision trees or occasionally other algorithms. Five of those studies applied the classifiers on the features that originated directly from the generative model. The remaining five studies generated time-series and two of them used the time-series data for classification as well. The other three studies calculated statistical, event-related potential (ERP), or connectivity features just for the classification.

#### 3.1.5.1. Overview of effects

For an overview of the effect of augmenting data with synthetic data, we first extracted the highest effect in terms of absolute accuracy increase from each study and classification task (Table 4, Figure 6).

When accuracies were only depicted in figures in the original paper, we estimated them visually.

A high baseline classification accuracy, i.e., classification performance for training with real data only, provides limited possibilities for improvement; therefore, we expected the highest increase for studies with low baseline accuracies. This is not immediately obvious from Figure 6 but we did indeed find a small negative correlation between baseline accuracy and the amount of accuracy increase when training on augmented data ($r = -0.37$; $t_{31} = -2.249$; $p = 0.032$).

TABLE 4 Mean baseline accuracies and their improvements with augmented data for classifiers with two to five classes.

| Number of classes | 2 | 3 | 4 | 5 |
|---|---|---|---|---|
| *n* | 24 | 4 | 4 | 1 |
| Baseline accuracy [%] | 76.91 ± 5.41 | 85.26 ± 4.45 | 51.22 ± 5.78 | 54.34 |
| Accuracy improvement [%] | 5.51 ± 1.65 | 5.41 ± 3.46 | 15.62 ± 16.03 | 8.53 |

#### 3.1.5.2. Effect dependent on the amount of generated data

Some studies provide data on the accuracy development dependent on the amount of generated data for training the classifier (Figure 7). On an intuitive notion, the classification accuracy should increase with increasing size of training data and eventually level out when the generated data cannot provide additional information. However, we saw in several studies that there seems to be an optimal amount of additional synthetic data, and the accuracies drop with even more data.

### 3.1.6. Publication

Fourteen studies from this review were journal articles, mainly published *via* IEEE Xplore (IEEE, New York, NY, United States) ($n = 7$), otherwise from Hindawi (Hindawi Limited, London, United Kingdom) with two articles, and one each from Elsevier (Elsevier B.V., Amsterdam, Netherlands), IOPscience (IOP Publishing, Bristol, United Kingdom), MDPI (MDPI AG, Basel, Switzerland), and Taylor & Francis (Taylor & Francis Groups, Abingdon,

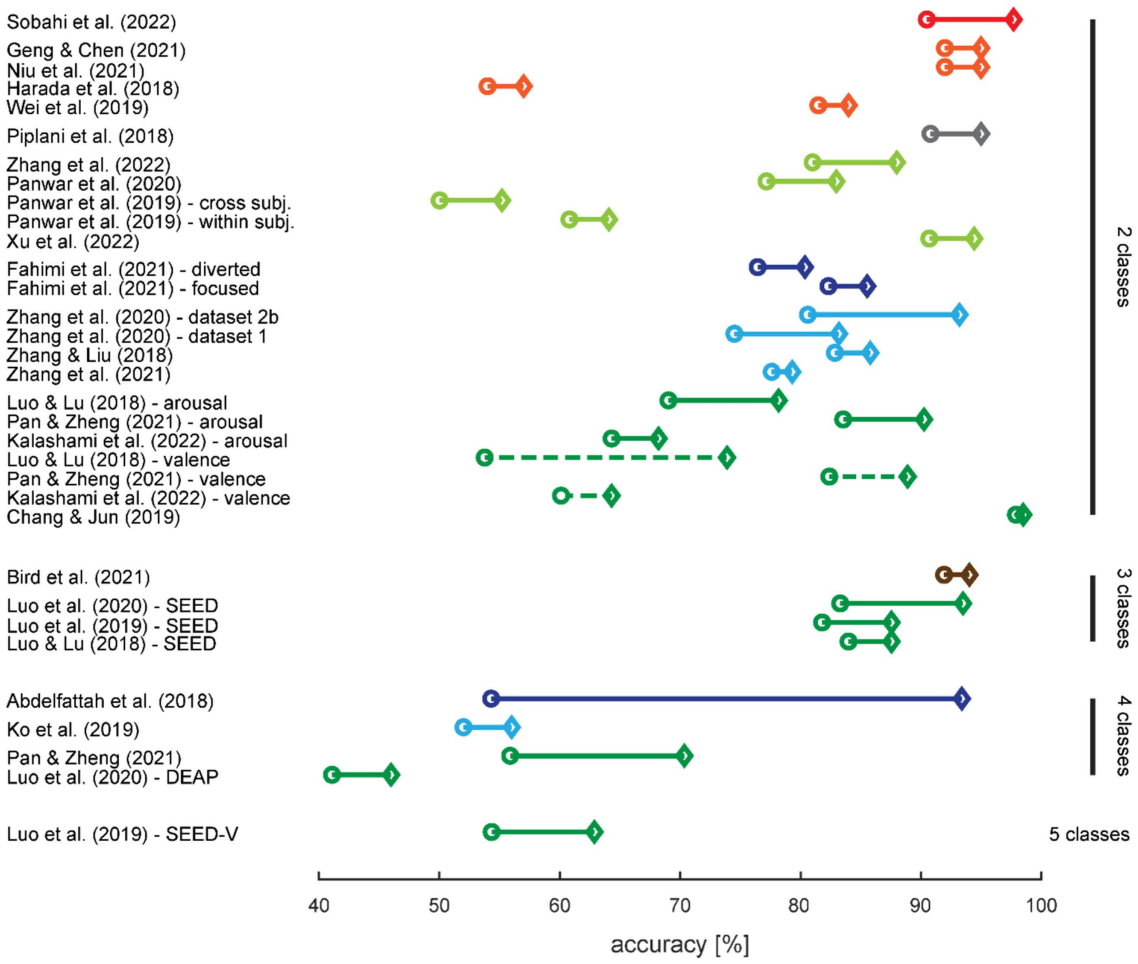


FIGURE 6
Effect of augmentation with synthetic data on classification performance. The circles denote the classification accuracies with training on real data only, and the diamonds denote the highest increase in accuracy with training on augmented data. Results are sorted first by number of classes in the classification task, then by use case (*cf.* color coding), and finally from the highest to lowest increase in accuracy. When more than one classification task was tested in a study, the results were split up. The colors are adopted from Figure 2; a dashed line differentiates two classification tasks for the same number of classes within a study.

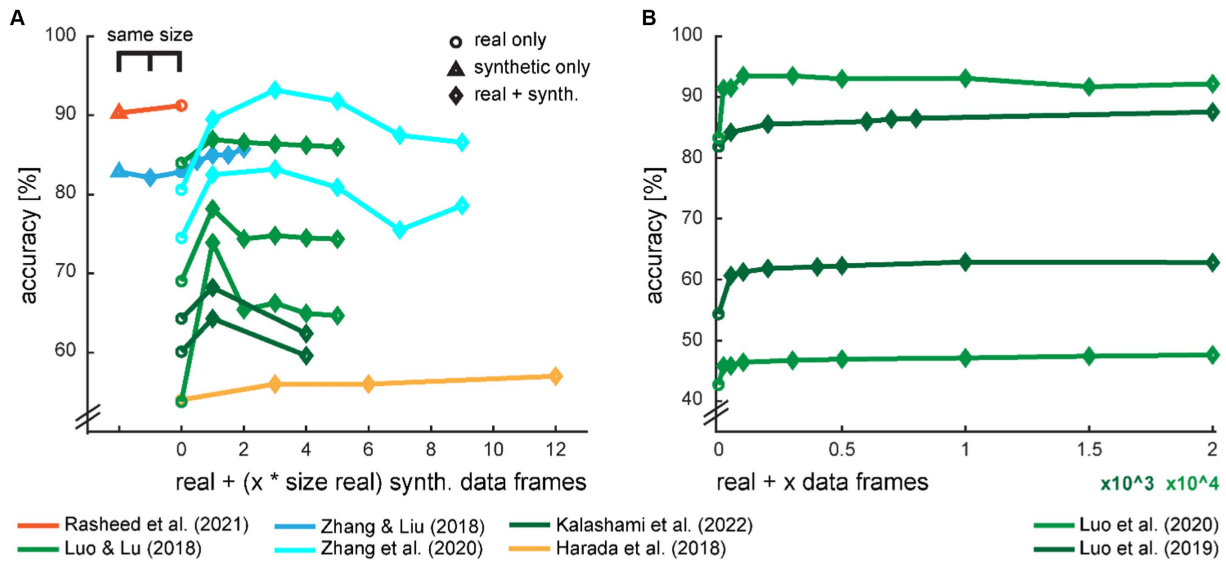


FIGURE 7
Development of classification accuracy with the ratio of real and synthetic data. The amount of synthetic data in the augmented dataset was either provided in multiples of the size of the real training dataset **(A)** or in the absolute amount of synthetic data frames **(B)**. Two studies also provide a comparison with the equal amount of training data, either with a fully synthetic dataset or a mixed set with half real and half synthetic data. The color scheme is loosely adopted from Figure 2.

United Kingdom). Eight of these articles were published in journals that are dedicated to methods in biology, medicine, or neuroscience or interdisciplinary journals comprising one of these disciplines and computation or engineering on the other side. One article was published in a journal specialized for architecture and building engineering. The remaining five articles were published in journals in the fields of computer science or engineering.

Eleven articles were full conference papers, also mainly published *via* IEEE Xplore ($n = 9$), as well as one each from ACM Digital Library (ACM, New York, NY, United States) and Springer (Springer-Verlag GmbH, Berlin, Germany). Five articles were presented at conferences dedicated to methods in biology, medicine, or neuroscience, with the remaining six at computer science or engineering conferences.

Two of the articles included in the review were preprints accessed from arXiv.

Ten articles had gaps in the methods that make them non-reproducible. These include missing information on the data source, preprocessing, data synthetization, and/or data evaluation.

## 3.2. Data augmentation

### 3.2.1. Synthetic data

Visual inspection of exemplary single time-series (Figure 8 top rows) and means across time-series from electrodes F3 and F4 (Figure 8 bottom row) revealed no conspicuous differences between real and synthetic data. The forms and distributions of the generated time-series are well within the range expected from the real data.

Transforming the time-series to power spectra revealed that the synthetic data capture some aspects of the frequency content well but some aspects less well (*cf.* Figure 9 for electrodes F7 and F8). Well represented was the finding that most of the signal power is contained in frequencies roughly below 15 Hz. The characteristics in the low-frequency bands with peaks in delta and alpha but a dip in theta (except for some HC subject in dataset 2) bands seemed to be smoothed in the synthetic signals. Averaging the spectral power within frequency bands (*cf.* insets in Figure 9) revealed for dataset 1 significant main effects of data type, i.e., real vs. synthetic data, in delta, theta, and alpha bands (all $F_{1,92} > 5.041$; $p < 0.027$) but neither main effects of diagnosis nor interactions (Figure 9A inset). Dataset 2 presented the opposite pattern, with significant main effects of diagnosis in delta and theta bands (all $F_{1,108} > 7.389$; $p < 0.008$) but neither main effects of data type nor interactions (Figure 9B inset). In the alpha band, we found no significant effects in the latter dataset.

In contrast to the synthetic data, we did not find any differences between real and noise data in the frequency bands. All main effects of data type failed to reach significance for dataset 1 (all $F_{1,92} < 2.948$; $p > 0.089$) and dataset 2 (all $F_{1,108} < 2.251$; $p > 0.137$).

### 3.2.2. Classification results

The diagnosis classifiers trained on the real data performed around chance level (accuracy: 50.9 ± 6.4%) for dataset 1 and well above chance level (accuracy: 79.8 ± 6.7%) for dataset 2 (Figure 10 pink lines). The classifiers trained on the noise data performed in the same range, independent of the augmentation ratio. The classifiers trained only on the synthetic data performed either similar in the case of the chance classifier for dataset 1, or worse in the case of the performant classifier for dataset 2. In the latter case, however, it performed still significantly above chance level ($t_{27} = 16.168$; $p < 0.001$). Substituting half of the real data by synthetic data brought back the performance of the original classifier for both datasets. Padding the real data with the same amount of synthetic data and therewith doubling the amount of training data yielded a significant accuracy increase of 9.96% in the case of dataset 1 ($t_{46} = 1.771$; $p = 0.042$) but no significant improvement for dataset 2. Further adding synthetic data did not

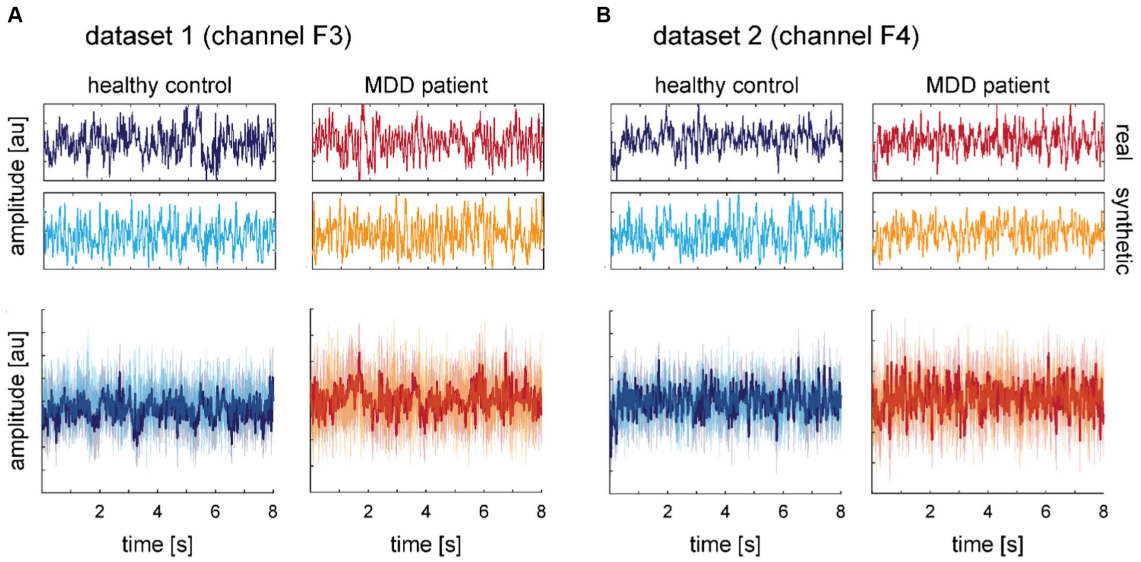


FIGURE 8
Comparison of time-series windows of 8 s in length for real and synthetic data for electrode F3 from dataset 1 **(A)** and electrode F4 from dataset 2 **(B)**. The top panels show exemplary single time-series for a random subject. Middle panels show exemplary single time-series for a random synthetic data frame. Bottom panels show the mean over 10 time-series from real subjects selected randomly and 10 time-series of synthetic data. The shaded areas depict 95% confidence intervals. Data is normalized from −1 to 1, therefore the amplitude has arbitrary units but y-axes match across graphs. The color scheme introduced in this figure is adopted in all subsequent figures showing real data (dark blue and red for HC and MDD, respectively) and synthetic data (light blue and orange for HC and MDD, respectively).

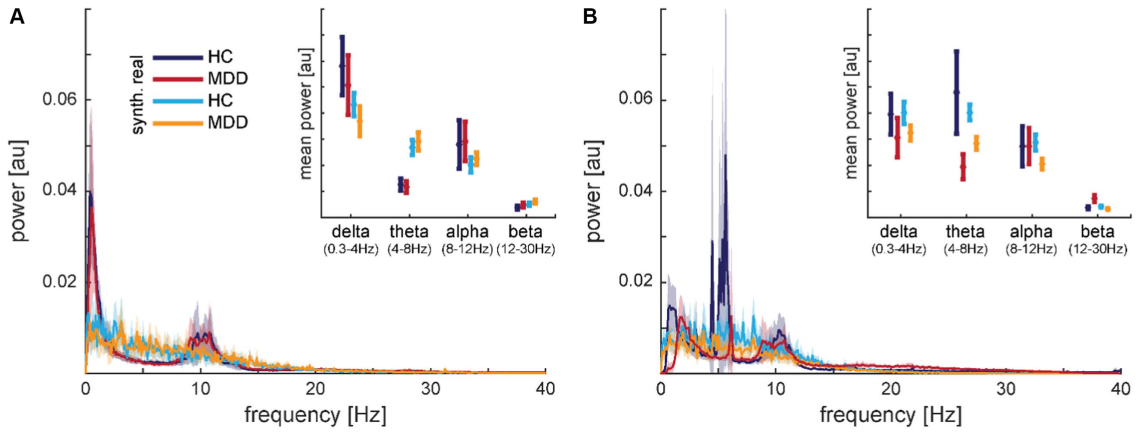


FIGURE 9
Comparison of mean spectra for real and synthetic data for electrode F7 from dataset 1 **(A)** and electrode F8 from dataset 2 **(B)**. The insets show the same data averaged within frequency bands. The shaded areas and error bars depict 95% confidence intervals. Data is normalized from −1 to 1, therefore, the amplitude has arbitrary units, but y-axes match across graphs.

lead to additional improvements in classification accuracy. Note that the classifiers were all **tested** on real data.

Investigating the other classification performance metrics (Figure A1 in Supplementary material) indicated for dataset 1 that the classification was rather balanced for the real data. The increase in classification accuracy was first driven by the precision, but with the amount of real data being maximal again, the classification was balanced once more. The classification for dataset 2 was already tipped toward recall, i.e., sensitivity, for the real data and this imbalance was particularly pronounced when the classifier was exclusively trained by the synthetic data. However, augmenting the real data with twice the synthetic or noise data, balanced this classification as well.

## 4. Discussion

The current study presents the status of the field of generative methods for EEG data focusing on the generation of synthetic data later used for a classification task, such as a clinical diagnosis, based on a systematic review. An in-depth analysis of the methods,

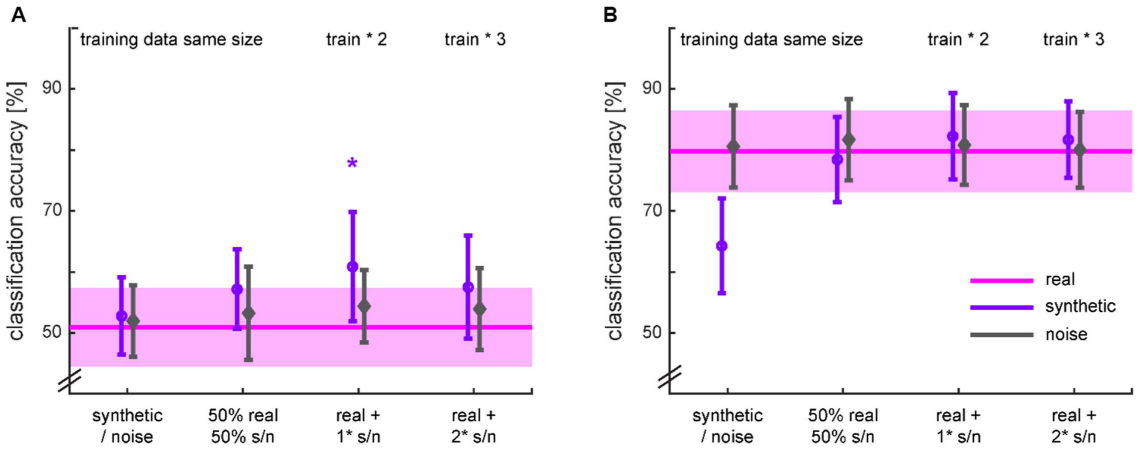


FIGURE 10
Classification accuracies for HC vs. MDD based on different ratios of real and synthetic or noise data for training (Table 2) from dataset 1 **(A)** and dataset 2 **(B)**. The classification with training on real data serves as baseline for comparison and is therefore spread across the x-axis. The shaded areas and error bars depict 95% confidence intervals. * $p < 0.05$ for the t-test in comparison to training on real data only.

opportunities, and pitfalls, as well as the interdependence between the sub-steps of the data generation and evaluation process, provides an overview of the possibilities and current weaknesses of the research field. Based on two EEG datasets, we then demonstrated the generation of synthetic data from random noise for the two clinical groups MDD and HC with a WGAN incorporating CNNs as the generator and critic. The data were used to train a "diagnosis classifier" based on a CNN separating HC from MDD and were partially able to improve classification accuracy. This is to our knowledge the first study generating EEG time-series data directly for two clinical populations. The evaluation of our synthetic data reveals strengths and weaknesses of the generated data that are well within the parameters of comparable studies presented in the review part. The methods may not be ripe yet to be applied in neuroscience or medical research at a large scale to produce data for methodological developments. However, the field will now benefit greatly from domain experts working with EEG on understanding psychiatric or neurodegenerative diseases.

Evaluation of our synthetic data first demonstrates the face validity of the generated signal. The synthetic time-series cannot be distinguished from the real time-series with the bare eye. Transforming the data into the frequency space, a common transformation for extracting features from EEG signals (Poil et al., 2013), e.g., in order to extract biomarkers for MDD (Greco et al., 2021), revealed some weaknesses of our synthetic data. The generated data maps some frequency characteristics of the real data well but also smooths frequency peaks and dips. This effect can also be observed in the two other studies generating continuous time-series EEG data and subsequently showing frequency spectra. A close look at Figure 6 in the study of Hartmann et al. (2018) shows that, e.g., the beta peaks in the Rest condition are smoothed over in the synthetic data generated with a WGAN-GP with CNN architecture. Similarly, Figure 5 in the study of Bird et al. (2021) demonstrates highly smoothed versions of the 50 Hz line noise artifact as well as the absence of alpha peaks in the synthetic data produced with a GPT model. Given the importance of the frequency content in EEG signals, especially in clinical use cases (Poil et al., 2013), this constitutes a serious weakness in current generative models that needs to be addressed in further studies. Categorizing our power spectra in the frequency bands used in clinical research provides contradictory results. The analyses for dataset 1 showed that the real and synthetic data were significantly different in all frequency bands. However, for dataset 2, we found significant differences for the MDD vs. HC groups in the low frequency bands without significant differences between real and synthetic data. This finding demonstrates a successful differentiated reconstruction of this frequency content for the two clinical groups. This holds at least true for the granularity the frequency content is often analyzed, i.e. condensed in commonly used frequency bands. Note that for this dataset, the classification accuracy based on the real data is with nearly 80% already well above chance level. This suggests that the conditional GAN might also have a better chance of generating separable classes for a dataset in which the classes are already better separable. Finally, yet importantly, we improved our diagnosis classifier by nearly 10% for dataset 1 when augmenting the real data with the same amount of synthetic data. This is well within the range of improvement we saw in the other studies analyzed for the review. This improvement is mainly driven by precision, i.e., an increase in the ratio of correctly classified patients among all data classified as patients. It might be that the diversity of the augmented training data was helpful in this case. However, we could not replicate this improvement with dataset 2, which already had a marked higher baseline classification accuracy than dataset 1. Here, training only on synthetic data steeply increased the imbalance biased toward recall, i.e., the sensitivity or the ratio of correctly classified patients, at the cost of precision and specificity. Augmenting the data with synthetic or noise data, however, lead to a more balanced classification without increasing the classification accuracy. Because the CNN used for classification behaves like a black box, we are blind as to whether the algorithm bases its decision on clinical meaningful features or not. The direct comparison of the synthetic data as well as the classification results for the two datasets demonstrates that these methods do not yet produce stable results and therefore cannot be readily applied in a clinical context.

Our clinical use case of generating data for two clinical populations has only been studied twice, but both times with

generating features from EEG instead of generating time-series data directly. An additional clinical study published after our search generated data for the minority class only (Sadegh-Zadeh et al., 2023). In contrast to within-subjects studies, like most other studies in the review, the differences between the classes arise here from disease-dependent changes to the resting state EEG signal and not from different mental states within the same subject. The inherent challenges of generating data resembling the original data persist, but the differentiation between classes is more subtle. In contrast to continuous EEG data, time locked signals are much more ordered in the time domain. Therefore, transferring methods between those two modes of EEG recordings should be considered with caution.

The type of generated data determines the degree of freedom for further processing the data. The less the EEG data is processed or condensed, the more options remain. The original EEG time-series can be reconstructed from a complex power spectrum, i.e., the amplitude and phase of the frequencies; therefore, this representation can also be used for obtaining data with the same possibilities as generating time-series data directly. Only one study used the real part of the power spectrum as input/output feature (Piplani et al., 2018), and four studies used images with TFR, i.e., spectral power amplitude over time. These representations do not allow for a full reconstruction of the signal since phase shifts between frequencies are lost, but the frequency content is still captured. Two of these studies presented exemplary synthetic TFR images (Zhang and Liu, 2018; Zhao et al., 2020) that seem to capture the frequencies rather well, but the overall quality of the generated data cannot be fully judged based on these images alone. Apart from data type, the structure of the input data is of relevance, at least for the generators using convolutional layers. Here, the neighborhood relations in the data structure are of essence. For time and frequency dimensions, these relationships are given but the spatial domain, i.e., the channels, were handled differently across studies. Choosing only one channel (Hartmann et al., 2018) or separately generating data for each channel (Zhang and Liu, 2018) bypasses this issue. However, the signal correlation between channels is discarded in the synthetic data in the latter case. Zhang et al. (2020) stacked the TFR images in the same dimension as the frequency while maintaining the neighboring relationships between their three channels. Several studies organized the channels in an additional dimension but did not report their order. Finally, the type of normalization of the EEG time-series is important to consider, especially when the synthetic dataset is supposed to be used for a clinical use case. Normalization from zero to one or minus one to one is a common preprocessing step for machine learning (Singh and Singh, 2020), i.e., also for the generator models. For many (clinical) applications, however, the relative signal strength across electrodes is meaningful as demonstrated by the common representation of EEG data in a topographic map. These differences should therefore not be factored out by, e.g., normalizing the channels individually. The same holds true for other common preprocessing steps which are out of scope for this review but can heavily influence further processing and should therefore be carefully chosen based on domain expertise. Domain knowledge of the use case and the data also aids in extracting features from the EEG data and generating those instead of time-series data. This is a viable option when the data is used directly to augment the training data for a specific classification task. However, this approach limits the use of the synthetic data beyond this immediate application.

For GANs, various architectural choices have already been tested for generating EEG data (*cf.* Figure 3). This toolbox provides a solid foundation for refining the models for generating EEG data usable for a clinical use case. Especially for time-series transformed into TFR images, CNN variants of the GAN provide the advantage of a large community working on image generation and with it the quick advances in methodological development (Wang et al., 2021). However, the issue of a potential spatial dimension with the EEG channels still needs to be addressed. Given the sequential nature of EEG signals, GAN architectures using RNN and GPT models seem to be a natural choice. However, these approaches have been studied less frequently, and their potential for the clinical use case needs more exploration. In light of the rapidly advancing fields of language and image generation (Zhang et al., 2023), researchers synthetizing EEG data should keep track of GPT and possible future classes of generative algorithms. Except for one study, VAE were only used for comparison with a GAN architecture and always performed worse than the GAN.

A third of the studies provided neither a qualitative nor a quantitative evaluation of the quality of the generated data. Given that data quality is of essence for any data-driven decision process, selective and meaningful metrics for assessing data quality, and in the case of synthetic data, faithfulness to the real data, are essential. Evaluation metrics for synthetic data are still a topic of ongoing research and debate (Theis et al., 2015; Borji, 2019). Face validity is a first important step. However, in the case of EEG time-series data, which cannot be judged as easily as, e.g., natural images by the naked eye, showing time-series data is not sufficient. Transformation into frequency space or visual representations like topographic maps aids visual judgment tremendously and does in fact reveal weaknesses of the synthetic data in the few studies that provided this information as well as in our own. Finding two- or three-dimensional mappings of the data that represent its distribution are popular methods that were also applied in some of the reviewed studies. However, the three studies that did show convincing 2D distributions of the time-series data (Fahimi et al., 2021; Geng and Chen, 2021; Xu et al., 2022) all worked with time locked data, e.g., the form of the ERP was represented in 2D space and not a continuous EEG signal. The only study showing a 2D representation of continuous time-series data with a principal component analysis (PCA) (Kalashami et al., 2022) could neither demonstrate a class nor dataset separation in this representation. We also tried to find a meaningful 2D representation with three popular dimension reduction approaches—PCA, locally linear embedding [LLE (Roweis and Saul, 2000)], and t-Distributed Stochastic Neighbor Embedding [t-SNE (Van der Maaten and Hinton, 2008)]—but failed to find one. Explaining only 8 to 9% of the variance in our data with the first two components of the PCA suggests that two dimensions might simply not suffice for meaningfully condensing continuous time-series EEG data. Quantitative metrics were provided by seven studies only and the details of the evaluation vary widely. For time locked paradigms, similarity between signals can be assessed more easily, e.g., DTW (Bellman and Kalaba, 1959) is a distance metric applied in one study that is well suited for a comparison between two time-series with defined beginning and ending. For continuous data, however, quantitative evaluation of the data quality might greatly benefit from domain expertise about the use case. In our study, we extracted the bandpower of the available frequency bands for a quantitative evaluation. These features, however, are only one example of the many biomarkers used in EEG research for MDD (Greco et al., 2021).

The gold standard evaluation of the synthetic data for most studies was improving a classifier's performance with training it on augmented data including the synthetic data. All studies succeeded in improving their classification accuracy. However, 18 studies used some kind of deep learning classifier and did not assess whether the synthetic data genuinely provided relevant information for the task or whether accuracy improvement was simply an artifact (Nguyen et al., 2015). An explanation for the pattern of only a transient accuracy increase with increasing amount of synthetic data observed in a few studies might be that the first couple of data frames counteract the effect of overtraining but further synthetic data tunes the classifier too far away from using task-relevant information. This hypothesis, however, is of a theoretical nature so far and needs further investigation. In our work, we compared the performance of a classifier trained on data augmented with synthetic data to one trained on data augmented with noise data. While adding noise data did not improve the classification performance significantly, adding synthetic data did in the case of dataset 1. However, we classified the data with a CNN used as a black box starting at the chance level. For the classifier starting well above chance level with dataset 2, we could not replicate this improvement.

The articles reviewed were mainly directed at a technical or methodologically interested and adept audience. Algorithms were developed or adapted from another data domain, and the main goal was to demonstrate the technical feasibility. In order to proceed to the generation of synthetic data with clinical relevance, i.e., faithfully representing clinically relevant features in the data, domain experts on EEG data analysis in a clinical area or in basic neuroscience research need to add their expertise to the research field. This review has identified two key issues where domain expertise is essential: the format of the input/output data and evaluation of the generated data. On a related note, the explainability of DL models processing EEG data needs to be enhanced, another task where domain expertise is most useful. This becomes relevant to the field when the DL model is used to evaluate the generated data. Finally, yet importantly, architectures specifically designed for continuous data such as GANs with RNN and GPT models should be further explored for their suitability for EEG data generation.

Our work carves out the opportunities and current weaknesses of generating synthetic EEG data for two clinical groups, such as MDD patients and HC, based on a systematic literature review in combination with an empirical study on two publicly available datasets. The generation of synthetic data constitutes a promising approach for (medical) fields in which large datasets are sparse. Still, biomarker research, especially methods based on (deep) machine learning, requires large datasets to produce generalizable models able to support clinical routine. A sound technical basis is set with the algorithms developed over the last decade, but the shortcomings of the data generated so far require further research before their broad application in clinical use cases. In order to address these shortcomings, more domain expertise from researchers specialized in EEG processing and EEG biomarkers for clinical applications needs to be incorporated into further developments in the field.

## Data availability statement

Publicly available datasets were analyzed in this study. This data can be found here: http://modma.lzu.edu.cn/data/index/; https://doi.org/10.6084/m9.figshare.4244171.v2.

## Ethics statement

The studies involving humans were approved by Ethics Committee for Biomedical Research at the Lanzhou University Second Hospital and Ethics Committee of Hospital Universiti Sains Malaysia. The studies were conducted in accordance with the local legislation and institutional requirements. The participants provided their written informed consent to participate in this study.

## Author contributions

YH organized and pre-processed the data. FC performed data augmentation and classification. FC and AR analyzed the results and performed the literature review. AR wrote the first draft of the manuscript. FC and YH wrote sections of the manuscript. All authors contributed to conception and design of the study. All authors contributed to manuscript revision, read, and approved the submitted version.

## Funding

YH is supported by grant KK5207801BM0 from the Federal Ministry for Economic Affairs and Climate Action (BMWK) on the basis of a decision by the German Bundestag.

## Acknowledgments

The authors thank R.-A. Windberger for helpful comments on an earlier version of the manuscript.

## Conflict of interest

The authors declare that the research was conducted in the absence of any commercial or financial relationships that could be construed as a potential conflict of interest.

## Publisher's note



## Supplementary material

The Supplementary material for this article can be found online at: https://www.frontiersin.org/articles/10.3389/fnins.2023.1219133/full#supplementary-material

# References


Abdelfattah, S. M., Abdelrahman, G. M., and Wang, M. (2018). Augmenting the size of EEG datasets using generative adversarial networks. Paper presented at the 2018 international joint conference on neural networks (IJCNN) 2018-07.

Arjovsky, M., Chintala, S., and Bottou, L. (2017). Wasserstein GAN.

Bellman, R., and Kalaba, R. (1959). On adaptive control processes. *IRE Trans. Autom. Control.* 4, 1–9. doi: 10.1109/TAC.1959.1104847

Bird, J. J., Pritchard, M., Fratini, A., Ekárt, A., and Faria, D. R. (2021). Synthetic biological signals machine-generated by GPT-2 improve the classification of EEG and EMG through data augmentation. *IEEE Robot. Autom. Lett.* 6, 3498–3504. doi: 10.1109/LRA.2021.3056355

Blankertz, B., Dornhege, G., Krauledat, M., Müller, K.-R., and Curio, G. (2007). The non-invasive Berlin brain–computer interface: fast acquisition of effective performance in untrained subjects. *NeuroImage* 37, 539–550. doi: 10.1016/j.neuroimage.2007.01.051

Borji, A. (2019). Pros and cons of Gan evaluation measures. *Comput. Vis. Image Underst.* 179, 41–65. doi: 10.1016/j.cviu.2018.10.009

Bundesärztekammer (BÄK), Kassenärztliche Bundesvereinigung (KBV), Arbeitsgemeinschaft der Wissenschaftlichen Medizinischen Fachgesellschaften (AWMF). (2022). *Nationale VersorgungsLeitlinie Unipolare Depression – Langfassung, Version 3.2*. Available at: www.leitlinien.de/depression

Cai, H., Gao, Y., Sun, S., Li, N., Tian, F., Xiao, H., et al. (2020). Modma dataset: a multi-modal open dataset for mental-disorder analysis. ar Xiv preprint ar Xiv: 2002.09283.

Chang, S., and Jun, H. (2019). Hybrid deep-learning model to recognise emotional responses of users towards architectural design alternatives. *J. Asian Arch. Build. Eng.* 18, 381–391. doi: 10.1080/13467581.2019.1660663

Cho, J., Lee, K., Shin, E., Choy, G., and Do, S. (2015). How much data is needed to train a medical image deep learning system to achieve necessary high accuracy? arXiv preprint arXiv: 1511.06348.

Dev, A., Roy, N., Islam, M. K., Biswas, C., Ahmed, H. U., Amin, M. A., et al. (2022). Exploration of EEG-based depression biomarkers identification techniques and their applications: a systematic review. IEEE Access.

Fahimi, F., Dosen, S., Ang, K. K., Mrachacz-Kersting, N., and Guan, C. (2021). Generative adversarial networks-based data augmentation for brain-computer Interface. *IEEE Trans. Neural Netw. Learn. Syst.* 32, 4039–4051. doi: 10.1109/TNNLS.2020.3016666

Geng, D., and Chen, Z. S. (2021). Auxiliary classifier generative adversarial network for interictal epileptiform discharge Modeling and EEG data augmentation. Paper presented at the 2021 10th international IEEE/EMBS conference on neural engineering (NER) 2021-05.

Goodfellow, I., Pouget-Abadie, J., Mirza, M., Xu, B., Warde-Farley, D., Ozair, S., et al. (2014). *Generative adversarial nets in advances in neural information processing systems (NIPS)*. Red Hook, NY, USA: Curran Associates, Inc. 2672–2680.

Gramfort, A., Luessi, M., Larson, E., Engemann, D. A., Strohmeier, D., Brodbeck, C., et al. (2014). MNE software for processing MEG and EEG data. *NeuroImage* 86, 446–460. doi: 10.1016/j.neuroimage.2013.10.027

Greco, C., Matarazzo, O., Cordasco, G., Vinciarelli, A., Callejas, Z., and Esposito, A. (2021). Discriminative power of EEG-based biomarkers in major depressive disorder: a systematic review. *IEEE Access* 9, 112850–112870. doi: 10.1109/ACCESS.2021.3103047

Gulrajani, I., Ahmed, F., Arjovsky, M., Dumoulin, V., and Courville, A. C. (2017). Improved training of wasserstein gans. *Adv. Neural Inf. Proces. Syst.* 30. doi: 10.48550/arXiv.1704.00028

Habashi, A. G., Azab, A. M., Eldawlatly, S., and Aly, G. M. (2023). Generative adversarial networks in EEG analysis: an overview. *J. Neuro Eng. Rehab.* 20:40. doi: 10.1186/s12984-023-01169-w

Habert, J., Katzman, M. A., Oluboka, O. J., McIntyre, R. S., McIntosh, D., Mac Queen, G. M., et al. (2016). Functional recovery in major depressive disorder: focus on early optimized treatment. *Prim. Care Comp. CNS Disord.* 18:24746. doi: 10.4088/PCC.15r01926

Haradal, S., Hayashi, H., and Uchida, S. (2018). Biosignal data augmentation based on generative adversarial networks. Paper presented at the 2018 40th Annual International Conference of the IEEE Engineering in Medicine and Biology Society (EMBC).

Hartmann, K. G., Schirrmeister, R. T., and Ball, T. (2018). EEG-GAN: generative adversarial networks for electroencephalograhic (EEG) brain signals.

He, C., Liu, J., Zhu, Y., and Du, W. (2021). Data augmentation for deep neural networks model in EEG classification task: a review. *Front. Hum. Neurosci.* 15:765525. doi: 10.3389/fnhum.2021.765525

Heusel, M., Ramsauer, H., Unterthiner, T., Nessler, B., and Hochreiter, S. (2017). Gans trained by a two time-scale update rule converge to a local Nash equilibrium. *Adv. Neural Inf. Proces. Syst.* 30. doi: 10.48550/arXiv.1706.08500

Kalashami, M. P., Pedram, M. M., and Sadr, H. (2022). EEG feature extraction and data augmentation in emotion recognition. *Comput. Intell. Neurosci.* 2022:7028517. doi: 10.1155/2022/7028517

Kingma, D. P., and Ba, J. (2014). Adam: a method for stochastic optimization. arXiv preprint arXiv: 1412.6980.

Kingma, D. P., and Welling, M. (2014). Auto-encoding variational Bayes.

Ko, W., Jeon, E., Lee, J., and Suk, H.-I. (2019). *Semi-supervised deep adversarial learning for brain-computer interface*. Paper presented at the 2019 7th international winter conference on brain-computer interface (BCI).

Koelstra, S., Muhl, C., Soleymani, M., Lee, J.-S., Yazdani, A., Ebrahimi, T., et al. (2011). Deap: a database for emotion analysis; using physiological signals. *IEEE Trans. Affect. Comput.* 3, 18–31. doi: 10.1109/T-AFFC.2011.15

Lashgari, E., Liang, D., and Maoz, U. (2020). Data augmentation for deep-learning-based electroencephalography. *J. Neurosci. Methods* 346:108885. doi: 10.1016/j.jneumeth.2020.108885

LeCun, Y., Bengio, Y., and Hinton, G. (2015). Deep learning. *Nature* 521, 436–444. doi: 10.1038/nature14539

Lee, S., and Lee, C. (2020). Revisiting spatial dropout for regularizing convolutional neural networks. *Multimed. Tools Appl.* 79, 34195–34207. doi: 10.1007/s11042-020-09054-7

Leeb, R., Lee, F., Keinrath, C., Scherer, R., Bischof, H., and Pfurtscheller, G. (2007). Brain–computer communication: motivation, aim, and impact of exploring a virtual apartment. *IEEE Trans. Neural Syst. Rehabil. Eng.* 15, 473–482. doi: 10.1109/TNSRE.2007.906956

Leiser, S. C., Dunlop, J., Bowlby, M. R., and Devilbiss, D. M. (2011). Aligning strategies for using EEG as a surrogate biomarker: a review of preclinical and clinical research. *Biochem. Pharmacol.* 81, 1408–1421. doi: 10.1016/j.bcp.2010.10.002

Li, A., Feitelberg, J., Saini, A. P., Höchenberger, R., and Scheltienne, M. (2022). MNE-ICALabel: automatically annotating ICA components with ICLabel in Python. *J. Open Sour. Softw.* 7:4484. doi: 10.21105/joss.04484

Liao, C., and Dong, M. (2022). ACWGAN: an auxiliary classifier wasserstein gan-based oversampling approach for multi-class imbalanced learning.

Liberati, A., Altman, D. G., Tetzlaff, J., Mulrow, C., Gøtzsche, P. C., Ioannidis, J. P. A., et al. (2009). The PRISMA statement for reporting systematic reviews and meta-analyses of studies that evaluate healthcare interventions: explanation and elaboration. *BMJ* 339:b2700. doi: 10.1136/bmj.b2700

Liu, W., Qiu, J.-L., Zheng, W.-L., and Lu, B.-L. (2021). Comparing recognition performance and robustness of multimodal deep learning models for multimodal emotion recognition. *IEEE Trans. Cogn. Dev. Syst.* 14, 715–729. doi: 10.1109/TCDS.2021.3071170

Luo, Y., and Lu, B.-L. (2018). EEG data augmentation for emotion recognition using a conditional Wasserstein GAN. Paper presented at the 2018 40th Annual International Conference of the IEEE Engineering in Medicine and Biology Society (EMBC).

Luo, Y., Zhu, L.-Z., and Lu, B.-L. (2019). "A GAN-based data augmentation method for multimodal emotion recognition" in *Advances in neural networks–ISNN 2019*. eds. H. Lu, H. Tang and Z. Wang (Cham: Springer International Publishing)

Luo, Y., Zhu, L.-Z., Wan, Z.-Y., and Lu, B.-L. (2020). Data augmentation for enhancing EEG-based emotion recognition with deep generative models. *J. Neural Eng.* 17:056021. doi: 10.1088/1741-2552/abb580

Mahato, S., and Paul, S. (2019). Electroencephalogram (EEG) signal analysis for diagnosis of major depressive disorder (MDD): a review. *Nanoelectr. Circ. Commun. Syst. Proc. NCCS* 2017, 323–335. doi: 10.1007/978-981-13-0776-8_30

Mirza, M., and Osindero, S. (2014). Conditional generative adversarial nets. arXiv preprint arXiv: 1411.1784.

Mumtaz, W. (2016). MDD patients and healthy controls EEG data (new). Figshare. Dataset. MDD patients and healthy controls EEG data generated. doi: 10.6084/m9.figshar, 4244171, v2

Naeem, M., Brunner, C., Leeb, R., Graimann, B., and Pfurtscheller, G. (2006). Seperability of four-class motor imagery data using independent components analysis. *J. Neural Eng.* 3:208. doi: 10.1088/1741-2560/3/3/003

Nguyen, A., Yosinski, J., and Clune, J. (2015). Deep neural networks are easily fooled: High confidence predictions for unrecognizable images. Paper presented at the Proceedings of the IEEE Conference on Computer Vision and Pattern Recognition.

Nikolenko, S. I. (2019). Synthetic data for deep learning. arXiv preprint arXiv: 1909.11512.

Niu, R., Wang, Y., Xi, H., Hao, Y., and Zhang, M. (2021). Epileptic seizure prediction by synthesizing EEG signals through GPT. Paper presented at the AIPR 2021: 2021 4th international conference on artificial intelligence and pattern recognition.

Otte, C., Gold, S. M., Penninx, B. W., Pariante, C. M., Etkin, A., Fava, M., et al. (2016). Major depressive disorder. *Nat. Rev. Dis. Prim.* 2, 1–20. doi: 10.1038/nrdp.2016.65

Pan, B., and Zheng, W. (2021). Emotion recognition based on EEG using generative adversarial nets and convolutional neural network. *Comput. Math. Methods Med.* 2021:2520394. doi: 10.1155/2021/2520394

Panwar, S., Rad, P., Jung, T.-P., and Huang, Y. (2020). Modeling EEG data distribution with a Wasserstein generative adversarial network to predict RSVP events. *IEEE Trans. Neural Syst. Rehabil. Eng.* 28, 1720–1730. doi: 10.1109/TNSRE.2020.3006180

Panwar, S., Rad, P., Quarles, J., and Huang, Y. (2019). Generating EEG signals of an RSVP experiment by a class conditioned Wasserstein generative adversarial network. Paper presented at the 2019 IEEE international conference on systems, man and cybernetics (SMC).

Peyré, G., and Cuturi, M. (2017). Computational optimal transport. Center for Research in economics and statistics working papers (2017-86).

Piplani, T., Merill, N., and Chuang, J. (2018). Faking it, making it: Fooling and improving brain-based authentication with generative adversarial networks. Paper presented at the 2018 IEEE 9th International Conference on Biometrics Theory, Applications and Systems (BTAS).

Poil, S.-S., De Haan, W., van der Flier, W. M., Mansvelder, H. D., Scheltens, P., and Linkenkaer-Hansen, K. (2013). Integrative EEG biomarkers predict progression to Alzheimer's disease at the MCI stage. *Front. Aging Neurosci.* 5:58. doi: 10.3389/fnagi.2013.00058

Radford, A., Narasimhan, K., Salimans, T., and Sutskever, I. (2018). *Improving language understanding by generative pre-training*.

Rakić, M., Cabezas, M., Kushibar, K., Oliver, A., and Lladó, X. (2020). Improving the detection of autism spectrum disorder by combining structural and functional MRI information. *Neuro Image Clin.* 25:102181. doi: 10.1016/j.nicl.2020.102181

Rasheed, K., Qadir, J., O'Brien, T. J., Kuhlmann, L., and Razi, A. (2021). A generative model to synthesize EEG data for epileptic seizure prediction. *IEEE Tran. Neural Syst. Rehab. Eng.* 29, 2322–2332. doi: 10.1109/TNSRE.2021.3125023

Robbins, K. A., Touryan, J., Mullen, T., Kothe, C., and Bigdely-Shamlo, N. (2020). How sensitive are EEG results to preprocessing methods: a benchmarking study. *IEEE Trans. Neural Syst. Rehabil. Eng.* 28, 1081–1090. doi: 10.1109/TNSRE.2020.2980223

Roweis, S. T., and Saul, L. K. (2000). Nonlinear dimensionality reduction by locally linear embedding. *Science* 290, 2323–2326. doi: 10.1126/science.290.5500.2323

Rüschendorf, L. (1985). The Wasserstein distance and approximation theorems. *Probab. Theory Relat. Fields* 70, 117–129. doi: 10.1007/BF00532240

Saatci, Y., and Wilson, A. G. (2017). Bayesian gan. *Adv. Neural Inf. Proces. Syst.* 30. doi: 10.48550/arXiv.1705.09558

Sadegh-Zadeh, S.-A., Fakhri, E., Bahrami, M., Bagheri, E., Khamsehashari, R., Noroozian, M., et al. (2023). An approach toward artificial intelligence Alzheimer's disease diagnosis using brain signals. *Diagnostics* 13:477. doi: 10.3390/diagnostics13030477

Saeb, S., Lonini, L., Jayaraman, A., Mohr, D. C., and Kording, K. P. (2017). The need to approximate the use-case in clinical machine learning. *Gigascience* 6:gix019. doi: 10.1093/gigascience/gix019

Sajda, P., Gerson, A., Muller, K.-R., Blankertz, B., and Parra, L. (2003). A data analysis competition to evaluate machine learning algorithms for use in brain-computer interfaces. *IEEE Trans. Neural Syst. Rehabil. Eng.* 11, 184–185. doi: 10.1109/TNSRE.2003.814453

Salimans, T., Goodfellow, I., Zaremba, W., Cheung, V., Radford, A., and Chen, X. (2016). Improved techniques for training gans. *Adv. Neural Inf. Proces. Syst.* 29. doi: 10.48550/arXiv.1606.03498

Schlögl, A., Lugger, K., and Pfurtscheller, G. (1997). Using adaptive autoregressive parameters for a brain-computer-interface experiment. Paper presented at the Proceedings of the 19th Annual International Conference of the IEEE Engineering in Medicine and Biology Society. Magnificent Milestones and Emerging Opportunities in Medical Engineering'(cat. No. 97CH36136).

Seal, A., Bajpai, R., Agnihotri, J., Yazidi, A., Herrera-Viedma, E., and Krejcar, O. (2021). DeprNet: a deep convolution neural network framework for detecting depression using EEG. *IEEE Trans. Instrum. Meas.* 70, 1–13. doi: 10.1109/TIM.2021.3053999

Singh, D., and Singh, B. (2020). Investigating the impact of data normalization on classification performance. *Appl. Soft Comput.* 97:105524. doi: 10.1016/j.asoc.2019.105524

Sobahi, N., Ari, B., Cakar, H., Alcin, O. F., and Sengur, A. (2022). A new signal to image mapping procedure and convolutional neural networks for efficient schizophrenia detection in EEG recordings. *IEEE Sensors J.* 22, 7913–7919. doi: 10.1109/JSEN.2022.3151465

Song, Z., Wang, J., Yi, G., and Deng, B. (2021). Improving EEG-based Alzheimer's disease identification with generative adversarial learning. Paper presented at the 2021 40th Chinese Control Conference (CCC).

Stewart, J. L., Bismark, A. W., Towers, D. N., Coan, J. A., and Allen, J. J. (2010). Resting frontal EEG asymmetry as an endophenotype for depression risk: sex-specific patterns of frontal brain asymmetry. *J. Abnorm. Psychol.* 119:502. doi: 10.1037/a0019196

Talavera, E., Iglesias, G., González-Prieto, Á., Mozo, A., and Gómez-Canaval, S. (2022). Data augmentation techniques in time series domain: a survey and taxonomy. arXiv preprint arXiv:2206.13508.

Theis, L., Oord, A. V. D., and Bethge, M. (2015). A note on the evaluation of generative models. arXiv preprint arXiv:1511.01844.

Van der Maaten, L., and Hinton, G. (2008). Visualizing data using t-SNE. *J. Mach. Learn. Res.* 9, 2579–2605. doi: 10.1145/3439723

Wang, Z., She, Q., and Ward, T. E. (2021). Generative adversarial networks in computer vision: a survey and taxonomy. *ACM Comp. Surv.* 54, 1–38.

Wei, Z., Zou, J., Zhang, J., and Xu, J. (2019). Automatic epileptic EEG detection using convolutional neural network with improvements in time-domain. *Biomed. Sig. Process. Control* 53:101551. doi: 10.1016/j.bspc.2019.04.028

World Health Organization. (2017). Depression and other common mental disorders: global health estimates. Available at: https://www.who.int/health-topics/depression

Xu, M., Chen, Y., Wang, Y., Wang, D., Liu, Z., and Zhang, L. (2022). BWGAN-GP: an EEG data generation method for class imbalance problem in RSVP tasks. *IEEE Trans. Neur. Syst. Rehabil. Eng.* 30, 251–263. doi: 10.1109/TNSRE.2022.3145515

Yang, B., Fan, C., Guan, C., Gu, X., and Zheng, M. (2019). A framework on optimization strategy for EEG motor imagery recognition. Paper presented at the 2019 41st Annual International Conference of the IEEE Engineering in Medicine and Biology Society (EMBC).

Yang, C., Xiao, C., Westover, M. B., and Sun, J. (2023). Self-supervised electroencephalogram representation learning for automatic sleep staging: model development and evaluation study. *JMIR AI.* 23:e46769.

Yao, D., Qin, Y., Hu, S., Dong, L., Bringas Vega, M. L., and Valdés Sosa, P. A. (2019). Which reference should we use for EEG and ERP practice? *Brain Topogr.* 32, 530–549. doi: 10.1007/s10548-019-00707-x

Yasin, S., Hussain, S. A., Aslan, S., Raza, I., Muzammel, M., and Othmani, A. (2021). EEG based major depressive disorder and bipolar disorder detection using neural networks: a review. *Comput. Methods Prog. Biomed.* 202:106007. doi: 10.1016/j.cmpb.2021.106007

Zhang, Z., Li, M., and Yu, J. (2018). On the convergence and mode collapse of GAN. In SIGGRAPH Asia 2018 technical briefs.

Zhang, Q., and Liu, Y. (2018). Improving brain computer interface performance by data augmentation with conditional deep convolutional generative adversarial networks. arXiv preprint arXiv:1806.07108.

Zhang, X., Wang, Z., Liu, D., Lin, Q., and Ling, Q. (2021). Deep adversarial data augmentation for extremely low data regimes. *IEEE Trans. Circuits Syst. Video Technol.* 31, 15–28. doi: 10.1109/TCSVT.2020.2967419

Zhang, K., Xu, G., Han, Z., Ma, K., Zheng, X., Chen, L., et al. (2020). Data augmentation for motor imagery signal classification based on a hybrid neural network. *Sensors* 20:E4485. doi: 10.3390/s20164485

Zhang, R., Zeng, Y., Tong, L., Shu, J., Lu, R., Yang, K., et al. (2022). ERP-WGAN: a data augmentation method for EEG single-trial detection. *J. Neurosci. Methods* 376:109621. doi: 10.1016/j.jneumeth.2022.109621

Zhang, X., Zhang, Z., Diao, W., Zhou, C., Song, Y., Wang, R., et al. (2022). Early-diagnosis of major depressive disorder: from biomarkers to point-of-care testing. *TrAC Trends Anal. Chem.* 159:116904

Zhang, C., Zhang, C., Zheng, S., Qiao, Y., Li, C., Zhang, M., et al. (2023). A complete survey on generative AI (AIGC): is chat GPT from GPT-4 to GPT-5 all you need? arXiv preprint arXiv:2303.11717.

Zhao, S., Liu, Z., Lin, J., Zhu, J.-Y., and Han, S. (2020). Differentiable augmentation for data-efficient GAN training.

Zheng, W.-L., and Lu, B.-L. (2015). Investigating critical frequency bands and channels for EEG-based emotion recognition with deep neural networks. *IEEE Trans. Auton. Ment. Dev.* 7, 162–175. doi: 10.1109/TAMD.2015.2431497

frontiers | Frontiers in Neuroscience

TYPE Original Research
PUBLISHED 13 October 2023
DOI 10.3389/fnins.2023.1278183



OPEN ACCESS

EDITED BY
Amelie Haugg,
Psychiatric University Hospital Zurich, Switzerland

REVIEWED BY
Masoumeh Kourosh Arami,
Iran University of Medical Sciences, Iran
Pishan Chang,
University College London, United Kingdom

*CORRESPONDENCE
Jing Wang
✉ Jing.Wang2@nyulangone.org
Lisa V. Doan
✉ lisa.doan@nyulangone.org

†These authors have contributed equally to this work and share first authorship

RECEIVED 15 August 2023
ACCEPTED 25 September 2023
PUBLISHED 13 October 2023

CITATION
Kenefati G, Rockholt MM, Ok D, McCartin M, Zhang Q, Sun G, Maslinski J, Wang A, Chen B, Voigt EP, Chen ZS, Wang J and Doan LV (2023) Changes in alpha, theta, and gamma oscillations in distinct cortical areas are associated with altered acute pain responses in chronic low back pain patients.
*Front. Neurosci.* 17:1278183.
doi: 10.3389/fnins.2023.1278183



# Changes in alpha, theta, and gamma oscillations in distinct cortical areas are associated with altered acute pain responses in chronic low back pain patients

George Kenefati[1,2†], Mika M. Rockholt[1,2†], Deborah Ok[1], Michael McCartin[1], Qiaosheng Zhang[1,2], Guanghao Sun[1,2], Julia Maslinski[1,2], Aaron Wang[1,2], Baldwin Chen[1,2], Erich P. Voigt[3], Zhe Sage Chen[4,5,6], Jing Wang[1,2,5*] and Lisa V. Doan[1,2*]

[1]Department of Anesthesiology, Perioperative Care and Pain Management, New York University Grossman School of Medicine, New York, NY, United States, [2]Interdisciplinary Pain Research Program, New York University Grossman School of Medicine, New York, NY, United States, [3]Department of Otolaryngology-Head and Neck Surgery, New York University Grossman School of Medicine, New York, NY, United States, [4]Department of Psychiatry, New York University Grossman School of Medicine, New York, NY, United States, [5]Department of Neuroscience and Physiology, Neuroscience Institute, New York University Grossman School of Medicine, New York, NY, United States, [6]Department of Biomedical Engineering, New York University Tandon School of Engineering, Brooklyn, NY, United States

**Introduction:** Chronic pain negatively impacts a range of sensory and affective behaviors. Previous studies have shown that the presence of chronic pain not only causes hypersensitivity at the site of injury but may also be associated with pain-aversive experiences at anatomically unrelated sites. While animal studies have indicated that the cingulate and prefrontal cortices are involved in this generalized hyperalgesia, the mechanisms distinguishing increased sensitivity at the site of injury from a generalized site-nonspecific enhancement in the aversive response to nociceptive inputs are not well known.

**Methods:** We compared measured pain responses to peripheral mechanical stimuli applied to a site of chronic pain and at a pain-free site in participants suffering from chronic lower back pain ($n = 15$) versus pain-free control participants ($n = 15$) by analyzing behavioral and electroencephalographic (EEG) data.

**Results:** As expected, participants with chronic pain endorsed enhanced pain with mechanical stimuli in both back and hand. We further analyzed electroencephalographic (EEG) recordings during these evoked pain episodes. Brain oscillations in theta and alpha bands in the medial orbitofrontal cortex (mOFC) were associated with localized hypersensitivity, while increased gamma oscillations in the anterior cingulate cortex (ACC) and increased theta oscillations in the dorsolateral prefrontal cortex (dlPFC) were associated with generalized hyperalgesia.

**Discussion:** These findings indicate that chronic pain may disrupt multiple cortical circuits to impact nociceptive processing.

KEYWORDS

**chronic pain, electroencephalography, source localization, oscillations, alpha, theta, gamma**

# 1. Introduction

Pain is a dynamic and multi-dimensional experience shaped by sensory, affective, and cognitive components (Melzack, 2001). Chronic pain, meanwhile, is characterized by both an altered brain state and an abnormal response to transient, evoked inputs (Apkarian et al., 2005; Tracey and Bushnell, 2009; Apkarian et al., 2011). Chronic pain has well-known associations with symptoms of allodynia and/or hypersensitivity at the site of tissue or nerve injury (Basbaum et al., 2009; Latremoliere and Woolf, 2009). At the same time, studies from pain syndromes such as fibromyalgia and knee osteoarthritis have shown that the presence of chronic pain also causes increased pain severity and a distorted pain intensity scale in a diffuse non-anatomic pattern (Petzke et al., 2003; Kudel et al., 2007; Rakel et al., 2015). Thus, chronic pain not only causes hypersensitivity at sites of tissue injury, but it can also lead to a generalized form of enhancement in aversion to evoked stimuli.

Previous neuroimaging studies based on functional magnetic resonance imaging (fMRI) and positron emission tomography (PET) have revealed that chronic pain causes maladaptive changes in a distributed cortical network including the primary somatosensory cortex (S1), the anterior cingulate cortex (ACC), dorsolateral prefrontal cortex (dlPFC), and the insular cortex (IC; Apkarian et al., 2004, 2005; Brooks and Tracey, 2005; Tracey, 2005; Tracey and Mantyh, 2007; Kucyi and Davis, 2015; Mouraux and Iannetti, 2018; Prichep et al., 2018; Van Der Miesen et al., 2019; Chen, 2021). These findings are further supported by studies in animal models (Bingel and Tracey, 2008; Zhang et al., 2017; Xiao et al., 2019; Sun et al., 2023). Less is known, however, about how the brain, in particular the cortex, dynamically responds to a temporally regulated stimulus (Wager et al., 2013; Sun et al., 2021). Electroencephalography (EEG) provides recordings of oscillatory activity in the cortex both at rest and in response to noxious input with high temporal resolution (Hutchison et al., 1999; Pinheiro et al., 2016; Ploner and May, 2018; Levitt and Saab, 2019; Davis et al., 2020). Resting-state EEG studies have shown both increased and decreased power in peak alpha frequency and theta bands, increased beta-band power with increased event-related desynchronization (ERD) in the same bands, mainly in the frontal, parietal, and occipital cortices, and these studies are in general agreement with fMRI and PET results (De Vries et al., 2013; González-Roldán et al., 2016; Levitt et al., 2020; Rockholt et al., 2023). Meanwhile, recent studies of evoked EEG potentials in response to acute painful stimuli, especially in the context of pre-existing chronic pain (Teixeira M. et al., 2021; Teixeira P. E. P. et al., 2021), allow for enhanced understanding of the mechanisms underlying nociception and hyperalgesia (Plaghki and Mouraux, 2005). These studies have shown that chronic pain causes neurons to undergo long-term plasticity that can manifest as increased spiking rates or increased power in high gamma (>60 Hz) and theta (4–8 Hz) oscillations in response to noxious stimuli (Babiloni et al., 2002; Wang et al., 2011; Schulz et al., 2012a; Misra et al., 2017; Zhou R. et al., 2018; Dinh et al., 2019; May et al., 2019; Vanneste et al., 2019; Vanneste and De Ridder, 2021). Some of these studies have applied source localization to infer the cortical sources for such oscillatory changes, showing that both chronic pain and acute pain are associated with abnormalities in regions such as the ACC (Babiloni et al., 2002; Vanneste et al., 2019; Vanneste and De Ridder, 2021). However, few studies have carefully examined source-localized oscillatory changes in response to stimuli targeting painful and non-painful sites in chronic pain conditions. Such studies, however, are critical for understanding brain mechanisms for impairments of endogenous pain processing leading to abnormal pain behaviors.

We conducted a prospective study to identify behavioral and electrophysiological responses to acute mechanical stimuli applied to participants with chronic low back pain (CLBP) as well as pain-free control participants. Our results show that participants with chronic pain demonstrate more intense pain in both their back and the dorsum of the hand. Further, when we analyzed source localized EEG data, we found that hypersensitivity to back is associated with enhanced theta and alpha oscillations in the contralateral medial orbitofrontal cortex (mOFC), whereas increased response to peripheral mechanical stimulation to hand correlates with increased gamma oscillations in the contralateral ACC and increased theta oscillations in the contralateral dlPFC. These results suggest distinct mechanisms for site-specific hypersensitivity and more generalized hyperalgesia.

# 2. Methods

## 2.1. Ethical considerations and participants

The study was approved by the New York University Grossman School of Medicine Institutional Review Board (8/22/2019, #i19-01088) and conducted in accordance with the latest version of the Declaration of Helsinki. Written informed consent was obtained from all participants before study enrollment.

## 2.2. Eligibility criteria

A total of 15 participants with CLBP and 15 control participants were recruited in this study. For participants with CLBP, inclusion criteria were diagnosis of CLBP, defined as pain lasting greater than 6 months, with a baseline average back pain intensity >4 on a 0–10 numerical rating scale OR pain-free participants, aged between 18 and 75 years, and ASA physical status 1–3. Exclusion criteria included acute lumbosacral radiculopathy with signs such as sensory loss, motor weakness, and decreased reflexes, low back pain with any systemic signs or symptoms, cognitive impairment (by history) or clinical signs of altered mental status, history of schizophrenia, daily benzodiazepine use, and pregnancy.

## 2.3. Mechanical stimulation and pain assessment

Participants were blindfolded by a mask and asked to stay relaxed and in a wakeful state during the behavioral tasks and EEG recordings. Weighted mechanical pinprick stimulators (MRC Systems GmbH, Heidelberg, Germany) exerting forces of 32 mN and 256 mN were used. Pinpricks were applied both to the lower back (in the painful

area in participants with CLBP) and the dorsum of the right hand. A total of ~10 trials per force were applied at each site, and stimulations were delivered in random order with an interstimulus interval of approximately 10 s. Participants were asked to rate each stimulus on a 0–10 numeric rating scale.

## 2.4. EEG recordings

Brain activity was recorded using a high density-EEG cap which includes four integrated bipolar leads for vertical and horizontal electrooculogram (EOG; 64-channel Quik-Cap Neo Net, Compumedics Neuroscan, Charlotte, NC, United States). The ground electrode was placed on the left cheek. The EEG cap was connected to the 64-channel Neuroscan SynAmps 2/RT and Nuevo Amplifier (Compumedics Neuroscan, Charlotte, NC, United States). For each session, two 5-min baseline recordings (one with eyes open and one with eyes closed) were performed before applying mechanical stimulations. All data was recorded using Curry 8 (Compumedics Neuroscan, Charlotte, NC, United States) at 1000 Hz.

## 2.5. EEG preprocessing

MNE-Python (version 1.0.3) was used for preprocessing (Gramfort et al., 2013; Larson et al., 2023). First, raw signals were down-sampled to a rate of 400 Hz and band-pass filtered between 1.0 and 100 Hz. A band-stop filter between 55 and 65 Hz removing line noise was applied. Further, noisy EEG channels were detected using PyPREP and subsequently interpolated in MNE-Python (Bigdely-Shamlo et al., 2015; Appelhoff et al., 2022). Criteria for noisy channel detection included low signal-to-noise ratio (SNR), lack of correlation with other channels, low or high relative deviations, presence of high-frequency noise, and poor prediction by other channels based on the random sample consensus approach. All signals were re-referenced to the average reference. An independent component analysis (ICA) based on the fast ICA algorithm was then conducted on the basis of the −0.2 to 0.8 s peri-stimulus time windows of the EEG data using a number of independent components (ICs) equal to half the number of EEG channels (Hyvarinen, 1999). Subsequently, ICs representing artifacts originating from eye movements recorded in the EOG electrode were removed from the EEG data. The cleaned data were analyzed using functions in MNE-Python as well as custom-written Python code. Data were segmented into epochs ranging from −0.2 to 0.8 s in peri-stimulus time. Noisy epochs were detected using the AutoReject package based on Bayesian optimization and were automatically marked for rejection (Jas et al., 2017). Following comparison to recording notes, automatically rejected epochs accurately matched trials marked as containing movement. For the 256 mN stimulation of the back, this resulted in a total of 144 trials for chronic pain and 143 trials for pain-free control participants. The numbers are 151 and 143 trials for the 32 mN stimulation for CLBP and pain-free participants, respectively. For the 256 mN stimulation of the hand, this resulted in 156 trials for chronic pain participants and 148 trials for control participants. The numbers are 156 and 147 trials for the 32 mN stimulation for CLBP and pain-free participants, respectively.

## 2.6. Source model

To project sensor-space time series to source space, we used dynamical statistical parametric mapping (dSPM) for noise-normalization, implemented in MNE-Python (Dale et al., 2000). The surface-based, three-shell boundary element model used for anatomical reconstruction is sourced from 'fsaverage', a template brain based on 40 MRI scans of real brains (Fischl et al., 1999, 2004; Destrieux et al., 2010). For each individual, a regularized noise covariance matrix was computed from a two-minute period in the resting condition before the start of the stimulus portion of the EEG recording. The inverse solution computed with a loose-orientation value of 0.2 was chosen to allow source space dipoles to have somewhat free orientation, but not too far from an orientation that is perpendicular to the cortex.

## 2.7. Assessment of source-space TFRs

Source-space time-frequency representations (TFRs) were obtained from the source time course epochs using a Slepian multitaper approach from 1 to 100 Hz, omitting the 55 to 65 Hz band-stop range. We selected event-related synchronization and desynchronization (ERS/ERD) as the preferred method for assessing changes in oscillatory activity following mechanical stimulation. ERS/ERD is defined as the percentage of power decrease or increase, respectively, according to the expression $ERD\% = (A - R)/R \times 100$ where the power within the frequency bands of interest in the period after the event is given by A and that that of the preceding baseline period is given by R (Pfurtscheller and Lopes Da Silva, 1999). Therefore, TFRs were referenced to the baseline period (−0.2 to 0.0 s) by subtracting the mean of the baseline and dividing by the mean of the baseline, resulting in percent-change power values. To compare responses to stimuli between the two groups, the source-space TFRs were first band-pass filtered to the frequency band of interest, theta (4 to 8 Hz), alpha (8 to 13 Hz), and high-gamma (65 to 100 Hz; May et al., 2019; Shirvalkar et al., 2023). We then averaged power values across time from 0.0 to 0.8 s post-stimulus onset for each trial of all participants in each group. To maximize the signal-to-noise ratio for visualization, TFRs represented by heat maps were averaged across epochs of the same stimulus site.

## 2.8. Statistical analyses

All data was analyzed using IBM SPSS Statistical software (Version 28, IBM, New York, United States) and GraphPad Prism (Version 9.4.1, GraphPad Software, Boston, United States). Results were expressed as mean ± standard error of mean (SEM) or median [interquartile range] for continuous variables and frequency and percentage for categorical variables. For all behavioral data, a non-parametric Mann–Whitney U test was used for hypothesis testing to compare the mean pain scores. A non-parametric Mann–Whitney U test was also used for hypothesis testing to compare the mean power values. We chose the Mann–Whitney U test to account for non-Gaussian distributions in the mean power values from the

trials of each participant. The mean power in each frequency band was tested independently. $p < 0.05$ was considered significant.

# 3. Results

## 3.1. Participant characteristics

The sample ($n = 30$) consisted of age and gender-matched participants with CLBP [$n = 15$; 11 male (73%), 4 female (27%)], with the majority suffering from chronic pain for 1–5 years (60%), and those who were pain-free [$n = 15$: 11 male (73%), 4 female (27%)] with the mean age of 49.9 ± 4.71 and 50.5 ± 3.76, respectively.

## 3.2. Participants with CLBP experience increased sensitivity at painful and non-painful sites

We used a 256 mN stimulus and a 32 mN stimulus to induce mechanical stimulations to the lower back and hand of all participants. For chronic pain patients, the lower back region represents the site of their chronic pain. Pain scores across all trials per stimulus intensity across all groups were analyzed and compared using the Mann–Whitney U test; both participants with CLBP, as well as control participants, reported higher pain scores with the 256 mN stimulus than the 32 mN stimulus at both the hand (3.1 [2.3–4.6] vs. 1.3 [0.7–2.4] and 1.9 [1.0–3.3] vs. 0.7 [0.3–1.1], respectively: $p < 0.001$) and the lower back (3.3 [2.3–4.5] vs. 2.1 [1.2–2.8] and 2.0 [1.1–3.8] vs. 1.2 [0.4–2.1], respectively: $p < 0.001$). Importantly, as presented in Figure 1, participants with CLBP reported statistically significantly higher scores than control participants for the noxious stimuli at both the lower back and hand ($p < 0.001$).

## 3.3. Sensitivity to the site of chronic pain is associated with increased theta and alpha oscillations in the OFC

We measured cortical activity using a 64-channel-EEG cap, for 5 min at baseline before and during mechanical stimulations to the lower back of all participants. EEG signals were sampled at 1000 Hz and band-pass filtered between 1 and 100 Hz. After band-pass filtering, we source localized our data using dSPM (Figure 2). To better understand mechanisms for both site-specific and anatomically nonspecific hyperalgesia, we focused our analysis on cortical areas such as the ACC, dlPFC, and mOFC which are known to be important for pain processing but demonstrate little or no somatotopy.

We quantitated EEG power in the control participants and CLBP participants, and measured power in canonical frequency bands while focusing on theta (4–8 Hz), alpha (8–13 Hz), and high-gamma (65–100 Hz) bands (Figure 3; Supplementary Figure S1). We then calculated changes in power from baseline in these frequencies in response to 32 mN or 256 mN stimuli applied to the back of these participants. We found that participants with CLBP demonstrated a statistically significant increase in the mean power at the alpha and theta frequencies in the contralateral medial OFC, compared with pain-free control participants (Figure 4) for the 256 mN stimulus (theta 1.243 ± 0.1453 vs. 0.8538 ± 0.1239, $p = 0.0028$, alpha 0.9887 ± 0.1040 vs. 0.6394 ± 0.0775, $p = 0.0034$) but not the 32 mN stimulus (theta 1.0494 ± 0.1606 vs. 0.8022 ± 0.1227, $p = 0.4737$, alpha 0.7735 ± 0.0857 vs. 0.9466 ± 0.0902, $p = 0.0924$).

## 3.4. Sensitivity to anatomically unrelated sites among chronic pain participants is associated with increased theta in dlPFC and gamma oscillations in the ACC

Next, we quantitated EEG powers in the control participants and CLBP participants, and measured power in the theta (4–8 Hz), alpha (8–13 Hz), and high-gamma (65–100 Hz) bands in response to mechanical stimulations to the hand of all participants (Figure 5; Supplementary Figure S2). We calculated changes in power from baseline across different frequencies in response to either 32 mN or 256 mN stimuli applied to the right hand of these participants. We found that participants with CLBP, compared with control participants, demonstrated a statistically significant increase in the mean power at the theta frequency in the dlPFC and the high gamma frequency band in the ACC (Figure 6) with the 256 mN stimulus (theta 0.9909 ± 0.1872 vs. 0.6138 ± 0.0799, $p = 0.0385$, high-gamma 1.8779 ± 0.5073 vs. 1.8198 ± 0.4141, $p = 0.0294$) but not the 32 mN stimulus (theta 0.7257 ± 0.0979 vs. 0.8179 ± 0.0915, $p = 0.2207$, high-gamma 1.1838 ± 0.2862 vs. 1.0532 ± 0.1777, $p = 0.3133$).

# 4. Discussion

In this study, we used EEG to record cortical responses to acute mechanical stimuli applied to participants with CLBP vs. pain-free control participants. Our data indicate that CLBP participants demonstrated hypersensitivity both at the site of chronic pain and at a non-painful site. Source localized EEG data, meanwhile, suggest distinct cortical mechanisms that underlie hypersensitivity to painful and non-painful sites in these participants.

There is accumulating evidence that specific oscillatory activity patterns in anatomically defined brain regions, as well as the synchronization between them, play a key role in acute and chronic pain processing. The use of source localization algorithms for high-density EEG recordings, in particular, is an emerging technical development in the pain field that has enabled insights into cortical mechanisms of both acute and chronic pain in human subjects (Stern et al., 2006; Jensen et al., 2013; Prichep et al., 2018; Seeber et al., 2019; Teixeira M. et al., 2021; Teixeira P. E. P. et al., 2021; Völker et al., 2021; Mussigmann et al., 2022; Bott et al., 2023; Rockholt et al., 2023). In this study, we have focused on the cortical response to evoked stimuli rather than resting measurements. There have already been a number of EEG studies examining resting cortical activity in pain states, and changes in power responses in various frequency bands have been reported (Stern et al., 2006; Michels et al., 2011; Van Den Broeke et al., 2013; Prichep et al., 2018; Teixeira M. et al., 2021; Teixeira P. E. P. et al., 2021; Vanneste and De Ridder, 2021; Heitmann et al., 2022; Rockholt et al., 2023). However, the evaluation of resting state EEG potentials can sometimes be confounded by other time-invariant brain processes (Hansen et al., 2017). In contrast, evoked EEG provides

10.3389/fnins.2023.1278183

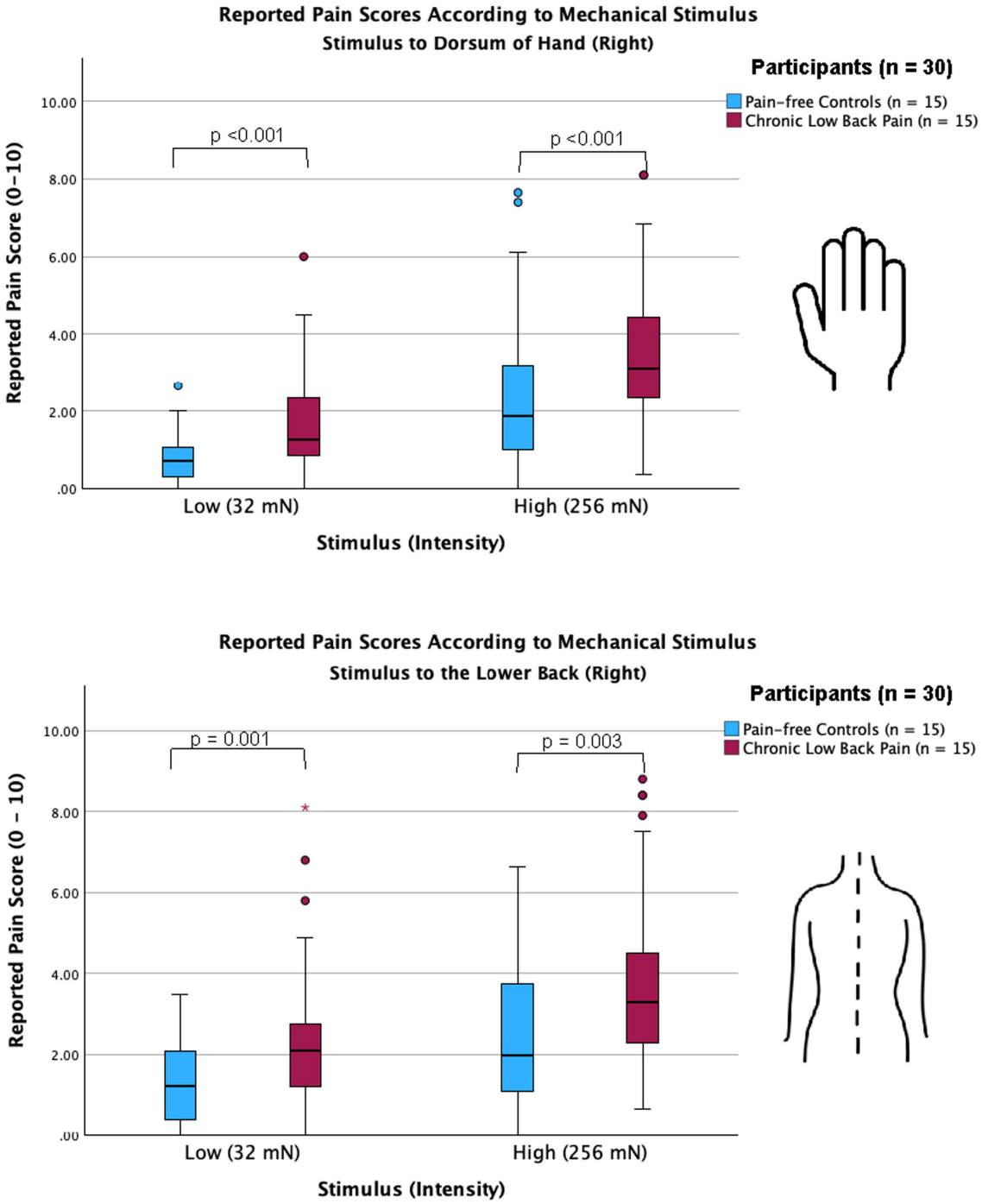


FIGURE 1
Chronic low back pain participants show increased sensitivity in both back and hand compared with pain-free controls. Clustered box plots with median [interquartile range] for pain scores (numerical rating scale, 0–10) for stimuli applied to the dorsum of right hand (upper graph) and the lower back (lower graph) of pain-free controls and chronic pain participants. Participants with chronic lower back pain, as well as pain-free control participants, reported significantly higher pain scores for both low-intensity (32 mN) and high-intensity stimuli (256 mN) when applied to the dorsum of the hand ($p < 0.001$) and the lower back ($p = 0.001$ and $p = 0.003$, respectively). Outliers are represented by red circles and stars. Hypothesis testing was performed using the non-parametric Mann–Whitney test for independent groups.

time-sensitive data, and thus can complement findings from resting EEG studies; in particular, evoked EEG allows assessment of how the presence of chronic pain alters normal nociceptive processing (Teixeira M. et al., 2021; Teixeira P. E. P. et al., 2021) and thus provide insights into mechanisms underlying pathological processes such as allodynia and hyperalgesia (Plaghki and Mouraux, 2005). This information is of particular interest when examining chronic pain participants, as the number of studies evaluating neural responses to evoked painful stimuli in this cohort is scarce (Apkarian et al., 2005; Mussigmann et al., 2022).

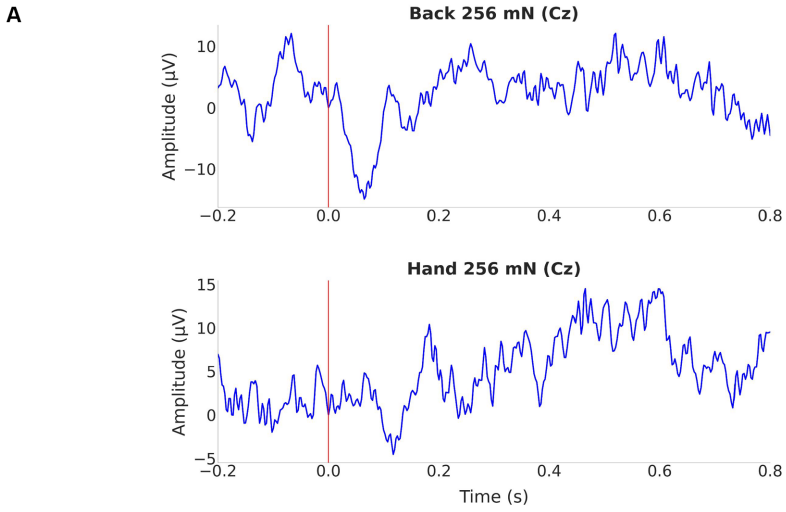


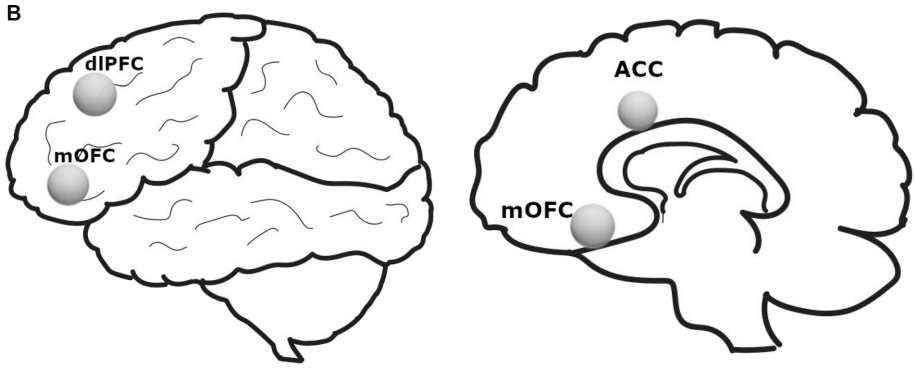


**MNI Coordinates (mm)**

| Region | x | y | z |
|---|---|---|---|
| *ACC* | -5.07 | 19.16 | 26.37 |
| *dlPFC* | -6.83 | 30.38 | 52.35 |
| *mOFC* | -5.13 | 37.25 | -20.34 |

FIGURE 2
EEG recording and source localization overview. **(A)** Example EEG from electrode Cz in a chronic pain participant during mechanical stimulation (256 mN) to the lower back (top) and hand (bottom). **(B)** Lateral and medial views of the brain and regions of interest (ROIs) used for source localization. Also shown are the MNI coordinates of the 3 (contralateral) ROIs in millimeter scale. ACC, anterior cingulate cortex; dlPFC, dorsolateral prefrontal cortex; mOFC, medial orbitofrontal cortex.

In this study, we found changes in alpha, theta and gamma oscillations in chronic pain participants, and indeed oscillatory activities in these frequency ranges have been repeatedly shown to play important roles in previous studies on pain, particularly when evaluating evoked pain stimuli from pain-free participants (Gross et al., 2007; Zhang et al., 2012; Schulz et al., 2012b, 2015; Peng and Tang, 2016; Taesler and Rose, 2016; Peng et al., 2017). The alpha oscillation is the predominant oscillatory activity observed in sensory cortices at resting states and is commonly studied in the context of pain research. In resting state studies, increased alpha power has been noted in frontal, sensory, temporal, and parietal areas (Kisler et al., 2020). Experimentally induced transient pain in chronic pain and healthy cohorts elicited decreases in alpha power in the frontal-central or parietal-occipital regions which were

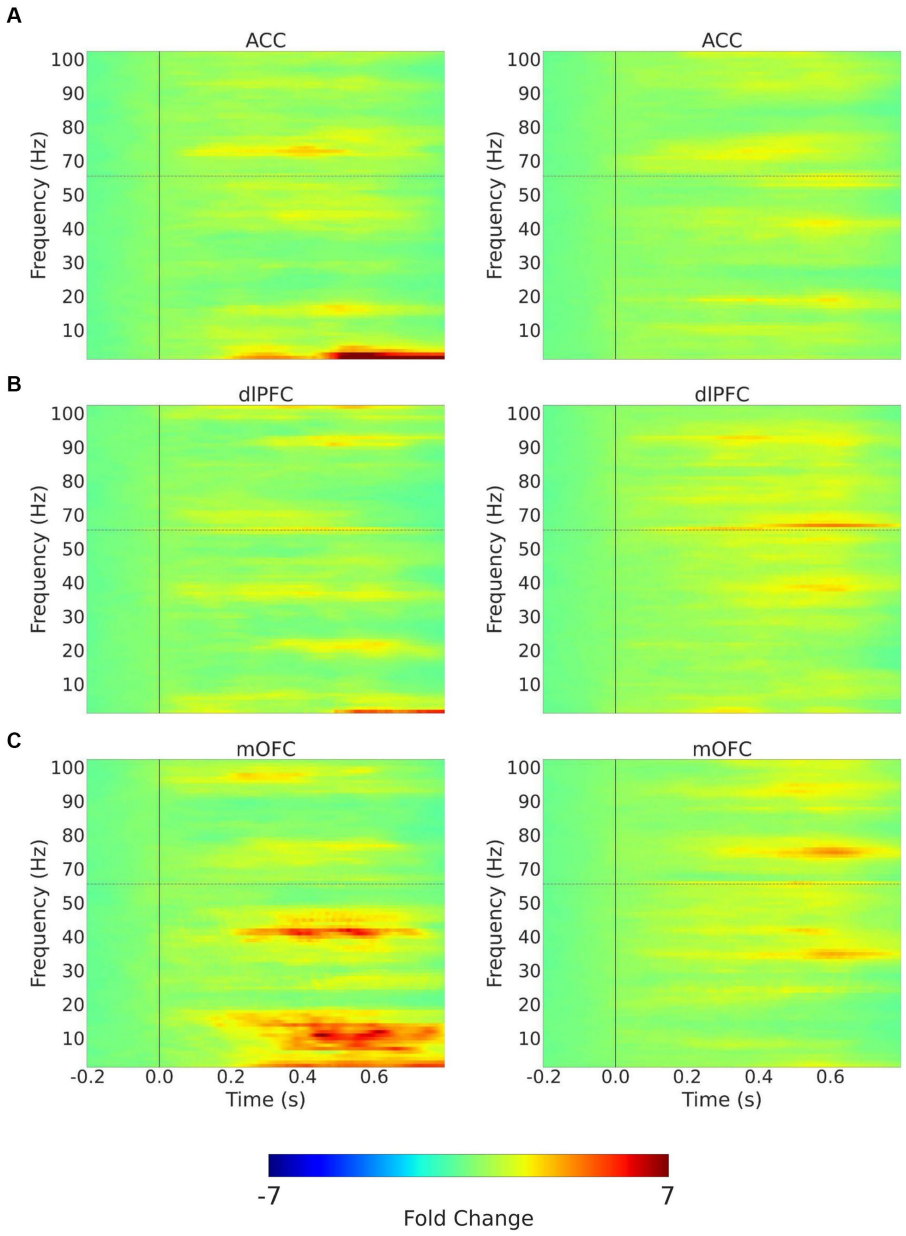


FIGURE 3
Trial-averaged time-frequency spectra with mechanical stimulation to the lower back with 256 mN. Time-frequency spectra (TFRs) are shown for example recordings from a chronic pain participant (left) and a pain-free control participant (right) for the 3 (contralateral) ROIs, **(A)** ACC; **(B)** dlPFC; **(C)** mOFC. Frequencies between 55 and 65 Hz (horizontal dashed line) omitted to remove electrical line noise. The TFRs represent percent change with respect to the baseline (−0.2–0.0 s before stimulus onset). ACC, anterior cingulate cortex; dlPFC, dorsolateral prefrontal cortex; mOFC, medial orbitofrontal cortex.

inversely associated with stimulus intensity (Peng et al., 2014, 2015; Schulz et al., 2015; Misra et al., 2017; Nickel et al., 2017; Wang et al., 2019, 2021; Baroni et al., 2020). Theta oscillations in the hippocampus and cortex, however, are not only known to be important for sleep and cognition in animal and human studies (Green and Arduini, 1954; Winson, 1978; Wang, 2010; Seger et al., 2023), but have also been found to contribute to pain modulation (Taesler and Rose, 2016) where increased theta activity has been reported in participants with various chronic pain conditions, both in resting state recordings as well as evoked EEG potentials (Sarnthein and Jeanmonod, 2008; Vuckovic et al., 2014; González-Roldán et al., 2016; Hansen et al., 2017; Lee et al., 2017; Fallon et al., 2018; Wang et al., 2019). In addition, theta rhythmicity can also reflect a brain state of social response to social and fearful stimuli, further contributing to the pain experience (Tendler and Wagner, 2015). Meanwhile, changes in amplitudes of gamma oscillations have been shown to correlate with both evoked stimulus intensity and subjective pain rating in several studies (Gross et al., 2007; Michels et al., 2011; Zhang et al., 2012; Schulz et al., 2015; Mouraux and Iannetti, 2018; Zhou R. et al., 2018; Dinh et al., 2019; May et al.,

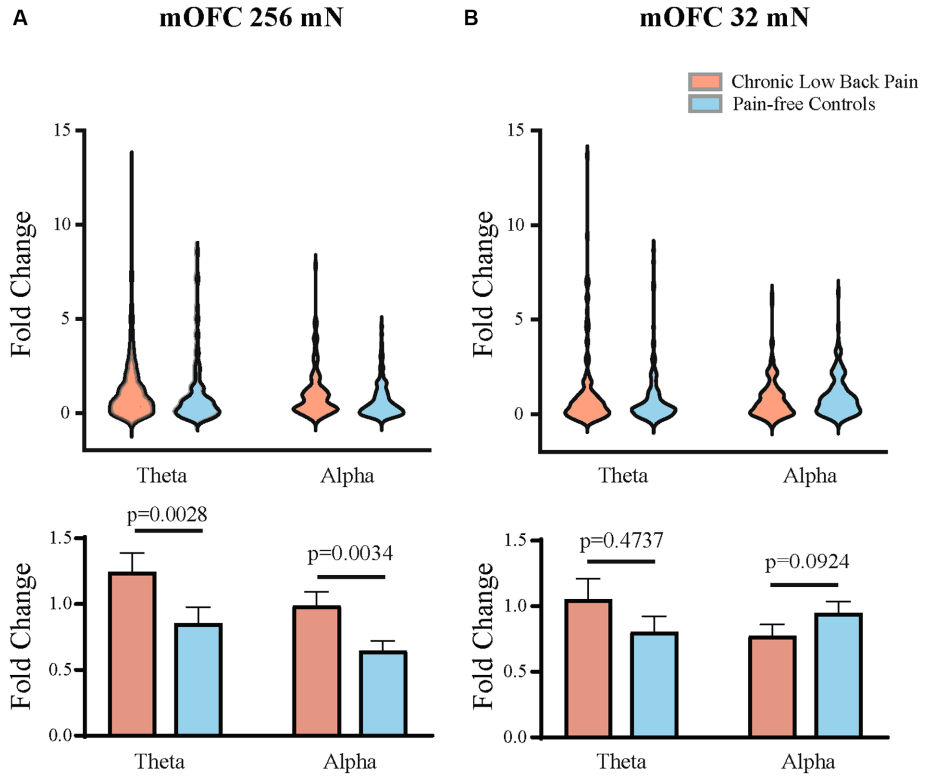


FIGURE 4
Mean theta and alpha band power are higher in the contralateral mOFC after mechanical stimulations to the lower back. **(A)** Mechanical stimulation with 256 mN results in a greater increase in the fold change of mean power in the theta ($p = 0.0028$) and alpha frequencies ($p = 0.0034$) of mOFC in participants with chronic low back pain ($n = 15$ participants and 144 trials) than pain-free controls ($n = 15$ participants and 143 trials). **(B)** Stimulation with 32 mN did not result in any statistically significant differences in the theta and alpha frequencies between chronic pain ($n = 15$ participants and 151 trials) and pain-free control participants ($n = 15$ participants and 143 trials). Data are shown as mean +/− SEM.

2019; Baroni et al., 2020; Vanneste and De Ridder, 2021), where recent animal studies have also shown that theta and gamma oscillations in the ACC and S1 may encode the intensity of pain (Harris-Bozer and Peng, 2016; Tan et al., 2019; Sun et al., 2022, 2023; Zhang et al., 2023).

A key finding in our study is that whereas hypersensitivity at the site of injury (back) is associated with enhanced theta and alpha oscillations in the contralateral OFC, more generalized, anatomically-nonspecific enhancement in nociceptive response is seen with increased gamma oscillations in the ACC and increased theta oscillations in the contralateral dlPFC. To our knowledge, we are among the first group to distinguish between the locations of peripheral noxious stimuli. Such distinction is important, however, from both clinical and scientific viewpoints. Clinically, there is a need to distinguish between peripheral hypersensitivity and a more generalized, anatomically diffuse, enhancement for pain sensitivity, as treatments are often different. Scientifically, peripheral and spinal mechanisms as well as mechanisms in the brain may contribute to hypersensitivity at the site of injury, whereas the brain likely plays a more dominant role in a more generalized form of hyperalgesia. Our results here are compatible with findings from multiple animal studies that specifically investigated hyperalgesia of diffuse distribution, where enhancement in high gamma oscillatory activities in the ACC has been shown to be important and likely play a causal role (Zhang et al., 2017; Zhou H. et al., 2018; Friesner et al., 2020; Sun et al., 2021). The dlPFC, meanwhile, is known to produce top-down pain regulation, and its activation in response to nociceptive inputs has been widely reported in both human and animal literature (Hardy, 1985; Lee et al., 2015; Zhang et al., 2015; Kiritoshi et al., 2016; Martinez et al., 2017; Dale et al., 2018). Interestingly, a recent study using chronic intracranial recordings in patients with refractory pain showed that sustained power changes from the OFC can be used to detect the presence of chronic pain, whereas transient, evoked pain processing may be found in the ACC (Shirvalkar et al., 2023). It is possible that peripheral hypersensitivity serves as an index of chronic pain, and that OFC, which has prominent roles in reward processing as well as placebo analgesia (Petrovic et al., 2002; Kringelbach, 2005), may integrate multiple cognitive functions including disease-threat assessment to process allodynic-type of experiences. Due to the lack of threat at the non-injured site, OFC activity may play a more minor role, as shown by results in the cortical response to hand stimulation in our study.

There are several limitations to this study. The sample size was limited, and thus it is possible that the study was not powered to detect changes in all cortical areas. Further, the study was focused on participants with CLBP, and there are many additional chronic pain conditions. Future investigations with larger sample sizes and the inclusion of other chronic pain conditions are needed to assess the generalizability of our findings. Large sample sizes may also facilitate

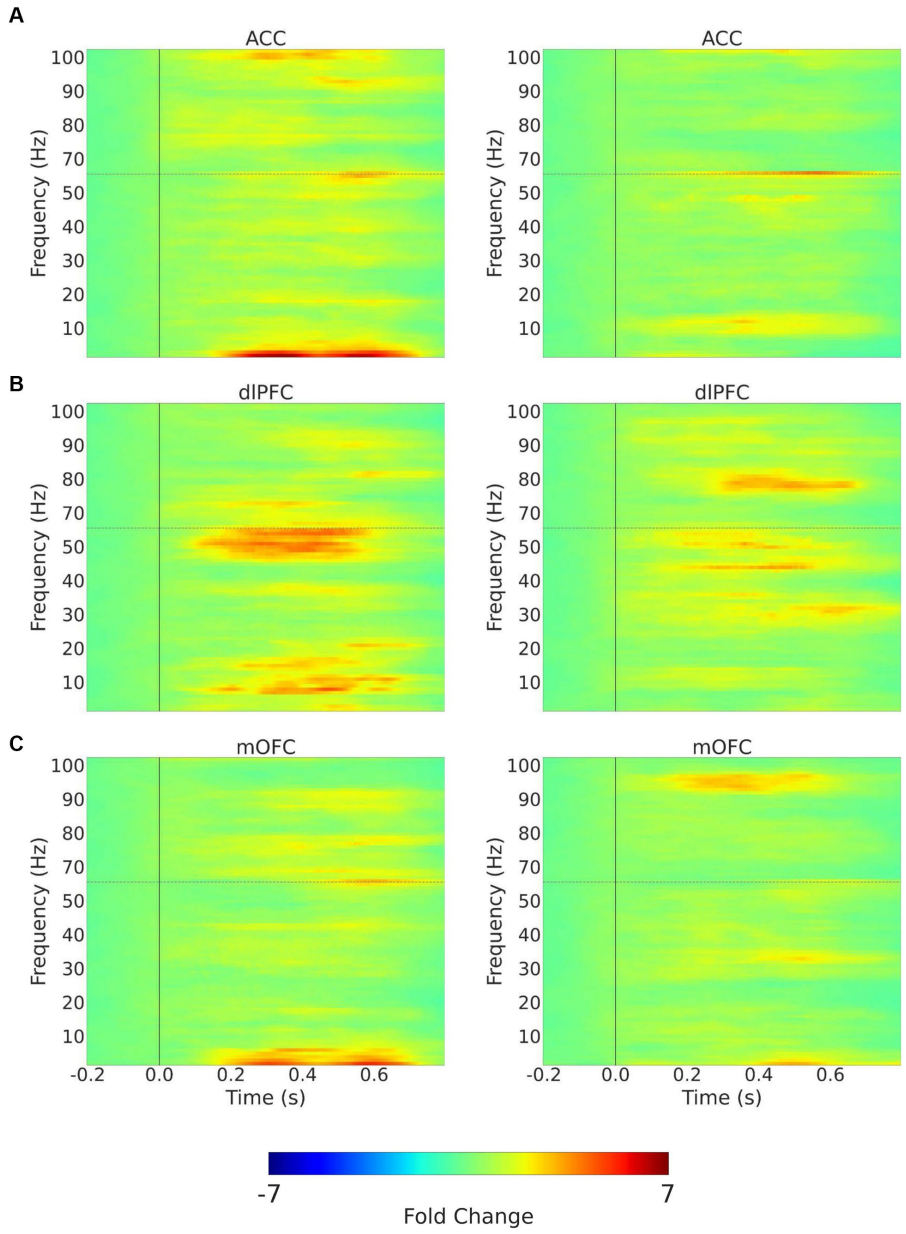


FIGURE 5
Trial-averaged time-frequency spectra with mechanical stimulation to the hand with 256 mN. Time-frequency spectra (TFRs) are shown for example recordings from a chronic pain participant (left) and a pain-free control participant (right) for the 3 (contralateral) ROIs, **(A)** ACC; **(B)** dlPFC; **(C)** mOFC. Frequencies between 55 and 65 Hz (hoirizontal dashed line) omitted to remove electrical line noise. The TFRs represent percent change with respect to the baseline (−0.2–0.0 s before stimulus onset). ACC, anterior cingulate cortex; dlPFC, dorsolateral prefrontal cortex; mOFC, medial orbitofrontal cortex.

functional connectivity studies to understand how nociceptive information flows among different regions. Further studies of larger sample sizes are also needed to carefully analyze sex differences in cortical pain processing. Another limitation of this study is the use of two pinprick stimulators with fixed forces applied to all participants. Due to our sample size, we have based our EEG analysis on stimulus intensity, rather than pain scores, as done in previous studies (Nickel et al., 2017). Our protocol did not include temporal summation, and thus overall, evoked pain was less intense, unlike in previous studies of ERP responses to more intense stimulations (Hu et al., 2014). Hence, future studies of larger sample sizes using a larger range of noxious stimuli during EEG recordings could further analyze changes in brain activity. In addition, due to the nature of the short-lived mechanical stimulations, the cortical response we observed is likely the result of sensitization to A fiber stimulation, rather than C fiber stimulation, and thus future studies using different protocols such as thermal stimulations can provide a more complete picture of cortical changes in response to nociceptive inputs.

In conclusion, we have identified multiple cortical circuit elements that may underlie potential mechanisms on how chronic pain not only confers hypersensitivity at the site of injury but also induces a more anatomically nonspecific form of generalized

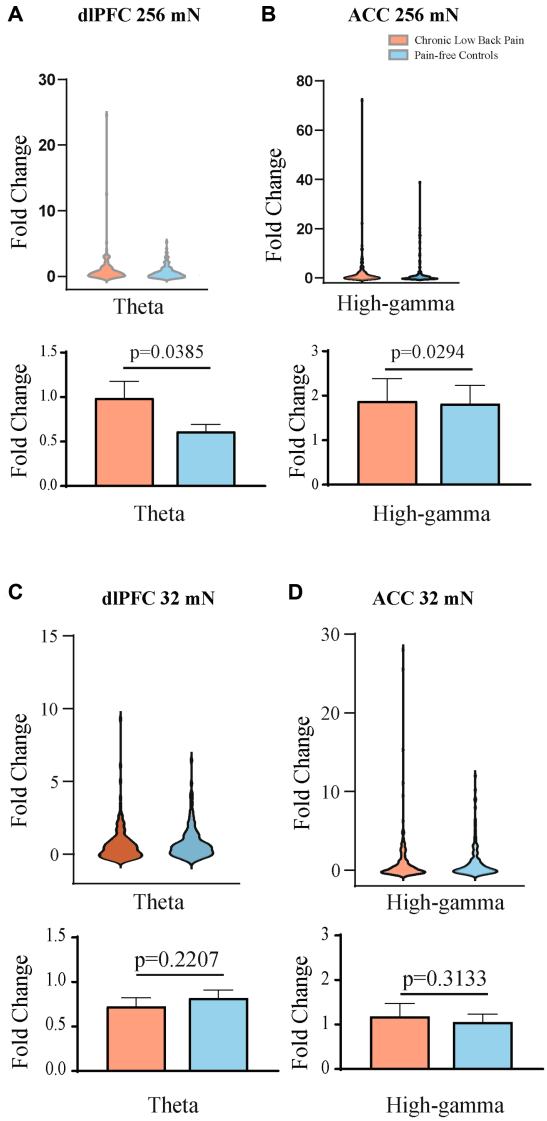


FIGURE 6
Mean theta and high gamma band power are higher in the contralateral dlPFC and contralateral ACC, respectively, after mechanical stimulations to the hand. **(A)** Mechanical stimulation with 256 mN results in a greater fold increase in the mean power of the theta frequency band in the dlPFC of participants with chronic low back pain ($n = 15$ participants and 156 trials) than that of pain-free controls ($n = 15$ participants and 148 trials), $p = 0.0385$. **(B)** Mechanical stimulation with 256 mN results in a greater fold increase in the mean power of the high-gamma frequency band in the ACC of participants with chronic low back pain than that of pain-free controls, $p = 0.0294$. **(C)** Stimulation with 32 mN did not result in any statistically significant differences in the mean power of the theta frequency band in the dlPFC between chronic pain and pain-free control participants. **(D)** Stimulation with 32 mN did not result in any statistically significant differences in the mean power of the high-gamma frequency band in the ACC between chronic pain ($n = 15$ participants and 156 trials) and pain-free control participants ($n = 15$ participants and 147 trials). Data are shown as mean +/− SEM.

hypersensitivity. Future studies of larger sample sizes utilizing more detailed analysis, including functional connectivity analysis, will provide further insights into how chronic pain alters normal nociceptive functions in the brain.

## Data availability statement

The original contributions presented in the study are included in the article/Supplementary material, further inquiries can be directed to the corresponding authors.

## Ethics statement

The studies involving humans were approved by Institutional Review Board of New York University Grossman School of Medicine. The studies were conducted in accordance with the local legislation and institutional requirements. The participants provided their written informed consent to participate in this study.

## Author contributions

GK: Data curation, Formal analysis, Methodology, Project administration, Software, Visualization, Writing – original draft, Writing – review & editing. MMR: Data curation, Formal analysis, Investigation, Project administration, Writing – original draft, Writing – review & editing. DO: Investigation, Project administration, Writing – review & editing. MM: Investigation, Project administration, Writing – review & editing. QZ: Data curation, Formal analysis, Methodology, Writing – review & editing. GS: Investigation, Methodology, Project administration, Writing – review & editing. JM: Data curation, Formal analysis, Writing – review & editing. AW: Data curation, Formal analysis, Writing – review & editing. BC: Data curation, Formal analysis, Writing – review & editing. EPV: Investigation, Project administration, Writing – review & editing. ZSC: Data curation, Formal analysis, Methodology, Writing – review & editing. JW: Conceptualization, Data curation, Formal analysis, Funding acquisition, Investigation, Methodology, Supervision, Writing – original draft, Writing – review & editing. LVD: Conceptualization, Data curation, Formal analysis, Funding acquisition, Investigation, Supervision, Writing – review & editing.

## Funding

The author(s) declare financial support was received for the research, authorship, and/or publication of this article. The authors acknowledge funding from the Interdisciplinary Pain Research Program; Department of Anesthesiology, Perioperative Care, and Pain Medicine, NYU Grossman School of Medicine. Any opinions, findings, and conclusions or recommendations expressed in this article are solely those of the authors and do not necessarily reflect the views of the funding agencies.

## Conflict of interest

JW is a cofounder of Pallas Technologies, Inc., and ZSC is a scientific advisor of Pallas Technologies, Inc. JW and ZSC are inventors of a pending US patent application of pain treatment technology.

The remaining authors declare that the research was conducted in the absence of any commercial or financial relationships that could be construed as a potential conflict of interest.

The author(s) declared that they were an editorial board member of Frontiers, at the time of submission. This had no impact on the peer review process and the final decision.

## Publisher's note

All claims expressed in this article are solely those of the authors and do not necessarily represent those of their affiliated organizations, or those of the publisher, the editors and the reviewers. Any product that may be evaluated in this article, or claim that may be made by its manufacturer, is not guaranteed or endorsed by the publisher.

## Supplementary material

The Supplementary material for this article can be found online at: https://www.frontiersin.org/articles/10.3389/fnins.2023.1278183/full#supplementary-material

## References


Apkarian, A. V., Bushnell, M. C., Treede, R. D., and Zubieta, J. K. (2005). Human brain mechanisms of pain perception and regulation in health and disease. *Eur. J. Pain* 9, 463–484. doi: 10.1016/j.ejpain.2004.11.001

Apkarian, A. V., Hashmi, J. A., and Baliki, M. N. (2011). Pain and the brain: specificity and plasticity of the brain in clinical chronic pain. *Pain* 152, S49–S64. doi: 10.1016/j.pain.2010.11.010

Apkarian, A. V., Sosa, Y., Sonty, S., Levy, R. M., Harden, R. N., Parrish, T. B., et al. (2004). Chronic back pain is associated with decreased prefrontal and thalamic gray matter density. *J. Neurosci.* 24, 10410–10415. doi: 10.1523/JNEUROSCI.2541-04.2004

Appelhoff, S. H., Austin, J., Lawrence, A., Li, A., Mantilla Ramos, Y. J., O'Reilly, C., et al. (2022). PyPREP: a Python implementation of the preprocessing pipeline (PREP) for EEG data. *Zenodo* 2. doi: 10.5281/zenodo.6363576

Babiloni, C., Babiloni, F., Carducci, F., Cincotti, F., Rosciarelli, F., Arendt-Nielsen, L., et al. (2002). Human brain oscillatory activity phase-locked to painful electrical stimulations: a multi-channel EEG study. *Hum. Brain Mapp.* 15, 112–123. doi: 10.1002/hbm.10013

Baroni, A., Severini, G., Straudi, S., Buja, S., Borsato, S., and Basaglia, N. (2020). Hyperalgesia and central sensitization in subjects with chronic orofacial pain: analysis of pain thresholds and EEG biomarkers. *Front. Neurosci.* 14:552650. doi: 10.3389/fnins.2020.552650

Basbaum, A. I., Bautista, D. M., Scherrer, G., and Julius, D. (2009). Cellular and molecular mechanisms of pain. *Cells* 139, 267–284. doi: 10.1016/j.cell.2009.09.028

Bigdely-Shamlo, N., Mullen, T., Kothe, C., Su, K. M., and Robbins, K. A. (2015). The PREP pipeline: standardized preprocessing for large-scale EEG analysis. *Front. Neuroinform.* 9:16. doi: 10.3389/fninf.2015.00016

Bingel, U., and Tracey, I. (2008). Imaging CNS modulation of pain in humans. *Physiology* 23, 371–380. doi: 10.1152/physiol.00024.2008

Bott, F. S., Nickel, M. M., Hohn, V. D., May, E. S., Gil Ávila, C., Tiemann, L., et al. (2023). Local brain oscillations and interregional connectivity differentially serve sensory and expectation effects on pain. *Sci. Adv.* 9:eadd7572. doi: 10.1126/sciadv.add7572

Brooks, J., and Tracey, I. (2005). From nociception to pain perception: imaging the spinal and supraspinal pathways. *J. Anat.* 207, 19–33. doi: 10.1111/j.1469-7580.2005.00428.x

Chen, Z. S. (2021). Decoding pain from brain activity. *J. Neural Eng.* 18:051002. doi: 10.1088/1741-2552/ac28d4

Dale, A. M., Liu, A. K., Fischl, B. R., Buckner, R. L., Belliveau, J. W., Lewine, J. D., et al. (2000). Dynamic statistical parametric mapping: combining fMRI and MEG for high-resolution imaging of cortical activity. *Neuron* 26, 55–67. doi: 10.1016/s0896-6273(00)81138-1

Dale, J., Zhou, H., Zhang, Q., Martinez, E., Hu, S., Liu, K., et al. (2018). Scaling up cortical control inhibits pain. *Cell Rep.* 23, 1301–1313. doi: 10.1016/j.celrep.2018.03.139

Davis, K. D., Aghaeepour, N., Ahn, A. H., Angst, M. S., Borsook, D., Brenton, A., et al. (2020). Discovery and validation of biomarkers to aid the development of safe and effective pain therapeutics: challenges and opportunities. *Nat. Rev. Neurol.* 16, 381–400. doi: 10.1038/s41582-020-0362-2

De Vries, M., Wilder-Smith, O. H., Jongsma, M. L., Van Den Broeke, E. N., Arns, M., Van Goor, H., et al. (2013). Altered resting state EEG in chronic pancreatitis patients: toward a marker for chronic pain. *J. Pain Res.* 6, 815–824. doi: 10.2147/JPR.S50919

Destrieux, C., Fischl, B., Dale, A., and Halgren, E. (2010). Automatic parcellation of human cortical gyri and sulci using standard anatomical nomenclature. *NeuroImage* 53, 1–15. doi: 10.1016/j.neuroimage.2010.06.010

Dinh, S. T., Nickel, M. M., Tiemann, L., May, E. S., Heitmann, H., Hohn, V. D., et al. (2019). Brain dysfunction in chronic pain patients assessed by resting-state electroencephalography. *Pain* 160, 2751–2765. doi: 10.1097/j.pain.0000000000001666

Fallon, N., Chiu, Y., Nurmikko, T., and Stancak, A. (2018). Altered theta oscillations in resting EEG of fibromyalgia syndrome patients. *Eur. J. Pain* 22, 49–57. doi: 10.1002/ejp.1076

Fischl, B., Sereno, M. I., Tootell, R. B. H., and Dale, A. M. (1999). High-resolution intersubject averaging and a coordinate system for the cortical surface. *Hum. Brain Mapp.* 8, 272–284. doi: 10.1002/(sici)1097-0193(1999)8:4<272::aid-hbm10>3.0.co;2-4

Fischl, B., Van Der Kouwe, A., Destrieux, C., Halgren, E., Ségonne, F., Salat, D. H., et al. (2004). Automatically parcellating the human cerebral cortex. *Cereb. Cortex* 14, 11–22. doi: 10.1093/cercor/bhg087

Friesner, I. D., Martinez, E., Zhou, H., Gould, J. D., Li, A., Chen, Z. S., et al. (2020). Ketamine normalizes high-gamma power in the anterior cingulate cortex in a rat chronic pain model. *Mol. Brain* 13:129. doi: 10.1186/s13041-020-00670-w

González-Roldán, A. M., Cifre, I., Sitges, C., and Montoya, P. (2016). Altered dynamic of EEG oscillations in fibromyalgia patients at rest. *Pain Med.* 17, 1058–1068. doi: 10.1093/pm/pnw023

Gramfort, A., Luessi, M., Larson, E., Engemann, D., Strohmeier, D., Brodbeck, C., et al. (2013). MEG and EEG data analysis with MNE-Python. *Front. Neurosci.* 7:267. doi: 10.3389/fnins.2013.00267

Green, J. D., and Arduini, A. A. (1954). Hippocampal electrical activity in arousal. *J. Neurophysiol.* 17, 533–557. doi: 10.1152/jn.1954.17.6.533

Gross, J., Schnitzler, A., Timmermann, L., and Ploner, M. (2007). Gamma oscillations in human primary somatosensory cortex reflect pain perception. *PLoS Biol.* 5:e133. doi: 10.1371/journal.pbio.0050133

Hansen, T. M., Mark, E. B., Olesen, S. S., Gram, M., Frøkjær, J. B., and Drewes, A. M. (2017). Characterization of cortical source generators based on electroencephalography during tonic pain. *J. Pain Res.* 10, 1401–1409. doi: 10.2147/JPR.S132909

Hardy, S. G. (1985). Analgesia elicited by prefrontal stimulation. *Brain Res.* 339, 281–284. doi: 10.1016/0006-8993(85)90093-9

Harris-Bozer, A. L., and Peng, Y. B. (2016). Inflammatory pain by carrageenan recruits low-frequency local field potential changes in the anterior cingulate cortex. *Neurosci. Lett.* 632, 8–14. doi: 10.1016/j.neulet.2016.08.016

Heitmann, H., Gil Ávila, C., Nickel, M. M., Ta Dinh, S., May, E. S., Tiemann, L., et al. (2022). Longitudinal resting-state electroencephalography in patients with chronic pain undergoing interdisciplinary multimodal pain therapy. *Pain* 163, e997–e1005. doi: 10.1097/j.pain.0000000000002565

Hu, L., Cai, M. M., Xiao, P., Luo, F., and Iannetti, G. D. (2014). Human brain responses to concomitant stimulation of Aδ and C nociceptors. *J. Neurosci.* 34, 11439–11451. doi: 10.1523/JNEUROSCI.1355-14.2014

Hutchison, W. D., Davis, K. D., Lozano, A. M., Tasker, R. R., and Dostrovsky, J. O. (1999). Pain-related neurons in the human cingulate cortex. *Nat. Neurosci.* 2, 403–405. doi: 10.1038/8065

Hyvarinen, A. (1999). Fast and robust fixed-point algorithms for independent component analysis. *IEEE Trans. Neural Netw.* 10, 626–634. doi: 10.1109/72.761722

Jas, M., Engemann, D. A., Bekhti, Y., Raimondo, F., and Gramfort, A. (2017). Autoreject: automated artifact rejection for MEG and EEG data. *NeuroImage* 159, 417–429. doi: 10.1016/j.neuroimage.2017.06.030

Jensen, M. P., Gertz, K. J., Kupper, A. E., Braden, A. L., Howe, J. D., Hakimian, S., et al. (2013). Steps toward developing an EEG biofeedback treatment for chronic pain. *App Psychophysiol Biofeedback.* 38, 101–108. doi: 10.1007/s10484-013-9214-9

Kiritoshi, T., Ji, G., and Neugebauer, V. (2016). Rescue of Impaired mGluR5-driven endocannabinoid signaling restores prefrontal cortical output to inhibit pain in arthritic rats. *J. Neurosci.* 36, 837–850. doi: 10.1523/JNEUROSCI.4047-15.2016

Kisler, L. B., Kim, J. A., Hemington, K. S., Rogachov, A., Cheng, J. C., Bosma, R. L., et al. (2020). Abnormal alpha band power in the dynamic pain connectome is a marker of chronic pain with a neuropathic component. *Neuroimage Clin.* 26:102241. doi: 10.1016/j.nicl.2020.102241

Kringelbach, M. L. (2005). The human orbitofrontal cortex: linking reward to hedonic experience. *Nat. Rev. Neurosci.* 6, 691–702. doi: 10.1038/nrn1747

Kucyi, A., and Davis, K. D. (2015). The dynamic pain connectome. *Trends Neurosci.* 38, 86–95. doi: 10.1016/j.tins.2014.11.006

Kudel, I., Edwards, R. R., Kozachik, S., Block, B. M., Agarwal, S., Heinberg, L. J., et al. (2007). Predictors and consequences of multiple persistent postmastectomy pains. *J. Pain Symptom Manag.* 34, 619–627. doi: 10.1016/j.jpainsymman.2007.01.013

Larson, E., Gramfort, A., Engemann, D. A., Leppakangas, J., Brodbeck, C., Jas, M., et al. (2023). MNE-Python (v1.3.1). *Zenodo*. doi: 10.5281/zenodo.7671973

Latremoliere, A., and Woolf, C. J. (2009). Central sensitization: a generator of pain hypersensitivity by central neural plasticity. *J. Pain* 10, 895–926. doi: 10.1016/j.jpain.2009.06.012

Lee, P. S., Low, I., Chen, Y. S., Tu, C. H., Chao, H. T., Hsieh, J. C., et al. (2017). Encoding of menstrual pain experience with theta oscillations in women with primary dysmenorrhea. *Sci. Rep.* 7:15977. doi: 10.1038/s41598-017-16039-4

Lee, M., Manders, T. R., Eberle, S. E., Su, C., D'amour, J., Yang, R., et al. (2015). Activation of corticostriatal circuitry relieves chronic neuropathic pain. *J. Neurosci.* 35, 5247–5259. doi: 10.1523/JNEUROSCI.3494-14.2015

Levitt, J., Edhi, M. M., Thorpe, R. V., Leung, J. W., Michishita, M., Koyama, S., et al. (2020). Pain phenotypes classified by machine learning using electroencephalography features. *NeuroImage* 223:117256. doi: 10.1016/j.neuroimage.2020.117256

Levitt, J., and Saab, C. Y. (2019). What does a pain 'biomarker' mean and can a machine be taught to measure pain? *Neurosci. Lett.* 702, 40–43. doi: 10.1016/j.neulet.2018.11.038

Martinez, E., Lin, H. H., Zhou, H., Dale, J., Liu, K., and Wang, J. (2017). Corticostriatal regulation of acute pain. *Front. Cell. Neurosci.* 11:146. doi: 10.3389/fncel.2017.00146

May, E. S., Nickel, M. M., Ta Dinh, S., Tiemann, L., Heitmann, H., Voth, I., et al. (2019). Prefrontal gamma oscillations reflect ongoing pain intensity in chronic back pain patients. *Hum. Brain Mapp.* 40, 293–305. doi: 10.1002/hbm.24373

Melzack, R. (2001). Pain and the Neuromatrix in the brain. *J. Dent. Educ.* 65, 1378–1382. doi: 10.1002/j.0022-0337.2001.65.12.tb03497.x

Michels, L., Moazami-Goudarzi, M., and Jeanmonod, D. (2011). Correlations between EEG and clinical outcome in chronic neuropathic pain: surgical effects and treatment resistance. *Brain Imaging Behav.* 5, 329–348. doi: 10.1007/s11682-011-9135-2

Misra, G., Wang, W. E., Archer, D. B., Roy, A., and Coombes, S. A. (2017). Automated classification of pain perception using high-density electroencephalography data. *J. Neurophysiol.* 117, 786–795. doi: 10.1152/jn.00650.2016

Mouraux, A., and Iannetti, G. D. (2018). The search for pain biomarkers in the human brain. *Brain* 141, 3290–3307. doi: 10.1093/brain/awy281

Mussigmann, T., Bardel, B., and Lefaucheur, J. P. (2022). Resting-state electroencephalography (EEG) biomarkers of chronic neuropathic pain. A systematic review. *NeuroImage* 258:119351. doi: 10.1016/j.neuroimage.2022.119351

Nickel, M. M., May, E. S., Tiemann, L., Schmidt, P., Postorino, M., Ta Dinh, S., et al. (2017). Brain oscillations differentially encode noxious stimulus intensity and pain intensity. *NeuroImage* 148, 141–147. doi: 10.1016/j.neuroimage.2017.01.011

Peng, W., Babiloni, C., Mao, Y., and Hu, Y. (2015). Subjective pain perception mediated by alpha rhythms. *Biol. Psychol.* 109, 141–150. doi: 10.1016/j.biopsycho.2015.05.004

Peng, W., Hu, L., Zhang, Z., and Hu, Y. (2014). Changes of spontaneous oscillatory activity to tonic heat pain. *PLoS One* 9:e91052. doi: 10.1371/journal.pone.0091052

Peng, W., and Tang, D. (2016). Pain related cortical oscillations: methodological advances and potential applications. *Front. Comput. Neurosci.* 10:9. doi: 10.3389/fncom.2016.00009

Peng, W. W., Xia, X. L., Yi, M., Huang, G., Zhang, Z. G., Iannetti, G. D., et al. (2017). Brain oscillations reflecting pain-related behavior in freely-moving rats. *Pain* 159, 106–118. doi: 10.1097/j.pain.0000000000001069

Petrovic, P., Kalso, E., Petersson, K. M., and Ingvar, M. (2002). Placebo and opioid analgesia – imaging a shared neuronal network. *Science* 295, 1737–1740. doi: 10.1126/science.1067176

Petzke, F., Clauw, D. J., Ambrose, K., Khine, A., and Gracely, R. H. (2003). Increased pain sensitivity in fibromyalgia: effects of stimulus type and mode of presentation. *Pain* 105, 403–413. doi: 10.1016/S0304-3959(03)00204-5

Pfurtscheller, G., and Lopes Da Silva, F. H. (1999). Event-related EEG/MEG synchronization and desynchronization: basic principles. *Clin. Neurophysiol.* 110, 1842–1857. doi: 10.1016/s1388-2457(99)00141-8

Pinheiro, E. S. D. S., Queirós, F. C. D., Montoya, P., Santos, C. L., Nascimento, M. A. D., Ito, C. H., et al. (2016). Electroencephalographic patterns in chronic pain: a systematic review of the literature. *PLoS One* 11:e0149085. doi: 10.1371/journal.pone.0149085

Plaghki, L., and Mouraux, A. (2005). EEG and laser stimulation as tools for pain research. *Curr. Opin. Investig. Drugs* 6, 58–64.

Ploner, M., and May, E. S. (2018). Electroencephalography and magnetoencephalography in pain research—current state and future perspectives. *Pain* 159, 206–211. doi: 10.1097/j.pain.0000000000001087

Prichep, L. S., Shah, J., Merkin, H., and Hiesiger, E. M. (2018). Exploration of the pathophysiology of chronic pain using quantitative EEG source localization. *Clin. EEG Neurosci.* 49, 103–113. doi: 10.1177/1550059417736444

Rakel, B., Vance, C., Zimmerman, M. B., Petsas-Blodgett, N., Amendola, A., and Sluka, K. A. (2015). Mechanical hyperalgesia and reduced quality of life occur in people with mild knee osteoarthritis pain. *Clin. J. Pain* 31, 315–322. doi: 10.1097/AJP.0000000000000116

Rockholt, M. M., Kenefati, G., Doan, L. V., Chen, Z. S., and Wang, J. (2023). In search of a composite biomarker for chronic pain by way of EEG and machine learning: where do we currently stand? *Front. Neurosci.* 17:1186418. doi: 10.3389/fnins.2023.1186418

Sarnthein, J., and Jeanmonod, D. (2008). High thalamocortical theta coherence in patients with neurogenic pain. *NeuroImage* 39, 1910–1917. doi: 10.1016/j.neuroimage.2007.10.019

Schulz, E., May, E. S., Postorino, M., Tiemann, L., Nickel, M. M., Witkovsky, V., et al. (2015). Prefrontal gamma oscillations encode tonic pain in humans. *Cereb. Cortex* 25, 4407–4414. doi: 10.1093/cercor/bhv043

Schulz, E., Tiemann, L., Witkovsky, V., Schmidt, P., and Ploner, M. (2012a). Gamma oscillations are involved in the sensorimotor transformation of pain. *J. Neurophysiol.* 108, 1025–1031. doi: 10.1152/jn.00186.2012

Schulz, E., Zherdin, A., Tiemann, L., Plant, C., and Ploner, M. (2012b). Decoding an individual's sensitivity to pain from the multivariate analysis of EEG data. *Cereb. Cortex* 22, 1118–1123. doi: 10.1093/cercor/bhr186

Seeber, M., Cantonas, L.-M., Hoevels, M., Sesia, T., Visser-Vandewalle, V., and Michel, C. M. (2019). Subcortical electrophysiological activity is detectable with high-density EEG source imaging. *Nat. Commun.* 10:753. doi: 10.1038/s41467-019-08725-w

Seger, S. E., Kriegel, J. L. S., Lega, B. C., and Ekstrom, A. D. (2023). Memory-related processing is the primary driver of human hippocampal theta oscillations. *Neuron* 13, S0896–S6273. doi: 10.1016/j.neuron.2023.06.015

Shirvalkar, P., Prosky, J., Chin, G., Ahmadipour, P., Sani, O. G., Desai, M., et al. (2023). First-in-human prediction of chronic pain state using intracranial neural biomarkers. *Nat. Neurosci.* 26, 1090–1099. doi: 10.1038/s41593-023-01338-z

Stern, J., Jeanmonod, D., and Sarnthein, J. (2006). Persistent EEG overactivation in the cortical pain matrix of neurogenic pain patients. *NeuroImage* 31, 721–731. doi: 10.1016/j.neuroimage.2005.12.042

Sun, G., Mccartin, M., Liu, W., Zhang, Q., Kenefati, G., Chen, Z. S., et al. (2023). Temporal pain processing in the primary somatosensory cortex and anterior cingulate cortex. *Mol. Brain* 16:3. doi: 10.1186/s13041-022-00991-y

Sun, G., Wen, Z., Ok, D., Doan, L., Wang, J., and Chen, Z. S. (2021). Detecting acute pain signals from human EEG. *J. Neurosci. Methods* 347:108964. doi: 10.1016/j.jneumeth.2020.108964

Sun, G., Zeng, F., Mccartin, M., Zhang, Q., Xu, H., Liu, Y., et al. (2022). Closed-loop stimulation using a multiregion brain-machine interface has analgesic effects in rodents. *Sci. Transl. Med.* 14:eabm5868. doi: 10.1126/scitranslmed.abm5868

Taesler, P., and Rose, M. (2016). Prestimulus Theta oscillations and connectivity modulate pain perception. *J. Neurosci.* 36, 5026–5033. doi: 10.1523/JNEUROSCI.3325-15.2016

Tan, L. L., Oswald, M. J., Heinl, C., Retana Romero, O. A., Kaushalya, S. K., Monyer, H., et al. (2019). Gamma oscillations in somatosensory cortex recruit prefrontal and descending serotonergic pathways in aversion and nociception. *Nat. Commun.* 10:983. doi: 10.1038/s41467-019-08873-z

Teixeira, M., Mancini, C., Wicht, C. A., Maestretti, G., Kuntzer, T., Cazzoli, D., et al. (2021). Beta electroencephalographic oscillation is a potential GABAergic biomarker of chronic peripheral neuropathic pain. *Front. Neurosci.* 15:594536. doi: 10.3389/fnins.2021.594536

Teixeira, P. E. P., Pacheco-Barrios, K., Uygur-Kucukseymen, E., Machado, R. M., Balbuena-Pareja, A., Giannoni-Luza, S., et al. (2021). Electroencephalography signatures for conditioned pain modulation and pain perception in nonspecific chronic Low Back pain—an exploratory study. *Pain Med.* 23, 558–570. doi: 10.1093/pm/pnab293

Tendler, A., and Wagner, S. (2015). Different types of theta rhythmicity are induced by social and fearful stimuli in a network associated with social memory. *elife* 4:e03614. doi: 10.7554/eLife.03614

Tracey, I. (2005). Nociceptive processing in the human brain. *Curr. Opin. Neurobiol.* 15, 478–487. doi: 10.1016/j.conb.2005.06.010

Tracey, I., and Bushnell, M. C. (2009). How neuroimaging studies have challenged us to rethink: is chronic pain a disease? *J. Pain* 10, 1113–1120. doi: 10.1016/j.jpain.2009.09.001

Tracey, I., and Mantyh, P. W. (2007). The cerebral signature for pain perception and its modulation. *Neuron* 55, 377–391. doi: 10.1016/j.neuron.2007.07.012

Van Den Broeke, E. N., Wilder-Smith, O. H. G., Van Goor, H., Vissers, K. C. P., and Van Rijn, C. M. (2013). Patients with persistent pain after breast Cancer treatment show enhanced alpha activity in spontaneous EEG. *Pain Med.* 14, 1893–1899. doi: 10.1111/pme.12216

Van Der Miesen, M. M., Lindquist, M. A., and Wager, T. D. (2019). Neuroimaging-based biomarkers for pain: state of the field and current directions. *Pain Rep.* 4:e751. doi: 10.1097/PR9.0000000000000751

Vanneste, S., and De Ridder, D. (2021). Chronic pain as a brain imbalance between pain input and pain suppression. *Brain Commun.* 3:fcab014. doi: 10.1093/braincomms/fcab014

Vanneste, S.To, W. T, and De Ridder, D. (2019). Tinnitus and neuropathic pain share a common neural substrate in the form of specific brain connectivity and microstate

profiles. *Prog. Neuro-Psychopharmacol. Biol. Psychiatry* 88, 388–400. doi: 10.1016/j.pnpbp.2018.08.015

Völker, J. M., Arguissain, F. G., Andersen, O. K., and Biurrun Manresa, J. (2021). Variability and effect sizes of intracranial current source density estimations during pain: systematic review, experimental findings, and future perspectives. *Hum. Brain Mapp.* 42, 2461–2476. doi: 10.1002/hbm.25380

Vuckovic, A., Hasan, M. A., Fraser, M., Conway, B. A., Nasseroleslami, B., and Allan, D. B. (2014). Dynamic oscillatory signatures of central neuropathic pain in spinal cord injury. *J. Pain* 15, 645–655. doi: 10.1016/j.jpain.2014.02.005

Wager, T. D., Atlas, L. Y., Lindquist, M. A., Roy, M., Woo, C.-W., and Kross, E. (2013). An fMRI-based neurologic signature of physical pain. *N. Engl. J. Med.* 368, 1388–1397. doi: 10.1056/NEJMoa1204471

Wang, X. J. (2010). Neurophysiological and computational principles of cortical rhythms in cognition. *Physiol. Rev.* 90, 1195–1268. doi: 10.1152/physrev.00035.2008

Wang, W. E., Ho, R. L., Gatto, B., Van Der Veen, S. M., Underation, M. K., Thomas, J. S., et al. (2021). Cortical dynamics of movement-evoked pain in chronic low back pain. *J. Physiol.* 599, 289–305. doi: 10.1113/JP280735

Wang, J., Li, D., Li, X., Liu, F.-Y., Xing, G.-G., Cai, J., et al. (2011). Phase–amplitude coupling between theta and gamma oscillations during nociception in rat electroencephalography. *Neurosci. Lett.* 499, 84–87. doi: 10.1016/j.neulet.2011.05.037

Wang, W.-E., Roy, A., Misra, G., Ho, R. L. M., Ribeiro-Dasilva, M. C., Fillingim, R. B., et al. (2019). Altered neural oscillations within and between sensorimotor cortex and parietal cortex in chronic jaw pain. *Neuroimage Clin.* 24:101964. doi: 10.1016/j.nicl.2019.101964

Winson, J. (1978). Loss of hippocampal theta rhythm results in spatial memory deficit in the rat. *Science* 201, 160–163. doi: 10.1126/science.663646

Xiao, Z., Martinez, E., Kulkarni, P. M., Zhang, Q., Hou, Q., Rosenberg, D., et al. (2019). Cortical pain processing in the rat anterior cingulate cortex and primary somatosensory cortex. *Front. Cell. Neurosci.* 13:165. doi: 10.3389/fncel.2019.00165

Zhang, Z., Gadotti, V. M., Chen, L., Souza, I. A., Stemkowski, P. L., and Zamponi, G. W. (2015). Role of Prelimbic GABAergic circuits in sensory and emotional aspects of neuropathic pain. *Cell Rep.* 12, 752–759. doi: 10.1016/j.celrep.2015.07.001

Zhang, Z. G., Hu, L., Hung, Y. S., Mouraux, A., and Iannetti, G. D. (2012). Gamma-band oscillations in the primary somatosensory cortex--a direct and obligatory correlate of subjective pain intensity. *J. Neurosci.* 32, 7429–7438. doi: 10.1523/JNEUROSCI.5877-11.2012

Zhang, Q., Hu, S., Talay, R., Xiao, Z., Rosenberg, D., Liu, Y., et al. (2023). A prototype closed-loop brain-machine interface for the study and treatment of pain. *Nat Biomed Eng* 7, 533–545. doi: 10.1038/s41551-021-00736-7

Zhang, Q., Manders, T., Tong, A. P., Yang, R., Garg, A., Martinez, E., et al. (2017). Chronic pain induces generalized enhancement of aversion. *elife* 6:e25302. doi: 10.7554/eLife.25302

Zhou, R., Wang, J., Qi, W., Liu, F.-Y., Yi, M., Guo, H., et al. (2018). Elevated resting state gamma oscillatory activities in electroencephalogram of patients with post-herpetic neuralgia. *Front. Neurosci.* 12:750. doi: 10.3389/fnins.2018.00750

Zhou, H., Zhang, Q., Martinez, E., Dale, J., Hu, S., Zhang, E., et al. (2018). Ketamine reduces aversion in rodent pain models by suppressing hyperactivity of the anterior cingulate cortex. *Nat. Commun.* 9:3751. doi: 10.1038/s41467-018-06295-x

frontiers | Frontiers in Neuroscience

TYPE Mini Review
PUBLISHED 15 November 2023
DOI 10.3389/fnins.2023.1307834



OPEN ACCESS

EDITED BY
Amelie Haugg,
Psychiatric University Hospital Zurich, Switzerland

REVIEWED BY
Jieying Zhang,
First Teaching Hospital of Tianjin University of Traditional Chinese Medicine, China

*CORRESPONDENCE
Ji Wang
✉ d201881399@hust.edu.cn

†These authors share first authorship

RECEIVED 05 October 2023
ACCEPTED 27 October 2023
PUBLISHED 15 November 2023

CITATION
Shao ZD, Gong YJ, Ren J and Wang J (2023) Exploring the arcuate fasciculus from a clinical perspective.
*Front. Neurosci.* 17:1307834.
doi: 10.3389/fnins.2023.1307834



# Exploring the arcuate fasciculus from a clinical perspective

Zhi Ding Shao†, Yu Juan Gong†, Jing Ren and Ji Wang*

Second Affiliated Hospital of Wannan Medical College, Wuhu, Anhui, China

In recent years, language function impairment caused by intracranial diseases has gained increasing interest, mainly due to its significant impact on the language and cognitive ability, leading to a serious decline in the quality of life of patients. Consequently, researchers aimed to clarify the quantitative degree of lesions of the arcuate fasciculus and therapeutic targets to promote nerve fiber remodeling. The arcuate fasciculus is extremely prone to damage caused by diseases such as stroke and brain tumor. Hallucinating schizophrenia, autism spectrum disorder, epilepsy, chronic fatigue syndrome, chronic tinnitus, and other diseases can also lead to changes in the fractional anisotropy value of arcuate fasciculus; however, different studies have different conclusions about how this change occurs. To obtain a better understanding, more clinical studies are required. Owing to various advancements in neuroimaging, a better understanding and identification of vital targets for restoration of neurological function are possible. The arcuate fasciculus is stratified into three substructures, each having unique neurological functions. Both diffusion tensor imaging (DTI) sequences and deterministic monitoring techniques render it possible to visually and quantitatively analyze the substructure in three parts. In this review, we examined the progress of the arcuate fasciculus and quantitative DTI technology in recent years.

KEYWORDS

**arcuate fasciculus, diffusion tensor imaging, stroke, language ability, brain tumor**

## Introduction

Complex language expression is a neurological function unique to humans. From birth to death, practicing language has been a continuous process, and concurrently, the progress of language has continuously promoted the exchange of information between people. In recent years, brain structures related to language function have been found to be closely associated with cognitive function (Yang et al., 2017; Cheema and Cummine, 2018). Research on post-stroke aphasia suggests that language-related white matter fiber tract pathways, such as arcuate fasciculus (AF), may have decreased FA values, which are related to language receptive and expressive abilities and language repetitive function (Yang et al., 2017). In patients with cerebral hemorrhage and aphasia, the left arcuate fasciculus was found to have varying degrees of changes in imaging characteristic values, such as FA values; another study on aphasia after cerebral infarction also suggested that the left arcuate fasciculus had decreased FA values, which were related to aphasia function (Koyama and Domen, 2016). Language function loss caused by various brain diseases has been found to not only affect the quality of life of patients but also lead to abnormalities in certain neurocognitive functions (Catani and Mesulam, 2008). Patients who had undergone brain glioma surgery were found to have significantly enhanced visualization of the left arcuate fasciculus, which was associated with the recovery of the patients' language function (Hayashi et al., 2012); another similar study pointed out that the FA of the arcuate fasciculus in the dominant hemisphere of patients with brain tumors before surgery was

elevated and predicted recovery of language function in patients after surgery (Kinoshita et al., 2014). To identify targets that can restore language ability or to use more precise methods for the reversal of an abnormal brain structure, over the past few years, many language scientists have discovered a remarkable correlation between brain regions and language cognition; examined the correlation among various neurons in the cortex, different neurotransmitters, and language; and finally determined the physical interconnectivities. Language functionality here mainly refers to the neural function produced by white matter fibers connecting different brain areas. The arcuate tract is one of the most well-known white matter fiber tracts. We believe that a broader understanding of this brain fiber structure can provide novel insights into clinical diagnosis and treatment (Breier et al., 2011; Raffa et al., 2017; Chawla et al., 2019).

## Review of simple neuroanatomy theory

In the human brain, the arcuate tract is an important nerve fiber bundle, which is closely related to the human language function and is the main contact fiber of the language dorsal pathway (Bernal and Ardila, 2009). The AF is believed to link the Broca's area within the dominant inferior frontal gyrus with the posterior Wernicke area to the dominant superior temporal gyrus (Geschwind, 1970). Anatomically, it is located lateral to the corticospinal tract, adjacent to the corpus callosum. The arcuate tract connects the prefrontal cortex and the posterior superior temporal gyrus on the dorsal side. The segment bends and enters the posterior temporal cortex (Catani and Mesulam, 2008; Axer et al., 2013). The AF is known to originate from Brodmann's areas (BA) 22, 21, and 37 and terminates in BA 44, 45, and 46 (Hong et al., 2009; Jehna et al., 2017). Currently, most literature divide it into three parts: deep, anterior, and posterior arcuate fasciculus (Martino et al., 2013; Falkenberg et al., 2020). Owing to the advancement in scanning techniques and post-processing methods, more nuanced anatomical forms can be identified from noninvasive diffusion tensor imaging (DTI) methods (Bernard et al., 2019). Based on the above anatomy, several studies based on EEG and MRI have found that when patients have language dysfunction, they are often accompanied by varying degrees of damage to the arcuate fasciculus, and the location of damage is related to the type and degree of aphasia (Zhang et al., 2010), which can be understood as differences in neural functions of substructures (Janssen et al., 2023). It was also found that the left and right arcuate tracts exert different roles in language function (di Cristofori et al., 2021; Gao et al., 2022), which is closely related to neural function formation in ontogeny. However, if the findings of previous studies are also evaluated using more neurological diseases, people may have a more varied and new understanding of the anatomical structure and function of the arcuate fasciculus (di Cristofori et al., 2021).

## Progress in the recognition of the arcuate fasciculus

The process of understanding the arcuate fasciculus is presented in Figure 1. First, confirm the existence of the arcuate fasciculus from the neuroanatomy, determine the brain regions connected by it, and then start exploring via noninvasive visualization to further understand a more detailed structural relationship, particularly, what are the major substructures. At this time, the completeness and quantitative accuracy of electroencephalogram (EEG), functional magnetic resonance imaging (fMRI), and DTI technologies were gradually attained. Furthermore, in combination with behavioral tests, it is found that in right-handed people, the left arcuate tract mainly participates in language function, whereas the right side participates in language adjustment. Thus, this verifies that both sides of the arcuate tract are involved in cognitive functions and that each part of the substructure has a different role in language participation, as evidenced from fMRI and EEG results, among others (Catani and Mesulam, 2008). Thus, understanding of the arcuate bundle is a constant process. With the ongoing technological advancements, more discoveries will be uncovered.

## Arcuate fasciculus and language

Traditionally, language is split into several subsystems as follows (van der Lely and Pinker, 2014): syntax, morphology, phonology, pragmatics, and lexicon. We have herein focused on the first three subsystems and proposed to cross-classify them via distinction of representation and processing. In the cranium, the brain structure related to it is described as follows: the main function of the dorsal pathway is a hierarchical phrase structure and syntactically complex sentences (extended syntax), rule-generated regular inflection (extended morphology), acoustic to articulatory network (sensorimotor interface), acoustic to articulatory network (speech segments; basic phonology), and acoustic to the articulatory network (syllables and larger prosodic domains; extended phonology); the main functions of the ventral and bilateral pathways are local phrase structure (basic syntax) and lexical and phrasal semantics (basic syntax), stored irregular forms (basic morphology), stored derived forms (basic morphology), and acoustic to semantic network (word recognition; basic phonology; van der Lely and Pinker, 2014). This article will not elaborate further on more biologically related issues of complex and delicate language as this review only aimed to illustrate the anatomy and function of the arcuate tract in combination with the clinical utility of advanced magnetic resonance sequences to help patients with language dysfunction. To realize the above functions, the coordination of different brain regions is required; thus, the connection between regions and neurotransmitter transmission depends on the white matter fiber structure. Certainly, current techniques still fail to clearly elucidate all brain structures related to language ability in the entire brain; however, the vital and main arcuate tracts have provided opportunities for research. A recent good study combined task fMRI and DTI to confirm the neural function of the substructure of the arcuate fasciculus in language execution and further differentiated the more accurate language-related tasks that different substructures are responsible for Janssen et al. (2023).

## Arcuate fasciculus and DTI

From the end of the 19th century to the present, the relationship between brain white matter fiber structure and language has been

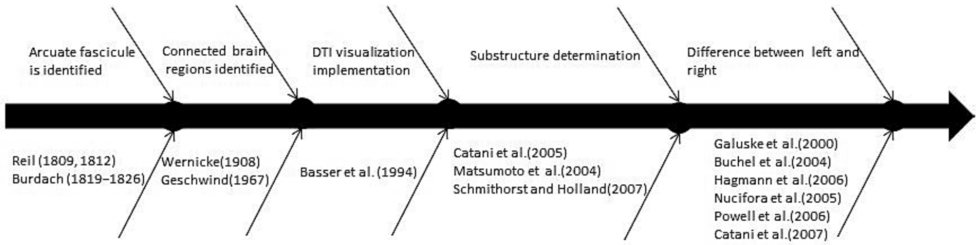


FIGURE 1
The timeline of the arcuate fasciculus is recognized by researchers.

perpetually explored, and the technological advancements are streamlined daily. Among these advancements, diffusion-weighted magnetic resonance imaging, also known as DTI, allowed tracking of white matter fiber structure *in vivo* (Janssen et al., 2023). The post-processing techniques of such sequence are mainly divided into deterministic and probabilistic fiber tracking. In the deterministic fiber tracking technology, through neuroanatomy, a variety of white matter fiber structures are confirmed; thus, it has a high degree of reliability and restoration authenticity. For example, the arcuate bundle, which is the highlight of this review, is difficult to display via conventional MRI techniques, let alone the substructure, while DTI sequences can provide very clear morphological structures such as that in Figure 2. After restoration of this brain structure noninvasively, as a clinician, a question is posed: how can it be used and researched? Thus far, we found that this technology can be utilized more in stroke and brain tumor. For brain tumors, it can be precisely positioned prior to surgery to significantly improve the quality of life of patients after surgery, and secondly, it can be used to predict neurological function recovery, such as language and cognition after surgery (Mori and van Zijl, 2002; Yang et al., 2017; Zimmermann et al., 2020). For stroke, the highlight is on predicting the recovery of language ability and exploring new methods of diagnosis and treatment, such as neuromodulation therapy (Puig et al., 2017; Wang et al., 2020).

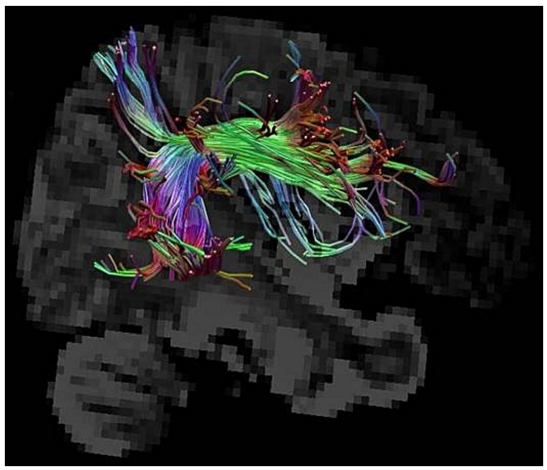

FIGURE 2
Visualization of the arcuate fasciculus by DTI.

## Visualization of the arcuate fasciculus structure

The visualized structure obtained by various post-processing methods allows an intuitive observation of morphological structure changes of a certain position of the arcuate tract. If it is determined that the changed structure is related to certain neural functions, the neural functions involved in the structure can be qualitatively determined. It is instrumental in helping patients better understand their own condition and can be used as a diagnostic marker for clinically investigating more treatment options (Yagmurlu et al., 2016). The current visualization of the arcuate tract is quite advanced and has been confirmed by neuroanatomists (Yagmurlu et al., 2016). This provides precise opportunities for conducting both cross-sectional and longitudinal studies (Figure 3). The presentation of its three-part substructure has also been realized, and many research groups have conducted studies on the correlation between the substructure and behavior and whether a relationship between the substructure and other brain regions exists or whether there is participation in the realization of certain neural functions. Reviewing past research data, varying scan parameter selections have different rendering quality for the three parts of the arcuate beam; therefore, a better quantification is also warranted. Regarding whether the identification is impaired, in the routine sequence, some studies have elucidated that even if no lesion is found on DWI, DTT can certainly demonstrate the absence of the arcuate tract in patients, which corroborates with the responsible area of the patient's language dysfunction. Yamada et al. reported a patient who showed conduction aphasia after corona infarction. The patient exhibited severe dysrepetition with speech errors. Although no lesions were observed in the Broca's or Wernicke's areas on brain diffusion-weighted images, DTT demonstrated partial damage to the left AF in terms of FA values and AF configuration: a decreased FA value and a smaller left AF size, compared with the right AF (Yamada et al., 2007). Another Korean research group revealed that patients with aphasia caused by cerebral hemorrhage presented with different types of aphasia under different AF structures, and visual AF allowed a clear observation of the morphological changes that generated obvious differences (Ryu and Park, 2020). These findings should fully attract the attention of clinicians. For patients who present with neurological deficits but with no abnormalities in routine examinations, improving more sequence examinations and conducting a follow-up analysis to provide an accurate diagnosis and prognosis and derive new treatment strategies are warranted.

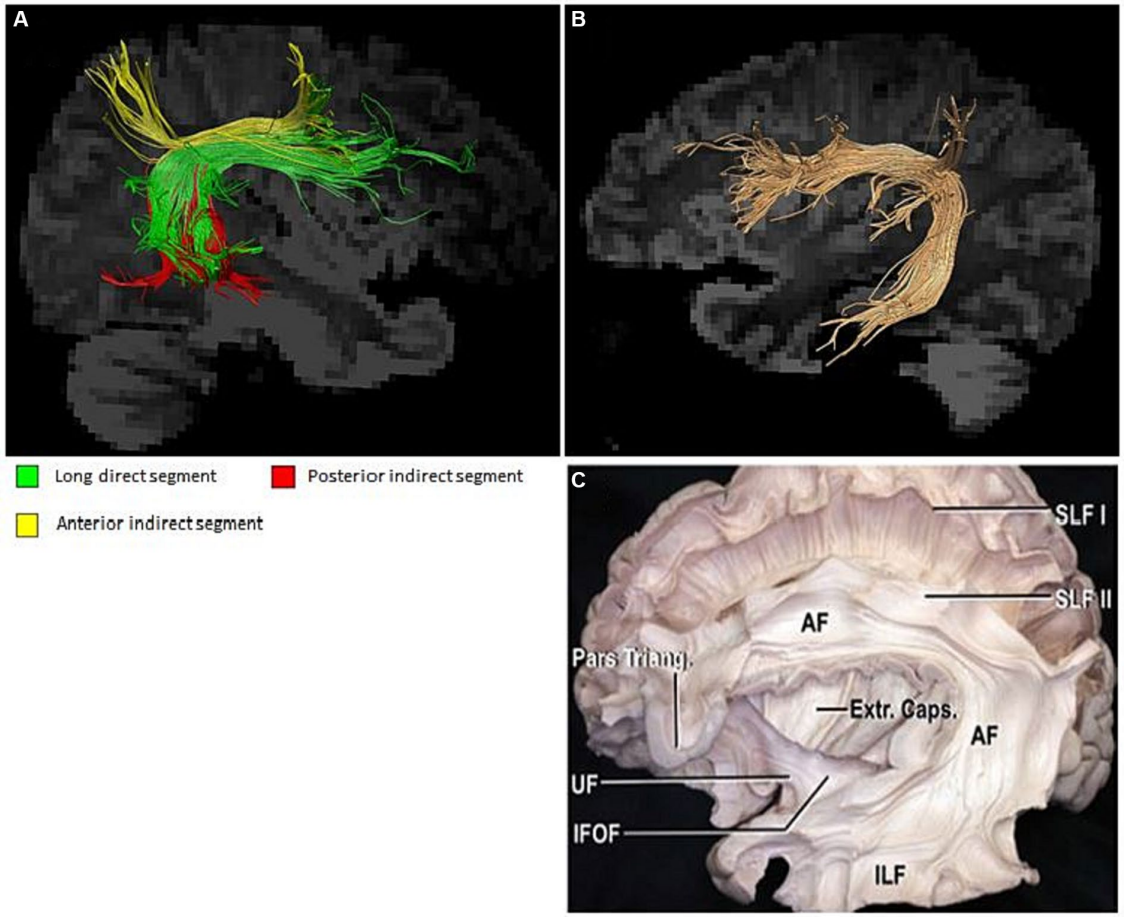


FIGURE 3
**(A)** Substructure of the arcuate fasciculus; **(B,C)** Arcuate fasciculus and neuroanatomy (Yagmurlu et al., 2016).

## Indices predicting language function recovery

If visualization aimed to match the neuroanatomy and help in better understanding the brain structure, then the core should be in its quantifiable characteristics, that is, values can be quantitatively identified under different degrees of damage to accurately predict the long-term prognosis of individuals. To predict the degree of language impairment recovery, the arcuate tract is not solely involved. If accuracy and precision are pursued, the nerve fiber structure near or distant from the lesion should also be included. The predicted value mainly comprised various types of eigenvalues from DTI sequences, such as FA, ADC, volume, and length values, among others (Wu et al., 2022). In recent years, the connection between post-stroke aphasia and arcuate tract changes has become one of the hotspots. Definitely, other different fiber tract pathways related to human language remain unexplored, and this review only elucidates on the arcuate tract. The more common arcuate tract injuries are still brain tumors and strokes, and the different degrees of damage can also predict whether the patient's language ability can be restored in a few months. For example, left arcuate fasciculus changes have been detected among right-handed patients after stroke. Some studies have discovered that approximately 24%–38% of stroke patients may develop aphasia in the acute phase (Laska et al., 2001; Engelter et al., 2006). However, in patients with aphasia, lesions could not be detected in conventional MRI scan sequences. Therefore, perfecting DTI sequences can help in accurately classifying the types of aphasia (Kim et al., 2011), which will bring opportunities for targeted diagnosis and treatment. Another research group compared the intracranial DTI of the arcuate tract of aphasia in the acute phase of stroke with the control group and found a significant decline in the FA value of the left arcuate tract, thus confirming that the left arcuate tract is responsible for aphasia in post-stroke patients (Koyama and Domen, 2016). In the study of brain tumors inducing arcuate tract damage, AF quantification provided relevant guidance preoperatively (Hayashi et al., 2012). Studies have demonstrated that the preoperative increase in the FA value of the arcuate tract in the dominant hemisphere can be used as a predictor of language recovery after tumor resection, that is, the increase in the preoperative FA value of the arcuate tract suggests a high possibility for postoperative language recovery, and thus, surgery should be exercised with extreme caution to avoid unnecessary injury (Kinoshita et al., 2014). Another study further demonstrated that the change of the characteristic value of the arcuate tract under DTI sequence may be correlated with malignancy of a tumor, which

indicates that noninvasive methods may help in determining the malignancy of the patient's lesion and guide treatment (Zoli et al., 2021). In a research group in China using the DTT method to predict postoperative language function in low-grade gliomas, the volume and number of the arcuate tract fibers can afford better reliability than the FA value, which once again confirms the noninvasive archetype. Also, the description of the eigenvalues of the bundle has predictability (Wu et al., 2022).

## Therapeutic targets, precise targeting, and individualized treatment

Damage to different brain regions may have varied treatment options, such as the treatment site and transcranial magnetic stimulation intensity, and different neural regulation methods. A study differentiated the structure of white matter fibers related to exercise under TMS treatment and found that DTI-based guided neural regulation research is feasible (Raffa et al., 2018). Professors from Harvard Medical School and Boston University performed a very systematic study on the relationship between TMS treatment and brain white matter fiber tracts, and the study findings showed that DTI can be used to describe the microstructural description of TMS and the connection abnormalities of the different brain regions (Naeser et al., 2010). More studies have revealed that the arcuate tract is also related to the cognitive function of patients, and it is more manifested on both sides, rather than the left side. Thus, to improve cognitive symptoms, treatment strategies employed for arcuate tract changes through neurological regulatory methods are worthy of attention. For patients with brain tumors, it is of crucial importance to determine the extent of tumor resection prior to surgery and to predict the degree of postoperative speech function recovery. Studies have demonstrated that the combination of DTI and nTMS is the most optimal preoperative strategy, and patients enrolled in this method showed better prognosis and exhibited reduction in movement and language damage secondary to surgery (Raffa et al., 2017). Another study emphasized that DTI is effective and feasible in awake surgery as the arcuate bundle is a common and easily damaged structure during surgery, and the current visualization technology is advanced. Its appropriate application during surgery can help in deterring nerve function damage, such as those related to speech and movement (D'Andrea et al., 2016). Many studies have been published for the treatment of post-stroke aphasia with TMS. Although the treatment site, time, and type of aphasia are varied, majority of the studies have achieved improvement in language function outcomes (Arheix-Parras et al., 2021). These researchers also acknowledged that a mechanism to explain these improvements is lacking. However, it is conjectured that the structural changes of the arcuate fasciculus may be the most intuitive factor (Arheix-Parras et al., 2021). Moreover, the relationship between the specific substructure changes of the arcuate fasciculus and TMS should be examined more to further refine diagnosis and treatment.

## Observing changes in neuroplasticity

One of the foundations of neurological recovery is neuroplasticity. For example, to evaluate the treatment outcomes, remodeling of nerve fibers at the damaged site should be observed. Evidence reveals that neural remodeling continuously occurs throughout a person's lifetime (Kong et al., 2016). Even with disease conditions, the brain tissue itself has a certain capacity to remodel. Therefore, the occurrence of neural remodeling indicates restoration of lost neural function. Furthermore, if this mechanism can be elucidated more clearly, the symptoms can be improved and the quality of life of affected patients can be enhanced by targeting the formation of nerve remodeling after the occurrence of various intracranial diseases. Studies have confirmed that in the magnetic resonance imaging and MEG detection of patients with brain tumors, additional activated sites can be found, which can be verified as a form of neural remodeling combined with behavioral studies (Breier et al., 2011). Moreover, this can further clarify the mechanism or the relevant brain region connection via further imaging and white matter fiber structure reconstruction. A research group administered a standardized treatment on a patient with post-stroke aphasia and concurrently completed behavioral and DTI examinations in the acute phase and 3 months after the stroke. Improvements were observed on both time periods, accompanied by the improvement of the patient's speech ability (Kierońska et al., 2021). Studies have also explored on post-stroke aphasia using various imaging modalities such as DTI, fMRI, and EEG and found changes in the brain structure or brain function related to language after 3 months of systemic treatment. The arcuate tract showed an increase in integrity and increase in the number and volume of fibers which directly correlate with recovery of language and cognitive functions (Breier et al., 2011). Another group of researchers also compared the structure of deep brain fiber tracts of gymnasts and non-athletes, in which the arcuate tract was found to have a regionally lower FA, which indirectly indicated that the arcuate tract may also be involved in motor regulation and spatial attention. The author speculates that the regular quantitative changes are associated with the time of exercise training received, and the researchers also used these quantitative fiber structure values to verify whether they can distinguish between athletes and non-exercise abilities (Deng et al., 2017).

## Discussion

Research on neuropsychological diseases using AF and/or in combination with other adjacent fiber tracts, such as diagnostic markers, has also been conducted (Chawla et al., 2019). For example, in hallucinating patients with schizophrenia, the left AF is longer, indicating increased connectivity between auditory areas in the temporal lobe and frontal and parietal areas associated with language (Fernández-Miranda et al., 2015). In bilateral AF, auditory hallucinations had significantly lower FA values (Chawla et al., 2019). Studies have found that toddlers with autism spectrum disorder (ASD) and left-sided AF have FA values significantly lower than those of normal individuals, suggesting the lack of speaking ability in the early stages of patients with ASD (Zhang et al., 2018). Clinically, it is common to observe personality changes in patients with epilepsy. A previous study reported that the intracranial white matter fiber tracts in patients with epilepsy undergo changes in multiple brain regions, thereby explaining the causes of personality changes. This study found

that AF did not differ between patients with epilepsy diagnosed 5 years ago and normal controls, but AF changed significantly in patients diagnosed with epilepsy 12 years ago (Mao et al., 2011). Recent studies have shown that the right arcuate fasciculus undergoes changes in patients with chronic fatigue syndrome (Zeineh et al., 2015). In right-handed patients, the FA value of the right arcuate fascicle is significantly increased. According to the authors of this study, CFS is the cause of this change, and this change may serve as a diagnostic biomarker (Zeineh et al., 2015). It was also surprising to find a correlation between behavioral scores and changes in the left arcuate fasciculus in patients with tinnitus (Ahmed et al., 2021). Thus, from the above researches, we can conclude that with the advancement of neuroimaging and anatomical techniques, a better understanding of the arcuate tract is also achieved. There are many cells involved in the damage and remodeling of nerve fiber bundles, and the relationship between these biological changes and imaging findings needs to be clarified. Thus, a more detailed and complete research on the arcuate tract in relation to clinical diagnosis and treatment is warranted, and the conclusion from multicenter big data is an exciting pursuit.

## Author contributions

ZS: Resources, Writing – review & editing. YG: Methodology, Writing – review & editing. JR: Formal analysis, Writing – review & editing. JW: Software, Writing – original draft, Writing – review & editing.

## Funding

The author(s) declare that no financial support was received for the research, authorship, and/or publication of this article.

## Conflict of interest

The authors declare that the research was conducted in the absence of any commercial or financial relationships that could be construed as a potential conflict of interest.

## Publisher's note

All claims expressed in this article are solely those of the authors and do not necessarily represent those of their affiliated organizations, or those of the publisher, the editors and the reviewers. Any product that may be evaluated in this article, or claim that may be made by its manufacturer, is not guaranteed or endorsed by the publisher.

## Supplementary material

The Supplementary material for this article can be found online at: https://www.frontiersin.org/articles/10.3389/fnins.2023.1307834/full#supplementary-material

## References

Ahmed, S., Mohan, A., Yoo, H. B., Kovacs, S., Sunaert, S., de Ridder, D., et al. (2021). Structural correlates of the audiological and emotional components of chronic tinnitus. *Prog. Brain Res.* 262, 487–509. doi: 10.1016/bs.pbr.2021.01.030

Arheix-Parras, S., Barrios, C., Python, G., Cogné, M., Sibon, I., Engelhardt, M., et al. (2021). A systematic review of repetitive transcranial magnetic stimulation in aphasia rehabilitation: leads for future studies. *Neurosci. Biobehav. Rev.* 127, 212–241. doi: 10.1016/j.neubiorev.2021.04.008

Axer, H., Klingner, C. M., and Prescher, A. (2013). Fiber anatomy of dorsal and ventral language streams. *Brain Lang.* 127, 192–204. doi: 10.1016/j.bandl.2012.04.015

Bernal, B., and Ardila, A. (2009). The role of the arcuate fasciculus in conduction aphasia. *Brain* 132, 2309–2316. doi: 10.1093/brain/awp206

Bernard, F., Zemmoura, I., Ter Minassian, A., Lemée, J. M., and Menei, P. (2019). Anatomical variability of the arcuate fasciculus: a systematical review. *Surg. Radiol. Anat.* 41, 889–900. doi: 10.1007/s00276-019-02244-5

Breier, J. I., Juranek, J., and Papanicolaou, A. C. (2011). Changes in maps of language function and the integrity of the arcuate fasciculus after therapy for chronic aphasia. *Neurocase* 17, 506–517. doi: 10.1080/13554794.2010.547505

Catani, M., and Mesulam, M. (2008). The arcuate fasciculus and the disconnection theme in language and aphasia: history and current state. *Cortex* 44, 953–961. doi: 10.1016/j.cortex.2008.04.002

Chawla, N., Deep, R., Khandelwal, S. K., and Garg, A. (2019). Reduced integrity of superior longitudinal fasciculus and arcuate fasciculus as a marker for auditory hallucinations in schizophrenia: a DTI tractography study. *Asian J. Psychiatr.* 44, 179–186. doi: 10.1016/j.ajp.2019.07.043

Cheema, K., and Cummine, J. (2018). The relationship between white matter and Reading acquisition, refinement and maintenance. *DevNeurosci* 40, 209–222. doi: 10.1159/000489491

D'Andrea, G., Familiari, P., Di Lauro, A., Angelini, A., and Sessa, G. (2016). Safe resection of gliomas of the dominant angular gyrus availing of preoperative FMRI and intraoperative DTI: preliminary series and surgical technique. *World Neurosurg.* 87, 627–639. doi: 10.1016/j.wneu.2015.10.076

Deng, F., Zhao, L., Liu, C., Lu, M., Zhang, S., Huang, H., et al. (2017). Plasticity in deep and superficial white matter: a DTI study in world class gymnasts. *Brain Struct. Funct.* 223, 1849–1862. doi: 10.1007/s00429-017-1594-9

di Cristofori, A., Basso, G., de Laurentis, C., Mauri, I., Sirtori, M. A., Ferrarese, C., et al. (2021). Perspectives on (a)symmetry of arcuate fasciculus. A short review about anatomy, Tractography and TMS for arcuate fasciculus reconstruction in planning surgery for gliomas in language areas. *Front. Neurol.* 12:639822. doi: 10.3389/fneur.2021.639822

Engelter, S. T., Gostynski, M., Papa, S., Frei, M., Born, C., Ajdacic-Gross, V., et al. (2006). Epidemiology of aphasia attributable to first ischemic stroke: incidence, severity, fluency, etiology, and thrombolysis. *Stroke* 37, 1379–1384. doi: 10.1161/01.STR.0000221815.64093.8c

Falkenberg, L. E., Westerhausen, R., Johnsen, E., Kroken, R., Løberg, E. M., Beresniewicz, J., et al. (2020). Hallucinating schizophrenia patients have longer left arcuate fasciculus fiber tracks: a DTI tractography study. *Psychiatry Res. Neuroimaging* 302:111088. doi: 10.1016/j.pscychresns.2020.111088

Fernández-Miranda, J. C., Wang, Y., Pathak, S., Stefaneau, L., Verstynen, T., et al. (2015). Asymmetry, connectivity, and segmentation of the arcuate fascicle in the human brain. *Brain Struct. Funct.* 220, 1665–1680. doi: 10.1007/s00429-014-0751-7

Gao, Y., Meng, X., Bai, Z., Liu, X., Zhang, M., Li, H., et al. (2022). Left and right arcuate fasciculi are uniquely related to word Reading skills in Chinese-English bilingual children. *Neurobiol Lang* 3, 109–131. doi: 10.1162/nol_a_00051

Geschwind, N. (1970). The organization of language and the brain. *Science* 170, 940–944. doi: 10.1126/science.170.3961.940

Hayashi, Y., Kinoshita, M., Nakada, M., and Hamada, J. (2012). Correlation between language function and the left arcuate fasciculus detected by diffusion tensor imaging tractography after brain tumor surgery. *J. Neurosurg.* 117, 839–843. doi: 10.3171/2012.8.JNS12348

Hong, J. H., Kim, S. H., Ahn, S. H., and Jang, S. H. (2009). The anatomical location of the arcuate fasciculus in the human brain: a diffusion tensor tractography study. *Brain Res. Bull.* 80, 52–55. doi: 10.1016/j.brainresbull.2009.05.011

Janssen, N., Kessels, R., Mars, R. B., Llera, A., Beckmann, C., and Roelofs, A. (2023). Dissociating the functional roles of arcuate fasciculus subtracts in speech production. *Cereb. Cortex* 33, 2539–2547. doi: 10.1093/cercor/bhac224

Jehna, M., Becker, J., Zaar, K., von Campe, G., Mahdy Ali, K., Reishofer, G., et al. (2017). Symmetry of the arcuate fasciculus and its impact on language performance of patients with brain tumors in the language-dominant hemisphere. *J. Neurosurg.* 127, 1407–1416. doi: 10.3171/2016.9.JNS161281

Kierońska, S., Świtońska, M., Meder, G., Piotrowska, M., and Sokal, P. (2021). Tractography alterations in the arcuate and Uncinate fasciculi in post-stroke aphasia. *Brain Sci.* 11:53. doi: 10.3390/brainsci11010053

Kim, S. H., Lee, D. G., You, H., Son, S. M., Cho, Y. W., Chang, M., et al. (2011). The clinical application of the arcuate fasciculus for stroke patients with aphasia: a diffusion tensor tractography study. *NeuroRehabilitation* 29, 305–310. doi: 10.3233/NRE-2011-0706

Kinoshita, M., Nakada, M., Okita, H., Hamada, J. I., and Hayashi, Y. (2014). Predictive value of fractional anisotropy of the arcuate fasciculus for the functional recovery of language after brain tumor resection: a preliminary study. *Clin. Neurol. Neurosurg.* 117, 45–50. doi: 10.1016/j.clineuro.2013.12.002

Kong, N. W., Gibb, W. R., and Tate, M. C. (2016). Neuroplasticity: insights from patients harboring gliomas. *Neural Plast.* 2016, 2365063–2365012. doi: 10.1155/2016/2365063

Koyama, T., and Domen, K. (2016). Reduced diffusion tensor fractional anisotropy in the left arcuate fasciculus of patients with aphasia caused by acute cerebral infarct. *Prog Rehabil Med* 1:8. doi: 10.2490/prm.20160008

Laska, A. C., Hellblom, A., Murray, V., Kahan, T., and Von Arbin, M. (2001). Aphasia in acute stroke and relation to outcome. *J. Intern. Med.* 249, 413–422. doi: 10.1046/j.1365-2796.2001.00812.x

Mao, L. Y., Ding, J., Peng, W. F., Ma, Y., Zhang, Y. H., Chen, C., et al. (2011). Disease duration and arcuate fasciculus abnormalities correlate with psychoticism in patients with epilepsy. *Seizure* 20, 741–747. doi: 10.1016/j.seizure.2011.07.002

Martino, J., de Witt Hamer, P. C., Berger, M. S., Lawton, M. T., Arnold, C. M., de Lucas, E., et al. (2013). Analysis of the subcomponents and cortical terminations of the perisylvian superior longitudinal fasciculus: a fiber dissection and DTI tractography study. *Brain Struct. Funct.* 218, 105–121. doi: 10.1007/s00429-012-0386-5

Mori, S., and van Zijl, P. C. (2002). Fiber tracking: principles and strategies—a technical review. *NMR Biomed.* 15, 468–480. doi: 10.1002/nbm.781

Naeser, M. A., Martin, P. I., Treglia, E., Ho, M., Kaplan, E., Bashir, S., et al. (2010). Research with rTMS in the treatment of aphasia. *Restor. Neurol. Neurosci.* 28, 511–529. doi: 10.3233/RNN-2010-0559

Puig, J., Blasco, G., Schlaug, G., Stinear, C. M., Daunis-i-Estadella, P., Biarnes, C., et al. (2017). Diffusion tensor imaging as a prognostic biomarker for motor recovery and rehabilitation after stroke. *Neuroradiology* 59, 343–351. doi: 10.1007/s00234-017-1816-0

Raffa, G., Conti, A., Scibilia, A., Cardali, S. M., Esposito, F., Angileri, F., et al. (2018). The impact of diffusion tensor imaging Fiber tracking of the corticospinal tract based on navigated transcranial magnetic stimulation on surgery of motor-eloquent brain lesions. *Neurosurgery* 83, 768–782. doi: 10.1093/neuros/nyx554

Raffa, G., Conti, A., Scibilia, A., Sindorio, C., Quattropani, M. C., Visocchi, M., et al. (2017). Functional reconstruction of motor and language pathways based on navigated transcranial magnetic stimulation and DTI Fiber tracking for the preoperative planning of low grade glioma surgery: a new tool for preservation and restoration of eloquent networks. *Acta Neurochir. Suppl.* 124, 251–261. doi: 10.1007/978-3-319-39546-3_37

Ryu, H., and Park, C. H. (2020). Structural characteristic of the arcuate fasciculus in patients with fluent aphasia following intracranial hemorrhage: a diffusion tensor Tractography study. *Brain Sci.* 10:280. doi: 10.3390/brainsci10050280

van der Lely, H. K., and Pinker, S. (2014). The biological basis of language: insight from developmental grammatical impairments. *Trends Cogn. Sci.* 18, 586–595. doi: 10.1016/j.tics.2014.07.001

Wang, H., Li, S., Dai, Y., and Yu, Q. (2020). Correlation between speech repetition function and the arcuate fasciculus in the dominant hemisphere detected by diffusion tensor imaging Tractography in stroke patients with aphasia. *Med. Sci. Monit.* 26:e928702. doi: 10.12659/MSM.928702

Wu, D., Zhang, M., Geng, J., and Chen, X. (2022). Noninvasive prediction of language lateralization through arcuate fasciculus Tractography in patients with low-grade gliomas: correlation with the Wada test. *Front. Oncol.* 12:936228. doi: 10.3389/fonc.2022.936228

Yagmurlu, K., Middlebrooks, E. H., Tanriover, N., and Rhoton, A. J. (2016). Fiber tracts of the dorsal language stream in the human brain. *J. Neurosurg.* 124, 1396–1405. doi: 10.3171/2015.5.JNS15455

Yamada, K., Nagakane, Y., Mizuno, T., Hosomi, A., Nakagawa, M., and Nishimura, T. (2007). MR tractography depicting damage to the arcuate fasciculus in a patient with conduction aphasia. *Neurology* 68:789. doi: 10.1212/01.wnl.0000256348.65744.b2

Yang, M., Li, Y., Li, J., Yao, D., Liao, W., and Chen, H. (2017). Beyond the arcuate fasciculus: damage to ventral and dorsal language pathways in aphasia. *Brain Topogr.* 30, 249–256. doi: 10.1007/s10548-016-0503-5

Zeineh, M. M., Kang, J., Atlas, S. W., Raman, M. M., Reiss, A. L., Norris, J., et al. (2015). Right arcuate fasciculus abnormality in chronic fatigue syndrome. *Radiology* 274, 517–526. doi: 10.1148/radiol.14141079

Zhang, L., Li, K., Zhang, C., Qi, X., Zheng, N., and Wang, G. (2018). Arcuate fasciculus in autism Spectrum disorder toddlers with language regression. *Open Med* 13, 90–95. doi: 10.1515/med-2018-0014

Zhang, Y., Wang, C., Zhao, X., Chen, H., Han, Z., and Wang, Y. (2010). Diffusion tensor imaging depicting damage to the arcuate fasciculus in patients with conduction aphasia: a study of the Wernicke-Geschwind model. *Neurol. Res.* 32, 775–778. doi: 10.1179/016164109X12478302362653

Zimmermann, M., Rössler, K., Kaltenhäuser, M., Grummich, P., Yang, B., Buchfelder, M., et al. (2020). Refined functional magnetic resonance imaging and magnetoencephalography mapping reveals reorganization in language-relevant areas of lesioned brains. *World Neurosurg.* 136, e41–e59. doi: 10.1016/j.wneu.2019.10.014

Zoli, M., Talozzi, L., Martinoni, M., Manners, D. N., Badaloni, F., Testa, C., et al. (2021). From neurosurgical planning to histopathological brain tumor characterization: potentialities of arcuate fasciculus along-tract diffusion tensor imaging Tractography measures. *Front. Neurol.* 12:633209. doi: 10.3389/fneur.2021.633209

frontiers | Frontiers in Neuroscience

TYPE Original Research
PUBLISHED 29 November 2023
DOI 10.3389/fnins.2023.1229729



OPEN ACCESS

EDITED BY
Amelie Haugg,
Psychiatric University Hospital Zurich, Switzerland

REVIEWED BY
Luka Milosevic,
University Health Network (UHN), Canada
David M. A. Mehler,
University Hospital RWTH Aachen, Germany

*CORRESPONDENCE
Andrew A. Nicholson
✉ andrew.nicholson@theroyal.ca

†These authors share senior authorship

RECEIVED 26 May 2023
ACCEPTED 24 October 2023
PUBLISHED 29 November 2023

CITATION
Lieberman JM, Rabellino D, Densmore M, Frewen PA, Steyrl D, Scharnowski F, Théberge J, Hosseini-Kamkar N, Neufeld RWJ, Jetly R, Frey BN, Ros T, Lanius RA and Nicholson AA (2023) A tale of two targets: examining the differential effects of posterior cingulate cortex- and amygdala-targeted fMRI-neurofeedback in a PTSD pilot study. *Front. Neurosci.* 17:1229729. doi: 10.3389/fnins.2023.1229729



# A tale of two targets: examining the differential effects of posterior cingulate cortex- and amygdala-targeted fMRI-neurofeedback in a PTSD pilot study

Jonathan M. Lieberman[1,2,3], Daniela Rabellino[3,4], Maria Densmore[3,5], Paul A. Frewen[4,6], David Steyrl[7], Frank Scharnowski[7], Jean Théberge[2,5,8,9], Niki Hosseini-Kamkar[1,10], Richard W. J. Neufeld[4,5,6,11], Rakesh Jetly[10], Benicio N. Frey[2,12], Tomas Ros[13], Ruth A. Lanius[3,4,5†] and Andrew A. Nicholson[2,8,10,14*†]

[1]Atlas Institute for Veterans and Families, Ottawa, ON, Canada, [2]Department of Psychiatry and Behavioural Neurosciences, McMaster University, Hamilton, ON, Canada, [3]Imaging, Lawson Health Research Institute, London, ON, Canada, [4]Department of Neuroscience, Western University, London, ON, Canada, [5]Department of Psychiatry, Western University, London, ON, Canada, [6]Department of Psychology, Western University, London, ON, Canada, [7]Department of Cognition, Emotion, and Methods in Psychology, University of Vienna, Vienna, Austria, [8]Department of Medical Biophysics, Western University, London, ON, Canada, [9]Department of Diagnostic Imaging, St. Joseph's Healthcare, London, ON, Canada, [10]The University of Ottawa Institute of Mental Health Research, Royal Ottawa Hospital, University of Ottawa, Ottawa, ON, Canada, [11]Department of Psychology, University of British Columbia, Kelowna, BC, Canada, [12]Mood Disorders Treatment and Research Clinic, St. Joseph's Healthcare Hamilton, Ontario, ON, Canada, [13]Department of Neuroscience and Psychiatry, University of Geneva, Geneva, Switzerland, [14]School of Psychology, University of Ottawa, Ottawa, ON, Canada

**Introduction:** Real-time fMRI-based neurofeedback (rt-fMRI-NFB) is a non-invasive technology that enables individuals to self-regulate brain activity linked to neuropsychiatric symptoms, including those associated with post-traumatic stress disorder (PTSD). Selecting the target brain region for neurofeedback-mediated regulation is primarily informed by the neurobiological characteristics of the participant population. There is a strong link between PTSD symptoms and multiple functional disruptions in the brain, including hyperactivity within both the amygdala and posterior cingulate cortex (PCC) during trauma-related processing. As such, previous rt-fMRI-NFB studies have focused on these two target regions when training individuals with PTSD to regulate neural activity. However, the differential effects of neurofeedback target selection on PTSD-related neural activity and clinical outcomes have not previously been investigated.

**Methods:** Here, we compared whole-brain activation and changes in PTSD symptoms between PTSD participants ($n = 28$) that trained to downregulate activity within either the amygdala ($n = 14$) or the PCC ($n = 14$) while viewing personalized trauma words.

**Results:** For the PCC as compared to the amygdala group, we observed decreased neural activity in several regions implicated in PTSD psychopathology – namely, the bilateral cuneus/precuneus/primary visual cortex, the left superior parietal lobule, the left occipital pole, and the right superior temporal gyrus/

temporoparietal junction (TPJ) – during target region downregulation using rt-fMRI-NFB. Conversely, for the amygdala as compared to the PCC group, there were no unique (i.e., over and above that of the PCC group) decreases in neural activity. Importantly, amygdala downregulation was not associated with significantly improved PTSD symptoms, whereas PCC downregulation was associated with reduced reliving and distress symptoms over the course of this single training session. In this pilot analysis, we did not detect significant between-group differences in state PTSD symptoms during neurofeedback. As a critical control, the PCC and amygdala groups did not differ in their ability to downregulate activity within their respective target brain regions. This indicates that subsequent whole-brain neural activation results can be attributed to the effects of the neurofeedback target region selection in terms of neurophysiological function, rather than as a result of group differences in regulatory success.

**Conclusion:** In this study, neurofeedback-mediated downregulation of the PCC was differentially associated with reduced state PTSD symptoms and simultaneous decreases in PTSD-associated brain activity during a single training session. This novel analysis may guide researchers in choosing a neurofeedback target region in future rt-fMRI-NFB studies and help to establish the clinical efficacy of specific neurofeedback targets for PTSD. A future multi-session clinical trial of rt-fMRI-NFB that directly compares between PCC and amygdala target regions is warranted.

KEYWORDS

**post-traumatic stress disorder, fMRI neurofeedback, posterior cingulate cortex, amygdala, default mode network**

## 1 Introduction

Over the past two decades, interest in real-time functional magnetic resonance imaging-based neurofeedback (rt-fMRI-NFB) has grown rapidly, largely owing to recent developments in real-time data processing and pattern analysis (Watanabe et al., 2017). rt-fMRI-NFB is a non-invasive brain-computer interface that enables individuals to self-regulate specific brain networks and functions, which can be particularly beneficial for treating various psychiatric conditions. Indeed, several studies have implemented rt-fMRI-NFB in a range of prevalent psychiatric conditions (Linden et al., 2012; Li et al., 2013; Schoenberg and David, 2014; Hamilton et al., 2016; Young et al., 2017; Mehler et al., 2018), including post-traumatic stress disorder (PTSD) (Gerin et al., 2016; Misaki et al., 2018, 2019, 2021; Nicholson et al., 2016a, 2018, 2021; Zotev et al., 2018; Zweerings et al., 2018, 2020; Chiba et al., 2019; Weaver et al., 2020; Lieberman et al., 2023; Zhao et al., 2023). In designing clinical rt-fMRI-NFB studies, multiple methodological factors require critical consideration; however, one of the most crucial decisions is the selection of the neurophysiological basis by which to generate the neurofeedback signal. While there are several possible approaches in this regard – including multi-voxel activation (i.e., decoded neurofeedback) and functional connectivity-based neurofeedback – the majority of previous rt-fMRI-NFB studies in PTSD have selected a target region as the basis for the neurofeedback signal (Gerin et al., 2016; Nicholson et al., 2016a, 2021; Misaki et al., 2018, 2019; Zotev et al., 2018; Zweerings et al., 2018; Weaver et al., 2020; Zhao et al., 2023).

In a clinical context, the selection of a neurofeedback target region is primarily informed by the neurobiological characteristics and desired clinical outcomes of the psychiatric condition being studied. Two main approaches are used for selecting a target region in the majority of clinical studies: the altered process approach and the compensatory process approach (Sulzer et al., 2013; Young et al., 2021). In the altered process approach, rt-fMRI-NFB is used to select regions with altered function or connectivity that are linked to the psychiatric condition being studied. This approach requires prior knowledge of the pathophysiological mechanisms underlying the condition to inform the choice of target region and the direction of regulation (i.e., upregulate vs. downregulate). The guiding assumption of this approach is that by normalizing pathophysiological alterations in brain activity, participants may be able to alleviate associated symptoms (Sulzer et al., 2013; Young et al., 2021). Alternatively, in the compensatory process approach, rt-fMRI-NFB is used to train participants to overcome impaired functionality by engaging compensatory neural mechanisms that have been well studied in healthy populations (Sulzer et al., 2013; Young et al., 2021). For instance, the putative brain regions underlying automatic and voluntary emotion regulation may serve as effective targets for neurofeedback training for several clinical populations in which emotion regulation deficits are present (Sulzer et al., 2013). Despite having these approaches available, it remains unclear how to select between several possible target regions that are all of neurobiological relevance to a particular psychiatric condition. Indeed, in the rt-fMRI-NFB literature, significant heterogeneity exists in the selection of target regions, even among studies with similar populations or clinical/behavioral objectives (Thibault et al., 2018). For instance, in a recent systematic review, multiple target regions (i.e., amygdala, insula, anterior cingulate cortex [ACC], prefrontal cortex [PFC]) were investigated across rt-fMRI-NFB studies in PTSD, depression, and anxiety-based disorders, all with the shared goal of improving emotion regulation capacities (Linhartová et al., 2019). This heterogeneity in neurofeedback target selection is unsurprising

as psychiatric conditions, including PTSD, involve complex neurobiological mechanisms in which pathophysiological alterations extend across several distinct brain regions.

Extensive research has established a strong link between PTSD symptoms and multiple functional disruptions in the brain (e.g., Lanius et al., 2015; Tursich et al., 2015; Fenster et al., 2018). Indeed, both at rest and during trauma-related processing, hyperactivity within the amygdala – a brain region associated with emotion generation and processing – has been strongly associated with PTSD symptoms (Lanius et al., 2010, 2015; Etkin et al., 2011; Mickleborough et al., 2011; Patel et al., 2012; Birn et al., 2014; Yehuda et al., 2015; Aghajani et al., 2016; Koch et al., 2016; Fenster et al., 2018; Fitzgerald et al., 2018). There are also PTSD-associated alterations in functional connectivity between the amygdala and the cingulate cortex (including the ACC), insula, and PFC (Fonzo et al., 2010; Rabinak et al., 2011; Sripada et al., 2012; Birn et al., 2014; Brown et al., 2014; Nicholson et al., 2015, 2016b). In particular, negative medial PFC-amygdala connectivity is associated with PTSD symptom severity during trauma-related emotion processing (Stevens et al., 2013; Jin et al., 2014; Sadeh et al., 2014; Wolf and Herringa, 2016). Taken together, PTSD-associated emotion dysregulation appears to result from a hyperactive limbic system (i.e., amygdala, insula) driven by the loss of top-down inhibition from frontal brain regions (i.e., PFC, ACC) (Rauch et al., 2006; Lanius et al., 2010; Shin and Liberzon, 2010; Aupperle et al., 2012; Pitman et al., 2012; Admon et al., 2013; Ronzoni et al., 2016). Given this neurobiological account of PTSD, it is fitting that the majority of previous rt-fMRI-NFB studies in PTSD have targeted the amygdala, wherein participants were trained to either downregulate regional activity during negative emotion induction (Gerin et al., 2016; Nicholson et al., 2016a, 2018; Zhao et al., 2023) or upregulate regional activity during positive emotion induction (Misaki et al., 2018, 2019; Zotev et al., 2018). Other studies have taken a related approach in which individuals with PTSD were trained to upregulate frontal brain regions involved in emotion regulation (Zweerings et al., 2018, 2020). For instance, in one study, participants upregulated left lateral PFC activity while performing cognitive reappraisal to reduce their emotion response to negative scenes (Zweerings et al., 2020). However, it is increasingly apparent that the fronto-limbic model, as previously described, does not explain the full range of symptoms experienced by PTSD patients or account for alterations within other brain regions (e.g., Akiki et al., 2017; Fenster et al., 2018; Kamiya and Abe, 2020). Therefore, exploration of novel neurofeedback targets in PTSD is of critical importance.

The posterior cingulate cortex (PCC), the major hub of the posterior default mode network (DMN) (Greicius et al., 2003; Buckner et al., 2008; Spreng et al., 2009; Qin and Northoff, 2011; Brewer et al., 2013), is another brain region that is critically implicated in PTSD psychopathology. Among individuals with PTSD, there are alterations in functional connectivity of the PCC and the DMN both at rest (Akiki et al., 2017, 2018, Bluhm et al., 2009; Sripada et al., 2012; Lanius, 2015; Tursich et al., 2015; Yehuda et al., 2015; Koch et al., 2016; Hinojosa et al., 2019; Nicholson et al., 2020a) and during executive functioning tasks (Daniels et al., 2010; Melara et al., 2018). Importantly, hyperactivity within the PCC during the reliving and reexperiencing of trauma-related autobiographical memories in PTSD has also been reported (Ramage et al., 2013; Frewen et al., 2017; Awasthi et al., 2020; Thome et al., 2020), including in a recent meta-analysis (Thome et al., 2020). In a longitudinal study, PTSD patients with recent exposure to traumatic events (i.e., within the past 2 months) demonstrated greater activation in the right PCC as compared to control participants in response to trauma-related cues (Ke et al., 2016). Notably, at a two-year follow-up, decreased activation in the PCC during a trauma provocation task was also predictive of PTSD symptom improvement (Ke et al., 2016). Taken together, these findings highlight the PCC's clinical relevance in PTSD psychopathology and suggest that regulating activity within the region via rt-fMRI-NFB may generate positive clinical outcomes. Critically, however, very few studies have examined the neurobiological mechanisms associated with the regulation of the PCC with rt-fMRI-NFB (Zhang et al., 2013; Garrison et al., 2013a,b; Kirlic et al., 2022; Yu et al., 2022), with only one study examining the regulation of this region in PTSD (Nicholson et al., 2021; Lieberman et al., 2023).

Previously, our group has used rt-fMRI-NFB to train individuals with PTSD to downregulate activity within both the amygdala and PCC during an identical trauma provocation paradigm in which individuals viewed personalized trauma words (Nicholson et al., 2016a, 2018, 2021; Lieberman et al., 2023). With regard to amygdala targeted neurofeedback, the involvement of the prefrontal cortex and its role in emotion regulation may be critical for facilitating successful downregulation. Indeed, our previous study showed that amygdala downregulation was associated with increased neural activity within the PFC (i.e., dlPFC, vlPFC), increased bidirectional amygdala-PFC (i.e., dlPFC, dmPFC) effective connectivity, and increased recruitment of the left central executive network (CEN; including the bilateral dlPFC) (Nicholson et al., 2016a, 2018). On the other hand, PCC downregulation was associated with simultaneous widespread decreases in neural activity within several brain regions implicated in PTSD psychopathology – namely, the dmPFC, postcentral gyrus, amygdala/hippocampus, cingulate cortex, and temporal pole/gyri (Nicholson et al., 2021). Additionally, PCC downregulation was also associated with increased PCC connectivity with the dmPFC, vmPFC, posterior insula, and amygdala (Lieberman et al., 2023). Hence, PCC downregulation may help to restore connectivity between functionally segregated posterior and anterior DMN structures and may also result in the concomitant regulation of brain regions involved in emotion generation/processing (i.e., amygdala) and embodiment (i.e., insula). Critically, however, no studies to date have conducted a direct comparison between multiple rt-fMRI-NFB target regions (i.e., the amygdala and the PCC) among individuals with PTSD. This novel analysis may help to elucidate unique neural mechanisms underlying rt-fMRI-NFB regulation and establish the clinical efficacy of specific neurofeedback targets.

## 1.1 Current study

In the current study, we aimed to explore differential neural mechanisms associated with rt-fMRI-NFB targeting the amygdala or PCC among individuals with PTSD. To do so, we compared whole-brain activation patterns between two groups of PTSD participants, who were trained to downregulate activity within either the amygdala or the PCC during an identical trauma provocation paradigm. Based on previous studies examining patterns of activation and connectivity associated with amygdala and PCC downregulation with rt-fMRI-NFB (Gerin et al., 2016; Nicholson et al., 2016a, 2018, 2021; Misaki et al., 2018, 2019; Zotev et al., 2018; Lieberman et al., 2023; Zhao et al.,

2023), we expected to observe unique neural mechanisms involved in the downregulation of these two target regions when comparing them directly. More specifically, we hypothesized that amygdala downregulation would be associated with increased neural activity in emotion regulation areas within the prefrontal cortex, as compared to the PCC group. In contrast, we hypothesized that PCC downregulation would be associated with concomitant widespread decreases in neural activity within regions involved in PTSD psychopathology, as compared to the amygdala group.

# 2 Methods

## 2.1 Participants

The sample for this study consisted of $n = 28$ participants with PTSD (Table 1) who were trained to downregulate activity within one of two target regions – either the amygdala ($n = 14$) or the PCC ($n = 14$) – using rt-fMRI-NFB. While not analyzed here, there was also a group of healthy control participants who were trained to downregulate activity within the PCC ($n = 15$) (Nicholson et al., 2021). The sample size of this pilot investigation was based on study feasibility during the recruitment period. All participants were recruited via clinician referrals, community organizations, and posters throughout the London, Ontario community. Inclusion criteria included a current primary diagnosis of PTSD as measured by the Clinician-Administered PTSD Scale (CAPS-5) (Weathers et al., 2018) and the Structured Clinical Interview for DSM-5 (SCID) (First, 2015). Exclusion criteria included: ongoing or recent (within the previous three months) alcohol or substance use disorders, suicidal ideations, self-injurious behaviors requiring medical attention, lifetime diagnoses of bipolar or psychotic disorders, previous biofeedback treatment, noncompliance with 3 T fMRI safety guidelines, untreated medical conditions, pregnancy, previous head injury with loss of consciousness, and neurological or pervasive developmental disorders. All scanning took place at the Lawson Health Research Institute in London, Ontario. This research was approved by the Research Ethics Board at Western University, and all participants provided written informed consent. A CRED-nf checklist (Ros et al., 2020) summarizing experimental design was completed via the standardized CRED-nf online tool[1] and is provided as Supplementary material.

Prior to scanning, participants completed several clinical assessments, including the Beck's Depression Inventory (BDI) (Beck et al., 1997), the Childhood Trauma Questionnaire (CTQ) (Bernstein et al., 2003) and the Multiscale Dissociation Inventory (MDI) (Briere et al., 2005). After each of the fMRI neurofeedback runs, participants completed the Response to Script Driven Imagery Scale (RSDI) (Hopper et al., 2007a), which included the following symptom subscales: reliving, distress, physical reactions, dissociation, and emotional numbing.

There were no significant differences between the groups in terms of age, or scores on the BDI, CTQ, and MDI (Table 1). However, there were significant differences between the groups in terms of biological sex (amygdala group: 4 males, 10 females; PCC group: 8 males, 6 females) and CAPS-5 scores (amygdala group: $M = 31.7$, SD = 9.4; PCC group: $M = 43.2$, SD = 8.3) (Table 1). As such, both biological sex and CAPS-5 scores were included as covariates within subsequent analyses. Notably, there was a single missing data point for one participant's CAPS-5 score. For the purposes of including CAPS-5 scores as a covariate in our analyses, we used the expectation–maximization (EM) algorithm to impute a value for this missing data point. To implement the EM algorithm, we used Python 3.9 and the scikit-learn library. Specifically, we used the 'LinearRegression' function to create a linear regression model, which we trained on the observed data from all participants (i.e., age, biological sex, CAPS-5 scores). We then used the trained model to impute a value for the missing data point for use as a covariate only. Among several possible approaches for imputing the missing data point, the EM algorithm with a linear regression model was optimal given the observed data. Previous publications by our group have analyzed the imaging data for each participant group separately (Nicholson et al., 2016a, 2018, 2021; Lieberman et al., 2023), but no previous study has assessed the differential neural and clinical effects associated with PCC as compared to amygdala-targeted fMRI-NFB.

TABLE 1 Demographic and clinical information.

| Measure | PCC ($n = 14$) | Amygdala ($n = 14$) |
|---|---|---|
| Age | 49.50 (±5.11) | 48.08 (±9.78) |
| **Biological sex** | **6F, 8M** | **10F, 4M** |
| **CAPS-5** | **43.21 (±8.26)** | **31.70 (±9.42)** |
| BDI | 32.14 (±12.55) | 26.60 (±13.33) |
| CTQ | 61.50 (±25.84) | 60.64 (±16.58) |
| MDI | 87.36 (±28.23) | 68.20 (±27.12) |
| Psychotropic medication | 10 | 11 |

Bolded measures (i.e., biological sex, CAPS-5) were found to differ significantly between groups and were included as covariates in subsequent analyses. Values in parentheses indicate standard deviation. CAPS-5, Clinician-Administered PTSD Scale (version 5); BDI, Beck's Depression Inventory; CTQ, Childhood Trauma Questionnaire (*none or minimal childhood trauma* = 25–36, *moderate* = 56–68, extreme trauma > 72); MDI, Multiscale Dissociation Inventory.

## 2.2 Real-time fMRI neurofeedback protocol

All participants underwent an identical experimental protocol and neurofeedback paradigm, with the exception of the neurofeedback target region (i.e., the amygdala or PCC) (Figure 1). During neurofeedback training, participants were presented with a signal corresponding to BOLD activation within the neurofeedback target region. This neurofeedback signal was presented as a virtual thermometer on both sides of the MRI screen that was visible to participants while they were inside the scanner. The bars on the thermometer increased or decreased in correspondence to changes in BOLD activation within the neurofeedback target region. Participants were instructed that they would be regulating an area of the brain related to emotion. To avoid biasing the selection and usage of regulatory mental strategies by participants, no specific instructions were provided on how to regulate the neurofeedback target region

1 http://www.rtfin.org/CREDnf

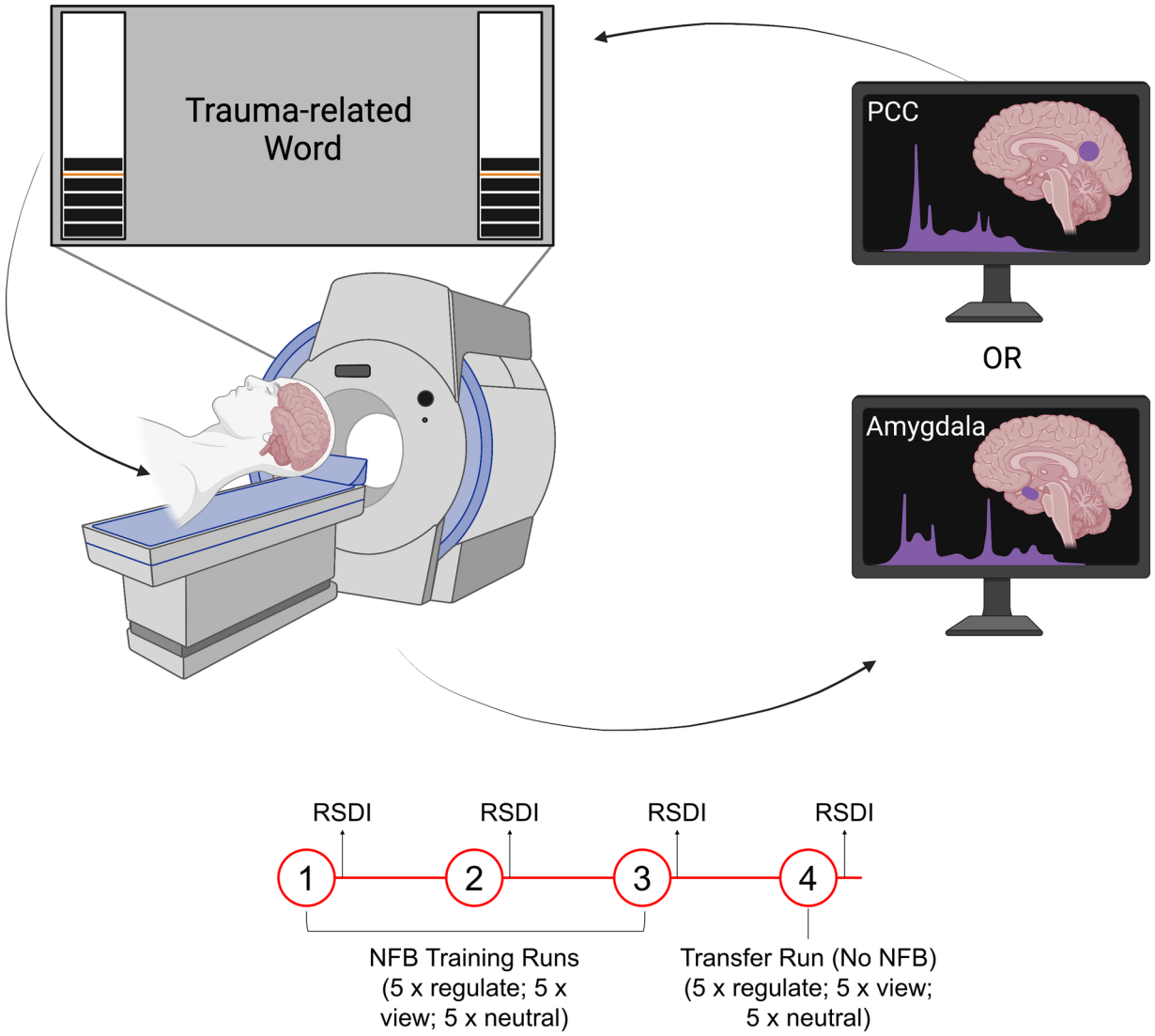


FIGURE 1
Illustration of the rt-fMRI-NFB experimental set-up. The neurofeedback signal took the form of a virtual thermometer whose level changed in response to fluctuating activity within the neurofeedback target region (PCC or amygdala). Participants viewed the neurofeedback signal during a trauma provocation paradigm while they were in the scanner. All participants completed three neurofeedback training runs, followed by a transfer run, in which they were not shown the neurofeedback signal. Figure adapted with permission from Nicholson et al. (2021).

(Paret et al., 2014, 2016a; Nicholson et al., 2016a, 2018, 2021). Rather, participants were instructed to use whichever strategies they personally found to work best for regulating the neurofeedback signal. Participants were asked to focus their gaze directly on the presented word for the duration of each condition and to use their peripheral vision to monitor the thermometers. Participants were also informed that the neurofeedback signal lags behind their brain activity by approximately 6–8 s (due to the BOLD signal time lag).

Our neurofeedback protocol consisted of three conditions: regulate, view, and neutral. In the *regulate* condition, participants were instructed to decrease the neurofeedback signal while viewing a personalized trauma-related word. In the *view* condition, participants viewed a trauma-related word but were instructed to respond naturally and not attempt to exert regulatory control over the neurofeedback signal. In the *neutral* condition, participants viewed a personalized neutral word and were instructed to respond naturally and not attempt to exert regulatory control over the neurofeedback signal. Personalized words were selected with the guidance of a trauma-informed clinician ($n = 10$ for both trauma-related and neutral words). Participants selected trauma-related words that were related to their individual experiences of trauma. The trauma-related words were matched on subjective units of distress to control for between subject/group variability. Stimuli were presented using Presentation software from Neurobehavioral Systems.

The experimental design included three consecutive neurofeedback training runs, followed by a single transfer run. In the transfer run, participants underwent an identical protocol except they were not shown a neurofeedback signal. Each run lasted 9 min and included 15 trials (5 per condition). The timing for all trials was as follows: 2 s for instructions, followed by 24 s for the condition, and then a 10 s implicit rest with an intertrial fixation cross. All trials were counterbalanced.

## 2.3 Real-time signal processing for neurofeedback

For all participants, we performed identical procedures to present real-time neural activation of the neurofeedback target region via a thermometer display. First, we imported anatomical scans into BrainVoyager (version QX2.4, Brain Innovations), skull-stripped and transformed them into Talairach space. We then added the normalization parameters into Turbo-BrainVoyager (TBV, version 3.0, Brain Innovations) which was the software used for real-time processing and analysis of BOLD signals. During real-time signal processing, TBV detected and corrected for small head movements (via rigid body transformation to the first recorded volume) and conducted spatial smoothing (4-mm full-width-half-maximum; FWHM). We discarded the first two volumes of the functional scans before real-time processing. Next, we defined the neurofeedback target region using TBV. For the amygdala, we used a bilateral anatomical mask from the PickAtlas software (WFU Pickatlas). For the PCC, we used a 6 mm sphere at the coordinate (MNI: 0–50 20) (Bluhm et al., 2009). In both cases, we then used the "best voxel selection" tool in TBV to calculate the BOLD signal amplitude in the defined target area. This method identifies the 33% most active (i.e., the highest beta-values) voxels for the *view* > *neutral* contrast. The first two trials of each neurofeedback run were the view and neutral conditions, which allowed us to select voxels based on the *view* > *neutral* contrast. This selection was dynamically updated throughout the duration of training. Indeed, as outlined in previous publications (Paret et al., 2014, 2016b; Nicholson et al., 2016a, 2018), dynamic voxel selection is based on (a) the voxel with the largest beta value, and (b) the magnitude of deviation from the mean of all condition betas (Goebel, 2014). This method ensures that there are no inter-subject differences in the number of voxels used for signal extraction. Additionally, it accounts for slight shifts in anatomical delineation resulting from changes in alignment across runs and/or movement-related slice shifts. The neurofeedback signal was calculated as the mean of the processed BOLD signal over the included voxels within the target brain region. In order to smooth out rapid BOLD signal fluctuations, the neurofeedback signal shown to participants via thermometer display was the mean of the neurofeedback signal of the current and 3 preceding TRs (Paret et al., 2014, 2016b; Nicholson et al., 2016a, 2021). At the start of each trial, the mean of the neurofeedback signal of the first 4 TRs (preceding stimuli onset) were utilized as a baseline and shown to participants as an orange line on the thermometer display. Subsequently, the level of the thermometer was continuously updated (at each TR) and shown to participants throughout the 3 neurofeedback training runs. Each segment of the thermometer corresponded to a 0.2% change in BOLD activation, with a maximum range of +2.8% and −1.2% from baseline (Paret et al., 2014, 2016b; Nicholson et al., 2016a, 2018, 2021).

## 2.4 fMRI image acquisition

We used the same 3 Tesla MRI Scanner (Siemens Biograph mMR) at the Lawson Health Research Institute for all participants. Functional whole-brain images of the BOLD contrast were acquired using a gradient echo T2*-weighted echo-planar-imaging sequence (TE = 30 ms, TR = 2 s, FOV = 192 mm × 192 mm, flip angle = 80°, in-plane resolution = 3 mm × 3 mm). Each volume consisted of 36 ascending interleaved slices tilted −20° from the AC-PC axis with a thickness of 3 mm and a slice gap of 1 mm. Participants' heads were stabilized using a 32-channel head coil. These scanning parameters enabled whole-brain coverage. The experimental runs comprised 284 volumes, and T1-weighted anatomical images were obtained using a Magnetization Prepared Rapid Acquisition Gradient Echo sequence (TE = 3.03 ms, TR = 2.3 s, 192 slices, FOV = 256 mm × 256 mm).

## 2.5 fMRI preprocessing

We preprocessed all neuroimaging data following identical procedures using SPM12 within MATLAB R2020a. We discarded the first four functional volumes for each subject and then performed slice time correction to the middle slice as well as reorientation to the AC-PC axis. Using a rigid body transformation, we performed spatial alignment to the mean functional image to correct for participant movement during the scan. The functional images were also resliced. T1 anatomical images were corrected for inhomogeneity. We then used the mean functional image to co-register the functional scans to the subject-specific T1-weighted anatomical image. Co-registration was visually inspected for each subject and was manually corrected if necessary. Subsequently, we performed segmentation of all tissue types with the co-registered images using the "New Segment" method in SPM. Volumes were then spatially normalized ($2\,mm^3 \times 2\,mm^3 \times 2\,mm^3$) to the MNI standard template via application of a deformation matrix. Functional images were then smoothed via a three-dimensional isotropic 6-mm FWHM Gaussian kernel. Lastly, we performed additional motion correction using the Artifact Detection Tool (ART) software package,[2] which computes regressors to account for outlier volumes, in addition to the six movement regressors computed during standard realignment procedures in general linear modeling. We selected the standard thresholds for outlier detection in ART (global signal threshold = 9.0 mm, absolute subject motion threshold = 2.0 mm, rotational threshold = 0.05 mm, scan-to-scan subject motion = 2.0 mm, and scan-to-scan subject rotation = 0.02 mm).

## 2.6 Statistical analyses

### 2.6.1 First-level analysis

Separate sessions were defined for each of the neurofeedback training runs and transfer run. All task events (initial rest, instructions, fixation cross, and conditions) were modeled as blocks of brain activation and convolved with the hemodynamic response function. At this stage, functional data was high-pass filtered and serial correlations were taken into account using an autoregressive model. Additionally, we included the ART regressors as nuisance variables to account for additional movement and outlier artifacts. The three experimental conditions (*regulate*, *view*, and *neutral*) were modeled separately.

2 https://www.nitrc.org/projects/artifact_detect

### 2.6.2 Whole-brain neural activation analysis – second-level

We conducted a mixed-effects model, split-plot factorial 2 (Neurofeedback target region: PCC, amygdala) × 3 (Run: 1, 2, 3) × 2 (Condition: regulate, view) ANCOVA with covariates for biological sex and CAPS-5 scores within SPM12 [hereafter referred to as, "training runs ANCOVA"]. We examined the transfer run separately by conducting a mixed-effects model, split-plot factorial 2 (Neurofeedback target region: PCC, amygdala) × 2 (Condition: regulate, view) ANCOVA with the same covariates [hereafter referred to as, "transfer run ANCOVA"]. We chose to include biological sex and CAPS-5 scores as covariates in both analyses as they differed significantly between the two participant groups. We were specifically interested in investigating differential neural activation between the two participant groups while they exerted regulatory control over activity within the neurofeedback target region. Therefore, we conducted *a priori* *t*-tests directly comparing whole-brain activation between the two groups during the *regulate* condition. All statistical tests were corrected for multiple comparisons using a cluster-level false discovery rate (FDR) significance threshold of $p < 0.05$, $k = 10$, with an initial cluster defining threshold at $p < 0.001$, $k = 10$ (Eklund et al., 2016; Roiser et al., 2016). As the SPM software version that was utilized only permits one-sided *t*-tests, we opted for a conservative approach by adjusting the statistical thresholds (i.e., $p < 0.05/2 = 0.025$) of the one-sided *t*-tests to achieve identical results to those that would be obtained through the use of a two-sided *t*-test (Chen et al., 2018).

### 2.6.3 Neurofeedback target downregulation analysis

To evaluate downregulation of the neurofeedback target region (i.e., neurofeedback success), we used rfxplot software to extract the event-related BOLD response (peristimulus time histogram) from the appropriate target region (i.e., PCC or amygdala during the *regulate* and *view* conditions) (Gläscher, 2009). Within the search volume, we extracted event-related BOLD responses from individual peaks for each subject and imported these values into SPSS (v.29) for statistical analyses. In rfxplot software, event-related BOLD responses are represented as the average height of the BOLD responses within a user-defined search volume and time window (Gläscher, 2009). Event-related BOLD responses are estimated using a condition-specific Finite Impulse Response (FIR) model (Gläscher, 2009). For the search volume, we used identical regional definitions as was used during participant scanning to generate the neurofeedback signal from each neurofeedback target region. For the time window, we parcellated the condition duration into temporal bins (TR = 2 s) starting at the onset of all trials belonging to a particular condition. The parameter estimate of each temporal bin within the FIR model is equivalent to that of the bin's mean BOLD response. Thus, the outcome of the FIR model is an event-related BOLD time course for each subject.

Previously, we observed that participants were able to successfully downregulate BOLD activity within both the amygdala (Nicholson et al., 2016a, 2018) and PCC (Nicholson et al., 2021). Here, we sought to determine whether participants' neurofeedback performance differed between the two target regions during rt-fMRI-NFB. Thus, we conducted a mixed-effects model, split-plot factorial 2 (Neurofeedback target region: PCC, amygdala) x 4 (Run: 1, 2, 3, 4) x 2 (Condition: regulate, view) repeated measures ANCOVA with covariates for biological sex and CAPS-5 scores. Subsequently, we conducted *a priori* defined independent sample *t*-tests, comparing average BOLD response between the two target regions for *regulate* and *view* conditions during each neurofeedback run.

### 2.6.4 State changes in PTSD symptoms over neurofeedback

We assessed state changes in PTSD symptoms to traumatic stimuli after each neurofeedback run (including the transfer run), as measured by the RSDI scale. As this data was not normally distributed, we conducted non-parametric Friedman's repeated measures ANOVAs for each RSDI subscale for the participant groups separately to measure within-group changes in state PTSD symptoms. We Bonferroni corrected our statistical threshold ($p < 0.05/5 = 0.01$) for multiple nonparametric ANOVAs. We then examined two *a priori* planned comparisons between RSDI subscale scores at different time points – post-run 1 vs. post-run 3 and post-run 1 vs. post-run 4 – using non-parametric tests for related samples (Wilcoxon signed-ranks test). Finally, we compared RSDI subscale scores between participant groups after each neurofeedback run (including the transfer run) using Mann–Whitney U tests. As an additional precaution, we performed a similar between-group comparison using a Quade's rank-transformed ANCOVA with CAPS-5 scores as a covariate which yielded identical results. Please note, within-group changes on RSDI subscale scores for the PCC group have been reported elsewhere (Nicholson et al., 2021; Lieberman et al., 2023).

## 3 Results

### 3.1 Downregulation of neurofeedback target brain region

Previously, we found that individuals with PTSD were able to significantly downregulate BOLD activity within the PCC (Nicholson et al., 2021) and amygdala (Nicholson et al., 2016a) during *regulate* as compared to *view* conditions for all three neurofeedback training runs, as well as the transfer run. Additionally, for both participant groups, activity within the target region during *regulate* did not significantly differ when directly comparing across neurofeedback runs (Nicholson et al., 2016a, 2021). Here, within the ANCOVA examining the down regulation of the neurofeedback target regions, we observed a significant main effect of condition [$F(1, 24) = 10.33$, $\eta^2 = 0.301$, $p = 0.004$]. We also observed non-significant main effects of run [$F(3, 72) = 0.668$, $\eta^2 = 0.027$, $p = 0.575$] and group [$F(1, 24) = 0.030$, $\eta^2 = 0.001$, $p = 0.864$], with non-significant interaction effects. Follow-up independent sample *t*-tests revealed that there was no significant difference in the average event-related BOLD response within the target region between the two groups during *regulate* or *view* in any individual neurofeedback run [regulate, run 1: $t(26) = 0.197$, $p = 0.846$, Cohen's $d = 0.074$; regulate, run 2: $t(26) = 0.342$, $p = 0.735$, Cohen's $d = 0.129$; regulate, run 3: $t(26) = 0.637$, $p = 0.530$, Cohen's $d = 0.241$; regulate, run 4: $t(26) = 0.794$, $p = 0.435$, Cohen's $d = 0.300$; view, run 1: $t(26) = -1.11$, $p = 0.278$, Cohen's $d = -0.419$; view, run 2: $t(26) = -0.064$, $p = 0.949$, Cohen's $d = -0.024$; view, run 3: $t(26) = 0.045$, $p = 0.965$, Cohen's $d = 0.017$; view, run 4: $t(26) = -0.645$, $p = 0.525$, Cohen's $d = -0.244$; Figure 2]. Importantly, this shows that both participant groups exhibited similar activation within the target

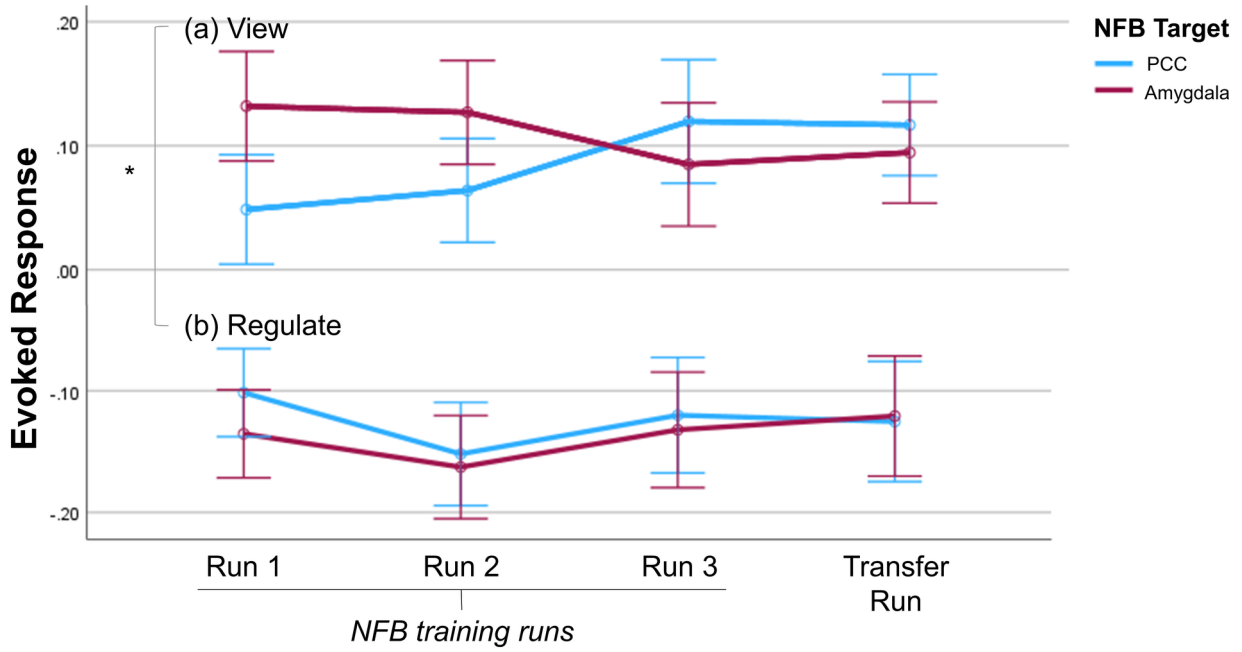


FIGURE 2
Average event-related BOLD response in the NFB target regions – PCC (blue) or amygdala (red) – is shown for the **(A)** *view* and **(B)** *regulate* conditions during the three NFB training runs and transfer run. For both the PCC and amygdala, average event-related BOLD response is significantly lower during *regulate* as compared to *view* conditions for each NFB training run and the transfer run. There were no significant differences in the average event-related BOLD response between the two NFB target regions during *regulate* or *view* in any individual NFB run. The x-axis of the graph indicates the NFB run; the y-axis indicates the average event-related BOLD response (peristimulus time histogram) across the entire duration of the condition. Error bars indicate standard error of the mean. PCC, posterior cingulate cortex; NFB, neurofeedback.

region in response to the trauma-related words (i.e., the *view* comparisons) and were similarly able to downregulate activation within their target region (i.e., the *regulate* comparisons). Therefore, neural activation results can be confidently attributed to the differential effect of the selected neurofeedback target region for each participant group rather than resulting from possible group differences in trauma-related responses or success in regulating the neurofeedback target (Sorger et al., 2019).

## 3.2 Whole-brain neural activation analysis

Our neurofeedback training runs ANCOVA revealed significant main effects for neurofeedback target and condition (Table 2). The main effect of neurofeedback target showed significant clusters within the bilateral cuneus/precuneus/primary visual cortex, the left superior parietal lobule, and the left occipital pole. The main effect of condition showed significant clusters within the left superior/middle frontal gyrus, the left angular gyrus, and the left precuneus. There was a non-significant main effect of run and non-significant interaction effects (Table 2).

For the amygdala as compared to the PCC group, we did not observe any significant unique (i.e., over and above that of the PCC group) decreases in neural activity during the *regulate* condition (Table 3). Conversely, for the PCC as compared to the amygdala group, we observed widespread whole-brain decreases in activity within the bilateral cuneus/precuneus/primary visual cortex, the left superior parietal lobule, the left occipital pole, and the right superior temporal gyrus/temporoparietal junction (TPJ) (Table 3; Figure 3).

Importantly, in conducting between-group comparisons of neural activity, any changes in neural activity that are shared by both groups would not be observable. As such, we conducted follow-up comparisons of neural activity during the *regulate* condition as compared to rest for each group separately (Table 4; Figure 4). During *regulate* as compared to rest, the PCC group showed widespread whole-brain decreases in activity including a large bilateral posterior cluster extending across the cuneus, precuneus, primary visual cortex, and PCC, as well as significant clusters within the dmPFC/ACC, left dlPFC, bilateral caudate/nucleus accumbens, right hippocampus/parahippocampal gyrus/amygdala, and bilateral angular gyri (Figure 4A – bottom panel). The PCC group only showed increased activity in posterior regions of the brain with significant clusters within the right superior parietal lobule, the left occipital gyrus/primary visual cortex, and the left cerebellum lobule VI (Figure 4A – top panel). Conversely, during *regulate* as compared to rest, the amygdala group did not show any significant whole-brain decreases in activity (Figure 4B – bottom panel). However, this group showed increased activity in several brain regions including the left vlPFC/inferior frontal gyrus, bilateral occipital gyri, bilateral cerebellum lobule VIIb, right precentral gyri, right anterior insula, and the bilateral supplementary motor cortex (Figure 4B – top panel).

Our transfer run ANCOVA did not reveal any significant main effects or interactions between factors. For the transfer run, *a priori*

TABLE 2 2 (Group) × 3 (NFB Run) × 2 (Condition) – training runs ANCOVA.

| | | | | MNI coordinate | | | | | |
|---|---|---|---|---|---|---|---|---|---|
| Comparison | Brain region | H | *k* | *x* | *y* | *z* | *F*-Stat. | *Z*-Score | *p*-FDR |
| Main effect of NFB target | Cuneus/precuneus/primary visual cortex | Right | 1,127 | 14 | −72 | 20 | 34.38 | 5.44 | <0.001 |
| | Cuneus/precuneus/primary visual cortex | Left | 97 | −18 | −68 | 10 | 15.89 | 3.71 | 0.03 |
| | Superior parietal lobule | Left | 175 | −22 | −60 | 38 | 24.26 | 4.6 | 0.004 |
| | Occipital pole | Left | 118 | −14 | −100 | 18 | 18.39 | 4 | 0.018 |
| Main effect of run | *ns* | | | | | | | | |
| Main effect of condition | Superior/middle frontal gyrus | Left | 132 | −18 | 26 | 44 | 21.87 | 4.37 | 0.022 |
| | Angular gyrus | Left | 144 | −50 | −72 | 30 | 18.7 | 4.03 | 0.022 |
| | Precuneus | Left | 110 | −10 | −54 | 38 | 16.52 | 3.79 | 0.033 |
| NFB target × run | *ns* | | | | | | | | |
| NFB target × condition | *ns* | | | | | | | | |
| Run × condition | *ns* | | | | | | | | |
| NFB target × run × condition | *ns* | | | | | | | | |

Results of the split-plot factorial 2 (group) by 3 (NFB run) by 2 (condition) ANCOVA evaluated at the FDR-cluster corrected threshold for multiple comparisons ($p < 0.05$, $k = 10$). The comparison, brain region, hemisphere of the region (H), cluster size (*k*), MNI coordinates (*x*,*y*,*z*), *F*-statistic (*F*-Stat.), *Z*-Score, and significance (*p*-FDR) of each significant cluster are included as columns. *ns*, not significant; NFB, neurofeedback.

TABLE 3 Neurofeedback training – between-group comparisons during *regulate*.

| | | | | | MNI coordinate | | | | | |
|---|---|---|---|---|---|---|---|---|---|---|
| Comparison | Condition | Brain region | H | *k* | *x* | *y* | *z* | *T*-Stat. | *Z*-Score | *p*-FDR |
| Amygdala < PCC | Regulate | *ns* | | | | | | | | |
| PCC < Amygdala | Regulate | Cuneus/precuneus/ primary visual cortex | Bilateral | 1,643 | 14 | −74 | 22 | 5.87 | 5.57 | <0.001 |
| | | Superior parietal lobule | Left | 856 | −22 | −60 | 38 | 5.12 | 4.91 | <0.001 |
| | | Occipital pole | Left | 198 | −20 | −90 | 8 | 4.24 | 4.12 | 0.007 |
| | | Superior temporal gyrus/ TPJ | Right | 194 | 56 | −38 | 16 | 3.99 | 3.89 | 0.007 |

Results of the *a-priori* between-group comparisons for the *regulate* condition during the NFB training runs evaluated at the FDR-cluster corrected threshold for multiple comparisons ($p < 0.025$, $k = 10$). The comparison, condition, brain region, hemisphere of the brain region (H), cluster size (*k*), MNI coordinates (*x*,*y*,*z*), *T*-statistic (*T*-Stat.), *Z*-Score, and significance (*p*-FDR) of each significant cluster are included as columns. *ns*, not significant; PCC, posterior cingulate cortex; TPJ, temporoparietal junction.

planned comparisons between the two participant groups during the *regulate* condition yielded non-significant results.

## 3.3 State changes in PTSD symptoms over neurofeedback

In summary, when assessing state changes in PTSD symptoms, we observed clear differences in terms of within-group results for the PCC and amygdala groups. As previously published, PCC downregulation was found to show a significant main effect of run for the nonparametric ANOVA investigating reliving [$\chi^2(3) = 11.49$, $p = 0.009$] and distress [$\chi^2(3) = 13.79$, $p = 0.003$] symptoms, and non-significant effects for the other RSDI subscales [physical reactions: $\chi^2(3) = 4.70$, $p = 0.195$; emotional numbing: $\chi^2(3) = 2.26$, $p = 0.520$; dissociation: $\chi^2(3) = 2.29$, $p = 0.515$] when controlling for multiple comparisons (Nicholson et al., 2021). Wilcoxon signed-rank tests revealed lower reliving scores during run 3 versus run 1 ($p = 0.016$) and lower distress scores during runs 3 ($p = 0.010$) and 4 ($p = 0.013$) versus run 1 for the PCC group (Nicholson et al., 2021; Table 5). By contrast, amygdala downregulation was not found to show a significant main effect of run for any of the nonparametric ANOVAs that were conducted for each of the RSDI subscales [reliving: $\chi^2(3) = 9.21$, $p = 0.027$; distress: $\chi^2(3) = 4.98$, $p = 0.173$; physical reactions: $\chi^2(3) = 10.24$, $p = 0.017$; emotional numbing: $\chi^2(3) = 0.240$, $p = 0.971$; dissociation: $\chi^2(3) = 0.241$, $p = 0.971$] when controlling for multiple comparisons. Wilcoxon signed-rank tests did not reveal any significant differences in RSDI scores between runs (i.e., run 1 vs. run 3; run 1 vs. run 4) for the amygdala group. When directly comparing the two groups during each run using Mann–Whitney U tests, there were no significant differences observed for any of the RSDI subscale scores (Table 6).

# 4 Discussion

## 4.1 Overview

The complexity of neurobiological alterations associated with PTSD poses a challenge for selecting an optimal target region for the regulation of neural activity using rt-fMRI-NFB. In the present analysis,

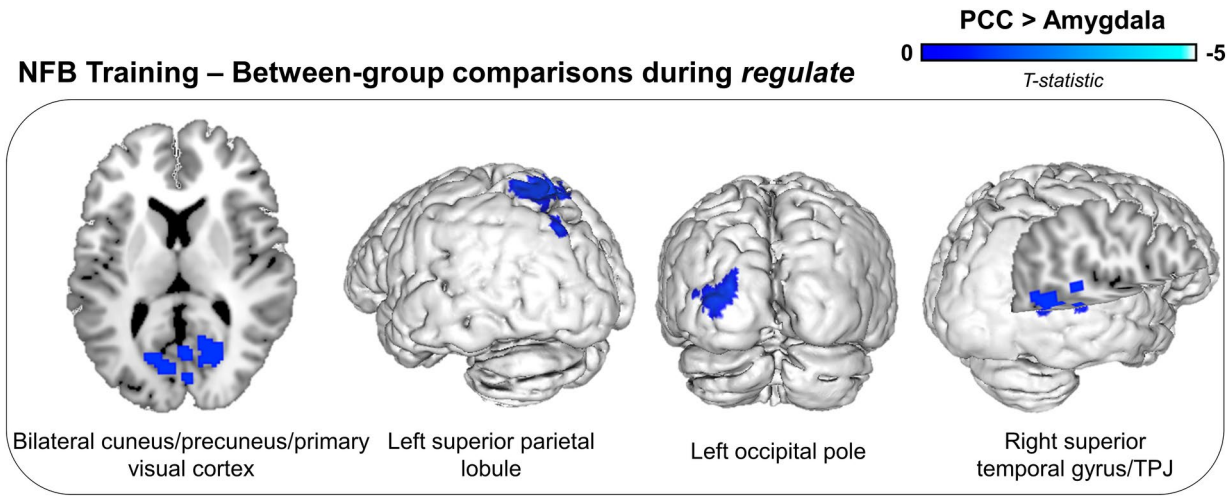


FIGURE 3
Between-group differences in neural activity during NFB downregulation of the target region (PCC or amygdala). Displayed brain regions show concomitant decreases in neural activity for the PCC as compared to the amygdala group during downregulation across NFB training runs. Results are corrected for multiple comparisons using a cluster-level false discovery rate (FDR) significance threshold of $p < 0.025$, $k = 10$. TPJ, temporoparietal junction.

we conducted a direct comparison of whole-brain activation patterns and changes in symptoms between two groups of PTSD participants who were trained to downregulate activity in clinically relevant target regions – either the amygdala or the PCC – using rt-fMRI-NFB. We observed significant differences in whole-brain activity during the *regulate* condition depending on the neurofeedback target region. For the PCC group as compared to the amygdala group, there were whole-brain decreases in activity within the bilateral cuneus/precuneus/primary visual cortex, the left superior parietal lobule, the left occipital pole, and the right superior temporal gyrus/TPJ (Figure 3). In contrast, for the amygdala group as compared to the PCC group, there were no unique (i.e., over and above that of the PCC group) decreases in neural activity. Interestingly, we observed clear differences in clinical outcomes between participants in the two groups with acute decreases in state PTSD symptoms observed for the PCC group only. Indeed, downregulation of amygdala activity via rt-fMRI-NFB did not lead to improvements in state PTSD symptoms among participants, whereas downregulation of PCC activity was associated with reduced reliving and distress symptoms (Nicholson et al., 2018, 2021; Lieberman et al., 2023). As previously reported, participants were able to successfully downregulate activity within both of these target brain regions (Nicholson et al., 2016a, 2021). Importantly, in the present analysis, we found that there was no significant difference between the two participant groups in terms of their neural response to trauma-related words within the target region or their ability to downregulate activity within their respective target brain regions, thus serving as a critical control for the between-group neural activation results. Moreover, participants in both groups reported using similar regulatory strategies including mindfulness-based techniques, positive self-talk, and the use of visual imagery.

## 4.2 Differential neural activation

Significant differences in neural activity based on the target region for rt-fMRI-NFB (during the *regulate* condition) were observed in the present analysis. For the PCC group as compared to the amygdala group, downregulation of the target region was concomitantly associated with whole-brain decreases in neural activity, with a particular focus toward posterior areas. Specifically, participants in the PCC as compared to the amygdala group, showed simultaneous downregulation within the bilateral cuneus/precuneus/primary visual cortex, the left superior parietal lobule, the left occipital pole, and the right superior temporal gyrus/TPJ (Figure 3), all of which have been linked to PTSD psychopathology (Lanius et al., 2002; Hopper et al., 2007b; Yin et al., 2011; Nilsen et al., 2016; Clancy et al., 2017; Kunimatsu et al., 2020; Sheynin et al., 2020). The precuneus is closely linked - both anatomically and functionally - with the PCC and comprises a critical node within the posterior DMN (Cavanna and Trimble, 2006; Fransson and Marrelec, 2008; Raichle, 2015), in which PTSD-associated alterations have been shown to be related to traumatic/negative autobiographical memories, dysregulated self-referential processing and altered social cognition (Bluhm et al., 2009; Daniels et al., 2010; Lanius, 2015; Tursich et al., 2015; Akiki et al., 2017; Fenster et al., 2018; Hinojosa et al., 2019; Lanius et al., 2020). Indeed, hyperactivity within the precuneus specifically has been associated with the presentation of trauma-related stimuli among individuals with PTSD (Ramage et al., 2013; Sartory et al., 2013; Thome et al., 2020) and negatively correlated with symptom improvements following treatment (Ke et al., 2016). The cuneus, primary visual cortex and occipital pole all lie within the occipital lobe and are necessary for processing visual information and contribute to the formation and perception of visual imagery (Le Bihan et al., 1993; Klein et al., 2000; Thiebaut de Schotten et al., 2014; Palejwala et al., 2021). In the context of PTSD, visual cortex hyperactivity has been shown to be positively correlated with symptom severity (Zhu et al., 2014, 2015; Neumeister et al., 2017; Suo et al., 2020). Indeed, hyperactivity (Rauch, 1996; Hendler et al., 2003; Todd et al., 2015; Neumeister et al., 2017) and elevated connectivity (Neumeister et al., 2017; Rabellino et al., 2018b; Suo et al., 2020) within the visual cortex during trauma-related cue exposure may specifically correspond to

TABLE 4 Neurofeedback training – within-group comparisons.

| | | | | | MNI coordinate | | | | | |
|---|---|---|---|---|---|---|---|---|---|---|
| NFB target | Condition | Brain region | H | *k* | *x* | *y* | *z* | *T*-Stat. | *Z*-Score | *p*-FDR |
| PCC | Regulate > Rest | Superior parietal lobule | Right | 994 | 32 | −78 | 14 | 7.18 | 6.66 | <0.001 |
| | | Occipital fusiform gyrus/primary visual cortex | Left | 239 | −14 | −90 | −10 | 5.84 | 5.54 | 0.001 |
| | | Cerebellum lobule VI | Left | 142 | −30 | −62 | −22 | 5.82 | 5.53 | 0.013 |
| Amygdala | Regulate > Rest | Occipital gyrus | Right | 4,554 | 18 | −88 | −2 | 7.87 | 7.21 | <0.001 |
| | | Occipital gyrus | Left | 4,942 | −16 | −92 | −8 | 7.6 | 6.99 | <0.001 |
| | | Cerebellum lobule VIIb | Left | 102 | −22 | −72 | −48 | 5.76 | 5.47 | 0.018 |
| | | Anterior insula | Right | 449 | 36 | 28 | −8 | 5.31 | 5.08 | <0.001 |
| | | Inferior frontal gyrus | Left | 261 | −48 | 46 | 0 | 5.14 | 4.93 | <0.001 |
| | | Precentral gyrus | Right | 295 | 36 | −4 | 44 | 4.77 | 4.6 | <0.001 |
| | | Cerebellum lobule VIIb | Right | 157 | 32 | −66 | −48 | 4.76 | 4.59 | 0.005 |
| | | vlPFC/Inferior frontal gyrus | Left | 117 | −54 | 14 | 8 | 4.75 | 4.58 | 0.014 |
| | | Supplementary motor cortex | Bilateral | 108 | 4 | 2 | 64 | 4.71 | 4.55 | 0.016 |
| PCC | Regulate < Rest | Cuneus/precuneus/primary visual cortex/PCC | Bilateral | 24,962 | 12 | −64 | 14 | 10.89 | >8 | <0.001 |
| | | dmPFC/ACC | Bilateral | 3,725 | 24 | 28 | 40 | 6.6 | 6.18 | <0.001 |
| | | dlPFC | Left | 693 | −22 | 26 | 42 | 6.32 | 5.95 | <0.001 |
| | | Caudate/nucleus accumbens | Bilateral | 147 | −8 | 6 | −4 | 4.71 | 4.55 | 0.01 |
| | | Hippocampus/parahippocampal gyrus/amygdala | Right | 195 | 28 | −18 | −16 | 4.54 | 4.39 | 0.003 |
| | | Angular gyrus | Left | 126 | −38 | −78 | 38 | 4.47 | 4.33 | 0.016 |
| | | Angular gyrus | Right | 291 | 42 | −70 | 36 | 4.12 | 4 | <0.001 |
| Amygdala | Regulate < Rest | *ns* | | | | | | | | |

Results of the follow-up within-group comparisons between *regulate* and rest during the NFB training runs evaluated at the FDR-cluster corrected threshold for multiple comparisons ($p < 0.025$, $k = 10$). The NFB target, condition, brain region, hemisphere of the brain region (H), cluster size (*k*), MNI coordinates (*x*,*y*,*z*), *T*-statistic (*T*-Stat.), *Z*-Score, and significance (*p*-FDR) of each significant cluster are included as columns. *ns*, not significant; PCC, posterior cingulate cortex; vlPFC, ventrolateral prefrontal cortex; dmPFC, dorsomedial prefrontal cortex; ACC, anterior cingulate cortex; dlPFC, dorsolateral prefrontal cortex.

the visual component of PTSD reliving and reexperiencing symptoms. Interestingly, decreased neural activity was also observed within brain regions that are closely linked to PTSD-associated alterations in other sensory domains and cognitive processing.

In the present neural activation analysis, decreased neural activity was also observed in the posterior region of the right superior temporal gyrus/TPJ, for the PCC as compared to the amygdala group. The temporal gyrus displays increased activation in response to trauma-related stimuli and is positively correlated to PTSD symptoms of avoidance and dissociation (Lanius et al., 2002; Hopper et al., 2007b; Nilsen et al., 2016). The TPJ is involved in multisensory (i.e., visual, vestibular, and somatosensory) integration, bodily self-consciousness, and embodiment (Arzy et al., 2006; Blanke, 2012; Igelström et al., 2015), processes whose impairment may underlie PTSD symptoms related to dissociation, emotion constriction/detachment, and altered interoception/exteroception (Hopper et al., 2007b; Lanius et al., 2012; Lanius, 2015; Harricharan et al., 2016, 2021; Rabellino et al., 2020; Kearney and Lanius, 2022). The superior temporal gyrus/TPJ are also involved in reperesenting one's peripersonal space (i.e., the area surrounding the body where one can reach or be reached by external entities, including objects or other individuals) (Bernasconi et al., 2018; Rabellino et al., 2020). It has been suggested that in PTSD one's peripersonal space is likely to be larger in size (for defensive purposes) and more rigid (less able to modify the body schema in response to shifting multisensory inputs) (Rabellino et al., 2020). Interestingly, neuroimaging data suggest the existence of a specific neural network involving the PCC, TPJ, and intraparietal sulcus, which together generate one's sense of self-location, a fundamental aspect of bodily self-consciousness (Park and Blanke, 2019). Hence, simultaneous downregulation of TPJ and PCC activity during trauma provocation may suggest a recalibration of the neural system that enables proper bodily self-consciousness functionality and multisensory integration, and thereby may reduce PTSD symptoms.

The left superior parietal lobule, which also showed decreased activity in the present neural activation analysis in the PCC as compared to the amygdala group, is pivotal in several sensory and cognitive processes, including somatosensory and visuomotor integration (Culham and Valyear, 2006; Iacoboni, 2006), motor learning (Weiss et al., 2003; Wenderoth et al., 2004) and exerting top-down attentional control (Behrmann et al., 2004). As a multimodal sensory integration region, the superior parietal lobule also helps to construct an awareness of one's internal state, body

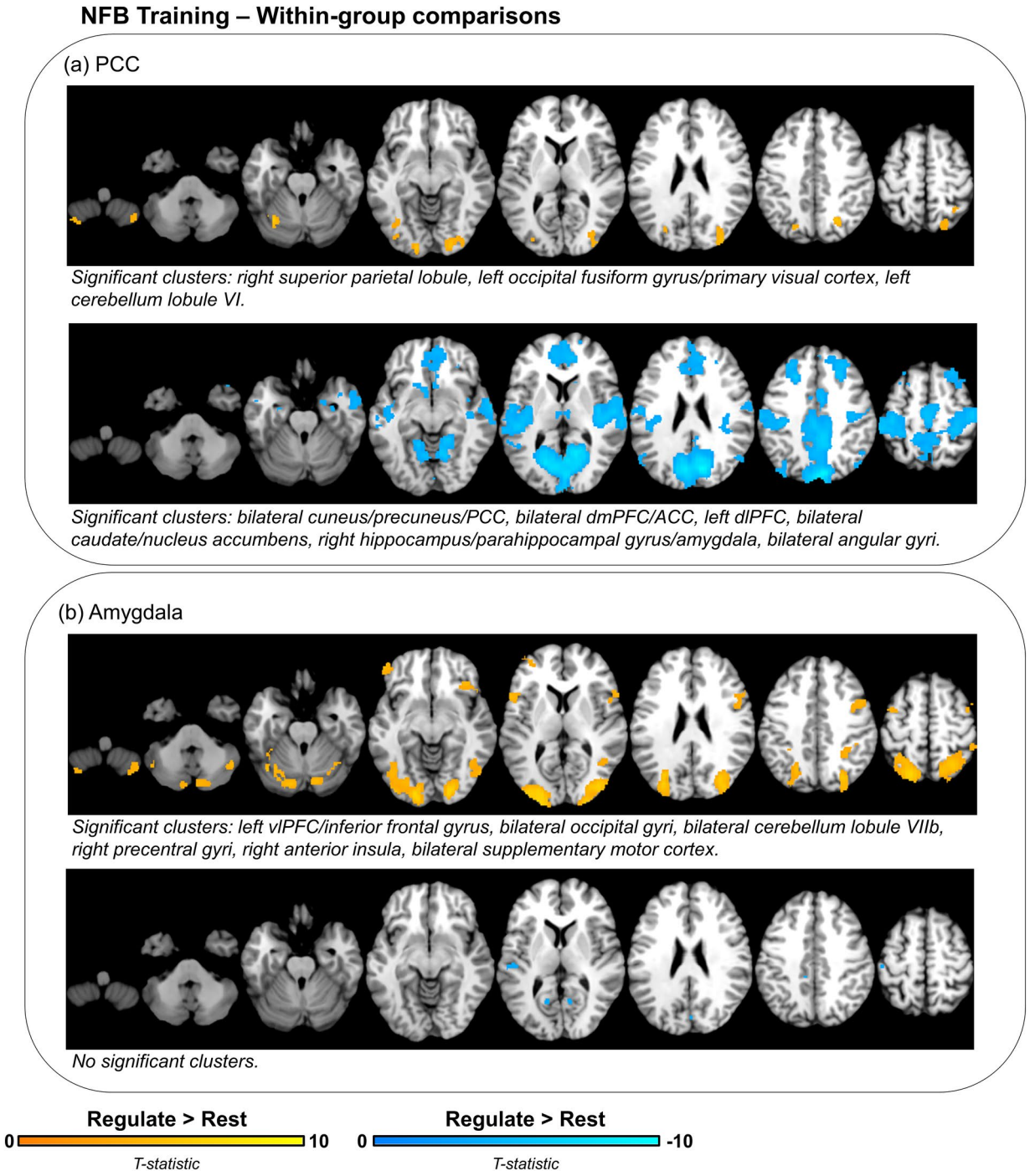


FIGURE 4
Within-group differences in neural activity during NFB downregulation of target region (PCC or amygdala) as compared to rest. Displayed brain regions show concomitant increases (yellow) or decreases (blue) in neural activity for the **(A)** PCC and **(B)** amygdala groups during *regulate* as compared to rest. Brain images are thresholded with an initial cluster defining threshold at $p < 0.001$, $k = 10$. Significant clusters are identified using a cluster-level false discovery rate (FDR) significance threshold of $p < 0.025$, $k = 10$. PCC, posterior cingulate cortex; vlPFC, ventrolateral prefrontal cortex; dmPFC, dorsomedial prefrontal cortex; ACC, anterior cingulate cortex; dlPFC, dorsolateral prefrontal cortex.

schema, and relation to external space (Pearson, 2009). In this regard, the superior parietal lobule shares functional overlap with the temporal gyrus/TPJ in contributing to body part localization (Felician et al., 2004), bodily self-consciousness (Tsakiris et al., 2007), and representing one's peripersonal space (Lloyd et al., 2006; Gallivan et al., 2011), processes which are often altered in PTSD (Rabellino et al., 2016, 2020; Rabellino et al., 2018a). During a memory retrieval paradigm, participants with PTSD showed hyperconnectivity between the posterior DMN and several sensorimotor network hubs (Kearney et al., 2023), including the left superior parietal lobule. This may reflect the integration of trauma-related sensorimotor imprints with autobiographical memory,

TABLE 5 Reliving and distress symptoms during NFB.

| | NFB training: Run 1 | | NFB training: Run 2 | | NFB training: Run 3 | | NFB transfer: Run 4 | | Run 1 vs Run 3 | | | Run 1 vs Run 4 | | |
|---|---|---|---|---|---|---|---|---|---|---|---|---|---|---|
| NFB Target | Mean | SD | Mean | SD | Mean | SD | Mean | SD | *Z*-Score | *p* | Effect Size (*r*) | *Z*-Score | *p* | Effect Size (*r*) |
| *Reliving* | | | | | | | | | | | | | | |
| PCC | 2.71 | 1.86 | 2.29 | 1.86 | 1.86 | 1.83 | 1.86 | 1.79 | −2.401 | 0.016* | −0.454* | −1.981 | 0.050 | −0.374 |
| Amygdala | 2.36 | 1.55 | 1.86 | 1.96 | 1.57 | 1.65 | 1.57 | 1.95 | −1.930 | 0.054 | −0.364 | −1.826 | 0.068 | −0.345 |
| *Distress* | | | | | | | | | | | | | | |
| PCC | 2.93 | 1.21 | 2.79 | 1.72 | 2.07 | 1.44 | 2.07 | 1.54 | −2.588 | 0.010* | −0.489* | −2.489 | 0.013* | −0.470* |
| Amygdala | 2.50 | 2.03 | 2.57 | 1.95 | 2.36 | 1.55 | 1.86 | 1.83 | −0.439 | 0.660 | −0.083 | −1.224 | 0.221 | −0.231 |

The left side of the table shows the mean and SD results for reliving and distress symptoms (as measured by RSDI) for the PCC and amygdala groups after each of the neurofeedback training runs and transfer run (i.e., Run 4). The right side of the table shows results of the a priori comparisons between reliving and distress symptoms for Run 1 as compared to Runs 3 and 4 using non-parametric tests for related samples (Wilcoxon signed-ranks test). The *Z*-Score, significance (*p*) and effect size (r) of each comparison are included as columns. Asterisks indicate significant results. PCC, posterior cingulate cortex; NFB, neurofeedback; SD, standard deviation.

thereby contributing to the vividness of reexperiencing and/or reliving of symptoms (van der Kolk and Fisler, 1995; Brewin et al., 1996; Kearney and Lanius, 2022). The superior parietal lobule is also a critical node within the dorsal attention network and is thought to play a key role in orienting visuospatial attention (Corbetta et al., 1993, 1995; Corbetta and Shulman, 2002; Lanssens et al., 2020). Altered connectivity of the dorsal attention network as a whole has been found among individuals with PTSD (Russman Block et al., 2017; Evans et al., 2022). Disrupted attentional processes, such as response inhibition and attention regulation, may represent a critical mechanism underlying PTSD symptom development and relate to PTSD symptom severity due to difficulties in disengaging from threat/defence processing and reorienting attention to task-relevant stimuli (Pineles et al., 2007, 2009; Aupperle et al., 2012; Russman Block et al., 2017; Evans et al., 2022). Taken together, decreased activity within the posterior DMN (i.e., precuneus), visual cortex (i.e., cuneus/primary visual cortex and occipital lobe), temporal gyrus/TPJ, and superior parietal lobule, may indicate that individuals with PTSD regulating activity within the PCC, as compared to the amygdala, show greater control over trauma-related autobiographical memory, emotion, and multisensory processing. Indeed, these findings may help make sense of the fact that only the PCC group showed improvements in state PTSD symptoms (i.e., reliving and distress) with rt-fMRI-NFB training during the trauma provocation paradigm (Nicholson et al., 2016a, 2018).

Conversely, for the amygdala group as compared to the PCC group, neurofeedback training was not associated with any significant unique (i.e., over and above that of the PCC group) decreases in neural activity during the *regulate* condition. This suggests that downregulating the amygdala, as compared to the PCC, does not result in unique regulatory decreases in neural activity elsewhere in the brain. Indeed, this finding raises a critical point for consideration. In conducting comparisons of neural activity on the basis of the neurofeedback target region, any changes in neural activity that were common to both groups would not be observable. As such, we conducted supplemental comparisons of neural activity during the regulate condition as compared to rest for each group separately. For *regulate* as compared to rest, there were significant whole-brain increases in neural activity – including significant clusters in the left vlPFC/inferior frontal gyrus, bilateral occipital gyri, bilateral cerebellum lobule VIIb, right precentral gyrus, right anterior insula, and bilateral supplementary motor cortex – for the amygdala group (Figure 4B – top panel). However, there were no significant decreases in neural activity (i.e., simultaneous downregulation) for the amygdala group during *regulate* as compared to rest (Figure 4B – bottom panel). Conversely, for the PCC group, during *regulate* as compared to rest, there were widespread whole-brain decreases in neural activity – including significant clusters in the bilateral cuneus/precuneus/primary visual cortex/PCC, left dlPFC, bilateral caudate/nucleus accumbens, right hippocampus/parahippocampal gyrus/amygdala, bilateral dmPFC/ACC, and bilateral angular gyri (Figure 4A – bottom panel). Significant increases in neural activity for the PCC group during *regulate* as compared to rest were restricted to posterior brain regions, including the right superior parietal lobule, left occipital gyrus/primary visual cortex, and the left cerebellum lobule VI (Figure 4A – top panel). Interestingly, these results indicate unique neural mechanisms – largely either increased or decreased concomitant whole-brain neural activity – that are associated with downregulation of the amygdala or PCC, respectively. Taken together, downregulating the PCC using rt-fMRI-NFB appears to be more strongly associated with whole-brain decreases in neural activity, whereas downregulating the amygdala is associated with persistent activation in several brain regions.

Accumulating evidence from several previous independent analyses by our group, in which we examined each neurofeedback target region separately, supports the notion that distinct neural mechanisms are associated with rt-fMRI-NFB downregulation of the amygdala and PCC (Nicholson et al., 2016a, 2018, 2021; Lieberman et al., 2023). More specifically, we previously found that during *regulate* as compared to *view* conditions, amygdala downregulation was associated with concomitant increased neural activity within the PFC (i.e., dlPFC, vlPFC) and increased bidirectional amygdala-PFC (i.e., dlPFC, dmPFC) connectivity (Nicholson et al., 2016a). Moreover, amygdala downregulation was associated with dynamic changes in intrinsic connectivity networks, where there was increased recruitment of the left CEN

TABLE 6 Between-group comparisons of PTSD symptoms during NFB.

| | | PCC vs Amygdala | | | |
|---|---|---|---|---|---|
| Run | Group | Mean rank | *Z*-Score | *p* | Effect size (*r*) |
| *Reliving* | | | | | |
| Run 1 | PCC | 15.39 | −0.588 | 0.556 | −0.111 |
| | Amygdala | 13.61 | | | |
| Run 2 | PCC | 15.54 | −0.683 | 0.495 | −0.129 |
| | Amygdala | 13.46 | | | |
| Run 3 | PCC | 14.96 | −0.310 | 0.757 | −0.059 |
| | Amygdala | 14.04 | | | |
| Run 4 (transfer) | PCC | 15.39 | −0.602 | 0.547 | −0.114 |
| | Amygdala | 13.61 | | | |
| *Distress* | | | | | |
| Run 1 | PCC | 15.61 | −0.723 | 0.470 | −0.137 |
| | Amygdala | 13.39 | | | |
| Run 2 | PCC | 14.75 | −0.165 | 0.869 | −0.031 |
| | Amygdala | 14.25 | | | |
| Run 3 | PCC | 13.75 | −0.498 | 0.619 | −0.094 |
| | Amygdala | 15.25 | | | |
| Run 4 (transfer) | PCC | 15.29 | −0.515 | 0.606 | −0.097 |
| | Amygdala | 13.71 | | | |
| *Physical reactions* | | | | | |
| Run 1 | PCC | 13.50 | −0.654 | 0.513 | −0.124 |
| | Amygdala | 15.50 | | | |
| Run 2 | PCC | 14.61 | −0.070 | 0.944 | −0.013 |
| | Amygdala | 14.39 | | | |
| Run 3 | PCC | 14.71 | −0.140 | 0.888 | −0.026 |
| | Amygdala | 14.29 | | | |
| Run 4 (transfer) | PCC | 14.86 | −0.235 | 0.814 | −0.044 |
| | Amygdala | 14.14 | | | |
| *Emotional numbing* | | | | | |
| Run 1 | PCC | 15.36 | −0.568 | 0.570 | −0.107 |
| | Amygdala | 13.64 | | | |
| Run 2 | PCC | 14.89 | −0.259 | 0.796 | −0.049 |
| | Amygdala | 14.11 | | | |
| Run 3 | PCC | 14.46 | −0.023 | 0.981 | −0.004 |
| | Amygdala | 14.54 | | | |
| Run 4 (transfer) | PCC | 15.14 | −0.423 | 0.672 | −0.080 |
| | Amygdala | 13.86 | | | |
| *Dissociation* | | | | | |
| Run 1 | PCC | 14.29 | −0.142 | 0.887 | −0.027 |
| | Amygdala | 14.71 | | | |
| Run 2 | PCC | 14.25 | −0.170 | 0.865 | −0.032 |
| | Amygdala | 14.75 | | | |
| Run 3 | PCC | 13.96 | −0.360 | 0.719 | −0.068 |
| | Amygdala | 15.04 | | | |
| Run 4 (transfer) | PCC | 15.00 | −0.335 | 0.737 | −0.063 |
| | Amygdala | 14.00 | | | |

Results of the between-group comparisons of PTSD symptoms (as measured by RSDI) after each run using Mann–Whitney U Tests. The run, group, mean rank, *Z*-Score, significance (*p*), and effect size (*r*) are included as columns. NFB, neurofeedback.

(including the bilateral dlPFC) (Nicholson et al., 2018). As such, the involvement of prefrontal cortex emotion regulation regions appears to be of primary importance for amygdala downregulation using rt-fMRI-NFB. On the other hand, we previously showed in a separate analysis that during *regulate* as compared to *view* conditions, PCC downregulation was associated with simultaneous decreases in neural activity within several brain regions involved in PTSD psychopathology – i.e., the dmPFC, postcentral gyrus, amygdala/hippocampus, cingulate cortex, and temporal pole/gyri (Nicholson et al., 2021) – as well as increased PCC connectivity with the dmPFC, vmPFC, posterior insula, and amygdala (Lieberman et al., 2023). Thus, in the context of PTSD, the neural mechanisms associated with PCC downregulation appear to primarily involve the reintegration of functionally segregated posterior and anterior DMN structures and may also result in the concomitant regulation of brain regions involved in emotion generation/processing (i.e., amygdala, mid-cingulate) and embodiment (i.e., insula). Taken together, despite both being of significant clinical relevance, downregulating the PCC and amygdala may recruit distinct neural mechanisms associated with emotion regulation. Indeed, while the involvement of prefrontal cortex brain regions in emotion regulation is well established (Rauch et al., 2006; Lanius et al., 2010; Shin and Liberzon, 2010; Aupperle et al., 2012; Pitman et al., 2012; Admon et al., 2013; Ronzoni et al., 2016), emerging neurobiological evidence is beginning to identify the critical role of the DMN and PCC in facilitating emotion regulation as well (Lanius et al., 2010; Zhou et al., 2012; Garrison et al., 2013a,b; Fresco et al., 2017; Garrett et al., 2019; Sheynin et al., 2020; Messina et al., 2021). For example, PCC regulation has been associated with emotional acceptance (Messina et al., 2021), mindfulness-based meditation (Garrison et al., 2013a,b), and reduced PTSD symptoms following trauma-focused cognitive behavioral therapy (Garrett et al., 2019). Together with the current findings, this suggests that the PCC/DMN may warrant inclusion within neural mechanistic models of emotion regulation in PTSD. In addition to its role in emotion regulation, further consideration of the PCC through the lens of network-level neuroscience, may help in understanding why it may serve as a particularly effective neurofeedback target region.

## 4.3 Network-level neuroscience

Within the vast network of neuronal connections that comprise the human brain (i.e., the connectome), certain network elements possess a relatively greater number of connections thus marking them as putative network hubs (Bassett and Bullmore, 2006; van den Heuvel and Sporns, 2013; Bassett and Sporns, 2017; Oldham and Fornito, 2019). Network hubs are critical in that they facilitate the integration between functionally specialized and anatomically distributed brain regions to enable higher-level cognitive and mental processing (Bassett and Bullmore, 2006; van den Heuvel and Sporns, 2013; Bassett and Sporns, 2017; Oldham and Fornito, 2019). While both the amygdala and PCC constitute critical hubs within each of their networks – the SN and DMN, respectively (Zuo et al., 2010; Menon, 2011, 2020) – research indicates that the PCC may be a particularly effective neurofeedback target region, from a network neuroscience-level perspective. Studies using both anatomical (Hagmann et al., 2008) and functional connectivity (Buckner et al., 2009; Tomasi and Volkow, 2011) measures have identified regions in the DMN, including the PCC specifically, as having the highest global brain connectivity values. Additionally, analysis of structural brain networks revealed that hubs of regional and global controllability – or the ability to influence subsequent neurophysiological dynamics in other regions – are preferentially located in the DMN (Gu et al., 2015). The PCC in particular plays a heterogeneous role in cortical dynamics by communicating with multiple large-scale brain networks (Leech et al., 2012; Leech and Smallwood, 2019). Such highly distributed patterns of cortical dynamics may underlie the diverse functionality of the PCC, which can be broadly categorized into task-negative (e.g., deactivation during complex external tasks), representational (e.g., self-related and social cognition), and dynamic (e.g., performance monitoring and exploration, regulation of neural dynamics) roles (Leech and Smallwood, 2019). Owing to its highly distributed functional connectivity, and the fact that it is a hub for regional and global controllability, the PCC is well positioned to regulate homeostatic balance between large-scale brain networks (Leech and Smallwood, 2019). In alignment with this proposed functionality of the PCC, EEG-NFB targeting regulation of alpha oscillations – which are correlated with PCC activation (Mantini et al., 2007; Jann et al., 2009; Clancy et al., 2020) – may promote the homeostatic normalization (i.e., self-tuning neuroplasticity) of pathological large-scale brain dynamics (Ros et al., 2014, 2017; Nicholson et al., 2023). Indeed, among individuals with PTSD, alpha-rhythm EEG-NFB was shown to recalibrate altered spontaneous long-range temporal correlations, where the degree of inter-individual recalibration was positively correlated with reduced hyperarousal symptoms (Ros et al., 2017). Furthermore, in a 20-week randomized controlled trial with PTSD participants, alpha-rhythm EEG-NFB resulted in significantly reduced PTSD severity scores and promoted neuroplastic resynchronization (i.e., homeostatic rebound) of alpha power within the anterior DMN, a region which showed decreased alpha power at baseline (Nicholson et al., 2023). Taken together, the PCC may be uniquely situated as a neurofeedback target region that can generate wide-reaching homeostatic regulation of pathological brain dynamics. As previously discussed, emerging research has identified the PCC as critically implicated in PTSD, where increased PCC activation is observed during the reliving and reexperiencing of trauma-related memories (Ramage et al., 2013; Frewen et al., 2017; Awasthi et al., 2020; Thome et al., 2020) and decreased PCC activation is associated with longitudinal improvements in PTSD symptoms (Ke et al., 2016; Garrett et al., 2019). In conjunction with the unique neural mechanisms and symptom decreases that were observed in the current study for the PCC group, these network-level perspectives on PCC functionality suggest that it may be a particularly effective neurofeedback target region in the context of PTSD.

## 4.4 Limitations and future directions

Limitations of the present analysis include a small sample size which may have limited our ability to detect significant between-group differences in state changes in PTSD symptoms and may also

impact the generalizability of the neural activation findings. Additionally, data for the two participant groups were collected sequentially which precluded randomized group assignment. Although broadly similar themes emerged for both groups regarding the use of regulatory strategies (i.e., mindfulness-based techniques, positive self-talk, visual imagery), future research is needed to comprehensively evaluate strategy use and its implications on training success. In order to further investigate the potential therapeutic effect of neurofeedback in PTSD, exploration of complementary neurofeedback modalities with optimized temporal resolution is warranted (i.e., EEG, MEG). Indeed, in a 20-week randomized controlled trial by our group, EEG-NFB targeting alpha oscillations (related to PCC activity) was shown to be associated with significant reductions in PTSD symptom severity (Nicholson et al., 2020b, 2023). Further research is needed to assess how the temporal and spatial resolutions of different neurofeedback modalities (i.e., fMRI, EEG, MEG) might impact regulation success and clinical outcomes. Lastly, it is important to note that the present study was not preregistered as data collection began before preregistration was a standard practice in the field. To address the limitations of the current study and further elucidate the effect of neurofeedback target selection in PTSD, our group has preregistered and is currently conducting a multisession, double-blind, randomized controlled trial comparing PCC and amygdala neurofeedback targets versus a sham-control arm (NCT05456958). As part of this study, we are also conducting semi-structured interviews with participants after each neurofeedback session in order to obtain qualitative data on their use of regulatory strategies. Including a sham control arm in the study will provide further insight into the neurophysiological specificity of both neurofeedback target regions. Examining the impact of multiple rt-fMRI-NFB sessions on brain activation and clinical outcomes will reveal the potential cumulative effects of rt-fMRI-NFB and inform the development of more effective treatment strategies.

## 5 Conclusion

In summary, we compared neural activation between two groups of PTSD participants who were trained to downregulate activity within one of two clinically relevant target regions – the amygdala or PCC – using rt-fMRI-NFB. Although both participant groups were able to downregulate activity within their respective target brain regions to a similar extent, we observed significant differences between the groups in terms of neural activity and clinical outcomes during neurofeedback-mediated regulation. Indeed, the PCC group as compared to the amygdala group showed widespread whole-brain decreases in activity within the bilateral cuneus/precuneus/primary visual cortex, the left superior parietal lobule, the left occipital pole, and the right superior temporal gyrus/TPJ. Conversely, for the amygdala group as compared to the PCC group, there were no significant unique (i.e., over and above that of the PCC group) decreases in neural activity. These differential neural results may help to explain the finding that only the PCC group showed improvements in state PTSD symptoms (i.e., reliving and distress) during neurofeedback training. Although altered activation within both the PCC and amygdala are widely reported among PTSD populations, emerging evidence from studies employing a network-level neuroscience perspective suggests that the PCC – due to its heterogeneous functionality, highly connected nature, and involvement in regulating both regional and global neural dynamics – may be a highly effective target for downregulation using rt-fMRI-NFB in PTSD.

## Data availability statement

The data that support the findings of this study are available from the corresponding author upon reasonable request. Requests to access these datasets should be directed to AN, andrew.nicholson@theroyal.ca.

## Ethics statement

The studies involving humans were approved by the Western University Health Sciences Research Ethics Board (HSREB) (project ID: 103933) and the Lawson Health Research Institute (project ID: 1975). The studies were conducted in accordance with the local legislation and institutional requirements. The participants provided their written informed consent to participate in this study.

## Author contributions

RL and AN conceived and designed the original research study. DR, MD, PF, DS, FS, JT, RN, RJ, TR, RL, and AN were involved in data collection and execution of the research study. JL and AN conceived of the research questions, conducted the statistical analyses and interpretation of the data, and drafted and revised the manuscript. BF and NH-K provided valuable input on statistical analyses and interpreting the results. All authors contributed to the editing and revision of the final manuscript for submission.

## Funding

This research was funded by the Canadian Institute for Veteran Health Research (CIMVHR). AN has received funding support from the European Union's Horizon 2020 research and innovation program under the Marie Sklodowska-Curie Individual Fellowship (grant agreement no. 897709), the Banting Research Foundation (award no. 2021-1424), and the Canadian Institutes of Health Research (CIHR) (project grant no. 483268). JL has received funding support from the Canadian Institutes of Health Research (CIHR) (funding reference no. 187470).

## Acknowledgments

We thank Suzy Southwell and Stephanie Nevill for their significant contributions with data collection and curation.

## Conflict of interest

The authors declare that the research was conducted in the absence of any commercial or financial relationships that could be construed as a potential conflict of interest.

## Publisher's note

All claims expressed in this article are solely those of the authors and do not necessarily represent those of their affiliated organizations, or those of the publisher, the editors and the reviewers. Any product that may be evaluated in this article, or claim that may be made by its manufacturer, is not guaranteed or endorsed by the publisher.

## Supplementary material

The Supplementary material for this article can be found online at: https://www.frontiersin.org/articles/10.3389/fnins.2023.1229729/full#supplementary-material

## References


Admon, R., Milad, M. R., and Hendler, T. (2013). A causal model of post-traumatic stress disorder: disentangling predisposed from acquired neural abnormalities. *Trends Cogn. Sci.* 17, 337–347. doi: 10.1016/j.tics.2013.05.005

Aghajani, M., Veer, I. M., van Hoof, M., Rombouts, S. A. R. B., van der Wee, N. J., and Vermeiren, R. R. J. M. (2016). Abnormal functional architecture of amygdala-centered networks in adolescent posttraumatic stress disorder. *Hum. Brain Mapp.* 37, 1120–1135. doi: 10.1002/hbm.23093

Akiki, T. J., Averill, C. L., and Abdallah, C. G. (2017). A network-based neurobiological model of PTSD: evidence from structural and functional neuroimaging studies. *Curr. Psychiatry Rep.* 19:81. doi: 10.1007/s11920-017-0840-4

Akiki, T. J., Averill, C. L., Wrocklage, K. M., Scott, J. C., Averill, L. A., Schweinsburg, B., et al. (2018). Default mode network abnormalities in posttraumatic stress disorder: A novel network-restricted topology approach. *NeuroImage* 176, 489–498. doi: 10.1016/j.neuroimage.2018.05.005

Arzy, S., Thut, G., Mohr, C., Michel, C. M., and Blanke, O. (2006). Neural basis of embodiment: distinct contributions of temporoparietal junction and extrastriate body area. *J. Neurosci. Off. J. Soc. Neurosci.* 26, 8074–8081. doi: 10.1523/JNEUROSCI.0745-06.2006

Aupperle, R. L., Melrose, A. J., Stein, M. B., and Paulus, M. P. (2012). Executive function and PTSD: disengaging from trauma. *Neuropharmacology* 62, 686–694. doi: 10.1016/j.neuropharm.2011.02.008

Awasthi, S., Pan, H., LeDoux, J. E., Cloitre, M., Altemus, M., McEwen, B., et al. (2020). The bed nucleus of the stria terminalis and functionally linked neurocircuitry modulate emotion processing and HPA axis dysfunction in posttraumatic stress disorder. *NeuroImage* 28:102442. doi: 10.1016/j.nicl.2020.102442

Bassett, D. S., and Bullmore, E. (2006). Small-world brain networks. *Neuroscientist* 12, 512–523. doi: 10.1177/1073858406293182

Bassett, D. S., and Sporns, O. (2017). Network neuroscience. *Nat. Neurosci.* 20, 353–364. doi: 10.1038/nn.4502

Beck, A. T., Guth, D., Steer, R. A., and Ball, R. (1997). Screening for major depression disorders in medical inpatients with the Beck depression inventory for primary care. *Behav. Res. Ther.* 35, 785–791. doi: 10.1016/S0005-7967(97)00025-9

Behrmann, M., Geng, J. J., and Shomstein, S. (2004). Parietal cortex and attention. *Curr. Opin. Neurobiol.* 14, 212–217. doi: 10.1016/j.conb.2004.03.012

Bernasconi, F., Noel, J.-P., Park, H. D., Faivre, N., Seeck, M., Spinelli, L., et al. (2018). Audio-tactile and peripersonal space processing around the trunk in human parietal and temporal cortex: an intracranial EEG study. *Cereb. Cortex* 28, 3385–3397. doi: 10.1093/cercor/bhy156

Bernstein, D. P., Stein, J. A., Newcomb, M. D., Walker, E., Pogge, D., Ahluvalia, T., et al. (2003). Development and validation of a brief screening version of the childhood trauma questionnaire. *Child Abuse Negl.* 27, 169–190. doi: 10.1016/S0145-2134(02)00541-0

Birn, R. M., Patriat, R., Phillips, M. L., Germain, A., and Herringa, R. J. (2014). Childhood maltreatment and combat post-traumatic stress differentially predict fear–related fronto-subcortical connectivity. *Depress. Anxiety* 31, 880–892. doi: 10.1002/da.22291

Blanke, O. (2012). Multisensory brain mechanisms of bodily self-consciousness. *Nat. Rev. Neurosci.* 13, 556–571. doi: 10.1038/nrn3292

Bluhm, R. L., Williamson, P. C., Osuch, E. A., Frewen, P. A., Stevens, T. K., Boksman, K., et al. (2009). Alterations in default network connectivity in posttraumatic stress disorder related to early-life trauma. *J. Psychiat. Neurosci.* 34, 187–194.

Brewer, J. A., Garrison, K. A., and Whitfield-Gabrieli, S. (2013). What about the "self" is processed in the posterior cingulate cortex? *Front. Hum. Neurosci.* 7:647. doi: 10.3389/fnhum.2013.00647

Brewin, C. R., Dalgleish, T., and Joseph, S. (1996). A dual representation theory of posttraumatic stress disorder. *Psychol. Rev.* 103, 670–686. doi: 10.1037/0033-295x.103.4.670

Briere, J., Weathers, F. W., and Runtz, M. (2005). Is dissociation a multidimensional construct? Data from the multiscale dissociation inventory. *J. Trauma. Stress.* 18, 221–231. doi: 10.1002/jts.20024

Brown, V. M., LaBar, K. S., Haswell, C. C., Gold, A. L., McCarthy, G., and Morey, R. A. (2014). Altered resting-state functional connectivity of basolateral and centromedial amygdala complexes in posttraumatic stress disorder. *Neuropsychopharmacology* 39, 351–359. doi: 10.1038/npp.2013.197

Buckner, R. L., Andrews-Hanna, J. R., and Schacter, D. L. (2008). The Brain's default network. *Ann. N. Y. Acad. Sci.* 1124, 1–38. doi: 10.1196/annals.1440.011

Buckner, R. L., Sepulcre, J., Talukdar, T., Krienen, F. M., Liu, H., Hedden, T., et al. (2009). Cortical hubs revealed by intrinsic functional connectivity: mapping, assessment of stability, and relation to Alzheimer's disease. *J. Neurosci. Off. J. Soc. Neurosci.* 29, 1860–1873. doi: 10.1523/JNEUROSCI.5062-08.2009

Cavanna, A. E., and Trimble, M. R. (2006). The precuneus: a review of its functional anatomy and behavioural correlates. *Brain* 129, 564–583. doi: 10.1093/brain/awl004

Chen, G., Cox, R. W., Glen, D. R., Rajendra, J. K., Reynolds, R. C., and Taylor, P. A. (2018). A tail of two sides: artificially doubled false positive rates in neuroimaging due to the sidedness choice with *t*-tests. *Hum. Brain Mapp.* 40, 1037–1043. doi: 10.1002/hbm.24399

Chiba, T., Kanazawa, T., Koizumi, A., Ide, K., Taschereau-Dumouchel, V., Boku, S., et al. (2019). Current status of neurofeedback for post-traumatic stress disorder: a systematic review and the possibility of decoded neurofeedback. *Front. Hum. Neurosci.* 13:233. doi: 10.3389/fnhum.2019.00233

Clancy, K. J., Andrzejewski, J. A., Simon, J., Ding, M., Schmidt, N. B., and Li, W. (2020). Posttraumatic stress disorder is associated with α dysrhythmia across the visual cortex and the default mode network. *Eneuro* 7:ENEURO.0053-20.2020. doi: 10.1523/ENEURO.0053-20.2020

Clancy, K., Ding, M., Bernat, E., Schmidt, N. B., and Li, W. (2017). Restless 'rest': intrinsic sensory hyperactivity and disinhibition in post-traumatic stress disorder. *Brain* 140, 2041–2050. doi: 10.1093/brain/awx116

Corbetta, M., Miezin, F. M., Shulman, G. L., and Petersen, S. E. (1993). A PET study of visuospatial attention. *J. Neurosci.* 13, 1202–1226. doi: 10.1523/JNEUROSCI.13-03-01202.1993

Corbetta, M., and Shulman, G. (2002). Control of goal-directed and stimulus-driven attention in the brain. *Nat. Rev. Neurosci.* 3, 201–215. doi: 10.1038/nrn755

Corbetta, M., Shulman, G. L., Miezin, F. M., and Petersen, S. E. (1995). Superior parietal cortex activation during spatial attention shifts and visual feature conjunction. *Science* 270, 802–805. doi: 10.1126/science.270.5237.802

Culham, J. C., and Valyear, K. F. (2006). Human parietal cortex in action. *Curr. Opin. Neurobiol.* 16, 205–212. doi: 10.1016/j.conb.2006.03.005

Daniels, J. K., McFarlane, A. C., Bluhm, R. L., Moores, K. A., Clark, C. R., Shaw, M. E., et al. (2010). Switching between executive and default mode networks in posttraumatic stress disorder: alterations in functional connectivity. *J. Psychiat. Neurosci.* 35, 258–266. doi: 10.1503/jpn.090175

Eklund, A., Nichols, T. E., and Knutsson, H. (2016). Cluster failure: why fMRI inferences for spatial extent have inflated false-positive rates. *Proc. Natl. Acad. Sci.* 113, 7900–7905. doi: 10.1073/pnas.1602413113

Etkin, A., Egner, T., and Kalisch, R. (2011). Emotional processing in anterior cingulate and medial prefrontal cortex. *Trends Cogn. Sci.* 15, 85–93. doi: 10.1016/j.tics.2010.11.004

Evans, T. C., Alonso, M. R., Jagger-Rickels, A., Rothlein, D., Zuberer, A., Bernstein, J., et al. (2022). PTSD symptomatology is selectively associated with impaired sustained attention ability and dorsal attention network synchronization. *NeuroImage* 36:103146. doi: 10.1016/j.nicl.2022.103146

Felician, O., Romaiguère, P., Anton, J.-L., Nazarian, B., Roth, M., Poncet, M., et al. (2004). The role of human left superior parietal lobule in body part localization. *Ann. Neurol.* 55, 749–751. doi: 10.1002/ana.20109

Fenster, R. J., Lebois, L. A. M., Ressler, K. J., and Suh, J. (2018). Brain circuit dysfunction in post-traumatic stress disorder: from mouse to man. *Nat. Rev. Neurosci.* 19, 535–551. doi: 10.1038/s41583-018-0039-7

First, M. B. (2015). "Structured clinical interview for the DSM (SCID)" in *The encyclopedia of clinical psychology* (New York: John Wiley & Sons, Ltd.), 1–6.

Fitzgerald, J. M., DiGangi, J. A., and Phan, K. L. (2018). Functional neuroanatomy of emotion and its regulation in PTSD. *Harv. Rev. Psychiatry* 26, 116–128. doi: 10.1097/HRP.0000000000000185

Fonzo, G. A., Simmons, A. N., Thorp, S. R., Norman, S. B., Paulus, M. P., and Stein, M. B. (2010). Exaggerated and disconnected insular-amygdalar blood oxygenation level-dependent response to threat-related emotional faces in women with intimate-partner violence posttraumatic stress disorder. *Biol. Psychiatry* 68, 433–441. doi: 10.1016/j.biopsych.2010.04.028

Fransson, P., and Marrelec, G. (2008). The precuneus/posterior cingulate cortex plays a pivotal role in the default mode network: evidence from a partial correlation network analysis. *NeuroImage* 42, 1178–1184. doi: 10.1016/j.neuroimage.2008.05.059

Fresco, D. M., Roy, A. K., Adelsberg, S., Seeley, S., García-Lesy, E., Liston, C., et al. (2017). Distinct functional Connectivities predict clinical response with emotion regulation therapy. *Front. Hum. Neurosci.* 11:86. doi: 10.3389/fnhum.2017.00086

Frewen, P., Thornley, E., Rabellino, D., and Lanius, R. (2017). Neuroimaging the traumatized self: fMRI reveals altered response in cortical midline structures and occipital cortex during visual and verbal self- and other-referential processing in women with PTSD. *Eur. J. Psychotraumatol.* 8:1314164. doi: 10.1080/20008198.2017.1314164

Gallivan, J. P., McLean, A., and Culham, J. C. (2011). Neuroimaging reveals enhanced activation in a reach-selective brain area for objects located within participants' typical hand workspaces. *Neuropsychologia* 49, 3710–3721. doi: 10.1016/j.neuropsychologia.2011.09.027

Garrett, A., Cohen, J. A., Zack, S., Carrion, V., Jo, B., Blader, J., et al. (2019). Longitudinal changes in brain function associated with symptom improvement in youth with PTSD. *J. Psychiatr. Res.* 114, 161–169. doi: 10.1016/j.jpsychires.2019.04.021

Garrison, K. A., Santoyo, J. F., Davis, J. H., Thornhill, T. A., Kerr, C. E., and Brewer, J. A. (2013a). Effortless awareness: using real time neurofeedback to investigate correlates of posterior cingulate cortex activity in meditators' self-report. *Front. Hum. Neurosci.* 7:440. doi: 10.3389/fnhum.2013.00440

Garrison, K. A., Scheinost, D., Worhunsky, P. D., Elwafi, H. M., Thornhill, T. A., Thompson, E., et al. (2013b). Real-time fMRI links subjective experience with brain activity during focused attention. *NeuroImage* 81, 110–118. doi: 10.1016/j.neuroimage.2013.05.030

Gerin, M. I., Fichtenholtz, H., Roy, A., Walsh, C. J., Krystal, J. H., Southwick, S., et al. (2016). Real-time fMRI neurofeedback with war veterans with chronic PTSD: a feasibility study. *Front. Psych.* 7:111. doi: 10.3389/fpsyt.2016.00111

Gläscher, J. (2009). Visualization of group inference data in functional neuroimaging. *Neuroinformatics* 7, 73–82. doi: 10.1007/s12021-008-9042-x

Goebel, R. (2014). Dynamic ROIs. TBV users guide. Available at: http://download.brainvoyager.com/tbv/TBVUsersGuide/Neurofeedback/DynamicROIs.html

Greicius, M. D., Krasnow, B., Reiss, A. L., and Menon, V. (2003). Functional connectivity in the resting brain: a network analysis of the default mode hypothesis. *Proc. Natl. Acad. Sci.* 100, 253–258. doi: 10.1073/pnas.0135058100

Gu, S., Pasqualetti, F., Cieslak, M., Telesford, Q. K., Yu, A. B., Kahn, A. E., et al. (2015). Controllability of structural brain networks. *Nat. Commun.* 6:8414. doi: 10.1038/ncomms9414

Hagmann, P., Cammoun, L., Gigandet, X., Meuli, R., Honey, C. J., Wedeen, V. J., et al. (2008). Mapping the structural core of human cerebral cortex. *PLoS Biol.* 6:e159. doi: 10.1371/journal.pbio.0060159

Hamilton, J. P., Glover, G. H., Bagarinao, E., Chang, C., Mackey, S., Sacchet, M. D., et al. (2016). Effects of salience-network-node neurofeedback training on affective biases in major depressive disorder. *Psychiatry Res. Neuroimaging* 249, 91–96. doi: 10.1016/j.pscychresns.2016.01.016

Harricharan, S., McKinnon, M. C., and Lanius, R. A. (2021). How processing of sensory information from the internal and external worlds shape the perception and engagement with the world in the aftermath of trauma: implications for PTSD. *Front. Neurosci.* 15:625490. doi: 10.3389/fnins.2021.625490

Harricharan, S., Rabellino, D., Frewen, P. A., Densmore, M., Théberge, J., McKinnon, M. C., et al. (2016). fMRI functional connectivity of the periaqueductal gray in PTSD and its dissociative subtype. *Brain Behav.* 6:e00579. doi: 10.1002/brb3.579

Hendler, T., Rotshtein, P., Yeshurun, Y., Weizmann, T., Kahn, I., Ben-Bashat, D., et al. (2003). Sensing the invisible: differential sensitivity of visual cortex and amygdala to traumatic context. *NeuroImage* 19, 587–600. doi: 10.1016/S1053-8119(03)00141-1

Hinojosa, C. A., Kaur, N., VanElzakker, M. B., and Shin, L. M. (2019). Cingulate subregions in posttraumatic stress disorder, chronic stress, and treatment. *Handb. Clin. Neurol.* 166, 355–370. doi: 10.1016/B978-0-444-64196-0.00020-0

Hopper, J. W., Frewen, P. A., Sack, M., Lanius, R. A., and van der Kolk, B. A. (2007a). The responses to script-driven imagery scale (RSDI): assessment of state posttraumatic symptoms for psychobiological and treatment research. *J. Psychopathol. Behav. Assess.* 29, 249–268. doi: 10.1007/s10862-007-9046-0

Hopper, J. W., Frewen, P. A., van der Kolk, B. A., and Lanius, R. A. (2007b). Neural correlates of reexperiencing, avoidance, and dissociation in PTSD: symptom dimensions and emotion dysregulation in responses to script-driven trauma imagery. *J. Trauma. Stress.* 20, 713–725. doi: 10.1002/jts.20284

Iacoboni, M. (2006). Visuo-motor integration and control in the human posterior parietal cortex: evidence from TMS and fMRI. *Neuropsychologia* 44, 2691–2699. doi: 10.1016/j.neuropsychologia.2006.04.029

Igelström, K. M., Webb, T. W., and Graziano, M. S. A. (2015). Neural processes in the human Temporoparietal cortex separated by localized independent component analysis. *J. Neurosci. Off. J. Soc. Neurosci.* 35, 9432–9445. doi: 10.1523/JNEUROSCI.0551-15.2015

Jann, K., Dierks, T., Boesch, C., Kottlow, M., Strik, W., and Koenig, T. (2009). BOLD correlates of EEG alpha phase-locking and the fMRI default mode network. *NeuroImage* 45, 903–916. doi: 10.1016/j.neuroimage.2009.01.001

Jin, C., Qi, R., Yin, Y., Hu, X., Duan, L., Xu, Q., et al. (2014). Abnormalities in whole-brain functional connectivity observed in treatment-naive post-traumatic stress disorder patients following an earthquake. *Psychol. Med.* 44, 1927–1936. doi: 10.1017/S003329171300250X

Kamiya, K., and Abe, O. (2020). Imaging of posttraumatic stress disorder. *Neuroimaging Clin. N. Am.* 30, 115–123. doi: 10.1016/j.nic.2019.09.010

Ke, J., Zhang, L., Qi, R., Li, W., Hou, C., Zhong, Y., et al. (2016). A longitudinal fMRI investigation in acute post-traumatic stress disorder (PTSD). *Acta Radiol.* 57, 1387–1395. doi: 10.1177/0284185115585848

Kearney, B. E., and Lanius, R. A. (2022). The brain-body disconnect: A somatic sensory basis for trauma-related disorders. *Front. Neurosci.* 16:1015749. doi: 10.3389/fnins.2022.1015749

Kearney, B. E., Terpou, B. A., Densmore, M., Shaw, S. B., Théberge, J., Jetly, R., et al. (2023). How the body remembers: examining the default mode and sensorimotor networks during moral injury autobiographical memory retrieval in PTSD. *NeuroImage* 38:103426. doi: 10.1016/j.nicl.2023.103426

Kirlic, N., Cohen, Z. P., Tsuchiyagaito, A., Misaki, M., McDermott, T. J., Aupperle, R. L., et al. (2022). Self-regulation of the posterior cingulate cortex with real-time fMRI neurofeedback augmented mindfulness training in healthy adolescents: A nonrandomized feasibility study. *Cogn. Affect. Behav. Neurosci.* 22, 849–867. doi: 10.3758/s13415-022-00991-4

Klein, I., Paradis, A.-L., Poline, J.-B., Kosslyn, S., and Le Bihan, D. (2000). Transient activity in the human Calcarine cortex during visual-mental imagery: an event-related fMRI study. *J. Cogn. Neurosci.* 12, 15–23. doi: 10.1162/089892900564037

Koch, S. B. J., van Zuiden, M., Nawijn, L., Frijling, J. L., Veltman, D. J., and Olff, M. (2016). Aberrant resting-state brain activity in posttraumatic stress disorder: a meta-analysis and systematic review. *Depress. Anxiety* 33, 592–605. doi: 10.1002/da.22478

Kunimatsu, A., Yasaka, K., Akai, H., Kunimatsu, N., and Abe, O. (2020). MRI findings in posttraumatic stress disorder. *J. Magn. Reson. Imaging* 52, 380–396. doi: 10.1002/jmri.26929

Lanius, R. A. (2015). Trauma-related dissociation and altered states of consciousness: a call for clinical, treatment, and neuroscience research. *Eur. J. Psychotraumatol.* 6. doi: 10.3402/ejpt.v6.27905

Lanius, R. A., Brand, B., Vermetten, E., Frewen, P. A., and Spiegel, D. (2012). The dissociative subtype of posttraumatic stress disorder: rationale, clinical and neurobiological evidence, and implications. *Depress. Anxiety* 29, 701–708. doi: 10.1002/da.21889

Lanius, R. A., Frewen, P. A., Tursich, M., Jetly, R., and McKinnon, M. C. (2015). Restoring large-scale brain networks in PTSD and related disorders: A proposal for neuroscientifically-informed treatment interventions. *Eur. J. Psychotraumatol.* 6:27313. doi: 10.3402/ejpt.v6.27313

Lanius, R. A., Terpou, B. A., and McKinnon, M. C. (2020). The sense of self in the aftermath of trauma: lessons from the default mode network in posttraumatic stress disorder. *Eur. J. Psychotraumatol.* 11:1807703. doi: 10.1080/20008198.2020.1807703

Lanius, R. A., Vermetten, E., Loewenstein, R. J., Brand, B., Schmahl, C., Bremner, J. D., et al. (2010). Emotion modulation in PTSD: clinical and neurobiological evidence for a dissociative subtype. *Am. J. Psychiatr.* 167, 640–647. doi: 10.1176/appi.ajp.2009.09081168

Lanius, R. A., Williamson, P. C., Boksman, K., Densmore, M., Gupta, M., Neufeld, R. W. J., et al. (2002). Brain activation during script-driven imagery induced dissociative responses in PTSD: A functional magnetic resonance imaging investigation. *Biol. Psychiatry* 52, 305–311. doi: 10.1016/s0006-3223(02)01367-7

Lanssens, A., Pizzamiglio, G., Mantini, D., and Gillebert, C. R. (2020). Role of the dorsal attention network in distracter suppression based on features. *Cogn. Neurosci.* 11, 37–46. doi: 10.1080/17588928.2019.1683525

Le Bihan, D., Turner, R., Zeffiro, T. A., Cuénod, C. A., Jezzard, P., and Bonnerot, V. (1993). Activation of human primary visual cortex during visual recall: A magnetic resonance imaging study. *Proc. Natl. Acad. Sci.* 90, 11802–11805. doi: 10.1073/pnas.90.24.11802

Leech, R., Braga, R., and Sharp, D. J. (2012). Echoes of the brain within the posterior cingulate cortex. *J. Neurosci.* 32, 215–222. doi: 10.1523/JNEUROSCI.3689-11.2012

Leech, R., and Smallwood, J. (2019). "Chapter 5 – the posterior cingulate cortex: insights from structure and function" in *Handbook of clinical neurology*. ed. B. A. Vogt, vol. *166* (Amsterdam: Elsevier), 73–85.

Li, X., Hartwell, K. J., Borckardt, J., Prisciandaro, J. J., Saladin, M. E., Morgan, P. S., et al. (2013). Volitional reduction of anterior cingulate cortex activity produces

decreased cue craving in smoking cessation: a preliminary real-time fMRI study. *Addict. Biol.* 18, 739–748. doi: 10.1111/j.1369-1600.2012.00449.x

Lieberman, J. M., Rabellino, D., Densmore, M., Frewen, P. A., Steyrl, D., Scharnowski, F., et al. (2023). Posterior cingulate cortex targeted real-time fMRI neurofeedback recalibrates functional connectivity with the amygdala, posterior insula, and default-mode network in PTSD. *Brain Behav.* 13:e2883. doi: 10.1002/brb3.2883

Linden, D. E. J., Habes, I., Johnston, S. J., Linden, S., Tatineni, R., Subramanian, L., et al. (2012). Real-time self-regulation of emotion networks in patients with depression. *PLoS One* 7:e38115. doi: 10.1371/journal.pone.0038115

Linhartová, P., Látalová, A., Kóša, B., Kašpárek, T., Schmahl, C., and Paret, C. (2019). fMRI neurofeedback in emotion regulation: a literature review. *NeuroImage* 193, 75–92. doi: 10.1016/j.neuroimage.2019.03.011

Lloyd, D., Morrison, I., and Roberts, N. (2006). Role for human posterior parietal cortex in visual processing of aversive objects in peripersonal space. *J. Neurophysiol.* 95, 205–214. doi: 10.1152/jn.00614.2005

Mantini, D., Perrucci, M. G., Del Gratta, C., Romani, G. L., and Corbetta, M. (2007). Electrophysiological signatures of resting state networks in the human brain. *Proc. Natl. Acad. Sci. U. S. A.* 104, 13170–13175. doi: 10.1073/pnas.0700668104

Mehler, D. M. A., Sokunbi, M. O., Habes, I., Barawi, K., Subramanian, L., Range, M., et al. (2018). Targeting the affective brain—A randomized controlled trial of real-time fMRI neurofeedback in patients with depression. *Neuropsychopharmacology* 43, 2578–2585. doi: 10.1038/s41386-018-0126-5

Melara, R. D., Ruglass, L. M., Fertuck, E. A., and Hien, D. A. (2018). Regulation of threat in post-traumatic stress disorder: associations between inhibitory control and dissociative symptoms. *Biol. Psychol.* 133, 89–98. doi: 10.1016/j.biopsycho.2018.01.017

Menon, V. (2011). Large-scale brain networks and psychopathology: a unifying triple network model. *Trends Cogn. Sci.* 15, 483–506. doi: 10.1016/j.tics.2011.08.003

Menon, V. (2020). Brain networks and cognitive impairment in psychiatric disorders. *World Psychiatry* 19, 309–310. doi: 10.1002/wps.20799

Messina, I., Grecucci, A., and Viviani, R. (2021). Neurobiological models of emotion regulation: A meta-analysis of neuroimaging studies of acceptance as an emotion regulation strategy. *Soc. Cogn. Affect. Neurosci.* 16, 257–267. doi: 10.1093/scan/nsab007

Mickleborough, M. J. S., Daniels, J. K., Coupland, N. J., Kao, R., Williamson, P. C., Lanius, U. F., et al. (2011). Effects of trauma-related cues on pain processing in posttraumatic stress disorder: an fMRI investigation. *J. Psychiat. Neurosci.* 36, 6–14. doi: 10.1503/jpn.080188

Misaki, M., Mulyana, B., Zotev, V., Wurfel, B. E., Krueger, F., Feldner, M., et al. (2021). Hippocampal volume recovery with real-time functional MRI amygdala neurofeedback emotional training for posttraumatic stress disorder. *J. Affect. Disord.* 283, 229–235. doi: 10.1016/j.jad.2021.01.058

Misaki, M., Phillips, R., Zotev, V., Wong, C.-K., Wurfel, B. E., Krueger, F., et al. (2018). Real-time fMRI amygdala neurofeedback positive emotional training normalized resting-state functional connectivity in combat veterans with and without PTSD: A connectome-wide investigation. *NeuroImage* 20, 543–555. doi: 10.1016/j.nicl.2018.08.025

Misaki, M., Phillips, R., Zotev, V., Wong, C.-K., Wurfel, B. E., Krueger, F., et al. (2019). Brain activity mediators of PTSD symptom reduction during real-time fMRI amygdala neurofeedback emotional training. *NeuroImage* 24:102047. doi: 10.1016/j.nicl.2019.102047

Neumeister, P., Feldker, K., Heitmann, C. Y., Helmich, R., Gathmann, B., Becker, M. P. I., et al. (2017). Interpersonal violence in posttraumatic women: brain networks triggered by trauma-related pictures. *Soc. Cogn. Affect. Neurosci.* 12, 555–568. doi: 10.1093/scan/nsw165

Nicholson, A. A., Densmore, M., Frewen, P. A., Neufeld, R. W. J., Théberge, J., Jetly, R., et al. (2023). Homeostatic normalization of alpha brain rhythms within the default-mode network and reduced symptoms in post-traumatic stress disorder following a randomized controlled trial of electroencephalogram neurofeedback. Brain. *Communications* 5:fcad068. doi: 10.1093/braincomms/fcad068

Nicholson, A. A., Densmore, M., Frewen, P. A., Théberge, J., Neufeld, R. W., McKinnon, M. C., et al. (2015). The dissociative subtype of posttraumatic stress disorder: unique resting-state functional connectivity of basolateral and centromedial amygdala complexes. *Neuropsychopharmacology* 40, 2317–2326. doi: 10.1038/npp.2015.79

Nicholson, A. A., Harricharan, S., Densmore, M., Neufeld, R. W. J., Ros, T., McKinnon, M. C., et al. (2020a). Classifying heterogeneous presentations of PTSD via the default mode, central executive, and salience networks with machine learning. *NeuroImage* 27:102262. doi: 10.1016/j.nicl.2020.102262

Nicholson, A. A., Rabellino, D., Densmore, M., Frewen, P. A., Paret, C., Kluetsch, R., et al. (2016a). The neurobiology of emotion regulation in posttraumatic stress disorder: amygdala downregulation via real-time fMRI neurofeedback. *Hum. Brain Mapp.* 38, 541–560. doi: 10.1002/hbm.23402

Nicholson, A. A., Rabellino, D., Densmore, M., Frewen, P. A., Paret, C., Kluetsch, R., et al. (2018). Intrinsic connectivity network dynamics in PTSD during amygdala downregulation using real-time fMRI neurofeedback: a preliminary analysis. *Hum. Brain Mapp.* 39, 4258–4275. doi: 10.1002/hbm.24244

Nicholson, A. A., Rabellino, D., Densmore, M., Frewen, P. A., Steryl, D., Scharnowski, F., et al. (2021). Differential mechanisms of posterior cingulate cortex downregulation and symptom decreases in posttraumatic stress disorder and healthy individuals using real-time fMRI neurofeedback. *Brain Behav.* 12:e2441. doi: 10.1002/brb3.2441

Nicholson, A. A., Ros, T., Densmore, M., Frewen, P. A., Neufeld, R. W. J., Théberge, J., et al. (2020b). A randomized, controlled trial of alpha-rhythm EEG neurofeedback in posttraumatic stress disorder: a preliminary investigation showing evidence of decreased PTSD symptoms and restored default mode and salience network connectivity using fMRI. *NeuroImage* 28:102490. doi: 10.1016/j.nicl.2020.102490

Nicholson, A. A., Sapru, I., Densmore, M., Frewen, P. A., Neufeld, R. W. J., Théberge, J., et al. (2016b). Unique insula subregion resting-state functional connectivity with amygdala complexes in posttraumatic stress disorder and its dissociative subtype. *Psychiatry Res. Neuroimaging* 250, 61–72. doi: 10.1016/j.pscychresns.2016.02.002

Nilsen, A. S., Blix, I., Leknes, S., Ekeberg, Ø., Skogstad, L., Endestad, T., et al. (2016). Brain activity in response to trauma-specific, negative, and neutral stimuli. A fMRI study of recent road traffic accident survivors. *Front. Psychol.* 7:1173. doi: 10.3389/fpsyg.2016.01173

Oldham, S., and Fornito, A. (2019). The development of brain network hubs. *Dev. Cogn. Neurosci.* 36:100607. doi: 10.1016/j.dcn.2018.12.005

Palejwala, A. H., Dadario, N. B., Young, I. M., O'Connor, K., Briggs, R. G., Conner, A. K., et al. (2021). Anatomy and white matter connections of the lingual gyrus and cuneus. *World Neurosurg.* 151, e426–e437. doi: 10.1016/j.wneu.2021.04.050

Paret, C., Kluetsch, R., Ruf, M., Demirakca, T., Hoesterey, S., Ende, G., et al. (2014). Down-regulation of amygdala activation with real-time fMRI neurofeedback in a healthy female sample. *Front. Behav. Neurosci.* 8:299. doi: 10.3389/fnbeh.2014.00299

Paret, C., Kluetsch, R., Zaehringer, J., Ruf, M., Demirakca, T., Bohus, M., et al. (2016a). Alterations of amygdala-prefrontal connectivity with real-time fMRI neurofeedback in BPD patients. *Soc. Cogn. Affect. Neurosci.* 11, 952–960. doi: 10.1093/scan/nsw016

Paret, C., Ruf, M., Gerchen, M. F., Kluetsch, R., Demirakca, T., Jungkunz, M., et al. (2016b). fMRI neurofeedback of amygdala response to aversive stimuli enhances prefrontal–limbic brain connectivity. *NeuroImage* 125, 182–188. doi: 10.1016/j.neuroimage.2015.10.027

Park, H.-D., and Blanke, O. (2019). Coupling inner and outer body for self-consciousness. *Trends Cogn. Sci.* 23, 377–388. doi: 10.1016/j.tics.2019.02.002

Patel, R., Spreng, R. N., Shin, L. M., and Girard, T. A. (2012). Neurocircuitry models of posttraumatic stress disorder and beyond: a meta-analysis of functional neuroimaging studies. *Neurosci. Biobehav. Rev.* 36, 2130–2142. doi: 10.1016/j.neubiorev.2012.06.003

Pearson, H. J. (2009). Present and accounted for: sensory stimulation and parietal neuroplasticity. *J. EMDR Pract. Res.* 3, 39–49. doi: 10.1891/1933-3196.3.1.39

Pineles, S. L., Shipherd, J. C., Mostoufi, S. M., Abramovitz, S. M., and Yovel, I. (2009). Attentional biases in PTSD: more evidence for interference. *Behav. Res. Ther.* 47, 1050–1057. doi: 10.1016/j.brat.2009.08.001

Pineles, S. L., Shipherd, J. C., Welch, L. P., and Yovel, I. (2007). The role of attentional biases in PTSD: is it interference or facilitation? *Behav. Res. Ther.* 45, 1903–1913. doi: 10.1016/j.brat.2006.08.021

Pitman, R. K., Rasmusson, A. M., Koenen, K. C., Shin, L. M., Orr, S. P., Gilbertson, M. W., et al. (2012). Biological studies of posttraumatic stress disorder. *Nat. Rev. Neurosci.* 13, 769–787. doi: 10.1038/nrn3339

Qin, P., and Northoff, G. (2011). How is our self related to midline regions and the default-mode network? *NeuroImage* 57, 1221–1233. doi: 10.1016/j.neuroimage.2011.05.028

Rabellino, D., Burin, D., Harricharan, S., Lloyd, C., Frewen, P. A., McKinnon, M. C., et al. (2018a). Altered sense of body ownership and agency in posttraumatic stress disorder and its dissociative subtype: a rubber hand illusion study. *Front. Hum. Neurosci.* 12:163. doi: 10.3389/fnhum.2018.00163

Rabellino, D., Densmore, M., Théberge, J., McKinnon, M. C., and Lanius, R. A. (2018b). The cerebellum after trauma: resting-state functional connectivity of the cerebellum in posttraumatic stress disorder and its dissociative subtype. *Hum. Brain Mapp.* 39, 3354–3374. doi: 10.1002/hbm.24081

Rabellino, D., Frewen, P. A., McKinnon, M. C., and Lanius, R. A. (2020). Peripersonal space and bodily self-consciousness: implications for psychological trauma-related disorders. *Front. Neurosci.* 14:586605. doi: 10.3389/fnins.2020.586605

Rabellino, D., Harricharan, S., Frewen, P. A., Burin, D., McKinnon, M. C., and Lanius, R. A. (2016). "I can't tell whether it's my hand": a pilot study of the neurophenomenology of body representation during the rubber hand illusion in trauma-related disorders. *Eur. J. Psychotraumatol.* 7:32918. doi: 10.3402/ejpt.v7.32918

Rabinak, C. A., Angstadt, M., Welsh, R. C., Kenndy, A. E., Lyubkin, M., Martis, B., et al. (2011). Altered amygdala resting-state functional connectivity in post-traumatic stress disorder. *Front. Psych.* 2:62. doi: 10.3389/fpsyt.2011.00062

Raichle, M. E. (2015). The brain's default mode network. *Annu. Rev. Neurosci.* 38, 433–447. doi: 10.1146/annurev-neuro-071013-014030

Ramage, A. E., Laird, A. R., Eickhoff, S. B., Acheson, A., Peterson, A. L., Williamson, D. E., et al. (2013). A coordinate-based meta-analytic model of trauma processing in posttraumatic stress disorder. *Hum. Brain Mapp.* 34, 3392–3399. doi: 10.1002/hbm.22155

Rauch, S. L. (1996). A symptom provocation study of posttraumatic stress disorder using positron emission tomography and script-driven imagery. *Arch. Gen. Psychiatry* 53:380. doi: 10.1001/archpsyc.1996.01830050014003

Rauch, S. L., Shin, L. M., and Phelps, E. A. (2006). Neurocircuitry models of posttraumatic stress disorder and extinction: human neuroimaging research—past, present, and future. *Biol. Psychiatry* 60, 376–382. doi: 10.1016/j.biopsych.2006.06.004

Roiser, J. P., Linden, D. E., Gorno-Tempini, M. L., Moran, R. J., Dickerson, B. C., and Grafton, S. T. (2016). Minimum statistical standards for submissions to Neuroimage: clinical. *NeuroImage* 12, 1045–1047. doi: 10.1016/j.nicl.2016.08.002

Ronzoni, G., del Arco, A., Mora, F., and Segovia, G. (2016). Enhanced noradrenergic activity in the amygdala contributes to hyperarousal in an animal model of PTSD. *Psychoneuroendocrinology* 70, 1–9. doi: 10.1016/j.psyneuen.2016.04.018

Ros, T., Baars, J., Lanius, R. A., and Vuilleumier, P. (2014). Tuning pathological brain oscillations with neurofeedback: a systems neuroscience framework. *Front. Hum. Neurosci.* 8:1008. doi: 10.3389/fnhum.2014.01008

Ros, T., Enriquez-Geppert, S., Zotev, V., Young, K. D., Wood, G., Whitfield-Gabrieli, S., et al. (2020). Consensus on the reporting and experimental design of clinical and cognitive-behavioural neurofeedback studies (CRED-nf checklist). *Brain* 143, 1674–1685. doi: 10.1093/brain/awaa009

Ros, T., Frewen, P., Théberge, J., Michela, A., Kluetsch, R., Mueller, A., et al. (2017). Neurofeedback Tunes scale-free dynamics in spontaneous brain activity. *Cereb. Cortex* 27, 4911–4922. doi: 10.1093/cercor/bhw285

Russman Block, S., King, A. P., Sripada, R. K., Weissman, D. H., Welsh, R., and Liberzon, I. (2017). Behavioral and neural correlates of disrupted orienting attention in posttraumatic stress disorder. *Cogn. Affect. Behav. Neurosci.* 17, 422–436. doi: 10.3758/s13415-016-0488-2

Sadeh, N., Spielberg, J. M., Warren, S. L., Miller, G. A., and Heller, W. (2014). Aberrant neural connectivity during emotional processing associated with posttraumatic stress. *Clin. Psychol. Sci.* 2, 748–755. doi: 10.1177/2167702614530113

Sartory, G., Cwik, J., Knuppertz, H., Schürholt, B., Lebens, M., Seitz, R. J., et al. (2013). In search of the trauma memory: a meta-analysis of functional neuroimaging studies of symptom provocation in posttraumatic stress disorder (PTSD). *PLoS One* 8:e58150. doi: 10.1371/journal.pone.0058150

Schoenberg, P. L. A., and David, A. S. (2014). Biofeedback for psychiatric disorders: a systematic review. *Appl. Psychophysiol. Biofeedback* 39, 109–135. doi: 10.1007/s10484-014-9246-9

Sheynin, J., Duval, E. R., King, A. P., Angstadt, M., Phan, K. L., Simon, N. M., et al. (2020). Associations between resting-state functional connectivity and treatment response in a randomized clinical trial for posttraumatic stress disorder. *Depress. Anxiety* 37, 1037–1046. doi: 10.1002/da.23075

Shin, L. M., and Liberzon, I. (2010). The neurocircuitry of fear, stress, and anxiety disorders. *Neuropsychopharmacology* 35, 169–191. doi: 10.1038/npp.2009.83

Sorger, B., Scharnowski, F., Linden, D. E. J., Hampson, M., and Young, K. D. (2019). Control freaks: towards optimal selection of control conditions for fMRI neurofeedback studies. *NeuroImage* 186, 256–265. doi: 10.1016/j.neuroimage.2018.11.004

Spreng, R. N., Mar, R. A., and Kim, A. S. N. (2009). The common neural basis of autobiographical memory, prospection, navigation, theory of mind, and the default mode: a quantitative meta-analysis. *J. Cogn. Neurosci.* 21, 489–510. doi: 10.1162/jocn.2008.21029

Sripada, R. K., King, A. P., Welsh, R. C., Garfinkel, S. N., Wang, X., Sripada, C. S., et al. (2012). Neural dysregulation in posttraumatic stress disorder: evidence for disrupted equilibrium between salience and default mode brain networks. *Psychosom. Med.* 74, 904–911. doi: 10.1097/PSY.0b013e318273bf33

Stevens, J. S., Jovanovic, T., Fani, N., Ely, T. D., Glover, E. M., Bradley, B., et al. (2013). Disrupted amygdala-prefrontal functional connectivity in civilian women with posttraumatic stress disorder. *J. Psychiatr. Res.* 47, 1469–1478. doi: 10.1016/j.jpsychires.2013.05.031

Sulzer, J., Haller, S., Scharnowski, F., Weiskopf, N., Birbaumer, N., Blefari, M. L., et al. (2013). Real-time fMRI neurofeedback: progress and challenges. *NeuroImage* 76, 386–399. doi: 10.1016/j.neuroimage.2013.03.033

Suo, X., Lei, D., Li, W., Yang, J., Li, L., Sweeney, J. A., et al. (2020). Individualized prediction of PTSD symptom severity in trauma survivors from whole-brain resting-state functional connectivity. *Front. Behav. Neurosci.* 14:563152. doi: 10.3389/fnbeh.2020.563152

Thibault, R. T., MacPherson, A., Lifshitz, M., Roth, R. R., and Raz, A. (2018). Neurofeedback with fMRI: a critical systematic review. *NeuroImage* 172, 786–807. doi: 10.1016/j.neuroimage.2017.12.071

Thiebaut de Schotten, M., Urbanski, M., Valabregue, R., Bayle, D. J., and Volle, E. (2014). Subdivision of the occipital lobes: an anatomical and functional MRI connectivity study. *Cortex* 56, 121–137. doi: 10.1016/j.cortex.2012.12.007

Thome, J., Terpou, B. A., McKinnon, M. C., and Lanius, R. A. (2020). The neural correlates of trauma-related autobiographical memory in posttraumatic stress disorder: a meta-analysis. *Depress. Anxiety* 37, 321–345. doi: 10.1002/da.22977

Todd, R. M., MacDonald, M. J., Sedge, P., Robertson, A., Jetly, R., Taylor, M. J., et al. (2015). Soldiers with posttraumatic stress disorder see a world full of threat: magnetoencephalography reveals enhanced tuning to combat-related cues. *Biol. Psychiatry* 78, 821–829. doi: 10.1016/j.biopsych.2015.05.011

Tomasi, D., and Volkow, N. D. (2011). Functional connectivity hubs in the human brain. *NeuroImage* 57, 908–917. doi: 10.1016/j.neuroimage.2011.05.024

Tsakiris, M., Hesse, M. D., Boy, C., Haggard, P., and Fink, G. R. (2007). Neural signatures of body ownership: a sensory network for bodily self-consciousness. *Cereb. Cortex* 17, 2235–2244. doi: 10.1093/cercor/bhl131

Tursich, M., Ros, T., Frewen, P. A., Kluetsch, R. C., Calhoun, V. D., and Lanius, R. A. (2015). Distinct intrinsic network connectivity patterns of post-traumatic stress disorder symptom clusters. *Acta Psychiatr. Scand.* 132, 29–38. doi: 10.1111/acps.12387

van den Heuvel, M. P., and Sporns, O. (2013). Network hubs in the human brain. *Trends Cogn. Sci.* 17, 683–696. doi: 10.1016/j.tics.2013.09.012

van der Kolk, B. A., and Fisler, R. (1995). Dissociation and the fragmentary nature of traumatic memories: overview and exploratory study. *J. Trauma. Stress.* 8, 505–525. doi: 10.1007/BF02102887

Watanabe, T., Sasaki, Y., Shibata, K., and Kawato, M. (2017). Advances in fMRI real-time neurofeedback. *Trends Cogn. Sci.* 21, 997–1010. doi: 10.1016/j.tics.2017.09.010

Weathers, F. W., Bovin, M. J., Lee, D. J., Sloan, D. M., Schnurr, P. P., Kaloupek, D. G., et al. (2018). The clinician-administered PTSD scale for DSM–5 (CAPS-5): development and initial psychometric evaluation in military veterans. *Psychol. Assess.* 30, 383–395. doi: 10.1037/pas0000486

Weaver, S. S., Birn, R. M., and Cisler, J. M. (2020). A pilot adaptive neurofeedback investigation of the neural mechanisms of implicit emotion regulation among women with PTSD. *Front. Syst. Neurosci.* 14:40. doi: 10.3389/fnsys.2020.00040

Weiss, P. H., Marshall, J. C., Zilles, K., and Fink, G. R. (2003). Are action and perception in near and far space additive or interactive factors? *NeuroImage* 18, 837–846. doi: 10.1016/S1053-8119(03)00018-1

Wenderoth, N., Debaere, F., Sunaert, S., van Hecke, P., and Swinnen, S. P. (2004). Parieto-premotor areas mediate directional interference during bimanual movements. *Cereb. Cortex* 14, 1153–1163. doi: 10.1093/cercor/bhh075

Wolf, R. C., and Herringa, R. J. (2016). Prefrontal–amygdala dysregulation to threat in pediatric posttraumatic stress disorder, Prefrontal-amygdala dysregulation to threat in pediatric posttraumatic stress disorder. *Neuropsychopharmacology* 41, 822–831. doi: 10.1038/npp.2015.209

Yehuda, R., Hoge, C. W., McFarlane, A. C., Vermetten, E., Lanius, R. A., Nievergelt, C. M., et al. (2015). Post-traumatic stress disorder. *Nat. Rev. Dis. Primers.* 1:15057. doi: 10.1038/nrdp.2015.57

Yin, Y., Li, L., Jin, C., Hu, X., Duan, L., Eyler, L. T., et al. (2011). Abnormal baseline brain activity in posttraumatic stress disorder: a resting-state functional magnetic resonance imaging study. *Neurosci. Lett.* 498, 185–189. doi: 10.1016/j.neulet.2011.02.069

Young, K., Fine, N., and Hendler, T. (2021). "Chapter 8—fMRI neurofeedback for disorders of emotion regulation" in *fMRI neurofeedback*. ed. M. Hampson (London: Academic Press), 187–205.

Young, K. D., Siegle, G. J., Zotev, V., Phillips, R., Misaki, M., Yuan, H., et al. (2017). Randomized clinical trial of real-time fMRI amygdala neurofeedback for major depressive disorder: effects on symptoms and autobiographical memory recall. *Am. J. Psychiatry* 174, 748–755. doi: 10.1176/appi.ajp.2017.16060637

Yu, X., Cohen, Z. P., Tsuchiyagaito, A., Cochran, G., Aupperle, R. L., Stewart, J. L., et al. (2022). Neurofeedback-augmented mindfulness training elicits distinct responses in the subregions of the insular cortex in healthy adolescents. *Brain Sci.* 12:363. doi: 10.3390/brainsci12030363

Zhang, G., Zhang, H., Li, X., Zhao, X., Yao, L., and Long, Z. (2013). Functional alteration of the DMN by learned regulation of the PCC using real-time fMRI. *IEEE Trans. Neural. Syst. Rehabil. Eng.* 21, 595–606. doi: 10.1109/TNSRE.2012.2221480

Zhao, Z., Duek, O., Seidemann, R., Gordon, C., Walsh, C., Romaker, E., et al. (2023). Amygdala downregulation training using fMRI neurofeedback in post-traumatic stress disorder: a randomized, double-blind trial. *Trans. Psychiatry* 13. doi: 10.1038/s41398-023-02467-6

Zhou, Y., Wang, Z., Qin, L., Wan, J., Sun, Y., Su, S., et al. (2012). Early altered resting-state functional connectivity predicts the severity of post-traumatic stress disorder symptoms in acutely traumatized subjects. *PLoS One* 7:e46833. doi: 10.1371/journal.pone.0046833

Zhu, H., Qiu, C., Meng, Y., Cui, H., Zhang, Y., Huang, X., et al. (2015). Altered spontaneous neuronal activity in chronic posttraumatic stress disorder patients before and after a 12-week paroxetine treatment. *J. Affect. Disord.* 174, 257–264. doi: 10.1016/j.jad.2014.11.053

Zhu, H., Zhang, J., Zhan, W., Qiu, C., Wu, R., Meng, Y., et al. (2014). Altered spontaneous neuronal activity of visual cortex and medial anterior cingulate cortex in treatment-naïve posttraumatic stress disorder. *Compr. Psychiatry* 55, 1688–1695. doi: 10.1016/j.comppsych.2014.06.009

Zotev, V., Phillips, R., Misaki, M., Wong, C. K., Wurfel, B. E., Krueger, F., et al. (2018). Real-time fMRI neurofeedback training of the amygdala activity with simultaneous EEG in veterans with combat-related PTSD. *NeuroImage* 19, 106–121. doi: 10.1016/j.nicl.2018.04.010

Zuo, X.-N., Kelly, C., Adelstein, J. S., Klein, D. F., Castellanos, F. X., and Milham, M. P. (2010). Reliable intrinsic connectivity networks: test–retest evaluation using ICA and dual regression approach. *NeuroImage* 49, 2163–2177. doi: 10.1016/j.neuroimage.2009.10.080

Zweerings, J., Pflieger, E. M., Mathiak, K. A., Zvyagintsev, M., Kacela, A., Flatten, G., et al. (2018). Impaired voluntary control in PTSD: probing self-regulation of the ACC with real-time fMRI. *Front. Psych.* 9:219. doi: 10.3389/fpsyt.2018.00219

Zweerings, J., Sarkheil, P., Keller, M., Dyck, M., Klasen, M., Becker, B., et al. (2020). Rt-fMRI neurofeedback-guided cognitive reappraisal training modulates amygdala responsivity in posttraumatic stress disorder. *NeuroImage* 28:102483. doi: 10.1016/j.nicl.2020.102483

frontiers | Frontiers in Neuroscience

TYPE Original Research
PUBLISHED 08 December 2023
DOI 10.3389/fnins.2023.1302318



OPEN ACCESS

EDITED BY
Vassiliy Tsytsarev,
University of Maryland, United States

REVIEWED BY
Ekaterina Levichkina,
The University of Melbourne, Australia
Steven Tobochnik,
Brigham and Women's Hospital and Harvard Medical School, United States

*CORRESPONDENCE
Yuan Peng
✉ py9746@163.com

RECEIVED 26 September 2023
ACCEPTED 20 November 2023
PUBLISHED 08 December 2023

CITATION
Tao T, Lu S, Hu N, Xu D, Xu C, Li F, Wang Q and Peng Y (2023) Prognosis of comatose patients with reduced EEG montage by combining quantitative EEG features in various domains. *Front. Neurosci.* 17:1302318. doi: 10.3389/fnins.2023.1302318



# Prognosis of comatose patients with reduced EEG montage by combining quantitative EEG features in various domains

Tao Tao[1], Shiqi Lu[2], Nan Hu[3], Dongyang Xu[4], Chenyang Xu[1], Fajun Li[1], Qin Wang[1] and Yuan Peng[1]*

[1]Intensive Care Unit, The First People's Hospital of Kunshan, Kunshan Affiliated Hospital of Jiangsu University, Kunshan, Jiangsu, China, [2]Emergency Department, The First Affiliated Hospital of Soochow University, Suzhou, Jiangsu, China, [3]School of Electronics and Information Engineering, Soochow University, Suzhou, Jiangsu, China, [4]Center for Intelligent Acoustics and Signal Processing, Huzhou Institute of Zhejiang University, Huzhou, China

**Objective:** As the frontoparietal network underlies recovery from coma, a limited frontoparietal montage was used, and the prognostic values of EEG features for comatose patients were assessed.

**Methods:** Collected with a limited frontoparietal EEG montage, continuous EEG recordings of 81 comatose patients in ICU were used retrospectively. By the 60-day Glasgow outcome scale (GOS), the patients were dichotomized into favorable and unfavorable outcome groups. Temporal-, frequency-, and spatial-domain features were automatically extracted for comparison. Partial correlation analysis was applied to eliminate redundant factors, and multiple correspondence analysis was used to explore discrimination between groups. Prognostic characteristics were calculated to assess the performance of EEG feature-based predictors established by logistic regression. Analyses were performed on all-patients group, strokes subgroup, and traumatic brain injury (TBI) subgroup.

**Results:** By analysis of all patients, raised burst suppression ratio (BSR), suppressed root mean square (RMS), raised power ratio of β to α rhythm (β/α), and suppressed phase-lag index between F3 and P4 (PLI [F3, P4]) were associated with unfavorable outcome, and yielded AUC of 0.790, 0.811, 0.722, and 0.844, respectively. For the strokes subgroup, the significant variables were BSR, RMS, θ/total, θ/δ, and PLI (F3, P4), while for the TBI subgroup, only PLI (F3, P4) was significant. BSR combined with PLI (F3, P4) gave the best predictor by cross-validation analysis in the all-patients group (AUC = 0.889, 95% CI: 0.819–0.960).

**Conclusion:** Features extracted from limited frontoparietal montage EEG served as valuable coma prognostic tools, where PLI (F3, P4) was always significant. Combining PLI (F3, P4) with features in other domains may achieve better performance.

**Significance:** A limited-montage EEG coupled with an automated algorithm is valuable for coma prognosis.

KEYWORDS

**coma prognosis, electroencephalography, frontoparietal network, limited frontoparietal EEG montage, functional connectivity**

## Highlights

- A limited frontoparietal EEG montage was employed for EEG monitoring.
- A combination of EEG features was used to build predictors for coma outcome in ICU.
- Significant variables were found in temporal, frequency, and spatial domains.
- Burst suppression ratio combined with PLI between F3 and P4 formed the best predictor.
- EEG monitoring for frontoparietal network can contribute to coma prognosis.

## 1 Introduction

Patients with acquired brain injuries (ABIs) often suffer from severe disorders of consciousness (DoC), whose preceding state is coma, an acute state lasting up to 2–4 weeks or even longer (Owen, 2015). The Glasgow Coma Scale (GCS) is a conventional assessment tool for comatose patients, including three sub-scales: eye-opening (E), verbal response (V), and motor response (M). A patient is considered in coma only when $E = 1$, $V \leq 2$, and $M \leq 4$ are satisfied simultaneously (Zubler et al., 2015), and in the meantime, the overall $GCS = E + V + M \leq 7$ is given. Otherwise, the patient is no longer in a coma state but has turned to a post-coma DoC state, including unresponsive wakefulness syndrome (UWS), minimally conscious state (MCS), or EMCS (emerged from minimally conscious state), as assessed by the Coma Recovery Scale–Revised (CRS-R; Giacino et al., 2004) instead. Early prognosis of comatose patients in intensive care unit (ICU) has the potential to assist clinical decision-making for further treatment. Though the frequently used GCS is based on standardized objective examination findings, it needs expert interpretation, and it does not consider the underlying pathophysiology, the trajectory of neuro-recovery, or the presence of various confounding factors. Hence, developing a new coma outcome predictor based on continuous neurophysiological monitoring coupled with an automated algorithm has drawn much attention in recent years.

Electroencephalography (EEG) is known for its advantage in monitoring the overall functionality of the cerebral cortex and the neural response to external stimuli. When applied in neuro-prognostication for comatose patients, continuous bedside EEG monitoring offers the possibility of objective assessments of the trajectory of neuro-recovery with high temporal resolution (Young, 2000). EEG signals include evoked potentials and resting-state EEG. Evoked potentials used in coma prognosis include brainstem auditory evoked potential (BAEP; Rothstein, 2000), mid-latency auditory evoked potential (MLAEP; Tsurukiri et al., 2013), somatosensory evoked potential (SEP; Zhang et al., 2015), and auditory steady-state response (ASSR; Chen et al., 2020). Compared with evoked potentials depending on additional stimulation and synchronization devices, resting-state EEG corresponds to recording the patients' spontaneous EEG only, which is more suitable for long-term monitoring.

The American Clinical Neurophysiology Society (ACNS) recommended some standardized EEG descriptors (terminologies) to assess the patients in ICU (Hirsch et al., 2021), including continuity, voltage, frequency, symmetry, organization of an anterior/posterior gradient of the background activity, presence of reactivity, spontaneous variability of the background activity, and occurrence of epileptic discharges. Most of the ACNS EEG descriptors can be obtained from resting-state EEG recordings reviewed visually by experts or processed automatically by algorithms. In Hofmeijer et al. (2016), EEG of consecutive comatose patients after cardiac arrest was reviewed to be classified as isoelectric, low-voltage, epileptiform, burst suppression, diffusely slowed, or normal, and the classified states were applied in coma outcome prediction. ACNS EEG descriptors were used in Benarous et al. (2019) to predict outcome of postanoxic coma and showed the necessity of standardized methods of evaluating EEG parameters. In Scarpino et al. (2020), ACNS EEG descriptors combined with SEPs recorded at 12 and 72 h from resuscitation were used for predicting 6-month neurological outcome in comatose patients after cardiac arrest. Background activity, the presence of rhythmic or periodic patterns, and the reactivity of ACNS EEG descriptors were used in Guedes et al. (2020) to illustrate that they can be reliable predictors for poor neurological outcome as well as death. ACNS EEG descriptors in a reduced EEG montage study in Backman et al. (2020) also showed significant value in assessing comatose cardiac arrest patients. As a weighted sum of resting-state EEG parameters at temporal and frequency domains, ranging from 0 to 100, the bispectral index (BIS) has also been used in prediction of coma outcome (Schnakers et al., 2008).

Most of the EEG features used for coma prognosis, including ACNS EEG descriptors, were derived from temporal domain or frequency domain (Hoedemaekers et al., 2023), and the current trend is to involve deep neural networks with larger datasets (Zheng et al., 2022). In recent years, spatial EEG features have also been explored in this field. Coupling between EEG signals on the left–right axis and on the anterior–posterior axis was measured with four synchronization measures in Zubler et al. (2015) and used in coma prognosis. Based on the similarity of instantaneous frequencies in EEG epochs, link rates (LRs) and link durations (LDs) in the $\alpha$, $\delta$, and $\theta$ bands were calculated for outcome prediction of comatose patients after cardiac arrest (Keijzer et al., 2021). Three functional connectivity metrics, coherence (COH), phase locking value (PLV), and mutual information (MI), were calculated in 19-channel EEGs at 12, 24, and 48 h after cardiac arrest (Carrasco-Gómez et al., 2021), and machine learning techniques were used to combine them in a model to predict outcome of postanoxic coma. An intrinsic network reactivity index (INRI; Khanmohammadi et al., 2018) based on whole-brain multi-channel resting-state EEG was formed to study its correlation with the consciousness level of coma patients. Despite the above preliminary studies, the combination of the temporal-, frequency-, and spatial-domain features of resting-state EEG has seldom been used in prognostic research for comatose patients.

Relative to the neurologic examination-based neuro-prognostication scales, EEG is time-intensive, much more expensive, and not available in much of the resource-limited world. Therefore, conventional full-montage-based EEG monitoring combined with expert visual interpretation or supervised quantification techniques needs to be improved for coma prognosis. In this context, it is meaningful to assess the prognostic value of a limited-montage EEG coupled with an automated algorithm. In Backman et al. (2020), with a reduced EEG montage including six channels (F3, T3, P3, F4, T4, and P4), visually interpreted ACNS EEG descriptors yielded high prognostic performance for postcardiac arrest comatose patients. In recent years, the anterior forebrain mesocircuit (Fridman et al., 2014) and the frontoparietal network (Wu et al., 2015) have been consistently implicated in circuit mechanisms underlying recovery from coma (Edlow et al., 2021). Inspired by these circuit mechanisms underlying the restoration of cerebral activity during recovery from coma, we only reserve frontal and parietal electrodes in the reduced EEG montage used in Backman et al. (2020). The quantitative EEG features in temporal domain, frequency domain, and spatial domain can be extracted automatically from this limited-montage EEG. The prognostic value of a combination of quantitative EEG features in various domains would then be assessed in predicting outcomes of comatose patients with ABIs in ICU. At last, ancillary neuro-prognostication methods would be developed for all comatose population or patients in specific subgroups.

# 2 Materials and methods

## 2.1 Study design

This study was a retrospective one. Comatose patients with ABIs admitted to the ICU of the First People's Hospital of Kunshan from 29 October 2019 to 7 April 2021, who underwent multi-channel EEG monitoring, were considered. Inclusion criteria were: (1) The patients were in coma, i.e., GCS $\leq$ 7 with E = 1, V $\leq$ 2, and M $\leq$ 4; (2) EEG monitoring was conducted within 4 weeks after admission, including at least four frontoparietal channels: F3, F4, P3, P4, and the EEG recording lasted for at least 30 min; (3) EEG monitoring was initiated at or later than 24 h after sedating medications (André-Obadia et al., 2018); (4) The 60-day Glasgow outcome scale (GOS; Jennett and Bond, 1975) of the patient could be obtained by follow-up; (5) The patient was not diagnosed as brain dead before or during EEG monitoring, which would also show isoelectric (<2 μV) EEG waveform; (6) The patient did not regain consciousness during EEG monitoring. Qualified patients of both sexes were eligible for the study. According to the above criteria, a total of 81 comatose patients were included in the study cohort, and their 60-day GOS scores were obtained in follow-up. Ranked from 1 to 5, the GOS provides a measurement of post-coma outcome: 1 = death; 2 = vegetative state or severe disability; 3 = moderate disability, able to follow commands but unable to live independently; 4 = able to live independently but unable to return to work or school; 5 = fully recovered. Among the 81 patients who participated, we had GOS = 1 ($n$ = 39), GOS = 2 ($n$ = 20), GOS = 3 ($n$ = 10), GOS = 4 ($n$ = 7), and GOS = 5 ($n$ = 5). According to the GOS, the patients were dichotomized into favorable (GOS $\geq$ 3) and unfavorable (GOS $\leq$ 2) outcome groups. Finally, there were 22 patients in the favorable outcome group and 59 patients in the unfavorable outcome group.

In this study, the determination of conducting quantitative EEG monitoring was given by each patient's physician, instead of our study purpose. Our study did not influence the treatment or decision to withdraw life-sustaining therapy. Since EEG monitoring is part of standard care in our ICU, the need for informed consent for EEG measurements and follow-up by telephone interview was waived. The study protocol was reviewed and approved by the Medical Ethics Committee of the First People's Hospital of Kunshan (Approval No. 00012098), which ensured that our study was conducted in accordance with the ethical guidelines of the Declaration of Helsinki.

## 2.2 EEG recording and feature extraction

Quantitative EEG monitoring was conducted using a multi-lead EEG device (Cadwell Industries, Kennewick, WA, United States). A limited frontoparietal EEG montage was used, where F3, F4, P3, and P4 were used as EEG recording electrodes, and Cz was reference. The sampling rate was 250 Hz, and high-quality EEG recording lasted for at least 30 min. Considering the particularity of sedation and analgesia in the treatment of critically ill patients, and especially analgesic drugs being the basis of medication, we used a combination regimen of short-acting low-dose remifentanil and low-dose dexmedetomidine for all patients. It was known that sedation may lead to alteration of some neurophysiological markers (André-Obadia et al., 2018; Benghanem et al., 2022), including decreased voltage, decreased slow wave, and raised fast rhythms. In our ICU, all EEG monitoring were initiated at or later than 24 h after short-acting low-dose sedating medications and ended before next sedating medications. The occurrence of epileptic discharges, which was mainly focused on non-convulsive status epilepticus, was also visually interpreted and recorded by physicians. The physicians were not blinded to the EEG as they determined the EEG monitoring and had to treat epileptic seizures.

Each patient's EEG recording was partitioned into 2-min non-overlapping epochs. EEG in each epoch underwent baseline calibration, bandpass filtering, and trajectory rejection. A 0.1–40 Hz forward–backward four-order Butterworth filter was used to eliminate noise and interference. For rejection of trajectories such as abnormal movements, an epoch would be discarded if there existed a point whose density was >200 μV. For each epoch, 8 temporal features, 16 frequency features, and 24 spatial features were calculated. Temporal features or frequency features were calculated for all channels, and the median value of each kind of feature across all channels was used. The features among all reserved epochs were averaged to give the final variables for coma prognosis study. The diagram of EEG recording and feature extraction is displayed in Figure 1. EEG preprocessing and feature extraction were performed using MATLAB 2022a and the EEGLAB toolbox.

The extracted temporal features were: BSR (burst suppression ratio), RMS (root mean square), activity, mobility, complexity, kurtosis, skewness, and entropy. BSR was defined as the ratio of duration of EEG in suppression state ($\leq$5 μV) to the total duration in one epoch (Nagaraj

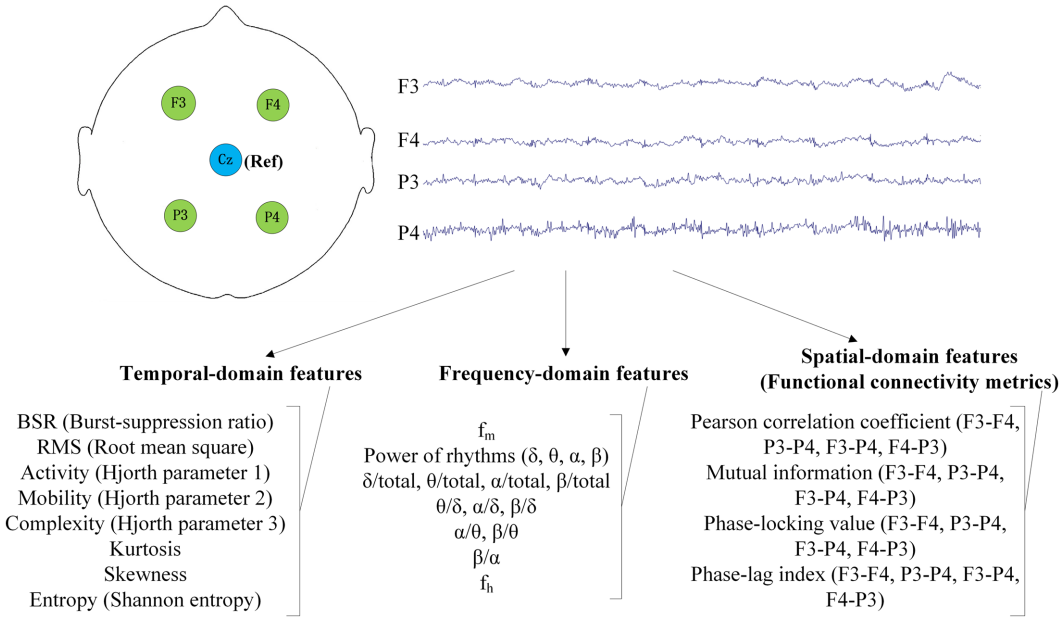


FIGURE 1
EEG recording and feature extraction in this study.

et al., 2018). If the EEG samples in one epoch are denoted as $x_n$, $n = 1, 2, \ldots, N$, where $N$ is the number of samples in one epoch, $\mathrm{RMS} = \sqrt{\mathrm{var}(x_n)} = \sqrt{\sum_{n=1}^{N}(x_n - \bar{x})^2 / N}$. Activity, mobility, and complexity are Hjorth parameters (Hjorth, 1970), given by activity = $\mathrm{var}(x_n)$, mobility = $\sqrt{\mathrm{var}(x_n') / \mathrm{var}(x_n)}$, and complexity = $\mathrm{mobility}(x_n') / \mathrm{mobility}(x_n)$, respectively. Kurtosis and skewness are frequently used higher-order statistics. Entropies were usually known as chaos features, but in this study, they were still categorized as temporal features, and Shannon entropy was used. The extracted frequency features were: the frequency corresponding to the maximum frequency component ($f_m$), power of δ rhythm (0.5–4 Hz), power of θ rhythm (4–8 Hz), power of α rhythm (8–13 Hz), power of β rhythm (13–30 Hz), power ratios (δ/total, θ/total, α/total, β/total, θ/δ, α/δ, β/δ, α/θ, β/θ, β/α), and the upper cutoff frequency ($f_h$). The spatial features used functional connectivity metrics, including Pearson correlation coefficient (PCC), mutual information (MI), phase locking value (PLV), and phase-lag index (PLI) for each couple of channels. If $x$ and $y$ denote two EEG channels, $\mathrm{PCC}(x,y) = \sum_{n=1}^{N}(x_n - \bar{x})(y_n - \bar{y}) / \left(N\sqrt{\mathrm{var}(x_n)\mathrm{var}(y_n)}\right)$, $\mathrm{MI}(x,y) = H_x + H_y - H_{xy}$, $\mathrm{PLV}(x,y) = \left|\left\langle e^{i\varphi_{x,y}(t)} \right\rangle\right|$, and $\mathrm{PLI}(x,y) = \left|\left\langle sign\varphi_{x,y}(t) \right\rangle\right|$, where $H_x$, $H_y$, and $H_{xy}$ denote entropy of $x$ channel, entropy of $y$ channel, and cross-entropy of $x$ channel and $y$ channel, respectively, $\varphi_{x,y}(t)$ denotes difference of unwrapped phases between $x$ channel and $y$ channel, and $\langle\cdot\rangle$ denotes expectation. In the existing EEG-based coma prognosis studies that exploited functional connectivity metrics (Zubler et al., 2015; Khanmohammadi et al., 2018; Carrasco-Gómez et al., 2021; Keijzer et al., 2021), a common reference or global average reference was used. As a limited montage is used in this study, we chose a common reference Cz for all four frontoparietal channels. It can be proved theoretically that, with a common reference, information of interaction between two coupled channels can still be derived, though attenuated by some interference terms.

## 2.3 Statistical analysis

To compare demographical or extracted feature variables in two patient groups, Fisher's exact test or $\chi^2$ test was used for categorical variables (presented as numbers [percentage]), and Student's $t$-test or Mann–Whitney $U$ test was performed for continuous variables, where the significance level was set at $p = 0.05$. The Benjamini–Hochberg correction of false discovery rate was employed for all EEG features. For continuous variables, Shapiro–Wilk test and Levene test were performed first to determine if the variable met normal distribution and homogeneity of variance, respectively. If a variable met normal distribution with homogeneous variance (presented as mean ± SD), the $t$-test was used; otherwise (presented as median [quartile]), the Mann–Whitney $U$ test was used. Partial correlation analysis was further applied to eliminate redundant factors. A multiple correspondence analysis (MCA) was used to explore discrimination between variables in two groups. Logistic regression was used to establish prognosis models for a single EEG feature-based predictor or a combination of multiple predictors in various domains. Area under the receiver operating characteristic curve (AUC-ROC) was calculated to assess the performances of the established prognosis models. Prognostic characteristics including sensitivity (Sen), specificity (Spec), positive predictive value (PPV), negative predictive value (NPV), and false positive rate for predicting unfavorable outcome by built predictors were also calculated, where the cutoff probability was set as 0.5. All

TABLE 1 Baseline characteristics of the study population.

| Variable | Favorable outcome (GOS ≥ 3) | Unfavorable outcome (GOS ≤ 2) | Statistical value | Value of *p* |
|---|---|---|---|---|
| | *n* = 22 | *n* = 59 | | |
| Sex (female) | 6 (27.3%) | 14 (23.7%) | 0.002 (Fisher) | 0.776 |
| Age | 49.32 ± 17.844 | 49.20 ± 17.966 | 0.026 (*t*) | 0.980 |
| GCS | 3.5 (3) | 3 (1) | 0.201 (U) | 0.841 |
| Etiology | 6/0/11/1/4 | 19/4/22/9/5 | 5.101 ($\chi^2$) | 0.292 |
| Time of EEG recording after brain injury (days) | 6 (15) | 3 (5) | 1.626 (U) | 0.104 |
| Occurrence of epileptic discharges | 2 (9.1%) | 2 (3.5%) | 0.227 (Fisher) | 0.297 |

The order of five etiology items in the table: hemorrhagic stroke, ischemic stroke, traumatic brain injury (TBI), postcardiac arrest, and others.

statistical analyses were conducted using SPSS Statistics 27 (IBM Corp., Armonk, NY, United States).

# 3 Results

Results in comparison of baseline characteristics between groups are displayed in Table 1. The baseline characteristics consist of sex, age, GCS evaluated during EEG recording, etiology, timing of EEG recording after brain injury, and occurrence of epileptic discharges. Among all patients in this study, the etiology included hemorrhagic stroke, ischemic stroke, traumatic brain injury (TBI), postcardiac arrest, and others (intoxication, tumor, pulmonary encephalopathy, etc.). From Table 1, it was found that none of the baseline characteristics showed significance.

## 3.1 Analysis of all patients

Comparison of EEG feature variables between the two groups is given in Table 2. It was found that BSR, RMS, activity, powers of δ, θ, α, and β rhythms, β/α, and PLI (F3, P4) showed significant differences between the two groups. RMS, similar to the "Voltage" in ACNS EEG descriptors, showed significance along with other eight EEG features. The EEG voltage amplitude is associated with many EEG features, e.g., rhythm densities extracted by Fourier transform $X(f)=\int x(t)e^{-j2\pi ft}\mathrm{d}t$ are in direct proportion to RMS. Partial correlation analysis is a useful tool to identify the true relationship between two variables while controlling for the effects of another variable. As the dichotomized outcomes are actually obtained from 60-day GOS, we performed partial correlation analysis between all significant EEG features (except RMS) and 60-day GOS, where RMS was used as controlled variable. Table 3 lists the partial correlation analysis results. It was found that activity and powers of δ, θ, α, and β rhythms were no longer significant, implying that their significance may be due to RMS, and hence these five variables would be pruned in the coma prognosis study. Spearman's correlations between the remaining significant variables (BSR, RMS, β/α, and PLI [F3, P4]) and 60-day GOS are presented in Table 4. High correlations between all these four variables and 60-day GOS can be found, and the trend of these variables along with the variation of GOS is also displayed in Figure 2 in the form of error bars. Henceforth, in this study, EEG features in temporal domain (BSR and RMS), frequency domain (β/α), and spatial domain (PLI [F3, P4]) would be considered in coma prognosis.

The task of establishing a prognosis model lies in discriminating between variables in two groups. Multiple correspondence analysis is a useful tool to map data from high-dimensional space to low-dimensional space, where visualization of discrimination among different groups can be achieved. The elements of row and column data in a contingency table are represented as category points in a 2-D space by MCA. In the output of MCA, the joint plot of category points shows separability of the corresponding variables belonging to different categories. If category points are close along some dimension or have close distances in the 2-D space, they are deemed to have close interactions. Discrimination measures give dimensional scores of category point separation, where a higher score implies that category points of a variable can be separated more easily along that dimension. The MCA results of the EEG features and the corresponding outcomes are presented in Figure 3. It can be found that, after being mapped to a 2-dimensional space, the four EEG features showed two discriminative clusters around the two coma outcomes along dimension 1. Note that the category points of BSR are perfectly overlapping with those of other features. Discrimination measures show that outcome can be separated along dimension 1, rather than dimension 2, and BSR, RMS, β/α, and PLI (F3, P4) all had high discrimination scores along dimension 1. This result implies that a combination of EEG features in various domains is promising to build a coma outcome predictor. The same discrimination score achieved by BSR, RMS, and β/α implies that these features may play similar roles in building a coma outcome predictor with combined features.

Logistic regression was performed to build coma outcome predictors using a single EEG feature or a combination of EEG features in various domains. Table 5 lists the results of single EEG feature-based unfavorable outcome predictors. It was found that BSR and β/α were risk factors, while RMS and PLI (F3, P4) were protective factors for predicting unfavorable outcome. All four features showed significance, i.e., AUC = 0.5 was rejected by Wilcoxon test of ranks. Multiple logistic regression for all four features was also performed, where likelihood ratio test was used to include or exclude variables. BSR and PLI (F3, P4) were reserved in the final prediction model, and the result is presented in Table 6. Partial correlation on EEG features with RMS was performed to adjust for interactions between frequency band powers and RMS, and hence powers of δ, θ, α, and β rhythms were excluded from building coma outcome predictors. Here we also performed multiple logistic regression with likelihood ratio test for all

TABLE 2 EEG features in various domains between favorable and unfavorable outcome groups.

| Variable | Favorable outcome (GOS ≥ 3) | Unfavorable outcome (GOS ≤ 2) | Statistical value | Value of *p* (after correction) |
|---|---|---|---|---|
| | *n* = 22 | *n* = 59 | | |
| BSR | 0.187 (0.120) | 0.358 (0.563) | −3.992 (U) | **<0.001*** |
| RMS | 22.73 (20.873) | 12.58 (15.077) | 4.290 (U) | **<0.001*** |
| Activity | 781.67 (1799.21) | 145.94 (406.64) | 3.961 (U) | **<0.001*** |
| Mobility | 12.69 (7.63) | 16.62 (13.54) | −1.688 (U) | 0.338 |
| Complexity | 4.58 (2.69) | 4.24 (2.81) | 1.487 (U) | 0.445 |
| Kurtosis | 3.49 (0.52) | 3.45 (1.21) | 0.680 (U) | 0.738 |
| Skewness | −0.075 (0.282) | −0.016 (0.211) | −1.179 (U) | 0.654 |
| Entropy | 4.077 (0.193) | 4.076 (0.356) | 0.074 (U) | 0.959 |
| $f_m$ | 0.549 (0.294) | 0.479 (0.446) | 0.812 (U) | 0.699 |
| δ | 91.30 (254.51) | 24.46 (64.33) | 4.141 (U) | **<0.001*** |
| θ | 2.834 (2.817) | 0.745 (2.045) | 3.589 (U) | **<0.001*** |
| α | 1.283 (1.227) | 0.273 (0.624) | 3.780 (U) | **<0.001*** |
| β | 0.438 (0.754) | 0.140 (0.363) | 3.292 (U) | **<0.001*** |
| δ/total | 0.923 (0.075) | 0.878 (0.192) | 1.593 (U) | 0.385 |
| θ/total | 0.042 (0.022) | 0.048 (0.052) | −0.892 (U) | 0.667 |
| α/total | 0.016 (0.019) | 0.023 (0.050) | −1.210 (U) | 0.653 |
| β/total | 0.007 (0.014) | 0.017 (0.079) | −1.858 (U) | 0.328 |
| θ/δ | 0.054 (0.045) | 0.054 (0.101) | −1.157 (U) | 0.642 |
| α/δ | 0.018 (0.025) | 0.031 (0.080) | −1.295 (U) | 0.596 |
| β/δ | 0.008 (0.019) | 0.022 (0.129) | −1.848 (U) | 0.307 |
| α/θ | 0.438 (0.313) | 0.537 (0.605) | −0.924 (U) | 0.740 |
| β/θ | 0.197 (0.241) | 0.512 (1.234) | −1.752 (U) | 0.346 |
| β/α | 0.474 (0.582) | 0.991 (1.275) | −3.058 (U) | **0.012*** |
| $f_h$ | 0.887 (0.342) | 0.814 (0.474) | 0.892 (U) | 0.691 |
| PCC (F3, F4) | 0.252 ± 0.333 | 0.335 ± 0.289 | −1.113 (*t*) | 0.666 |
| MI (F3, F4) | 0.184 (0.163) | 0.186 (0.304) | 0.276 (U) | 0.904 |
| PLV (F3, F4) | 0.241 (0.220) | 0.247 (0.273) | 0.457 (U) | 0.864 |
| PLI (F3, F4) | 0.851 (0.266) | 0.796 (0.228) | 0.849 (U) | 0.686 |
| PCC (P3, P4) | 0.415 ± 0.242 | 0.404 ± 0.267 | 0.158 (*t*) | 0.948 |
| MI (P3, P4) | 0.269 (0.361) | 0.228 (0.287) | 0.913 (U) | 0.722 |
| PLV (P3, P4) | 0.397 (0.355) | 0.321 (0.290) | 0.807 (U) | 0.683 |
| PLI (P3, P4) | 0.803 (0.209) | 0.842 (0.208) | −0.924 (U) | 0.771 |
| PCC (F3, P3) | 0.435 ± 0.296 | 0.457 ± 0.242 | −0.355 (*t*) | 0.918 |
| MI (F3, P3) | 0.313 (0.409) | 0.286 (0.348) | 0.786 (U) | 0.681 |
| PLV (F3, P3) | 0.442 ± 0.209 | 0.412 ± 0.203 | 0.583 (*t*) | 0.790 |
| PLI (F3, P3) | 0.854 (0.416) | 0.755 (0.257) | 0.903 (U) | 0.707 |
| PCC (F4, P4) | 0.412 ± 0.231 | 0.468 ± 0.226 | −0.997 (*t*) | 0.728 |
| MI (F4, P4) | 0.284 (0.315) | 0.287 (0.346) | −0.181 (U) | 0.948 |
| PLV (F4, P4) | 0.402 ± 0.185 | 0.422 ± 0.203 | −0.404 (*t*) | 0.894 |
| PLI (F4, P4) | 0.776 (0.181) | 0.840 (0.178) | −0.319 (U) | 0.929 |
| PCC (F3, P4) | 0.139 ± 0.334 | 0.272 ± 0.302 | −1.718 (*t*) | 0.360 |
| MI (F3, P4) | 0.174 (0.228) | 0.187 (0.151) | 0.149 (U) | 0.936 |
| PLV (F3, P4) | 0.230 (0.252) | 0.254 (0.222) | −0.117 (U) | 0.943 |
| PLI (F3, P4) | 0.886 ± 0. 095 | 0.713 ± 0.135 | 5.537 (*t*) | **<0.001*** |
| PCC (F4, P3) | 0.206 ± 0.268 | 0.248 ± 0.318 | −0.546 (*t*) | 0.803 |
| MI (F4, P3) | 0.171 (0.166) | 0.192 (0.228) | −0.595 (U) | 0.797 |
| PLV (F4, P3) | 0.209 (0.238) | 0.270 (0.220) | −0.701 (U) | 0.739 |
| PLI (F4, P3) | 0.882 (0.348) | 0.826 (0.204) | 0.287 (U) | 0.936 |

The symbol * indicates significance after correction. For EEG rhythms, powers or power ratios were calculated as frequency-domain features.

TABLE 3 Partial correlations between EEG feature variables and 60-day GOS, where RMS was used as a controlled variable.

| Variable | Rho | Value of *p* |
|---|---|---|
| BSR | −0.331 | **0.003*** |
| Activity | 0.077 | 0.496 |
| δ | −0.118 | 0.299 |
| θ | −0.111 | 0.328 |
| α | −0.075 | 0.508 |
| β | −0.077 | 0.498 |
| β/α | −0.321 | **0.004*** |
| PLI (F3, P4) | 0.224 | **0.046*** |

*Significant results ≤ 0.05.

TABLE 4 Spearman's correlations between EEG feature variables and 60-day GOS.

| Variable | Rho | Value of *p* |
|---|---|---|
| BSR | −0.547 | **<0.001*** |
| RMS | 0.578 | **<0.001*** |
| β/α | −0.422 | **<0.001*** |
| PLI (F3, P4) | 0.264 | **0.017*** |

*Significant results ≤ 0.05.

nine significant univariate features, and the result is identical to that in Table 6. Compared with the four significant features reserved after partial correlation, RMS and β/α were excluded from the final prediction model, which is also consistent with the MCA result where BSR, RMS, and β/α have identical discrimination scores along two dimensions.

The training and testing datasets were merged above in building coma outcome predictors, and hence the ROC curves reflecting prognostic performances were not considered in this combined cohort. To further illustrate the generalizability of the proposed method, *K*-fold cross-validation was performed. The involved 81 comatose patients were uniformly partitioned into $K = 3$ folds, and the distribution of outcome and etiology among 3 folds was as uniform as possible. In the *i*th round of cross-validation, the data in the *i*th fold formed the testing set, while the data in the rest folds were used for training the parameters of logistic regression. The prognostic characteristics of the coma outcome predictors built by EEG features in each round of 3-fold cross-validation are summarized in Table 7. It was found that in all rounds of cross-validation, all predictors achieved sensitivity ≥ 0.80 along with different levels of false positives. Among predictors using single EEG features, PLI (F3, P4) achieved the lowest false positives in all rounds of cross-validation. As expected, these single EEG feature-based predictors all suffered from medium to high false positives, indicating that cutoff probabilities can be set as larger than 0.5 for practical usage of these predictors, with degradation of sensitivity to some extent. It is noticed that the coma outcome predictor built by combining BSR and PLI (F3, P4) performed much better than those with single features in terms of low false positives. The cross-validated results on three testing datasets were merged, and then the comprehensive ROC curves of all predictors are plotted in Figure 4. Among all single variable-based predictors, PLI (F3, P4) achieved the largest AUC = 0.820 (95% CI: 0.716–0.925). Compared with these single variable-based predictors, the predictor with combined features, i.e., BSR + PLI (F3, P4), gave a larger AUC = 0.889 (95% CI: 0.819–0.960).

## 3.2 Subgroup analysis

Subgroup analyses were performed on patients with strokes as well as patients with TBI. The stroke subgroup included 29 patients, of whom 6 had favorable outcomes and 23 had unfavorable outcomes. By comparison of EEG features between favorable and unfavorable outcome groups and then partial correlation analysis with RMS controlled, BSR, RMS, θ/total, θ/δ, and PLI (F3, P4) were preserved as significant parameters. The results are summarized in Table 8, and it was found that raised BSR, suppressed RMS, raised θ/total, raised θ/δ, or suppressed PLI (F3, P4) may be associated with unfavorable coma outcome for stroke patients. Due to the limited number of patients in the strokes subgroup, cross-validation was not carried out in this group, and the prognostic characteristics of the significant variables or combined model were not evaluated by logistic regression.

The TBI subgroup included 33 patients, of whom 11 had favorable outcomes and 22 had unfavorable outcomes. By comparison between favorable and unfavorable outcome groups, only PLI (F3, P4) was found significant (corrected value of $p = 0.048$) in the TBI subgroup, and the comparative details are summarized in Table 9. Due to the limited number of patients in the TBI subgroup, cross-validation logistic regression was also not performed, and the corresponding prognostic characteristics were not displayed here.

# 4 Discussion

A retrospective study on coma prognosis in ICU using EEG feature-based predictors was conducted, with a limited frontoparietal EEG montage. This study was motivated by a common real-world requirement of a limited-montage EEG coupled with an automated algorithm and an important role played by frontoparietal network in underlying recovery from coma (Wu et al., 2015). Continuous EEG is recommended for the monitoring of critically ill patients (André-Obadia et al., 2015), and ACNS EEG descriptors have been studied in prognosis of coma or DoC in the past decade. ACNS EEG descriptors not only include some continuous variables but also concern the occurrence of some pathological patterns. The persistence of electrical status epilepticus was usually used as one ACNS EEG descriptor (Hirsch et al., 2021) and has been associated with a greater mortality rate (Rossetti et al., 2005), while in this study low occurrences of epileptiform discharges coincided in both groups. Hence, in this study, detection of epileptiform pattern was not considered, which usually depends on visual inspection or artificial intelligence (AI)-assisted methods trained on a large dataset. Standard interpretation of some ACNS EEG patterns still remains difficult in visual inspection (Westhall et al., 2015). Instead, in this study, features were extracted by quantitative analysis, and the EEG features in temporal domain (BSR and RMS), frequency domain (β/α), and spatial domain (PLI [F3, P4]) all showed their prognostic values by analysis of all patients, with a limited frontoparietal EEG montage.

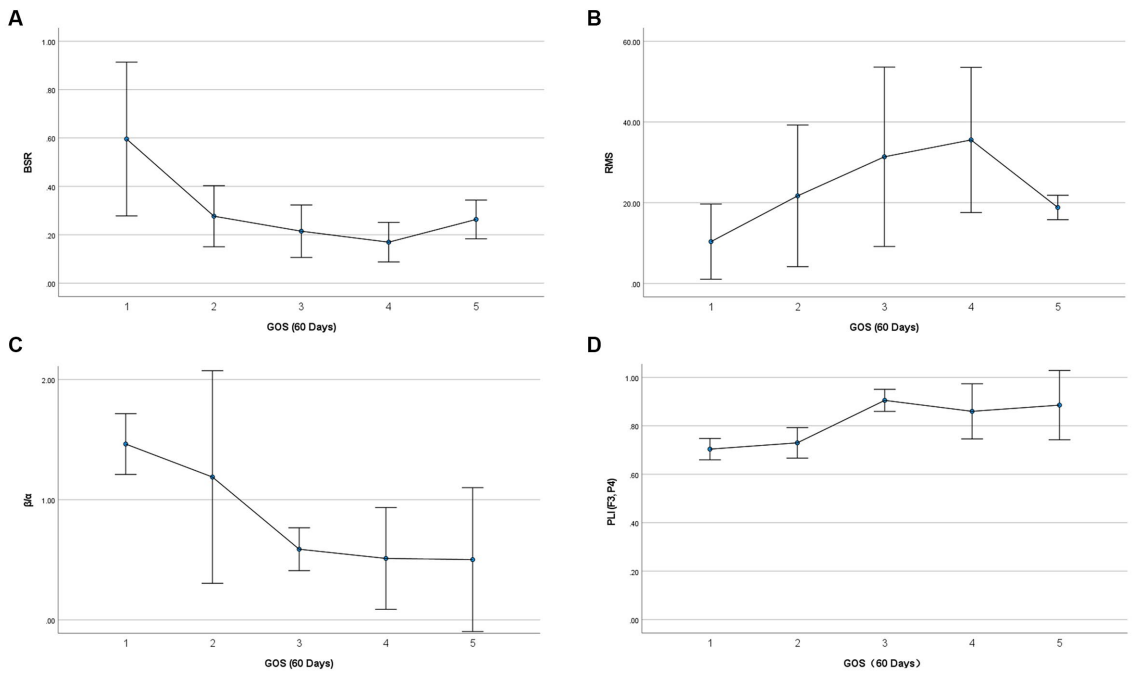


FIGURE 2
Relationship between selected EEG feature variables and 60-day GOS. Vertical error bars indicate the 95% confidence intervals, and the central points denote mean values.

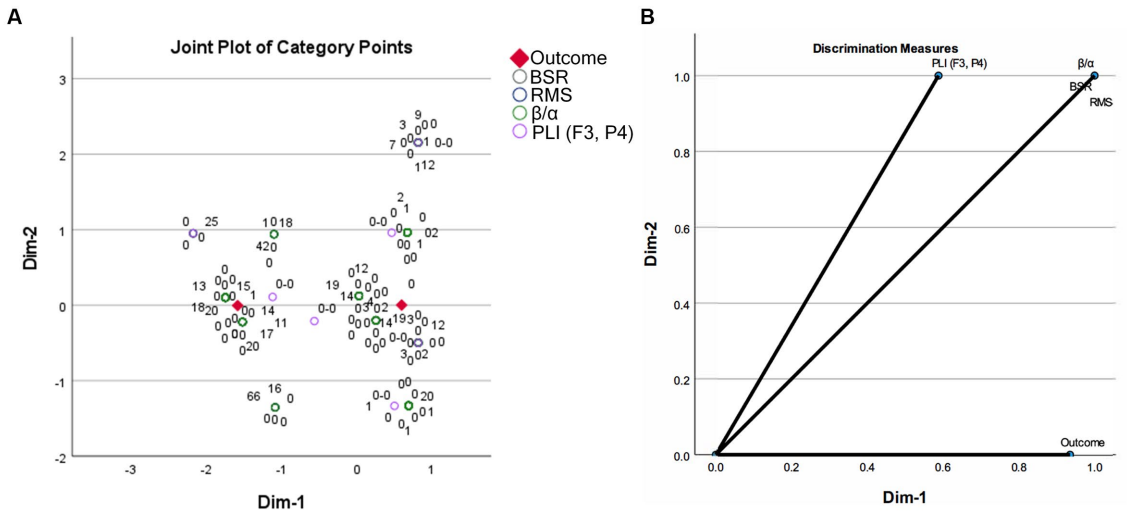


FIGURE 3
Multiple correspondence analysis results on the EEG features between two coma outcome groups: **(A)** joint plot of category points; **(B)** discrimination measures of all variables.

Timing of EEG recording after brain injury was considered important in the existing studies. In a prospective observational cohort study (Bauerschmidt et al., 2021), predictors established with quantitative EEG features at postanoxic days 4–6 achieved highest prediction accuracy. In our retrospective study, it was hard to control the EEG recording of all patients on the same days after brain injury. In spite of this, a comparison of timing of EEG recording between favorable and unfavorable outcome groups showed no significant difference, and the median EEG recording times are all within 1 week after brain injury.

In ACNS EEG descriptors, burst suppression and suppressed background EEG voltage (<10 μV) were usually considered as highly "malignant" patterns (Sandroni et al., 2014; Hofmeijer et al., 2016; Benarous et al., 2019; Backman et al., 2020; Guedes et al., 2020;

TABLE 5 Logistic regression results of single features predicting unfavorable outcomes.

| Variable | OR (95% CI) | Value of *p* |
|---|---|---|
| BSR | 1041.015 (9.395–115,347.064) | **<0.001*** |
| RMS | 0.942 (0.908–0.978) | **<0.001*** |
| β/α | 5.021 (1.612–15.639) | **0.002*** |
| PLI (F3, P4) | <0.001 (0.000–0.002) | **<0.001*** |

*Significant results ≤ 0.05.

TABLE 6 Multiple logistic regression results of combining EEG features for predicting unfavorable outcomes.

| Prediction model | Variable | OR (95% CI) | Value of *p* |
|---|---|---|---|
| BSR + PLI (F3, P4) | BSR | 470.161 (2.872–76957.79) | **0.018*** |
| | PLI (F3, P4) | <0.001 (0.000–0.008) | **<0.001*** |

*Significant results ≤ 0.05.

Scarpino et al., 2020; Nolan et al., 2021; Hoedemaekers et al., 2023), which were associated with poor neurological outcome. The presence of burst suppression was associated with an unfavorable prognosis with 100% specificity (Benarous et al., 2019). A suppressed EEG was considered as a reliable predictor of poor outcome if it persisted beyond 24 h after the arrest (Hoedemaekers et al., 2023). At 72 h, an isoelectric, suppression, or burst suppression pattern on EEG predicted poor outcome with 100% specificity (Scarpino et al., 2020). According to our analytical results on all patients as well as the strokes subgroup, among all temporal features, raised BSR and diminished RMS (i.e., suppressed voltage or diminished EEG power) were predictors of unfavorable outcome. This result is highly consistent with the conclusions in the literature. It is also noticed that BSR + PLI (F3, P4) formed the ultimate predictor by multiple logistic regression on all patients, indicating that diminished EEG power may be a reliable but not the best predictor for unfavorable coma outcome with our limited frontoparietal EEG montage.

Among the rhythms (δ, θ, α, and β), dominant δ and θ oscillations and attenuated α oscillations were considered as indicators for unfavorable outcome (Benarous et al., 2019; Kustermann et al., 2019; Scarpino et al., 2020). For analysis on all patients, the powers of δ, θ, α, and β all showed significance in comparison between groups, while they were then discarded according to the results of partial correlation analysis. As attenuation and overall suppression are negative prognostic factors, decreased power across frequency bands in the unfavorable outcome group can be found. The raised power ratio β/α was found associated with unfavorable coma outcome. α oscillations were known to appear only during wakefulness, reflecting basal forebrain, thalamus, and cortical interactions (Babiloni et al., 2009). β oscillations, or higher frequency rhythms, were associated with enhanced alertness following the onset of activity in cholinergic aggregates of the brainstem and basal forebrain. In the favorable outcome group, raised α and β oscillations can all be found, and it seems that α oscillations were dominant compared to β oscillations. For the analysis of the strokes subgroup, raised θ/total and raised θ/δ were found associated with unfavorable coma outcome, which is consistent with the existing conclusions. It seems that dominant θ oscillations may play a more important role in coma prognosis of the strokes subgroup among all frequency-domain features. For the TBI subgroup, none of the frequency-domain features were found significant. This result may be attributed to that localization and extent of the brain damage of various TBI patients were not considered in this study. As aforementioned, because sedation may lead to decreased voltage, decreased slow wave, or raised fast rhythm, all EEG monitoring were initiated at or later than 24 h after short-acting low-dose sedating medications in our ICU. Even so, the influence of sedation after 24 h cannot be totally avoided, and the bias may still exist.

Functional connectivity metrics were used as spatial features. One study showed that postanoxic comatose patients with poor neurological outcome had less dynamics of brain functional connectivity (Keijzer et al., 2021). In Zubler et al. (2015), patients with recovery on day 10 showed higher coherence across various bands. The study in Carrasco-Gómez et al. (2021) showed that postanoxic comatose patients with raised PLV in θ and α rhythms at 12 and 24 h were associated with favorable outcome. In a recent study (Jiang et al., 2023), the whole-brain connectivity based on coherence, phase synchronization, PLI, and cross-correlation was found to be significantly enhanced for favorable outcome. Full montage used to be employed in past studies, while in our study, a limited frontoparietal montage including four EEG channels was used. It was shown that even with a small number of frontoparietal channels, there is still a significant functional connectivity metric, PLI (F3, P4), achieving best prognosis performance among features in all domains. As an indicator of favorable outcome, raised PLI (F3, P4) may reflect enhanced connection between bilateral hemispheres, as well as increasing connection between cortical/subcortical structures in frontal and parietal lobes. It is known that the metabolic activity and functional connectivity within the anterior forebrain mesocircuit and the frontoparietal network are associated with the restoration of cerebral activity (Edlow et al., 2021). Inspired by this discovery, though with a reduced EEG montage including only four channels, the calculated functional connectivity metrics can reflect the frontoparietal network activities. By analysis of all patients as well as the strokes and TBI subgroups, it was found that during recovery from coma, restoration of frontoparietal network may be accompanied by an enhanced PLI (F3, P4).

There are few studies involving a combination of automatically extracted EEG features in temporal, frequency, and spatial domains. The temporal- and frequency-domain features were combined to give predictive values of the revised cerebral recovery index (rCRI) in Nagaraj et al. (2018), where random forest classification was used. Features in frequency domain and spatial domain were considered in prognosis of coma in Jiang et al. (2023), but they were not combined to form a better predictor. A comprehensive study in Carrasco-Gómez et al. (2021) used COH, PLV, and MI as spatial features and combined non-coupling features in Nagaraj et al. (2018) for outcome prediction of comatose patients, achieving a sensitivity of 73% at 100% specificity. The above studies used full EEG montages, which were believed to be essential for functional connectivity analysis in the past. However, full-montage monitoring has also been recognized as labor-intensive and resource-demanding, making it inconvenient for practical applications. Enlightened by Backman et al. (2020), a reduced montage consisting of only four frontoparietal EEG channels was used for monitoring.

10.3389/fnins.2023.1302318

TABLE 7 Prognostic performance of predictors built by EEG features in 3-fold cross-validation.

| Round of cross-validation | Predictors | Sensitivity (95% CI) | Specificity (95% CI) | PPV (95% CI) | NPV (95% CI) | False positives |
|---|---|---|---|---|---|---|
| 1 | BSR | 0.85 (0.64–0.95) | 0.14 (0.03–0.51) | 0.74 (0.54–0.87) | 0.25 (0.05–0.87) | 0.86 |
| | RMS | 1.00 (0.84–1.00) | 0.14 (0.03–0.51) | 0.77 (0.58–0.89) | 1.00 (0.21–1.00) | 0.86 |
| | β/α | 0.80 (0.58–0.92) | 0.00 (0.00–0.35) | 0.70 (0.49–0.84) | 0.00 (0.00–0.49) | 1.00 |
| | PLI (F3, P4) | 1.00 (0.84–1.00) | 0.57 (0.25–0.84) | 0.87 (0.68–0.95) | 1.00 (0.51–1.00) | 0.43 |
| | BSR + PLI (F3, P4) | 0.95 (0.76–0.99) | 0.71 (0.36–0.92) | 0.90 (0.71–0.97) | 0.83 (0.44–0.97) | 0.29 |
| 2 | BSR | 0.95 (0.75–0.99) | 0.25 (0.07–0.59) | 0.75 (0.55–0.88) | 0.67 (0.21–0.94) | 0.75 |
| | RMS | 0.95 (0.75–0.99) | 0.13 (0.02–0.47) | 0.72 (0.52–0.86) | 0.50 (0.09–0.91) | 0.87 |
| | β/α | 0.95 (0.75–0.99) | 0.13 (0.02–0.47) | 0.72 (0.52–0.86) | 0.50 (0.09–0.91) | 0.87 |
| | PLI (F3, P4) | 0.79 (0.57–0.91) | 0.38 (0.14–0.69) | 0.75 (0.53–0.89) | 0.43 (0.16–0.75) | 0.62 |
| | BSR + PLI (F3, P4) | 0.89 (0.69–0.97) | 0.63 (0.31–0.86) | 0.85 (0.64–0.95) | 0.71 (0.36–0.92) | 0.37 |
| 3 | BSR | 0.85 (0.64–0.95) | 0.57 (0.25–0.84) | 0.85 (0.64–0.95) | 0.57 (0.25–0.84) | 0.43 |
| | RMS | 0.95 (0.76–0.99) | 0.43 (0.16–0.75) | 0.83 (0.63–0.93) | 0.75 (0.30–0.95) | 0.57 |
| | β/α | 0.85 (0.64–0.95) | 0.57 (0.25–0.84) | 0.85 (0.64–0.95) | 0.57 (0.25–0.84) | 0.43 |
| | PLI (F3, P4) | 0.80 (0.58–0.92) | 0.71 (0.36–0.92) | 0.89 (0.67–0.97) | 0.56 (0.27–0.81) | 0.29 |
| | BSR + PLI (F3, P4) | 0.80 (0.58–0.92) | 0.86 (0.49–0.97) | 0.94 (0.73–0.99) | 0.60 (0.31–0.83) | 0.14 |

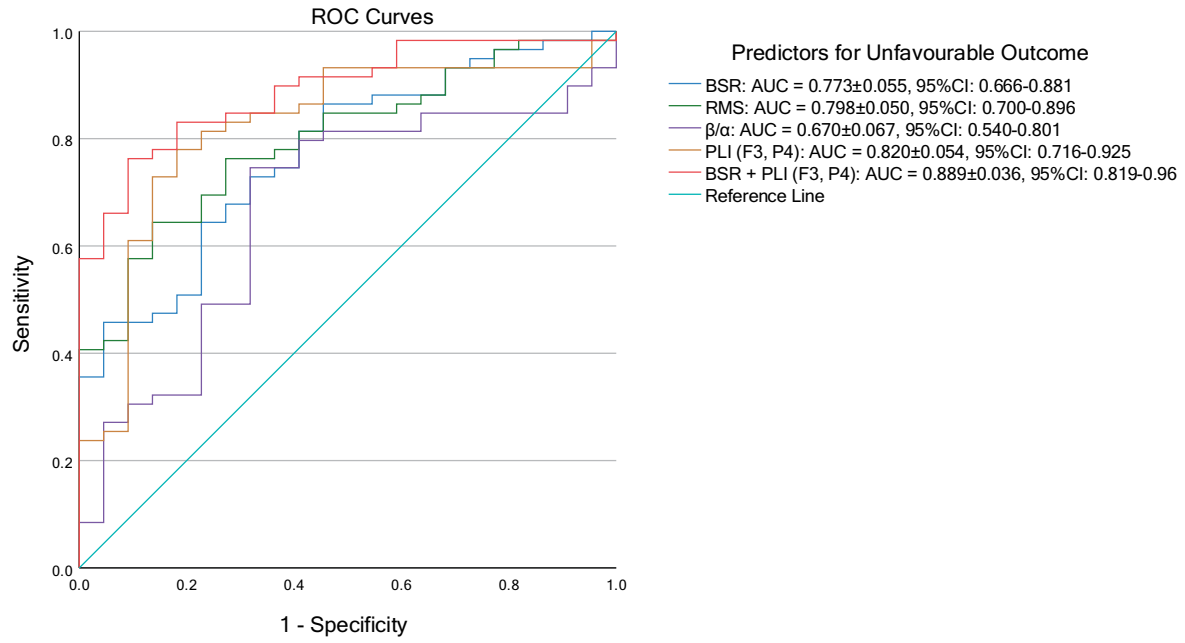


FIGURE 4
ROC curves of predictors for unfavorable coma outcomes established by 3-fold cross-validated logistic regression results.

Nevertheless, the results showed that features in all domains had their own prognostic value. Combination of features in various domains was found well suited to coma prognosis with reduced frontoparietal EEG montage, where the combination of BSR and PLI (F3, P4) brought great promotion of prognostic performance by analysis of all patients, compared with the predictors based on each feature alone.

The main limitation is that this study was a retrospective one. Whether and when a comatose patient should adopt bedside EEG monitoring was decided by the patient's physician, and a bias risk of subject selection may occur. The included critically ill patients had mixed etiologies, and the sample size in each subgroup was also limited, hindering performance evaluation of the coma outcome predictors established by logistic regression in each subgroup.

TABLE 8 Significant EEG features by comparison between favorable and unfavorable outcome groups in the stroke subgroup.

| Variable | Favorable outcome (GOS ≥ 3) | Unfavorable outcome (GOS ≤ 2) | Statistical value | Value of *p* (after correction) |
|---|---|---|---|---|
| | *n* = 6 | *n* = 23 | | |
| BSR | 0.140 (0.061) | 0.312 (0.172) | −3.284 (U) | <0.001* |
| RMS | 38.765 ± 16.93 | 15.046 ± 8.46 | 4.902 (t) | <0.001* |
| θ/total | 0.026 (0.013) | 0.052 (0.071) | −3.069 (U) | 0.048* |
| θ/δ | 0.028 (0.016) | 0.075 (0.118) | −2.907 (U) | 0.016* |
| PLI (F3, P4) | 0.877 ± 0.103 | 0.679 ± 0.130 | 3.455 (*t*) | 0.019* |

The symbol * indicates significance after correction. For EEG rhythms, powers or power ratios were calculated as frequency-domain features.

TABLE 9 The significant EEG feature derived by comparison between favorable and unfavorable outcome groups for analysis of the TBI subgroup.

| Variable | Favorable outcome (GOS ≥ 3) | Unfavorable outcome (GOS ≤ 2) | Statistical value | Value of *p* (after correction) |
|---|---|---|---|---|
| | *n* = 11 | *n* = 22 | | |
| PLI (F3, P4) | 0.880 ± 0.083 | 0.711 ± 0.126 | 4.022 (*t*) | 0.048* |

The symbol * indicates significance after correction.

Additionally, for each patient, EEG recording was not performed at an identical time after admission. The future work would be a prospective study, in which EEG recording would be performed at specific time nodes, to investigate the best time for EEG monitoring for coma prognosis with our limited frontoparietal montage. The sample size in each subgroup still needs to be enlarged in future research to facilitate the development and performance evaluation of separate coma outcome predictors for each subgroup. Furthermore, as in cross-validations, most of the models yielded low to moderate specificities, i.e., clinically significant false positive rates for predicting unfavorable outcomes; further investigation is still needed to translate the findings into a clinically applicable model.

## 5 Conclusion

For purpose of practical applications of quantitative EEG monitoring in coma prognosis in ICU, a limited frontoparietal EEG montage was used in this study. By using only four frontoparietal channels of EEG recording, features in temporal, frequency, and spatial domains all found their own prognostic value for critically ill comatose patients. By cross-validation analysis on all patients, the combination of EEG features in multiple domains outperformed the prediction based on the feature in each of the domains alone. The verified prognostic value in this study may lead to an easy-to-implement quantitative assessment approach in ICU and hold valuable implications for future automatic coma prognosis applications if further investigation is performed to control the false positive rates at a low level.

## Data availability statement

The original contributions presented in the study are included in the article/supplementary material, further inquiries can be directed to the corresponding author.

## Ethics statement

The studies involving humans were approved by the First People's Hospital of Kunshan Ethics Committee (Approval No. 00012098). The studies were conducted in accordance with the local legislation and institutional requirements. The participants provided their written informed consent to participate in this study.

## Author contributions

TT: Writing – original draft, Conceptualization, Investigation. SL: Conceptualization, Methodology. NH: Data curation, Methodology, Writing – review & editing. DX: Software, Methodology, Validation. CX: Formal Analysis, Resources. FL: Data curation, Investigation. QW: Formal Analysis, Visualization. YP: Writing – review & editing, Conceptualization, Funding acquisition, Project administration.

## Funding

The author(s) declare financial support was received for the research, authorship, and/or publication of this article. This study was supported by the Jiangsu University Medication Education Cooperation Key Innovation Project (JDY2022014), the Suzhou Youth Science and Technology Project (Grant KJXW2021074), the Suzhou Science and Technology Project (Grant SKYD2022096), as well as the Huzhou Science and Technology Project (Grant 2022GZ46).

## Conflict of interest

The authors declare that the research was conducted in the absence of any commercial or financial relationships that could be construed as a potential conflict of interest.

## Publisher's note



## References

André-Obadia, N., Parain, D., and Szurhaj, W. (2015). Continuous EEG monitoring in adults in the intensive care unit (ICU). *Neurophysiol. Clin.* 45, 39–46. doi: 10.1016/j.neucli.2014.11.003

André-Obadia, N., Zyss, J., Gavaret, M., Lefaucheur, J. P., Azabou, E., Boulogne, S., et al. (2018). Recommendations for the use of electroencephalography and evoked potentials in comatose patients. *Neurophysiol. Clin.* 48, 143–169. doi: 10.1016/j.neucli.2018.05.038

Babiloni, C., Sarà, M., Vecchio, F., Pistoia, F., Sebastiano, F., Onorati, P., et al. (2009). Cortical sources of resting-state alpha rhythms are abnormal in persistent vegetative state patients. *Clin. Neurophysiol.* 120, 719–729. doi: 10.1016/j.clinph.2009.02.157

Backman, S., Cronberg, T., Rosén, I., and Westhall, E. (2020). Reduced EEG montage has a high accuracy in the post cardiac arrest setting. *Clin. Neurophysiol.* 131, 2216–2223. doi: 10.1016/j.clinph.2020.06.021

Bauerschmidt, A., Eliseyev, A., Doyle, K. W., Velasquez, A., Egbebike, J., Chiu, W., et al. (2021). Predicting early recovery of consciousness after cardiac arrest supported by quantitative electroencephalography. *Resuscitation* 165, 130–137. doi: 10.1016/j.resuscitation.2021.06.008

Benarous, L., Gavaret, M., Soda Diop, M., Tobarias, J., de Ghaisne, S., de Bourmont, C., et al. (2019). Sources of interrater variability and prognostic value of standardized EEG features in post-anoxic coma after resuscitated cardiac arrest. *Clin. Neurophysiol. Pract.* 4, 20–26. doi: 10.1016/j.cnp.2018.12.001

Benghanem, S., Pruvost-Robieux, E., Bouchereau, E., Gavaret, M., and Cariou, A. (2022). Prognostication after cardiac arrest: how EEG and evoked potentials may improve the challenge. *Ann. Intensive Care* 12:111. doi: 10.1186/s13613-022-01083-9

Carrasco-Gómez, M., Keijzer, H. M., Ruijter, B. J., Bruña, R., Tjepkema-Cloostermans, M. C., Hofmeijer, J., et al. (2021). EEG functional connectivity contributes to outcome prediction of postanoxic coma. *Clin. Neurophysiol.* 132, 1312–1320. doi: 10.1016/j.clinph.2021.02.011

Chen, T., Lu, S., Qian, P., Chen, G., and Hu, N. (2020). An automatic detection method for 40-Hz auditory steady state response and its application in prognosis of comatose patients. *Clin. Neurophysiol.* 131, 703–715. doi: 10.1016/j.clinph.2020.01.002

Edlow, B. L., Claassen, J., Schiff, N. D., and Greer, D. M. (2021). Recovery from disorders of consciousness: mechanisms, prognosis and emerging therapies. *Nat. Rev. Neurol.* 17, 135–156. doi: 10.1038/s41582-020-00428-x

Fridman, E. A., Beattie, B. J., Broft, A., Laureys, S., and Schiff, N. D. (2014). Regional cerebral metabolic patterns demonstrate the role of anterior forebrain mesocircuit dysfunction in the severely injured brain. *Proc. Natl. Acad. Sci. U. S. A.* 111, 6473–6478. doi: 10.1073/pnas.1320969111

Giacino, J. T., Kalmar, K., and Whyte, J. (2004). The JFK coma recovery scale-revised: measurement characteristics and diagnostic utility. *Arch. Phys. Med. Rehabil.* 85, 2020–2029. doi: 10.1016/j.apmr.2004.02.033

Guedes, B., Manita, M., Peralta, A. R., Franco, A. C., Bento, L., and Bentes, C. (2020). Prognostic significance of specific EEG patterns after cardiac arrest in a Lisbon cohort. *Clin. Neurophysiol. Pract.* 5, 147–151. doi: 10.1016/j.cnp.2020.07.001

Hirsch, L. J., Fong, M. W., Leitinger, M., LaRoche, S. M., Beniczky, S., Abend, N. S., et al. (2021). American clinical neurophysiology Society's standardized critical care EEG terminology: 2021 version. *J. Clin. Neurophysiol.* 38, 1–29. doi: 10.1097/WNP.0000000000000806

Hjorth, B. (1970). EEG analysis based on time domain properties. *Electroencephalogr. Clin. Neurophysiol.* 29, 306–310. doi: 10.1016/0013-4694(70)90143-4

Hoedemaekers, C., Hofmeijer, J., and Horn, J. (2023). Value of EEG in outcome prediction of hypoxic-ischemic brain injury in the ICU: a narrative review. *Resuscitation* 189:109900. doi: 10.1016/j.resuscitation.2023.109900

Hofmeijer, J., Beernink, T. M. J., Bosch, F. H., Beishuizen, A., Tjepkema-Cloostermans, M. C., and van Putten, M. J. A. M. (2016). Early EEG contributes to multimodal outcome prediction of postanoxic coma. *Neurology* 86, 137–143. doi: 10.1212/WNL.0000000000001742

Jennett, B., and Bond, M. (1975). Assessment of outcome after severe brain damage: a practical scale. *Lancet* 305, 480–484. doi: 10.1016/s0140-6736(75)92830-5

Jiang, M., Niu, Z., Liu, G., Huang, H., Li, X., and Su, Y. (2023). Quantitative EEG and brain network analysis predicting awakening from early coma after cardiopulmonary resuscitation. *Neurol. Res.* 45, 969–978. doi: 10.1080/01616412.2023.2252281

Keijzer, H. M., Tjepkema-Cloostermans, M. C., Klijn, C. J. M., Blans, M., van Putten, M. J. A. M., and Hofmeijer, J. (2021). Dynamic functional connectivity of the EEG in relation to outcome of postanoxic coma. *Clin. Neurophysiol.* 132, 157–164. doi: 10.1016/j.clinph.2020.10.024

Khanmohammadi, S., Lauridosoto, O., Eisenman, L. N., Kummer, T. T., and Ching, S. N. (2018). Intrinsic network reactivity differentiates levels of consciousness in comatose patients. *Clin. Neurophysiol.* 129, 2296–2305. doi: 10.1016/j.clinph.2018.08.004

Kustermann, T., Nguissi, N. A. N., Pfeiffer, C., Haenggi, M., Kurmann, R., Zubler, F., et al. (2019). Electroencephalography-based power spectra allow coma outcome prediction within 24 h of cardiac arrest. *Resuscitation* 142, 162–167. doi: 10.1016/j.resuscitation.2019.05.021

Nagaraj, S. B., Tjepkema-Cloostermans, M. C., Ruijter, B. J., Hofmeijer, J., and van Putten, M. J. A. M. (2018). The revised cerebral recovery index improves predictions of neurological outcome after cardiac arrest. *Clin. Neurophysiol.* 129, 2557–2566. doi: 10.1016/j.clinph.2018.10.004

Nolan, J. P., Sandroni, C., Böttiger, B. W., Cariou, A., Cronberg, T., Friberg, H., et al. (2021). European resuscitation council and European Society of Intensive Care Medicine guidelines 2021: post-resuscitation care. *Intensive Care Med.* 47, 369–421. doi: 10.1016/j.resuscitation.2021.02.012

Owen, A. M. (2015). Using functional magnetic resonance imaging and electroencephalography to detect consciousness after severe brain injury. *Handb. Clin. Neurol.* 127, 277–293. doi: 10.1016/B978-0-444-52892-6.00018-0

Rossetti, A. O., Logroscino, G., and Bromfield, E. B. (2005). Refractory statusepilepticus: effect of treatment aggressiveness on prognosis. *Arch. Neurol.* 62, 1698–1702. doi: 10.1001/archneur.62.11.1698

Rothstein, T. L. (2000). The role of evoked potentials in anoxic-ischemic coma and severe brain trauma. *J. Clin. Neurophysiol.* 17, 486–497. doi: 10.1097/00004691-200009000-00007

Sandroni, C., Cariou, A., Cavallaro, F., Cronberg, T., Friberg, H., Hoedemaekers, C., et al. (2014). Prognostication in comatose survivors of cardiac arrest: an advisory statement from the European resuscitation council and the European Society of Intensive Care Medicine. *Intensive Care Med.* 40, 1816–1831. doi: 10.1007/s00134-014-3470-x

Scarpino, M., Carrai, R., Lolli, F., Lanzo, G., Spalletti, M., Valzania, F., et al. (2020). Neurophysiology for predicting good and poor neurological outcome at 12 and 72 h after cardiac arrest: the ProNeCA multicentre prospective study. *Resuscitation* 147, 95–103. doi: 10.1016/j.resuscitation.2019.11.014

Schnakers, C., Ledoux, D., Majerus, S., Damas, P., Damas, F., Lambermont, B., et al. (2008). Diagnostic and prognostic use of bispectral index in coma, vegetative state and related disorders. *Brain Inj.* 22, 926–931. doi: 10.1080/02699050802530565

Tsurukiri, J., Nagata, K., Okita, T., and Oomura, T. (2013). Middle latency auditory-evoked potential index for predicting the degree of consciousness of comatose patients in eds. *Am. J. Emerg. Med.* 31, 1556–1559. doi: 10.1016/j.ajem.2013.06.012

Westhall, E., Rosén, I., Rossetti, A. O., van Rootselaar, A. F., Kjaer, T. W., Friberg, H., et al. (2015). Interrater variability of EEG interpretation in comatose cardiac arrest patients. *Clin. Neurophysiol.* 126, 2397–2404. doi: 10.1016/j.clinph.2015.03.017

Wu, X., Zou, Q., Hu, J., Tang, W., Mao, Y., Gao, L., et al. (2015). Intrinsic functional connectivity patterns predict consciousness level and recovery outcome in acquired brain injury. *J. Neurosci.* 35, 12932–12946. doi: 10.1523/JNEUROSCI.0415-15.2015

Young, G. B. (2000). The EEG in coma. *J. Clin. Neurophysiol.* 17, 473–485. doi: 10.1097/00004691-200009000-00006

Zhang, Y., Su, Y., Xiao, S., and Liu, Y. (2015). Somatosensory and brainstem auditory evoked potentials assessed between 4 and 7 days after severe stroke onset predict unfavorable outcome. *Biomed. Res. Int.* 2015:196148. doi: 10.1155/2015/196148

Zheng, W. L., Amorim, E., Jing, J., Wu, O., Ghassemi, M., Lee, J. W., et al. (2022). Predicting neurological outcome from electroencephalogram dynamics in comatose patients after cardiac arrest with deep learning. *I.E.E.E. Trans. Biomed. Eng.* 69, 1813–1825. doi: 10.1109/TBME.2021.3139007

Zubler, F., Koenig, C., Steimer, A., Jakob, S. M., Schindler, K. A., and Gast, H. (2015). Prognostic and diagnostic value of EEG signal coupling measures in coma. *Clin. Neurophysiol.* 127, 2942–2952. doi: 10.1016/j.clinph.2015.08.022

frontiers | Frontiers in Neuroscience

TYPE Original Research
PUBLISHED 14 December 2023
DOI 10.3389/fnins.2023.1291608



OPEN ACCESS

EDITED BY
Fabien B. Wagner,
UMR5293 Institut des Maladies Neurodégénératives (IMN), France

REVIEWED BY
Guokai Zhang,
Tongji University, China
Kusumika Krori Dutta,
Ramaiah Institute of Technology, India

*CORRESPONDENCE
Jin Zhou
✉ sisun819@outlook.com
Changyong Wang
✉ wcy2000_zm@163.com

†These authors have contributed equally to this work

RECEIVED 09 September 2023
ACCEPTED 20 November 2023
PUBLISHED 14 December 2023

CITATION
Wang B, Yang X, Li S, Wang W, Ouyang Y, Zhou J and Wang C (2023) Automatic epileptic seizure detection based on EEG using a moth-flame optimization of one-dimensional convolutional neural networks.
*Front. Neurosci.* 17:1291608.
doi: 10.3389/fnins.2023.1291608



# Automatic epileptic seizure detection based on EEG using a moth-flame optimization of one-dimensional convolutional neural networks

Baozeng Wang[1†], Xingyi Yang[1,2†], Siwei Li[1], Wenbo Wang[1], Yichen Ouyang[1], Jin Zhou[1,3*] and Changyong Wang[1*]

[1]Beijing Institute of Basic Medical Sciences, Beijing, China, [2]State Key Laboratory of Intelligent Manufacturing System Technology, Beijing Institute of Electronic System Engineering, Beijing, China, [3]Chinese Institute for Brain Research, Beijing, China

**Introduction:** Frequent epileptic seizures can cause irreversible damage to the brains of patients. A potential therapeutic approach is to detect epileptic seizures early and provide artificial intervention to the patient. Currently, extracting electroencephalogram (EEG) features to detect epileptic seizures often requires tedious methods or the repeated adjustment of neural network hyperparameters, which can be time- consuming and demanding for researchers.

**Methods:** This study proposes an automatic detection model for an EEG based on moth-flame optimization (MFO) optimized one-dimensional convolutional neural networks (1D-CNN). First, according to the characteristics and need for early epileptic seizure detection, a data augmentation method for dividing an EEG into small samples is proposed. Second, the hyperparameters are tuned based on MFO and trained for an EEG. Finally, the softmax classifier is used to output EEG classification from a small-sample and single channel.

**Results:** The proposed model is evaluated with the Bonn EEG dataset, which verifies the feasibility of EEG classification problems that involve up to five classes, including healthy, preictal, and ictal EEG from various brain regions and individuals.

**Discussion:** Compared with existing advanced optimization algorithms, such as particle swarm optimization, genetic algorithm, and grey wolf optimizer, the superiority of the proposed model is further verified. The proposed model can be implemented into an automatic epileptic seizure detection system to detect seizures in clinical applications.

KEYWORDS

**moth-flame optimization, convolutional neural networks, hyperparameter optimization, electroencephalogram, epileptic seizure detection**

## 1 Introduction

According to the World Health Organization (2023), ~50 million people of all ages suffer from daily or weekly seizures worldwide, making it one of the most common neurological disorders. Epilepsy is a disorder caused by brain injury or abnormal discharges of neurons in the brain. Its characteristic is the repeated occurrence of transient brain dysfunction, mainly manifested as motor impairment, sensory impairment, or impaired consciousness, which can lead to limb convulsions, confusion, and even life-threatening situations (Bhattacharyya et al., 2017; Kong et al., 2022). The suddenness of epileptic seizures, as well as their self-sustained discharges lasting from a few minutes to several hours, greatly increases the

difficulty of detecting them. Therefore, it is clinically important to detect seizures early and intervene to reduce greater suffering for patients (Islam et al., 2022).

In general, in addition to computed tomography, single-photon emission computed tomography, and positron emission tomography, the convenient and fast conventional EEG remains the main means for detecting epileptic seizures (Nikodijevic et al., 2016). In 1964, the International League Against Epilepsy proposed a classification scheme for epileptic seizures for the first time (Caveness et al., 1964). According to the EEG of epileptic patients at different stages, it is clear that EEG features and clinical manifestations have equal diagnostic significance. To overcome the limitations of traditional epileptic seizure detection methods, the automatic detection of seizure type based on an EEG has become a hot research topic in the industry (Zhang Y. et al., 2022). In early clinical testing, epileptic seizure detection and analysis mainly rely on the visual observation and manual annotation of clinicians with specialized knowledge. This process is not only prone to omissions or errors but also increases the burden on doctors. Additionally, it has the disadvantage of relying on physician experience, individual subjectivity, and randomness to detect the presence or absence of epilepsy (Jing et al., 2021). Therefore, it is of great significance to seek automatic, efficient, and objective methods to classify multi-type epileptic EEGs.

Numerous researchers have conducted studies on the automatic detection of epileptic seizures based on an EEG. In the traditional detection methods of epileptic seizure, feature extraction of an EEG is performed using time-domain, frequency-domain, and time-frequency methods, which achieve good results (Hernández et al., 2018). However, these methods require domain expertise and complex EEG feature extraction tasks. Although the recognition model is relatively simple, it has a low recognition rate and poor generalization ability (Kurdthongmee, 2020). With the rapid development of deep learning technology, it is increasingly being applied in the field of brain science, such as neural signal recognition (Zhang H. et al., 2022), EEG classification (Li et al., 2022), and seizure detection (Hernández et al., 2018). In recent years, a plethora of deep learning algorithms, such as convolutional neural networks (CNN) (Sallam et al., 2018), artificial neural networks (Emami et al., 2019), recurrent neural networks (Bongiorni and Balbinot, 2020), long- and short-term memory artificial neural networks (LSTM) (Tsiouris et al., 2018), have received increasing attention and achieved encouraging results in epileptic seizure detection for two-class, three-class, four-class, and five-class classification problems (Zhao et al., 2020). In particular, the time-delay networks model proposed by Alexander Waibel et al. and the first one-dimensional CNN (1D-CNN) were successfully applied to speech recognition (Waibel, 1989). Subsequently, lots of 1D-CNN models have been applied to the research work of sequence models and achieved better recognition results for detecting epileptic seizures from an EEG (Wang et al., 2021; Ra et al., 2023). However, the performance of these deep neural network models directly depends on their hyperparameters (Aliyu and Lim, 2023; Lebal et al., 2023). In practice, the training models require the configuration of several, or even dozens, of network parameters (e.g., number of layers, number of cells, activation function, kernel size, and learning rate) (Kwasigroch et al., 2018; Chetana et al., 2023); the adjustment of these hyperparameters is extremely complex, requiring high-level technical expertise from the designers, and can be tedious and time-consuming. In addition, the optimization cost is high, and repeating the adjustment of hyperparameters through experiments is both inefficient and incomplete, often resulting in unsatisfactory results (Irmak, 2020). Thus, ensuring that the deep neural network framework adapts to a specific dataset and achieves optimal generalization remains one of the important tasks in optimizing the hyperparameters.

Although deep learning models can achieve better epilepsy recognition, no model can optimally adapt to all datasets. However, the optimization of deep learning models has posed new challenges in the field of model hyperparameter tuning (Hoang and Kang, 2019), and scholars from various countries have conducted extensive research. The recognition rate is stable and robust based on time-invariant features extracted from a single-channel EEG using two CNNs for patients with seizures (Zhao and Wang, 2020). The particle swarm optimization algorithm (PSO) is used to adaptively optimize the parameters of the CNN model, and the PSO-CNN model is built to improve the recognition rate of epileptic seizure detection (Lv et al., 2022). Based on the confidence function defined by the complex normal distribution, a new PSO variant named cPSO-CNN is proposed to determine the hyperparameter configuration of CNN (Wang et al., 2019). Similarly, the proposed neural network optimization method has a better performance by optimizing CNN hyperparameters using the genetic algorithm (GA) (Fatyanosa and Aritsugi, 2020). The generalized CNN extracts the most relevant features that can be interpreted and processed based on the Grey Wolf Algorithm (GWO). It has achieved the detection of an abnormal EEG associated with epilepsy, thereby improving the classification accuracy (Thanuja et al., 2023). Usually, numerous hyperparameters can produce a better performance. However, the PSO evaluates and tests the efficiency of forming models with different parameter combinations, which is not only inefficient and time-consuming but also easily falls into the local optimum (Mezzah and Tari, 2023). Therefore, it is necessary to investigate an efficient search solution that can quickly and effectively find an optimal hyperparameter combination (Kim et al., 2020). The moth-flame optimization algorithm (MFO) is a novel meta-heuristic swarm intelligence method that has good global optimization ability and faster convergence speed and optimality seeking as well as few parameters and a simple structure. It has received extensive attention from scholars all over the world (Mirjalili, 2015) and has been successfully applied to many optimization problems, such as scheduling (Elsakaan et al., 2018), parameter estimation (Hazir et al., 2018), and classification (Zawbaa et al., 2016; Shehab et al., 2020). The effectiveness of this optimization algorithm in solving different complex problems in a reasonable time has been demonstrated (Khurma et al., 2020). So far, no effective method has been found to optimize the hyperparameters of 1D-CNN for seizure detection based on MFO. Therefore, the aforementioned research results motivated us to propose a new method for automatically optimizing 1D-CNN hyperparameters based on MFO, without manually adjusting the network structure and hyperparameters.

The main motivation behind the proposed MFO is to find the optimal combination of hyperparameters without manually adjusting the hyperparameters of the network structure. The MFO is then applied to existing CNN models to adjust the hyperparameters. This enables the automatic detection of seizures in a small-sample single-channel EEG and improves the accuracy and universality of the seizure detection system.

# 2 Materials and methods

## 2.1 Epileptic seizure detection system based on 1D-CNN

The composition diagram of an epileptic seizure detection system based on the optimized 1D-CNN neural network detector in clinical applications is shown in Figure 1. The system consists of four main modules: (1) the EEG input module, which divides the input EEG into signal segments with a fixed size; (2) the optimization module, which optimizes the 1D-CNN model using the MFO; (3) the EEG feature extraction module, which passes the intercepted signal segments to the optimized 1D-CNN model and extracts EEG features; and (4) the fusion decision module, which inputs the EEG feature matrix to the softmax classifier layer, obtains the corresponding types of the input EEG, and presents the detection result to the doctor or issues an alarm.

The core part of the epileptic seizure detection system is the optimization algorithm in Figure 1. First, the MFO is used to automatically optimize the hyperparameters of the 1D-CNN model. Second, the proposed model is used to automatically classify the EEG time series of these five classes.

## 2.2 Dataset and data partitioning

### 2.2.1 Description of the EEG dataset

The available EEG dataset produced by the University of Bonn has the characteristics of diversity, large scale, high openness, and widespread use (Andrzejak et al., 2001). This database consists of five different subsets ($Z$, $O$, $N$, $F$, and $S$) denoted by $A \sim E$, respectively. The subsets $A$ and $B$ are collected using the international $10-20$ system from five healthy individuals in an awake state with eyes open and eyes closed, respectively. The datasets $C$, $D$, and $E$ are derived from EEG archives of presurgical diagnoses of five patients. The datasets $C$ and $D$ are acquired separately from the hippocampal structure of the opposite hemisphere and within the epileptogenic zone during seizure-free intervals. Then, dataset $E$ contains EEG activity during seizure from five patients (Xu et al., 2020).

Each subset contains 100 single-channel EEG segments with a duration of 23.6 s, and each segment has 4,097 samples with a sampling frequency of 173.61 Hz. These subsets are collected through a 128-channel amplifier system using an average standard reference. A bandpass filter is utilized to remove the noise and artifacts, with low and high cutoff frequencies of 0.53 and 40 Hz respectively set.

To illustrate these datasets, the EEG time series of these five classes corresponding to a certain channel is depicted in Figure 2.

The EEG characteristics corresponding to each EEG subset can be observed. The EEG waveforms are almost identical in datasets $A$ and $B$ from five healthy individuals. Similarly, the EEG amplitudes between datasets $C$ and $D$ are not substantially different, which increases the difficulty in classifying the EEG. By contrast, the EEG voltages in dataset $E$ exceed $1,000\ \mu$V during the ictal phase, which is considerably higher than that of the other EEG datasets.

### 2.2.2 EEG data augmentation

To extract effective EEG features from a smaller sample, a fixed sliding window is used to divide the EEG time series into segments (Zhang et al., 2017; Ullah et al., 2018). It is important to consider that the data augmentation not only shortens the duration of the EEG segment but also enables timely intervention for epileptic seizures. Additionally, it reduces data redundancy and computational load, making data processing more efficient. This study proposes a sliding window technique with a fixed sliding window of 1 s, as shown in Figure 3.

To increase the number of EEG samples, a single-channel EEG segment of each class is divided every 4,097 data points into 23 chunks, and the 2,300 chunks of EEG are obtained for each EEG subset. So a total of 11,500 samples from five classes are used to evaluate the performance of the proposed method.

## 2.3 Building the MFO-1D-CNN model

### 2.3.1 Building a 1D-CNN architecture

Owing to the fact that an EEG is time-series data, a 1D-CNN model is selected for detecting the EEG to improve the accuracy and generalization ability. This network includes the input layer, convolutional layer, pooling layer, dropout layer, and fully connected layer. Unlike the 2D-CNN model, the 1D-CNN model has the advantages of few parameters, easy training, and low computational effort, as shown in Figure 4.

First, it provides alternating layers of convolutional, batch normalization, dropout, and maximum pooling to extract more complex EEG features. Second, it also reduces the dimensionality of EEG features and ensures that some neurons are randomly discarded to prevent overfitting of the detection model. Then, the tiling layer is used to convert the EEG feature vector into 1D data to the fully connected layer. Finally, the result is output by the multi-classifier of the softmax layer.

To improve the detection effectiveness, this study focuses on optimizing the hyperparameters of the 1D-CNN model (Ullah et al., 2018; Yu et al., 2022). The related layers of convolutional, pooling, and fully connected are constructed sequentially as follows.

Each neuron is only associated with a local region of the neuron in the previous layer, which serves to divide the neural network into smaller parts. Then, the EEG features are extracted by the convolutional kernel to reduce the complexity of the network. The

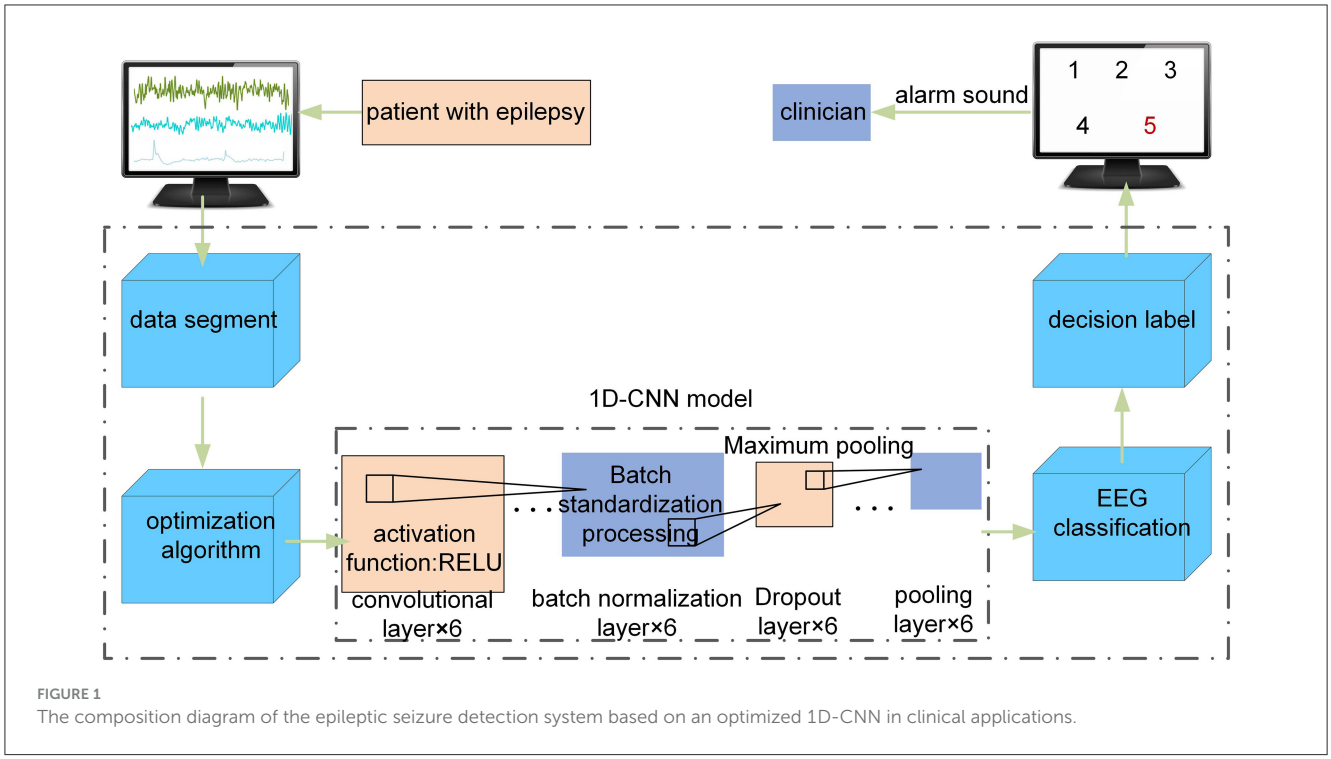


FIGURE 1
The composition diagram of the epileptic seizure detection system based on an optimized 1D-CNN in clinical applications.

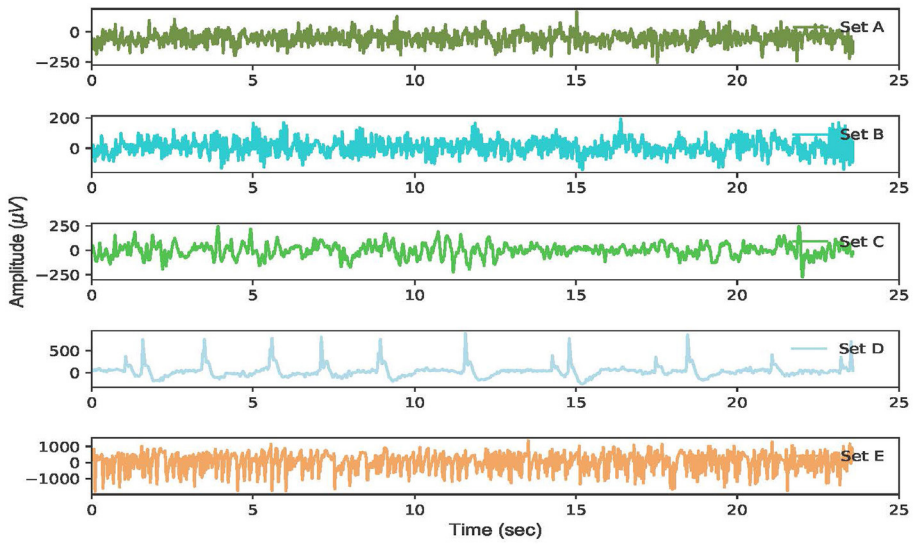


FIGURE 2
The raw EEG signal waveform corresponding to each of the five datasets of the Bonn dataset.

convolutional model with $l$ layers is characterized as:

$$y_j^l = f(\sum_{i \in M_j} x_i^{l-1} \omega_{ij}^l + b_i^l), j = 1, 2, ..., M \quad (1)$$

Where $l$ represents the current layer network; $j$ is the previous layer network; $x_i^{l-1}$ is the $i^{th}$ feature mapping of the previous layer; $\omega_{ij}^l$ represents the convolution kernel of the $i^{th}$ and $j^{th}$ layers; $b_i^l$ is the bias unit; $y_j^l$ is the $j^{th}$ feature mapping of the current layer; and $f(\bullet)$ is the activation function.

A pooling layer is generally set behind the convolutional layer to capture the key information. The pooling layers mainly include maximum pooling and average pooling, and the mathematical model of the pooling process is given by

$$y_j^l = f[\text{down}(y_j^{l-1}) + b_j^l] \quad (2)$$

Where *down*() is the pooling function.

Each neuron of the fully connected layer is connected to the neuron of the previous layer to extract EEG features. After the

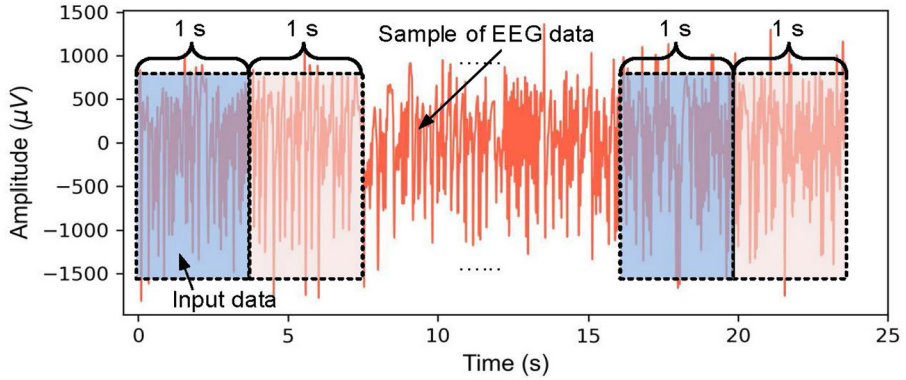


FIGURE 3
Schematic diagram of EEG data augmentation based on a fixed sliding window.

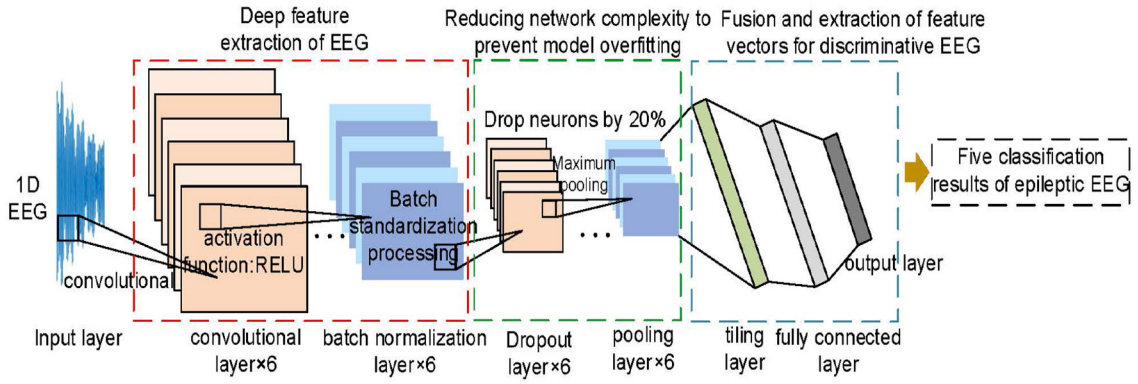


FIGURE 4
Schematic diagram of the 1D-CNN model for detecting EEG.

stacking of several convolutional and pooling layers, one or more fully connected layers are bridged by a tiling layer, and then the mathematical model of the fully connected layer is calculated as:

$$h(x^l) = f(\omega x^{l-1} + b) \tag{3}$$

Where $x^{l-1}$ is the input of the fully connected layer, that is, the output of the previous $l-1$ layer, $h(x^l)$ is the output of the fully connected layer, and $\omega$ and $b$ are the weight coefficients and bias values of the neurons, respectively.

Finally, the EEG is classified by the full connection layer using the softmax activation function. The final layer reduces the vector of length 178–5. The maximum probability of the corresponding types is obtained, and the different EEG classifications are automatically identified.

### 2.3.2 The hyperparameters of the 1D-CNN model

The hyperparameters are generally classified into two types, including network structure-related and network training-related (Kolar et al., 2021). Among them, the main hyperparameters related to network structure include the number of convolution kernels—the number of filters, convolutional kernel size—the filter size, number of hidden layers—a layer of neurons between the input and output layers, dropout—random deactivation of a certain percentage of neurons, and activation function—whether a neuron should be activated or not. The other hyperparameters include loss function—a measure of how far the predictions deviate from the true value, batch size—the selection of a sample set to update the weights, the number of iterations—the number of times the entire process is repeated, and learning rate—an adjustment parameter in optimization algorithms.

Hyperparameter selection has a significant impact on the performance of the detection model, which takes more time and requires an enriching experience with manual hyperparameter tuning. However, it is difficult to find the optimal set of hyperparameters through manual experience alone; hyperparameter selection can be quickly searched using intelligent optimization algorithms.

## 2.4 Building the MFO optimization model

The MFO takes the moth position as the optimization problem to be solved using the moth lateral positioning mechanism. The

algorithm is good at local development and global searching and is highly robust when solving optimization problems and convergence (Mirjalili, 2015).

In the MFO, the moths and flames are the candidate solutions for the algorithm; the flames are the optimal locations and the moths are the motives that keep moving around the search space. Suppose there are $n$ moths $X = [x_1, x_2, ..., x_n]^T$ and the $i$-th moth is $x_i = [x_{i,1}, x_{i,2}, ...x_{i,d}]^T$, where $d$ is the dimension of the optimization parameter. The flame is the best position obtained by the current iteration, then the $i$-th flame is $f_i = [f_{i,1}, f_{i,2}, ..f_{i,d}]^T$.

The MFO is inspired by the behavior of natural moths, and the individual moths iteratively update their position around a flame until the best solution is found. The mathematical description is divided into flame-catching and flame-discarding behavior.

Flame-catching behavior: moths $M_i$ with phototropic behavior in nature move toward the nearest flame $F_i$ to themselves, and the mathematical model of its logarithmic spiral flame-catching trajectory is as follows:

$$S(M_i, F_i) = D_i \cdot e^{bt} \cdot \cos(2\pi t) + F_j \tag{4}$$

Where $S(M_i, F_i)$ is the updated moth position, $b$ denotes the constant associated with the spiral shape, $t$ is a random number in the interval $[-1, 1]$, and $D_i = M_i - F_i$ denotes the distance between the moth $M_i$ and the flame $F_i$.

Flame abandonment behavior: the adaptive mechanism is used to reduce the number of flames, and the mathematical model of flame abandonment operation is as follows:

$$F_{flame} = round(N - t * \frac{N-1}{T}) \tag{5}$$

Where $t$ and $T$ are the current and maximum iterations, respectively, and $N$ is the maximum number of flames.

## 2.5 Hyperparameter of 1D-CNN based on MFO

The hyperparameters of 1D-CNN are still a major obstacle for a small-sample EEG. Setting appropriate hyperparameters not only improves the accuracy of the detection model but also accelerates the speed of model training. Therefore, the MFO automatically optimizes the hyperparameters of the 1D-CNN model, which can improve the feature extraction ability, training efficiency, and detection accuracy. The MFO-1D-CNN model, which combines the MFO with a 1D-CNN model, is proposed, as shown in Figure 5.

The specific process of hyperparameter tuning for the 1D-CNN model using MFO is as follows:

Step 1 initializes the 1D-CNN structure and determines the hyperparameters to be optimized by the MFO. In this work, the 6-dimensional hyperparameter vector is constructed from

$$\lambda = [\delta, s, a, d, \eta, m] \tag{6}$$

where $\lambda$ is the optimized hyperparameter vector, $\delta$ is the initial number of kernels, $s$ is the size of the kernel, $a$ is the activation function, $d$ is the probability value of dropped neurons in the Dropout layer, $\eta$ is the learning rate, and $m$ is the pooling window size.

Step 2 adopts the cross-entropy loss function as the objective function and determines the optimization objective functions and restricted conditions; then, the mathematical model is:

$$\min L(\hat{y}, y) = -\sum_{j=1}^{n} y_j \log \hat{y_j} \tag{7}$$

where $y$ is the predicted result of the $j_{th}$ type, $y_j$ is the true result of the $j_{th}$ type, $n$ is the total number of types, and $L$ is the error between the predicted and true value.

The constraints on the mathematical model using the cross-entropy loss function are:

$$\begin{cases} 40 \le \delta \le 100, \delta \in N \\ 1 \le s \le 20, s \in N \\ 0 \le a \le 2, a \in Z \\ 0 \le d \le 0.6 \\ 0.00001 \le \eta < 1 \\ 2 \le m \le 20 \end{cases} \tag{8}$$

where $a = 0$, $a = 1$, and $a = 2$ represent the ReLU, sigmoid, and tanh activation functions, respectively.

Step 3 initializes the MFO by setting parameters based on the objective function and constraint conditions and initializes the position of moths in the search space.

Step 4 calculates the distance between the moth and the flame according to the spiral function to update the position of the moth, as shown in Equation (4).

Step 5 calculates the fitness value according to the updated position of the moth and ranks the fitness values in increasing order. The moth position corresponding to the better fitness value is selected as the position of the next generation flame, and the number of flames is updated through the adaptive reduction mechanism, as shown in Equation (5).

Step 6 obtains the position of the optimal flame, which is the current optimal value of each hyperparameter, and the adaptation value of the optimal flame is the current minimum loss value after 1D-CNN training.

Step 7 checks whether the MFO has reached the maximum number of iterations. If not, it returns to step 4. If yes, it sets the optimized hyperparameters to the 1D-CNN network structure and determines the number of epochs, sample batch size, and weight update optimizer.

Step 8 calculates the error between the actual and expected target value by forward propagation based on the EEG dataset and adjusts the weights and biases in the network layer by layer through backpropagation.

Step 9 calculates the validation loss value and accuracy of the current network using the validation dataset at the end of each training cycle. If the validation accuracy is greater than the current optimal value, the currently trained completed network is saved as the optimal model.

Step 10 calculates the number of trainings; if the number is less than or equal to epoch, the process returns to step 8 to continue a new training. If the number is greater than an epoch, this step inputs the test dataset into the saved optimal model and classifies the EEG according to the detection results.

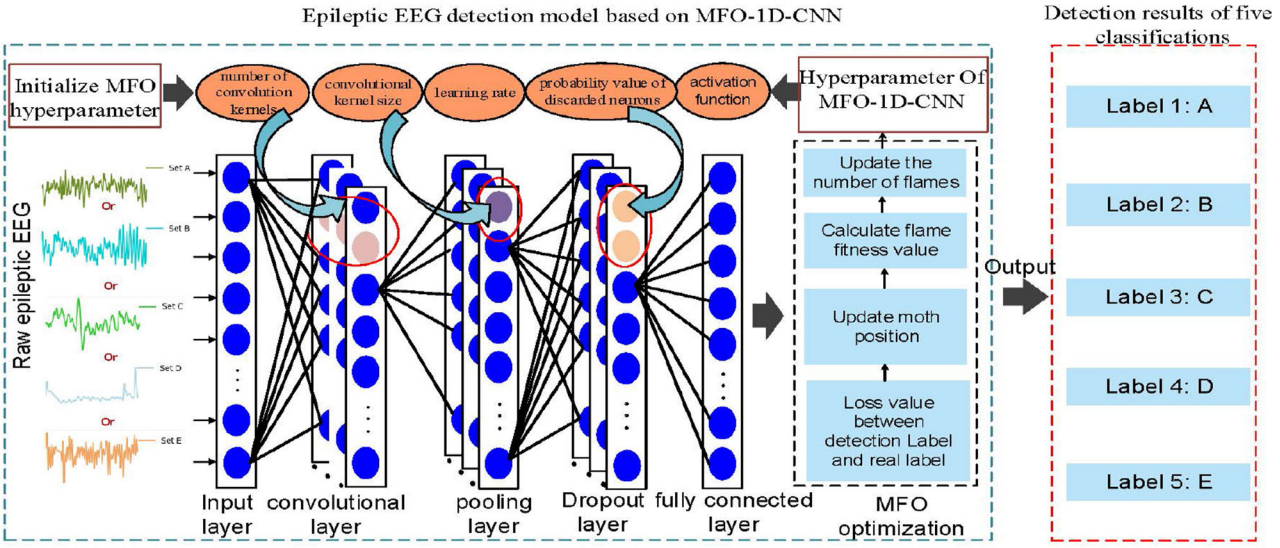


FIGURE 5
The 1D-CNN hyperparameter tuning based on MFO for detecting EEG classifications.

# 3 Experiment setup

## 3.1 Model evaluation and implementation

To achieve a comprehensive evaluation with the optimized 1D-CNN model, the EEG datasets are split at an 80-20 ratio of training and testing data. The tensorflow 2.6.0 in a Python 3.7.13 environment creates the detection models for a Windows workstation equipped with an Intel Xeon Silver 4215*R* CPU, a 64GB memory, and a GTX3080 GPU.

## 3.2 Evaluation metrics

The most important and commonly used parameters for evaluating performance mainly include accuracy, precision, recall, and F1-score (Liu et al., 2020). Among them, accuracy is used to measure the recognition ability of the detection model, precision is used to measure the model's recognition ability to identify an EEG correctly, recall is used to measure the model's ability to find EEGs that are actually positive and predicted to be positive, and F1-score is used as a comprehensive index to comprehensively evaluate a classifier by balancing the effects of accuracy and recall. The specific formulas for evaluating the performance of the detection model are as follows:

$$Accuracy = \frac{TP + TN}{TP + TN + FP + FN} \times 100 \quad (9)$$

$$Recall = \frac{TP}{TP + FN} \times 100 \quad (10)$$

$$Precision = \frac{TP}{TP + FP} \times 100 \quad (11)$$

$$F1 - score = \frac{2 \times recall \times precision}{recall + precision} \times 100 \quad (12)$$

where *TP* (true positive) represents the number of EEG samples correctly classified as positive, *TN* (true negative) represents the number of EEG samples correctly classified as negative, *FP* (false positive) represents the number of EEG samples incorrectly classified as positive, and *FN* (false negative) represents the number of EEG samples incorrectly classified as negative.

# 4 Results and discussion

## 4.1 The effect of different batch sizes on the CNN detection rate

The batch size affects the accuracy of the estimate of the error gradient in the process of training neural networks. If the batch size is too small, it takes too much time, and the gradient oscillates severely, which is not conducive to convergence. However, if the batch size is too large, it definitely causes memory overflow. Meanwhile, there is no gradient descent in the gradient direction of different batches, making it easy to fall into the local minimum (Lai et al., 2022). The hyperparameters of the 1D-CNN are optimized based on MFO, and the batch sizes are set to 32, 64, 128, 256, 512, and 1, 024. The new models are evaluated using the detection rate with different batch sizes, and the loss curves under different batch size conditions are shown in Figure 6.

The loss curve tends to stabilize with batch sizes of 32 or 64 when the number of iterations reaches 200. The batch size continues to increase to 128 or 256, and there is a trend of decreasing the loss value. When the batch size is 256, the loss value is the smallest, and when the batch size is further increased to 512 or 1, 024, the trend of the loss value is not decreasing but increasing. The optimal model of the 1D-CNN framework is obtained with a batch size of 256. In addition, the loss value stabilizes at a certain

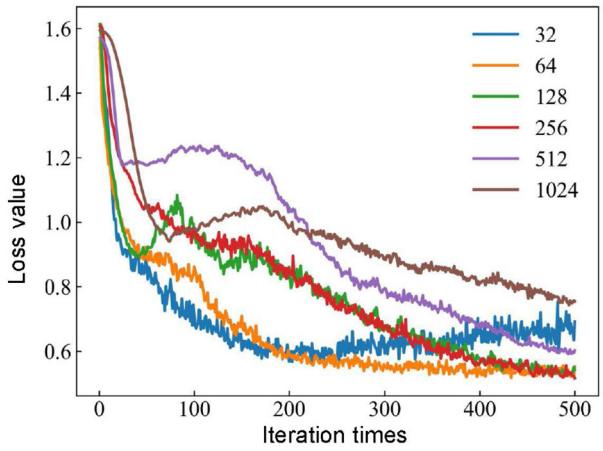


FIGURE 6
Influence of different batch size conditions for loss curves based on the MFO-1D-CNN model.

value when the number of iterations reaches 500. Therefore, a good balance between computational efficiency and convergence speed is obtained when the batch size is 256 and the number of iterations reaches 500.

## 4.2 Hyperparameter optimization of the 1D-CNN model

To obtain the optimal solution for improving the detection rate based on a 1D-CNN model, the combination of 6 hyperparameters is considered as the overall dataset, which includes the number of convolution kernels $\delta$, the size of the convolution kernels $s$, the activation function $a$, the probability value of discarded neurons $d$, the learning rate $\eta$, and the size of the pooling window $m$. Taking the five-class EEG classification as an example, the neural network hyperparameters are set to achieve the optimal value.

The parameters of the 1D-CNN model can be set to convolutional layers, normalization layers, and dropout layers. The pooling layer uses maximum pooling followed by a tiling layer and a fully connected layer to construct the model of epileptic seizure detection. In addition, the parameters of the 1D-CNN model optimized by PSO are set as follows: the maximum speed of the particle update is 6, the individual learning factor $c1$ is 2, the population learning factor $c2$ is 2, the maximum value of the inertia weight is 0.9, and the minimum value is 0.2. The parameters of the 1D-CNN model optimized by GWO are set as follows: the wolf swarm size is 20, the variable dimension is 6, and the maximum number of iterations is 100. The parameters of the 1D-CNN model optimized by GA are set as follows: the population size is 20, the crossover probability is 1, and the variation probability is 0.01. The parameters of the 1D-CNN model optimized by MFO are set as follows: the moth population size is 20, the variable dimension is 6, and the maximum number of iterations is 30. Through the above optimization parameter settings, the optimal value of the 1D-CNN model is obtained using multiple optimization algorithms, which are iterated 4,000 times. The different hyperparameters of the 1D-CNN model are shown in Table 1.

TABLE 1 The optimal hyperparameters of 1D-CNN model for the different optimization algorithms.

| Model | $\delta$ | $s$ | $a$ | $d$ | $\eta$ | $m$ |
|---|---|---|---|---|---|---|
| 1D-CNN | 40 | 6 | 0 | 3 | 3 | 5 |
| PSO-1D-CNN | 60 | 17 | 0 | 1 | 1 | 2 |
| GA-1D-CNN | 80 | 18 | 0 | 2 | 2 | 2 |
| GWO-1D-CNN | 79 | 12 | 0 | 1 | 1 | 2 |
| MFO-1D-CNN | 50 | 10 | 0 | 2 | 2 | 2 |

The results of six hyperparameters obtained with different optimization algorithms show obvious differences, and it is very important to select appropriate hyperparameter settings for epileptic seizure detection. Therefore, it is recommended to try multiple optimization algorithms and tune the hyperparameters to find the best training strategy. Therefore, the initial six hyperparameter values are set separately according to the detection results of the 1D-CNN model. In addition, the Adam optimization algorithm is used in the training process, which is an improvement on the random gradient descent algorithm and usually achieves good performance.

## 4.3 The effect of epileptic seizure detection with different optimization algorithms

As each combination of network hyperparameters represents a new model, it takes a lot of time and effort to randomly search for each network parameter. Then, tuning hyperparameters manually is even more time-consuming, and improving efficiency is highly dependent on personal experience. Therefore, this study uses optimization algorithms to find a method that can replace manual parameter adjustment for automatically and effectively finding appropriate network parameters.

To verify the effectiveness of the MFO-1D-CNN model for EEG detection, the representative methods, such as 1D-CNN, PSO-1D-CNN, GA-1D-CNN, and GWO-1D-CNN, are selected to detect seizure using the same EEG dataset and segment with a length of 1 s is selected from the Bonn EEG dataset. As the confusion matrix can be used to summarize the performance of the detection model, the confusion matrices of the five recognition algorithms are compared and analyzed, as shown in Figure 7.

The kappa values calculated by a confusion matrix are used to measure the performance of the detection model. The kappa values corresponding to the 1D-CNN, PSO-1D-CNN, GA-1D-CNN, GWO-1D-CNN, and MFO-1D-CNN models are 0.7300, 0.8717, 0.8600, 0.8697, and 0.8722, respectively. The Kappa level of the optimized 1D-CNN models is almost perfect except for the highly consistent Kappa level of the 1D-CNN model. Although the Kappa levels of all optimization methods perform very similarly, the Kappa values of the MFO-1D-CNN model can still maintain the highest among optimization methods.

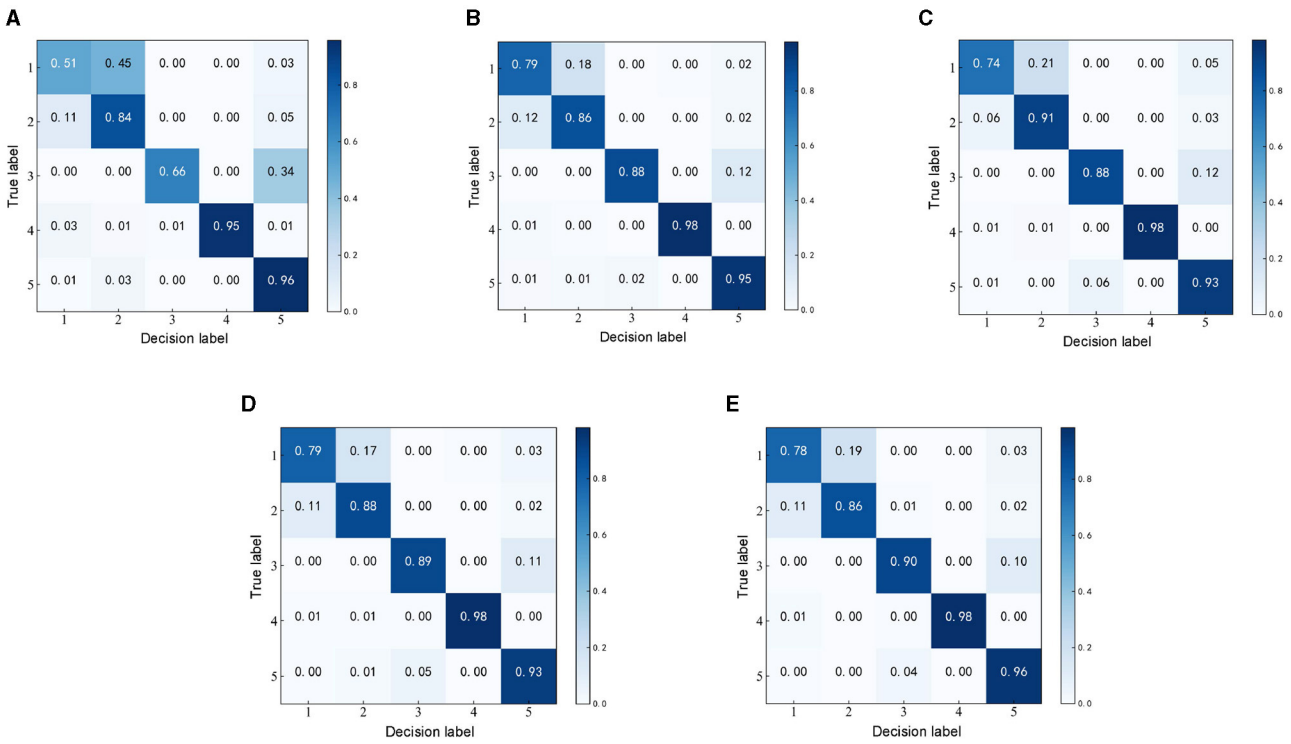


FIGURE 7
Confusion matrices of the detection models based on different optimization algorithms. **(A)** Confusion matrix of 1D-CNN. **(B)** Confusion matrix of PSO-1D-CNN. **(C)** Confusion matrix of GA-1D-CNN. **(D)** Confusion matrix of GWO-1D-CNN. **(E)** Confusion matrix of MFO-1D-CNN.

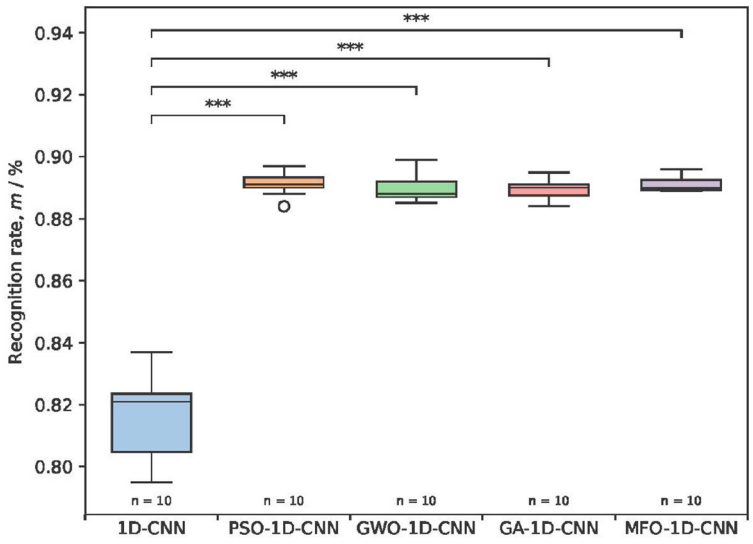


FIGURE 8
The recognition rates and *p*-values of the detection rates for different optimization models. ***$P < 0.001$.

To further compare the effectiveness of the differently optimized 1 D-CNN model, the box plots reflect the distribution of the recognition rates and p-values with the different results for the same dataset during each run. To ensure the effectiveness of detection, the result is obtained ten times for the 1D-CNN and four optimized models, and boxes are drawn to show the overall distribution of the detection results, as shown in Figure 8.

The detection rate using the 1D-CNN model ranges from 79.5 to 83.7%, and the recognition rates of the four optimized 1D-CNN models ranged from 88.9 to 89.1%. The recognition rates of the four optimized models are all higher than those before optimization

and show significant differences. The distribution of detection rates using the MFO-1D-CNN model is more concentrated, and the time of each detection is 4.10 s, which is slightly better than the 4.16 s for the PSO-1D-CNN model, indicating that the proposed model has a more stable mean recognition rate and a slightly faster detection time. Overall, the comparison with the previous three optimized 1D-CNN models indicates that the MFO-optimized 1D-CNN model is effective at classifying a multi-type EEG.

According to the influence of the 1D-CNN model with different optimization algorithms, the detection results of the proposed model are all better than the other three optimization algorithms based on the Kappa value, recognition rates, and their *P*-values. Therefore, the MFO-1D-CNN model was selected for the subsequent analysis to automatically detect EEG classifications. The hyperparameters of the MFO-1D-CNN model mainly include the number of network layers, the size and number of convolution kernels, and the activation function, as shown in Table 2.

The MFO-optimized 1D-CNN model has 26 network layers, including the input layer, convolutional layer, batch normalization layer, dropout layer, pooling layer, tiling layer, and fully connected layer. Among them, the convolutional layer, the normalization layer of samples, the dropout layer, and the pooling layer are reused several times to improve the EEG recognition rate. According to the results of the proposed model, the hyperparameters are as follows: the initial number of convolutional kernels is (50), the kernel size is (101), the activation function is relu, the probability value is set to (0.2), and the optimizer is Adam. In the last layer of the network, the detection layer is set to (5, 1). The feature vectors are inputted into the detection layer to obtain different probability vectors (5, 1). The parameters of the MFO-1D-CNN model are selected to detect EEG classification so that the proposed model is used for classifying EEG detection in the subsequent study.

## 4.4 Discussion of epileptic seizure detection results

According to the detection need of clinicians, the 4 types of experiments (including 40 sub-experiments) are set up from several different EEG classifications, and these experiments are frequently considered in most studies of epileptic seizure detection. The performance of the MFO-1D-CNN model is analyzed and compared with existing advanced models.

### 4.4.1 Two-class EEG classification

The seven different two-class classification groups are selected based on the actual needs for detecting an EEG in clinical practice, and the performance of the MFO-1D-CNN model for 23 sub-experiments is calculated based on the proposed model, as shown in Table 3.

The detection rates of the proposed model for 23 small experiments have a high recognition performance of above 90.00%, except for the one in the *C* vs. *D* dataset; the maximum detection rates of an EEG corresponding to normal vs. ictal and non-ictal vs. ictal are even close to 100.00%. This indicates that the MFO-1D-CNN model has excellent classification performance for two-class detection tasks. In addition, the proposed model has good recognition performance for the distribution problems of imbalanced datasets (such as *AB* vs. *CDE*, *CD* vs. *E*, *BCD* vs. *E*, *ABCD* vs. *E*, etc.), and their detection rate reaches ∼ 99.00%.

### 4.4.2 Three-class EEG classification

The five different three-class classification groups including 11 sub-experiments are chosen from five different subsets. The proposed model is used to calculate the evaluation results, as shown in Table 4.

The MFO-1D-CNN model performs well in 11 sub-experiments with an accuracy ranging from 87.75 to 99.42%, and most recognition rates are above 90%. Then, the proposed model achieves an accuracy of 87.75, 89.53, and 89.74% in datasets *A* vs. *C* vs. *D*, *B* vs. *C* vs. *D*, and *C* vs. *D* vs. *E*, respectively. From the above recognition results, the performance of the MFO-optimized 1D-CNN model is still good for three-class EEG classification recognition.

### 4.4.3 Four-class EEG classification

Similarly, the three different four-class classifications with three sub-experiments are selected. The MFO-1D-CNN model is used to calculate the detection results, as shown in Table 5.

The performance of the proposed model has an accuracy range of 86.16 to 94.70%, and the recognition rates of the last four groups are above 90%, except for the one in the *A* vs.*B* vs.*C* vs.*D* datasets. Generally, the proposed model can adapt to different datasets and has better robustness.

### 4.4.4 Five-class EEG classification

The five-class classification group consisting of only one sub-experiment is constructed in the *A* vs. *B* vs. *C* vs. *D* vs. *E* datasets. The performance of the proposed model is calculated and evaluated for five-class EEG classification, as shown in Table 6.

The five-class EEG classification is more complex and difficult to classify than the two-class, three-class, and four-class ones. The reason for the difficulty lies in the same category but in different states, such as datasets *A* and *B*, and *C* and *D*. Although there are multiple categories and small differences in the paired datasets, the proposed model still achieves good results, and its average detection rate can still reach 88.34%. This suggests that the MFO-1D-CNN model has excellent recognition performance in five-class EEG classification.

## 4.5 Comparison with existing state-of-the-art detection algorithms

To effectively and reasonably compare and analyze the performance of the proposed model and existing state-of-the-art detection models, the same EEG dataset and segment with a length of 1 s is selected from the Bonn EEG dataset. If there are no studies related to epileptic seizure detection with an EEG segment of 1 s, studies with a similar duration of EEG detection are selected.

TABLE 2 The MFO-1D-CNN model for epileptic seizure detection.

| Layer number | Input shape | Layer type | Activation size | Convolution kernel | Output shape |
|---|---|---|---|---|---|
| 1 | (178, 1) | Conv1D | Relu | 10 ∗ 1 | (178, 50) |
| 2 | (178, 50) | Batch_Normalization | – | – | (178, 50) |
| 3 | (178, 50) | Dropout | – | 0.2 | (178, 50) |
| 4 | (178, 50) | MaxPooling1D | – | 2 ∗ 1 | (89, 50) |
| 5 | (89, 50) | Conv1D | Relu | 10 ∗ 1 | (89, 40) |
| 6 | (89, 40) | Batch_Normalization | – | – | (89, 40) |
| 7 | (89, 40) | Dropout | – | 0.2 | (89, 40) |
| 8 | (89, 40) | MaxPooling1D | – | 2 ∗ 1 | (45, 40) |
| 9 | (45, 40) | Conv1D | Relu | 10 ∗ 1 | (45, 35) |
| 10 | (45, 35) | Batch_Normalization | – | – | (45, 35) |
| 11 | (45, 35) | Dropout | – | 0.2 | (45, 35) |
| 12 | (45, 35) | MaxPooling1D | – | 2 ∗ 1 | (23, 35) |
| 13 | (23, 35) | Conv1D | Relu | 10 ∗ 1 | (23, 30) |
| 14 | (23, 30) | Batch_Normalization | – | – | (23, 30) |
| 15 | (23, 30) | Dropout | – | 0.2 | (23, 30) |
| 16 | (23, 30) | MaxPooling1D | – | 2 ∗ 1 | (12, 30) |
| 17 | (12, 30) | Conv1D | Relu | 10 ∗ 1 | (12, 25) |
| 18 | (12, 25) | Batch_Normalization | – | – | (12, 25) |
| 19 | (12, 25) | Dropout | – | 0.2 | (12, 25) |
| 20 | (12, 25) | MaxPooling1D | – | 2 ∗ 1 | (6, 25) |
| 21 | (6, 25) | Conv1D | Relu | 10 ∗ 1 | (6, 20) |
| 22 | (6, 20) | Batch_Normalization | – | – | (6, 20) |
| 23 | (6, 20) | Dropout | – | 0.2 | (6, 20) |
| 24 | (6, 20) | MaxPooling1D | – | 2 ∗ 1 | (3, 20) |
| 25 | (3, 20) | Flatten | – | – | 60 |
| 26 | 60 | Dense | Sofmax | 5 | 5 |

First, many researchers have already considered the performance of two-class classification for EEG detection. Subsequently, most of them only focus on the recognition rate of epileptic seizure detection without considering the effect of the duration of the EEG segment, and fewer researchers have studied short-term segments with a duration of 1 s. This study takes 23 combinations of two-class subsets into account to verify the performance of the epileptic seizure detection model using an EEG, and the performance of the proposed model is analyzed and compared with existing advanced detection models, as shown in Table 7.

From the above chart, the recognition rates of the proposed model are all above 90%, except for the one in the *C* vs. *D* datasets, which is below 90%. Although the performance of the MFO-1D-CNN model is mostly better than the other existing models on two-class classifications using an EEG, it is worse than the other models in the *A* vs.*B*, *A* vs.*D*, and *B* vs. *D* datasets, and the size of the EEG segment length of the proposed model is far less than the ones of the EEG epoch for the other models. From the comparative analysis of the above research results, it can be observed that the proposed model has a better performance and generalization than the most advanced existing models.

Second, there are also many researchers considering 11 combinations of three-class subsets to verify the performance evaluation based on an EEG. The recognition rate of the proposed model was compared and analyzed with the existing advanced detection model, as shown in Table 8.

The detection rates of the proposed model are all higher than those of the novel recognition models from the three categories in Abbasi et al. (2019), Zhao et al. (2020), and Qiu et al. (2023). Again, the recognition rate of the proposed model in the *C* vs. *D* vs. *E* datasets is better than that of the detection model in Türk and Özerdem (2019). Although the performance of the proposed model is slightly lower than that of Türk's detection model in the *A* vs. *B* vs. *C*, *A* vs. *B* vs. *D*, *A* vs. *B* vs. *E*, *A* vs.*C* vs. *D*, and *B* vs. *C* vs. *D* datasets, the length of the inputted EEG data of 1 s is much shorter than that of Türk's detection model. From the comparison results, the proposed model is better than that of the known advanced models.

TABLE 3 The performance of the proposed model for two-class classification with 10-fold cross-validation.

| Group | Class | Accuracy | Precision | Recall | *F*1-score |
|---|---|---|---|---|---|
| Normal vs. normal | *A* vs. *B* | 91.41% | 91.56% | 91.41% | 91.40% |
| Normal vs. preictal | *A* vs. *C* | 98.35% | 98.36% | 98.35% | 98.35% |
| | *A* vs. *D* | 98.65% | 98.66% | 98.65% | 98.65% |
| | *B* vs. *C* | 99.50% | 99.50% | 99.50% | 99.50% |
| | *B* vs. *D* | 99.78% | 99.78% | 99.78% | 99.78% |
| | *AB* vs. *CD* | 98.93% | 98.94% | 98.93% | 98.93% |
| Normal vs. ictal | *A* vs. *E* | 99.96% | 99.96% | 99.96% | 99.96% |
| | *B* vs. *E* | 99.96% | 99.96% | 99.96% | 99.96% |
| | *AB* vs. *E* | 99.90% | 99.90% | 99.90% | 99.90% |
| Normal vs. preictal and ictal | *AB* vs. *CDE* | 99.09% | 99.09% | 99.09% | 99.09% |
| Preictal vs. preictal | *C* vs. *D* | 84.63% | 85.08% | 84.63% | 84.57% |
| Preictal vs. ictal | *C* vs. *E* | 99.78% | 99.78% | 99.78% | 99.78% |
| | *D* vs.*E* | 99.54% | 99.55% | 99.54% | 99.54% |
| | *CD* vs. *E* | 99.70% | 99.70% | 99.70% | 99.70% |
| Non-ictal vs. ictal | *AC* vs. *E* | 99.83% | 99.83% | 99.83% | 99.83% |
| | *AD* vs. *E* | 99.65% | 99.65% | 99.65% | 99.65% |
| | *BC* vs. *E* | 99.84% | 99.84% | 99.84% | 99.84% |
| | *BD* vs. *E* | 99.59% | 99.60% | 99.59% | 99.59% |
| | *ABC* vs. *E* | 99.88% | 99.88% | 99.88% | 99.88% |
| | *ACD* vs. *E* | 99.74% | 99.74% | 99.74% | 99.74% |
| | *ABD* vs. *E* | 99.67% | 99.67% | 99.67% | 99.67% |
| | *BCD* vs. *E* | 99.72% | 99.72% | 99.72% | 99.72% |
| | *ABCD* vs. *E* | 99.77% | 99.77% | 99.77% | 99.77% |

TABLE 4 The performance of the proposed model for three-class classification with 10-fold cross-validation.

| Group | Class | Accuracy | Precision | Recall | F1-score |
|---|---|---|---|---|---|
| Normal vs. preictal vs. ictal | *A* vs. *C* vs. *E* | 98.64% | 98.66% | 98.64% | 98.64% |
| | *A* vs. *D* vs. *E* | 98.77% | 98.78% | 98.77% | 98.77% |
| | *B* vs. *C* vs. *E* | 99.42% | 99.42% | 99.42% | 99.42% |
| | *B* vs. *D* vs. *E* | 98.97% | 98.99% | 98.97% | 98.97% |
| | *AB* vs. *CD* vs. *E* | 98.71% | 98.72% | 98.71% | 98.71% |
| Normal vs. normal vs. preictal | *A* vs. *B* vs. *C* | 92.98% | 93.30% | 92.98% | 93.02% |
| | *A* vs. *B* vs. *D* | 93.39% | 93.57% | 93.39% | 93.41% |
| Normal vs. normal vs. ictal | *A* vs. *B* vs. *E* | 94.17% | 94.31% | 94.17% | 94.18% |
| Normal vs. preictal vs. preictal | *A* vs. *C* vs. *D* | 87.75% | 87.72% | 87.75% | 87.67% |
| | *B* vs. *C* vs. *D* | 89.53% | 89.67% | 89.53% | 89.52% |
| Preictal vs. preictal vs. ictal | *C* vs. *D* vs. *E* | 89.74% | 89.94% | 89.74% | 89.75% |

Third, some scholars have also studied five different combinations of four-class subsets to verify the performance of the detection model. Similarly, the performance of the proposed model is further analyzed and compared with existing advanced models, as shown in Table 9.

Compared with the detection results in a previous study on four-class classifications (Türk and Özerdem, 2019), the recognition rates of the proposed model are not only slightly higher than those of the previous study for the *A* vs. *C* vs.*D* vs. *E* and *B* vs. *C* vs. *D* vs. *E* datasets but are also obtained through the significantly

TABLE 5 The performance of the proposed model for four-class classification with 10-fold cross-validation.

| Group | Class | Accuracy | Precision | Recall | F1-score |
|---|---|---|---|---|---|
| Normal vs. normal vs. preictal vs. preictal | *A* vs. *B* vs. *C* vs. *D* | 86.16% | 86.56% | 86.16% | 86.16% |
| Normal vs. normal vs. preictal vs. ictal | *A* vs. *B* vs. *C* vs. *E* | 94.45% | 94.68% | 94.45% | 94.47% |
| | *A* vs. *B* vs. *D* vs. *E* | 94.70% | 94.83% | 94.70% | 94.71% |
| Normal vs. preictal vs. preictal vs. ictal | *A* vs. *C* vs. *D* vs. *E* | 90.86% | 90.98% | 90.86% | 90.84% |
| | *B* vs. *C* vs. *D* vs. *E* | 91.74% | 91.93% | 91.74% | 91.74% |

TABLE 6 The performance of the proposed model for five-class classification with 10-fold cross-validation.

| Group | Class | Accuracy | Precision | Recall | F1-score |
|---|---|---|---|---|---|
| Normal vs. normal vs. preictal vs. preictal vs. ictal | *A* vs. *B* vs. *C* vs. *D* vs. *E* | 88.34% | 88.69% | 88.34% | 88.32% |

TABLE 7 Comparison of the performances between the proposed model and existing models on two-class classifications using the same EEG datasets.

| Dataset combination | Methods/segment(s) | State of the art | Acc (%) | Our acc (%) |
|---|---|---|---|---|
| *A* vs. *B* | CNN + scalogram /23.6 s | Türk and Özerdem, 2019 | 95.50% | 91.41% |
| *A* vs. *C* | LSTM and SVM/1.12 s | Abbasi et al., 2019 | 97.78% | 98.35% |
| *A* vs. *D* | 1D-LBPall and BayesNet/0.56 s | Kaya et al., 2014 | 99.50% | 98.65% |
| *B* vs. *C* | CNN + scalogram /23.6 s | Türk and Özerdem, 2019 | 99.00% | 99.50% |
| *B* vs. *D* | Epileptic-Net /7.87 s | Islam et al., 2022 | 100.00% | 99.78% |
| *AB* vs. *CD* | LS-SVM/2 s | Sharma et al., 2017 | 92.50% | 98.93% |
| *A* vs. *E* | 1D - CNN/1 s | Zhao et al., 2020 | 99.52% | 99.96% |
| *B* vs. *E* | 1D - CNN/1 s | Zhao et al., 2020 | 99.11% | 99.96% |
| *AB* vs. *E* | 1D - CNN/1 s | Zhao et al., 2020 | 99.38% | 99.90% |
| *AB* vs. *CDE* | 1D-LBPall and BayesNet/0.56 s | Kaya et al., 2014 | 93.00% | 99.09% |
| *C* vs. *D* | CNN + scalogram /23.6 s | Türk and Özerdem, 2019 | 80.00% | 84.63% |
| *C* vs. *E* | 1D - CNN/1 s | Zhao et al., 2020 | 99.02% | 99.78% |
| *D* vs. *E* | 1D - CNN/1 s | Zhao et al., 2020 | 97.63% | 99.54% |
| *CD* vs. *E* | 1D - CNN/1 s | Zhao et al., 2020 | 98.03% | 99.70% |
| *AC* vs. *E* | 1D - CNN/1 s | Zhao et al., 2020 | 99.03% | 99.83% |
| *AD* vs. *E* | 1D - CNN /1 s | Zhao et al., 2020 | 98.85% | 99.65% |
| *BC* vs. *E* | 1D - CNN /1 s | Zhao et al., 2020 | 98.68% | 99.84% |
| *BD* vs. *E* | 1D - CNN /1 s | Zhao et al., 2020 | 97.83% | 99.59% |
| *ABC* vs. *E* | 1D - CNN /1 s | Zhao et al., 2020 | 98.89% | 99.88% |
| *ACD* vs. *E* | DWT and kNN /23.6s | Kumar et al., 2012 | 95.00% | 99.74% |
| *ABD* vs. *E* | 1D - CNN /1 s | Zhao et al., 2020 | 98.56% | 99.67% |
| *BCD* vs. *E* | 1D - CNN /1 s | Zhao et al., 2020 | 98.36% | 99.72% |
| *ABCD* vs. *E* | 1D - CNN/1 s | Zhao et al., 2020 | 98.76% | 99.77% |

shorter duration of EEG detection than that of the previous study, with 23.6s. Although the recognition rate of the MFO-optimized 1D-CNN model on the *A* vs. *B* vs. *C* vs. *D*, *A* vs. *B* vs. *C* vs. *E*, and *A* vs. *B* vs. *D* vs. *E* datasets is lower than that of the Epileptic-Net model in the study by Islam et al. (2022), the length of the inputted EEG with 1 s is considerably lower than that of the Epileptic-Net model. In a comprehensive comparison, the proposed model still has advantages with four-class classifications.

Finally, there are relatively few scholars studying the five-class classification because of the difficulty in detecting the five-class EEG. When analyzed and compared with existing advanced models, there is only 1 combination of five-class subsets to verify the performance of the proposed model, as shown in Table 10.

For the detection results of five categories, a hybrid 1D-CNN and LSTM model is proposed in the study by Xu et al. (2020), and its recognition rate for the *A* vs. *B* vs. *C* vs. *D*

TABLE 8 Comparison of the performances between the proposed model and existing models on three-class classifications using the same EEG datasets.

| Dataset combination | Methods/segment(s) | State of the art | Acc (%) | Our acc (%) |
|---|---|---|---|---|
| *A* vs. *C* vs. *E* | LSTM and SVM/1.12 s | Abbasi et al., 2019 | 94.81% | 98.64% |
| *A* vs. *D* vs. *E* | 1D - CNN/1 s | Zhao et al., 2020 | 97.04% | 98.77% |
| *B* vs. *C* vs. *E* | 1D - CNN /1 s | Zhao et al., 2020 | 97.91% | 99.42% |
| *B* vs. *D* vs. *E* | 1D - CNN/1 s | Zhao et al., 2020 | 98.06% | 98.97% |
| *AB* vs. *CD* vs. *E* | ResNet-LSTM/1 s | Qiu et al., 2023 | 98.17% | 98.71% |
| *A* vs. *B* vs. *C* | CNN + scalogram /23.6 s | Türk and Özerdem, 2019 | 95.00% | 92.98% |
| *A* vs. *B* vs. *D* | CNN + scalogram /23.6 s | Türk and Özerdem, 2019 | 96.67% | 93.39% |
| *A* vs. *B* vs. *E* | CNN + scalogram /23.6 s | Türk and Özerdem, 2019 | 95.67% | 94.17% |
| *A* vs. *C* vs. *D* | CNN + scalogram /23.6 s | Türk and Özerdem, 2019 | 88.00% | 87.75% |
| *B* vs. *C* vs. *D* | CNN + scalogram /23.6 s | Türk and Özerdem, 2019 | 91.33% | 89.53% |
| *C* vs. *D* vs. *E* | CNN + scalogram /23.6 s | Türk and Özerdem, 2019 | 89.00% | 89.94% |

TABLE 9 Comparison of the performances between the proposed model and existing models on four-class classifications using the same EEG datasets.

| Dataset combination | Methods/segment(s) | State-of-the-art | Acc (%) | Our acc (%) |
|---|---|---|---|---|
| *A* vs. *B* vs. *C* vs. *D* | Epileptic-Net/7.87 s | Islam et al., 2022 | 99.91% | 86.16% |
| *A* vs. *B* vs. *C* vs. *E* | Epileptic-Net/7.87 s | Islam et al., 2022 | 100.00% | 94.45% |
| *A* vs. *B* vs. *D* vs. *E* | Epileptic-Net/7.87 s | Islam et al., 2022 | 100.00% | 94.70% |
| *A* vs. *C* vs. *D* vs. *E* | CNN + scalogram /23.6 s | Türk and Özerdem, 2019 | 90.50% | 90.86% |
| *B* vs. *C* vs. *D* vs. *E* | CNN + scalogram /23.6 s | Türk and Özerdem, 2019 | 91.50% | 91.74% |

TABLE 10 Comparison of the performances between the proposed model and existing models on five-class classifications using the same EEG datasets.

| Dataset combination | Methods/segment(s) | State-of-the-art | Acc (%) | Our acc (%) |
|---|---|---|---|---|
| *A* vs. *B* vs.*C* vs. *D* vs.*E* | 1D - CNN-LSTM/1 s | Xu et al., 2020 | 82.00% | 88.34% |
| *A* vs. *B* vs. *C* vs. *D* vs. *E* | 1D - CNN/1 s | Zhao et al., 2020 | 93.55% | 88.34% |

vs. *E* datasets is lower than that of the proposed model. The best recognition rate is 93.55% using the 8 optimized models by configuring network parameters manually, the detection rate of which is higher than that of the proposed model in the study by Zhao et al. (2020). Then, considering that configuring the network model requires appropriate professional knowledge and involves tedious processes, the MFO-1D-CNN model has advantages in the two-class, three-class, four-class, and five-class EEG classification problems.

Based on the above analysis, the proposed method can achieve better detection results within 500 iterations. This model is suitable for the 40 different two-class, three-class, four-class, and five-class classifications and has good generalization ability. The MFO-optimized 1D-CNN model not only extends the adaptive adaptability of the model to an EEG but also significantly improves the detection ability of epileptic seizure. Despite achieving good results in epileptic seizure detection, the model still has some shortcomings. First, the proposed model requires a large amount of EEGs. Second, this study does not fully consider the ability to optimize MFO in the optimization process. Finally, the proposed model needs to further reduce the number of neural network layers and neurons to reduce complexity and improve the epileptic seizure detection capability of the MFO-1 D-CNN model.

## 5 Conclusion

This study proposes an automatic epileptic seizure detection model based on 1D-CNN optimized by MFO. The novelty lies in its ability to automatically search for the optimal combination of CNN hyperparameters based on MFO, without manually adjusting the network structure and hyperparameters. This can further improve the effectiveness of the epileptic seizure detection model. The performance of the proposed model in detecting an EEG is experimentally validated with the highest accuracy of 99.96, 99.42, 94.70, and 88.34% in two-class, three-class, four-class, and five-class detection tasks, respectively. In particular, MFO-1D-CNN significantly reduces the time required to detect epileptic seizures. Compared with advanced optimization algorithms such as PSO, GA, and GWO, the proposed model has certain benefits in terms of detection rate and time efficiency. At present, the proposed model is mainly used for the detection of single-channel

EEGs. In the future, its ability to predict epileptic seizures will be investigated, and it may be implanted into epileptic seizure detection systems in clinical applications to achieve prediction using EEGs.

## Data availability statement

The original contributions presented in the study are included in the article/supplementary material, further inquiries can be directed to the corresponding authors.

## Ethics statement

Written informed consent was obtained from the individual(s) for the publication of any potentially identifiable images or data included in this article.

## Author contributions

BW: Writing—original draft, Writing—review & editing. XY: Visualization, Writing—original draft. SL: Data curation, Writing—original draft. WW: Software, Writing—original draft. YO: Writing—review & editing. JZ: Project administration, Writing—review & editing. CW: Funding acquisition, Writing—review & editing.

## Funding

The author(s) declare financial support was received for the research, authorship, and/or publication of this article. This study was financially supported by the STI 203—Major Projects (2021*ZD*0201600 and 2021*ZD*0201604).

## Acknowledgments

The authors are grateful to the Bonn University seizure dataset and reviewers for their valuable comments.

## Conflict of interest

The authors declare that the research was conducted in the absence of any commercial or financial relationships that could be construed as a potential conflict of interest.

## Publisher's note



## References

Abbasi, M. U., Rashad, A., Basalamah, A., and Tariq, M. (2019). Detection of epilepsy seizures in neo-natal EEG using LSTM architecture. *IEEE Access* 7, 179074–179085. doi: 10.1109/ACCESS.2019.2959234

Aliyu, I., and Lim, C. G. (2023). Selection of optimal wavelet features for epileptic EEG signal classification with LSTM. *Neural Comp. Appl.* 35, 1–21. doi: 10.1007/s00521-020-05666-0

Andrzejak, R. G., Lehnertz, K., Mormann, F., Rieke, C., David, P., and Elger, C. E. (2001). Indications of nonlinear deterministic and finite-dimensional structures in time series of brain electrical activity: dependence on recording region and brain state. *Phy. Rev. E* 64, 061907. doi: 10.1103/PhysRevE.64.061907

Bhattacharyya, A., Pachori, R. B., Upadhyay, A., and Acharya, U. R. (2017). Tunable-Q wavelet transform based multiscale entropy measure for automated classification of epileptic EEG signals. *Appl. Sci.* 7, 385. doi: 10.3390/app7040385

Bongiorni, L., and Balbinot, A. (2020). Evaluation of recurrent neural networks as epileptic seizure predictor. *Array* 8, 100038. doi: 10.1016/j.array.2020.100038

Caveness, W., Am Lorentz, H., and Radermecker, J. (1964). A proposed international classification of epileptic seizures. *Epilepsia* 5, 297–306. doi: 10.1111/j.1528-1157.1964.tb03337.x

Chetana, R., Shubha Rao, A., and Mahantesh, K. (2023). Application of conv-1D and Bi-LSTM to classify and detect epilepsy in EEG Data. *Int. J. Adv. Comp. Sci. Appl.* 14, 253–261.

Elsakaan, A. A., El-Sehiemy, R. A., Kaddah, S. S., and Elsaid, M. I. (2018). An enhanced moth-flame optimizer for solving non-smooth economic dispatch problems with emissions. *Energy* 157, 1063–1078. doi: 10.1016/j.energy.2018.06.088

Emami, A., Kunii, N., Matsuo, T., Shinozaki, T., Kawai, K., and Takahashi, H. (2019). Seizure detection by convolutional neural network-based analysis of scalp electroencephalography plot images. *NeuroImage Clin.* 22, 101684. doi: 10.1016/j.nicl.2019.101684

Fatyanosa, T. N., and Aritsugi, M. (2020). "Effects of the number of hyperparameters on the performance of GA-CNN," in *2020 IEEE/ACM International Conference on Big Data Computing, Applications and Technologies (BDCAT)* (Leicester: IEEE), 144–153.

Hazir, E., Erdinler, E. S., and Koc, K. H. (2018). Optimization of CNC cutting parameters using design of experiment (DOE) and desirability function. *J. For. Res.* 29, 1423–1434. doi: 10.1007/s11676-017-0555-8

Hernández, D., Trujillo, L., Flores, E., Villanueva, O., and Romo-Fewell, O. (2018). "Detecting epilepsy in eeg signals using time, frequency and time-frequency domain features," in *Computer Science and Engineering—Theory and Applications* (Springer), 167–182.

Hoang, D.-T., and Kang, H.-J. (2019). Rolling element bearing fault diagnosis using convolutional neural network and vibration image. *Cogn. Syst. Res.* 53, 42–50. doi: 10.1016/j.cogsys.2018.03.002

Irmak, E. (2020). Implementation of convolutional neural network approach for COVID-19 disease detection. *Physiol. Genom.* 52, 590–601. doi: 10.1152/physiolgenomics.00084.2020

Islam, M. S., Thapa, K., and Yang, S.-H. (2022). Epileptic-net: an improved epileptic seizure detection system using dense convolutional block with attention network from EEG. *Sensors* 2, 728. doi: 10.3390/s22030728

Jing, J., d'Angremont, E., Ebrahim, S., Tabaeizadeh, M., Ng, M., Herlopian, A., et al. (2021). Rapid annotation of seizures and interictal-ictal-injury continuum EEG patterns. *J. Neurosci. Methods* 347, 108956. doi: 10.1016/j.jneumeth.2020.108956

Kaya, Y., Uyar, M., Tekin, R., and Yıldırım, S. (2014). 1d-local binary pattern based feature extraction for classification of epileptic EEG signals. *Appl. Math. Comput.* 243, 209–219. doi: 10.1016/j.amc.2014.05.128

Khurma, R. A., Aljarah, I., and Sharieh, A. (2020). "Rank based moth flame optimisation for feature selection in the medical application," in *2020 IEEE Congress on Evolutionary Computation (CEC)* (Glasgow: IEEE), 1–8.

Kim, S.-H., Geem, Z. W., and Han, G.-T. (2020). Hyperparameter optimization method based on harmony search algorithm to improve performance of 1D CNN human respiration pattern recognition system. *Sensors* 20, 3697. doi: 10.3390/s20133697

Kolar, D., Lisjak, D., Pajk, M., and Gudlin, M. (2021). Intelligent fault diagnosis of rotary machinery by convolutional neural network with automatic hyper-parameters tuning using bayesian optimization. *Sensors* 21, 2411. doi: 10.3390/s21072411

Kong, L.-Z., Zhang, R.-L., Hu, S.-H., and Lai, J.-B. (2022). Military traumatic brain injury: a challenge straddling neurology and psychiatry. *Milit. Med. Res.* 9, 2. doi: 10.1186/s40779-021-00363-y

Kumar, Y., Dewal, M. L., and Anand, R. S. (2012). Relative wavelet energy and wavelet entropy based epileptic brain signals classification. *Biomed. Eng. Lett.* 2, 147–157. doi: 10.1007/s13534-012-0066-7

Kurdthongmee, W. (2020). Optimisation of deep neural networks for identification of epileptic abnormalities from electroencephalogram signals. *Heliyon* 6, e05694. doi: 10.1016/j.heliyon.2020.e05694

Kwasigroch, A., Jarzembinski, B., and Grochowski, M. (2018). "Deep CNN based decision support system for detection and assessing the stage of diabetic retinopathy," in *2018 International Interdisciplinary PhD Workshop (IIPhDW)* (Świnoujście: IEEE), 111–116.

Lai, H., Zhang, L., and Zhang, S. (2022). Improving network training on resource-constrained devices via habituation normalization. *Sensors* 22, 9940. doi: 10.3390/s22249940

Lebal, A., Moussaoui, A., and Rezgui, A. (2023). Epilepsy-Net: attention-based 1D-inception network model for epilepsy detection using one-channel and multi-channel EEG signals. *Multimed. Tools Appl.* 82, 17391–17413. doi: 10.1007/s11042-022-13947-0

Li, H., Ding, M., Zhang, R., and Xiu, C. (2022). Motor imagery eeg classification algorithm based on cnn-lstm feature fusion network. *Biomed. Signal Process. Control* 72, 103342. doi: 10.1016/j.bspc.2021.103342

Liu, J., Sun, S., Liu, Y., Guo, J., Li, H., Gao, Y., et al. (2020). A novel megnet for classification of high-frequency oscillations in magnetoencephalography of epileptic patients. *Complexity* 2020, 1–9. doi: 10.1155/2020/9237808

Lv, C., Nian, J., Yaru, X., and Bo, S. (2022). "Epilepsy EEG classification and recognition algorithm based on PSO-CNN," in *Second International Conference on Digital Signal and Computer Communications (DSCC 2022)*, *Vol. 12306* (Changchun: SPIE), 320–324.

Mezzah, S., and Tari, A. (2023). Practical hyperparameters tuning of convolutional neural networks for EEG emotional features classification. *Intell. Syst. Appl.* 18, 200212. doi: 10.1016/j.iswa.2023.200212

Mirjalili, S. (2015). Moth-flame optimization algorithm: a novel nature-inspired heuristic paradigm. *Knowl. Based Syst.* 89, 228–249. doi: 10.1016/j.knosys.2015.07.006

Nikodijevic, D., Baneva-Dolnenec, N., Petrovska-Cvetkovska, D., and Caparoska, D. (2016). Refractory epilepsy-MRI, EEG and CT scan, a correlative clinical study. *Maced. J. Med. Sci.* 4, 98. doi: 10.3889/oamjms.2016.029

Qiu, X., Yan, F., and Liu, H. (2023). A difference attention ResNet-LSTM network for epileptic seizure detection using EEG signal. *Biomed. Signal Process. Control* 83, 104652. doi: 10.1016/j.bspc.2023.104652

Ra, J. S., Li, T., and Li, Y. (2023). A novel epileptic seizure prediction method based on synchroextracting transform and 1-dimensional convolutional neural network. *Comput. Methods Progr. Biomed.* 240, 107678. doi: 10.1016/j.cmpb.2023.107678

Sallam, A. A., Kabir, M. N., Ahmed, A. A., Farhan, K., and Tarek, E. (2018). "Epilepsy detection from EEG signals using artificial neural network," in *International Conference on Intelligent Computing & Optimization* (Cham: Springer), 320–327.

Sharma, M., Pachori, R. B., and Acharya, U. R. (2017). A new approach to characterize epileptic seizures using analytic time-frequency flexible wavelet transform and fractal dimension. *Pattern Recognit. Lett.* 94, 172–179. doi: 10.1016/j.patrec.2017.03.023

Shehab, M., Abualigah, L., Al Hamad, H., Alabool, H., Alshinwan, M., and Khasawneh, A. M. (2020). Moth-flame optimization algorithm: variants and applications. *Neural Comp. Appl.* 32, 9859–9884. doi: 10.1007/s00521-019-04570-6

Thanuja, K., Shoba, M., and Patil, K. (2023). Epileptic seizure classification and feature optimization technique using grey wolf algorithm on dynamic datasets. *SN Comp. Sci.* 4, 311. doi: 10.1007/s42979-023-01741-0

Tsiouris, K. M., Pezoulas, V. C., Zervakis, M., Konitsiotis, S., Koutsouris, D. D., and Fotiadis, D. I. (2018). A long short-term memory deep learning network for the prediction of epileptic seizures using EEG signals. *Comput. Biol. Med.* 99, 24–37. doi: 10.1016/j.compbiomed.2018.05.019

Türk, Ö. and Özerdem, M. S. (2019). Epilepsy detection by using scalogram based convolutional neural network from EEG signals. *Brain Sci.* 9, 115. doi: 10.3390/brainsci9050115

Ullah, I., Hussain, M., Qazi, E., and Aboalsamh, H. (2018). An automated system for epilepsy detection using EEG brain signals based on deep learning approach. *Expert Syst. Appl.* 107, 61–71. doi: 10.1016/j.eswa.2018.04.021

Waibel, A., Hanazawa, T., Hinton, G., Shikano, K., and Lang, K. J. (1989). Phoneme recognition using time-delay neural networks. *IEEE Trans. Acoust. Speech Signal Process.* 37, 328–339. doi: 10.1109/29.21701

Wang, X., Wang, X., Liu, W., Chang, Z., Kärkkäinen, T., and Cong, F. (2021). One dimensional convolutional neural networks for seizure onset detection using long-term scalp and intracranial EEG. *Neurocomputing* 459, 212–222. doi: 10.1016/j.neucom.2021.06.048

Wang, Y., Zhang, H., and Zhang, G. (2019). cPSO-CNN: An efficient PSO-based algorithm for fine-tuning hyper-parameters of convolutional neural networks. *Swarm Evol. Comp.* 49, 114–123. doi: 10.1016/j.swevo.2019.06.002

World Health Organization (2023). *Epilepsy*. Available online at: https://www.who.int/news-room/fact-sheets/detail/epilepsy/ (accessed August 5, 2023).

Xu, G., Ren, T., Chen, Y., and Che, W. (2020). A one-dimensional CNN-LSTM model for epileptic seizure recognition using EEG signal analysis. *Front. Neurosci.* 14, 578126. doi: 10.3389/fnins.2020.578126

Yu, Z., Lu, Y., An, Q., Chen, C., Li, Y., and Wang, Y. (2022). Real-time multiple gesture recognition: application of a lightweight individualized 1D CNN model to an edge computing system. *IEEE Transact. Neural Syst. Rehabil. Eng.* 30, 990–998. doi: 10.1109/TNSRE.2022.3165858

Zawbaa, H. M., Emary, E., Parv, B., and Sharawi, M. (2016). "Feature selection approach based on moth-flame optimization algorithm," in *2016 IEEE Congress on Evolutionary Computation (CEC)* (Vancouver, BC: IEEE), 4612–4617.

Zhang, H., Liu, J., Wang, B., Dai, J., Lian, J., Ke, A., et al. (2022). Motion direction prediction through spike timing based on micro capsnet networks. *Science China Technol. Sci.* 65, 2763–2775. doi: 10.1007/s11431-022-2072-9

Zhang, T., Chen, W., and Li, M. (2017). Ar based quadratic feature extraction in the VMD domain for the automated seizure detection of EEG using random forest classifier. *Biomed. Signal Process. Control* 31, 550–559. doi: 10.1016/j.bspc.2016.10.001

Zhang, Y., Yao, S., Yang, R., Liu, X., Qiu, W., Han, L., et al. (2022). Epileptic seizure detection based on bidirectional gated recurrent unit network. *IEEE Transact. Neural Syst. Rehabil. Eng/* 30, 135–145. doi: 10.1109/TNSRE.2022.3143540

Zhao, W., and Wang, W. (2020). SeizureNet: a model for robust detection of epileptic seizures based on convolutional neural network. *Cogn. Comp. Syst.* 2, 119–124. doi: 10.1049/ccs.2020.0011

Zhao, W., Zhao, W., Wang, W., Jiang, X., Zhang, X., Peng, Y., et al. (2020). A novel deep neural network for robust detection of seizures using EEG signals. *Comput. Math. Methods Med.* doi: 10.1155/2020/9689821

frontiers | Frontiers in Neuroscience

TYPE Original Research
PUBLISHED 11 January 2024
DOI 10.3389/fnins.2023.1286665



OPEN ACCESS

EDITED BY
Kymberly Young,
University of Pittsburgh, United States

REVIEWED BY
Miguel Castelo-Branco,
Coimbra Institute for Biomedical Imaging and Translational Research (CIBIT), Portugal
Masaya Misaki,
Coimbra Institute for Biomedical Imaging and Translational Research (CIBIT), Portugal;
Laureate Institute for Brain Research,
United States

*CORRESPONDENCE
Ronald Sladky
✉ ronald.sladky@univie.ac.at

RECEIVED 31 August 2023
ACCEPTED 18 December 2023
PUBLISHED 11 January 2024

CITATION
Watve A, Haugg A, Frei N, Koush Y, Willinger D, Bruehl AB, Stämpfli P, Scharnowski F and Sladky R (2024) Facing emotions: real-time fMRI-based neurofeedback using dynamic emotional faces to modulate amygdala activity. *Front. Neurosci.* 17:1286665. doi: 10.3389/fnins.2023.1286665



# Facing emotions: real-time fMRI-based neurofeedback using dynamic emotional faces to modulate amygdala activity

Apurva Watve[1], Amelie Haugg[2], Nada Frei[2], Yury Koush[3], David Willinger[2,4,5], Annette Beatrix Bruehl[1,6], Philipp Stämpfli[1], Frank Scharnowski[1,5,7,8] and Ronald Sladky[1,9]*

[1]Department of Psychiatry, Psychotherapy, and Psychosomatics, Psychiatric University Hospital, University of Zürich, Zürich, Switzerland, [2]Department of Child and Adolescent Psychiatry, Psychiatric Hospital, University of Zürich, Zürich, Switzerland, [3]Magnetic Resonance Research Center (MRRC), Department of Radiology and Biomedical Imaging, Yale University, New Haven, CT, United States, [4]Division of Psychodynamics, Department of Psychology and Psychodynamics, Karl Landsteiner University of Health Sciences, Krems an der Donau, Lower Austria, Austria, [5]Neuroscience Center Zürich, University of Zürich and Swiss Federal Institute of Technology, Zürich, Switzerland, [6]Center for Affective, Stress and Sleep Disorders, Psychiatric University Hospital Basel, Basel, Switzerland, [7]Zurich Center for Integrative Human Physiology, Faculty of Medicine, University of Zürich, Zürich, Switzerland, [8]Department of Cognition, Emotion, and Methods in Psychology, Faculty of Psychology, University of Vienna, Vienna, Austria, [9]Social, Cognitive and Affective Neuroscience Unit, Department of Basic Psychological Research and Research Methods, Faculty of Psychology, University of Vienna, Vienna, Austria

**Introduction:** Maladaptive functioning of the amygdala has been associated with impaired emotion regulation in affective disorders. Recent advances in real-time fMRI neurofeedback have successfully demonstrated the modulation of amygdala activity in healthy and psychiatric populations. In contrast to an abstract feedback representation applied in standard neurofeedback designs, we proposed a novel neurofeedback paradigm using naturalistic stimuli like human emotional faces as the feedback display where change in the facial expression intensity (from neutral to happy or from fearful to neutral) was coupled with the participant's ongoing bilateral amygdala activity.

**Methods:** The feasibility of this experimental approach was tested on 64 healthy participants who completed a single training session with four neurofeedback runs. Participants were assigned to one of the four experimental groups ($n$ = 16 per group), i.e., happy-up, happy-down, fear-up, fear-down. Depending on the group assignment, they were either instructed to "try to make the face happier" by upregulating (happy-up) or downregulating (happy-down) the amygdala or to "try to make the face less fearful" by upregulating (fear-up) or downregulating (fear-down) the amygdala feedback signal.

**Results:** Linear mixed effect analyses revealed significant amygdala activity changes in the fear condition, specifically in the fear-down group with significant amygdala downregulation in the last two neurofeedback runs as compared to the first run. The happy-up and happy-down groups did not show significant amygdala activity changes over four runs. We did not observe significant improvement in the questionnaire scores and subsequent behavior. Furthermore, task-dependent effective connectivity changes between the amygdala, fusiform face area (FFA), and the medial orbitofrontal cortex (mOFC) were examined using dynamic causal modeling. The effective connectivity between FFA and the amygdala was significantly increased in the happy-up group (facilitatory effect) and decreased in the fear-down group. Notably, the amygdala was downregulated through an inhibitory mechanism mediated by mOFC during the first training run.

**Discussion:** In this feasibility study, we intended to address key neurofeedback processes like naturalistic facial stimuli, participant engagement in the task, bidirectional regulation, task congruence, and their influence on learning success. It demonstrated that such a versatile emotional face feedback paradigm can be tailored to target biased emotion processing in affective disorders.

KEYWORDS

**real-time fMRI, neurofeedback, amygdala, emotion regulation, dynamic faces**

## Introduction

Worldwide, nearly a billion people suffer from mental health problems in some form of mood disorder that significantly affects their quality of life (World Health Organization, 2022). Among the most common mood disorders are affective disorders, such as major depressive disorder (MDD), and anxiety disorder (AD), which have the highest global prevalence rate and cause a social and economic burden (Steel et al., 2014). Epidemiological data from Europe suggest that AD (14.0%) has the highest 12-month prevalence rate with MDD (6.9%) in the third position (Wittchen et al., 2011). They have become even more prominent with the emergence of the COVID-19 pandemic in 2020 (Santomauro et al., 2021). In addition to disrupting emotional well-being and behavior, affective disorders also affect somatic health (Momen et al., 2020), which can lead to reduced life expectancy (Nordentoft et al., 2013). They are substantially associated with high treatment costs, disability, and chronicity (Cuijpers et al., 2012; Baxter et al., 2014). Considerable financial and scientific resources have been invested in the development of efficient and cost-effective treatments for MDD and AD in the fields of neuropsychopharmacology, brain stimulation, and psychotherapy. However, further research into different treatment approaches for the improvement of AD and MDD symptoms is warranted due to the significant number of non-responders.

In terms of symptomatology, affective disorders are mainly characterized by affective biases, dysfunctional self-belief (Hofmann et al., 2012), and deficits in emotion regulation (Joormann and Siemer, 2014). Established research suggests that the maladaptive functioning of cortico-limbic regions, particularly the amygdala, is involved in the development and propagation of these symptoms (Disner et al., 2011). Altered amygdala responses to affective stimuli trigger emotion dysregulation, manifesting hallmark MDD symptoms such as anhedonia, i.e., diminished positive affectivity (McMakin et al., 2012), and amplified negative emotional responses, resulting in dysphoria, i.e., feelings of fear, anxiety, distress, etc. (Siegle et al., 2007). Neural signatures of MDD reveal that these affective biases are associated with decreased amygdala activity in response to positive stimuli and increased reactivity to negative stimuli (Suslow et al., 2010; Victor et al., 2010; Young et al., 2016). Reduced amygdala reactivity to happy faces in MDD patients correlates with higher anhedonia scores and poorer or inappropriate salience attributions to positive environmental cues (Victor et al., 2010). Such impaired processing of positive affect is also associated with an increased bias toward sad faces, which correlates with MDD severity (Suslow et al., 2010).

In anxiety disorders such as posttraumatic stress disorder (PTSD) and social anxiety disorder (SAD), attentional and emotion-processing biases lead to exaggerated responses to negative stimuli that are perceived as threatening. Fear is one of the core symptoms of anxiety disorders, e.g., fear of negative social evaluation and speech anxiety in SAD (Tillfors et al., 2002; Davies et al., 2017). Studies suggest that hyperactivation of the amygdala is associated with the biased processing of negative emotions that trigger fear responses in individuals with AD. There is evidence that amygdala activity scales with the intensity of emotional images (Karlsson et al., 2010) and faces (Wang et al., 2017). Amygdala hyperactivity has been observed in response to negative (Etkin and Wager, 2007) and neutral facial expressions in AD (Cooney et al., 2006). For example, patients suffering from SAD showed increased amygdala activity compared to healthy controls when presented with emotional faces (Stein et al., 2002; Phan et al., 2006; Schneier et al., 2009).

These findings of impaired neural processing of affective stimuli, such as emotional faces, are replicated in depression and anxiety disorders (Stein et al., 2002; Campbell et al., 2007; Etkin and Wager, 2007). Although the amygdala is not the only brain region relevant to the perception and regulation of mood and emotion (Pessoa and Adolphs, 2010; Grupe and Nitschke, 2013), its critical involvement in these processes remains undisputed. Current empirical evidence confirms that the amygdala not only plays a critical role in the detection and processing of emotionally salient stimuli but is also involved in emotional memory formation, fear conditioning, social cognition, and reward processing (Bickart et al., 2011; Inman et al., 2020; Domínguez-Borràs and Vuilleumier, 2022). These neural mechanisms are necessary for appropriately processing emotional cues and subsequent behavioral responses. Thus, the ability to regulate amygdala responses may indicate successful context-dependent affect processing. Unfortunately, its location deep within the temporal lobe limits the applicability of non-invasive exogenous brain stimulation methods such as transcranial magnetic and electrical stimulation. Therefore, a new form of non-invasive and individualized treatment is needed to address the heterogeneous symptoms of affective disorders.

The application of a novel form of endogenous brain stimulation method, such as real-time functional magnetic resonance imaging-based neurofeedback (rt-fMRI NF), could be a promising alternative or adjunct to current treatment regimens for affective disorders. Using this technique, participants can learn to voluntarily control their neural responses by modulating their brain activity, which is presented in the form of a real-time feedback signal. Previous rtfMRI-NF studies of amygdala self-regulation have already demonstrated the benefits of this new non-invasive approach in improving emotion regulation in healthy individuals and various psychiatric disorders (e.g., Linden et al., 2012; Brühl et al., 2014; Zotev et al., 2016; Young et al., 2017; Koush et al., 2017b; Paret et al., 2018; Zaehringer et al., 2020).

However, these previous studies used a symbolic representation of the feedback signal, such as a thermometer-like scale. Here,

we investigated the applicability of a novel feedback approach using adaptive naturalistic face stimuli. Instead of a discrete and abstract representation of the neurofeedback signal, we used a sequence of human faces displaying smooth transformations of varying intensities of neutral to happy or neutral to fearful facial emotions that were generated using face-morphing algorithms. This novel feedback modality might have several advantages over conventional feedback. First, social feedback is highly relevant because it reflects interactions that humans encounter in their natural habitat, and thus emotional faces are more ecologically valid than abstract symbolic feedback representations (Mathiak et al., 2015). Second, previous studies simultaneously presented the visual cue and the feedback signal at different locations or subsequently, in order to modulate stimulus-induced activity through neurofeedback training (Brühl et al., 2014; Paret et al., 2014; Hartwell et al., 2016). Such dual-task interference between stimulus perception and feedback monitoring can be avoided by combining amygdala-relevant pictorial cues (Geissberger et al., 2020) and the feedback signal. Third, interactive emotional faces (i.e., a fearful face that gradually becomes less fearful, and a neutral face that becomes happier) are more socially motivating as the participant's regulation effort has real motivational consequences in terms of approach and avoidance of the task-relevant feedback signal (Carver, 2006; Ihssen et al., 2017).

A few neurofeedback studies have used interactive feedback interfaces such as human avatars that dynamically change emotional expressions corresponding to the targeted neural activity (Mathiak et al., 2015; Direito et al., 2019, 2021). The current study paradigm included a more realistic and dynamic feedback presentation of human face stimuli. We argue that this type of innovative feedback could be more naturalistic, ecologically valid, and socially rewarding as compared to virtual avatars (Philip et al., 2018). Finally, this setup also allows for more complex research designs inspired by closed-loop control theory to shape brain dynamics through positive (i.e., a strong brain response causes a stronger stimulus) and negative (i.e., a strong brain response causes a weaker stimulus) feedback loops that increase or decrease neural responsivity, respectively (Toates, 1975; Mulholland and Eberlin, 1977; Mulholland et al., 1979; Pope et al., 1995).

In this study, we tested the efficacy of this novel closed-loop neurofeedback approach in healthy participants. The prospective goal is to use this tailored adaptive experimental therapy to target affective biases and associated symptoms in psychiatric disorders. Participants were randomly assigned to four groups based on the emotional face stimuli and task congruency. Participants were instructed to make the neutral face happier by increasing their amygdala activity in the happy-up (task-congruent) and decreasing it in the happy-down (task-incongruent) groups. Whereas participants were instructed to reduce the fearfulness of the face by downregulating their amygdala activity in the fear-down (task-congruent) group and upregulating it in the fear-up (task-incongruent) group, respectively (Figure 1). Perceiving facial expressions can help regulate emotional responses, such as enhancing positive mood or reducing negative affective state, especially when the expression of the face stimulus matches one's intentions, in other words, is congruent with one's regulatory efforts. For example, in the happy-up (task-congruent) group, the task goal was to increase the happiness of the face stimulus by upregulating amygdala activity, i.e., the face stimulus is rewarding the inherent human tendency to perceive happy faces by upregulating the amygdala. On the other hand, being exposed to emotional stimuli that are not in alignment with one's regulatory efforts can lead to task incongruency. For example, in the happy-down group, the goal was to increase the happiness of the face stimulus by decreasing amygdala activity. In this condition, the rewarding face stimuli (happy faces) contradict the task goal of downregulating the amygdala. This type of feedback setup may require greater cognitive effort due to internal conflict of pursuing a reward by engaging contrasting neural patterns and may provide a training opportunity akin to exposure therapy. With such a versatile and comprehensive feedback design, we hypothesized that healthy participants would learn to upregulate and downregulate their amygdala activity in the task-congruent groups, i.e., happy-up and fear-down, respectively, as compared to the respective task-incongruent groups (happy-down and fear-up).

Next, we hypothesized that the task-dependent effective connectivity between the amygdala and the prefrontal cortex and/or face-sensitive regions in the temporal lobe would increase over the course of the neurofeedback training session. In the context of affective disorders, maladaptive emotional responses are manifested due to dysfunctional inhibitory control of higher order cognitive top-down processes on the maladaptive bottom-up pathways regulated by subcortical regions like the amygdala (Nicholson et al., 2017). Previous work has already demonstrated the role of the fusiform face area (FFA) and the medial orbitofrontal cortex (mOFC) in face processing and amygdala regulation (Kanwisher et al., 1997; Almeida et al., 2009; de Almeida et al., 2011; Sabatinelli et al., 2011; Roy et al., 2012; Sladky et al., 2015). We employed dynamic causal modeling (DCM; Friston et al., 2003), a Bayesian framework, to assess the directionality of neural dynamics involved in emotion processing (Krylova et al., 2021; Sladky et al., 2022). Specifically, we hypothesized that upregulation of the amygdala would result in positive (facilitatory), and downregulation would entail negative (inhibitory) connectivity between the mOFC and the amygdala. Finally, we assessed the intervention-induced mood changes in the participants using self-rated psychometric questionnaires such as the Positive And Negative Affect Schedule (PANAS, Watson et al., 1988) and the Self-rating Depression Scale (SDS, Zung, 1965). We hypothesized that the naturalistic closed-loop training would improve participants' positive affectivity scores on the PANAS scale while decreasing PANAS negative affectivity scores, and SDS scores post-training, specifically, in the task-congruent groups (happy-up and fear-down).

# Methods

## Participants

Sixty-four healthy adults between 18 and 65 years of age, fluent in German, right-handed with normal vision and without any MRI contraindications such as pregnancy, claustrophobia, metallic implants, clinically significant somatic diseases, brain surgery, neurological disorders, and substance abuse, were recruited for the study. The participants (mean age = 25.07 ± 4.46 years) were assigned to one of the four age- and gender-matched neurofeedback intervention groups with 16 participants in each group, i.e., happy-up (mean age = 26.59 ± 4.87 years, gender = 8 m:8f), happy-down (mean age = 25.93 ± 5.93 years, gender = 8 m:8f), fear-up (mean age = 23.85 ± 3.54 years, gender = 7 m:9f), and fear-down (mean

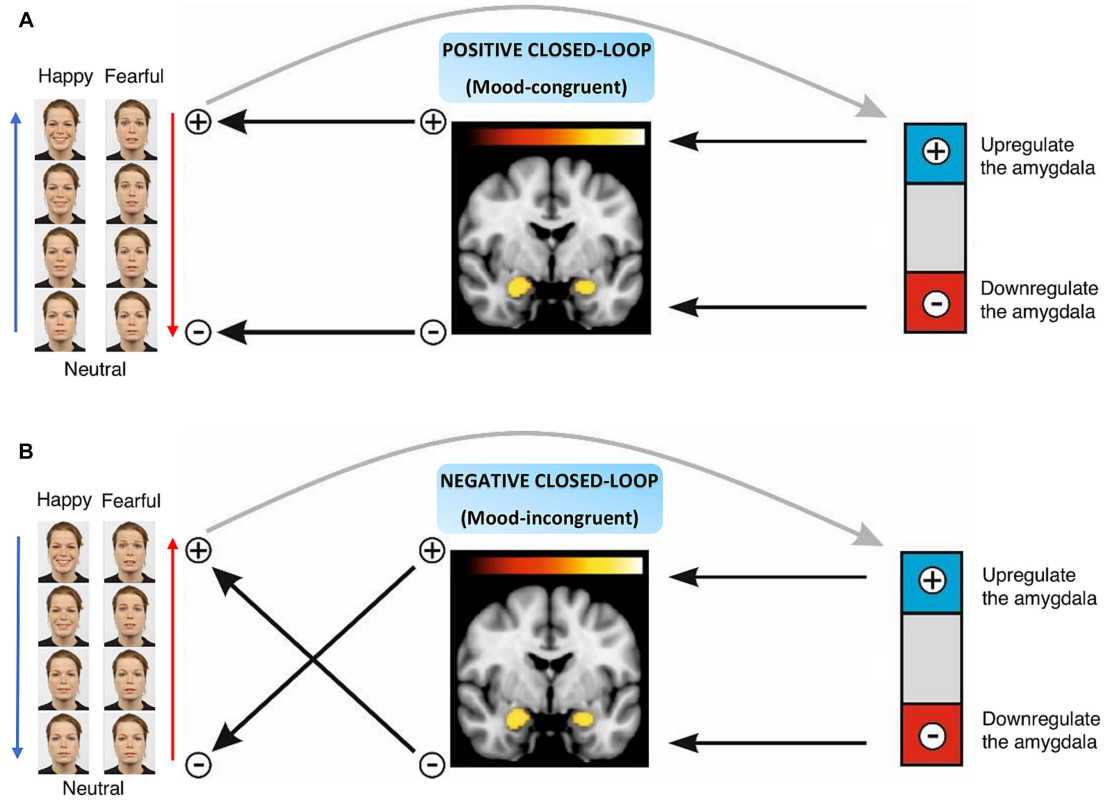


FIGURE 1
Naturalistic closed-loop neurofeedback design. **(A)** Positive closed-loop includes task-congruent conditions, i.e., happy-up and fear-down groups, where an increase in the amygdala activity enhances the intensity of the facial affect. **(B)** Negative closed-loop characterizes task-incongruent conditions, i.e., happy-down and fear-up groups where an increase in the amygdala activity reduces the intensity of the facial affect and vice versa.

age = 23.63 ± 2.85 years, gender = 8 m:8f). They were instructed to either up or downregulate the amygdala neurofeedback signal while they were presented with neutral to happy or neutral to fearful human faces (Figure 2). Participants were asked to abstain from psychotropic substances for a minimum of 3 days and from alcohol for at least 24 h prior and nicotine/caffeine 1 h prior to the imaging session. All participants provided written informed consent in accordance with the Declaration of Helsinki and were compensated for their participation. The study was approved by the local ethics committee of the canton Zurich.

## Neurofeedback task

The neurofeedback session consisted of four training runs with each neurofeedback run having four 40-s regulation blocks interleaved with four 20-s baseline blocks, during which participants were instructed to mentally count slowly (starting from one in increments of one) while fixating on a dot. During each regulation block, a new face from the Radboud Faces Database (Langner et al., 2010) was presented continuously. The faces were randomized, unique (i.e., novel for the participant), and counterbalanced for gender. Based on the group assignment, the faces expressed some degree of positive (i.e., happy) or negative (i.e., fearful) affective state. The intensity of the emotional expression was proportional to the mean blood oxygenation level dependent (BOLD) signal intensity of the participant's bilateral amygdala. The varying degrees of emotional intensity were achieved by smoothly blending faces with different emotional intensity using a face morphing software written in Python[1] (Willinger et al., 2019). Thus, participants were presented with highly naturalistic face stimuli that dynamically changed depending on their amygdala activity (Figure 2). Depending on the emotional stimulus and regulation condition, participants were assigned to one of the four experimental groups and received group-specific instructions as described below:

1. happy-up: "Try to make the face happier by up-regulating the amygdala."
2. happy-down: "Try to make the face happier by down-regulating the amygdala."
3. fear-down: "Try to make the face less fearful by down-regulating the amygdala."
4. fear-up: "Try to make the face less fearful by up-regulating the amygdala."

For all groups, ongoing bilateral amygdala activity was translated into facial expression intensity either from neutral to

1 https://github.com/alyssaq/face_morpher

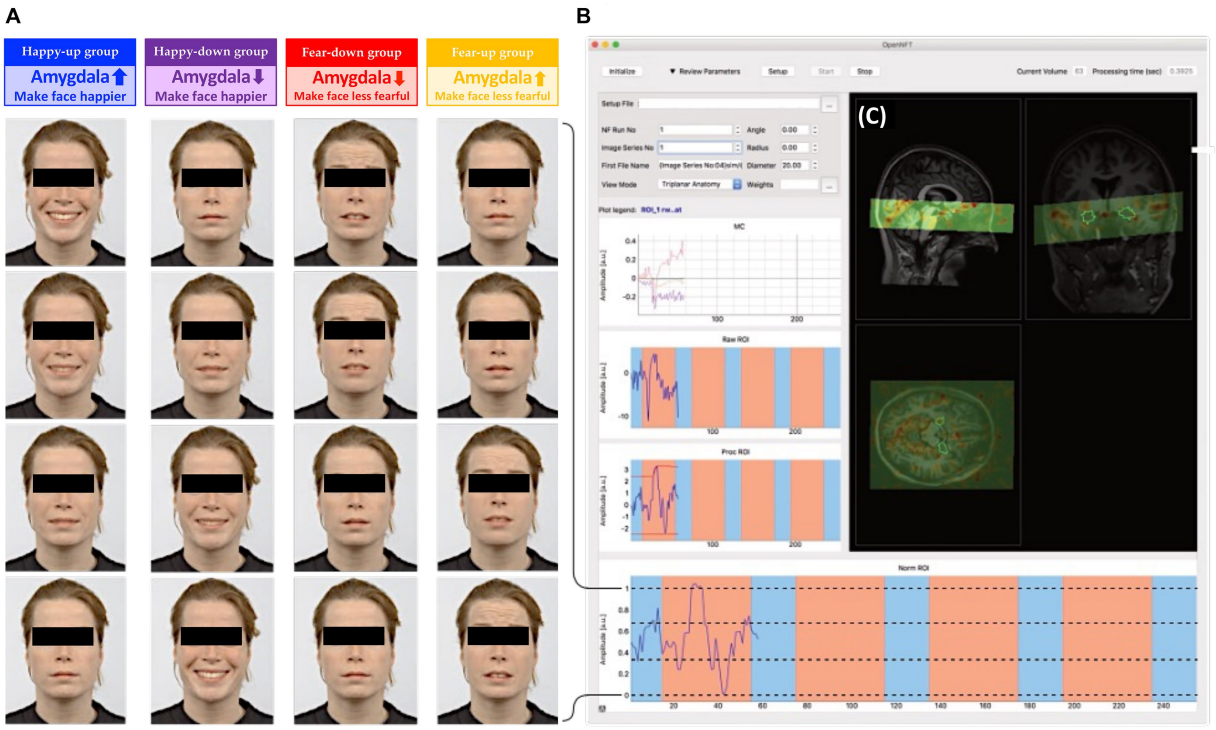


FIGURE 2
**(A)** Dynamic emotional face stimuli: Faces were digitally morphed in 30 steps from neutral to happy (happy groups) or neutral to fearful (fear groups). Subjects were instructed to either upregulate (up groups) or downregulate (down groups) the amygdala, and thus change the valence of the faces according to the group assignment. **(B)** OpenNFT display: Feedback from bilateral amygdala was continuously estimated using OpenNFT, an open-source framework for neurofeedback training (http://www.opennft.org, Koush et al., 2017a). **(C)** The field of view (green) projected on a participant's structural scan covered the mOFC, temporal lobe (amygdala, fusiform gyrus) and parts of the visual cortex. The stimulus intensities were calculated based on an anatomical mask of the bilateral amygdala (Tyszka and Pauli, 2016), and were presented as feedback using PsychoPy.

happy (first and second groups), or from fearful to neutral (third and fourth groups), as depicted in Figure 2. Participants were informed about the amygdala's involvement in affect processing and that the change in the expression of the face stimulus was based on their amygdala activity. They were given the freedom to use the emotion regulation strategies of their choice and to modify the strategies between runs. They were also asked to verbalize the experimental mental strategy beforehand and to remain focused during the task. Repeated sampling of participants' feedback between each run also ensured that participants remained engaged in the task.

## Naturalistic face feedback

The naturalistic face stimuli consisted of human faces of 30 Caucasian models (15 females) from the Radboud Face Database depicting neutral, fearful, and happy emotions (Langner et al., 2010). A face morphing algorithm developed in Python was used to create dynamic emotional faces with gradually changing facial expressions in 30 steps,[2] such that 0 corresponded to the lowest valence or neutral emotion (0%) and 30 to the highest valence (100%), i.e., fearful or happy (smiling) expressions. The intensity of the emotional valence was coupled to the average BOLD signal of the participant's bilateral amygdalae.

The estimation and presentation of the feedback signal was achieved using the Open NeuroFeedback Training (OpenNFT) software, an open-source neurofeedback framework implemented using Python and Matlab (Koush et al., 2017a). The feedback was scaled to the normalized amygdala time-series using OpenNFT's default dynamic range to estimate the maximum and minimum limits of the scaling (Koush et al., 2017a) by using the average of the 5% highest and lowest signal intensities observed so far. The preprocessed amygdala signal was then mapped to the intensity of the emotional expression ranging between the lowest and the highest valence of the face stimulus that served as the feedback signal.

## Region of Interest (ROI)

A high spatial resolution, three-dimensional, probabilistic *in vivo* anatomical mask of the bilateral amygdala used in the current study was based on the California Institute of Technology (CIT168) human brain templates (Tyszka and Pauli, 2016), and was co-registered non-linearly in individual MNI space (Figure 2C). The template mask was created using the SPM normalization function through inverse warping.

2 https://github.com/alyssaq/facemorpher

## Brain image acquisition

MRI acquisitions were performed using an Achieva 3-Tesla MRI scanner (Philipps Healthcare, Best, The Netherlands) and the manufacturer's 32 channel head coil at the MR Centre of the Psychiatric Hospital, University of Zurich. We acquired 265 volumes covering the mOFC, temporal lobe (amygdala, fusiform gyrus) and parts of the visual cortex per training run using a gradient echo T2*-weighted echo planar imaging (EPI) sequence with the following parameters: TR = 1,000 ms, TE = 35 ms, 15 interleaved ascending axial slices, $2 \times 2 \times 2\,mm^3$ voxel size, 1 mm slice gap, $112 \times 110$ matrix, field of view (FOV) = $224 \times 224 \times 44\,mm^3$, flip angle of 65°, SENSE factor 2. The first five volumes were discarded as dummy scans. Additionally, a whole brain EPI volume (same parameters as above except 70 slices and a TR = 5,000 ms) and a whole brain T1-weighted structural scan (TR = 9 ms, TE = 5 ms, 160 coronal slices, $1 \times 1 \times 1\,mm^3$ voxel size, $240 \times 240$ matrix, FOV = $240 \times 160 \times 240\,mm^3$, flip angle = 8°) were acquired for online and offline data processing and to localize the bilateral amygdala. For rt-fMRI NF, brain images were exported in real-time to a high-performance computer using the proprietary Philips DRIN export system.

## Online data processing and analysis

A spatial transformation Statistical Parametric Mapping (SPM12, v7771, https://www.fil.ion.ucl.ac.uk/spm/software/spm12/) batch pipeline was used to transform the participant's structural MRI scan, whole brain EPI volume, test EPI volume with the FOV, and a bilateral amygdala mask (Tyszka and Pauli, 2016) into the individual's space to serve as a volume of interest for neurofeedback training. The test EPI volume was used as a reference for online realignment.

Online rt-fMRI data analysis and neurofeedback signal calculation were performed using OpenNFT (Koush et al., 2017a). OpenNFT's default online preprocessing pipeline was used which comprised real-time realignment for motion correction and spatial smoothing (Gaussian kernel, 5 mm FWHM). Temporal data processing included spike removal using a Kalman filter, drift removal using a cumulative general linear model (GLM), a first-order autoregressive model AR (1) to account for serial correlations, and OpenNFT's default dynamical range scaling. The extracted, preprocessed amygdala timeseries data were used to dynamically scale the intensity of the emotional expression in the faces and served as a feedback signal for the participant.

## Offline data processing and analysis

Offline data processing and analysis of the four neurofeedback runs were performed in SPM12 and comprised slice-timing correction (Sladky et al., 2013), realignment, coregistration to the participant's whole brain EPI volume and T1-weighted structural MRI image, normalization to MNI space, and spatial smoothing with a 6 mm FWHM Gaussian kernel.

A subject-level analyses were performed using SPM12-based GLM only on the first neurofeedback run due to the groups' different regulation instructions. We aimed at differentiating the individual contributions of the experimental manipulations. We expected that the task-relevant brain responses could be modeled using three orthogonalized regressors: x1 models the effects of the fMRI task condition in general, i.e., the blocks where participants were asked to regulate their amygdala response (Figure 3A, green) by convolving the box car function that encodes the regulation blocks (20s *off*, 40s *on* period) with SPM's canonical hemodynamic response function (*cHRF*). x2 modeled the subject's response to the emotional face that scaled proportionally to the intensity of the neurofeedback signal (Figure 3A, orange), calculated by convolving the online-extracted, normalized amygdala BOLD signal (i.e., OpenNFT's Norm ROI signal, which was also used for neurofeedback stimulus presentation) with the *cHRF*, which corresponds to a parametric modulator of the block design. x3 was used to model the source of the neurofeedback signal (Figure 3A, magenta), which is confounded by both the regulation task (x1) and the response to the stimulus intensity (x2). To account for this, x1 and x2 were regressed out of the normalized amygdala BOLD signal, i.e., yielding a regressor (x3) that corresponds to the residual amygdala signal independent of the BOLD response to the neurofeedback stimulus intensity (x2) and regulation blocks (x1). Six realignment parameter estimates were included as nuisance regressors to account for residual movement artifacts not accounted for by the realignment preprocessing step. This design matrix captured the circularity that is inherent to the closed-loop paradigm of this study, where the stimulus intensity depends on the activity of the target region, which in turn is influenced by the stimulus intensity.

The second-level random effects group analysis consisted of a one-sample t-test of the individual contrasts between faces and baseline to identify neurofeedback-selective brain regions in the first neurofeedback run. Significance threshold for the resulting statistical parametric map was set to $p < 0.001$ (voxel-wise threshold) and $p < 0.05$ FWE cluster-level corrected.

Amygdala time-series analyses were based on OpenNFT logs from the neurofeedback experiment. We used the pre-processed amygdala signal (i.e., kalmanProc data). Each neurofeedback run consisted of four regulation blocks (dynamic face stimulus) interleaved with the four baseline blocks (a dot). Preprocessed data were modeled using GLM analysis with four regressors for the four individual regulation blocks to estimate the mean amygdala BOLD signal in the regulation condition. Contrasts were designed as a boxcar function with the 20s off (baseline) and 40s on (regulation) period convolved with SPM's cHRF. Average values (beta weights) were extracted from the ROI beta maps associated with each regulation block and utilized in subsequent statistical analyses.

Amygdala activity changes over four neurofeedback runs were analyzed based on linear mixed-effect model (LMM) using "lme4" package (version 1.1–31, Bates et al., 2015) in R (version 4.2.0, R Core Team, 2022). LMM analysis was performed separately for the happy (happy-up and happy-down groups) and fear (fear-up and fear-down groups) conditions. For each condition, we modeled neurofeedback runs (4 runs) and groups (congruent and incongruent) categorical variables that served as fixed effects of interest with the participant as a random effect factor. For example, in the "Happy" condition, we analyzed amygdala activity changes over four runs in task-congruent (happy-up, $N = 16$) and task-incongruent (happy-down, $N = 16$) groups with a run x group interaction. The statistical model was fitted with restricted maximum likelihood (REML) using Satterthwaite's method. A similar analysis was performed for the "Fear" condition by testing an interaction between training runs and groups (fear-down, fear-up) to assess amygdala activity changes.

10.3389/fnins.2023.1286665

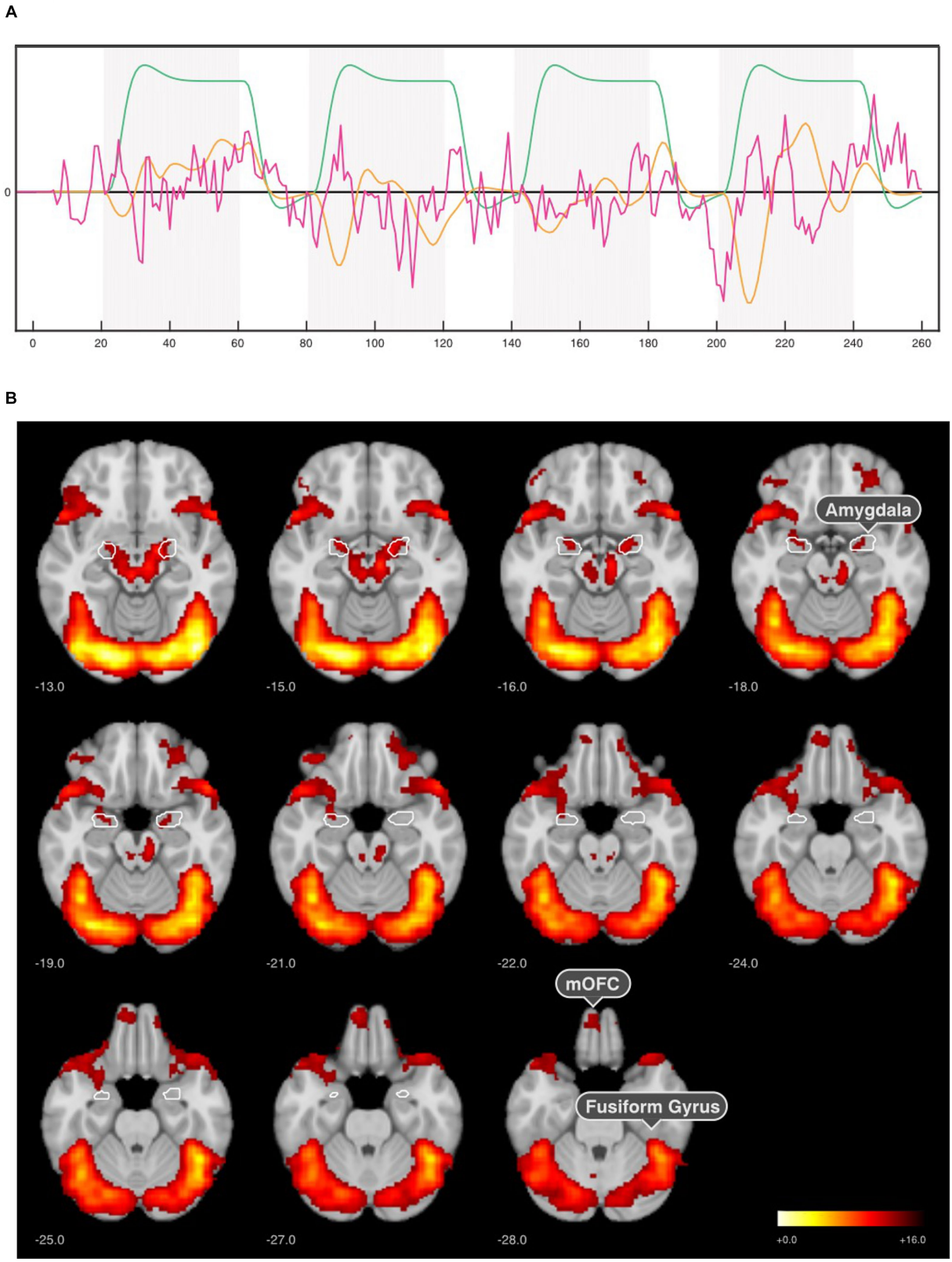


FIGURE 3
SPM-based GLM analysis results for the first neurofeedback run. **(A)** GLM model comprising three orthogonalized regressors of interest: $x_1$—regulation blocks (green), $x_2$ -neurofeedback response (amygdala signal x cHRF, orange), and $x_3$—neurofeedback signal (residual amygdala signal, magenta). **(B)** Regulation > Baseline contrasts for $x_1$ regressor in the first neurofeedback run across all groups ($n = 64$) revealed activation in the amygdala, medial orbitofrontal cortex (mOFC), fusiform gyrus (fusiform face area). The results were corrected for $p < 0.001$ voxel-wise threshold and $p < 0.05$ cluster-level family wise error (FWE).

## Dynamic causal modeling

Based on previous research (de Almeida et al., 2011; Sabatinelli et al., 2011; Sladky et al., 2022), we assumed that the amygdala (Amy) receives task-relevant input from the fusiform face area (FFA; Kanwisher et al., 1997) and the medial orbitofrontal cortex (mOFC; Roy et al., 2012). The primary visual cortex (V1) was considered to be the input for the experimental perturbation, i.e., the visual stimulation by emotional faces, and connected to the other regions. FFA is part of the ventral visual processing stream originating from V1 extending to the amygdala. In addition, the amygdala and mOFC also receive low-level visual input from other sources, e.g., thalamic pathways. This means in this case the direct connections from V1 do not reflect direct anatomical connectivity but a relevant task-specific, functional relationship. Omitting these connections would bias the model toward FFA-centered processing of emotional stimuli.

Dynamic causal modeling (DCM12 as implemented in SPM12, build 6,906) was used to estimate effective connectivity between task regions. Temporally filtered and detrended time courses of V1, bilateral FFA, bilateral amygdala, and medial orbitofrontal cortex were extracted for each subject using SPM's volume of interest (VOI) extraction batch script (single-subject significance threshold $p < 0.05$, first eigenvariate used as summary statistic, adjusted for effect of interest). For the amygdala, we used the same mask that was used in the neurofeedback experiment. For the other regions, 8 mm spheres were centered around the local maximum in the group-level SPMs: V1 x/y/z = −0.0/−87.0/−6.0 mm [MNI], rFFA x/y/z = +42.0/−51.0/−24.0 mm [MNI], left FFA x/y/z = −45.0/−45.0/−25.0 mm [MNI], and mOFC x/y/z = −8.00/56.00/−26.00 mm [MNI].

The model space comprised Amy, V1, FFA, and mOFC. It was assumed *a priori* that V1 receives the driving input (i.e., modeled as the neurofeedback face regressor). Different DCM models were created where forward connections between V1 and Amy, FFA, and mOFC as well es bidirectional connections between amygdala and mOFC and FFA were considered, which resulted in 128 models. All models were estimated and analyzed using random effects Bayesian model averaging (BMA; Penny et al., 2010) to estimate the mean effective connectivity for each connection, depending on the neurofeedback run (i.e., 1–4) and group assignment (happy-up, happy-down, fear-up, fear-down).

## Clinical assessment

The influence of closed-loop amygdala neurofeedback on participants' affectivity was investigated using self-reporting psychometric questionnaires. Participants' positive and negative affective state changes were measured using 20-item Positive And Negative Affect Schedule (PANAS, Watson et al., 1988). The Self-rating Depression Scale (SDS, Zung, 1965) was used to screen the symptoms relating to depression. These questionnaires were filled out by the participants on a desktop computer immediately before and after their MRI measurement. Training-induced behavioral changes were assessed by fitting a LMM with PANAS and SDS scores as the outcome variable, time (pre- vs. post-training) and group (task-congruent vs. incongruent) as a fixed effect of interest, and an intercept for each participant as random effect in happy and fear conditions.

The Consensus on Reporting and Experimental Design of Clinical and Cognitive-Behavioral Neurofeedback Studies checklist (CRED-nf, Ros et al., 2020), which summarizes the current rtfMRI-NF study design, is provided in Supplementary material.

# Results

Based on SPM's GLM analysis, the three regressors of interest were analyzed ($x_1$—regulation blocks, $x_2$—neurofeedback response, and $x_3$—neurofeedback signal). For the face regulation blocks ($x_1$), highest activation was observed in the visual cortex (occipital lobe) and fusiform face area (inferior temporal lobe) in the first neurofeedback run. The peak MNI coordinates [42, −78, −10] implied an activation in the occipital face-selective area. Besides the obvious maximum in the bilateral amygdala, this model indicated a strong BOLD response in a distributed network encompassing the mOFC, temporal, and occipital lobe in the first neurofeedback run across all participants (Figure 3B).

## Amygdala BOLD signal changes during neurofeedback training

Neural correlates of neurofeedback training were examined using LMM analysis by modeling run (1–4) and group (congruent and incongruent) as the fixed effects and a random intercept for participant separately in the happy and fear conditions. We observed a significant effect of run [$F(3,90) = 5.28$, $p = 0.0002$] in the fear condition with decreased amygdala activity in the third run [$\beta = -0.34$, SE = 0.11, $t(90) = -3.04$, $p = 0.003$], and the fourth run [$\beta = -0.34$, SE = 0.11, $t(90) = -3.02$, $p = 0.003$] compared to the first neurofeedback run in the fear-down group. We did not observe a significant effect of group (fear-down, fear-up) or the interaction between fixed effects, i.e., run x group. In the happy condition, LMM analyses revealed no significant effect of run, group (happy-up, happy-down), or their interaction. Amygdala activity changes over four training runs in all groups are depicted in Figure 4.

## Amygdala habituation effects within runs

Potential amygdala habituation effects within runs were investigated using a linear regression model of mean amygdala BOLD signal for each block in all participants. The resulting parameter estimates for habituation effects of each participant and run were further analyzed on a group level. No significant within-run habituation effects were observed for the happy-up and the happy-down groups. However, amygdala habituation effects were present in the last runs in the fear-down and fear-up groups. In the fear-down group, a statistically significant amygdala habituation occurred mainly in the third [Run 3: $\beta = -0.449 \pm 0.770$, $t(15) = -2.33$, $p = 0.034$] and fourth runs [Run 4: $\beta = -0.799 \pm 0.853$, $t(15) = -3.75$, $p = 0.002$]. Participants in the fear-up group exhibited an amygdala upregulation in the first three training runs with a significant habituation effect in the fourth run [Run 4: $\beta = -0.622 \pm 0.740$, $t(15) = -3.36$, $p = 0.004$]. The results are summarized in Table 1.

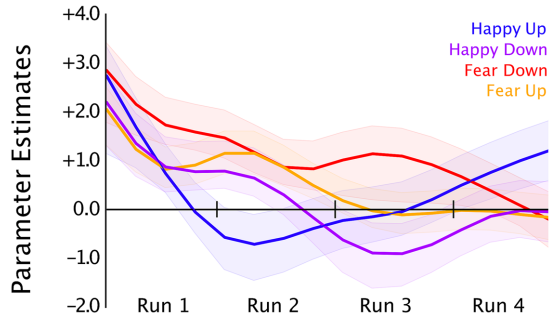


FIGURE 4
Bilateral amygdala time courses averaged (OpenNFT's kalmanProc timeseries) over four neurofeedback training runs in the happy-up (blue, n = 16), happy-down (purple, *n* = 16), fear-down (red, *n* = 16), and fear-up (orange, n = 16) groups. OpenNFT's filtered timeseries were modeled using a GLM with each regulation blocks as regressors, which resulted in a parameter estimate that represents the single subject mean of the block's time course corrected for the hemodynamic delay. For display purposes, the plot of group means is smoothed using a Gaussian window (window length = 6).

**TABLE 1** Estimated coefficients (β), standard errors (SE), *t* (degrees of freedom) and *p* values of the change in the amygdala activity within four training runs in four experimental groups.

| Groups | NFB runs | β | SE | $t_{(15)}$ | *p* |
|---|---|---|---|---|---|
| Happy-up | 1 | −1.066 | 2.512 | −1.70 | 0.110 |
| | 2 | −0.547 | 1.707 | −1.28 | 0.220 |
| | 3 | −0.103 | 0.919 | −0.45 | 0.659 |
| | 4 | 0.362 | 1.549 | 0.93 | 0.367 |
| Happy-down | 1 | 0.304 | 1.890 | 0.64 | 0.532 |
| | 2 | 0.196 | 0.996 | 0.79 | 0.442 |
| | 3 | −0.148 | 0.652 | −0.91 | 0.377 |
| | 4 | −0.402 | 0.761 | −2.11 | 0.052 |
| Fear-up | 1 | 0.559 | 0.889 | 2.52 | 0.024 |
| | 2 | 0.616* | 0.942 | 2.62 | 0.019 |
| | 3 | 0.030 | 0.862 | 0.14 | 0.891 |
| | 4 | −0.622* | 0.740 | −3.36 | 0.004 |
| Fear-down | 1 | 0.264 | 1.176 | 0.90 | 0.382 |
| | 2 | 0.088 | 0.907 | 0.39 | 0.702 |
| | 3 | −0.449* | 0.770 | −2.33 | 0.034 |
| | 4 | −0.799* | 0.853 | −3.75 | 0.002 |

*Significance at $p < 0.05$.

## Effective connectivity changes using DCM

DCM Bayesian model averaging over 128 models is illustrated in Figure 5. The extrinsic inputs into V1 were similar in all groups. Positive connections were observed from V1 to FFA, Amygdala, and mOFC between groups. Task-dependent effective connectivity between FFA to amygdala and the mOFC to amygdala during the first and the fourth runs and in between group comparisons were performed using t-tests. The results revealed that participants in the happy-up group exhibited a significant task-dependent (i.e., intrinsic connectivity [A] + modulation by faces [$B_1$] and the intensity of the emotion [$B_2$]) upregulation of the amygdala induced by the FFA and mOFC in the last run as compared to the first run. On the contrary, the fear-down group exhibited strong upregulation of the amygdala in the first run, which is counteracted by inhibitory feedback of the mOFC. This downregulation effect persisted until the last run. While participants from happy-up group maintained the positive influence of FFA and mOFC on the amygdala over runs, connectivity in the fear-down group reduced over time. This could indicate a training-related learning mechanism in the fear-down group. Other groups did not show significant connectivity changes. The group differences in the effective connectivity between V1, FFA, amygdala and mOFC are depicted in Table 2.

Within groups significant changes for FFA and amygdala connectivity were observed in happy-up (M = 0.83 ± 0.21) vs. happy-down [M = 0.19 ± 0.23, $t(15) = 8.30$, $p < 0.001$], happy-up (M = 0.83 ± 0.21) vs. fear-down [M = 0.32 ± 0.17, $t(15) = 7.50$, $p < 0.001$], and happy-up (M = 0.83 ± 0.21) vs. fear-up [M = 0.25 ± 0.19, $t(15) = 8.26$, $p < 0.001$]. Whereas, the significant mOFC and amygdala connectivity changes were observed in the happy-up (M = 0.22 ± 0.19) vs. fear-down [M = −0.08 ± 0.19, $t(15) = 4.48$, $p < 0.001$], happy-down (M = 0.19 ± 0.23) vs. fear-down [M = −0.08 ± 0.18, $t(15) = 3.71$, $p < 0.001$], and fear-down (M = 0.08 ± 0.18) vs. fear-up [M = 0.09 ± 0.22, $t(15) = -2.35$, $p = 0.03$].

## Psychometric changes

LMM analyses of psychometric measures revealed no significant effect of time, group, and interaction on PANAS and SDS scores in any group in the happy and fear conditions.

# Discussion

In the current study, we introduced an innovative neurofeedback design using dynamically adapting naturalistic face stimuli (happy and fearful faces) as a feedback signal coupled to the participant's ongoing amygdala activity. Healthy participants were trained in four groups to upregulate or downregulate their amygdala explicitly by modulating the valence of the face stimulus. Participants in the happy condition were instructed to make the face happier either by upregulating (happy-up group, task-congruent) or downregulating (happy-down group, task-incongruent) their amygdala activity. Meanwhile, participants in the fear condition were instructed to reduce fearfulness of the face through amygdala downregulation (fear-down group, task-congruent) and through upregulation (fear-up group, task-incongruent). Thus, with such a versatile neurofeedback design, we investigated the effects of the stimulus (happy vs. fearful faces), regulation condition (upregulation vs. downregulation), and task congruency (task-congruent vs. incongruent) on learning success.

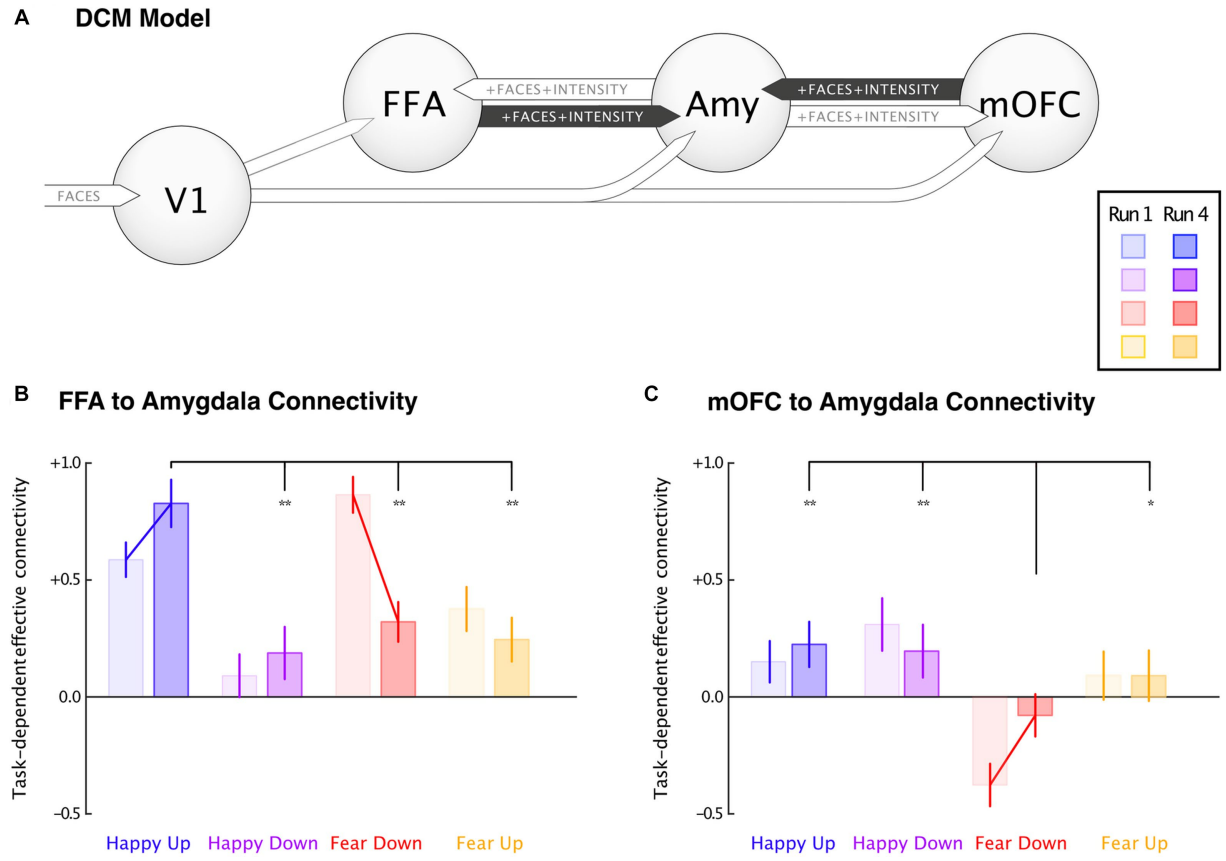


FIGURE 5
Dynamic causal modeling. Task-dependent connectivity changes were depicted between the first (light-colored bar) and the fourth (dark-colored bar) runs, and between groups. **(A)** A DCM model comprising primary visual cortex (V1), fusiform face area (FFA), medial orbitofrontal cortex (mOFC), and bilateral amygdala (Amy). **(B)** Effective connectivity changes between FFA to amygdala revealed a significant increase in the happy-up and decrease in the fear-down group, and **(C)** mOFC to amygdala connectivity showed significant negative responses in the fear-down group. Significantly decreased negative connectivity parallels reduced input from FFA. Error bars indicate 95% confidence interval, and the connecting lines denote mean significance computed using paired *t*-test. *Significance at $p < 0.05$, and **Significance at $p < 0.001$.

## Training-induced amygdala regulation

We assessed changes in the amygdala activity across four runs using LMM analysis which revealed a significant effect of run, mainly in the fear-down group (Figure 3). Higher amygdala activity was observed in all groups during the first training run which may contribute to the novelty of the emotionally salient facial stimulus (Balderston et al., 2011). Particularly, we observed a decrease in the amygdala activity in the fear-down group in the last two runs as compared to the first run. Decreasing amygdala activity in the fear-down group is congruent with the task instruction, but not in the fear-up group. It is possible that a task-congruent condition may have facilitated the perception of reward which might have encouraged the participant's regulatory effort. Whereas, in the fear-up group, a conflict between the high-level goal of amygdala upregulation (by making the face less fearful) and intrinsic desire to perceive neutral or less intense faces as rewarding (by implicitly downregulating the amygdala) may have contributed to unsuccessful upregulation.

However, contrary to our hypothesis, we did not observe a significant increase in the amygdala BOLD signal in the happy-up group, where the task instructions were congruent. A possible explanation is a ceiling effect, as reported by Paret et al. (2018), where healthy participants could not achieve successful amygdala upregulation while exposed to aroused pictures.

## Habituation effects

Some of the observed effects, particularly in the fear conditions, could be attributed to amygdala habituation. Similar effects have been observed previously (Plichta et al., 2012; Geissberger et al., 2020), however, these studies did not address the internal regulatory mechanisms and goal-directed behavior of the participants. We propose that the amygdala is not a passive processor of emotional stimuli that becomes habituated when the stimuli are no longer novel. Instead, it is part of a complex network that is also influenced by the participant's ongoing motivational goals, expectations, and other cognitive processes. We observed that the amygdala habituated in the fear-down and fear-up groups, but not in the happy-up and happy-down groups. This suggests that the participant's goal-directed behavior and the valence of the stimulus influence potential amygdala habituation effects.

TABLE 2 DCM Bayesian Model Averaging results.

| VOI | Group | Run | Intrinsic [A] | Face [$B_1$] | Intensity [$B_2$] | Total [$A + B_1 + B_2$] |
|---|---|---|---|---|---|---|
| V1 → FFA | Happy-up | 1 | +0.17 ± 0.02** | | | +0.17 ± 0.02** |
| | | 4 | +0.09 ± 0.02** | | | +0.09 ± 0.02** |
| | Happy-down | 1 | +0.03 ± 0.02** | | | +0.03 ± 0.02** |
| | | 4 | +0.06 ± 0.02** | | | +0.06 ± 0.02** |
| | Fear-down | 1 | +0.16 ± 0.02** | | | +0.16 ± 0.02** |
| | | 4 | +0.09 ± 0.02** | | | +0.09 ± 0.02** |
| | Fear-up | 1 | +0.14 ± 0.02** | | | +0.14 ± 0.02** |
| | | 4 | +0.12 ± 0.02** | | | +0.12 ± 0.02** |
| V1 → Amy | Happy-up | 1 | +0.13 ± 0.02** | | | +0.13 ± 0.02** |
| | | 4 | +0.04 ± 0.02** | | | +0.04 ± 0.02** |
| | Happy-down | 1 | +0.04 ± 0.02** | | | +0.04 ± 0.02** |
| | | 4 | +0.01 ± 0.02 | | | +0.01 ± 0.02 |
| | Fear-down | 1 | +0.16 ± 0.02** | | | +0.16 ± 0.02** |
| | | 4 | +0.04 ± 0.02** | | | +0.04 ± 0.02** |
| | Fear-up | 1 | +0.04 ± 0.02** | | | +0.04 ± 0.02** |
| | | 4 | +0.08 ± 0.02** | | | +0.08 ± 0.02** |
| V1 → mOFC | Happy-up | 1 | +0.05 ± 0.02** | | | +0.05 ± 0.02** |
| | | 4 | +0.04 ± 0.02** | | | +0.04 ± 0.02** |
| | Happy-down | 1 | −0.00 ± 0.02 | | | −0.00 ± 0.02 |
| | | 4 | +0.01 ± 0.02* | | | +0.01 ± 0.02* |
| | Fear-down | 1 | +0.12 ± 0.02** | | | +0.12 ± 0.02** |
| | | 4 | +0.01 ± 0.02* | | | +0.01 ± 0.02* |
| | Fear-up | 1 | +0.11 ± 0.02** | | | +0.11 ± 0.02** |
| | | 4 | +0.04 ± 0.02** | | | +0.04 ± 0.02** |
| FFA → Amy | Happy-up | 1 | +0.07 ± 0.03** | +0.16 ± 0.09** | +0.36 ± 0.14** | +0.59 ± 0.15** |
| | | 4 | −0.01 ± 0.03 | +0.56 ± 0.12** | +0.27 ± 0.17** | +0.83 ± 0.21** |
| | Happy-down | 1 | +0.10 ± 0.02** | −0.03 ± 0.13 | +0.02 ± 0.14 | +0.09 ± 0.19 |
| | | 4 | +0.03 ± 0.02** | +0.14 ± 0.15* | +0.02 ± 0.17 | +0.19 ± 0.23* |
| | Fear-down | 1 | +0.01 ± 0.02 | +0.55 ± 0.09** | +0.31 ± 0.13** | +0.86 ± 0.16** |
| | | 4 | +0.04 ± 0.02** | +0.29 ± 0.10** | −0.01 ± 0.16 | +0.32 ± 0.17** |
| | Fear-up | 1 | +0.04 ± 0.02** | +0.23 ± 0.13** | +0.11 ± 0.15* | +0.38 ± 0.19** |
| | | 4 | +0.01 ± 0.02* | +0.04 ± 0.12 | +0.19 ± 0.14** | +0.24 ± 0.19** |
| Amy → FFA | Happy-up | 1 | +0.13 ± 0.02** | +0.05 ± 0.04** | +0.01 ± 0.07 | +0.18 ± 0.06** |
| | | 4 | +0.04 ± 0.02** | +0.10 ± 0.09** | −0.02 ± 0.11 | +0.12 ± 0.15* |
| | Happy-down | 1 | +0.12 ± 0.02** | −0.04 ± 0.14 | +0.48 ± 0.16** | +0.56 ± 0.21** |
| | | 4 | +0.06 ± 0.02** | +0.08 ± 0.15* | −0.03 ± 0.15 | +0.11 ± 0.21 |
| | Fear-down | 1 | +0.12 ± 0.02** | −0.02 ± 0.07 | −0.02 ± 0.08 | +0.08 ± 0.10* |
| | | 4 | +0.06 ± 0.02** | +0.13 ± 0.08** | +0.04 ± 0.11 | +0.23 ± 0.13** |
| | Fear-up | 1 | +0.06 ± 0.02** | −0.02 ± 0.12 | −0.06 ± 0.14 | −0.03 ± 0.18 |
| | | 4 | +0.04 ± 0.02** | +0.00 ± 0.13 | +0.12 ± 0.15* | +0.17 ± 0.20* |
| Amy → mOFC | Happy-up | 1 | +0.03 ± 0.02** | +0.21 ± 0.04** | −0.14 ± 0.07** | +0.10 ± 0.07** |
| | | 4 | −0.01 ± 0.02* | +0.15 ± 0.09** | −0.15 ± 0.11** | −0.01 ± 0.15 |
| | Happy-down | 1 | +0.01 ± 0.02 | +0.05 ± 0.13 | −0.03 ± 0.14 | +0.03 ± 0.19 |

*(Continued)*

TABLE 2 (Continued)

| VOI | Group | Run | Intrinsic [A] | Face [$B_1$] | Intensity [$B_2$] | Total [$A + B_1 + B_2$] |
|---|---|---|---|---|---|---|
| | | 4 | +0.04 ± 0.02** | +0.04 ± 0.14 | +0.05 ± 0.15 | +0.13 ± 0.21* |
| | Fear-down | 1 | +0.08 ± 0.02** | +0.03 ± 0.07 | +0.24 ± 0.09** | +0.34 ± 0.11** |
| | | 4 | +0.03 ± 0.02** | +0.09 ± 0.08** | +0.01 ± 0.11 | +0.13 ± 0.13* |
| | Fear-up | 1 | +0.03 ± 0.02** | +0.01 ± 0.12 | −0.07 ± 0.13 | −0.02 ± 0.17 |
| | | 4 | +0.00 ± 0.02 | +0.03 ± 0.13 | +0.03 ± 0.14 | +0.05 ± 0.20 |
| mOFC → Amy | Happy-up | 1 | +0.13 ± 0.03** | +0.06 ± 0.10* | −0.03 ± 0.15 | +0.15 ± 0.18* |
| | | 4 | −0.03 ± 0.02** | +0.24 ± 0.12** | +0.02 ± 0.15 | +0.22 ± 0.20** |
| | Happy-down | 1 | −0.02 ± 0.03* | +0.19 ± 0.15** | +0.14 ± 0.16* | +0.31 ± 0.23** |
| | | 4 | +0.00 ± 0.02 | +0.02 ± 0.16 | +0.17 ± 0.17* | +0.20 ± 0.23* |
| | Fear-down | 1 | +0.02 ± 0.02* | −0.24 ± 0.12** | −0.16 ± 0.15** | −0.38 ± 0.19** |
| | | 4 | −0.03 ± 0.02** | +0.01 ± 0.11 | −0.06 ± 0.15 | −0.08 ± 0.18 |
| | Fear-up | 1 | +0.02 ± 0.02* | +0.13 ± 0.14* | −0.05 ± 0.16 | +0.09 ± 0.21 |
| | | 4 | −0.01 ± 0.02 | +0.11 ± 0.15* | −0.01 ± 0.17 | +0.09 ± 0.22 |

Intrinsic connectivity [A], modulation by faces [$B_1$] and intensity [$B_2$], and total task-dependent connectivity [$A + B_1 + B_2$]. *Significance at $p < 0.05$. **Significance at $p < 0.001$.

## Connectivity changes associated with the amygdala

We also observed amygdala effective connectivity changes using DCM that were specific to the experimental condition. We found that FFA to amygdala connectivity increased in the happy-up group and decreased in the fear-down group over four training runs. Consistent with our hypothesis, amygdala upregulation is associated with positive (i.e., facilitatory) and downregulation with negative (i.e., inhibitory) connectivity between the mOFC and the amygdala. This finding is supported by the previous effective connectivity studies suggesting that amygdala downregulation is mediated by the mOFC when participants view emotional faces (Sladky et al., 2015; Minkova et al., 2017). In the first run, the amygdala was strongly downregulated by the mOFC in the fear-down group as compared to the other groups. This downregulation effect persisted until the last run. It appears that during the first run most of the regulation occurs top-down via the mOFC, while in the last run, the bottom-up influence of the FFA is increased. While the present study cannot provide a definitive answer for the underlying mechanisms, we can speculate that upregulating (happy-up) or downregulating (fear-down) the influence of the external stimulus would be more efficient than prefrontal regulation, both neuronally (i.e., because of long-range connections) and psychologically (i.e., because of cognitive effort). Conceptualizing neurofeedback learning as a metabolically efficient adaptation of hierarchical regulation loops contrasts the view that the amygdala is a statically mapped, stimulus-driven system. Instead, viewing the amygdala as a dynamic control circuit would be in line with an active inference interpretation of amygdala function, where amygdala communication occurs via flexible perceptual predictions and resulting prediction errors (Sladky et al., 2023).

Reduced effective connectivity between the OFC and the amygdala has also been observed during increased cognitive workload (Minkova et al., 2017) and in patients with social anxiety disorder (Sladky et al., 2015). The orbitofrontal cortex appears to play a central role in social anhedonia (Germine et al., 2011). Consistent with this model, MDD patients showed a decreased amygdala upregulation by the orbitofrontal cortex when exposed to happy faces as compared to healthy controls (de Almeida et al., 2009). In our study, significant affect-specific changes were observed only in the task-congruent groups such as happy-up and fear-down, supporting an innate tendency of neural processes to increase positive and decrease negative affectivity. This may suggest an adaptive learning process guided by mOFC activity during the training. It is highly plausible that the connectivity between mOFC and amygdala is rapidly updated during task performance, as mOFC is thought to be involved in regulation mechanisms that enable adaptive behavior (Lichtenberg et al., 2017).

## Behavioral changes

We did not observe significant changes in the psychometric questionnaire scores of the participants in any of the groups. As this feasibility study was conducted in healthy participants to test the efficacy of the naturalistic feedback approach, it is less likely that the training will produce lasting or strong changes in the affectivity in participants without mood impairments. Therefore, the plausibility of this novel training approach in reducing negative mood and anxiety symptoms should be evaluated in a clinical sample such as MDD and AD patients. In addition, the pragmatic utility of the amygdala dynamic face feedback training for improving affective responses in real-life environment needs to be investigated in future studies.

## Applications of the naturalistic closed-loop neurofeedback

This innovative approach allowed participants to train self-regulation of their amygdala by changing the emotional expression of facial stimuli. Previous rtfMRI-NF studies have reported successful amygdala downregulation in healthy participants while viewing negative emotional faces (Brühl et al., 2014) or aversive situations

(Sarkheil et al., 2015; Paret et al., 2016; Herwig et al., 2018), and in clinical populations such as patients suffering with PTSD (Nicholson et al., 2016) and bipolar disorder (Zaehringer et al., 2020). Amygdala upregulation was also achieved through positive autobiographical memory recall in healthy subjects (Zotev et al., 2016; Hellrung et al., 2018) and MDD patients (Young et al., 2017). Moreover, Paret et al. (2018) demonstrated concurrent upregulation and downregulation of the amygdala in healthy female participants while viewing emotional images. Our new experimental setup extends these previous findings by providing an ecologically valid, naturalistic face feedback training that could be a versatile neuroscience research tool and a novel experimental therapy.

Compared to the abstract feedback representations used in these studies, the use of emotional faces is highly relevant to studies investigating how we perceive emotions and regulate subsequent neural responses. Social cognition involves the processing of verbal and nonverbal social cues by identifying, perceiving, and interpreting other people's behaviors, intentions, feelings, and beliefs (Frith and Frith, 2006). Faces are an important source of information relevant to the perception of the mental state of others (Weightman et al., 2014). As a result, humans are highly trained to discriminate static (e.g., identity, gender, age) and dynamic features (e.g., gaze direction and emotional expression) of other peoples' faces (Bruce and Young, 1986). While static features are processed in the fusiform gyrus (Haxby et al., 2000), their dynamicity is processed in the superior temporal sulcus (STS) with the amygdala and insula for processing of emotional expressions (Haxby et al., 2000). Thus, using a facial feedback with dynamically adapting affect is more realistic, socially rewarding and increases the sense of agency as compared to the symbolic feedback representation. Furthermore, it reduces the cognitive load associated with participants' explicit regulatory efforts by preventing dual-task interference between visual cues and feedback signal (Ihssen et al., 2017; Sitaram et al., 2017).

Naturalistic face feedback could lead to more rewarding social interactions which is specifically relevant for autism spectrum disorders (Dichter, 2018), SAD (Sladky et al., 2012), and addiction disorders, where the hedonic value of social rewards is reduced. Regarding the latter, most studies address the "wanting" component of addiction (e.g., compulsive thoughts; Koob and Le Moal, 1997; Sulzer et al., 2013; Kirschner et al., 2018), which is thought to be mediated by the dopaminergic reward network. Amygdala neurofeedback using naturalistic social rewards could be a complementary method to address the "liking" component of hedonic experience (Robinson and Berridge, 2000; Haugg et al., 2022). Thus, presenting social feedback in the form of emotional faces may be beneficial in training healthy individuals and psychiatric patients to improve social cognition.

Given the variety of methodological and psychological questions that can be addressed with such an adaptive facial feedback design, its use is not solely restricted to training a single brain region such as the amygdala. It can be tailored to address other affect processing brain regions like the anterior cingulate cortex (ACC; Mathiak et al., 2010, 2015) or even functional networks (Ramot et al., 2017; Koush et al., 2017b; Zich et al., 2020; Taylor et al., 2022) to regulate neural responses that govern emphatic behavior and social cognition. Thus, dynamic emotional faces serve as suitable naturalistic feedback stimuli for shaping clinically relevant amygdala activity.

## Limitations

This feasibility study has several limitations. We used a high-resolution anatomical mask to define the region of interest (ROI), i.e., bilateral amygdalae (Tyszka and Pauli, 2016). The amygdala is a small subcortical structure that is functionally dynamic and anatomically diverse (Tyszka and Pauli, 2016; Wang et al., 2017), so using a predefined mask to generate the feedback signal could be a limitation. Comparatively, a functional localizer task may have higher accuracy in defining participant-specific ROI that facilitates neurofeedback learning, but there is currently no supporting evidence (Haugg et al., 2021). A more refined ROI definition based on amygdala sub-nuclei may improve the quality of the neurofeedback signal which can be achieved with ultra-high field imaging at 7-Tesla fMRI, which provides a higher signal-to-noise ratio, improving spatial specificity in the subcortex (Hahn et al., 2013; Sladky et al., 2018).

Another limitation could be a restricted field of view (temporal lobe, visual cortex, and mOFC), which hindered understanding the potential influence of affect processing brain regions other than the amygdala, specifically, the cortical areas and other face processing areas such as STS and occipital face area (OFA). We restricted our data acquisition to the ventral brain because we wanted to investigate the involvement of the FFA and mOFC in addition to the amygdala. While prefrontal regions such as dorsolateral prefrontal cortex (DLPFC) play an important role in reappraisal mechanisms (Morawetz et al., 2016), we previously identified the mOFC as the most relevant causal influence on amygdala regulation (Sladky et al., 2022). However, other PFC regions engaged through the participants' explicit cognitive regulatory efforts and emotion perception regions like STS which is responsible for social cognition (Direito et al., 2021) are highly relevant and require further exploration. Future studies using faster acquisition methods such as multiband EPI sequences and higher field strengths will allow for better brain coverage without compromising the image resolution.

The main limiting factor could be the short duration of the neurofeedback training. In this proof-of-concept study, participants completed only four training runs within a single session of neurofeedback training. It is possible that such short-duration training is not enough to induce learning and subsequent behavioral changes. Hence, it is difficult to make any causal inferences regarding the effectiveness of the novel naturalistic face neurofeedback design. Currently, there is no consensus on the optimal number of neurofeedback runs or sessions required to achieve desired neural and behavioral changes in healthy and in clinical populations (Paret et al., 2019). Furthermore, recent evidence suggests that patients are more successful than healthy participants at learning self-regulation of brain activity (Haugg et al., 2021). Therefore, enrolling more participants in intensive longitudinal neurofeedback training and testing this novel approach in psychiatric disorders may lead to clinically relevant neural and behavioral changes.

Another main limitations of the study are the lack of a control group and the no-feedback practice (i.e., baseline) and transfer runs. The inclusion of a control condition is necessary to improve the specificity of the training and to rule out non-specific factors influencing the regulation success (Sorger et al., 2019). Thus, without a control group in the current study, it is difficult to ascertain causal

effects of the naturalistic face neurofeedback training. A recent meta-analysis has reported a positive correlation between the learning success and pre-training practice run without feedback (Haugg et al., 2021). While a practice run may enhance the effectiveness of the chosen regulation strategies during the actual training, a post-training no-feedback run, or a transfer run is a prerequisite for improving the transferability of the learned behavior to real life. These aspects of neurofeedback training are not addressed in the current study.

The type of adaptive emotional face feedback used in the current study may pose a challenge in determining whether the observed changes in amygdala activity are attributed to participants' conscious regulatory efforts based on the feedback they receive (feedback-driven) or are solely a response to the facial stimuli (stimulus-driven). This is because face feedback not only represents the brain's response to external stimuli (e.g., dynamic facial emotions) but also simultaneously influences the person's ability to regulate brain activity (Direito et al., 2019). This distinction is crucial for ascertaining the effectiveness of neurofeedback training. However, disentangling these two aspects is methodologically complex given the small sample size and beyond the scope of the current study. Larger and more diverse study samples (e.g., including clinical populations) might allow investigating the individual differences in emotion and amygdala regulation success at the level of effective connectivity differences. Furthermore, follow-up studies could employ specifically designed transfer runs or sham feedback conditions. Future neurofeedback studies using an adaptive feedback interface should aim to investigate the stimulus-driven and self-regulation-driven changes in brain activity.

The unavailability of the data on subjective performance during the training could be another confound. Participants included in the study were given the freedom to use emotion regulation strategies of their choice and were briefed about the amygdala neurofeedback and subsequent training goals (i.e., to make the face happier or less fearful). They were asked to verbalize the mental strategy that they intended to use before each neurofeedback run to avoid mind-wandering and rumination during the training. The most common strategies reported by the participants to make the face happier were mentally telling a joke, imagining positive memories, imagining tickling a person etc., whereas, to reduce the fearfulness of the face, calming the person down, imagining walking by the lake, hugging a person etc., were used. However, we did not include the individual regulation strategies used by the participants during the training in our analysis as we did not perform a structured qualitative interview. The use of appropriate and effective mental strategies may be central to the cognitive learning and may have an influence on neural processes and subsequent behavior, especially, in patients with psychiatric disorders (Mac Duffie et al., 2018; Herwig et al., 2019). Hence, future neurofeedback studies should consider including subjective data to address regulatory success.

## Conclusion

In conclusion, the results of this proof-of-concept study in healthy participants have demonstrated that the dynamic emotional face neurofeedback design offers a powerful experimental approach for investigating complex interactions between stimuli, regulation conditions, and adaptive feedback signals to efficiently shape brain activity. Although the present study did not confirm the clinical efficacy of closed-loop naturalistic face neurofeedback, the literature has demonstrated the therapeutic benefits of interactive feedback interfaces such as dynamic face stimuli in clinical settings (Direito et al., 2021). In this context, such a novel naturalistic face feedback design could be an extension of currently developing adaptive neurofeedback protocols for affective and other psychiatric disorders.

## Data availability statement

The raw data supporting the conclusions of this article will be made available by the authors on request, without undue reservation.

## Ethics statement

The studies involving humans were approved by Kantonale Ethikkommission Zürich. The studies were conducted in accordance with the local legislation and institutional requirements. The participants provided their written informed consent to participate in this study.

## Author contributions

AW: Data curation, Formal analysis, Project administration, Writing – original draft, Methodology. AH: Data curation, Writing – review & editing. NF: Data curation, Writing – review & editing. YK: Software, Writing – review & editing. DW: Software, Writing – review & editing. AB: Conceptualization, Methodology, Writing – review & editing. PS: Software, Writing – review & editing. FS: Conceptualization, Funding acquisition, Investigation, Methodology, Resources, Supervision, Validation, Writing – review & editing. RS: Conceptualization, Data curation, Formal analysis, Funding acquisition, Investigation, Methodology, Project administration, Supervision, Writing – original draft, Writing – review & editing.

## Funding

The author(s) declare financial support was received for the research, authorship, and/or publication of this article. This study was supported by the Swiss National Science Foundation (BSSG10_155915, 100014_178841, and 32003B_166566), the Foundation for Research in Science and the Humanities at the University of Zurich (STWF-17-012), and the Baugarten Stiftung.

## Acknowledgments

The authors would like to thank Bingjie Cheng, Margrith Kramis Jordi, Cindy Lor, and Vivian Steiger for their assistance during data acquisition, recruitment, and preparation. We would like to thank Lydia Hellrung and Hanne Scheerer for their valuable research inputs.

## Conflict of interest

The authors declare that the research was conducted in the absence of any commercial or financial relationships that could be construed as a potential conflict of interest.

## Publisher's note

All claims expressed in this article are solely those of the authors and do not necessarily represent those of their affiliated organizations, or those of the publisher, the editors and the reviewers. Any product that may be evaluated in this article, or claim that may be made by its manufacturer, is not guaranteed or endorsed by the publisher.

## Supplementary material

The Supplementary material for this article can be found online at: https://www.frontiersin.org/articles/10.3389/fnins.2023.1286665/full#supplementary-material

## References


Almeida, J. R. C., Mechelli, A., Hassel, S., Versace, A., Kupfer, D. J., and Phillips, M. L. (2009). Abnormally increased effective connectivity between parahippocampal gyrus and ventromedial prefrontal regions during emotion labeling in bipolar disorder. *Psychiatry Res. Neuroimaging* 174, 195–201. doi: 10.1016/j.pscychresns.2009.04.015

Balderston, N. L., Schultz, D. H., and Helmstetter, F. J. (2011). The human amygdala plays a stimulus specific role in the detection of novelty. *Neuroimage* 55, 1889–1898. doi: 10.1016/j.neuroimage.2011.01.034

Bates, D., Mächler, M., Bolker, B., and Walker, S. (2015). Fitting linear mixed-effects models using lme 4. *J. Stat. Softw.* 67, 1–48. doi: 10.18637/jss.v067.i01

Baxter, A. J., Vos, T., Scott, K. M., Ferrari, A. J., and Whiteford, H. A. (2014). The global burden of anxiety disorders in 2010. *Psychol. Med.* 44, 2363–2374. doi: 10.1017/S0033291713003243

Bickart, K. C., Wright, C. I., Dautoff, R. J., Dickerson, B. C., and Barrett, L. F. (2011). Amygdala volume and social network size in humans. *Nat. Neurosci.* 14, 163–164. doi: 10.1038/nn.2724

Bruce, V., and Young, A. (1986). Understanding face recognition. *Br. J. Psychol.* 77, 305–327. doi: 10.1111/j.2044-8295.1986.tb02199.x

Brühl, A. B., Scherpiet, S., Sulzer, J., Stämpfli, P., Seifritz, E., and Herwig, U. (2014). Real-time neurofeedback using functional MRI could improve down-regulation of amygdala activity during emotional stimulation: a proof-of-concept study. *Brain Topogr.* 27, 138–148. doi: 10.1007/s10548-013-0331-9

Campbell, D. W., Sareen, J., Paulus, M. P., Goldin, P. R., Stein, M. B., and Reiss, J. P. (2007). Time-varying amygdala response to emotional faces in generalized social phobia. *Biol. Psychiatry* 62, 455–463. doi: 10.1016/j.biopsych.2006.09.017

Carver, C. S. (2006). Approach, avoidance, and the self-regulation of affect and action. *Motiv. Emot.* 30, 105–110. doi: 10.1007/s11031-006-9044-7

Cooney, R. E., Atlas, L. Y., Joormann, J., Eugène, F., and Gotlib, I. H. (2006). Amygdala activation in the processing of neutral faces in social anxiety disorder: is neutral really neutral? *Psychiatry Res.* 148, 55–59. doi: 10.1016/j.pscychresns.2006.05.003

Cuijpers, P., Beekman, A. T. F., and Reynolds, C. F. (2012). Preventing depression: a global priority. *JAMA* 307, 1033–1034. doi: 10.1001/jama.2012.271

Davies, C. D., Young, K., Torre, J. B., Burklund, L. J., Goldin, P. R., Brown, L. A., et al. (2017). Altered time course of amygdala activation during speech anticipation in social anxiety disorder. *J. Affect. Disord.* 209, 23–29. doi: 10.1016/j.jad.2016.11.014

de Almeida, J. R. C., Kronhaus, D. M., Sibille, E. L., Langenecker, S. A., Versace, A., LaBarbara, E. J., et al. (2011). Abnormal left-sided Orbitomedial prefrontal cortical-amygdala connectivity during happy and fear face processing: a potential neural mechanism of female MDD. *Front. Psych.* 2:69. doi: 10.3389/fpsyt.2011.00069

de Almeida, J. R. C., Versace, A., Mechelli, A., Hassel, S., Quevedo, K., Kupfer, D. J., et al. (2009). Abnormal amygdala-prefrontal effective connectivity to happy faces differentiates bipolar from major depression. *Biol. Psychiatry* 66, 451–459. doi: 10.1016/j.biopsych.2009.03.024

Dichter, G. S. (2018). Motivational impairments in autism may be broader than previously thought. *JAMA Psychiatry* 75:773. doi: 10.1001/jamapsychiatry.2018.1078

Direito, B., Lima, J., Simões, M., Sayal, A., Sousa, T., Lührs, M., et al. (2019). Targeting dynamic facial processing mechanisms in superior temporal sulcus using a novel fMRI neurofeedback target. *Neuroscience* 406, 97–108. doi: 10.1016/j.neuroscience.2019.02.024

Direito, B., Mouga, S., Sayal, A., Simões, M., Quental, H., Bernardino, I., et al. (2021). Training the social brain: clinical and neural effects of an 8-week real-time functional magnetic resonance imaging neurofeedback phase IIa clinical trial in autism. *Autism* 25, 1746–1760. doi: 10.1177/13623613211002052

Disner, S. G., Beevers, C. G., Haigh, E. A. P., and Beck, A. T. (2011). Neural mechanisms of the cognitive model of depression. *Nat. Rev. Neurosci.* 12, 467–477. doi: 10.1038/nrn3027

Domínguez-Borràs, J., and Vuilleumier, P. (2022). Amygdala function in emotion, cognition, and behavior. *Handb. Clin. Neurol.* 187:8. doi: 10.1016/b978-0-12-823493-8.00015-8

Etkin, A., and Wager, T. D. (2007). Functional neuroimaging of anxiety: a Meta-analysis of emotional processing in PTSD, social anxiety disorder, and specific phobia. *Am. J. Psychiatry* 164, 1476–1488. doi: 10.1176/appi.ajp.2007.07030504

Friston, K. J., Harrison, L., and Penny, W. (2003). Dynamic causal modelling. *Neuroimage* 19, 1273–1302. doi: 10.1016/S1053-8119(03)00202-7

Frith, C. D., and Frith, U. (2006). How we predict what other people are going to do. *Brain Res.* 1079, 36–46. doi: 10.1016/j.brainres.2005.12.126

Geissberger, N., Tik, M., Sladky, R., Woletz, M., Schuler, A.-L., Willinger, D., et al. (2020). Reproducibility of amygdala activation in facial emotion processing at 7T. *Neuroimage* 211:116585. doi: 10.1016/j.neuroimage.2020.116585

Germine, L. T., Garrido, L., Bruce, L., and Hooker, C. (2011). Social anhedonia is associated with neural abnormalities during face emotion processing. *Neuroimage* 58, 935–945. doi: 10.1016/j.neuroimage.2011.06.059

Grupe, D. W., and Nitschke, J. B. (2013). Uncertainty and anticipation in anxiety: an integrated neurobiological and psychological perspective. *Nat. Rev. Neurosci.* 14, 488–501. doi: 10.1038/nrn3524

Hahn, A., Kranz, G. S., Seidel, E. M., Sladky, R., Kraus, C., Kublböck, M., et al. (2013). Comparing neural response to painful electrical stimulation with functional MRI at 3 and 7T. *Neuroimage* 82, 336–343. doi: 10.1016/j.neuroimage.2013.06.010

Hartwell, K. J., Hanlon, C. A., Li, X., Borckardt, J. J., Canterberry, M., Prisciandaro, J. J., et al. (2016). Individualized real-time fMRI neurofeedback to attenuate craving in nicotine-dependent smokers. *J. Psychiatry Neurosci.* 41, 48–55. doi: 10.1503/jpn.140200

Haugg, A., Manoliu, A., Sladky, R., Hulka, L. M., Kirschner, M., Brühl, A. B., et al. (2022). Disentangling craving- and valence-related brain responses to smoking cues in individuals with nicotine use disorder. *Addict. Biol.* 27:83. doi: 10.1111/adb.13083

Haugg, A., Renz, F. M., Nicholson, A. A., Lor, C., Götzendorfer, S. J., Sladky, R., et al. (2021). Predictors of real-time fMRI neurofeedback performance and improvement – a machine learning mega-analysis. *Neuroimage* 237:118207. doi: 10.1016/j.neuroimage.2021.118207

Haxby, J. V., Hoffman, E. A., and Gobbini, M. I. (2000). The distributed human neural system for face perception. *Trends Cogn. Sci.* 4, 223–233. doi: 10.1016/s1364-6613(00)01482-0

Hellrung, L., Dietrich, A., Hollmann, M., Pleger, B., Kalberlah, C., Roggenhofer, E., et al. (2018). Intermittent compared to continuous real-time fMRI neurofeedback boosts control over amygdala activation. *Neuroimage* 166, 198–208. doi: 10.1016/j.neuroimage.2017.10.031

Herwig, U., Lutz, J., Scherpiet, S., Scheerer, H., Kohlberg, J., Opialla, S., et al. (2019). Training emotion regulation through real-time fMRI neurofeedback of amygdala activity. *Neuroimage* 184, 687–696. doi: 10.1016/j.neuroimage.2018.09.068

Herwig, U., Opialla, S., Cattapan, K., Wetter, T. C., Jäncke, L., and Brühl, A. B. (2018). Emotion introspection and regulation in depression. *Psychiatry Res. Neuroimaging* 277, 7–13. doi: 10.1016/j.pscychresns.2018.04.008

Hofmann, S. G., Ellard, K. K., and Siegle, G. J. (2012). Neurobiological correlates of cognitions in fear and anxiety: a cognitive–neurobiological information-processing model. *Cognit. Emot.* 26, 282–299. doi: 10.1080/02699931.2011.579414

Ihssen, N., Sokunbi, M. O., Lawrence, A. D., Lawrence, N. S., and Linden, D. E. J. (2017). Neurofeedback of visual food cue reactivity: a potential avenue to alter incentive sensitization and craving. *Brain Imaging Behav.* 11, 915–924. doi: 10.1007/s11682-016-9558-x

Inman, C. S., Bijanki, K. R., Bass, D. I., Gross, R. E., Hamann, S., and Willie, J. T. (2020). Human amygdala stimulation effects on emotion physiology and emotional experience. *Neuropsychologia* 145:106722. doi: 10.1016/j.neuropsychologia.2018.03.019

Joormann, J., and Siemer, M. (2014). "Emotion regulation in mood disorders" in *Handbook of emotion regulation*. ed. J. J. Gross. *2nd* ed (New York, NY: Guilford Press), 3–20.

Kanwisher, N., McDermott, J., and Chun, M. M. (1997). The fusiform face area: a module in human Extrastriate cortex specialized for face perception. *J. Neurosci.* 17, 4302–4311. doi: 10.1523/JNEUROSCI.17-11-04302.1997

Karlsson, K. A., Windischberger, C., Gerstl, F., Mayr, W., Siegel, J. M., and Moser, E. (2010). Modulation of hypothalamus and amygdalar activation levels with stimulus valence. *Neuro Image* 51, 324–328. doi: 10.1016/j.neuroimage.2010.02.029

Kirschner, M., Sladky, R., Haugg, A., Stämpfli, P., Jehli, E., Hodel, M., et al. (2018). Self-regulation of the dopaminergic reward circuit in cocaine users with mental imagery and neurofeedback. *EBioMedicine* 37, 489–498. doi: 10.1016/j.ebiom.2018.10.052

Koob, G. F., and Le Moal, M. (1997). Drug abuse: hedonic homeostatic dysregulation. *Science* 278, 52–58. doi: 10.1126/science.278.5335.52

Koush, Y., Ashburner, J., Prilepin, E., Sladky, R., Zeidman, P., Bibikov, S., et al. (2017a). Open NFT: an open-source Python/Matlab framework for real-time fMRI neurofeedback training based on activity, connectivity and multivariate pattern analysis. *Neuroimage* 156, 489–503. doi: 10.1016/j.neuroimage.2017.06.039

Koush, Y., Meskaldji, D. E., Pichon, S., Rey, G., Rieger, S. W., Linden, D. E. J., et al. (2017b). Learning control over emotion networks through connectivity-based neurofeedback. *Cereb. Cortex* 27, 1193–1202. doi: 10.1093/cercor/bhv311

Krylova, M., Skouras, S., Razi, A., Nicholson, A. A., Karner, A., Steyrl, D., et al. (2021). Progressive modulation of resting-state brain activity during neurofeedback of positive-social emotion regulation networks. *Sci. Rep.* 11:23363. doi: 10.1038/s41598-021-02079-4

Langner, O., Dotsch, R., Bijlstra, G., Wigboldus, D. H. J., Hawk, S. T., and van Knippenberg, A. (2010). Presentation and validation of the Radboud faces database. *Cognit. Emot.* 24, 1377–1388. doi: 10.1080/02699930903485076

Lichtenberg, N. T., Pennington, Z. T., Holley, S. M., Greenfield, V. Y., Cepeda, C., Levine, M. S., et al. (2017). Basolateral amygdala to orbitofrontal cortex projections enable Cue-triggered reward expectations. *J. Neurosci.* 37, 8374–8384. doi: 10.1523/JNEUROSCI.0486-17.2017

Linden, D. E. J., Habes, I., Johnston, S. J., Linden, S., Tatineni, R., Subramanian, L., et al. (2012). Real-time self-regulation of emotion networks in patients with depression. *PloS One* 7:e38115. doi: 10.1371/journal.pone.0038115

Mac Duffie, K. E., Mac Innes, J., Dickerson, K. C., Eddington, K. M., Strauman, T. J., and Adcock, R. A. (2018). Single session real-time fMRI neurofeedback has a lasting impact on cognitive behavioral therapy strategies. *Neuro Image. Clin* 19, 868–875. doi: 10.1016/j.nicl.2018.06.009

Mathiak, K. A., Alawi, E. M., Koush, Y., Dyck, M., Cordes, J. S., Gaber, T. J., et al. (2015). Social reward improves the voluntary control over localized brain activity in fMRI-based neurofeedback training. *Front. Behav. Neurosci.* 9:136. doi: 10.3389/fnbeh.2015.00136

Mathiak, K. A., Koush, Y., Dyck, M., Gaber, T. J., Alawi, E. A., Zepf, F. D., et al. (2010). Social reinforcement can regulate localized brain activity. *Eur. Arch. Psychiatry Clin. Neurosci.* 260, 132–136. doi: 10.1007/s00406-010-0135-9

McMakin, D. L., Olino, T. M., Porta, G., Dietz, L. J., Emslie, G., Clarke, G., et al. (2012). Anhedonia predicts poorer recovery among youth with selective serotonin reuptake inhibitor treatment-resistant depression. *J. Am. Acad. Child Adolesc. Psychiatry* 51, 404–411. doi: 10.1016/j.jaac.2012.01.011

Minkova, L., Sladky, R., Kranz, G. S., Woletz, M., Geissberger, N., Kraus, C., et al. (2017). Task-dependent modulation of amygdala connectivity in social anxiety disorder. *Psychiatry Res. Neuroimaging* 262, 39–46. doi: 10.1016/j.pscychresns.2016.12.016

Momen, N. C., Plana-Ripoll, O., Agerbo, E., Benros, M. E., Børglum, A. D., Christensen, M. K., et al. (2020). Association between mental disorders and subsequent medical conditions. *N. Engl. J. Med.* 382, 1721–1731. doi: 10.1056/NEJMoa1915784

Morawetz, C., Bode, S., Baudewig, J., Kirilina, E., and Heekeren, H. R. (2016). Changes in effective connectivity between dorsal and ventral prefrontal regions moderate emotion regulation. *Cereb. Cortex* 26, 1923–1937. doi: 10.1093/cercor/bhv005

Mulholland, T., Boudrot, R., and Davidson, A. (1979). Feedback delay and amplitude threshold and control of the occipital EEG. *Biofeedback Self Regul.* 4, 93–102. doi: 10.1007/BF01007104

Mulholland, T., and Eberlin, P. (1977). Effect of feedback contingencies on the control of occipital alpha. *Biofeedback Self Regul.* 2, 43–57. doi: 10.1007/BF01001719

Nicholson, A. A., Friston, K. J., Zeidman, P., Harricharan, S., McKinnon, M. C., Densmore, M., et al. (2017). Dynamic causal modeling in PTSD and its dissociative subtype: bottom–up versus top–down processing within fear and emotion regulation circuitry. *Hum. Brain Mapp.* 38, 5551–5561. doi: 10.1002/hbm.23748

Nicholson, A. A., Ros, T., Frewen, P. A., Densmore, M., Théberge, J., Kluetsch, R. C., et al. (2016). Alpha oscillation neurofeedback modulates amygdala complex connectivity and arousal in posttraumatic stress disorder. *Neuroimage Clin* 12, 506–516. doi: 10.1016/j.nicl.2016.07.006

Nordentoft, M., Wahlbeck, K., Hällgren, J., Westman, J., Ösby, U., Alinaghizadeh, H., et al. (2013). Excess mortality, causes of death and life expectancy in 270,770 patients with recent onset of mental disorders in Denmark, Finland and Sweden. *PloS One* 8:e55176. doi: 10.1371/journal.pone.0055176

Paret, C., Goldway, N., Zich, C., Keynan, J. N., Hendler, T., Linden, D., et al. (2019). Current progress in real-time functional magnetic resonance-based neurofeedback: methodological challenges and achievements. *Neuroimage* 202:116107. doi: 10.1016/j.neuroimage.2019.116107

Paret, C., Kluetsch, R., Ruf, M., Demirakca, T., Hoesterey, S., Ende, G., et al. (2014). Down-regulation of amygdala activation with real-time fMRI neurofeedback in a healthy female sample. *Front. Behav. Neurosci.* 8:299. doi: 10.3389/fnbeh.2014.00299

Paret, C., Ruf, M., Gerchen, M. F., Kluetsch, R., Demirakca, T., Jungkunz, M., et al. (2016). fMRI neurofeedback of amygdala response to aversive stimuli enhances prefrontal–limbic brain connectivity. *Neuroimage* 125, 182–188. doi: 10.1016/j.neuroimage.2015.10.027

Paret, C., Zähringer, J., Ruf, M., Gerchen, M. F., Mall, S., Hendler, T., et al. (2018). Monitoring and control of amygdala neurofeedback involves distributed information processing in the human brain. *Hum. Brain Mapp.* 39, 3018–3031. doi: 10.1002/hbm.24057

Penny, W. D., Stephan, K. E., Daunizeau, J., Rosa, M. J., Friston, K. J., Schofield, T. M., et al. (2010). Comparing families of dynamic causal models. *PLoS Comput. Biol.* 6:e1000709. doi: 10.1371/journal.pcbi.1000709

Pessoa, L., and Adolphs, R. (2010). Emotion processing and the amygdala: from a "low road" to "many roads" of evaluating biological significance. *Nat. Rev. Neurosci.* 11, 773–782. doi: 10.1038/nrn2920

Phan, K. L., Fitzgerald, D. A., Nathan, P. J., and Tancer, M. E. (2006). Association between amygdala hyperactivity to harsh faces and severity of social anxiety in generalized social phobia. *Biol. Psychiatry* 59, 424–429. doi: 10.1016/j.biopsych.2005.08.012

Philip, L., Martin, J.-C., and Clavel, C. (2018). Rapid facial reactions in response to facial expressions of emotion displayed by real versus virtual faces. *Iperception* 9:204166951878652. doi: 10.1177/2041669518786527

Plichta, M. M., Schwarz, A. J., Grimm, O., Morgen, K., Mier, D., Haddad, L., et al. (2012). Test–retest reliability of evoked BOLD signals from a cognitive–emotive fMRI test battery. *Neuroimage* 60, 1746–1758. doi: 10.1016/j.neuroimage.2012.01.129

Pope, A. T., Bogart, E. H., and Bartolome, D. S. (1995). Biocybernetic system evaluates indices of operator engagement in automated task. *Biol. Psychol.* 40, 187–195. doi: 10.1016/0301-0511(95)05116-3

R Core Team, (2022). R: A language and environment for statistical computing. R Foundation for Statistical Computing, Vienna, Austria. Available at: https://www.R-project.org/.

Ramot, M., Kimmich, S., Gonzalez-Castillo, J., Roopchansingh, V., Popal, H., White, E., et al. (2017). Direct modulation of aberrant brain network connectivity through real-time neuro feedback. *Elife* 6:e28974. doi: 10.7554/eLife.28974

Robinson, T. E., and Berridge, K. C. (2000). The psychology and neurobiology of addiction: an incentive–sensitization view. *Addiction* 95, 91–117. doi: 10.1080/09652140050111681

Ros, T., Enriquez-Geppert, S., Zotev, V., Young, K. D., Wood, G., Whitfield-Gabrieli, S., et al. (2020). Conensus on the reporting and experimental design of clinical and cognitive behavioural neurofeedback studies (CRED-nf checklist). *Brain.* 143, 1674–1685. doi: 10.1093/brain/awaa009

Roy, M., Shohamy, D., and Wager, T. D. (2012). Ventromedial prefrontal-subcortical systems and the generation of affective meaning. *Trends Cogn. Sci.* 16, 147–156. doi: 10.1016/j.tics.2012.01.005

Sabatinelli, D., Fortune, E. E., Li, Q., Siddiqui, A., Krafft, C., Oliver, W. T., et al. (2011). Emotional perception: Meta-analyses of face and natural scene processing. *Neuroimage* 54, 2524–2533. doi: 10.1016/j.neuroimage.2010.10.011

Santomauro, D. F., Mantilla Herrera, A. M., Shadid, J., Zheng, P., Ashbaugh, C., Pigott, D. M., et al. (2021). Global prevalence and burden of depressive and anxiety disorders in 204 countries and territories in 2020 due to the COVID-19 pandemic. *Lancet* 398, 1700–1712. doi: 10.1016/S0140-6736(21)02143-7

Sarkheil, P., Zilverstand, A., Kilian-Hütten, N., Schneider, F., Goebel, R., and Mathiak, K. (2015). fMRI feedback enhances emotion regulation as evidenced by a reduced amygdala response. *Behav. Brain Res.* 281, 326–332. doi: 10.1016/j.bbr.2014.11.027

Schneier, F. R., Kent, J. M., Star, A., and Hirsch, J. (2009). Neural circuitry of submissive behavior in social anxiety disorder: a preliminary study of response to direct eye gaze. *Psychiatry Res. Neuroimaging* 173, 248–250. doi: 10.1016/j.pscychresns.2008.06.004

Siegle, G. J., Thompson, W., Carter, C. S., Steinhauer, S. R., and Thase, M. E. (2007). Increased amygdala and decreased dorsolateral prefrontal BOLD responses in unipolar depression: related and independent features. *Biol. Psychiatry* 61, 198–209. doi: 10.1016/j.biopsych.2006.05.048

Sitaram, R., Ros, T., Stoeckel, L., Haller, S., Scharnowski, F., Lewis-Peacock, J., et al. (2017). Closed-loop brain training: the science of neurofeedback. *Nat. Rev. Neurosci.* 18, 86–100. doi: 10.1038/nrn.2016.164

Sladky, R., Baldinger, P., Kranz, G. S., Tröstl, J., Höflich, A., Lanzenberger, R., et al. (2013). High-resolution functional MRI of the human amygdala at 7T. *Eur. J. Radiol.* 82, 728–733. doi: 10.1016/j.ejrad.2011.09.025

Sladky, R., Geissberger, N., Pfabigan, D. M., Kraus, C., Tik, M., Woletz, M., et al. (2018). Unsmoothed functional MRI of the human amygdala and bed nucleus of the stria terminalis during processing of emotional faces. *Neuroimage* 168, 383–391. doi: 10.1016/j.neuroimage.2016.12.024

Sladky, R., Hahn, A., Karl, I. L., Geissberger, N., Kranz, G. S., Tik, M., et al. (2022). Dynamic causal modeling of the prefrontal/amygdala network during processing of emotional faces. *Brain Connect.* 12, 670–682. doi: 10.1089/brain.2021.0073

Sladky, R., Hoflich, A., Atanelov, J., Kraus, C., Baldinger, P., Moser, E., et al. (2012). Increased neural habituation in the amygdala and orbitofrontal cortex in social anxiety disorder revealed by fMRI. *PloS One* 7:e50050. doi: 10.1371/journal.pone.0050050

Sladky, R., Höflich, A., Küblböck, M., Kraus, C., Baldinger, P., Moser, E., et al. (2015). Disrupted effective connectivity between the amygdala and orbitofrontal cortex in social anxiety disorder during emotion discrimination revealed by dynamic causal modeling for fMRI. *Cereb. Cortex* 25, 895–903. doi: 10.1093/cercor/bht279

Sladky, R., Kargl, D., Haubensak, W., and Lamm, C. (2023). An active inference perspective for the amygdala complex. *Trends Cogn. Sci.* 15, S1364–6613. doi: 10.1016/j.tics.2023.11.004

Sorger, B., Scharnowski, F., Linden, D. E. J., Hampson, M., and Young, K. D. (2019). Control freaks: towards optimal selection of control conditions for fMRI neurofeedback studies. *Neuroimage* 186, 256–265. doi: 10.1016/j.neuroimage.2018.11.004

Steel, Z., Marnane, C., Iranpour, C., Chey, T., Jackson, J. W., Patel, V., et al. (2014). The global prevalence of common mental disorders: a systematic review and meta-analysis 1980–2013. *Int. J. Epidemiol.* 43, 476–493. doi: 10.1093/ije/dyu038

Stein, M. B., Goldin, P. R., Sareen, J., Zorrilla, L. T. E., and Brown, G. G. (2002). Increased amygdala activation to angry and contemptuous faces in generalized social phobia. *Arch. Gen. Psychiatry* 59, 1027–1034. doi: 10.1001/archpsyc.59.11.1027

Sulzer, J., Haller, S., Scharnowski, F., Weiskopf, N., Birbaumer, N., Blefari, M. L., et al. (2013). Real-time fMRI neurofeedback: Progress and challenges. *Neuroimage* 76, 386–399. doi: 10.1016/j.neuroimage.2013.03.033

Suslow, T., Konrad, C., Kugel, H., Rumstadt, D., Zwitserlood, P., Schöning, S., et al. (2010). Automatic mood-congruent amygdala responses to masked facial expressions in major depression. *Biol. Psychiatry* 67, 155–160. doi: 10.1016/j.biopsych.2009.07.023

Taylor, J. E., Yamada, T., Kawashima, T., Kobayashi, Y., Yoshihara, Y., Miyata, J., et al. (2022). Depressive symptoms reduce when dorsolateral prefrontal cortex-precuneus connectivity normalizes after functional connectivity neurofeedback. *Sci. Rep.* 12:2581. doi: 10.1038/s41598-022-05860-1

Tillfors, M., Furmark, T., Marteinsdottir, I., and Fredrikson, M. (2002). Cerebral blood flow during anticipation of public speaking in social phobia: a PET study. *Biol. Psychiatry* 52, 1113–1119. doi: 10.1016/S0006-3223(02)01396-3

Toates, F. M. (1975). *Control theory in biology and experimental psychology*. London: Hutchinson Educational Ltd.

Tyszka, J. M., and Pauli, W. M. (2016). In vivo delineation of subdivisions of the human amygdaloid complex in a high-resolution group template. *Hum. Brain Mapp.* 37, 3979–3998. doi: 10.1002/hbm.23289

Victor, T. A., Furey, M. L., Fromm, S. J., Öhman, A., and Drevets, W. C. (2010). Relationship between amygdala responses to masked faces and mood state and treatment in major depressive disorder. *Arch. Gen. Psychiatry* 67, 1128–1138. doi: 10.1001/archgenpsychiatry.2010.144

Wang, S., Yu, R., Tyszka, J. M., Zhen, S., Kovach, C., Sun, S., et al. (2017). The human amygdala parametrically encodes the intensity of specific facial emotions and their categorical ambiguity. *Nat. Commun.* 8:14821. doi: 10.1038/ncomms14821

Watson, D., Clark, L. A., and Tellegen, A. (1988). Development and validation of brief measures of positive and negative affect: the PANAS scales. *J. Pers. Soc. Psychol.* 54, 1063–1070. doi: 10.1037//0022-3514.54.6.1063

Weightman, M. J., Air, T. M., and Baune, B. T. (2014). A review of the role of social cognition in major depressive disorder. *Front. Psych.* 5:179. doi: 10.3389/fpsyt.2014.00179

Willinger, D., Karipidis, I. I., Beltrani, S., Di Pietro, S. V., Sladky, R., Walitza, S., et al. (2019). Valence-dependent coupling of prefrontal-amygdala effective connectivity during facial affect processing. *eNeuro* 6:ENEURO.0079-19.2019. doi: 10.1523/ENEURO.0079-19.2019

Wittchen, H. U., Jacobi, F., Rehm, J., Gustavsson, A., Svensson, M., Jönsson, B., et al. (2011). The size and burden of mental disorders and other disorders of the brain in Europe 2010. *Eur. Neuropsychopharmacol.* 21, 655–679. doi: 10.1016/j.euroneuro.2011.07.018

World Health Organization. (2022). Mental Disorders. https://www.who.int/news-room/fact-sheets/detail/mental-disorders (Accessed 8 June 2022).

Young, K. D., Bodurka, J., and Drevets, W. C. (2016). Differential neural correlates of autobiographical memory recall in bipolar and unipolar depression. *Bipolar Disord.* 18, 571–582. doi: 10.1111/bdi.12441

Young, K. D., Siegle, G. J., Zotev, V., Phillips, R., Misaki, M., Yuan, H., et al. (2017). Randomized clinical trial of real-time fMRI amygdala neurofeedback for major depressive disorder: effects on symptoms and autobiographical memory recall, in. *Am. J. Psychiatry* 174, 748–755. doi: 10.1176/appi.ajp.2017.16060637

Zaehringer, J., Jennen-Steinmetz, C., Schmahl, C., Ende, G., and Paret, C. (2020). Psychophysiological effects of downregulating negative emotions: insights from a Meta-analysis of healthy adults. *Front. Psychol.* 11:470. doi: 10.3389/fpsyg.2020.00470

Zich, C., Johnstone, N., Lührs, M., Lisk, S., Haller, S. P. W., Lipp, A., et al. (2020). Modulatory effects of dynamic fMRI-based neurofeedback on emotion regulation networks in adolescent females. *Neuroimage* 220:117053. doi: 10.1016/j.neuroimage.2020.117053

Zotev, V., Yuan, H., Misaki, M., Phillips, R., Young, K. D., Feldner, M. T., et al. (2016). Correlation between amygdala BOLD activity and frontal EEG asymmetry during real-time fMRI neurofeedback training in patients with depression. *Neuroimage Clin* 11, 224–238. doi: 10.1016/j.nicl.2016.02.003

Zung, W. W. K. (1965). A self-rating depression scale. *Arch. Gen. Psychiatry* 12:63. doi: 10.1001/archpsyc.1965.01720310065008

10.3389/fnins.2023.1286665

## Glossary

| | |
|---|---|
| WHO | World Health Organization |
| MDD | Major depressive disorder |
| AD | Anxiety disorders |
| PTSD | Posttraumatic stress disorder |
| SAD | Social anxiety disorder |
| fMRI | Functional magnetic resonance imaging |
| rtfMRI-NF | Real-time fMRI neurofeedback |
| TR | Repetition time |
| TE | Echo-time |
| EPI | Echo planar imaging |
| FOV | Field of view |
| ROI | Region of interest |
| FWHM | Full width at half maximum |
| MNI | Montreal Neurologic Institute |
| GLM | General linear model |
| SPM | Statistical parametric mapping |
| DCM | Dynamic causal modeling |
| BMA | Bayesian model averaging |
| cHRF | Canonical hemodynamic response function |
| BOLD | Blood oxygenation level dependent |
| FFA | Fusiform face area |
| mOFC | Medial orbitofrontal cortex |
| ACC | Anterior cingulate cortex |
| DLPFC | Dorsolateral prefrontal cortex |
| PANAS | Positive and negative affect schedule |
| SDS | Self-rating depression scale |
| ANOVA | Analysis of variance |
| STS | Superior temporal sulcus |

frontiers | Frontiers in Neuroscience

TYPE Original Research
PUBLISHED 14 February 2024
DOI 10.3389/fnins.2024.1245791



OPEN ACCESS

EDITED BY
Stavros Skouras,
University of Bergen, Norway

REVIEWED BY
Amaresh K. Ranjan,
Pharmazz Inc., United States
David M. A. Mehler,
University Hospital RWTH Aachen, Germany

*CORRESPONDENCE
Noah S. Molinski
✉ noah.molinski@charite.de

†These authors have contributed equally to this work

RECEIVED 23 June 2023
ACCEPTED 31 January 2024
PUBLISHED 14 February 2024

CITATION
Molinski NS, Kenda M, Leithner C, Nee J, Storm C, Scheel M and Meddeb A (2024) Deep learning-enabled detection of hypoxic–ischemic encephalopathy after cardiac arrest in CT scans: a comparative study of 2D and 3D approaches.
*Front. Neurosci.* 18:1245791.
doi: 10.3389/fnins.2024.1245791



# Deep learning-enabled detection of hypoxic–ischemic encephalopathy after cardiac arrest in CT scans: a comparative study of 2D and 3D approaches

Noah S. Molinski[1]*, Martin Kenda[2,3], Christoph Leithner[2], Jens Nee[4], Christian Storm[4], Michael Scheel[1†] and Aymen Meddeb[1,3†]

[1]Department for Neuroradiology, Charité – Universitätsmedizin Berlin, Freie Universität Berlin and Humboldt-Universität zu Berlin, Berlin, Germany, [2]Department of Neurology with Experimental Neurology, Charité – Universitätsmedizin Berlin, Freie Universität Berlin and Humboldt-Universität zu Berlin, Berlin, Germany, [3]Berlin Institute of Health at Charité – Universitätsmedizin Berlin, BIH Biomedical Innovation Academy, Berlin, Germany, [4]Department of Nephrology and Medical Intensive Care, Charité – Universitätsmedizin Berlin, Freie Universität Berlin and Humboldt-Universität zu Berlin, Berlin, Germany

**Objective:** To establish a deep learning model for the detection of hypoxic–ischemic encephalopathy (HIE) features on CT scans and to compare various networks to determine the best input data format.

**Methods:** 168 head CT scans of patients after cardiac arrest were retrospectively identified and classified into two categories: 88 (52.4%) with radiological evidence of severe HIE and 80 (47.6%) without signs of HIE. These images were randomly divided into a training and a test set, and five deep learning models based on based on Densely Connected Convolutional Networks (DenseNet121) were trained and validated using different image input formats (2D and 3D images).

**Results:** All optimized stacked 2D and 3D networks could detect signs of HIE. The networks based on the data as 2D image data stacks provided the best results (*S100:* AUC: 94%, ACC: 79%, *S50:* AUC: 93%, ACC: 79%). We provide visual explainability data for the decision making of our AI model using Gradient-weighted Class Activation Mapping.

**Conclusion:** Our proof-of-concept deep learning model can accurately identify signs of HIE on CT images. Comparing different 2D- and 3D-based approaches, most promising results were achieved by 2D image stack models. After further clinical validation, a deep learning model of HIE detection based on CT images could be implemented in clinical routine and thus aid clinicians in characterizing imaging data and predicting outcome.

KEYWORDS

**artificial intelligence, cardiac arrest, CT, hypoxic-ischemic encephalopathy, classification, GradCAM**

# 1 Introduction

Globally, up to six million people suffer from sudden cardiac arrest each year, with less than 10% surviving (Zeppenfeld et al., 2022). Hypoxic ischemic encephalopathy (HIE) is a major cause of mortality and long-term disability among survivors in the acute phase (Geocadin et al., 2019). Accurate neuroprognostication is crucial, and current guidelines recommend combining several prognostic factors to predict poor outcomes (Deutsche Gesellschaft für Neurologie e.V, 2017). Besides neurological examination, laboratory tests and electrophysiology, computed tomography (CT) of the brain is vital in predicting of neurological outcome in patients with suspected HIE. Cerebral edema with decreased attenuation of gray matter in CT is a typical finding in patients with severe HIE, and a loss of boundary between gray and white matter has been shown to be associated with poor outcome (Kjos et al., 1983).

The early detection of HIE is especially important for choosing the right treatment protocol because the approach for patients with HIE differs significantly from that of patients without HIE. For patients with HIE, the primary goal of treatment is to minimize brain damage and promote neurological recovery. This may involve therapeutic hypothermia to reduce metabolic activity and protect the brain (Nolan et al., 2015). Additionally, supportive care, including maintaining adequate blood pressure, oxygenation, and fluid balance, is essential. In contrast, patients without HIE typically receive supportive care and monitoring, with a focus on preventing complications from the cardiac arrest itself (Nolan et al., 2021).

A reliable prognostic factor for poor outcome is the cerebral gray–white matter ratio (GWR) (Scheel et al., 2013; Lee et al., 2015; Na et al., 2018; Streitberger et al., 2019). Several studies determined that a GWR below 1.16–1.22 highly predicted poor neurological outcome (Kim et al., 2013; Scheel et al., 2013; Cristia et al., 2014; Lee et al., 2015). Various approaches exist to assess the GWR and predict poor outcome with high specificity and low-to-moderate sensitivity, depending on imaging timing (Na et al., 2018). Commonly, GWR is measured through manual placement of up to 16 regions of interest (ROIs) by a neuroradiologist (Metter et al., 2011). The manual placement of ROIs is however time consuming and prone to interrater variability (Kenda et al., 2022). More recently, Kenda et al. developed a simplified method with an automated placement of atlas ROIs (bilateral putamen and internal capsule) with comparable outcome prediction to the 16 ROIs method (Kenda et al., 2021).

The recent development of machine and deep learning has significantly progressed and advanced the field of medical image analysis. Deep convolutional neural networks (CNNs) became widespread in the last decade and successfully addressed tasks such as object detection, image segmentation and classification. Several studies have demonstrated promising results in organ segmentation (Akkus et al., 2017; Livne et al., 2019; Hssayeni et al., 2020; Meddeb et al., 2021) and disease classification (Artzi et al., 2019; Burduja et al., 2020; Li et al., 2020; Meddeb et al., 2022; Nishio et al., 2022). In neuro-imaging, deep learning models have been successfully applied to intracranial hemorrhage detection and segmentation using CT images (Xu et al., 2021), as well as brain tumor classification using magnetic resonance imaging (MRI) (Gao et al., 2022).

The purpose of this investigation was to develop a deep learning framework capable of identifying imaging features of hypoxic–ischemic encephalopathy (HIE) in CT scans of resuscitated cardiac arrest patients. The principal emphasis was on investigating the feasibility and constraints of deep learning in HIE detection, along with technical and clinical prerequisites. Various model architectures were evaluated using 2D and 3D data formats to develop a state-of-the-art model with the highest achievable classification accuracy.

# 2 Methods

## 2.1 Study design

This retrospective observational study used prospectively collected data from adult (aged ≥18 years) comatose CA survivors treated with targeted temperature management (TTM) at a single tertiary academic hospital between 2010 and 2019. This study was approved by the institutional review board of the Charité (No.: EA2/066/17, EA4/136/21). The recommendations of the CLAIM checklist of the RSNA and the DECIDE-AI checklist were largely adhered to and are attached as Supplementary materials (Mongan et al., 2020; Vasey et al., 2022). Due to the retrospective design of this study, new informed consent was not required. All patient data was strictly protected and anonymized prior to analysis.

## 2.2 Study population

We included 168 patients from a previously published cohort of 483 cardiac arrest (CA) survivors with suspected HIE from our institution (Kenda et al., 2021). After admission to the intensive care unit (ICU), patients were treated with TTM (body temperature of 33°C for 24 h) according to the European Resuscitation Council Guidelines (Nolan et al., 2015). All patients received CT-imaging within seven days after *CA*. The head CT images were taken by several GE Lightspeed and Revolution scanners as well as on Toshiba Aquilion. Neurological outcome was assessed by treating physicians at hospital discharge using the cerebral performance category (CPC) scale. For prognostic evaluation in this study, the outcome was dichotomized into "good" (CPC 1–3) and "poor" outcome (CPC 4–5). A board-certified radiologist (AM) and a board-certified neuroradiologist (MS) classified CTs with the labels "HIE" or "no HIE." Both radiologists were blinded to the clinical parameters of the study population. All patient data was handled only using anonymized identifiers based on patient cohort and a number in the form of X123 which still enables future de-identification A graphical representation of the patient selection and data flow of this study can be found in the Supplementary Figure S1.

## 2.3 CT imaging characteristics and preprocessing

All CT images were reformatted from standard DICOM to Neuroimaging Informatics Technology Initiative (NIfTI) format. In a second stage, they were co-registered in a linear and non-linear mode to a standardized CT template in an MRI-based standard space using FNIRT and FLIRT functions from FSL (FMRIB Software Library v6.0, FMRIB, Oxford, UK) (Jenkinson et al., 2012). To reduce superfluous information, we evaluated different preprocessing techniques: The first technique consisted of thresholding the skull bone and obtaining CT images with brain and head ridge visible (THRESH), the second

technique used the FSL brain extraction tool (BET). Following standard best practices of the train-test split for machine learning models, 134 CTs were used for training and validation, and the remaining 34 CTs for independent testing after training. Examples of CT images obtained from both preprocessing pipelines with different degrees of HIE and no HIE are shown in Figure 1.

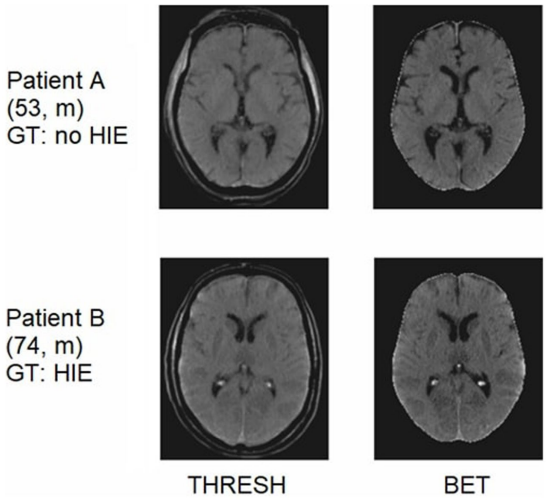


FIGURE 1
CT images of two different patients after passing through the two preprocessing pipelines. Patient A showing no signs of HIE. Patient B showing signs of severe HIE ("reversal sign"). GT, ground truth.

## 2.4 Deep learning models and input data

The 2D and 3D DenseNets presented in this paper were implemented using the Python programming language (version 3.7, Python Software Foundation[1]) on the open-source deep learning framework MONAI (version 0.9[2]) in conjunction with PyTorch (version 1.13.0[3]).

All these networks are based on DenseNet121 architecture, which is characterized by four dense blocks with three transition layers and a final classification layer (Huang et al., 2016). DenseNets show a very high performance in deep learning classification (Zhou et al., 2022). Figure 2 shows a schematic diagram of the data processing within the neural network.

To determine the highest classification performance, five networks were trained with different data formats for both the BET and THRESH preprocessed data:

- 3D-NET-ALL: all CT data as 3D images
- 2D-NET-ALL: all CT data as 2D images
- 2D-NET-*S100*: a stack of 100 2D images per CT scan (from the skull base until centrum semiovale)
- 2D-NET-*S50*: a stack of 50 2D images per CT scan (50 slices containing basal ganglia)
- 2D-NET-BG: one slice at the level of the anterior commissure

Evidence from previous studies (Singh et al., 2020) indicates that certain layers of the CT images contain significantly more relevant information than others, which is why a 2D model with all images (2D-NET-all, 181 images per CT), two 2D models with image stacks (2D-NET-*S100*, 100 images per CT; 2D-NET-*S50*, 50 images per CT) and one model with only a single slice at the level of the anterior commissure (2D-NET-BG, 1 slice per CT) were tested. A schematic visualization of the used images per CT scan can be found in Figure 3.

The preprocessed data were subjected to various transformations such as intensity scaling, rescaling, and rotations to obtain a higher variance of the input data. During training, a cross entropy loss function was used (Selvaraju et al., 2016). As a hyperparameter of interest, the learning rate was fine-tuned for each model in the range of $10^{-5}$ to $10^{-2}$. This was achieved by using the Adam optimizer and determining the steepest gradient of the loss function over the learning rate. Each model was trained for a maximum of up to 100 epochs. For internal validation after each epoch, a subset of 34 CT scans was used. The best training epoch was determined based on the highest AUC value. To optimize for highest specificity/lowest FPR, the threshold for the decision certainty of the model was increased from 0.5 to 0.95 resp. 0.99. Subsequently, the result was obtained by binarizing the probability values using the adjusted threshold. Additionally, GradCAM images were created for visual verification of the model predictions (Selvaraju et al., 2016).

## 2.5 Statistical analysis

Continuous variables between two groups were compared using a Welch's t-tests or Mann–Whitney U tests according to the normality of the data. Classification performances were evaluated using the area under the receiver operating characteristic curve (AUC), accuracy (ACC), sensitivity (SEN), and specificity (SPE) for the training and test set. Inter-rater reliability was determined using Cohen's kappa (k) for nominal variables, such as the presence/absence of HIE signs on CT images and classified according to Altmann's scheme (Altman, 1990). $p$-values <0.05 were considered statistically significant at 95% CIs. Statistical analysis was performed using Python 3.7, the scipy library [version 1.8.1[4] (Pedregosa et al., 2012) and R Studio (Version 2022.12.0+353)].

# 3 Results

## 3.1 Study population

Of 168 patients, 50 (29.8%) were female, the average age was 60 (±12) years. According to the labeling of the neuroradiologist, 88 (52.4%) showed signs of HIE in their CT images while the other 80 (47.6%) showed no signs of HIE. Among all patients, 128 (76.2%) of CT images were from patients with out-of-hospital cardiac arrests

1 https://www.python.org (accessed on 18 July, 2022).
2 https://docs.monai.io
3 https://pytorch.org
4 https://scipy.org/

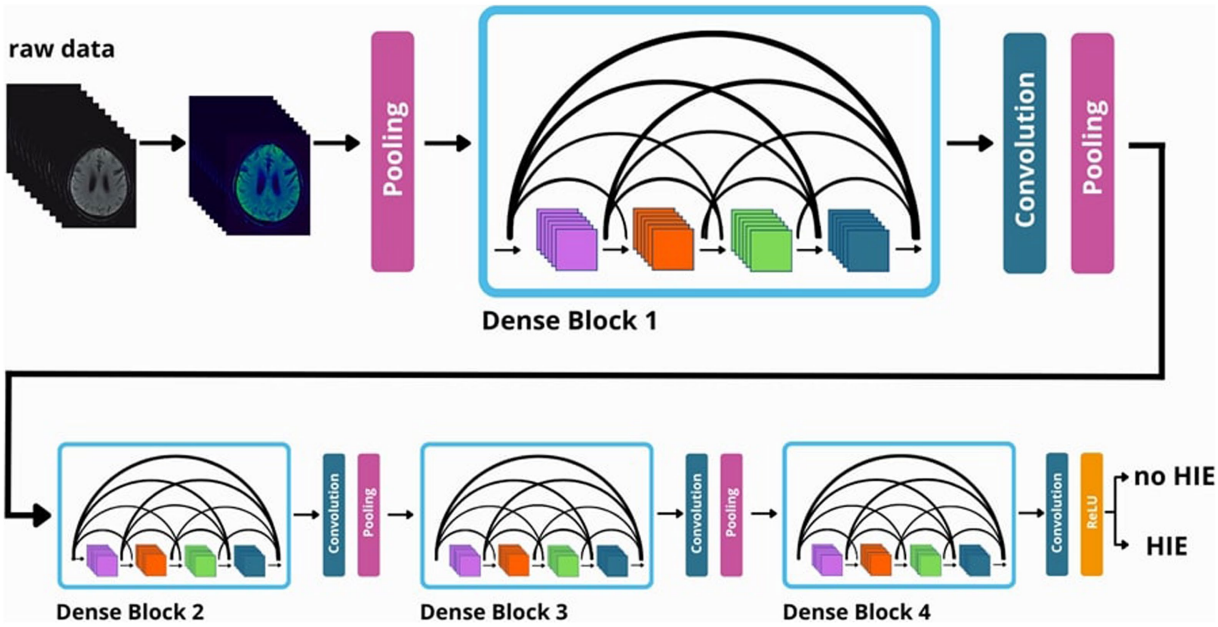


FIGURE 2
Visualization of the data processing flow in a 3D-DenseNet network.

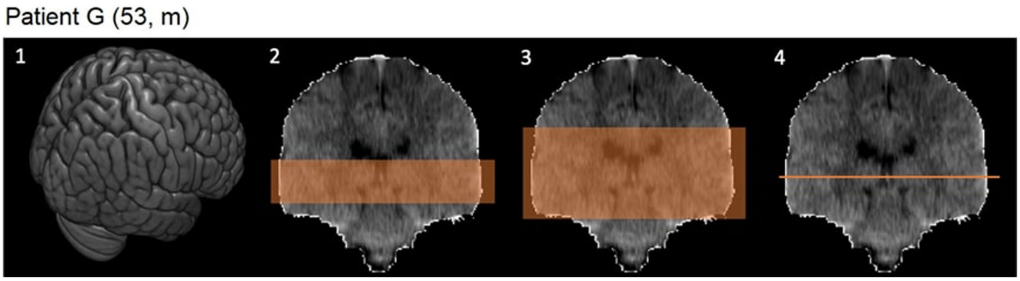


FIGURE 3
CT images in 3D and coronal reconstruction. 1: 3D image of the whole brain. 2: Image stack of 50 slices including the basal ganglia. 3: Image stack of 100 slices. 4: One slice at the level of the anterior commissure.

(OHCA). While almost 87 (98.9%) patients labeled with "HIE" by the radiologist had poor outcome (CPC 4–5 at hospital discharge), the "no HIE" group included 22 (25.0%) cases with CPC 4–5. An overview of the analyzed demographic and clinical characteristics of the study population is shown in Table 1.

To verify the correct classification between the two groups, 20% of the CT images were reviewed by a second board-certified neuroradiologist and the interobserver variability was determined. The independent radiological reviews yielded a Cohens kappa of 0.758, which is a "good agreement" according to Altmann's scheme.

For missing data, the parameters are calculated on the basis of the available data and their new total number is specified.

## 3.2 Evaluation of classification performance and further metrics

Overall, the 2D-NET-*S100* and 2D-NET-*S50* achieved the highest AUCs (AUC: 94% resp. 93%) and accuracies (both ACC: 79%), 2D-NET-all (AUC: 89%, ACC: 76%) performed worse than the stack models but still a lot better than the 3D-NET-all (AUC: 70%, ACC: 50%). The 2D-NET-BG (AUC: 47%, ACC: 50%) performed on the same level as a random guess. The receiver operating characteristic curves with their corresponding AUCs are shown in Supplementary Figure S2. An overview of the most relevant performance metrics for all networks on the BET data can be found in Table 2. Networks using the THRESH data performed less stable than on the BET data. A table of all performance parameters for all networks including both kinds of preprocessed input data as well as two probability thresholds is displayed in the Supplementary Table S1.

## 3.3 Deep learning visualization

To better understand the decision-making process of our models, Gradient-weighted Class Activation Mapping (GradCAM) was implemented and evaluated for each patient. GradCAM utilizes the activation gradient information of the last convolutional layer to

TABLE 1 Demographic and clinical characteristics of the study population.

| Parameter | Total | HIE | no HIE | *p*-value* |
|---|---|---|---|---|
| *n* | 168 | 88 | 80 | |
| Age | 60 [48–70] | 57 [44–68] | 63 [54–72] | 0.021 |
| Sex | | | | |
| Male | 118 (70.2%) | 60 (68.2%) | 58 (72.5%) | 0.271 |
| OHCA | 128 (76.2%) | 73 (83.0%) | 55 (68.8%) | 0.033 |
| Shockable Rhythm (*n* = 167/88/79) | 78 (46.7%) | 37 (42.0%) | 41 (51.9%) | 0.205 |
| Primary cause of arrest (*n* = 166/87/79) | | | | 0.075 |
| Cardiac | 69 (41.6%) | 29 (33.3%) | 40 (50.6%) | |
| Respiratory | 39 (23.5%) | 24 (27.6%) | 15 (19.0%) | |
| Other ** | 58 (34.9%) | 34 (39.1%) | 24 (30.4%) | |
| Time to ROSC (min) (*n* = 157/81/76) | 20 [10–30] | 22 [15–60] | 12 [8–21] | 0.007 |
| Total Adrenalin Dose (mg) (*n* = 157/87/70) | 2 [1–5] | 4 [2–7] | 2 [1–3] | <0.001 |
| APACHE Score (*n* = 165/86/79) | 36 [30–40] | 37 [31–41] | 34 [29–39] | 0.1 |
| Length of ICU stay (days) | 10 [5–17] | 5 [3–11] | 15 [10–28] | <0.001 |
| Time on Ventilator (hours) | 170 [96–334] | 123 [60–235] | 242 [135–432] | 0.003 |
| CT acquisition (hours after CA) (*n* = 167/88/79) | 20 [3–93] | 18 [3–85] | 34 [4–125] | 0.004 |
| Neurological outcome at hospital discharge | | | | <0.001 |
| CPC 1 | 36 | 0 | 36 | |
| CPC 2 | 22 | 0 | 22 | |
| CPC 3 | 4 | 1 | 3 | |
| CPC 4 | 11 | 9 | 2 | |
| CPC 5 | 95 | 78 | 17 | |

*Mann–Whitney U test (resp. Welch's *t*-tests). **Intoxication, metabolic and unknown cases.

TABLE 2 Overview of the various key metrics for comparing the different neuronal networks on the BET data.

| Parameter | 3D-NET-all | 2D-NET-all | 2D-NET-*S100* | 2D-NET-*S50* | 2D-NET-BG |
|---|---|---|---|---|---|
| SEN [%] | 0 | 53 | 59 | 59 | 0 |
| SPE [%] | 100 | 100 | 100 | 100 | 100 |
| ACC [%] | 50 | 76 | 79 | 79 | 50 |
| AUC [%] | 70 | 89 | 94 | 93 | 47 |

All metrics are based on the test dataset including 34 CT scans and a network probability threshold of 0.99. SEN, sensitivity; SPE, specificity; ACC, accuracy; AUC, area under the curve.

highlight the regions of highest importance for the prediction of the model and visualizes these regions similar to heatmaps (Selvaraju et al., 2016). Figure 4 contains examples of GradCAM images implemented on 2D THRESH Ct scans. The first images on the left-hand side depict the original CT scans. The second image in each row presents a comprehensive GradCAM image. The third image overlays the entire GradCAM image with 60% opacity onto the original CT scan. The fourth image showcases the region encompassing the 30th percentile of the most vigorous activations in the Gradcam images, superimposed over the original CT. All test data is visualized in the same manner in Supplementary Figure S3.

In general, the GradCAM visualizations showed that the highest information density for the decision on the presence of HIE was based on the expression strands of the sulci in the area of the centrum semiovale and the basal ganglia. This presentation was quite analogous for all true-positive and true-negative cases. With the exception of true-positive cases, in which no sulci were visible and the GWR was already visually expected to be very low, further brain areas were also displayed.

Furthermore, the GradCAM images also made it possible to determine that false positive or false negative cases mostly marked areas outside the brain or the limits of the FSL brain extraction tool.

## 4 Discussion

The aim of this study was to develop a convolutional neural network (CNN) that could detect HIE in CA patients and to explore which data types and network architectures are best to establish a state-of-the-art model. All trained models were able to detect HIE with varying accuracies. Both 2D-NETs (*S100*, *S50*) trained on image stacks from brain extracted images (BET-images) achieved best

10.3389/fnins.2024.1245791

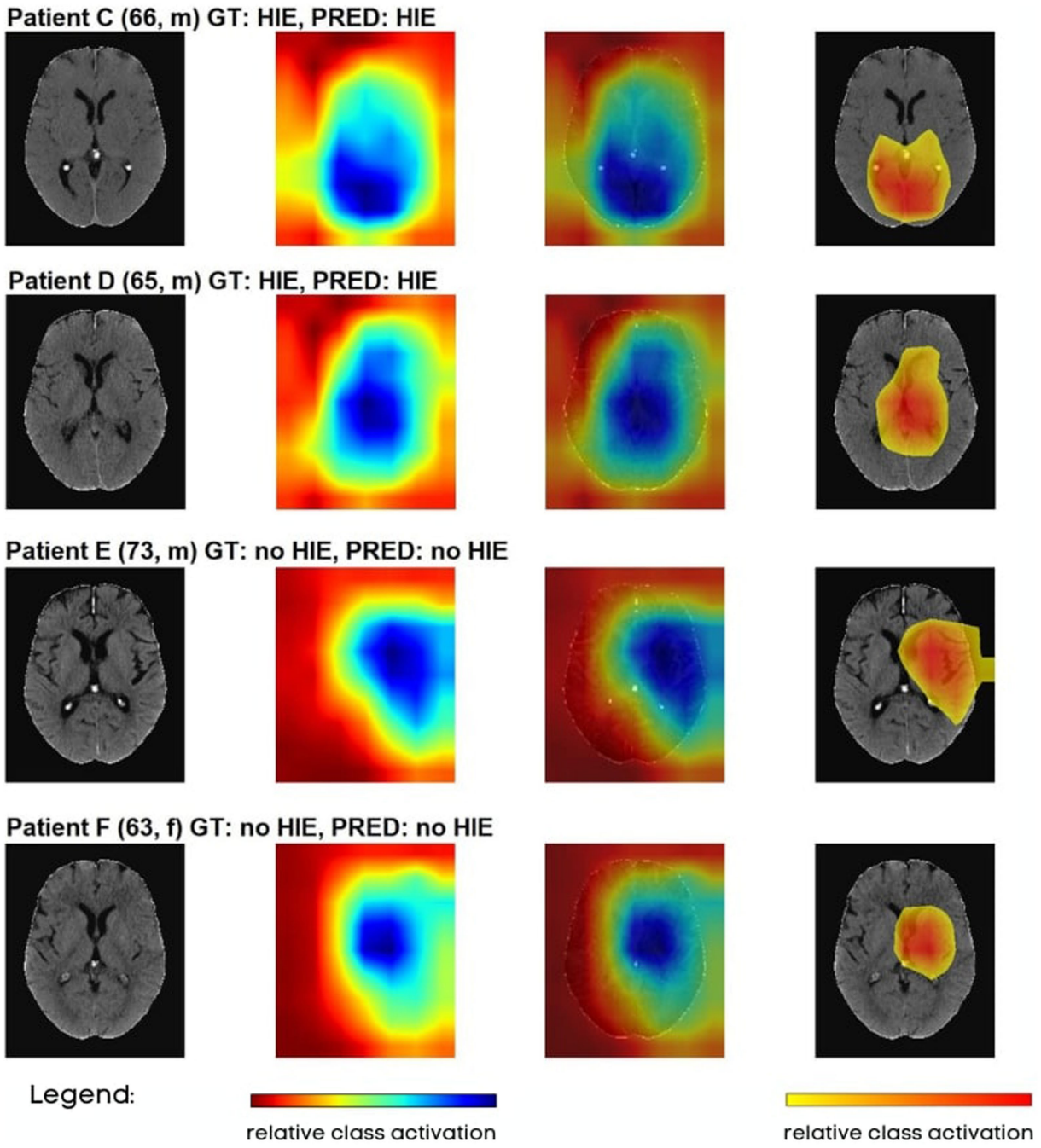


FIGURE 4
Visualization of various CT images tested on 2D-NET-*S100* network, where the test images were partially overlaid with GradCAM images. GT, ground truth; PRED, prediction.

predictive performance and highest accuracy in the training/validation as well as in the test set.

In recent years, CT imaging has played a central role in a multimodal approach to estimate the prognosis and consequently decide on continuation or withdrawal of life-sustaining therapy in CA patients. Grey-White Matter Ratio (GWR) measurement has proven to be a strong prognosticator of poor outcome with high specificity and low- to moderate sensitivity (Lee et al., 2015; Na et al., 2018). However, GWR measurement needs neuroradiological expertise that is rarely found outside of referral care centers and university hospitals (Elmer et al., 2023). In this study, we established a deep learning model for detection of HIE signs on CT images that can be easily implemented in clinical routine.

We tested two different preprocessing pipelines for our data. The first pipeline involved thresholding to strip the skull, while the second pipeline involved brain extraction. The use of thresholding technique in the first pipeline was faster to implement but resulted in some prediction bias. This may have been due to the presence of superfluous information through the head ridge, e.g., subcutaneous edema that could indicate continuous heart failure after CA and lead to a poor outcome regardless of HIE. On the other hand, brain extraction removed superfluous information, but resulted in some partial

information loss through removal of cerebrospinal fluid, veins, and superficial cortex. The brain extraction technique was found to produce better predictive performance as well as a more plausible predictions judging from the GradCAM images.

After performing the necessary preprocessing steps, we trained multiple models using different data formats, including 3D images, 2D images of the entire brain, 2D stacks of the most significant brain regions, and 2D slices at the level of the anterior commissure. Our results demonstrated that networks trained on the 2D image stacks, which included 50 resp. 100 image slices but not all images of each CT scan, delivered the best performance. One possible explanation for this is the significantly larger amount of training data available for the 2D stack format, with 13,400 images (for 2D Stack-100) compared to only 134 images for the 3D data in the training set. Our results are corroborated by Crespi et al., who described that 2D networks outperformed 3D networks on medical data despite the lower number of parameters (Crespi et al., 2022). These findings highlight the importance of carefully selecting the appropriate data format for training CNN models in medical imaging applications to achieve optimal performance.

Moreover, GradCAM visualization provides a valuable tool for understanding the decision-making process of the CNN models. These maps helped us gain insight into the reasoning behind the model's predictions and identify areas that may require further investigation or attention from treating clinicians. According to our GradCAM images, our models predominantly use information in the basal ganglia and cortical sulci when discriminating between HIE and no HIE. To further analyze this observation systematically, we divided the GradCAMs into subgroups based on the model's decisions (true positive, true negative, false negative, false positive) and visualized them again as group overlay plots. These visualizations are presented in Supplementary Figure S4, where the metrics of the subgroups correspond to rows 34–37 of columns I and J in Supplementary Table S1. First, the overlays of the THRESH method highlight significantly more areas from outside the brain than in the brain extraction group (BET), which was the main reason why we developed the BET pipeline. The subgroup overlays indicate that for both types of CT data, similar regions were highlighted for both true positive and false positive decisions, as well as for both true negative and false negative decisions, respectively. While the heatmaps for true positive focuses more on deep grey matter including basal ganglia, the heatmaps in true negative are more diffused, suggesting the model is not focusing on any particular area indicative of HIE. This observation emphasizes again the critical importance of interpretability neural networks for medical imaging analysis, as it can help identify false predictions caused by information loss or other factors.

In addition, we also complied with 37 of the 42 checklist items on the RSNA's CLAIM checklist during the study. The open items were either not applicable and indicated external validation, which we have already identified as a limitation of our study and will be addressed in future work. Of the DECIDE-AI checklist, 28 of the 37 items were adhered to. The open points are all in the area of implementation in everyday clinical practice and usability by other medical users, which was not yet planned as part of this study. We would like to point out that the scope of this checklist is aimed at other areas than this initial proof of concept study was intended to investigate.

In a recent publication by Mansour et al. (2022), machine and deep learning were utilized to identify patients who would exhibit radiologic evidence of apparent HIE on follow-up CT scans. Although this study demonstrates the potential of deep learning in detecting features that may not be visible to human raters, their proposed method included various significant limitations (i.e., high risk of overfitting due to small data set, questionable training pipeline and principal component analysis), which could result in partially erroneous results (Molinski et al., 2022). Our approach involved training our deep learning models from scratch, with direct class prediction as the output, without manual feature selection or additional machine learning modeling. Additionally, we believe that interpretability of the model's predictions is crucial, which is why we utilized GradCAM visualization.

Our deep learning-based classification method differs significantly from GWR measurement. Unlike GWR, which relies on placing ROIs in the basal ganglia and white matter and may miss important information in other regions such as the cerebellum, our model considers all spatial information in the images. In addition, GWR only takes into account the Hounsfield units of the ROI, neglecting other relevant anatomical factors such as sulcal relief and ventricular enlargement. Our multi-class deep learning classification method uses a neural network with output nodes equal to the number of classes (in our case two: "HIE" and "no HIE"). Each output node is associated with a class and generates a score for that class, which is then passed through an activation layer to obtain probability values. As prediction probability threshold is set at 0.5 by default, we adjusted for the optimal threshold to achieve 0% FPR, which is necessary for clinical implementation (Geocadin et al., 2019).

Our study has several potential limitations that should be considered. First, as the study has a retrospective, single-center design, our model has yet to be externally and prospectively validated. Furthermore, our cohort of 168 patients is relatively small, and a larger dataset is needed to ensure the reproducibility of results and reduce the risk of overfitting. We tried to reduce this risk as much as possible by utilizing raw image transforms, a learning rate finder and an Adam gradient optimizer. Additionally, choosing a standard training-validation split instead of cross-validation can also be seen as limitation, as cross-validation could probably deliver a more robust assessment of generalization ability and facilitate a more comprehensive evaluation of hyperparameters. But we still opted for a conventional training-test split instead of employing cross-validation in this proof-of-concept study, because (i) this study was designed to minimize computational overhead, (ii) repeatedly training and evaluating the model on different subsets of a small dataset may cause the model to memorize specific patterns rather than learning the underlying patterns of the data and thereby increases the risk of overfitting and (iii) a standard training-test split allows for a more straightforward visualization of the model's performance and thus enables better comparability of the different models used in the study. Another point of concern is the choice of ground truth: In our study, we used neuroradiological expertise as the ground truth for "HIE" and "no HIE" labels. However, this may not necessarily reflect the underlying pathology or clinical status of the patients. The main reason for this choice is the difficulty to clinically determine the real cause of poor outcome, as many patients with HIE develop other complications such as cardiac or pulmonary complications, which may lead to death. Given the complexity of clinical cases like HIE, it is important to note that the ground truth of our training data corresponds to the expert opinion of a radiologist, which may already contain errors. To minimize this risk, a portion of the data was reviewed by another neuroradiologist to

determine interrater variability. Our analysis found a high level of agreement between raters, which was significantly better than what is typically observed for HIE (Caraganis et al., 2020). However, there is still a small possibility that the ground truth of certain images may be incorrect. Another limitation is the quality of the data itself. Despite various preprocessing techniques, there is always the possibility that the individual CTs are not sufficiently homogenized since our data originated from three different scanner types of two manufactures. In a phantom study, Li et al. (2021) showed a high variability of image quality between different CT scanners. Roa et al. (2015) demonstrated that the image quality of a same CT scanner decreased over time. The data quality is also partially impaired by variability in patient characteristics, such as age and the timing of the CT scan after *CA*. It is well known that age-related cerebral atrophy and hypoattenuation of white matter in chronic small vessel ischemic disease can complicate neuroradiological diagnosis. Furthermore, HIE diagnosis on later CT scans is also significantly more sensitive for poor outcomes (GWR decreases over time in patients with severe HIE), so the sensitivity for prediction of poor outcome is higher for late CTs (>24 h after CA) as compared to early CTs (<6 h after CA) (Streitberger et al., 2019). As these aspects confound the outcome prognosis for a human rater, they also confound the training of a neural network, especially on a small dataset.

For our future work, we first want to address the current limitations especially in regards to the data sampling (i.e., cross-validation) and retest and retrain it on a larger dataset. We will also explore newer techniques of CT quality harmonization such as the ComBat method (Johnson et al., 2007; Orlhac et al., 2021). Moreover, as the timing of brain computed tomography and accuracy of outcome prediction are correlated, we will investigate the influence of CT timing on the predictive performance of our model. Our vision is to develop a multimodal model, for which we will integrate further parameters such as serum biomarkers and electrophysiology data to improve outcome prediction. Transfer learning in combination with an external multi-center validation approach can be used to further optimize this pilot study (Weiss et al., 2016).

## 5 Conclusion

In this study we established a state-of-the-art, deep learning-based model for detection of hypoxic–ischemic encephalopathy on CT images which can be trained on 2D or 3D images.

The best performance was achieved by neuronal networks trained on 2D image stacks of brain extracted CT data. After implementing the described improvements and external validation, our model can be implemented in clinical routine and help clinicians with outcome prediction of HIE in CA patients.

## Data availability statement

The data analyzed in this study is subject to the following licenses/restrictions: the developed code, additional data and/or materials will be disclosed upon reasonable request to the corresponding author. Requests to access these datasets should be directed to noah.molinski@charite.de.

## Ethics statement

The studies involving humans were approved by Institutional review board of the Charité (Nos.: EA2/066/17, EA4/136/21). The studies were conducted in accordance with the local legislation and institutional requirements. Written informed consent for participation was not required from the participants or the participants' legal guardians/next of kin in accordance with the national legislation and institutional requirements.

## Author contributions

NM: conceptualization, formal analysis, investigation, methodology, software, visualization, writing – original draft, and writing – review and editing. MK: data curation, formal analysis, methodology, software, and writing – review and editing. CL: data curation, methodology, and writing – review and editing. JN: data curation and writing – review and editing. CS: data curation and writing – review and editing. MS: conceptualization, formal analysis, project administration, supervision, and writing – review and editing. AM: conceptualization, formal analysis, project administration, software, visualization, writing – original draft, and writing – review and editing. All authors contributed to the article and approved the submitted version.

## Funding

MK is fellow of the BIH Charité Junior Digital Clinician Scientist Program funded by the Charité – Universitätsmedizin Berlin, and the Berlin Institute of Health at Charité (BIH). AM is fellow of the BIH Charité Digital Clinician Scientist Program funded by the Charité – Universitätsmedizin Berlin, and the Berlin Institute of Health at Charité (BIH).

## Conflict of interest

The authors declare that the research was conducted in the absence of any commercial or financial relationships that could be construed as a potential conflict of interest.

## Publisher's note



## Supplementary material

The Supplementary material for this article can be found online at: https://www.frontiersin.org/articles/10.3389/fnins.2024.1245791/full#supplementary-material

# References


Akkus, Z., Galimzianova, A., Hoogi, A., Rubin, D. L., and Erickson, B. J. (2017). Deep learning for brain MRI segmentation: state of the art and future directions. *J. Digit. Imaging* 30, 449–459. doi: 10.1007/s10278-017-9983-4

Altman, D. G. *Practical statistics for medical research*. (1990). CRC Press: Boca Raton, FL.

Artzi, M., Bressler, I., and Bashat, D. B. (2019). Differentiation between glioblastoma, brain metastasis and subtypes using Radiomics analysis. *J. Magn. Reson. Imaging* 50, 519–528. doi: 10.1002/jmri.26643

Burduja, M., Ionescu, R. T., and Verga, N. (2020). Accurate and efficient intracranial hemorrhage detection and subtype classification in 3D CT scans with convolutional and long short-term memory neural networks. *Sensors* 20:5611. doi: 10.3390/s20195611

Caraganis, A., Mulder, M., Kempainen, R. R., Brown, R. Z., Oswood, M., Hoffman, B., et al. (2020). Interobserver variability in the recognition of hypoxic–ischemic brain injury on computed tomography soon after out-of-hospital cardiac arrest. *Neurocrit. Care.* 33, 414–421. doi: 10.1007/s12028-019-00900-7

Crespi, L., Loiacono, D., and Sartori, P. (2022). Are 3D better than 2D convolutional neural networks for medical imaging semantic segmentation? *2022 Int. Jt. Conf. Neural Netw.*, 1–8. doi: 10.1109/ijcnn55064.2022.9892850

Cristia, C., Ho, M.-L., Levy, S., Andersen, L. W., Perman, S. M., Giberson, T., et al. (2014). The association between a quantitative computed tomography (CT) measurement of cerebral edema and outcomes in post-cardiac arrest—a validation study. *Resuscitation* 85, 1348–1353. doi: 10.1016/j.resuscitation.2014.05.022

Deutsche Gesellschaft für Neurologie e.V. *S1-Leitlinie Hypoxisch-Ischämische Enzephalopathie (HIE) Im Erwachsenenalter*. Kommission Leitlinien der Deutschen Gesellschaft für Neurologie. (2017).

Elmer, J., Steinberg, A., and Callaway, C. W. (2023). Paucity of Neuroprognostic testing after cardiac arrest in the United States. *Resuscitation* 188:109762. doi: 10.1016/j.resuscitation.2023.109762

Gao, P., Shan, W., Guo, Y., Wang, Y., Sun, R., Cai, J., et al. (2022). Development and validation of a deep learning model for brain tumor diagnosis and classification using magnetic resonance imaging. *JAMA Netw. Open* 5:e2225608. doi: 10.1001/jamanetworkopen.2022.25608

Geocadin, R. G., Callaway, C. W., Fink, E. L., Golan, E., Greer, D. M., Ko, N. U., et al. (2019). Standards for studies of neurological prognostication in comatose survivors of cardiac arrest: a scientific statement from the American Heart Association. *Circulation* 140, e517–e542. doi: 10.1161/cir.0000000000000702

Hssayeni, M. D., Croock, M. S., Salman, A. D., Al-khafaji, H. F., Yahya, Z. A., and Ghoraani, B. (2020). Intracranial hemorrhage segmentation using a deep convolutional model. *Data* 5:14. doi: 10.3390/data5010014

Huang, G., Liu, Z., van der Maaten, L., and Weinberger, K. Q. (2016). Densely connected convolutional networks. *Arxiv*:1608.06993.

Jenkinson, M., Beckmann, C. F., Behrens, T. E. J., Woolrich, M. W., and Smith, S. M. (2012). FSL. *NeuroImage* 62, 782–790. doi: 10.1016/j.neuroimage.2011.09.015

Johnson, W. E., Li, C., and Rabinovic, A. (2007). Adjusting batch effects in microarray expression data using empirical Bayes methods. *Biostatistics* 8, 118–127. doi: 10.1093/biostatistics/kxj037

Kenda, M., Cheng, Z., Guettler, C., Storm, C., Ploner, C. J., Leithner, C., et al. (2022). Inter-rater agreement between humans and Computer in Quantitative Assessment of computed tomography after cardiac arrest. *Front. Neurol.* 13:990208. doi: 10.3389/fneur.2022.990208

Kenda, M., Scheel, M., Kemmling, A., Aalberts, N., Guettler, C., Streitberger, K. J., et al. (2021). Automated assessment of brain CT after cardiac arrest—an observational derivation/validation cohort study. *Crit. Care Med.* 49, e1212–e1222. doi: 10.1097/ccm.0000000000005198

Kim, S. H., Choi, S. P., Park, K. N., Youn, C. S., Oh, S. H., and Choi, S. M. (2013). Early brain computed tomography findings are associated with outcome in patients treated with therapeutic hypothermia after out-of-hospital cardiac arrest. *Scand J. Trauma Resusc. Emerg. Med.* 21:57. doi: 10.1186/1757-7241-21-57

Kjos, B., Brant-Zawadzki, M., and Young, R. (1983). Early CT findings of global central nervous system Hypoperfusion. *Am. J. Roentgenol.* 141, 1227–1232. doi: 10.2214/ajr.141.6.1227

Lee, B. K., Jeung, K. W., Song, K. H., Jung, Y. H., Choi, W. J., Kim, S. H., et al. (2015). Prognostic values of gray matter to white matter ratios on early brain computed tomography in adult comatose patients after out-of-hospital cardiac arrest of cardiac etiology. *Resuscitation* 96, 46–52. doi: 10.1016/j.resuscitation.2015.07.027

Li, J., Fu, G., Chen, Y., Li, P., Liu, B., Pei, Y., et al. (2020). A multi-label classification model for full slice brain computerised tomography image. *BMC Bioinformat.* 21:200. doi: 10.1186/s12859-020-3503-0

Li, Y., Jiang, Y., Liu, H., Yu, X., Chen, S., Ma, D., et al. (2021). A phantom study comparing low-dose CT physical image quality from five different CT scanners. *Quant. Imaging Med. Surg.* 12, 766–780. doi: 10.21037/qims-21-245

Livne, M., Rieger, J., Aydin, O. U., Taha, A. A., Akay, E. M., Kossen, T., et al. (2019). A U-net deep learning framework for high performance vessel segmentation in patients with cerebrovascular disease. *Front. Neurosci.* 13:97. doi: 10.3389/fnins.2019.00097

Mansour, A., Fuhrman, J. D., Ammar, F. E., Loggini, A., Davis, J., Lazaridis, C., et al. (2022). Machine learning for early detection of hypoxic-ischemic brain injury after cardiac arrest. *Neurocrit. Care.* 36, 974–982. doi: 10.1007/s12028-021-01405-y

Meddeb, A., Kossen, T., Bressem, K. K., Hamm, B., and Nagel, S. N. (2021). Evaluation of a deep learning algorithm for automated spleen segmentation in patients with conditions directly or indirectly affecting the spleen. *Tomogr* 7, 950–960. doi: 10.3390/tomography7040078

Meddeb, A., Kossen, T., Bressem, K. K., Molinski, N., Hamm, B., and Nagel, S. N. (2022). Two-stage deep learning model for automated segmentation and classification of splenomegaly. *Cancers* 14:5476. doi: 10.3390/cancers14225476

Metter, R. B., Rittenberger, J. C., Guyette, F. X., and Callaway, C. W. (2011). Association between a quantitative CT scan measure of brain edema and outcome after cardiac arrest. *Resuscitation* 82, 1180–1185. doi: 10.1016/j.resuscitation.2011.04.001

Molinski, N. S., Meddeb, A., Kenda, M., and Scheel, M. (2022). Comment on "machine learning for early detection of hypoxic-ischemic brain injury after cardiac arrest". *Neurocrit. Care.* 37, 363–364. doi: 10.1007/s12028-022-01526-y

Mongan, J., Moy, L., and Kahn, C. E. Jr. (2020). Checklist for artificial intelligence in medical imaging (CLAIM): a guide for authors and reviewers. *Radiol. Artif. Intell.* 2:e200029. doi: 10.1148/ryai.2020200029

Na, M. K., Kim, W., Lim, T. H., Jang, B., Cho, Y., Choi, K.-S., et al. (2018). Gray matter to white matter ratio for predicting neurological outcomes in patients treated with target temperature management after cardiac arrest: a systematic review and meta-analysis. *Resuscitation* 132, 21–28. doi: 10.1016/j.resuscitation.2018.08.024

Nishio, M., Kobayashi, D., Nishioka, E., Matsuo, H., Urase, Y., Onoue, K., et al. (2022). Deep learning model for the automatic classification of COVID-19 pneumonia, non-COVID-19 pneumonia, and the healthy: a multi-center retrospective study. *Sci. Rep.* 12:8214. doi: 10.1038/s41598-022-11990-3

Nolan, J. P., Sandroni, C., Böttiger, B. W., Cariou, A., Cronberg, T., Friberg, H., et al. (2021). European resuscitation council and European Society of Intensive Care Medicine Guidelines 2021: post-resuscitation care. *Intensiv. Care Med.* 47, 369–421. doi: 10.1007/s00134-021-06368-4

Nolan, J. P., Soar, J., Cariou, A., Cronberg, T., Moulaert, V. R. M., Deakin, C. D., et al. (2015). European resuscitation council and European Society of Intensive Care Medicine Guidelines for post-resuscitation care 2015 section 5 of the European resuscitation council guidelines for resuscitation 2015. *Resuscitation* 95, 202–222. doi: 10.1016/j.resuscitation.2015.07.018

Orlhac, F., Eertink, J. J., Cottereau, A.-S., Zijlstra, J. M., Thieblemont, C., Meignan, M. A., et al. (2021). A guide to ComBat harmonization of imaging biomarkers in multicenter studies. *J. Nucl. Med.* 63, 172–179. doi: 10.2967/jnumed.121.262464

Pedregosa, F., Varoquaux, G., Gramfort, A., Michel, V., Thirion, B., Grisel, O., et al. (2012). Scikit-learn: machine learning in Python. *J. Mach. Learn. Res.* 12, 2825–2830

Roa, A. M. A., Andersen, H. K., and Martinsen, A. C. T. (2015). CT image quality over time: comparison of image quality for six different CT scanners over a six-year period. *J. Appl. Clin. Méd. Phys.* 16, 350–365. doi: 10.1120/jacmp.v16i2.4972

Scheel, M., Storm, C., Gentsch, A., Nee, J., Luckenbach, F., Ploner, C. J., et al. (2013). The prognostic value of gray-white-matter ratio in cardiac arrest patients treated with hypothermia. *Scand J. Trauma Resusc. Emerg. Med.* 21:23. doi: 10.1186/1757-7241-21-23

Selvaraju, R. R., Cogswell, M., Das, A., Vedantam, R., Parikh, D., and Batra, D. (2016). Grad-CAM: visual explanations from deep networks via gradient-based localization. *Arxiv* 128, 336–359. doi: 10.1007/s11263-019-01228-7

Singh, S. P., Wang, L., Gupta, S., Goli, H., Padmanabhan, P., and Gulyás, B. (2020). 3D deep learning on medical images: a review. *Sensors* 20:5097. doi: 10.3390/s20185097

Streitberger, K. J., Endisch, C., Ploner, C. J., Stevens, R., Scheel, M., Kenda, M., et al. (2019). Timing of brain computed tomography and accuracy of outcome prediction after cardiac arrest. *Resuscitation* 145, 8–14. doi: 10.1016/j.resuscitation.2019.09.025

Vasey, B., Nagendran, M., Campbell, B., Clifton, D. A., Collins, G. S., Denaxas, S., et al. (2022). Reporting guideline for the early-stage clinical evaluation of decision support systems driven by artificial intelligence: DECIDE-AI. *Nat. Med.* 28, 924–933. doi: 10.1038/s41591-022-01772-9

Weiss, K., Khoshgoftaar, T. M., and Wang, D. (2016). A survey of transfer learning. *J. Big Data* 3:9. doi: 10.1186/s40537-016-0043-6

Xu, J., Zhang, R., Zhou, Z., Wu, C., Gong, Q., Zhang, H., et al. (2021). Deep network for the automatic segmentation and quantification of intracranial hemorrhage on CT. *Front. Neurosci.* 14:541817. doi: 10.3389/fnins.2020.541817

Zeppenfeld, K., Tfelt-Hansen, J., de Riva, M., Winkel, B. G., Behr, E. R., Blom, N. A., et al. (2022). ESC guidelines for the Management of Patients with ventricular arrhythmias and the prevention of sudden cardiac death. *Eur. Heart J.* 43, 3997–4126. doi: 10.1093/eurheartj/ehac262

Zhou, T., Ye, X., Lu, H., Zheng, X., Qiu, S., and Liu, Y. (2022). Dense convolutional network and its application in medical image analysis. *Biomed. Res. Int.* 2022, 2384830–2384822. doi: 10.1155/2022/2384830

frontiers | Frontiers in Neuroscience

TYPE Systematic Review
PUBLISHED 11 March 2024
DOI 10.3389/fnins.2024.1286130



OPEN ACCESS

EDITED BY
Yumie Ono,
Meiji University, Japan

REVIEWED BY
Kazuyori Yagyu,
Health Sciences University of Hokkaido, Japan
Takayuki Nozawa,
University of Toyama, Japan

*CORRESPONDENCE
Kerstin Konrad
✉ k.konrad@fz-juelich.de

RECEIVED 30 August 2023
ACCEPTED 30 January 2024
PUBLISHED 11 March 2024

CITATION
Konrad K, Gerloff C, Kohl SH, Mehler DMA, Mehlem L, Volbert EL, Komorek M, Henn AT, Boecker M, Weiss E and Reindl V (2024) Interpersonal neural synchrony and mental disorders: unlocking potential pathways for clinical interventions.
*Front. Neurosci.* 18:1286130.
doi: 10.3389/fnins.2024.1286130



# Interpersonal neural synchrony and mental disorders: unlocking potential pathways for clinical interventions

Kerstin Konrad[1,2]*, Christian Gerloff[1,2,3], Simon H. Kohl[1,2], David M. A. Mehler[4,5,6], Lena Mehlem[1], Emily L. Volbert[1], Maike Komorek[1], Alina T. Henn[1], Maren Boecker[1,7], Eileen Weiss[1,7] and Vanessa Reindl[1,8]

[1]Child Neuropsychology Section, Department of Child and Adolescent Psychiatry, Psychosomatics and Psychotherapy, University Hospital RWTH, Aachen, Germany, [2]JARA Brain Institute II, Molecular Neuroscience and Neuroimaging (INM-11), Jülich Research Centre, Jülich, Germany, [3]Department of Applied Mathematics and Theoretical Physics, Cambridge Centre for Data-Driven Discovery, University of Cambridge, Cambridge, United Kingdom, [4]Department of Psychiatry, Psychotherapy and Psychosomatics, Medical School, RWTH Aachen University, Aachen, Germany, [5]Institute for Translational Psychiatry, University of Münster, Münster, Germany, [6]School of Psychology, Cardiff University Brain Research Imaging Center (CUBRIC), Cardiff University, Cardiff, United Kingdom, [7]Institute of Medical Psychology and Medical Sociology, University Hospital RWTH, Aachen, Germany, [8]Department of Psychology, School of Social Sciences, Nanyang Technological University, Singapore, Singapore

**Introduction:** Interpersonal synchronization involves the alignment of behavioral, affective, physiological, and brain states during social interactions. It facilitates empathy, emotion regulation, and prosocial commitment. Mental disorders characterized by social interaction dysfunction, such as Autism Spectrum Disorder (ASD), Reactive Attachment Disorder (RAD), and Social Anxiety Disorder (SAD), often exhibit atypical synchronization with others across multiple levels. With the introduction of the "second-person" neuroscience perspective, our understanding of interpersonal neural synchronization (INS) has improved, however, so far, it has hardly impacted the development of novel therapeutic interventions.

**Methods:** To evaluate the potential of INS-based treatments for mental disorders, we performed two systematic literature searches identifying studies that directly target INS through neurofeedback (12 publications; 9 independent studies) or brain stimulation techniques (7 studies), following PRISMA guidelines. In addition, we narratively review indirect INS manipulations through behavioral, biofeedback, or hormonal interventions. We discuss the potential of such treatments for ASD, RAD, and SAD and using a systematic database search assess the acceptability of neurofeedback (4 studies) and neurostimulation (4 studies) in patients with social dysfunction.

**Results:** Although behavioral approaches, such as engaging in eye contact or cooperative actions, have been shown to be associated with increased INS, little is known about potential long-term consequences of such interventions. Few proof-of-concept studies have utilized brain stimulation techniques, like transcranial direct current stimulation or INS-based neurofeedback, showing feasibility and preliminary evidence that such interventions can boost behavioral synchrony and social connectedness. Yet, optimal brain stimulation protocols and neurofeedback parameters are still undefined. For ASD, RAD, or SAD, so far no randomized controlled trial has proven the efficacy of direct

INS-based intervention techniques, although in general brain stimulation and neurofeedback methods seem to be well accepted in these patient groups.

**Discussion:** Significant work remains to translate INS-based manipulations into effective treatments for social interaction disorders. Future research should focus on mechanistic insights into INS, technological advancements, and rigorous design standards. Furthermore, it will be key to compare interventions directly targeting INS to those targeting other modalities of synchrony as well as to define optimal target dyads and target synchrony states in clinical interventions.

KEYWORDS

**interpersonal neural synchrony (INS), hyperscanning neurofeedback, mental disorders, social dysfunction, brain stimulation**

## 1 Introduction

The evolution of humans as social creatures has prepared our brains to be ideally primed for interpersonal interactions (Hari and Kujala, 2009). When we naturally mirror each other's smiles or laughter during social engagement or unintentionally align our body language with those we are speaking to, these are moments of behavioral synchrony. Moreover, interpersonal synchrony is evident in hormonal states and the autonomous nervous system (physiological synchrony), as well as in neural responses among two (or more) individuals interacting with each other (interpersonal neural synchrony, INS).

Measures of the autonomous nervous system (ANS) become synchronized in interacting dyads, reflecting the activity of the sympathetic and parasympathetic nervous system. This includes, e.g., heartbeat, electrodermal activity, or breathing rhythm (Davis et al., 2018; Bell, 2020). Furthermore, hormonal levels like oxytocin or cortisol get attuned in interacting dyads. This phenomenon can be seen from birth on and in the case, e.g., of parents and their infants critically depends on the quality of their behavioral synchrony (Feldman et al., 2011; Feldman, 2012b).

Interpersonal neural synchrony (INS) is the temporal relationship between two person's brain signals while interacting and seems to reflect a fundamental mechanism of bi-directional attunement (Azhari et al., 2019). In particular, neural activity is coordinated in frontotemporal cortices when humans are interacting (see Lotter et al., 2023 for a review). INS can be captured by hemodynamic or electrophysiological measures. Electroencephalography (EEG) / magnetoencephalography (MEG), near-infrared spectroscopy (fNIRS), and functional magnetic resonance imaging (fMRI) are the most widely used imaging techniques to capture neural synchrony patterns of two or more subjects concurrently, which is called hyperscanning (Czeszumski et al., 2022).

INS is associated with both external and internal factors: External influences might include non-social triggers such as common sensory input, as well as social triggers like shared eye contact, language, or movement. On the other hand, internal synchronizers might encompass personality traits, the mental states of those interacting, the social closeness between them, and motivational states (Dikker et al., 2021).

Synchrony across all known modalities, such as in behavior, hormonal states, autonomous nervous and central nervous activity can be seen as a crucial underlying factor of social participation and social cohesion (Feldman, 2017). Being able to adaptively get "in-sync" and "out-of-sync" with others may represent important requirements for successful interaction in terms of communication, social bonding, and affiliation (Hove and Risen, 2009; Rennung and Göritz, 2016; Vicaria and Dickens, 2016; Mogan et al., 2017; Hu et al., 2022). Some of these requirements are the individuals' adaptive capacities to access another's internal arousal state (Mizugaki et al., 2015), share and regulate emotions (Davis et al., 2018; Birk et al., 2022), to learn from each other (Pan et al., 2021), and to adapt to collective behaviors and group norms (Wiltermuth and Heath, 2009; Reinero et al., 2021).

A lack of social interaction abilities and maladaptive relationships during the early formative years as well as throughout the life span are among the most significant factors leading to mental disorders (Schilbach, 2016; Schilbach and Lahnakoski, 2023). Vice versa, mental disorders can affect our abilities to successfully interact with others and to enjoy social interactions. Psychotherapy, an effective treatment for many mental disorders, utilizes the structured therapeutic relationship to favor the patients' well-being. Thus, it has been suggested that mental disorders in general can be construed as disorders of social interaction (Schilbach, 2016). However, there are some mental disorders, such as autism spectrum disorder (ASD), (Reactive) attachment disorder (RAD), or social anxiety disorder (SAD), that are particularly characterized by disruption of social interaction and communication as an essential part of their underlying patho-mechanisms. In line with this, there is first evidence derived from recent hyperscanning studies that decreased INS is associated with (i) increased level of social difficulties in everyday life in subjects with ASD (Quiñones-Camacho et al., 2021), (ii) predictive of poor attachment quality in high-risk mother–child dyads (Miller et al., 2019) and (iii) linked to symptom severity in SAD when assessed in emotionally negative situations (Deng et al., 2022).

However, despite the compelling evidence for the broad relevance of social interaction in mental health and the emerging evidence for a specific role of synchrony as an important underlying mechanism, so far, the majority of neuroscientific studies focused on the mechanisms, antecedents, and consequences of INS under typical and atypical conditions largely ignoring INS as a therapeutic target for mental health interventions. However, the recent technical advances in the field of hyperscanning, real-time neurofeedback, and neurostimulation techniques open up new avenues to translate this second-person

neuroscience approach into interactive-based neuroscientific interventions. Tackling directly the neural mechanism involved in social function and dysfunction might thus help to develop novel effective prevention strategies and interventions for a variety of mental disorders.

In principle, a range of methods can be employed to influence INS. Neural synchrony can be targeted through direct manipulation or indirectly by targeting alternative modalities of synchrony to enhance INS. Directly INS can be targeted using brain stimulation and hyperscanning neurofeedback (hyper-NF), indirectly it can be targeted using pharmacological approaches, ANS-biofeedback and behavioral interventions aiming to enhance INS (Figure 1).

In this work, we will outline these translational approaches and provide an overview how they impact on INS. We will systematically review those approaches that directly target INS by (i) hyper-NF and (ii) neurostimulation approaches, and (iii) how well such approaches are generally accepted by patients. Furthermore, we will exemplify how manipulation of INS can contribute to treatment of three selected mental disorders, all characterized by social interactions deficits, ASD, RAD and SAD. While here we highlight these three mental disorders, we note that INS-based approaches may also be relevant to other psychiatric or neurological diseases that are characterized by impaired social interactions. Finally, we will provide a critical outlook on open research questions, technical challenges, and clinical caveats to be considered in future studies.

## 2 Methods

In this review, we offer a concise overview of indirect strategies for manipulating INS, while also presenting a comprehensive state-of-the-art illustration of all translational techniques that directly target INS. The latter insights are derived from systematic database searches, providing a thorough analysis of the current landscape. To foster discussions about progress towards clinical utility, open technical challenges for these novel approaches will be outlined. Finally, we will narratively review promising clinical applications for improving interaction-based mental health outcomes in the future along with a systematic review on their general acceptability by patients. Of note, in the clinical translation part we will exclusively focus on future avenues for INS-based approaches for treatment of social interaction disorder while leaving out the scope in terms of INS-based diagnostics or patient stratification.

To provide a comprehensive overview of techniques directly targeting INS and assess their feasibility and acceptability, we conducted three structured literature searches (i: neurostimulation, ii: hyper-NF, iii: feasibility / acceptability). Literature searches were conducted using the open-source search engine SetYouFree (v. 0.1.2, https://github.com/ChristianGerloff/set-you-free, Gerloff et al., 2022b) following the best practices of the PRISMA guidelines for systematic reviews. As the reviewed techniques are in their early stages, the search was conducted across scientific publication databases as well as preprint servers. All searches were performed starting from 1st January 2000 up to the 31th December 2023 (date of conduction of ii), which includes the first hyperscanning studies (Montague et al., 2002). Publications were screened in SetYouFree using deterministic exclusion criteria, which were *a-priori*-defined (see Supplementary Tables S1–S3). For one of the searches (ii), the screening was conducted by two independent reviewers to assess their interrater reliability (Cohen's kappa = 0.95). To ensure reproducibility, technical details, parameters, search flows and human readable SetYouFree files are provided in the Supplementary materials (Text

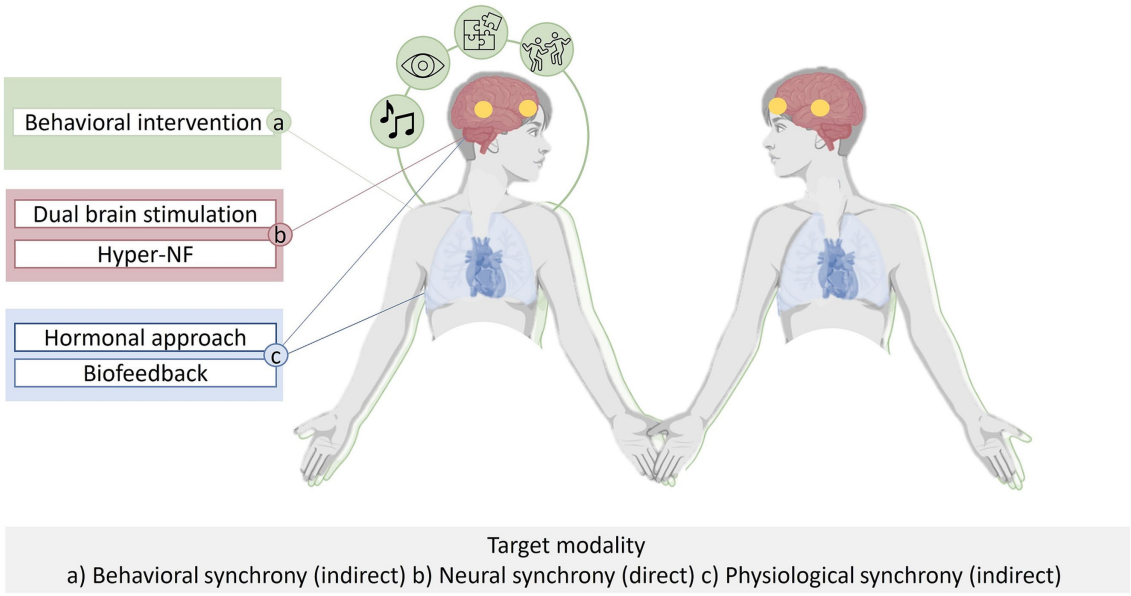


FIGURE 1
Interpersonal Synchrony occurs at multiple levels (i.e., behavior, autonomous nervous system, hormones and brain) in interacting subjects. Interpersonal neural synchrony (INS) can be targeted through *direct* manipulation (depicted in RED) via dual brain stimulation or hyperscanning neurofeedback (hyper-NF). INS can be targeted *indirectly* by behavioral interventions (depicted in GREEN), or by peripher-physiological biofeedback or pharmacological approaches (depicted in BLUE).

"Structured Literature Search", Supplementary Tables S1–S3, Supplementary Figures S1–S3).

To guide the reader, the kind of search (systematic or unsystematic) is explicitly described at the beginning of each paragraph in the Result section. In Section 3.2.1 we provide an overview of brain stimulation results based on a systemic literature search using search strings that combined "neurostimulation", "TMS", "tDCS" or "tACS" with hyperscanning-related terms. From the initial pool of $N = 695$ studies, we identified seven studies that applied tACS ($N = 5$), tDCS ($N = 1$) or both ($N = 1$) in one or both members of a dyad with the goal to manipulate INS and examining changes in behavioral and/or neural synchrony.

In Section 3.2.2 we investigated the general feasibility and training success of hyper-NF based on twelve eligible publications (EEG: $N = 10$, fNIRS: $N = 1$; fMRI: $N = 1$) out of 129 initial search results, using a search string that combined "neurofeedback" with hyperscanning-related terms (see i).

Finally, in Section 3.4 we analyzed the general acceptability and feasibility of direct intervention techniques in patients with social interaction dysfunction across 8 out of 321 studies based on neurofeedback ($N = 4$) and neurostimulation ($N = 4$). For this search, we combined the search terms from (i) and (ii) with relevant disorder related terms ("social", "autism", "attachment") and outcome specific terms ("acceptability", "feasibility", "acceptance", "compliance", "adherence"). The specific search terms are provided in Supplementary Tables S1–S3.

# 3 Results

## 3.1 Techniques targeting INS indirectly through other modalities of synchrony

One of the most widely used indirect approaches to target INS is through behavioral techniques that aim to modify behavior and foster shared experiences and emotional bonding. Hyperscanning studies using EEG/MEG, fNIRS, and fMRI have shown increased INS in a variety of social-interactive tasks, e.g., emotional sharing, joint action, coordinated and synchronized movement, communication, making music, eye contact and joint attention, cooperation and competition, decision making and learning tasks (e.g., see Nam et al., 2020 for a review). Based on these studies, we will non-systematically summarize several behavioral techniques that may be particularly well-suited for increasing INS and promoting positive outcomes in Section 3.1.1. Given the close link between the brain and other bodily systems, INS may additionally be enhanced by targeting synchrony in the ANS and by hormonal manipulations. These techniques will be non-systematically summarized in Section 3.1.2.

### 3.1.1 Behavioral techniques

Some promising candidates for enhancing INS include (i) coordinating or synchronizing body movements, (ii) making music together, (iii) playing cooperative or interactive games, and (iv) engaging in shared eye contact or joint attention. Of note is that while these possibilities are not the exclusive ones, they are highlighted here because there is fairly robust evidence for all four of them.

#### 3.1.1.1 Coordinated and synchronized movements

Evidence suggests that coordinated or synchronized body movements are associated with increased INS. Examples of tasks that induce INS include synchronized button press after counting a time in mind (Hu et al., 2017), synchronized arm movement (Nozawa et al., 2019) and imitation tasks (Dumas et al., 2010; Holper et al., 2012; Miyata et al., 2021), as well as many cooperative tasks that involve action coordination or synchronization (e.g., Cui et al., 2012; Li et al., 2020; see below for more information). Further, experimental manipulations of movement synchrony have been shown to induce higher affiliation (Hove and Risen, 2009), altruistic and prosocial behavior (Valdesolo and DeSteno, 2011; Cirelli et al., 2014), cooperation (Wiltermuth and Heath, 2009) and joint action performance (Valdesolo et al., 2010). Some of these effects may be facilitated through increased INS (Hu et al., 2017). While most hyperscanning studies have measured the effects of behavioral synchrony on INS concurrently, Nozawa et al. (2019) have probed the prolonged effects of an experimental movement synchrony manipulation on subsequent social interaction. In their study, pairs of participants had to move their arm to a beat of a sound, presented either at the same or at a different tempo. After the rhythmic movement block, participants engaged in an educational communication where they taught and learned unknown words to/from each other during which their neural activities in medial and left lateral prefrontal cortices were measured using fNIRS hyperscanning. Results showed that prior movement synchrony enhanced both teacher-learner rapport and INS in the left lateral prefrontal cortex in the subsequent teaching-learning task, and these changes were interrelated. Thus, although these findings need to be replicated, this suggests that movement synchrony induction can have at least short-term carry-over effects on social interaction.

#### 3.1.1.2 Cooperative behavior and games

As shown by a recent systematic review and quantitative meta-analysis, cooperative behavior has been associated with statistically significant INS, with a large overall effect sizes in frontal and temporoparietal areas, across diverse cooperative tasks, including Jenga game, Tangram puzzle, creativity tasks, joint finger tapping, drawing and singing, realistic problem solving and a math task ($N = 13$ fNIRS-based hyperscanning studies with 890 human subjects; Czeszumski et al., 2022). Many of the cooperative tasks have been applied or are potentially suitable for children and adolescents (e.g., Reindl et al., 2018, 2022; Kruppa et al., 2021). Importantly, compared to simple movement coordination/synchronization tasks, gamifying behavioral synchrony induction tasks (e.g., as in Cui et al., 2012 or Reindl et al., 2018) may make the tasks more engaging, particularly for developmental populations, and thus potentially more suitable for behavioral interventions.

#### 3.1.1.3 Music

Singing or humming together, drumming, playing musical instruments like guitar or piano, musical improvisation and listening to music have been associated with INS in multiple studies (e.g., Lindenberger et al., 2009; Sänger et al., 2012; Müller et al., 2013, 2018; Osaka et al., 2015; Zamm et al., 2018; Müller and Lindenberger, 2019, 2022, 2023; Hou et al., 2020; Liu et al., 2021; Chabin et al., 2022; Gugnowska et al., 2022). The close link between music and INS is not surprising given that making music involves sensorimotor coupling

in musicians, being entrained to the same pace and rhythm as well as coordinating and synchronizing actions. Further, music is a pleasurable experience that is linked to emotional sharing in musicians, audience as well as between musicians and audience. In addition to its emotional effects, it promotes social functions, such as communication, cooperation, and social attachment, and thereby might possess inherent therapeutic potential (Koelsch, 2014).

#### 3.1.1.4 Eye contact

Irrespective of the specific task, ostensive signals have been proposed to entrain oscillatory brain signals during the social interaction (e.g., via mutual phase resetting in sender and receiver; Wass et al., 2020). Ostensive signals are cues that a communicator uses to convey their communicative intention to an addressee (Wass et al., 2020); one of the most notable is eye contact. Studies in adults and adult-child dyads show that eye contact elicits increased INS (e.g., Dikker et al., 2017; Hirsch et al., 2017; Koike et al., 2019; Dravida et al., 2020; Noah et al., 2020; Guglielmini et al., 2022; Luft et al., 2022; but see Haresign et al., 2023 for contradictory findings). This has been demonstrated both in naturalistic tasks, e.g., during communication (Piazza et al., 2020), as well as in well-controlled experimental set-ups, e.g., eye-to-eye contact compared to mutual gaze at the eyes of a picture face (Hirsch et al., 2017). Further, Dikker et al. (2017) demonstrated that engaging in a short eye-to-eye contact activity could serve as an intervention to enhance subsequent INS. In their study, the EEGs were recorded of 12 students simultaneously over the course of a semester during regular classroom activities. Prior to the class, students engaged in a 2-min eye contact with an assigned peer. Students showed highest INS with their face-to-face partner during class, which was correlated with student's mutual closeness rating. Such a correlation was only observed for face-to-face partners; thus, it seemed to "activate" interpersonal relationship features.

Taken together, behavioral studies indicate that social interactions that involve coordinating or synchronizing actions, cooperation, music and eye contact are associated with increased INS, and thus are potentially suitable as behavioral interventions. However, the majority of studies have evaluated INS during the behavioral intervention or experimental condition. Only a very limited number of studies have explored the effects of behavioral interventions on INS measured shortly thereafter, indicating that these tasks may have carry-over effects (Dikker et al., 2017; Nozawa et al., 2019; Khalil et al., 2022). While long-term effects on INS manipulations are rather unexplored, some of these techniques have been implemented in therapeutic approaches (e.g., in a dance/movement interventions based on interpersonal movement imitation and synchronization; Koehne et al., 2016) (for further information see Section 3.3). Nevertheless, before moving behavioral synchrony manipulations towards clinical application in patients with social dysfunction more research is needed to demonstrate whether they do show longer-lasting effects on social interactive behaviors, INS or both.

### 3.1.2 ANS-based biofeedback and hormonal manipulations

Another indirect technique to manipulate synchrony in interacting individuals is to provide feedback systems to measures of the ANS. This form of biofeedback training can for instance be provided based on heart rate variability. As such, it can not only be employed in single-person designs to entrain self-regulation of the underlying biological signal (Mather and Thayer, 2018), but is also considered a suitable approach for dyadic contexts to increase interpersonal synchrony. For example, it may help to increase interpersonal synchrony in a therapeutic setting (Fiskum, 2019) or promote empathy and social entrainment between two people (Tennant et al., 2019). Besides heart rate variability, skin conductance has been used to provide (simulated) dyadic feedback (Feijt et al., 2020) and other studies have provided ANS-based biofeedback based on breathing rhythm (Järvelä et al., 2019, 2021; Stepanova et al., 2020; Salminen et al., 2022). Popular feedback modalities in this context are pure visual (Feijt et al., 2020), or auditory feedback (Tennant et al., 2019) as well as a multisensorial approach via virtual realities (Järvelä et al., 2019, 2021; Stepanova et al., 2020; Salminen et al., 2022).

Along with biofeedback, hormonal approaches can be employed to intentionally enhance INS. Notably, maternal chemo-signals have been found to heighten INS between parents and infants and can also foster increased INS between an infant and an unfamiliar person (Endevelt-Shapira et al., 2021). Moreover, studies have demonstrated that the administration of intranasal oxytocin can effectively boost INS (Mu et al., 2016) and promote behavioral synchrony in adult participants (Spengler et al., 2017). Again, nothing is known about any longer-lasting effects of such manipulations.

## 3.2 Techniques directly targeting INS

Promising manipulation approaches that target synchrony directly on the neural level include brain stimulation through methods like transcranial direct current stimulation (tDCS) or transcranial alternating current stimulation (tACS), as well as hyper-NF. These techniques aim to directly influence INS in the brain.

Both tDCS and tACS pass a low electrical current through the brain to modulate neural activity (Kropotov, 2016) and can be used to influence the activity of specific brain regions, such as regions that are involved in social cognition and interpersonal interaction. Specifically, tDCS delivers a weak, direct current to the brain through scalp electrodes and can thereby manipulate the membrane potential of neurons and modulate spontaneous firing rates, producing facilitatory or inhibitory effects upon a variety of behaviors (Paulus, 2011; Thair et al., 2017). Instead of using a direct current, tACS delivers sinusoidally varying transcranial stimulation that may interact with ongoing rhythms in the cortex (Paulus, 2011). tDCS may create a stable environment that predisposes neural circuits towards synchronization, potentially affecting INS through sustained shifts in excitability and plasticity. tACS, on the other hand, could immediately and dynamically entrain neural oscillations and directly modulate the temporal dynamics of brain activity, providing a more immediate but possibly less enduring impact on INS. Thus, while both, tDCS and tACS can modulate INS, they may do so through different mechanisms and with different temporal dynamics. tDCS might promote a general state of heightened plasticity and readiness for synchronization, while tACS could directly entrain and synchronize oscillatory activity in real-time, which is typically considered the foundation of INS (Lu et al., 2023). In comparison, tDCS applies a constant stimulation and can thus modulate brain activities in regions associated with the mental processes that are being probed. tDCS can also reduce INS, e.g., by applying stimulation to one participant but not the other (Long et al., 2023). The influence of those two brain stimulation techniques

has been shown to impact on INS in dyads with respect to synchrony in communication (Long et al., 2023), movement (Novembre et al., 2017; Szymanski et al., 2017; Pan et al., 2021) as well as enhanced learning performances (Pan et al., 2021).

While brain stimulation influences the brain signal most directly, neurofeedback allows participants to intentionally manipulate their neural activity through real-time information about their brain activity (Marzbani et al., 2016). Recently, initial studies have focused on hyper-NF also called dual neurofeedback or so-called cross-brain neurofeedback (Duan et al., 2013; Zhang and Zhao, 2018). In this context, mainly EEG (Järvelä et al., 2019, 2021; Dikker et al., 2021; Müller et al., 2021; Putri et al., 2022; Salminen et al., 2022; Ceccato et al., 2023; Vrins et al., 2023) but also fNIRS (Duan et al., 2013) and fMRI (Kerr et al., 2022) have been used.

So far, little is known about how direct approaches can be used to manipulate INS intentionally, even though brain stimulation and hyper-NF are promising techniques and represent two of the most suitable, practicable, and relatively cost-effective methods for clinical translation. Therefore, we will provide a systematic overview of the current literature on brain stimulation approaches in section 3.2.1 and hyper-NF in Section 3.2.2. Additionally, we will discuss considerations of optimizing technical and design issues for hyper-NF (Boxes 1, 2).

### 3.2.1 Brain stimulation

Seven studies were identified that used brain stimulation protocols with the goal to modify INS and measure its effects on behavioral outcomes, with five studies using tACS (Novembre et al., 2017; Szymanski et al., 2017; Pan et al., 2021; Chen et al., 2022; Liu et al., 2023), one study using tDCS (Long et al., 2023) and one study using both (Lu et al., 2023) (see Table 1 for an overview). In a hyper-tACS protocol, the brains of a pair of participants are simultaneously stimulated and a behavioral outcome, such a movement synchrony, is measured during the stimulation. The stimulation can be applied with the same or different frequency and with the same or different phase. While same-phase-same-frequency stimulation is expected to enhance INS, different-phase-same-frequency or different-phase-different-frequency stimulation are expected to reduce INS, although it should be noted that INS was not actually measured in three hyper-tACS studies. In the first study, Novembre et al. (2017) showed that in-phase 20 Hz stimulation over the participants' left motor cortices (same-phase-same-frequency) enhanced interpersonal movement synchrony in a finger tapping task, compared with anti-phase or sham stimulation, particularly for the initial taps following a preparatory period. This effect was specific for 20 Hz (beta oscillations) stimulation and was not found for 10 Hz (alpha oscillations) or 2 Hz (finger tapping frequency). In contrast to these findings, Szymanski et al. (2017) demonstrated that same-phase-same-frequency and different-phase-different-frequency stimulation over right frontal and parietal sites in the theta frequency range were associated with greater dyadic drumming asynchrony relative to a sham condition. This indicates that artificial modulation of inter-brain synchronization can actually impair rather than improve joint action coordination and highlight the importance of finding the optimal stimulation protocol to enhance synchrony. Investigating the potential of brain stimulation for social learning, Pan et al. (2021) found that tACS stimulation of learners and instructors over inferior frontal brain regions with in-phase 6 Hz alternating currents (same-phase-same-frequency) led to spontaneous and synchronized body movements and enhanced song learning performance (intonation accuracy) compared to a sham condition. Interestingly, the effects of in-phase stimulation on learning performance were partially mediated by interpersonal movement synchrony, suggesting that brain stimulation can facilitate learning through enhancing interpersonal synchrony. Similarly, Chen et al. (2022) found an increased gamma-band INS in left temporoparietal region for successful versus unsuccessful conceptual alignment. This was paralleled by an observed enhancement in conceptual alignment when gamma-band in-phase tACS was applied. Notably, these findings were derived from two distinct experiments. Liu et al. (2023) used a semiotics paradigm in which participants had to establish a novel interpersonal symbolic communication system using arbitrary symbols and figures prior to which the two brains were stimulated simultaneously using either 40 Hz in-phase, 40 Hz anti-phase or sham stimulation targeting the right superior temporal gyrus (rSTG). Throughout the stimulation period and communication task, brain activities were measured using fNIRS. Results showed that in-phase stimulation not only enhanced INS in the rSTG, but also improved communicative accuracy compared to the sham or anti-phase stimulation. Importantly, higher INS in the rSTG was observed both during the stimulation and task periods for in-phase compared to anti-phase and sham stimulation, showing that it was effective in increasing INS.

While tACS may modulate the frequency of brain oscillations, e.g., in beta frequency band, tDCS does not target a specific frequency but induces subthreshold alterations in neuronal resting membrane potentials. In a tDCS protocol, stimulation was delivered to one participant of the dyad for 20 min. after which a resting-state session and social interaction task were conducted while measuring the brain activities using fNIRS hyperscanning (Long et al., 2023). Results showed that INS in the communication task was reduced after true compared to sham stimulation. Further, true stimulation decreased emotional empathy but importantly, the relationship between INS and emotional empathy was fully mediated through nonverbal behaviors. Thus, although there is ample correlational evidence for the importance of INS for learning, interpersonal understanding and affiliative bonding (e.g., Zheng et al., 2020; Zhang et al., 2022), the functional role of INS without behavior as a mediator is yet to be determined. Lu et al. (2023) compared the effects of 20 Hz in-phase tACS, tDCS and sham stimulation delivered to both participants over the right inferior frontal gyrus (rIFG) while their brain activities were measured simultaneous using fNIRS during a behavioral coordination task. They showed that tACS led to greater INS in the prefrontal cortex (PFC) for coordination after the stimulation while tDCS led to a reduced activation, indicating enhanced efficiency, in the rIFG. Importantly, tACS had longer lasting positive effects on behavioral coordination than tDCS. This shows that a comparison of tACS and tDCS can yield valuable insights into the unique effects of INS, yet these differences need to be interpreted with caution since effects may depend on parameter settings and intervention formulations, including the targeted cortex, intensity and frequency of stimulation (Lu et al., 2023).

To summarize, few studies exist examining the effects of brain stimulation on interpersonal synchrony. These studies have primarily focused on exploring the casual relationships between INS and behavioral synchrony and other outcome measures, however in some of the studies without directly assessing INS. Although some conflicting evidence exists, studies suggest that behavioral synchrony

BOX 1: Methodological considerations for hyper-NF.

From the reviewed hyper-NF studies, we will explore key methodological and design considerations, aiming to provide a comprehensive overview of the selected parameters and methodological considerations.

Typically, in neurofeedback, predefined brain regions are selected that have been shown to be associated with the psychological or biological construct of interest to calculate the feedback. The selection of these target regions varies considerably across studies. Some studies focus on distinct parietal regions targeted by a single EEG channel (Susnoschi Luca et al., 2021; Putri et al., 2022) while others consider multiple regions, such as the left and bilateral sensorimotor cortex in motor-related experiments (Duan et al., 2013; Zhang and Zhao, 2018). Dikker et al. (2021) and Vrins et al. (2023) performed whole-brain-based neurofeedback. Notably, all studies targeted only homologous brain regions between participants in a dyad or averaged the signals across regions.

The neural recordings from these targeted regions are subsequently online preprocessed. Online preprocessing can be performed either directly on an infinite stream of data or by slicing a finite number of subsequent samples into batches, termed batch processing (Marz and Warren, 2015). The reported batch sizes varied considerably across studies, ranging from 0.5 s up to 9 s for EEG experiments. Increasing the overlap of batches allows for a higher refresh frequency (the frequency at which the preprocessed signal is updated) of the preprocessed signal, approaching the sampling frequency. The refresh frequency in the reviewed studies ranged from 0.5 Hz in fMRI up to 60 Hz in EEG, enabling continuously perceived visual feedback. Signal processing operations on these batches involved signal averaging across target regions and time, transformations (e.g., Hilbert Transform), and applying filters, e.g., to select the desired frequency band in EEG studies. The choice of frequency band differed across EEG studies. For instance, Müller et al. (2021) targeted both the theta band and the delta band in separate training runs. In fNIRS, an important methodological consideration pertains to the signal type since fNIRS measures changes in oxyhemoglobin (HbO) and deoxyhemoglobin concentrations in the brain. Duan et al. (2013) targeted HbO to derive feedback features, a common approach in fNIRS neurofeedback studies (see Kohl et al., 2020). Notably, none of the studies applied bad channel detection or artifact correction beyond filters (see Nolan et al., 2010; Mullen et al., 2015; Aranyi et al., 2016; Kohl et al., 2023).

Based on the preprocessed signals, a single or a set of features are derived, forming the basis of the subsequently presented feedback. The features in the studies reviewed here can be differentiated into three categories: amplitude and power-based estimators, or functional connectivity estimators. Both amplitude and power-based feedback provide independent metrics for each subject ($f(x_1), f(x_2)$). These can be feedbacked independently, e.g., as two bars, or a difference between subjects' features can be calculated and presented to the participants, e.g., as a see-saw, resulting in symmetric feedback ($f(x_1, x_2) = |f(x_2, x_1)|$, see Figure 2 ) In contrast to amplitude and power-based feedback features, connectivity estimators quantify synchrony directly ($f(x_1, x_2)$). Here, generally, non-directed and directed estimators can be differentiated (Bastos and Schoffelen, 2016). While non-directed metrics aim to capture some form of interdependence between signals, without considering any direction of influence, directed metrics seek to establish a statistical causation from the data that is based on the principle that cause precedes effect (e.g., from parent to child or vice versa). Among the reviewed studies, only undirected functional connectivity estimators were used. These undirected estimators, such as the Pearson correlation, provide a single value that is equal for both participants ($f(x_1, x_2) = f(x_2, x_1)$). This value indicating high or low INS is feedbacked to the participants, e.g., as a pendulum (joint feedback; Figure 2). In contrast, directed FC, such as Granger causality, can provide individual feedback for each person which is dependent but non-symmetric ($f(x_1, x_2)$ != $f(x_2, x_1)$), thus allowing to remove individual training differences within a dyad. The feedback signal should fit the task at hand. For example, joint feedback may be less applicable for a competitive task where the winner should be displayed, while in a cooperative task both joint and individual feedback can provide valuable information.

To quantify success based on the feedback signal, either the continuous feedback signal itself can be used, for example, in an offline analysis, or a discrete performance measure can be calculated from the feedback signal. For instance, three studies thresholded feedback signals to estimate discrete states of synchronization or desynchronization, and then counted the occurrence of the desired state if the state lasted over a period, such as 1 s (Müller et al., 2021; Susnoschi Luca et al., 2021; Putri et al., 2022).

and related behavioral outcomes (e.g., coordination, learning, communication or conceptual understanding) may be enhanced by hyper-tACS.

### 3.2.2 Hyperscanning based neurofeedback (hyper-NF)

Twelve publications including nine independent experimental data sets were identified that investigated the general feasibility and training success of hyper-NF using EEG ($N = 10$), fNIRS ($N = 1$), or fMRI ($N = 1$). Detailed information on methodological and design characteristics of the studies can be found in Boxes 1, 2. In a typical hyper-NF setup, the brain activations of two or more individuals are simultaneously measured to provide feedback on a shared target parameter (amplitudes or a measure of synchrony). This feedback allows individuals to collectively learn self-regulation of the target parameter. From a clinical perspective, the ultimate goal is to modify outcomes such as empathy, social affiliation or affective mental states. To assess whether participants were able to successfully regulate their brain activities / INS, we followed established regulation success classifications from single-person neurofeedback research (Thibault et al., 2018; Kohl et al., 2020). Specifically, we explored whether a study reported a significant effect as compared to a baseline control condition (CTB), for an early session as compared to a late session (ECTL), a linear increase (linear) and lastly if a study reported a significant effect as compared to a control condition (CTC). Results are depicted in Table 2 and study details provided in Supplementary Table S4. Findings are either based on the online analysis which was used for the calculation of the neurofeedback signal or an INS derived from an additional offline analysis.

In a strictly controlled within-subject design, Müller et al. (2021) subjected participants to two different tasks in which they received real feedback, fake feedback (an enhanced signal meant to motivate the participants by giving them the impression that they are performing well) and inverted feedback (reinforcing desynchronization) of theta or delta frequencies ($N = 25$ dyads). Specifically, participants either had to move two balls as close as

BOX 2: Design considerations for hyper-NF.

Conceptually, cooperative, and competitive tasks can be differentiated. Cooperative tasks typically reinforce a synchronization of neural activity between dyads. In contrast, competitive tasks reinforce a desynchronization, e.g., by targeting the upregulation of one's neural activities above those of the opponent, or by targeting neural activities into opposite directions (i.e., bidirectional training). However, whether indeed competition leads to lower, or possibly higher, INS than cooperation remains to be explored. Most studies employed a cooperative task, such as dyadic meditation (Järvelä et al., 2019, 2021; Salminen et al., 2022) or generating live music together (Ceccato et al., 2023; Vrins et al., 2023), while other studies employed competitive tasks, such as tug-of-war games (Duan et al., 2013; Zhang and Zhao, 2018). Depending on the task and neurofeedback target region, studies provide either specific instructions, e.g., motor imagery to regulate motor areas (Duan et al., 2013; Zhang and Zhao, 2018), or empathic, warm and compassionate feelings to regulate prefrontal EEG frequency bands (Järvelä et al., 2019, 2021; Salminen et al., 2022), or rather loose instructions as in Müller et al. (2021) who provide a few exemplary strategies but encourage a trial-and-error approach. A conceptional exception is the study by Kerr et al. (2022), in which mothers are instructed to regulate not their own brain activation but that of their daughters.

The presentation of feedback may differ with regard to (1) sensory modality (e.g., visual, auditory), (2) timing (immediate vs. delayed), (3) complexity (simple vs. complex), (4) reward (reward vs. no reward, type and time point of reward, see also Kohl et al. (2020). In previous hyper-NF studies, the feedback animations ranged from very simple visual designs such moving bar designs (Kerr et al., 2022) or intuitive approaching-ball-, pendulum- or seesaw-designs reflecting the IBS of both participants (Müller et al., 2021) to complex immersive audiovisual VR environments of a campfire scene using glowing connecting bridges between two avatars (Järvelä et al., 2019, 2021; Salminen et al., 2022). In the artistic approach of Dikker et al. (2021) participants sat face-to-face in a dome-like neurofeedback environment that immerses pairs of participants in a real-time audiovisual (AV) reflection of their EEG signals. In the study by Ceccato et al. (2023) and Vrins et al. (2023) participants received musical feedback. The pitch, intensity and pleasantness of the tone were determined by the different EEG features of the participants. Notably, nearly all studies provided immediate feedback on brain activity or synchrony. None of the studies provided delayed or post-block feedback, i.e., feedback after regulation. Two studies (Susnoschi Luca et al., 2021; Putri et al., 2022) presented additional rewards in the form of points that participants could collect throughout the training. Notably none of the studies used a form of social or monetary reward, which may boost regulation performance (Mathiak et al., 2015; Sepulveda et al., 2016; Kohl et al., 2023).

A hyper-NF protocol can be organized into trials/blocks, nested in runs, nested in sessions, although it should be noted that taxonomies differ between hyper-NF studies. A training run can be defined as a sequence of trials or blocks which is presented once or several times in one session, whereas different sessions are conducted on different days. Past protocols consisted of several training runs (1–8) on each day/session and up to six regulation trials per run. Besides the study by Susnoschi Luca et al. (2021) and Putri et al. (2022) (3 sessions) all studies employed singles-session training regimes. Whereas studies based on hemodynamic neuroimaging followed blocked designs with alternating regulation and resting/baseline blocks of 40 s each (Duan et al., 2013; Kerr et al., 2022), EEG studies involved longer regulation trials/blocks without breaks in between up to 5 min (Susnoschi Luca et al., 2021; Putri et al., 2022) or with breaks only after 5–10 trials (Müller et al., 2021), but resting baselines before the experiment, which was used for normalization purposes (Susnoschi Luca et al., 2021; Putri et al., 2022).

Neurofeedback experiments can employ several different control conditions (Sorger et al., 2019). Most studies were lacking a control condition, while some used sham or implicit feedback (i.e., participants were unaware that they received neurofeedback) (Dikker et al., 2021), no feedback, solo-neurofeedback or biofeedback (Järvelä et al., 2019, 2021; Salminen et al., 2022) and fake or inverted feedback (Müller et al., 2021). The implementation of random sham feedback can be challenging. For example, in Vrins et al. (2023), participants anticipated whether they were assigned to the control group and reported that the sham feedback was perceived as noisy music. Although no statistical comparison between cooperation and competition was conducted, the approach proposed by Susnoschi Luca et al. (2021) offers conceptually a bidirectional control mechanism that involves for one party a collaborative task to reinforce synchronization and for the other party a competitive task to reinforce desynchronization.

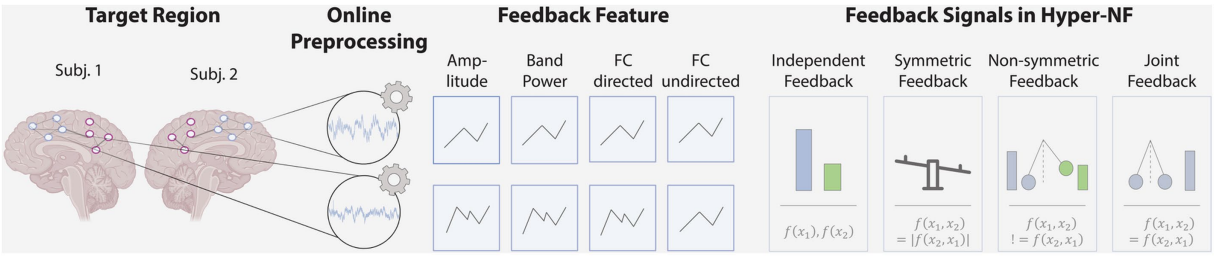


FIGURE 2
Study design considerations. Hyper-NF begins with the observation of neural activity of multiple persons using EEG/MEG, fNIRS or fMRI in target brain regions or network of regions. In an online analysis, signals are preprocessed and a feedback signal is calculated based on features such as the signal's amplitude, band power or directed / undirected functional connectivity. This is then fed back to the participants through visual, auditory, or other modalities using independent, symmetric, non-symmetric or joint feedback.

possible to each other by synchronizing their brain activities or they had to make two pendulums, each reflecting the oscillatory activity of one of the two participants, swing in phase. Across task and feedback conditions, participants demonstrated increased INS at theta and beta frequencies and partly also at delta frequencies compared to a resting state whereas INS at alpha frequencies decreased. Further validating their approach, they showed that INS at theta and beta was relatively strongly related to test partner

TABLE 1 Brain stimulation study results.

| Author | *N* dyads | Type of stimulation | Stimulation conditions | Stimulation target | Task | Outcome | |
|---|---|---|---|---|---|---|---|
| | | | | | | Neural | Behavioral |
| Chen et al. (2022) | 27 (experiment 2) | Dual-tACS | 40 Hz in-phase, sham (between-subjects) | Left STG | tACS during rest and semiotic game | NA | No significant differences in number of people in success / failure group;<br>Accuracy higher for tACS vs. sham in success but not failure group |
| Liu et al. (2023) | 70 (experiment 3) | Dual-tACS | 40 Hz in-phase, 40 Hz anti-phase, sham (between-subjects) | Right STG | tACS prior to coordinating symbolic communication task | Higher INS in right STG during baseline and task for in-phase compared to anti-phase and sham stimulation | Communicative accuracy higher for in-phase compared to sham and anti-phase stimulation |
| Long et al. (2023) | 30 | Single tDCS | True, sham and control stimulation (within-subjects) | *True / sham*: Right ATL;<br>*Control*: Occipital lobe | tDCS applied to *one* member of the dyad (women) prior to naturalistic communication task | Decreased INS for true compared to the sham and control stimulation | No significant differences in verbal or nonverbal behaviors;<br>Reduced emotional empathy for true compared to sham and control stimulation |
| Lu et al. (2023) | 62 | Dual-tACS, dual-tDCS | 20 Hz in-phase tACS, tDCS, sham (between subjects) | Right IFG | Six coordination blocks with stimulation in blocks 3 and 4 | Higher INS in PFC for tACS compared to tDCS and sham in block 5;<br>Higher INS in right IFG during rest period after stimulation for tACS compared to tDCS;<br>Reduced activation in right IFG for tDCS during stimulation compared to poststimulation | Numbers of wins in blocks 3–6 higher than at baseline (block 1) in tACS and tDCS but not sham group, positive effect on number of wins in block 6 only for tACS not tDCS;<br>Higher difference in reaction times (weaker coordination) in block 6 for tDCS compared to sham |
| Novembre et al. (2017) | 30 | Dual-tACS | frequency (within-subjects: 2 Hz, 10 Hz, 20 Hz) × relative phase (within-subjects: in-phase, anti-phase), sham stimulation | Left primary motor cortex | tACS during joint finger tapping task | NA | Increased synchrony for 20 Hz in-phase stimulation compared to anti-phase stimulation |
| Pan et al. (2021) | 24 | Dual-tACS | frequency (between-subjects: 6 Hz, 10 Hz) x relative phase (within-subjects: in-phase, antiphase, sham) | Left IFC | tACS during song learning task | NA | Increased synchrony for 6 Hz in-phase stimulation compared to 6 Hz sham stimulation;<br>Improved intonation learning performance for 6 Hz in-phase compared to 6 Hz sham stimulation |
| Szymanski et al. (2017) | 38 | Dual-tACS | same-phase-same-frequency (6 Hz), different-phase-different-frequency (5 Hz and 7 Hz with 1 degree offset), 6 Hz sham (within-subjects) | Right frontal and parietal sites | tACS during joint drumming task | NA | Decreased synchrony for same-phase-same-frequency and the different-phase-different-frequency compared to sham |

tACS, transcranial alternating current stimulation; tDCS, transcranial direct current stimulation; IFC, inferior frontal cortex; ATL, anterior temporal lobe; IFG, inferior frontal gyrus; PFC, prefrontal cortex; STG, superior temporal gyrus; N/A, not applicable.



10.3389/fnins.2024.1286130

TABLE 2 Hyper-NF study results.

| Author | *N* dyads | Imaging modality | Target region | Task type | Regulation success as compared to | | | |
|---|---|---|---|---|---|---|---|---|
| | | | | | CTB | ECTL | Linear | CTC |
| Ceccato et al. (2023) | 1 | EEG | NR | Coop | Only 1 dyad and no statistics were reported | | | |
| Dikker et al. (2021) | 784 | EEG | Whole-brain | Coop | NR | Yes (offline[1]) | NR | Yes (offline[1]) |
| Duan et al. (2013) | 1 | fNIRS | Left sensorimotor cortex | Comp | Yes (offline[1]) | NR | NR | N/A |
| Järvelä et al. (2019) | 21 | EEG | Frontal cortex | Coop | NR | NR | NR | Yes |
| Järvelä et al. (2021) | 39 | | | | NR | NR | NR | NR |
| Salminen et al. (2022) (incl. Overlapping data sets) | 36 | | | | NR | NR | NR | NR |
| Kerr et al. (2022) | 6 | fMRI | Right anterior insular cortex | Coop | NR | NR | NR | N/A |
| Müller et al. (2021) | 25 | EEG | Frontal cortex | Coop | Yes | NR | NR | No |
| Putri et al. (2022) and Susnoschi Luca et al. (2021)[2] (same data sets) | Comp.: 10<br>Coop.: 10 | EEG | Parietal cortex | Both | **Comp**:<br>Alpha power: no<br>Synchrony (offline[1]): yes<br>**Coop:**<br>Alpha power: no<br>Synchrony (offline[1]): yes | **Comp**:<br>Alpha power: yes<br>Synchrony (offline[1]): no<br>**Coop:** NR | **Comp**: NR<br>**Coop**: NR | **Comp**: NR<br>**Coop**: NR |
| Vrins et al. (2023) | 8 | EEG | Whole-brain | Coop | Synchrony (offline[1]): yes<br>Sham feedback (offline[1]): no | NR | NR | Yes (offline[1]) |
| Zhang and Zhao (2018) | 1 | EEG | Bilateral sensorimotor cortex | Comp | Only 1 dyad and no statistics were reported | | | |

Comp, Competition; Coop, Cooperation; CTB, compared to a baseline control condition; ECTL, early session as compared to a late session; Linear, linear increase over several sessions; CTC, compared to a within- or between-control condition; NR, not reported; N/A, not applicable.

[1]Some studies analyzed regulation success based on results from an additional offline analysis of neural synchrony which was different from the online analysis used to calculate the feedback signal.

[2]Susnoschi Luca et al. (2021) did not compare synchrony to a within subject baseline, but used permutation testing against a null distribution created from fake pairs.

likability and estimated ability to influence the feedback signal, as assessed using survey items. However, no significant differences between real and manipulated NF (enhanced and inverted) in INS emerged.

While in the study by Müller et al. (2021) both tasks were cooperative in nature, in the experiment by Susnoschi Luca et al. (2021) and Putri et al. (2022) participants controlled a virtual seesaw either in a cooperative or competitive interaction ($N = 10$ dyads each). Cooperating dyads had to maintain their Relative Alpha (RA) within 5% of each other to win shared points, while competing dyads won points if their RA was 10% above their opponent's. The authors observed a decrease in alpha power in both competitive and cooperative tasks compared to rest. Further, significant INS in theta, alpha and beta frequency bands was found for both tasks, however, unfortunately cooperative, and competitive tasks were not directly compared in the study (Susnoschi Luca et al., 2021).

Three publications reported different analyses from the same experimental set-up (Järvelä et al., 2019, 2021; Salminen et al., 2022). In a virtual reality meditation environment, dyadic neurofeedback targeting EEG frontal asymmetry (neurophysiological measure of

approach motivation) was combined with respirational biofeedback ($N = 21$, 39 and 36 dyads, respectively). Higher frontal asymmetry was observed in participants engaging in a dyadic neurofeedback condition compared to those in a solo neurofeedback condition. Additionally, increased synchrony of frontal asymmetry was observed when dyadic neurofeedback was combined with respiratory synchrony biofeedback, surpassing the effects of dyadic neurofeedback alone (Järvelä et al., 2019). Note, that the two later publications (Järvelä et al., 2021; Salminen et al., 2022) did not report respiratory or neural synchrony data. However, higher levels of empathy, emotion and social presence were reported following EEG-feedback and respiratory feedback, compared to a no-feedback condition, as well as after dyadic meditation compared to solo meditation conditions. Furthermore, the synchronization of EEG-frontal asymmetries between participants was associated with higher levels of empathy, with the highest ratings observed when both participants exhibited high values of frontal asymmetry (Järvelä et al., 2021; Salminen et al., 2022). Thus, these findings indicate that combining dyadic neurofeedback with biofeedback may augment both self-reported and neurophysiologically measured empathy.

Ceccato et al. (2023) built a dual brain-computer interface (BCI) that generates live music by measuring three EEG signal characteristics, which was adopted in a recent preprint by Vrins et al. (2023) to assess the effect of audio-based hyper-NF on interpersonal neural synchrony using a blinded protocol. Specifically, eight dyads ($N = 4$ dyads per group) listened to generated music. While in one group, three EEG signal characteristics (mean amplitude, frontal alpha asymmetry, and inter-brain phase-lock value) were mapped to the pitch, intensity, and consonance of the music, the control group was exposed to sham feedback based on randomly adjusted sound characteristics. The results showed a significant increase in INS through Hyper-NF compared to baseline only in the actual group, not in the control group. The authors also found that increased INS was associated with increased perceived synchrony and that the actual group reported a significant increased enjoyment, and changes in perceived mental state. However, it should be noted that participants anticipated ex-post correctly their group assignment. Hence, this study may indicate the potential of audio-based Hyper-NF.

In the so far largest hyper-NF study sample, Dikker et al. (2021) took a "crowdsourcing neuroscience" approach, in which they invited museum and festival visitors to sit in a "Mutual Wave Machine," a dome-like neurofeedback environment that translates real-time correlations of each pair's EEG activity into light patterns (final sample size: $N = 784$). Participants showed an increase in synchrony in the second compared to the first half of the experiment, however only if they were explicitly told that the visuals were derived from their correlated EEG signal. Further, this increase in synchrony in the second compared to first half was also observed in a sham feedback group, in which visualizations were randomly generated, indicating that the mere belief that the feedback signal was related to the success of the interaction could lead to higher social engagement irrespective of the actual relationship between inter-brain coupling and the feedback animation. Moreover, dyads´ relationship duration, social closeness, focus level, and social behavior (joint action and eye contact) positively and personal distress negatively predicted synchronization. While this crowdsourcing approach generated a very large sample, the authors also acknowledge its methodological limitations, in particular, the high likelihood of noise contamination, rendering it difficult to draw meaningful conclusions about the participants' INS based on their online feedback.

Finally, three studies have developed and probed new experimental setups but with very limited samples sizes ($N = 1$–6; Duan et al., 2013; Zhang and Zhao, 2018; Kerr et al., 2022). Duan et al. (2013) developed a hyper-NF setup for fNIRS with a competitive "tug-of-war" game in which the target of both participants was to upregulate their left sensorimotor brain activities more strongly than the opponent in order to pull a ribbon to their side. Similarly, Zhang and Zhao (2018) developed a hyper-NF setup for EEG, testing it using a similar competitive "tug-of-war" game. Finally, Kerr et al. (2022) did not provide dyadic neurofeedback in the sense that the brain signals of two persons were fed back simultaneously but rather they probed whether mothers were able to downregulate the right anterior insular cortex signal of their adolescent daughter during an emotion discussion task.

To summarize, the field of hyper-NF is at a very early stage consisting mainly of proof-of-concept studies involving only limited sample sizes and oftentimes lacking stringent control conditions. These studies provide preliminary evidence that EEG-based hyper-NF is effective in modulating specifically targeted measures of INS. Not enough studies employing fMRI or fNIRS-based hyper-NF are available. While there is evidence that INS can be modulated by hyper-NF, neurofeedback based on amplitudes, based on a noisy signal or even sham neurofeedback may also enhance INS (Dikker et al., 2021; Müller et al., 2021).

## 3.3 *Clinical translation:* integration of INS-based manipulations in the treatment of mental disorders characterized by social interaction dysfunction

The three cases, presented in Box 3, although representing distinct clinical pictures, demonstrate the tremendous impact of social interaction dysfunction on our everyday functioning leading to severe impairments in building up trust and emotional connections in (close) relationships, in forming friendships with peers, and in overall academic development. Despite advancements in the last decade regarding our understanding of the neural basis of ASD, attachment issues, and anxiety disorders, the application of these insights into clinical practice remains largely confined. Over the past ten years, there have been few significant breakthroughs in the development of new therapeutic approaches, whether in psychotherapy or pharmacological treatments, for any of these mental conditions. Direct application of a transdiagnostic second-person neuroscience perspective-moving from a single brain towards at least two interacting brains—might open novel avenues for prevention and intervention of social interaction disorders.

Coming back to the three cases presented above: Imagine, forming a secure attachment pattern between Sally's foster parents and herself could be supported by engaging them in synchronous activities along with direct feedback to improve synchronization of their biological parameters in the caregiver-child dyad, such as synchronized oxytocin, cortisol levels, or simultaneous brain activities in those brain regions associated with mentalizing and trust. Imagine Brian's learning difficulties in the classroom could be reduced by facilitating neural entrainment between the teacher and himself. For example, providing

BOX 3: Clinical case presentations.

Imagine the following scenarios:

A foster mother seeks psychotherapeutic help for her 2-year-old daughter Sally, whom she took into foster care 6 months ago due to neglect and suspicion of child abuse in her biological family. Sally seems withdrawn and anxious, shows no attachment to her foster parents, and does not play with other children in kindergarten. When she cries, Sally cannot be comforted by anyone, not even by the foster mother, who overall appears sensitive and empathetic when interacting with Sally.

Brian, a six-year-old boy, diagnosed with ASD three years ago, had been treated with intensive behavioral interventions, including applied behavioral analysis (ABA). Although his parents report that overall, Brian seems to profit from those interventions showing more adequate interactions within his family and with his little sister and less ASD-stereotypic behavior (i.e., less body rocking) he still suffers from marked social interaction deficits in the classroom. He typically misses the overall context of the lesson while focusing on specific details and he does not engage in any group activities which impairs both his integration into joint classroom activities with his peers as well as the acquisition of academic skills.

Susan, an 18-year-old university student, has always been shy and has consistently faced difficulties speaking in front of strangers. After moving to a new town for college, where she is unfamiliar with her peers and surroundings, she experiences a noticeable exacerbation of her social anxiety, including intense physical symptoms such as trembling, sweating, and palpitations as soon as she steps onto the campus. She seeks psychotherapeutic help as she is unable to attend her classes, participate in group projects, or engage in any typical social interactions on campus.

him with social ostensive signals that trigger transient moments of interpersonal teacher-pupil entrainment, in which the information presented by the teacher might arrive at a high receptivity phase for optimal encoding in Brian's brain. And finally, imagine the effectiveness of a cognitive-behavioral therapy (CBT) for Susan's social anxiety could be improved or shortened by synchronizing her ANS and neural activity with a socially non-anxious role model in prototype situations of social interactions.

In the following paragraphs, we will briefly describe what is already known about interpersonal synchrony, and INS in particular, in the three mental disorders, all characterized by social interaction dysfunction: ASD, RAD and SAD. We will summarize the current treatment standards according to clinical guidelines for each of these disorders and finally stimulate a critical discussion about the potential of tailored intervention to enhance INS in clinical treatment of these disorders and conclude with aspects of acceptability by participants and cost-effectiveness.

### 3.3.1 Autism spectrum disorder (ASD)

ASD is a very heterogeneous, pervasive developmental disorder with life-long difficulties in social affect, including social interaction and communication, as well as restricted and repetitive behaviors. It affects approximately 1–3% of children and by the year of 2025 the cost of caring only for Americans with ASD will approximately reach up to 461 billion USD in the absence of more-effective interventions and support across the life span (Autism Statistics and Facts, 2023).

More recently, temporal synchrony has been in the focus of interest and might provide new insights for the understanding of social communication and sensory difficulties in ASD as experienced in everyday tasks and in naturalistic settings such as speaking back-and-forth on the telephone without visual cues, engaging in "flowing" one-to-one in-person conversation, and taking turns in social interactions. McNaughton and Redcay (2020) and Baldwin et al. (2022) reviewed existing studies on synchrony in ASD. Results demonstrated that participants with ASD tended to show more temporally asynchronous behavior when performing tasks that required audio-visual, audio-motor, visuo-tactile, visuo-motor, social motor, and conversational sensory integration.

In line with, a growing number of studies investigated interpersonal synchrony in ASD, and more recently also focused on INS (e.g., Lyons et al., 2020; Kruppa et al., 2021; Quiñones-Camacho et al., 2021; Wang et al., 2021; Key et al., 2022). Since these studies vary tremendously in the participants' age (children, adolescents, and adults), as well as in tasks and imaging techniques (EEG, fMRI and fNIRS), it is difficult at this point to draw any strong conclusions. Kruppa et al. (2021) for instance found differences in behavioral synchrony between typically developing children and children with ASD, but no difference with respect to INS measures (i.e., wavelet coherence was calculated for oxy- and deoxyhemoglobin brain signals during a fNIRS task). However, using the same sample, Gerloff et al. (2022a) was able to predict ASD diagnosis based on non-linear connectivity estimators and network embeddings. Quiñones-Camacho et al. (2021) on the other hand, reported that healthy adults showed more neural synchrony than participants with ASD in the TPJ during a conversation task in an fNIRS study. Similarly, Key et al. (2022) reported that in typically developing adolescents and in adolescents with ASD, lower levels of synchrony, as measured with EEG, were associated with increased behavioral symptoms of social difficulties. Furthermore, Tanabe et al. (2012) used a real-time joint-attention task combined with dual-fMRI recordings and found that detecting gaze direction was impaired in both healthy subjects and subjects with ASD, when they were paired together and inter-brain coherence in the right inferior frontal gyrus (IFG) together with intra-brain functional connectivity between the right IFG and right superior temporal sulcus (STS) was diminished in ASD. These studies – although not completely consistent—point to impaired interpersonal synchrony across multiple levels in subjects with ASD.

Up to now, numerous interventions have been developed to improve ASD symptomatology. During early childhood, intensive behavioral interventions, including applied behavioral analysis (ABA, Cooper et al., 1987) and TEAACH (Mesibov et al., 2005), aim to improve difficulties in communication and social interaction. Nonetheless, its evidence is heterogenous, and randomized control trials (RCTs) are scarce. However, increasing evidence now supports the efficacy, and in some instances, the long-term impact of interventions focusing on parent–child interactions during the early

years (e.g., European Child and Adolescent Psychiatry practice parameters). From school-age on, social skills training programs are commonly applied, mostly in high-functioning children with ASD, and just like early behavioral interventions, some evidence exists that show improvement in social functioning, including, i.e., social motivation, social anxiety, social cognition, and social skills (e.g., Spain and Blainey, 2015; Freitag et al., 2016). Nevertheless, so far, no interventions are available that can provide "cure" for ASD across the lifespan. In line with this, clinical guidelines refer to a multi-sensory, multi-disciplinary approach for the treatment of ASD (Subramanyam et al., 2019). Existing behavioral, psychosocial, educational, medical, and complementary approaches are recommended to be chosen based on the age and developmental status of the individual to maximize functional independence and quality of life by minimizing core deficits in social skills and communication, facilitating development and learning, promoting socialization, reducing maladaptive behaviors, and educating and supporting families. Intervention studies targeting interpersonal synchrony are still scarce yet, however, they provide first evidence for effectiveness and give hope for a whole new branch of intervention studies in ASD. Until now four interventions exist that target synchrony in individuals with ASD. Koehne et al. (2016) included 55 adults with ASD who either received 10 weeks of a dance movement intervention focusing on interpersonal movement imitation and synchronization (SI-DMI) or a control movement intervention (CMI). Patients in the SI-SMI group increased their synchronization skills and imitation tendencies, as well as whole-body imitation/synchronization and movement reciprocity/dialogue, compared to patients in the CMI group. In a RCT Landa et al. (2011) provided 50 toddlers with 10 h/week of classroom intervention, parent education setting (38 h) and 1.5 h of home-based parent training and instructional strategies. Additionally, half of the participants received a supplementary curriculum targeting socially engaged imitation, joint attention, and affect sharing. The authors report an increase in socially engaged imitation with eye contact in autistic toddlers, who participated in the supplementary curriculum. In a more recent study, Griffioen et al. (2020) provided six weekly sessions of 30-min-long dog-assisted therapy with children with ASD and children with Down's syndrome focusing on psychomotor and socialization skills that would ensure aligned motor action between the child and the therapy dog. The authors also report an increase in synchronous interaction between children with ASD and their therapy dog. However, the number of participants ($N = 10$) in the study limits the generalizability of the findings. And last, in a pilot RCT (Srinivasan et al., 2015) 36 children with ASD between 5 and 12 years of age received one of three interventions (rhythm, robotic or standard-of-care) for eight weeks four times per week. In the rhythm and robot groups children got engaged in socially embedded whole-body movement games, whereas the children in the standard-of-care group engaged in tabletop activities promoting fine motor, social communication, and academic skills within a group setting. The rhythm and robot groups improved on the body coordination assessment, whereas the standard-of-care group improved on the fine manual control assessment. All three groups improved in imitation/praxis. The rhythm and robot groups also showed improved interpersonal synchrony performance.

These studies provide first and very preliminary evidence for behavioral joint-action interventions manipulating INS indirectly in dyadic interactions (person–person, child-dog, person-robot) in individuals with ASD. Other interventions to improve INS in ASD, such as neurofeedback or neurostimulation, have not been published yet. By contrast, neurofeedback interventions based on single-brain information using EEG, thus not including/targeting INS, have *not* been shown to be effective to improve ASD symptoms (Holtmann et al., 2011).

### 3.3.2 Reactive attachment disorder (RAD)

RAD is characterized by absent or aberrant attachment behaviors in young children which are observable across settings. Children with RAD rarely interact with caregivers and they do not seek comfort or respond to comfort when distressed (American Psychiatric Association, 2013; Zeanah et al., 2016). In addition, they show limited or no positive affect, often appear socially and emotionally unresponsive and may display episodes of unexplained irritability, sadness, or fearfulness even if (familiar) adults are around. A child diagnosed with RAD should have a cognitive age of at least 9 months as this is the time, when infants usually have formed preferred attachments, and the symptomatology should develop before the age of 5 (American Psychiatric Association, 2013). RAD is a rather rare disorder, however in high-risk populations as, e.g., in children being raised in institutional care the prevalence rate is much higher and might reach up to 40% (O'Connor and Zeanah, 2003).

Children with RAD partly present similar symptoms as children diagnosed with ASD, e.g., social withdrawal and reduced social reciprocity. Both disorders are often associated with cognitive delays and stereotypes (Zeanah et al., 2016). The phenotypic similarity between the two disorders can be such that children exposed to sustained extreme early life institutional deprivation may present a symptom pattern that Rutter et al. (2007) termed "quasi-autism". Importantly, in contrast to ASD, RAD is caused by the experience of adverse, neglectful caregiving environments including social neglect or deprivation, for example when being raised in institutions with high child-to-caregiver ratios or after having repeated changes of primary caregivers. As such, inadequate care is etiologic regarding the development of RAD as the deficits and the aberrant attachment behaviors develop in children who would have been able to develop functional social interaction processes if they had been raised in more favourable caregiving environments. Faced with severely limited opportunities to form selective attachments, affected children fail to develop attachments to any caregiver. However, it is important to bear in mind, that the RAD symptoms should not be reduced to a unique dysregulation of the children's attachment system. Instead, the RAD symptoms rather seem to reflect a more general emotional and behavioral dysregulation (Rutter et al., 2009). This general pattern of dysregulation might be seen as a direct consequence of the lack of biobehavioral synchrony experience with a sensitive caregiver in early development. The important role of early synchrony experiences for the child's social–emotional development has been shown in several studies. The quality of the early caregiver-child synchrony has been shown to predict the child's later emotion and stress regulation capabilities, the expression of core social behaviors like engagement with peers and displaying empathy, as well as the exhibition of cognitive control (Feldman, 2012a, 2015b; Bell, 2020). Up to now, there are no studies investigating either behavioral synchrony or INS in children diagnosed with

RAD. However, some studies considered biobehavioral synchrony in the context of insecure or disorganized attachment styles in high-risk caregiver-child conditions, such as in premature infants, in families who experienced multiple traumata or in mothers with postpartum depression (e.g., Feldman, 2015a; Granat et al., 2017; Pratt et al., 2019; Ulmer-Yaniv et al., 2023). For instance, it could be shown that depressed mothers and their infants were less synchronous, i.e., had lower levels of gaze and touch synchrony, reduced coordination of affectionate touch with mutual gazing, and diminished maternal behavior (Granat et al., 2017). Pratt et al. (2019) investigated the impact of early and persistent maternal depression on the child's brain and general development in a prospective longitudinal study. They not only found an increased prevalence of affective disorders in these children, but also a longitudinal impact of maternal depression on the children's oxytocin levels across early childhood and aberrant neural responses to attachment-specific and social cues in preadolescence.

Research regarding the relationship between attachment quality and INS is still in its infancy (Long et al., 2020) and so far, studies with children with RAD or with high-risk dyads are missing. Using fNIRS hyperscanning in 28 mother–child dyads during the performance of a cooperation task Miller et al. (2019) found some preliminary evidence in an ROI-based correlation analysis that avoidant attachment in the child was associated with reduced INS in the right frontopolar PFC. Another fNIRS hyperscanning study in 42 dyads of mothers and their preschool children demonstrated that INS was positively correlated with behavioral reciprocity (Nguyen et al., 2020).

With regard to treatment, the clinical guidelines for RAD recommend as treatment of first choice the child's placement in a safe and sensitive caregiving environment with an emotionally available attachment figure as early as possible to minimize the consequences of the psychosocial deprivation on the child's development (Practice Parameter of the American Academy of Child and Adolescent Psychiatry (AACAP); Zeanah et al., 2016). However, due to a lack of research in this field, it is less clear whether children who recover from RAD still have an enhanced risk for subsequent interpersonal difficulties. To help the child and the caregivers to attune to each other and to interact more positively, the AACAP-Parameter additionally recommend psychotherapeutic interventions targeting the caregiver-child-dyad (Zeanah et al., 2016). Among them the child–parent psychotherapy (CPP; Lieberman, 2004) and the Attachment and Biobehavioral Catch Up intervention (ABC; Bernard et al., 2012; Dozier and Bernard, 2017) were found to be effective in RCTs, though in samples of children with disturbed attachment relationships, not specifically in toddlers with attachment disorders. ABC, a manualized, in-home treatment program includes synchrony-based interventions and is targeted to "catch up" the missed experience of nurturing and sensitive caregiving. Consequently, ABC focuses on directly changing caregivers' behaviors by, e.g., using direct behavior-focused in-the-moment comments when caregivers interact with the child as well as video feedback. Three main parenting targets are addressed during the intervention, namely nurturing the child when distressed, following the child's lead (synchronous behavior), and behaving in nonfrightening ways (Dozier and Bernard, 2017). In ABC-T for toddlers the third target is replaced by helping the caregivers to serve as co-regulators when toddlers show signs of dysregulation as, e.g., anger or frustration or aggressive behavior (Lind et al., 2017; Imrisek et al., 2018). It could be shown that the ABC intervention led to enhanced caregivers' synchronous behaviors and improved attachment behavior, cortisol production, and executive functioning in the child (Dozier et al., 2013).

These first studies addressing the enhancement of biobehavioral synchrony as a core intervention target provide evidence that attachment- and synchrony-based interventions can help to attenuate the consequences of psychosocial deprivation. However, treatment interventions directly targeting INS in socially deprived children have not been published yet.

### 3.3.3 Social anxiety disorder (SAD)

SAD is a persistent anxiety and avoidance reaction triggered by social or performance situations. SAD may escalate to panic attacks when facing fearful situations such as speaking or eating in the presence of others or engaging in social activities. Individuals with SAD experience distress and/or impairment in occupational and social functioning. SAD often becomes chronic without intervention. The anxiety reaction typically extends to all social contexts and varies in severity, influenced by stressors and life changes (Stein and Stein, 2008; Steinert et al., 2013). SAD is highly prevalent, with a lifetime and 12-month prevalence of 13 and 8%, respectively, among adults in the United States and similar rates in adolescents (Kessler et al., 2005, 2012; Kessler and Üstün, 2008). Onset is typically during adolescence (mean age: 13 years) and rarely after age 25 (Stein and Stein, 2008; Steinert et al., 2013).

Given the considerable difficulties individuals with SAD face in interpersonal scenarios, investigating interpersonal synchrony within this patient group holds substantial promise. Asher et al. (2020) recently examined behavioral and heart rate (HR) synchrony during closeness-generating and small talk conversation in opposite-sex dyads including subjects with and without SAD. It was shown that closeness-generating conversation compared to small-talk conversation led to increased behavioral synchrony (as derived from computer-based video analysis) in control dyads but not in subjects with SAD. Furthermore, the authors found that during intimate conversations, social anxiety correlated with increased HR synchrony in control dyads but decreased HR synchrony in SAD dyads, suggesting that SAD may hinder the ability to establish HR synchrony in closer social contexts, potentially affecting relationships negatively (Asher et al., 2021). So far, INS has been hardly addressed in the context of SAD. However, one study conducted an EEG hyperscanning study with parent-adolescent dyads, revealing that SAD in adolescents is associated with heightened gamma interbrain synchrony in positive emotional contexts and diminished gamma interbrain synchrony in emotionally negative context during socioemotional interactions (Deng et al., 2022).

Clinical guidelines for the treatment of SAD (e.g., Germany: S3 guideline, Bandelow et al., 2014); United Kingdom: NICE guidelines (National Institute for Health and Care Excellence, 2013); Canada: Canadian Clinical Practice Guidelines (Katzman et al., 2014) recommend both, cognitive behavioral therapy and pharmacotherapy for treatment. Several RCT studies in subjects with SAD demonstrated high efficacy for exposure therapy and cognitive restructuring (effect size: 1.8) and for selective serotonin reuptake inhibitors (effect size: 1.5) (Fedoroff and Taylor, 2001; Stein et al., 2004; Canton et al., 2012). While divergent study designs hinder direct effect size comparisons between psychotherapy and pharmacotherapy, emerging evidence suggests faster effects with pharmaceuticals and potentially more

enduring effects with CBT (Gelernter et al., 1991; Heimberg et al., 1998; Liebowitz et al., 1999; Haug et al., 2003; Davidson et al., 2004; Nordahl et al., 2016). RCTs comparing monotherapies with combined CBT and psychotropics yield heterogeneous results (Knijnik et al., 2008; Stein and Stein, 2008; Canton et al., 2012; Baldwin et al., 2014; Nordahl et al., 2016).

Moreover, given that individuals with SAD inherently fear social interactions, the question emerges about the potential of therapeutic approaches aimed at reinforcing synchronization for therapeutic efficacy. As of now and to our knowledge, no study has explicitly targeted synchronization between therapist and patient with SAD, despite its assessment as an outcome measure in previous research. Altmann et al. (2020) investigated the effect of movement synchrony in interactions between individuals with SAD and psychotherapists, without putting synchrony in the therapeutic focus. The study revealed that heightened synchrony led by the therapist correlated with improved therapeutic alliance and decreased interpersonal issues. Similarly, Schoenherr et al. (2019) found that therapist-patient pairs, which included patients with SAD who prematurely terminated psychotherapy, exhibited lower movement synchrony at the therapy onset compared to patients who completed therapy. Ramseyer and Tschacher (2011) reported analogous results across more diverse disease profiles. Notably, if patients took a leading role in synchrony at the end of the psychotherapy, a reduced therapeutic alliance was observed along with increased scores for interpersonal problems and depression (Altmann et al., 2020). Furthermore, studies on vocal synchrony in patient-therapist interactions (Schoenherr et al., 2021) revealed that heightened patient-led vocal synchrony correlated with elevated symptom severity, attachment anxiety, avoidance, and interpersonal problems in subjects with SAD.

Previous studies have demonstrated that the inclusion of neurofeedback as a treatment tool can produce effects in reducing symptoms in generalized anxiety disorder (Hou et al., 2021) and specific phobia (Zilverstand et al., 2015). In an initial pilot study, NIRS-based neurofeedback targeting the dlPFC in individuals with SAD was deemed feasible (Kimmig et al., 2019). Participants improved dlPFC control, altering social threat-related attention bias. Decreased social anxiety severity was linked to reduced attentional threat processing and successful NF training. NIRS-based NF offers potential to explore attention biases and the dlPFC's role in SAD. Nevertheless, subsequent research should encompass larger sample sizes and suitable control groups to validate and extend these initial findings. While these studies focused on a single-subject, Saul et al. (2022) were the first to introduce hyper-NF protocol (called "InBS-NF-paradigm") for clinical application in SAD employing multi-user neurofeedback for intervention. The paradigm aims to integrate neural activities of interacting partners with external sources to minimize subjective distortions. It enables real-time observation and treatment of SAD symptoms by updating the mental self-representation using objective external cues. This work exemplifies the first attempts to directly target INS in clinical treatment.

## 3.4 Feasibility of neuroscience-based intervention approaches in patients with social interaction disorders

If interventions that directly target the neural basis of a mental disorder in at least two interacting individuals, e.g., by hyper-NF or by brain stimulation, could represent novel treatment options, implementation depends not only on the effectiveness of such approaches but is also heavily influenced by the patients' perspective on tolerability and acceptance of such treatment approaches as well as cost-effectiveness and safety of the intervention. The systematic database search for feasibility of neurofeedback and neurostimulation approaches in subjects with social interaction disorders provided overall good support for such methods (see Table 3 for study results). NF studies in patients with social interaction disorders reported no clinically meaningful adverse events. Generally, both EEG and fNIRS, typically used in NF, are considered safe and can be used in all patient groups (Strehl et al., 2017; Pinti et al., 2020). Similarly, non-invasive brain stimulation methods used in the therapy of mental disorders, such as tDCS, trigeminal nerve stimulation (TNS) or transcutaneous electrical nerve stimulation (TENS), are well tolerated with mild side effects like skin irritations from electrodes (Matsumoto and Ugawa, 2017; Wei et al., 2017). One neuromodulation study conducted with participants with social interaction disorders used TENS and reported no adverse events (Foldes et al., 2021). Three studies used tDCS in patients with ASD and reported no adverse events as well as low drop-out rates (D'Urso et al., 2015, 2022; Wang et al., 2023).

In NF studies, acceptability was high. In a study by Kimmig et al. (2019), 9 out of 12 of participants in a NF training for social anxiety disorder would recommend the treatment. A fMRI-based NF study examining adolescents with ASD reported high fidelity, feasibility, and acceptability (Direito et al., 2021). Some studies reported that children had difficulty concentrating on the NF task (Steiner et al., 2014; LaMarca et al., 2018). LaMarca et al. (2018) conducted an EEG-NF intervention with children with ASD and reported that some participants displayed problems with concentration, compliance as well as sensory issues associated with the NF protocol (e.g., electrode placement, noises).

Note, however, that the studies included here had few participants and reported on few measures of acceptability. However, the findings are in line with NF studies in other patient groups. A meta-analysis from Catalá-López et al. (2017) found lower drop-out rates for NF treatment for children and adolescents with ADHD compared to cognitive training, and no difference to a wide range of other pharmaceutical and non-pharmaceutical treatments, suggesting high acceptability.

While acceptability of single-brain-based neuroscience-based interventions was high in patients with social interaction disorders, this cannot be automatically generalized to dual-brain-based interventions. Targeting the INS requires interventions of social interacting partners. This could pose an additional challenge. Therefore, future studies need to specifically assess acceptability for neuroscience-based interventions involving synchrony.

## 3.5 Considerations of cost-effectiveness of neuroscience-based interventions in patients with social interaction disorders

In addition to acceptability and safety, cost-effectiveness is a crucial factor for the implementation of any novel treatment option. Commonly used behavioral therapies for patients with ASD are costly, e.g., ABA-based interventions are estimated to cost around 45,000 USD annually per patient (Hodgson et al., 2022). Treatments for social

TABLE 3 Study results for feasibility of neuroscience-based intervention approaches for social interaction disorders.

| Author | Patient group | *N* | Intervention | Outcome measures | Results |
|---|---|---|---|---|---|
| Direito et al. (2021) | ASD (16-22y) | 15 | NF (fMRI, facial expression task) | Fidelity; feasibility; acceptability | All measures 100%; 1 drop-out |
| D'Urso et al. (2015) | ASD (18-26y) | 12 | tDCS | Drop-out rate | No adverse events; 2 drop-outs |
| D'Urso et al. (2022) | ASD (9-13y) | 7 | tDCS | Drop-out rate | No adverse events; no drop-outs |
| Foldes et al. (2021) | ASD (10-21y) | 7 | Transdermal electrical neuromodulation | Adverse events (AE); tolerability (sham-controlled) | No significant AEs reported during the trial; no participant reported discomfort from the study procedures (including the electrodes) |
| Kimmig et al. (2019) | SAD (over 18y) | 12 | NF (NIRS, social threat-processing experiment) | Enjoyment; importance of performing; effort they put into the training; if they would recommend it | 2 drop-outs; 9 would recommend it to others, 3 were unsure; motivation to perform well: $M = 3.58$, $SD = 0.52$; enjoyment of training: $M = 3.00$, $SD = 0.74$ (scale was 0 to 4) |
| LaMarca et al. (2018) | ASD (6-8y) | 8 | NF (EEG, TAGteach-assisted NF) | Case study; description of fidelity, feasibility, and acceptability for each case | Method is feasible; some patients showed difficulties with focus fatigue, disruptive behavior, and tolerability of sensory aspects of NF, but issues could be resolved by the instructor |
| Steiner et al. (2014) | ASD (7-12y) | 10 | NF (EEG, play attention & academic tasks) | Motivation; feedback of intervention questionnaire (parents & child) | All children reported it was easy to understand, follow, and that the sessions helped them concentrate; 3 had low motivation scores; 5 said sessions were "boring"; 90% of parents reported that the intervention was helpful |
| Wang et al. (2023) | ASD (4–12 y) | 45 | tDCS | Adverse events | With adaptations, all children tolerated the treatment; all children developed scalp erythema, but it disappeared after 30 min; 3 had symptoms of excitement and night terrors which improved on their own; no serious AEs occurred |

ASD, Autism Spectrum Disorder; SAD, Social Anxiety Disorder; NF, Neurofeedback; tDCS, transcranial direct current stimulation.

anxiety disorders, such as cognitive behavioral group therapy, typically amount to approximately 2,500 USD for a 15-session program consisting of two-hour sessions (Stuhldreher et al., 2014). Cost for neuroscience-based interventions using hyperscanning depend on the specific protocol and the type of neuroimaging method that is used. In an EEG NF study, Arnold et al. (2013) reported that after 24 sessions, the parent rating of ADHD symptom improvement plateaued. Assuming a similar number of treatment sessions for NF treatment of social interaction disorders and calculating the costs for one-person NF intervention (according to the remuneration of the German health insurance funds for NF training), the total cost of one-person NF intervention is around 1,500 USD (for 24 sessions). Two-person NF requires two neuroimaging devices, but no additional therapeutic personnel are needed, so the cost of each session for hyper-NF should be comparable to one-person NF. In contrast, fMRI-based hyper-NF constitutes an exception as it requires twice costly scanner time and additional technical personnel. Recent developments of low-cost neuroimaging devices for EEG (Niso et al., 2023) and fNIRS (Vidal-Rosas et al., 2023) have increased accessibility to mobile NF equipment. Taken together, compared to standard treatment of social interaction disorders, NF training based on EEG and fNIRS can be considered relatively low-cost. Thus, such approaches might yield high potential to develop cost-effective interventions, however, as a first step, the field requires a robust evaluation of the effectiveness of such non-pharmacological interventions.

## 4 Conclusion

Despite their preliminary nature, early findings outline the potential of INS-based manipulations, such as hyper-NF. Although predominantly conducted in healthy adult cohorts in the past, the

findings motivate the extension of this technique to clinical and developmental samples, along with further developments of methodological approaches. Hyper-NF may exhibit greater transferability to everyday situations, particularly through its association with social experience and learning, compared to traditional neurofeedback approaches which have often struggled to demonstrate substantial real-world transfer (Kohl et al., 2020). Even other innovative and motivating treatment options, such as "serious games", may not fully address this aspect (Dewhirst et al., 2022). In contrast, targeting directly the INS might be distinct, as it couples learning mechanisms with physiological processes, linking a natural synchronization process with a conditioned stimulus.

Nevertheless, for clinical applications, first several technical and data analytical challenges must be solved. In particular, well-controlled studies with larger samples are needed to determine the most suitable hyper-NF parameters, such as experimental task and instructions, target brain regions and feedback signal, presentation of the feedback signal, required number of trials, runs and sessions etc. (see Boxes 1, 2). In addition to neurofeedback control conditions, e.g., sham neurofeedback, it will be key to compare feedback of neural synchrony to synchrony feedback in other modalities, such as heart rate or breathing (see also Järvelä et al., 2019, 2021; Salminen et al., 2022), as well as to behavioral interventions to determine the most effective technique or combination of techniques for enhancing INS. Furthermore, task and hyper-NF settings have to be evaluated with respect to their transferability. For instance, for patients with SAD, a training that involves no or little direct interaction between participants (e.g., back-to-back setting, Müller et al., 2021) may be less suitable although it allows for better experimental control. Similarly, for dual-brain stimulation more methodological groundwork is needed. In particular, previously conflicting findings suggest that identifying the optimal stimulation protocol, e.g., with respect to the specific frequencies and stimulation sites, will be crucial for developing this technique further. In addition, it will be necessary to assess short- and long-term changes in INS in response to single and repeated stimulation. In this review, we outline the importance of tailored design and method considerations (see Section 3.2.2), as well as key factors to report (see Supplementary Table S4) when combining hyperscanning with interventional techniques. Moving forward, future work may substantially benefit from an improved mechanistic understanding of INS (Lotter et al., 2023), e.g., to efficiently target relevant brain regions, as well as from further developments of technique-specific designs, reporting standards (Ros et al., 2020) and methods and from fostering the application of open science practices (Allen and Mehler, 2019; Niso et al., 2022; Botvinik-Nezer and Wager, 2023).

Based on the evidence of the current review, one can conclude that although direct strategies have shown some promise for improving INS, there is no concrete evidence that the effects of direct stimulation are more substantial than those achieved through indirect strategies. Furthermore, so far, no data are available how long such direct effects might last. Thus, given that few studies have attempted a comparison between direct and indirect INS-based manipulations (for exceptions see Järvelä et al., 2019, 2021 and Salminen et al., 2022) and none have examined their transferability, no clear conclusions can be drawn about the efficiency of direct versus indirect techniques. Interestingly, the findings of Järvelä et al. (2019) indicate that a combination of different types of feedback (here EEG neurofeedback and respiratory-based biofeedback) could potentially surpass the effects of one type of feedback alone. This is in line with many other areas of clinical applications of direct brain manipulations, such as in depression (Xu et al., 2023) neurological rehabilitation (Xu et al., 2022) or pain management (Goudra et al., 2017). In this regard it should also be noted that not all patients may profit equally from different types of interventions. Thus, identifying which types of interventions work best for certain groups of individuals (see also "precision medicine") may be an important avenue for future research.

The current review emphasizes the unique role of INS in selected mental disorders characterized by core deficits in social interactions. However, as outlined in this review, before INS-based interventions can be applied in clinical contexts there is quite a long way to go from the current state of knowledge towards RCTs testing the efficacy of INS-based interventions either as a stand-alone or as an add-on intervention to the current standard treatment approaches of the respective disorder. For example, in the case of ASD, future trials need to demonstrate that combined approaches including social competence trainings together with targeted interventions incorporating Hyper-NF or dual neurostimulation might be more effective than social competence training alone to facilitate not only cognitive but also affective empathy, thus creating a more holistic approach to managing social interaction dysfunctions in subjects with ASD.

Clinical applications based on a second-person neuroscience approach must be built on specific dysfunction in interpersonal synchrony. They should target those modalities of synchrony that have the largest effects to achieve the "optimal" or the "most healthy state" (see also Gordon et al., 2023). Gordon et al. (2023) proposed an alternative theory of flexible multimodal synchrony which highlights the context as a key component that defines "pulls" towards synchrony and "pulls" towards segregation inherent to the social situation. In the case of the mental disorders described above, this aspect becomes particularly relevant in the context of allostasis co-regulation in relationships, such as in the mother–child bond in RAD or in the patient-therapist-relationship in SAD. For instance, if a mother is comforting her crying child, it is intuitive to assume that maximal synchrony will not be most goal-conducive but that a temporary "desynchronization" may be more beneficial instead which allows the mother to down-regulate the child's affective state (Long et al., 2020). Thus, clinical intervention that include a monitoring of functional and dysfunctional synchrony patterns in interacting partners should enable and support the participants not only to pull towards synchrony but also to push out of maladaptive interpersonal synchrony. Furthermore, as there is growing evidence that synchrony of body and mind is distinct and their relationship is dependent on context (Reindl et al., 2022), a second challenge concerns the identification of the most efficient target of the different (i.e., behavioral, physiological, endocrine, and neural) measures of interpersonal synchrony. For example, increasing INS between caregivers and their children might support mentalizing and empathy towards their children's needs while ANS synchrony in some situations might be associated with higher overall distress in the dyads. Finally, for clinical translations, selecting the best patient's partner for INS-based intervention, e.g., a therapist, romantic partner, peer or the child's primary caregiver, will be crucial for treatment success and strongly depend on disorder-specific social dysfunction.

While further research is necessary to fine-tune these interventions and establish their efficacy, this exploration of interpersonal synchrony paves the way for promising advancements in the realm of mental health which may—in principle—be relevant

for many other mental disorders as well as for neurological diseases that are characterized by impaired social interactions.

## Data availability statement

The original contributions presented in the study are included in the article/Supplementary material, further inquiries can be directed to the corresponding author.

## Author contributions

KK: Conceptualization, Funding acquisition, Resources, Supervision, Writing – original draft, Writing – review & editing. CG: Methodology, Software, Visualization, Writing – original draft, Writing – review & editing. SK: Methodology, Writing – original draft, Writing – review & editing. DM: Writing – original draft, Writing – review & editing. LM: Visualization, Writing – original draft, Writing – review & editing. EV: Methodology, Writing – original draft, Writing – review & editing. MK: Writing – review & editing. AH: Writing – original draft, Writing – review & editing. MB: Writing – original draft, Writing – review & editing. EW: Writing – original draft, Writing – review & editing. VR: Conceptualization, Methodology, Resources, Supervision, Writing – original draft, Writing – review & editing.

## Funding

The author(s) declare financial support was received for the research, authorship, and/or publication of this article. KK has received funding for this research by the German Research Foundation –DFG: Project-ID 431549029 –SFB 1451.

## Conflict of interest

SK is working for MEDIACC GmbH, Berlin, an independent clinical research organization. SK and DM received payments to consult with Mendi Innovations AB, Stockholm, Sweden. None of these activities were related to the work presented in the current manuscript.

The remaining authors declare that the research was conducted in the absence of any commercial or financial relationships that could be construed as a potential conflict of interest.

## Publisher's note

All claims expressed in this article are solely those of the authors and do not necessarily represent those of their affiliated organizations, or those of the publisher, the editors and the reviewers. Any product that may be evaluated in this article, or claim that may be made by its manufacturer, is not guaranteed or endorsed by the publisher.

## Supplementary material

The Supplementary material for this article can be found online at: https://www.frontiersin.org/articles/10.3389/fnins.2024.1286130/full#supplementary-material

## References

Allen, C., and Mehler, D. M. A. (2019). Open science challenges, benefits and tips in early career and beyond. *PLoS Biol.* 17:e3000246. doi: 10.1371/journal.pbio.3000246

Altmann, U., Schoenherr, D., Paulick, J., Deisenhofer, A.-K., Schwartz, B., Rubel, J. A., et al. (2020). Associations between movement synchrony and outcome in patients with social anxiety disorder: evidence for treatment specific effects. *Psychother. Res.* 30, 574–590. doi: 10.1080/10503307.2019.1630779

American Psychiatric Association (2013). *Diagnostic and statistical manual of mental disorders DSM-5*. Washington, DC: American Psychiatric Association

Aranyi, G., Pecune, F., Charles, F., Pelachaud, C., and Cavazza, M. (2016). Affective interaction with a virtual character through an fNIRS brain-computer interface. *Front. Comput. Neurosci.* 10:70. doi: 10.3389/fncom.2016.00070

Arnold, L. E., Lofthouse, N., Hersch, S., Pan, X., Hurt, E., Bates, B., et al. (2013). EEG neurofeedback for ADHD: double-blind sham-controlled randomized pilot feasibility trial. *J. Atten. Disord.* 17, 410–419. doi: 10.1177/1087054712446173

Asher, M., Barthel, A. L., Hofmann, S. G., Okon-Singer, H., and Aderka, I. M. (2021). When two hearts beat as one: heart-rate synchrony in social anxiety disorder. *Behav. Res. Ther.* 141:103859. doi: 10.1016/j.brat.2021.103859

Asher, M., Kauffmann, A., and Aderka, I. M. (2020). Out of sync: nonverbal synchrony in social anxiety disorder. *Clin. Psychol. Sci.* 8, 280–294. doi: 10.1177/2167702619894566

Autism Statistics and Facts (2023). Autism speaks. Available at: https://www.autismspeaks.org/autism-statistics-asd (Accessed August 25, 2023).

Azhari, A., Leck, W. Q., Gabrieli, G., Bizzego, A., Rigo, P., Setoh, P., et al. (2019). Parenting stress undermines mother-child brain-to-brain synchrony: a hyperscanning study. *Sci. Rep.* 9:11407. doi: 10.1038/s41598-019-47810-4

Baldwin, D. S., Anderson, I. M., Nutt, D. J., Allgulander, C., Bandelow, B., den Boer, J. A., et al. (2014). Evidence-based pharmacological treatment of anxiety disorders, post-traumatic stress disorder and obsessive-compulsive disorder: a revision of the 2005 guidelines from the British Association for Psychopharmacology. *J. Psychopharmacol.* 28, 403–439. doi: 10.1177/0269881114525674

Baldwin, M. M., Xiao, Z., and Murray, A. (2022). Temporal synchrony in autism: a systematic review. *Rev. J. Autism Dev. Disord.* 9, 596–617. doi: 10.1007/s40489-021-00276-5

Bandelow, B., Wiltink, J., Alpers, G. W., Benecke, C., Deckert, J., Eckhardt-Henn, A., et al. (2014). Deutsche S3-Leitlinie Behandlung von Angststörungen. Available at: www.awmf.org/leitlinien.html.

Bastos, A. M., and Schoffelen, J.-M. (2016). A tutorial review of functional connectivity analysis methods and their interpretational pitfalls. *Front. Syst. Neurosci.* 9:175. doi: 10.3389/fnsys.2015.00175

Bell, M. A. (2020). Mother-child behavioral and physiological synchrony. *Adv. Child Dev. Behav.* 58, 163–188. doi: 10.1016/bs.acdb.2020.01.006

Bernard, K., Dozier, M., Bick, J., Lewis-Morrarty, E., Lindhiem, O., and Carlson, E. (2012). Enhancing attachment organization among maltreated children: results of a randomized clinical trial. *Child Dev.* 83, 623–636. doi: 10.1111/j.1467-8624.2011.01712.x

Birk, S. L., Stewart, L., and Olino, T. M. (2022). Parent–child synchrony after early childhood: a systematic review. *Clin. Child. Fam. Psychol. Rev.* 25, 529–551. doi: 10.1007/s10567-022-00383-7

Botvinik-Nezer, R., and Wager, T. D. (2023). Reproducibility in neuroimaging analysis: challenges and solutions. *Biol. Psychiatry. Cogn. Neurosci. Neuroimaging.* 8, 780–788. doi: 10.1016/j.bpsc.2022.12.006

Canton, J., Scott, K. M., and Glue, P. (2012). Optimal treatment of social phobia: systematic review and meta-analysis. *Neuropsychiatr. Dis. Treat.* 8, 203–215. doi: 10.2147/NDT.S23317

Catalá-López, F., Hutton, B., Núñez-Beltrán, A., Page, M. J., Ridao, M., Saint-Gerons, D. M., et al. (2017). The pharmacological and non-pharmacological

treatment of attention deficit hyperactivity disorder in children and adolescents: a systematic review with network meta-analyses of randomised trials. *PLoS One* 12:e0180355. doi: 10.1371/journal.pone.0180355

Ceccato, C., Pruss, E., Vrins, A., Prinsen, J., and Alimardani, M. (2023). BrainiBeats: a dual brain-computer interface for musical composition using inter-brain synchrony and emotional valence. In Extended abstracts of the 2023 CHI conference on human factors in computing systems (CHI EA '23) (New York, NY, USA: ACM), 1–7. doi: 10.1145/3544549.3585910

Chabin, T., Gabriel, D., Comte, A., Haffen, E., Moulin, T., and Pazart, L. (2022). Interbrain emotional connection during music performances is driven by physical proximity and individual traits. *Ann. N. Y. Acad. Sci.* 1508, 178–195. doi: 10.1111/nyas.14711

Chen, D., Zhang, R., Liu, J., Wang, P., Bei, L., Liu, C.-C., et al. (2022). Gamma-band neural coupling during conceptual alignment. *Hum. Brain Mapp. 43*, 2992–3006. doi: 10.1002/hbm.25831

Cirelli, L. K., Einarson, K. M., and Trainor, L. J. (2014). Interpersonal synchrony increases prosocial behavior in infants. *Dev. Sci.* 17, 1003–1011. doi: 10.1111/desc.12193

Cooper, J. O., Heron, T. E., and Heward, W. L. (1987). *Applied behavior analysis*. Columbus: Merrill Publishing Co.

Cui, X., Bryant, D. M., and Reiss, A. L. (2012). NIRS-based hyperscanning reveals increased interpersonal coherence in superior frontal cortex during cooperation. *NeuroImage* 59, 2430–2437. doi: 10.1016/j.neuroimage.2011.09.003

Czeszumski, A., Liang, S. H.-Y., Dikker, S., König, P., Lee, C.-P., Koole, S. L., et al. (2022). Cooperative behavior evokes interbrain synchrony in the prefrontal and temporoparietal cortex: a systematic review and meta-analysis of fNIRS hyperscanning studies. *eNeuro* 9:ENEURO.0268–21.2022. doi: 10.1523/ENEURO.0268-21.2022

D'Urso, G., Bruzzese, D., Ferrucci, R., Priori, A., Pascotto, A., Galderisi, S., et al. (2015). Transcranial direct current stimulation for hyperactivity and noncompliance in autistic disorder. *World J. Biol. Psychiatry* 16, 361–366. doi: 10.3109/15622975.2015.1014411

D'Urso, G., Toscano, E., Sanges, V., Sauvaget, A., Sheffer, C. E., Riccio, M. P., et al. (2022). Cerebellar transcranial direct current stimulation in children with autism spectrum disorder: a pilot study on efficacy, feasibility, safety, and unexpected outcomes in tic disorder and epilepsy. *J. Clin. Med.* 11:143. doi: 10.3390/jcm11010143

Davidson, J. R. T., Foa, E. B., Huppert, J. D., Keefe, F. J., Franklin, M. E., Compton, J. S., et al. (2004). Fluoxetine, comprehensive cognitive behavioral therapy, and placebo in generalized social phobia. *Arch. Gen. Psychiatry* 61, 1005–1013. doi: 10.1001/archpsyc.61.10.1005

Davis, M., West, K., Bilms, J., Morelen, D., and Suveg, C. (2018). A systematic review of parent-child synchrony: it is more than skin deep. *Dev. Psychobiol.* 60, 674–691. doi: 10.1002/dev.21743

Deng, X., Chen, X., Zhang, L., Gao, Q., Li, X., and An, S. (2022). Adolescent social anxiety undermines adolescent-parent interbrain synchrony during emotional processing: a hyperscanning study. *Int. J. Clin. Health Psychol.* 22:100329. doi: 10.1016/j.ijchp.2022.100329

Dewhirst, A., Laugharne, R., and Shankar, R. (2022). Therapeutic use of serious games in mental health: scoping review. *BJPsych. Open.* 8:e37. doi: 10.1192/bjo.2022.4

Dikker, S., Michalareas, G., Oostrik, M., Serafimaki, A., Kahraman, H. M., Struiksma, M. E., et al. (2021). Crowdsourcing neuroscience: inter-brain coupling during face-to-face interactions outside the laboratory. *NeuroImage* 227:117436. doi: 10.1016/j.neuroimage.2020.117436

Dikker, S., Wan, L., Davidesco, I., Kaggen, L., Oostrik, M., McClintock, J., et al. (2017). Brain-to-brain synchrony tracks real-world dynamic group interactions in the classroom. *Curr. Biol.* 27, 1375–1380. doi: 10.1016/j.cub.2017.04.002

Direito, B., Mouga, S., Sayal, A., Simões, M., Quental, H., Bernardino, I., et al. (2021). Training the social brain: clinical and neural effects of an 8-week real-time functional magnetic resonance imaging neurofeedback phase IIa clinical trial in autism. *Autism* 25, 1746–1760. doi: 10.1177/13623613211002052

Dozier, M., and Bernard, K. (2017). Attachment and biobehavioral catch-up: addressing the needs of infants and toddlers exposed to inadequate or problematic caregiving. *Curr. Opin. Psychol.* 15, 111–117. doi: 10.1016/j.copsyc.2017.03.003

Dozier, M., Zeanah, C. H., and Bernard, K. (2013). Infants and toddlers in foster care. *Child Dev. Perspect.* 7, 166–171. doi: 10.1111/cdep.12033

Dravida, S., Noah, J. A., Zhang, X., and Hirsch, J. (2020). Joint attention during live person-to-person contact activates rTPJ, including a sub-component associated with spontaneous eye-to-eye contact. *Front. Hum. Neurosci.* 14:201. doi: 10.3389/fnhum.2020.00201

Duan, L., Liu, W.-J., Dai, R.-N., Li, R., Lu, C.-M., Huang, Y.-X., et al. (2013). Cross-brain neurofeedback: scientific concept and experimental platform. *PLoS One* 8:e64590. doi: 10.1371/journal.pone.0064590

Dumas, G., Nadel, J., Soussignan, R., Martinerie, J., and Garnero, L. (2010). Inter-brain synchronization during social interaction. *PLoS One* 5:e12166. doi: 10.1371/journal.pone.0012166

Endevelt-Shapira, Y., Djalovski, A., Dumas, G., and Feldman, R. (2021). Maternal chemosignals enhance infant-adult brain-to-brain synchrony. *Sci. Adv.* 7:eabg6867. doi: 10.1126/sciadv.abg6867

Fedoroff, I. C., and Taylor, S. (2001). Psychological and pharmacological treatments of social phobia: a meta-analysis. *J. Clin. Psychopharmacol.* 21, 311–324. doi: 10.1097/00004714-200106000-00011

Feijt, M., De Kort, Y., Westerink, J., Okel, S., and Ijsselsteijn, W. (2020). "The effect of simulated feedback about psychophysiological synchronization on perceived empathy and connectedness" in *Virtual reality meets COVID-19: the potential of positive technology against the burden of coronavirus*. eds. B. K. Wiederhold and G. Riva (San Diego, CA: Interactive Media Institute), 117–121.

Feldman, R. (2012a). Bio-behavioral synchrony: a model for integrating biological and microsocial behavioral processes in the study of parenting. *Parent. Sci. Pract.* 12, 154–164. doi: 10.1080/15295192.2012.683342

Feldman, R. (2012b). Oxytocin and social affiliation in humans. *Horm. Behav.* 61, 380–391. doi: 10.1016/j.yhbeh.2012.01.008

Feldman, R. (2015a). Sensitive periods in human social development: new insights from research on oxytocin, synchrony, and high-risk parenting. *Dev. Psychopathol.* 27, 369–395. doi: 10.1017/S0954579415000048

Feldman, R. (2015b). The adaptive human parental brain: implications for children's social development. *Trends Neurosci.* 38, 387–399. doi: 10.1016/j.tins.2015.04.004

Feldman, R. (2017). The neurobiology of human attachments. *Trends Cogn. Sci.* 21, 80–99. doi: 10.1016/j.tics.2016.11.007

Feldman, R., Magori-Cohen, R., Galili, G., Singer, M., and Louzoun, Y. (2011). Mother and infant coordinate heart rhythms through episodes of interaction synchrony. *Infant Behav. Dev.* 34, 569–577. doi: 10.1016/j.infbeh.2011.06.008

Fiskum, C. (2019). Psychotherapy beyond all the words: dyadic expansion, vagal regulation, and biofeedback in psychotherapy. *J. Psychother. Integr.* 29, 412–425. doi: 10.1037/int0000174

Foldes, S. T., Jensen, A. R., Jacobson, A., Vassall, S., Foldes, E., Guthery, A., et al. (2021). Transdermal electrical neuromodulation for anxiety and sleep problems in high-functioning autism Spectrum disorder: feasibility and preliminary findings. *J. Pers. Med.* 11:1307. doi: 10.3390/jpm11121307

Freitag, C. M., Jensen, K., Elsuni, L., Sachse, M., Herpertz-Dahlmann, B., Schulte-Rüther, M., et al. (2016). Group-based cognitive behavioural psychotherapy for children and adolescents with ASD: the randomized, multicentre, controlled SOSTA-net trial. *J. Child Psychol. Psychiatry* 57, 596–605. doi: 10.1111/jcpp.12509

Gelernter, C. S., Uhde, T. W., Cimbolic, P., Arnkoff, D. B., Vittone, B. J., Tancer, M. E., et al. (1991). Cognitive-behavioral and pharmacological treatments of social phobia: a controlled study. *Arch. Gen. Psychiatry* 48, 938–945. doi: 10.1001/archpsyc.1991.01810340070009

Gerloff, C., Konrad, K., Kruppa, J., Schulte-Rüther, M., and Reindl, V. (2022a). "Autism spectrum disorder classification based on interpersonal neural synchrony: can classification be improved by dyadic neural biomarkers using unsupervised graph representation learning?" in *Machine learning in clinical neuroimaging lecture notes in computer science*. eds. A. Abdulkadir, D. R. Bathula, N. C. Dvornek, M. Habes, S. M. Kia and V. Kumar et al. (Cham: Springer Nature Switzerland), 147–157. doi: 10.1007/978-3-031-17899-3_15

Gerloff, C., Lotter, L. D., and Maheshwari, K. (2022b). Set you free: automated structured literature search. doi: 10.5281/zenodo.6907681

Gordon, I., Tomashin, A., and Mayo, O. (2023). A theory of flexible multimodal synchrony. PsyArXiv [preprint]. doi: 10.31234/osf.io/9u7q8

Goudra, B., Shah, D., Balu, G., Gouda, G., Balu, A., Borle, A., et al. (2017). Repetitive transcranial magnetic stimulation in chronic pain: a meta-analysis. *Anesth. Essays Res.* 11, 751–757. doi: 10.4103/aer.AER_10_17

Granat, A., Gadassi, R., Gilboa-Schechtman, E., and Feldman, R. (2017). Maternal depression and anxiety, social synchrony, and infant regulation of negative and positive emotions. *Emotion* 17, 11–27. doi: 10.1037/emo0000204

Griffioen, R. E., van der Steen, S., Verheggen, T., Enders-Slegers, M.-J., and Cox, R. (2020). Changes in behavioural synchrony during dog-assisted therapy for children with autism spectrum disorder and children with down syndrome. *J. Appl. Res. Intellect. Disabil.* 33, 398–408. doi: 10.1111/jar.12682

Guglielmini, S., Bopp, G., Marcar, V. L., Scholkmann, F., and Wolf, M. (2022). Systemic physiology augmented functional near-infrared spectroscopy hyperscanning: a first evaluation investigating entrainment of spontaneous activity of brain and body physiology between subjects. *Neurophotonics.* 9:026601. doi: 10.1117/1.NPh.9.2.026601

Gugnowska, K., Novembre, G., Kohler, N., Villringer, A., Keller, P. E., and Sammler, D. (2022). Endogenous sources of interbrain synchrony in duetting pianists. *Cereb. Cortex* 32, 4110–4127. doi: 10.1093/cercor/bhab469

Haresign, I. M., Phillips, E. A. M., Whitehorn, M., Lamagna, F., Eliano, M., Goupil, L., et al. (2023). Gaze onsets during naturalistic infant-caregiver interaction associate with 'sender' but not 'receiver' neural responses, and do not lead to changes in inter-brain synchrony. *Sci. Rep.* 13, 3555–3519. doi: 10.1038/s41598-023-28988-0

Hari, R., and Kujala, M. V. (2009). Brain basis of human social interaction: from concepts to brain imaging. *Physiol. Rev.* 89, 453–479. doi: 10.1152/physrev.00041.2007

Haug, T. T., Blomhoff, S., Hellstrøm, K., Holme, I., Humble, M., Madsbu, H. P., et al. (2003). Exposure therapy and sertraline in social phobia: 1-year follow-up of a randomised controlled trial. *Br. J. Psychiatry* 182, 312–318. doi: 10.1192/bjp.182.4.312

Heimberg, R. G., Liebowitz, M. R., Hope, D. A., Schneier, F. R., Holt, C. S., Welkowitz, L. A., et al. (1998). Cognitive behavioral group therapy vs phenelzine therapy for social phobia: 12-week outcome. *Arch. Gen. Psychiatry* 55, 1133–1141. doi: 10.1001/archpsyc.55.12.1133

Hirsch, J., Zhang, X., Noah, J. A., and Ono, Y. (2017). Frontal temporal and parietal systems synchronize within and across brains during live eye-to-eye contact. *NeuroImage* 157, 314–330. doi: 10.1016/j.neuroimage.2017.06.018

Hodgson, R., Biswas, M., Palmer, S., Marshall, D., Rodgers, M., Stewart, L., et al. (2022). Intensive behavioural interventions based on applied behaviour analysis (ABA) for young children with autism: a cost-effectiveness analysis. *PLoS One* 17:e0270833. doi: 10.1371/journal.pone.0270833

Holper, L., Scholkmann, F., and Wolf, M. (2012). Between-brain connectivity during imitation measured by fNIRS. *NeuroImage* 63, 212–222. doi: 10.1016/j.neuroimage.2012.06.028

Holtmann, M., Steiner, S., Hohmann, S., Poustka, L., Banaschewski, T., and Bölte, S. (2011). Neurofeedback in autism spectrum disorders. *Dev. Med. Child Neurol.* 53, 986–993. doi: 10.1111/j.1469-8749.2011.04043.x

Hou, Y., Song, B., Hu, Y., Pan, Y., and Hu, Y. (2020). The averaged inter-brain coherence between the audience and a violinist predicts the popularity of violin performance. *NeuroImage* 211:116655. doi: 10.1016/j.neuroimage.2020.116655

Hou, Y., Zhang, S., Li, N., Huang, Z., Wang, L., and Wang, Y. (2021). Neurofeedback training improves anxiety trait and depressive symptom in GAD. *Brain Behav.* 11:e02024. doi: 10.1002/brb3.2024

Hove, M. J., and Risen, J. L. (2009). It's all in the timing: interpersonal synchrony increases affiliation. *Soc. Cogn.* 27, 949–960. doi: 10.1521/soco.2009.27.6.949

Hu, Y., Cheng, X., Pan, Y., and Hu, Y. (2022). The intrapersonal and interpersonal consequences of interpersonal synchrony. *Acta Psychol.* 224:103513. doi: 10.1016/j.actpsy.2022.103513

Hu, Y., Hu, Y., Li, X., Pan, Y., and Cheng, X. (2017). Brain-to-brain synchronization across two persons predicts mutual prosociality. *Soc. Cogn. Affect. Neurosci. Neuroscience* 12, 1835–1844. doi: 10.1093/scan/nsx118

Imrisek, S. D., Castaño, K., and Bernard, K. (2018). Developing self-regulation in a dysregulating world: attachment and biobehavioral catch-up for a toddler in foster care. *J. Clin. Psychol.* 74, 1308–1318. doi: 10.1002/jclp.22642

Järvelä, S., Cowley, B., Salminen, M., Jacucci, G., Hamari, J., and Ravaja, N. (2021). Augmented virtual reality meditation: shared dyadic biofeedback increases social presence via respiratory synchrony. *ACM Trans. Soc. Comput.* 4, 1–19. doi: 10.1145/3449358

Järvelä, S., Salminen, M., Ruonala, A., Timonen, J., Mannermaa, K., Ravaja, N., et al. (2019). DYNECOM: augmenting empathy in VR with dyadic synchrony neurofeedback. In Proceedings of the 52nd Hawaii international conference on system sciences, 4212–4220. doi: 10.24251/HICSS.2019.509

Katzman, M. A., Bleau, P., Blier, P., Chokka, P., Kjernisted, K., Van Ameringen, M., et al. (2014). Canadian clinical practice guidelines for the management of anxiety, posttraumatic stress and obsessive-compulsive disorders. *BMC Psychiatry* 14:S1. doi: 10.1186/1471-244X-14-S1-S1

Kerr, K. L., Ratliff, E. L., Cohen, Z. P., Fuller, S., Cosgrove, K. T., DeVille, D. C., et al. (2022). Real-time functional magnetic resonance imaging dyadic neurofeedback for emotion regulation: a proof-of-concept study. *Front. Hum. Neurosci.* 16:910951. doi: 10.3389/fnhum.2022.910951

Kessler, R. C., Berglund, P., Demler, O., Jin, R., Merikangas, K. R., and Walters, E. E. (2005). "Lifetime prevalence and age-of-onset distributions of DSM-IV disorders in the National Comorbidity Survey replication": erratum. *Arch. Gen. Psychiatry* 62:768. doi: 10.1001/archpsyc.62.7.768

Kessler, R. C., Petukhova, M., Sampson, N. A., Zaslavsky, A. M., and Wittchen, H.-U. (2012). Twelve-month and lifetime prevalence and lifetime morbid risk of anxiety and mood disorders in the United States. *Int. J. Methods Psychiatr. Res.* 21, 169–184. doi: 10.1002/mpr.1359

Kessler, R. C., and Üstün, T. B. eds. (2008). *The WHO world mental health survey: global perspectives on the epidemiology of mental disorders*. Cambridge: Cambridge University Press.

Key, A. P., Yan, Y., Metelko, M., Chang, C., Kang, H., Pilkington, J., et al. (2022). Greater social competence is associated with higher interpersonal neural synchrony in adolescents with autism. *Front. Hum. Neurosci.* 15:790085. doi: 10.3389/fnhum.2021.790085

Khalil, A., Musacchia, G., and Iversen, J. R. (2022). It takes two: interpersonal neural synchrony is increased after musical interaction. *Brain Sci.* 12:409. doi: 10.3390/brainsci12030409

Kimmig, A.-C., Dresler, T., Hudak, J., Häußinger, F., Wildgruber, D., Fallgatter, A., et al. (2019). Feasibility of NIRS-based neurofeedback training in social anxiety disorder: behavioral and neural correlates. *J. Neural Transm.* 126, 1175–1185. doi: 10.1007/s00702-018-1954-5

Knijnik, D. Z., Blanco, C., Salum, G. A., Moraes, C. U., Mombach, C., Almeida, E., et al. (2008). A pilot study of clonazepam versus psychodynamic group therapy plus clonazepam in the treatment of generalized social anxiety disorder. *Eur. Psychiatry* 23, 567–574. doi: 10.1016/j.eurpsy.2008.05.004

Koehne, S., Behrends, A., Fairhurst, M. T., and Dziobek, I. (2016). Fostering social cognition through an imitation- and synchronization-based dance/movement intervention in adults with autism spectrum disorder: a controlled proof-of-concept study. *Psychother. Psychosom.* 85, 27–35. doi: 10.1159/000441111

Koelsch, S. (2014). Brain correlates of music-evoked emotions. *Nat. Rev. Neurosci.* 15, 170–180. doi: 10.1038/nrn3666

Kohl, S. H., Mehler, D. M. A., Lührs, M., Thibault, R. T., Konrad, K., and Sorger, B. (2020). The potential of functional near-infrared spectroscopy-based neurofeedback—a systematic review and recommendations for best practice. *Front. Neurosci.* 14:594. doi: 10.3389/fnins.2020.00594

Kohl, S. H., Melies, P., Uttecht, J., Lührs, M., Bell, L., Mehler, D. M. A., et al. (2023). Successful modulation of temporoparietal junction activity and stimulus-driven attention by fNIRS-based neurofeedback— a randomized controlled proof-of-concept study. *Imaging Neurosci.* 1, 1–26. doi: 10.1162/imag_a_00014

Koike, T., Sumiya, M., Nakagawa, E., Okazaki, S., and Sadato, N. (2019). What makes eye contact special? Neural substrates of on-line mutual eye-gaze: a hyperscanning fMRI study. *eNeuro* 6:ENEURO.0284-18.2019. doi: 10.1523/ENEURO.0284-18.2019

Kropotov, J. D. (2016). "Transcranial direct current stimulation" in *Functional neuromarkers for psychiatry*. ed. J. D. Kropotov (San Diego, CA: Academic Press), 273–280.

Kruppa, J. A., Reindl, V., Gerloff, C., Oberwelland Weiss, E., Prinz, J., Herpertz-Dahlmann, B., et al. (2021). Brain and motor synchrony in children and adolescents with ASD-a fNIRS hyperscanning study. *Soc. Cogn. Affect. Neurosci.* 16, 103–116. doi: 10.1093/scan/nsaa092

LaMarca, K., Gevirtz, R., Lincoln, A. J., and Pineda, J. A. (2018). Facilitating neurofeedback in children with autism and intellectual impairments using TAGteach. *J. Autism Dev. Disord.* 48, 2090–2100. doi: 10.1007/s10803-018-3466-4

Landa, R. J., Holman, K. C., O'Neill, A. H., and Stuart, E. A. (2011). Intervention targeting development of socially synchronous engagement in toddlers with autism spectrum disorder: a randomized controlled trial. *J. Child Psychol. Psychiatry* 52, 13–21. doi: 10.1111/j.1469-7610.2010.02288.x

Li, L., Wang, H., Luo, H., Zhang, X., Zhang, R., and Li, X. (2020). Interpersonal neural synchronization during cooperative behavior of basketball players: a fNIRS-based hyperscanning study. *Front. Hum. Neurosci.* 14:169. doi: 10.3389/fnhum.2020.00169

Lieberman, A. F. (2004). "Child-parent psychotherapy: a relationship-based approach to the treatment of mental health disorders in infancy and early childhood" in *Treating parent-infant relationship problems: strategies for intervention*. eds. A. J. Sameroff and K. L. Rosenblum (New York, NY: The Guilford Press), 97–122.

Liebowitz, M. R., Heimberg, R. G., Schneier, F. R., Hope, D. A., Davies, S., Holt, C. S., et al. (1999). Cognitive-behavioral group therapy versus phenelzine in social phobia: long-term outcome. *Depress. Anxiety* 10, 89–98. doi: 10.1002/(SICI)1520-6394(1999)10:3<89::AID-DA1>3.0.CO;2-5

Lind, T., Lee Raby, K., Caron, E. B., Roben, C. K. P., and Dozier, M. (2017). Enhancing executive functioning among toddlers in foster care with an attachment-based intervention. *Dev. Psychopathol.* 29, 575–586. doi: 10.1017/S0954579417000190

Lindenberger, U., Li, S.-C., Gruber, W., and Müller, V. (2009). Brains swinging in concert: cortical phase synchronization while playing guitar. *BMC Neurosci.* 10:22. doi: 10.1186/1471-2202-10-22

Liu, Y., Wang, T., Wang, K., and Zhang, Y. (2021). Collaborative learning quality classification through physiological synchrony recorded by wearable biosensors. *Front. Psychol.* 12:674369. doi: 10.3389/fpsyg.2021.674369

Liu, J., Zhang, R., Xie, E., Lin, Y., Chen, D., Liu, Y., et al. (2023). Shared intentionality modulates interpersonal neural synchronization at the establishment of communication system. *Commun. Biol.* 6:832. doi: 10.1038/s42003-023-05197-z

Long, M., Verbeke, W., Ein-Dor, T., and Vrtička, P. (2020). A functional neuro-anatomical model of human attachment (NAMA): insights from first- and second-person social neuroscience. *Cortex* 126, 281–321. doi: 10.1016/j.cortex.2020.01.010

Long, Y., Zhong, M., Aili, R., Zhang, H., Fang, X., and Lu, C. (2023). Transcranial direct current stimulation of the right anterior temporal lobe changes interpersonal neural synchronization and shared mental processes. *Brain Stimul.* 16, 28–39. doi: 10.1016/j.brs.2022.12.009

Lotter, L. D., Kohl, S. H., Gerloff, C., Bell, L., Niephaus, A., Kruppa, J. A., et al. (2023). Revealing the neurobiology underlying interpersonal neural synchronization with multimodal data fusion. *Neurosci. Biobehav. Rev.* 146:105042. doi: 10.1016/j.neubiorev.2023.105042

Lu, H., Wang, X., Zhang, Y., Huang, P., Xing, C., Zhang, M., et al. (2023). Increased interbrain synchronization and neural efficiency of the frontal cortex to enhance human coordinative behavior: a combined hyper-tES and fNIRS study. *NeuroImage 282*:120385. doi: 10.1016/j.neuroimage.2023.120385

Luft, C. D. B., Zioga, I., Giannopoulos, A., Di Bona, G., Binetti, N., Civilini, A., et al. (2022). Social synchronization of brain activity increases during eye-contact. *Commun. Biol.* 5:412. doi: 10.1038/s42003-022-03352-6

Lyons, K. M., Stevenson, R. A., Owen, A. M., and Stojanoski, B. (2020). Examining the relationship between measures of autistic traits and neural synchrony during movies in children with and without autism. *NeuroImage Clin.* 28:102477. doi: 10.1016/j.nicl.2020.102477

Marz, N., and Warren, J. (2015). *Big data: principles and best practices of scalable realtime data systems. 1st ed*. Shelter Island, NY: Manning Publications Co.

Marzbani, H., Marateb, H. R., and Mansourian, M. (2016). Neurofeedback: a comprehensive review on system design, methodology and clinical applications. *Basic Clin. Neurosci.* 7, 143–158. doi: 10.15412/J.BCN.03070208

Mather, M., and Thayer, J. F. (2018). How heart rate variability affects emotion regulation brain networks. *Curr. Opin. Behav. Sci.* 19, 98–104. doi: 10.1016/j.cobeha.2017.12.017

Mathiak, K. A., Alawi, E. M., Koush, Y., Dyck, M., Cordes, J. S., Gaber, T. J., et al. (2015). Social reward improves the voluntary control over localized brain activity in fMRI-based neurofeedback training. *Front. Behav. Neurosci.* 9:136. doi: 10.3389/fnbeh.2015.00136

Matsumoto, H., and Ugawa, Y. (2017). Adverse events of tDCS and tACS: a review. *Clin. Neurophysiol. Pract.* 2, 19–25. doi: 10.1016/j.cnp.2016.12.003

McNaughton, K. A., and Redcay, E. (2020). Interpersonal synchrony in autism. *Curr. Psychiatry Rep.* 22:12. doi: 10.1007/s11920-020-1135-8

Mesibov, G. B., Shea, V., and Schopler, E. (2005). *The TEACCH approach to autism spectrum disorders*. New York, NY: Springer Science + Business Media.

Miller, J. G., Vrtička, P., Cui, X., Shrestha, S., Hosseini, S. M. H., Baker, J. M., et al. (2019). Inter-brain synchrony in mother-child dyads during cooperation: an fNIRS hyperscanning study. *Neuropsychologia* 124, 117–124. doi: 10.1016/j.neuropsychologia.2018.12.021

Miyata, K., Koike, T., Nakagawa, E., Harada, T., Sumiya, M., Yamamoto, T., et al. (2021). Neural substrates for sharing intention in action during face-to-face imitation. *NeuroImage* 233:117916. doi: 10.1016/j.neuroimage.2021.117916

Mizugaki, S., Maehara, Y., Okanoya, K., and Myowa-Yamakoshi, M. (2015). The power of an Infant's smile: maternal physiological responses to infant emotional expressions. *PLoS One* 10:e0129672. doi: 10.1371/journal.pone.0129672

Mogan, R., Fischer, R., and Bulbulia, J. A. (2017). To be in synchrony or not? A meta-analysis of synchrony's effects on behavior, perception, cognition and affect. *J. Exp. Soc. Psychol.* 72, 13–20. doi: 10.1016/j.jesp.2017.03.009

Montague, P. R., Berns, G. S., Cohen, J. D., McClure, S. M., Pagnoni, G., Dhamala, M., et al. (2002). Hyperscanning: simultaneous fMRI during linked social interactions. *NeuroImage* 16, 1159–1164. doi: 10.1006/nimg.2002.1150

Mu, Y., Guo, C., and Han, S. (2016). Oxytocin enhances inter-brain synchrony during social coordination in male adults. *Soc. Cogn. Affect. Neurosci.* 11, 1882–1893. doi: 10.1093/scan/nsw106

Mullen, T. R., Kothe, C. A. E., Chi, Y. M., Ojeda, A., Kerth, T., Makeig, S., et al. (2015). Real-time neuroimaging and cognitive monitoring using wearable dry EEG. *I.E.E.E. Trans. Biomed. Eng.* 62, 2553–2567. doi: 10.1109/TBME.2015.2481482

Müller, V., and Lindenberger, U. (2019). Dynamic orchestration of brains and instruments during free guitar improvisation. *Front. Integr. Neurosci.* 13:50. doi: 10.3389/fnint.2019.00050

Müller, V., and Lindenberger, U. (2022). Probing associations between interbrain synchronization and interpersonal action coordination during guitar playing. *Ann. N. Y. Acad. Sci.* 1507, 146–161. doi: 10.1111/nyas.14689

Müller, V., and Lindenberger, U. (2023). Intra- and interbrain synchrony and hyperbrain network dynamics of a guitarist quartet and its audience during a concert. *Ann. N. Y. Acad. Sci.* 1523, 74–90. doi: 10.1111/nyas.14987

Müller, V., Perdikis, D., Mende, M. A., and Lindenberger, U. (2021). Interacting brains coming in sync through their minds: an interbrain neurofeedback study. *Ann. N. Y. Acad. Sci.* 1500, 48–68. doi: 10.1111/nyas.14605

Müller, V., Sänger, J., and Lindenberger, U. (2013). Intra- and inter-brain synchronization during musical improvisation on the guitar. *PLoS One* 8:e73852. doi: 10.1371/journal.pone.0073852

Müller, V., Sänger, J., and Lindenberger, U. (2018). Hyperbrain network properties of guitarists playing in quartet. *Ann. N. Y. Acad. Sci.* 1423, 198–210. doi: 10.1111/nyas.13656

Nam, C. S., Choo, S., Huang, J., and Park, J. (2020). Brain-to-brain neural synchrony during social interactions: a systematic review on hyperscanning studies. *Appl. Sci.* 10:6669. doi: 10.3390/app10196669

National Institute for Health and Care Excellence (2013). Social anxiety: recognition, assessment and treatment: clinical guideline (NICE guideline 159). Available at: https://www.nice.org.uk/guidance/cg159 (Accessed August 5, 2023).

Nguyen, T., Schleihauf, H., Kayhan, E., Matthes, D., Vrtička, P., and Hoehl, S. (2020). The effects of interaction quality on neural synchrony during mother-child problem solving. *Cortex* 124, 235–249. doi: 10.1016/j.cortex.2019.11.020

Niso, G., Botvinik-Nezer, R., Appelhoff, S., De La Vega, A., Esteban, O., Etzel, J. A., et al. (2022). Open and reproducible neuroimaging: from study inception to publication. *NeuroImage* 263:119623. doi: 10.1016/j.neuroimage.2022.119623

Niso, G., Romero, E., Moreau, J. T., Araujo, A., and Krol, L. R. (2023). Wireless EEG: a survey of systems and studies. *NeuroImage* 269:119774. doi: 10.1016/j.neuroimage.2022.119774

Noah, A., Zhang, X., Dravida, S., Ono, Y., Naples, A., McPartland, J., et al. (2020). Real-time eye-to-eye contact is associated with cross-brain neural coupling in angular gyrus. *Front. Hum. Neurosci.* 14:19. doi: 10.3389/fnhum.2020.00019

Nolan, H., Whelan, R., and Reilly, R. B. (2010). FASTER: fully automated statistical thresholding for EEG artifact rejection. *J. Neurosci. Methods* 192, 152–162. doi: 10.1016/j.jneumeth.2010.07.015

Nordahl, H. M., Vogel, P. A., Morken, G., Stiles, T. C., Sandvik, P., and Wells, A. (2016). Paroxetine, cognitive therapy or their combination in the treatment of social anxiety disorder with and without avoidant personality disorder: a randomized clinical trial. *Psychother. Psychosom.* 85, 346–356. doi: 10.1159/000447013

Novembre, G., Knoblich, G., Dunne, L., and Keller, P. E. (2017). Interpersonal synchrony enhanced through 20 Hz phase-coupled dual brain stimulation. *Soc. Cogn. Affect. Neurosci.* 12, 662–670. doi: 10.1093/scan/nsw172

Nozawa, T., Sakaki, K., Ikeda, S., Jeong, H., Yamazaki, S., Kawata, K. H. D. S., et al. (2019). Prior physical synchrony enhances rapport and inter-brain synchronization during subsequent educational communication. *Sci. Rep.* 9:12747. doi: 10.1038/s41598-019-49257-z

O'Connor, T. G., and Zeanah, C. H. (2003). Attachment disorders: assessment strategies and treatment approaches. *Attach. Hum. Dev.* 5, 223–244. doi: 10.1080/1461673031000159397 4

Osaka, N., Minamoto, T., Yaoi, K., Azuma, M., Shimada, Y. M., and Osaka, M. (2015). How two brains make one synchronized mind in the inferior frontal cortex: fNIRS-based hyperscanning during cooperative singing. *Front. Psychol.* 6:1811. doi: 10.3389/fpsyg.2015.01811

Pan, Y., Novembre, G., Song, B., Zhu, Y., and Hu, Y. (2021). Dual brain stimulation enhances interpersonal learning through spontaneous movement synchrony. *Soc. Cogn. Affect. Neurosci.* 16, 210–221. doi: 10.1093/scan/nsaa080

Paulus, W. (2011). Transcranial electrical stimulation (tES – tDCS; tRNS, tACS) methods. *Neuropsychol. Rehabil.* 21, 602–617. doi: 10.1080/09602011.2011.557292

Piazza, E. A., Hasenfratz, L., Hasson, U., and Lew-Williams, C. (2020). Infant and adult brains are coupled to the dynamics of natural communication. *Psychol. Sci.* 31, 6–17. doi: 10.1177/0956797619878698

Pinti, P., Tachtsidis, I., Hamilton, A., Hirsch, J., Aichelburg, C., Gilbert, S., et al. (2020). The present and future use of functional near-infrared spectroscopy (fNIRS) for cognitive neuroscience. *Ann. N. Y. Acad. Sci.* 1464, 5–29. doi: 10.1111/nyas.13948

Pratt, M., Zeev-Wolf, M., Goldstein, A., and Feldman, R. (2019). Exposure to early and persistent maternal depression impairs the neural basis of attachment in preadolescence. *Prog. Neuro-Psychopharmacol. Biol. Psychiatry* 93, 21–30. doi: 10.1016/j.pnpbp.2019.03.005

Putri, F., Susnoschi Luca, I., Garcia Pedro, J. A., Ding, H., and Vučković, A. (2022). Winners and losers in brain computer interface competitive gaming: directional connectivity analysis. *J. Neural Eng.* 19:046037. doi: 10.1088/1741-2552/ac8451

Quiñones-Camacho, L. E., Fishburn, F. A., Belardi, K., Williams, D. L., Huppert, T. J., and Perlman, S. B. (2021). Dysfunction in interpersonal neural synchronization as a mechanism for social impairment in autism spectrum disorder. *Autism Res.* 14, 1585–1596. doi: 10.1002/aur.2513

Ramseyer, F., and Tschacher, W. (2011). Nonverbal synchrony in psychotherapy: coordinated body movement reflects relationship quality and outcome. *J. Consult. Clin. Psychol.* 79, 284–295. doi: 10.1037/a0023419

Reindl, V., Gerloff, C., Scharke, W., and Konrad, K. (2018). Brain-to-brain synchrony in parent-child dyads and the relationship with emotion regulation revealed by fNIRS-based hyperscanning. *NeuroImage* 178, 493–502. doi: 10.1016/j.neuroimage.2018.05.060

Reindl, V., Wass, S., Leong, V., Scharke, W., Wistuba, S., Wirth, C. L., et al. (2022). Multimodal hyperscanning reveals that synchrony of body and mind are distinct in mother-child dyads. *NeuroImage* 251:118982. doi: 10.1016/j.neuroimage.2022.118982

Reinero, D. A., Dikker, S., and Van Bavel, J. J. (2021). Inter-brain synchrony in teams predicts collective performance. *Soc. Cogn. Affect. Neurosci.* 16, 43–57. doi: 10.1093/scan/nsaa135

Rennung, M., and Göritz, A. S. (2016). Prosocial consequences of interpersonal synchrony. *Z. Psychol.* 224, 168–189. doi: 10.1027/2151-2604/a000252

Ros, T., Enriquez-Geppert, S., Zotev, V., Young, K. D., Wood, G., Whitfield-Gabrieli, S., et al. (2020). Consensus on the reporting and experimental design of clinical and cognitive-behavioural neurofeedback studies (CRED-nf checklist). *Brain* 143, 1674–1685. doi: 10.1093/brain/awaa009

Rutter, M., Kreppner, J., Croft, C., Murin, M., Colvert, E., Beckett, C., et al. (2007). Early adolescent outcomes of institutionally deprived and non-deprived adoptees. III. Quasi-autism. *J. Child Psychol. Psychiatry* 48, 1200–1207. doi: 10.1111/j.1469-7610.2007.01792.x

Rutter, M., Kreppner, J., and Sonuga-Barke, E. (2009). Emanuel Miller lecture: attachment insecurity, disinhibited attachment, and attachment disorders: where do research findings leave the concepts? *J. Child Psychol. Psychiatry* 50, 529–543. doi: 10.1111/j.1469-7610.2009.02042.x

Salminen, M., Järvelä, S., Ruonala, A., Harjunen, V. J., Hamari, J., Jacucci, G., et al. (2022). Evoking physiological synchrony and empathy using social VR with biofeedback. *IEEE Trans. Affect. Comput.* 13, 746–755. doi: 10.1109/TAFFC.2019.2958657

Sänger, J., Müller, V., and Lindenberger, U. (2012). Intra- and interbrain synchronization and network properties when playing guitar in duets. *Front. Hum. Neurosci.* 6:312. doi: 10.3389/fnhum.2012.00312

Saul, M. A., He, X., Black, S., and Charles, F. (2022). Corrigendum: a two-person neuroscience approach for social anxiety: a paradigm with interbrain synchrony and neurofeedback. *Front. Psychol.* 13:871022. doi: 10.3389/fpsyg.2022.871022

Schilbach, L. (2016). Towards a second-person neuropsychiatry. *Philos. Trans. R. Soc. Lond. Ser. B Biol. Sci.* 371:20150081. doi: 10.1098/rstb.2015.0081

Schilbach, L., and Lahnakoski, J. M. (2023). "Clinical neuroscience meets second-person neuropsychiatry," in *Social and affective neuroscience of everyday human interaction: From theory to methodology*, eds. P. S. Boggio, T. S. H. Wingenbach, Silveira CoêlhoM. L. da, W. E. Comfort, L. Murrins Marques and M. V. C. Alves (Cham: Springer International Publishing), 177–191.

Schoenherr, D., Paulick, J., Strauss, B. M., Deisenhofer, A.-K., Schwartz, B., Rubel, J. A., et al. (2019). Nonverbal synchrony predicts premature termination of psychotherapy for social anxiety disorder. *Psychotherapy* 56, 503–513. doi: 10.1037/pst0000216

Schoenherr, D., Strauss, B., Stangier, U., and Altmann, U. (2021). The influence of vocal synchrony on outcome and attachment anxiety/avoidance in treatments of social anxiety disorder. *Psychotherapy* 58, 510–522. doi: 10.1037/pst0000393

Sepulveda, P., Sitaram, R., Rana, M., Montalba, C., Tejos, C., and Ruiz, S. (2016). How feedback, motor imagery, and reward influence brain self-regulation using real-time fMRI. *Hum. Brain Mapp.* 37, 3153–3171. doi: 10.1002/hbm.23228

Sorger, B., Scharnowski, F., Linden, D. E. J., Hampson, M., and Young, K. D. (2019). Control freaks: towards optimal selection of control conditions for fMRI neurofeedback studies. *NeuroImage* 186, 256–265. doi: 10.1016/j.neuroimage.2018.11.004

Spain, D., and Blainey, S. H. (2015). Group social skills interventions for adults with high-functioning autism spectrum disorders: a systematic review. *Autism* 19, 874–886. doi: 10.1177/1362361315587659

Spengler, F. B., Scheele, D., Marsh, N., Kofferath, C., Flach, A., Schwarz, S., et al. (2017). Oxytocin facilitates reciprocity in social communication. *Soc. Cogn. Affect. Neurosci.* 12, 1325–1333. doi: 10.1093/scan/nsx061

Srinivasan, S. M., Kaur, M., Park, I. K., Gifford, T. D., Marsh, K. L., and Bhat, A. N. (2015). The effects of rhythm and robotic interventions on the imitation/praxis, interpersonal synchrony, and motor performance of children with autism spectrum disorder (ASD): a pilot randomized controlled trial. *Autism Res. Treat.* 2015:736516, 1–18. doi: 10.1155/2015/736516

Stein, D. J., Ipser, J. C., and Balkom, A. J. (2004). Pharmacotherapy for social phobia. *Cochrane Database Syst. Rev.* 18:CD001206. doi: 10.1002/14651858.CD001206.pub2

Stein, M. B., and Stein, D. J. (2008). Social anxiety disorder. *Lancet* 371, 1115–1125. doi: 10.1016/S0140-6736(08)60488-2

Steiner, N. J., Frenette, E., Hynes, C., Pisarik, E., Tomasetti, K., Perrin, E. C., et al. (2014). A pilot feasibility study of neurofeedback for children with autism. *Appl. Psychophysiol. Biofeedback* 39, 99–107. doi: 10.1007/s10484-014-9241-1

Steinert, C., Hofmann, M., Leichsenring, F., and Kruse, J. (2013). What do we know today about the prospective long-term course of social anxiety disorder? A systematic literature review. *J. Anxiety Disord.* 27, 692–702. doi: 10.1016/j.janxdis.2013.08.002

Stepanova, E. R., Desnoyers-Stewart, J., Pasquier, P., and Riecke, B. E. (2020). JeL: breathing together to connect with others and nature. In Proceedings of the 2020 ACM Designing Interactive Systems Conference (DIS '20) (New York, NY, USA: Association for Computing Machinery), 641–654. doi: 10.1145/3357236.3395532

Strehl, U., Aggensteiner, P., Wachtlin, D., Brandeis, D., Albrecht, B., Arana, M., et al. (2017). Neurofeedback of slow cortical potentials in children with attention-deficit/hyperactivity disorder: a multicenter randomized trial controlling for unspecific effects. *Front. Hum. Neurosci.* 11:135. doi: 10.3389/fnhum.2017.00135

Stuhldreher, N., Leibing, E., Leichsenring, F., Beutel, M. E., Herpertz, S., Hoyer, J., et al. (2014). The costs of social anxiety disorder: the role of symptom severity and comorbidities. *J. Affect. Disord.* 165, 87–94. doi: 10.1016/j.jad.2014.04.039

Subramanyam, A. A., Mukherjee, A., Dave, M., and Chavda, K. (2019). Clinical practice guidelines for autism Spectrum disorders. *Indian J. Psychiatry* 61, 254–269. doi: 10.4103/psychiatry.IndianJPsychiatry_542_18

Susnoschi Luca, I., Putri, F. D., Ding, H., and Vuckovič, A. (2021). Brain synchrony in competition and collaboration during multiuser neurofeedback-based gaming. *Front. Neuroergon.* 2:749009. doi: 10.3389/fnrgo.2021.749009

Szymanski, C., Müller, V., Brick, T. R., von Oertzen, T., and Lindenberger, U. (2017). Hyper-transcranial alternating current stimulation: experimental manipulation of inter-brain synchrony. *Front. Hum. Neurosci.* 11:539. doi: 10.3389/fnhum.2017.00539

Tanabe, H. C., Kosaka, H., Saito, D. N., Koike, T., Hayashi, M. J., Izuma, K., et al. (2012). Hard to "tune in": neural mechanisms of live face-to-face interaction with high-functioning autistic spectrum disorder. *Front. Hum. Neurosci.* 6:268. doi: 10.3389/fnhum.2012.00268

Tennant, J. M., Cook, S., Moldoveanu, M. C., Peterson, J. B., and Cunningham, W. A. (2019). "Interpersonal resonance: developing interpersonal biofeedback for the promotion of empathy and social entrainment" in *Advances in human factors in wearable technologies and game design advances in intelligent systems and computing*. ed. T. Z. Ahram (Cham: Springer International Publishing), 208–214.

Thair, H., Holloway, A. L., Newport, R., and Smith, A. D. (2017). Transcranial direct current stimulation (tDCS): a beginner's guide for design and implementation. *Front. Neurosci.* 11:641. doi: 10.3389/fnins.2017.00641

Thibault, R. T., MacPherson, A., Lifshitz, M., Roth, R. R., and Raz, A. (2018). Neurofeedback with fMRI: a critical systematic review. *NeuroImage* 172, 786–807. doi: 10.1016/j.neuroimage.2017.12.071

Ulmer-Yaniv, A., Yirmiya, K., Peleg, I., Zagoory-Sharon, O., and Feldman, R. (2023). Developmental cascades link maternal-newborn skin-to-skin contact with Young adults' psychological symptoms, oxytocin, and immunity; charting mechanisms of developmental continuity from birth to adulthood. *Biology* 12:847. doi: 10.3390/biology12060847

Valdesolo, P., and DeSteno, D. (2011). Synchrony and the social tuning of compassion. *Emotion* 11, 262–266. doi: 10.1037/a0021302

Valdesolo, P., Ouyang, J., and DeSteno, D. (2010). The rhythm of joint action: synchrony promotes cooperative ability. *J. Exp. Soc. Psychol.* 46, 693–695. doi: 10.1016/j.jesp.2010.03.004

Vicaria, I. M., and Dickens, L. (2016). Meta-analyses of the intra- and interpersonal outcomes of interpersonal coordination. *J. Nonverbal Behav.* 40, 335–361. doi: 10.1007/s10919-016-0238-8

Vidal-Rosas, E. E., Lühmann, A.Von, Pinti, P., and Cooper, R. J. (2023). Wearable, high-density fNIRS and diffuse optical tomography technologies: a perspective. *Neurophotonics.* 10:023513. doi: 10.1117/1.NPh.10.2.023513

Vrins, A., Pruss, E., Ceccato, C., Prinsen, J., and Alimardani, M. (2023). Investigating the impact of a dual musical brain-computer interface on interpersonal synchrony: a pilot study. doi: 10.48550/ARXIV.2309.02079

Wang, H., Suveg, C., West, K. B., Han, Z. R., Zhang, X., Hu, X., et al. (2021). Synchrony of respiratory sinus arrhythmia in parents and children with autism Spectrum disorder: moderation by interaction quality and child behavior problems. *Autism Res.* 14, 512–522. doi: 10.1002/aur.2401

Wang, Y., Wang, F., Kong, Y., Gao, T., Zhu, Q., Han, L., et al. (2023). High definition transcranial direct current stimulation of the Cz improves social dysfunction in children with autism spectrum disorder: a randomized, sham, controlled study. *Autism Res. 16*, 2035–2048. doi: 10.1002/aur.3018

Wass, S. V., Whitehorn, M., Marriott Haresign, I., Phillips, E., and Leong, V. (2020). Interpersonal neural entrainment during early social interaction. *Trends Cogn. Sci.* 24, 329–342. doi: 10.1016/j.tics.2020.01.006

Wei, Y., Zhu, J., Pan, S., Su, H., Li, H., and Wang, J. (2017). Meta-analysis of the efficacy and safety of repetitive transcranial magnetic stimulation (rTMS) in the treatment of depression. *Shanghai Arch. Psychiatry* 29, 328–342. doi: 10.11919/j.issn.1002-0829.217106

Wiltermuth, S. S., and Heath, C. (2009). Synchrony and cooperation. *Psychol. Sci.* 20, 1–5. doi: 10.1111/j.1467-9280.2008.02253.x

Xu, W.-W., Liao, Q.-H., and Zhu, D.-W. (2022). The effect of transcranial magnetic stimulation on the recovery of attention and memory impairment following stroke: a systematic review and meta-analysis. *Expert. Rev. Neurother.* 22, 1031–1041. doi: 10.1080/14737175.2022.2155515

Xu, X., Xu, M., Su, Y., Cao, T. V., Nikolin, S., Moffa, A., et al. (2023). Efficacy of repetitive transcranial magnetic stimulation (rTMS) combined with psychological interventions: a systematic review and Meta-analysis of randomized controlled trials. *Brain Sci.* 13:1665. doi: 10.3390/brainsci13121665

Zamm, A., Debener, S., Bauer, A.-K. R., Bleichner, M. G., Demos, A. P., and Palmer, C. (2018). Amplitude envelope correlations measure synchronous cortical oscillations in performing musicians. *Ann. N. Y. Acad. Sci.* 1423, 251–263. doi: 10.1111/nyas.13738

Zeanah, C. H., Chesher, T., Boris, N. W., Walter, H. J., Bukstein, O. G., Bellonci, C., et al. (2016). Practice parameter for the assessment and treatment of children and adolescents with reactive attachment disorder and disinhibited social engagement disorder. *J. Am. Acad. Child Adolesc. Psychiatry* 55, 990–1003. doi: 10.1016/j.jaac.2016.08.004

Zhang, L., Xu, X., Li, Z., Chen, L., and Feng, L. (2022). Interpersonal neural synchronization predicting learning outcomes from teaching-learning interaction: a meta-analysis. *Front. Psychol.* 13:835147. doi: 10.3389/fpsyg.2022.835147

Zhang, R., and Zhao, X. (2018). "A cross-brain interaction platform based on neurofeedback using electroencephalogram" in *Augmented cognition: intelligent technologies lecture notes in computer science*. eds. D. D. Schmorrow and C. M. Fidopiastis (Cham: Springer International Publishing), 222–230.

Zheng, L., Liu, W., Long, Y., Zhai, Y., Zhao, H., Bai, X., et al. (2020). Affiliative bonding between teachers and students through interpersonal synchronisation in brain activity. *Soc. Cogn. Affect. Neurosci.* 15, 97–109. doi: 10.1093/scan/nsaa016

Zilverstand, A., Sorger, B., Sarkheil, P., and Goebel, R. (2015). fMRI neurofeedback facilitates anxiety regulation in females with spider phobia. *Front. Behav. Neurosci.* 9:148. doi: 10.3389/fnbeh.2015.00148

# Frontiers in Neuroscience

**Provides a holistic understanding of brain function from genes to behavior**

Part of the most cited neuroscience journal series which explores the brain - from the new eras of causation and anatomical neurosciences to neuroeconomics and neuroenergetics.

---

## Discover the latest Research Topics

See more →

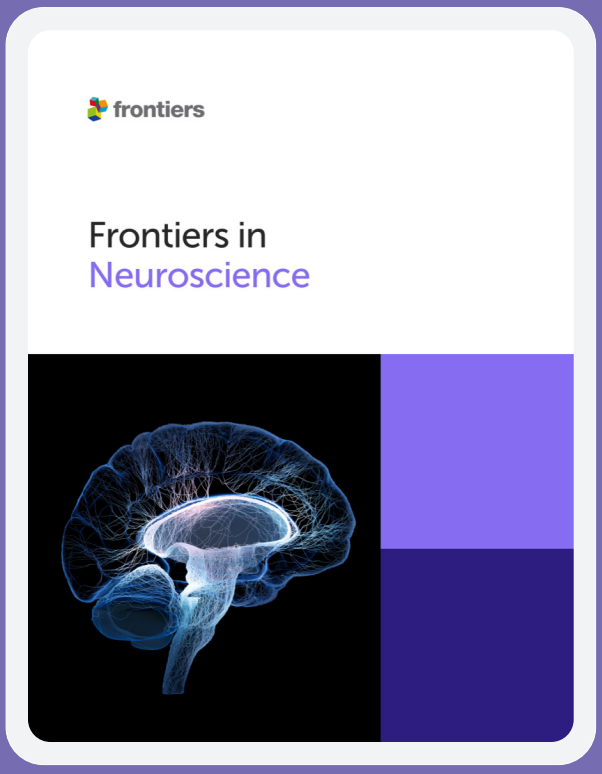


**Frontiers**

Avenue du Tribunal-Fédéral 34
1005 Lausanne, Switzerland
frontiersin.org

**Contact us**

+41 (0)21 510 17 00
frontiersin.org/about/contact